NASA CR-165275
RI/RD80-237

(NASA-CR-165275) LOW-THRUST CHEMICAL ROCKET ENGINE STUDY Final Progress Report, Jul. 1979 - Nov. 1980 (Rocketdyne) 340 p
HC A15/MF A01 CSCL 21H

N81-21125

Unclas
G3/20 42060

NASA

FINAL REPORT
LOW-THRUST CHEMICAL ROCKET ENGINE STUDY

by

J. M. Shoji

Rockwell International
Rocketdyne Division

prepared for
NATIONAL AERONAUTICS AND SPACE ADMINISTRATION

NASA-Lewis Research Center
Contract NAS3-21941

FOREWORD

This program was conducted by the Rocketdyne Division of Rockwell International for NASA-Lewis Research Center under Contract NAS3-21941 during the period July 1979 to November 1980. Mr. Dean Scheer was the NASA Project Manager. Mr. Harold Diem was the Rocketdyne Program Manager, and Mr. James Shoji was the Project Engineer.

The work presented in this report represents the concerted effort and expertise of many members of the Rocketdyne organization. Contributions of major significance were made by the following personnel:

P. Chen	- Engine Cycle Balance Analysis, Parametric Engine Performance Analysis, and Off-Design Engine Balance Analysis
D. P. Lim	- Boundary Layer and Heat Transfer Analysis
C. A. Laren	- Heat Transfer Analysis
A. P. Swift	- Engine Design
N. Djordjenic	- Engine Cycle Balance Analysis
W. H. Geniec	- Thrust Chamber Performance Analysis
D. F. Carson	- Engine Weight Analysis
R. B. Furst	- Pump Analysis
F. C. O'Hern	- Off-Design Pump Analysis
L. H. Russell	- Engine Complexity Rating
J. L. Boynton	- Turbine Analysis
M. Jensen	- Turbine Analysis
V. W. Jaqua	- Injector Performance and Design
J. Q. Weber	- Thereotical Propellant Performance and Properties
W. R. Bissell	- Turbopump Trends

TABLE OF CONTENTS

ILLUSTRATIONS

TABLES

SUMMARY

Over the specified range of thrust level (444.8 N or 100 lbf to 13345 N or 3000 lbf) and chamber pressure (13.8 N/cm^2 or 20 psia to 689.5 N/cm^2 or 1000 psia) the thrust chamber cooling limits were established for regenerative/radiation and film / radiation cooling using specified analysis guidelines. For regenerative/radiation-cooled thrust chambers, the maximum chamber pressure at a given thrust was limited primarily by the maximum coolant Mach number and the material wall temperature limit. The minimum chamber pressure was limited by two-phase heat transfer. The LO_2/H_2 regenerative/radiation-cooled thrust chamber provided the largest chamber pressure versus thrust operational envelope. Using the specified analysis guidelines, LO_2/RP-1 regenerative/radiation cooling was found unfeasible; however, with a gas-side carbon layer (physical thermal barrier), a feasible operational regime was achieved. An extended thrust chamber cooling capability analysis was also performed using physical thermal barriers and more optimistic analysis guidelines.

The LO_2/H_2 and LO_2/RP-1 film/radiation-cooled thrust chambers were limited to low chamber pressures, and LO_2/CH_4 film/radiation-cooled thrust chambers were not feasible. These thrust chambers were limited by the maximum material temperature limit and the film-cooled performance loss limit of 10%.

The results of thrust chamber heat transfer analysis were used to perform the initial engine cycle/configuration matrix screening. For the resulting engine cycle/configuration matrix, the engine cycle limits were determined by performing individual cycle balances. The fuel-cell-powered cycle engine achieved the maximum study chamber pressure over the entire thrust range. The other pump-fed engines achieved cycle limits below the thrust chamber cooling limits for most of the thrust range. Therefore, for the most part, the engine cycle limited the maximum achievable chamber pressure at a given thrust level. In addition, parametric thrust chamber performance and engine weight were generated for a 400-to-1 area ratio nozzle.

To select the two engine cycle/configurations for the preliminary engine design, the candidate engine cycle/configurations were rated according to the maximum achievable chamber pressure, delivered specific impulse, engine weight, and configuration complexity. For the LO_2/H_2 engines, the direct expander cycle engine achieved the highest overall rating. For the LO_2/Hydrocarbon engines, the LO_2/CH_4 direct expander cycle engine obtained the highest overall rating. Therefore, these two engine configurations were recommended and approved for preliminary engine design. NASA-LeRC selected a design thrust of 2224.1 N (500 lbf) for the preliminary designs.

The design chamber pressures for these two engines were established through an iteration of engine cycle balances and detailed pump, turbine, and thrust chamber heat transfer analyses. A summary of the pertinent preliminary design point engine data is presented for the LO_2/H_2 and LO_2/CH_4 engines in Table 1. The LO_2/H_2 engine resulted in a higher design chamber pressure and, therefore, had slightly smaller dimensions. However, the LO_2/CH_4 engine achieved a lighter engine due to smaller pumps. The LO_2/H_2 engine attained a significantly higher specific impulse (approximately 29% higher) due to the lighter-molecular-weight propellant and the higher design chamber pressure. Engine cycle balances were performed at the design point (nominal mixture ratio) and at ±10%/mixture off-design conditions.

TABLE 1. PRELIMINARY ENGINE DESIGN SUMMARY

PROPELLANT COMBINATION	LO_2/H_2	LO_2/CH_4
THRUST, N (lbf)	500	500
CYCLE	DIRECT EXPANDER	DIRECT EXPANDER
COOLING	REGENERATIVE/RADIATION	REGENERATIVE/RADIATION
CHAMBER PRESSURE, N/cm^2 (PSIA)	328.9 (477)	307.5 (446)
MIXTURE RATIO	6	3.7
AREA RATIO - NOZZLE EXTENSION - FIXED NOZZLE	 400 200	 400 200
SPECIFIC IMPULSE, N-sec/kg (LBF-SEC/LBM)	4564.5 (465.45)	3543 (361.29)
WEIGHT, kg (LBM)	28.46 (62.75)	25.8 (56.87)
RETRACTED ENGINE LENGTH, cm (INCHES)	56.2 (22.13)	56.6 (22.28)
TOTAL ENGINE (EXTENDED) LENGTH, cm (INCHES)	91.9 (36.19)	94.1 (37.06)
MAXIMUM ENGINE DIAMETER, cm (INCHES)	42.29 (16.65)	43.7 (17.22)

Engine design drawings were prepared for both engines, and pump and injector component drawings were prepared to illustrate preliminary component designs.

Updated parametric engine performance, engine dimensions, and engine weights were generated for the study thrust, chamber pressure, and nozzle area ratio range. The LO_2/H_2 engines offer a 30% delivered specific impulse increase with a slight engine weight penalty as compared to the LO_2/CH_4 engines. For the same thrust, chamber pressure, and area ratio, the engine length and diameter were essentially the same for the two propellant combinations. The parametric engine performance data for LO_2/H_2 engines indicated a significant performance gain with high area ratio nozzles.

Engine technology advancement required and those which could lead to further engine performance, weight, and size improvement are presented and discussed.

INTRODUCTION

An analytical study was performed to evaluate thrust chamber cooling, engine cycles, and preliminary engine designs for low-thrust chemical rocket engines for orbit-transfer vehicles. This evaluation was conducted for oxygen/hydrogen (LO_2/H_2), oxygen/methane (LO_2/CH_4), and oxygen/RP-1 (LO_2/RP-1) engines with thrust levels from 444.8 N (100 pounds) to 13345 N (3000 pounds) and chamber pressures from 13.8 N/cm^2 (20 psia) to 689.5 N/cm^2 (1000 psia). The study provides NASA and vehicle designers with theoretical propellant performance data, thrust chamber cooling limits, parametric engine data, preliminary engine designs, and identification of required technology items and advances.

Propellant physical and thermodynamic properties, theoretical propellant performance data, and transport properties were generated, organized, and documented for the three propellant combinations. The thrust chamber cooling limits for regenerative/radiation and film/radiation cooling were defined and parametric heat transfer data were generated for use in the engine cycle analysis. A conceptual evaluation of a number of engine cycles, including both pump- and pressure-fed engines was performed along with the generation of parametric engine data. Based on this evaluation, one LO_2/H_2 engine cycle/configuration and one LO_2/CH_4 engine cycle/configuration were chosen and recommended to NASA-LeRC for preliminary engine design. These low-thrust engine cycle/configurations were approved by NASA-LeRC, and preliminary engine designs were formulated and updated parametric engine data (delivered specific impulse, engine dimensions, and engine weight) were generated. Engine design drawings were prepared and an assessment of technology required was performed.

DISCUSSION

PROPELLANT PROPERTIES AND PERFORMANCE

The theoretical propellant performance data (characteristic velocity and specific impulse) and the propellant transport property data for LO_2/H_2, LO_2/CH_4, and LO_2/RP-1) generated for this program are presented in Appendixes A and B. The format of the plotted theoretical data is illustrated in Fig. 1 .

The characteristic velocity is plotted versus mixture ratio for parametric chamber pressure and two fuel injection temperatures. The theoretical vacuum specific impulse is plotted versus mixture ratio for parametric area ratio and five chamber pressures and two fuel injection temperatures.

The variation of the following combustion chamber gas transport properties with chamber pressure and mixture ratio were plotted for each propellant:

1. Combustion temperature
2. Molecular weight
3. Specific heat ($C_{p_{frozen}}$)
4. Specific heat ratio (γ)
5. Density
6. Thermal conductivity (k_{frozen})
7. Viscosity

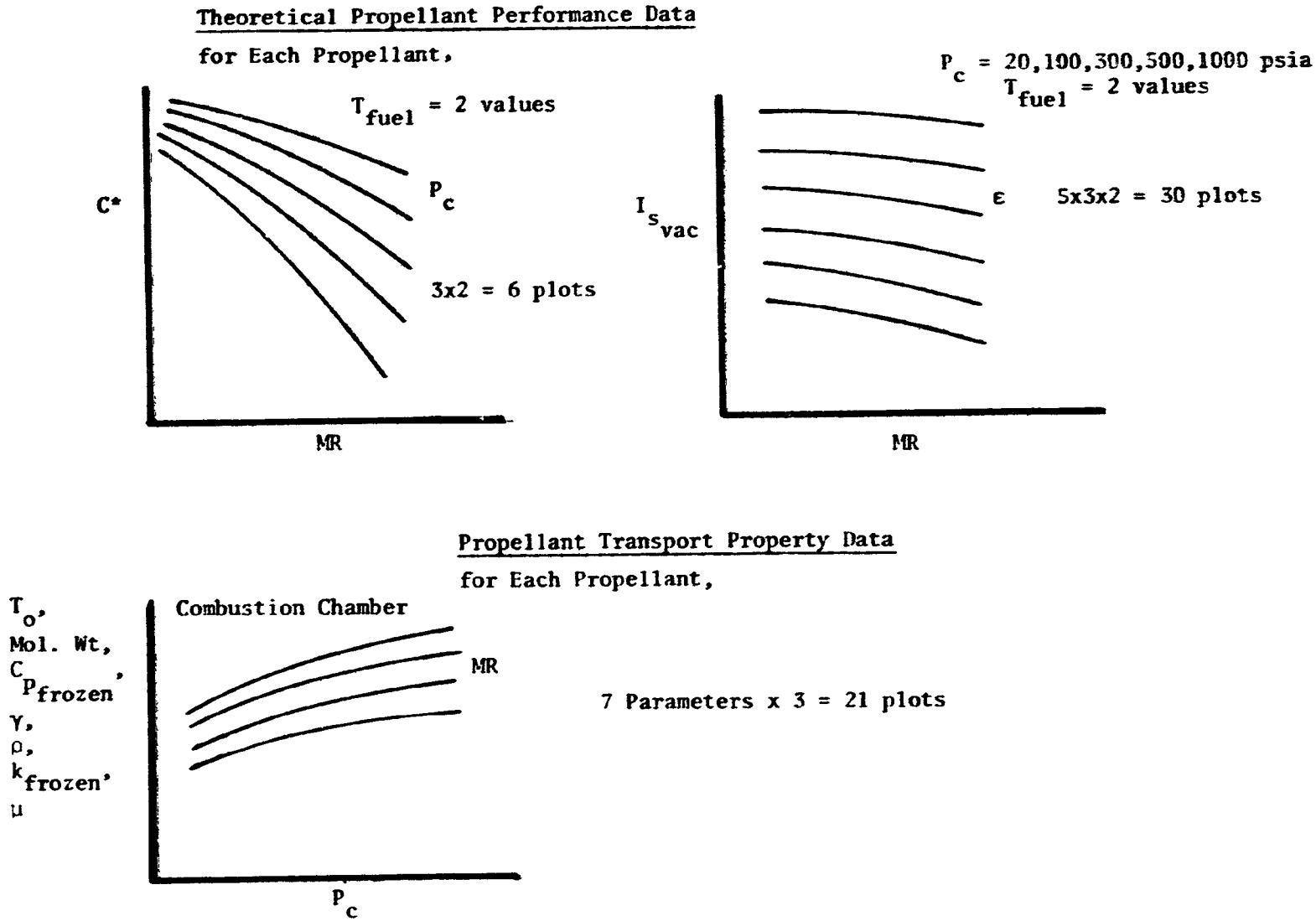

Figure 1 . Task I Data Plot Format

THRUST CHAMBER COOLING ANALYSIS

The thrust chamber cooling limits (maximum and minimum chamber pressures) were established for LO_2/H_2, LO_2/CH_4, and LO_2/RP-1 using fuel regenerative/radiation-cooling and film/radiation-cooling. Detailed coolant passage geometry and wall temperature data were calculated for a number of thrust chamber designs. In addition, the thrust chamber heat input and coolant pressure drop parametric data were determined for the three propellant combinations for use in the engine cycle/configuration evaluation.

Analysis Guidelines

The major analysis guidelines used in the thrust chamber cooling evaluation are presented in Table 2 . The combustion chambers were to be sized (chamber length and contraction ratio) to achieve a combustion efficiency of 98% or greater. The nozzle contour evaluated was an aerodynamic optimum 90% length, 400-to-1 area ratio nozzle.

In the heat transfer analysis, the existence of a gas-side carbon layer for the hydrocarbon-fueled propellants (LO_2/CH_4 and LO_2/RP-1) was to be neglected and for RP-1, a coking temperature limit of 561 K (550 F) was to be assumed. A gas-side carbon layer can greatly reduce the local heat flux and coolant heat input through the insulating characteristic of the carbon layer. However, the existence of carbon layer subsequent to an engine shutdown and its transient buildup to sufficient protective thicknesses during an engine start has been questioned and, therefore, the carbon layer influence was neglected as specified by the analysis guidelines. The coking of the hydrocarbon fuel is the thermal decomposition of the fuel on the coolant side of the regenerative-cooled thrust chamber coolant passage. The resulting thermal insulating deposits on the coolant side wall are detrimental and eventually result in wall failure. Increasing this coking limit through fuel refinement and/or surface catalytic influence would improve the cooling of RP-1 cooled thrust chambers.

In addition to the analysis guidelines presented in Table 2 , assumptions were made that included:

1. Maximum coolant curvature enhancement factor = 1.4
2. Internal tube or channel roughness = 60 microinches
3. Ripple factor $\left(\frac{\text{Heat Input Surface Area}}{\text{Project Area}}\right)$
   a. Tube ripple factor = 1.11
   b. Channel ripple factor = 1.00
4. Coolant pressure drop included:
   a. Two velocity head return manifold loss
   b. One velocity head exit loss

TABLE 2. THRUST CHAMBER STUDY GUIDELINES

Parameter	Guideline
Propellant	• O_2/H_2 at a mixture ratio of 6.0 • O_2/CH_4 at a mixture ratio of 3.7 • O_2/RP-1 at a mixture ratio of 3.0
Engine Size	• Thrust: 100 to 4000 pounds • Chamber Pressure: 20 to 1000 psia • 400:1 area ratio nozzle with 90% length
Performance	• 98% combustion efficiency • Film/radiation cooled configuration $P_{c_{max}}$: $(\eta_{t_h})_{FILM}$ = 0.90 $P_{c_{min}}$: $(\eta_{t_h})_{FILM}$ = 0.97

Combustor Geometry	Regenerative-Cooled Configuration:
	• Nontubular construction (i.e., channels)
	• Coolant channel dimension limits
	  • Minimum channel width = 0.01 inch
	  • Minimum web thickness = 0.01 inch
	  • Minimum wall thickness = 0.025 inch
	  • Maximum channel depth-to-width ratio = 4:1

Nozzle Geometry	• 400:1 area ratio nozzle with 90% length
	• Radiation-cooled section (criterion to be determined)
	• Regenerative/radiation cooled configuration
	  • Tubular construction
	  • Minimum wall thickness = 0.010 inch

Thrust Chamber Material	• Regenerative/radiation cooling
	  • Combustor: copper-base alloy or nickel
	  • Nozzle: stainless steel
	  • Radiation section: TBD
	  } With NASA-LeRC concurrence
	• Film/radiation cooling
	  • TBD

Thrust Chamber Wall Temperature Limits	• Regenerative/radiation cooling
	  • 1460 R for copper-base alloy (with NASA-LeRC concurrence)
	  • Coking temperature limits (see coolant heat transfer)
	  • Radiation section: TBD
	• Film/radiation cooling
	  • TBD

Hot-Gas Heat Transfer	• Contractor in-house methods and correlations to be used • Benefit of carbon deposition and hot-gas wall will be neglected

Coolant Heat Transfer	• Coolant inlet temperature
	  H_2: 17.8 R
	  RP-1: 537 R
	  CH_4: 201 R
	  } Fuels
	• Coolant discharge pressure
	  Liquid: 1.176 x P_c
	  Gas: 1.087 x P_c
	  } Minimum regenerative discharge or film coolant inlet
	• Maximum coolant velocity (regenerative)
	  Liquid: 200 ft/sec
	  Gas: Mach No. = 0.3
	• Coking Limits
	  RP-1: $(T_{wc})_{max}$ = 1010 R
	  CH_4: $(T_{wc})_{max}$ = 1760 R
	• Coolant state at jacket discharge will be single phase
	• Coolant flow through jacket must be stable (stability criteria to be approved by NASA-LeRC)

Cycle Life	• Five terminal cycles times a safety factor of four • Accumulative run time as specified in Fig. 1 of RFP

Subsequent to the analysis using these study guidelines, an extended thrust chamber cooling analysis was performed using more optimistic criteria and thermal barriers which included a carbon layer for LO_2/RP-1.

Although many types of thrust chamber cooling approaches could be applied for these low-thrust engines, the more conventional and promising regenerative/radiation and film/radiation cooling methods were specified. These methods are illustrated schematically in Fig. 2 . The regenerative/radiation cooling consists of two separately cooled sections which include a regenerative-cooled section using fuel forced convection cooling and a radiation-cooled nozzle section. In the film/radiation cooled thrust chamber, the combustion chamber is film cooled and the nozzle is cooled using a combination of film and radiation cooling. The film cooling in this study was assumed to be injected at the injector. In general, regenerative cooling is used in the high heat flux applications, and film and radiation cooling are used in low heat flux applications and low heat flux regions of a thrust chamber.

A maximum coolant gaseous Mach No. of 0.3 and a maximum liquid velocity of 200 ft/sec were specified. For the regenerative-cooled portion, the combined channel wall combustor (NARloy-Z for hydrogen and RP-1 and nickel for methane) and tubular nozzle (stainless steel) configuration was selected to achieve maximum cooling with a lightweight thrust chamber. For the film- and radiation-cooled portions, conventional materials (L-605 alloy and molybdenum) were evaluated, although more advanced materials such as carbon-carbon composites may potentially be incorporated.

Thrust Chamber Geometry

Combustion Chamber. The combustion chamber injector-to-throat length and contraction ratio were sized to deliver greater than the required 98% combustion efficiency. The LO_2/RP-1 and LO_2/H_2 data were obtained using an analytical-empirical computer program based on a curve-fit of existing engine test data. This type of data does not exist for LO_2/CH_4; therefore, an interpolating sizing criteria was used.

The LO_2/RP-1 sizing criteria have been developed around the vaporization characteristics of the fuel. RP-1 is a liquid hydrocarbon with relatively low vapor pressure at standard conditions of temperature and pressure. The fuel viscosity and surface tension tend to restrict atomization and vaporization when compared to the more volatile oxidizer. As a result, combustion performance is usually limited by vaporization of the fuel, and the combustion chamber size is optimized to provide a combination of residence time and relatively high gas velocity for "stripping" drops, enhancing "secondary breakup", and droplet heating. These required features lead to long combustion chamber length and low contraction ratios.

For LO_2/H_2, the fuel is typically injected as a gas and, therefore, fuel vaporization is not a problem. Liquid oxygen vaporization can be limiting; however, the low viscosity, low surface tensions, and high vapor pressure of liquid oxygen results in relative ease of atomization and rapid vaporization.

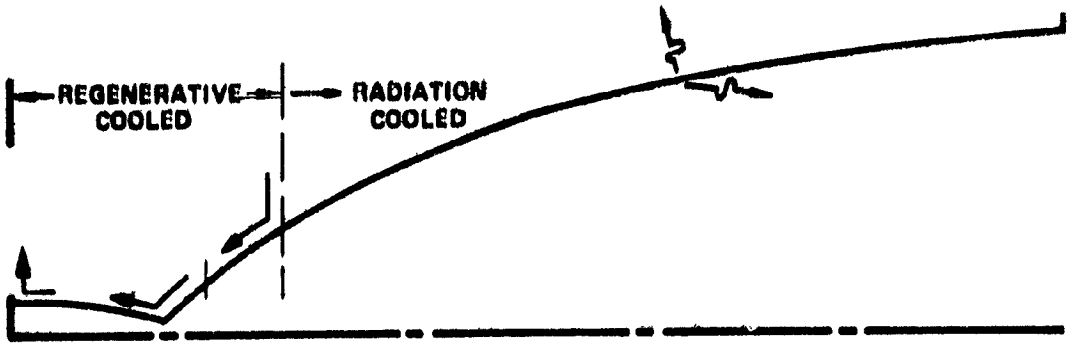

(A) REGENERATIVE/RADIATION COOLED CONFIGURATION

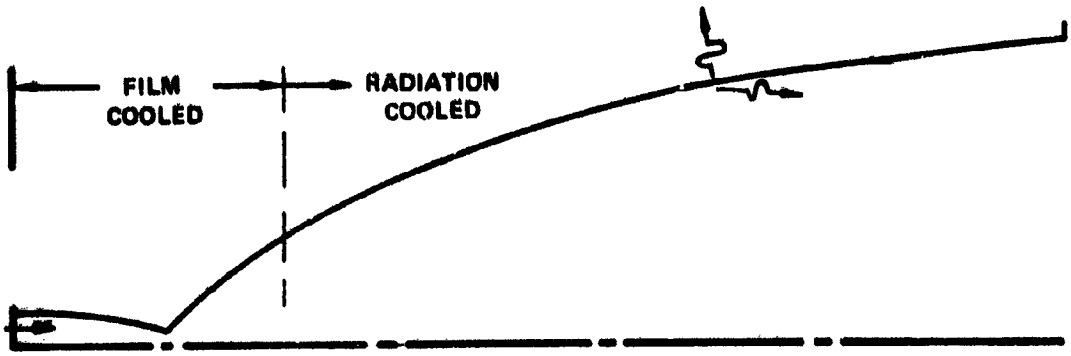

(B) FILM/RADIATION COOLED CONFIGURATION

Figure 2 . Candidate Thrust Chamber Cooling Methods

Therefore, for LO_2/H_2 vaporization it is seldom a problem. Since the combustion performance of LO_2/H_2 is not particularly sensitive to mixture ratio striations, mixing is usually accomplished with relative ease. These characteristics result in a short compact combustion chamber for LO_2/H_2, with a higher contraction ratio than for LO_2/hydrocarbon systems.

The characteristics of LO_2/CH_4 result in a sizing criteria which is between that for $LO_2/RP\text{-}1$ and LO_2/H_2. The LO_2/CH_4 combustion chamber length was determined as an average of the $LO_2/RP\text{-}1$ and LO_2/H_2 lengths. For the determination of the chamber contraction ratio, an average area was chosen.

The resulting combustion chamber lengths and contraction ratio for the three propellants are presented in Fig. 3 and Fig. 4 , respectively. In general, the lower thrusts and higher chamber pressure result in the shorter chamber lengths and also less variation in length. Over the 444.8 N (100 pounds) to 13345 N (3000 pounds) thrust range and the 13.8 N/cm^2 (20 psia) to 689.5 N/cm^2 (1000 psia) chamber pressure range, the injector-to-throat varied from 8.26 cm (3.25 inches) to 55.65 cm (21.91 inches). At a fixed thrust and low chamber pressure, the contraction ratio for LO_2/CH_4 is higher than for $LO_2/RP\text{-}1$. As chamber pressure is increased, the contraction ratio curves for LO_2/CH_4 and $LO_2/RP\text{-}1$ merge together. At high thrusts and low chamber pressures, low contraction ratios are preferred. For the analyzed range of thrusts and chamber pressures, the chamber contraction ratio varied from 2.15 to 8.55.

In addition to length and contraction ratio, the other geometrical parameters required are the upstream radius ratio and the maximum convergence ramp angle. The upstream radius ratio determines the surface length of the peak heat flux location and, therefore, a small value of 1.0 is used. A high convergence ramp angle could result in local boundary layer separation and resultant increase in heat fluxes. A maximum angle of 20 degrees was selected to provide a smooth flow transition.

A comparison of the combustion chamber contours for the three propellants at 4448.2 N (1000 lbf) thrust and a chamber pressure of 344.6 N/cm^2 (500 psia) is presented in Fig. 5 .

Nozzle Contour. The definition of the thrust chamber nozzle contour for a specific area ratio and percent length is dependent on the upstream and downstream throat radii of curvature and the combustion gas properties. Previous 88,964 N (20,000 lbf) thrust Advanced Space Engines studies (Ref. 1) utilized an upstream radius ratio of 1.0 and a downstream radius ratio of 0.392, and achieved high aerodynamic (geometric) performance. Extensive subscale nozzle testing was performed with a 400-to-1 nozzle contour and nozzle wall pressure distributions, and wall heat transfer distributions were verified.

For the low-thrust engine, an increase in the downstream radius ratio was originally thought to significantly improve the reaction kinetic efficiency by decreasing the initial rate of expansion of the nozzle flow. However, a One-Dimensional Kinetic (ODK) analysis of a 4448.2 N (1000 lbf) thrust LO_2/H_2 engine at a chamber pressure of 344.7 N/cm^2 (500 psia) resulted in only 0.05% increase in kinetic efficiency for an increase in the downstream radius ratio

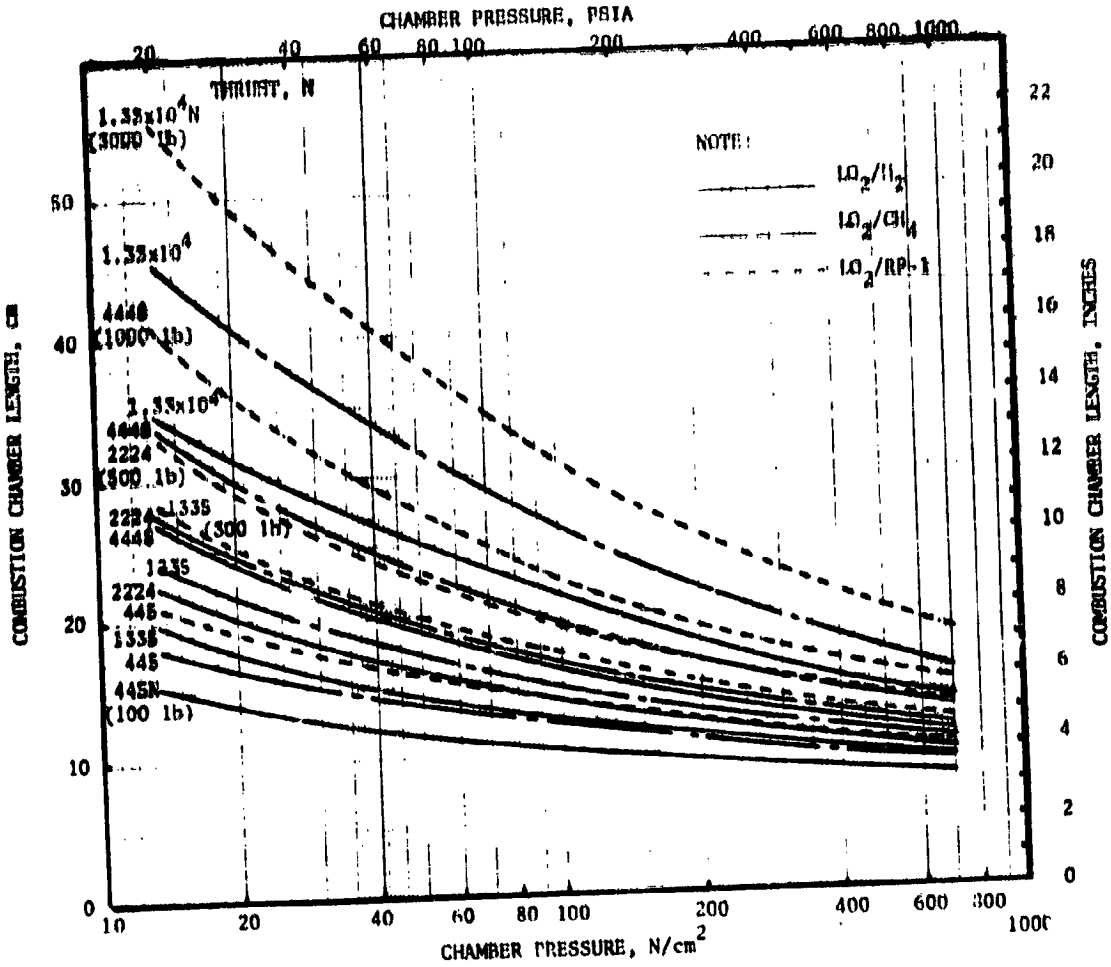

Figure 3 . Combustion Chamber Injector-to-Throat Length

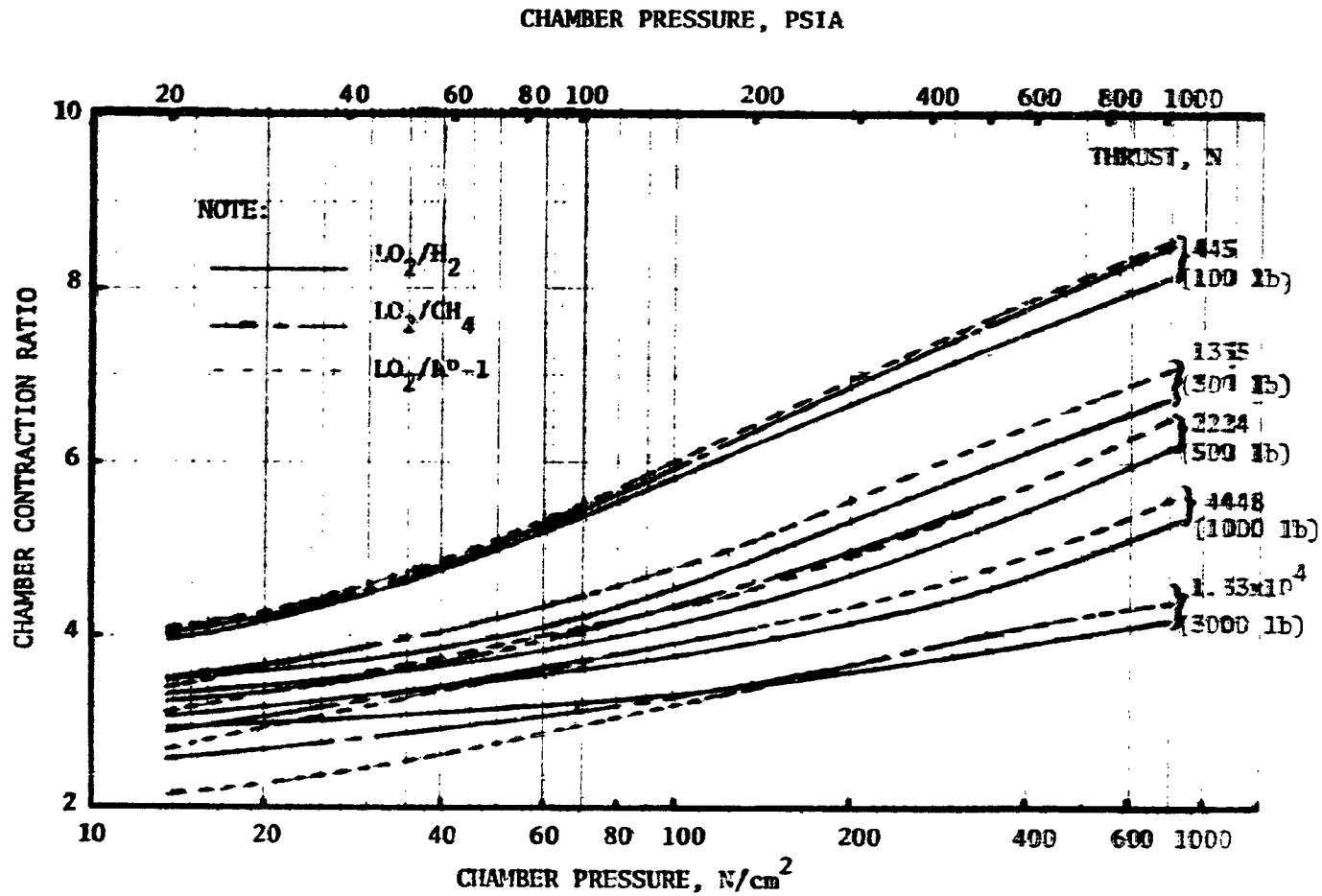

Figure 4 . Combustion Chamber Contraction Ratio

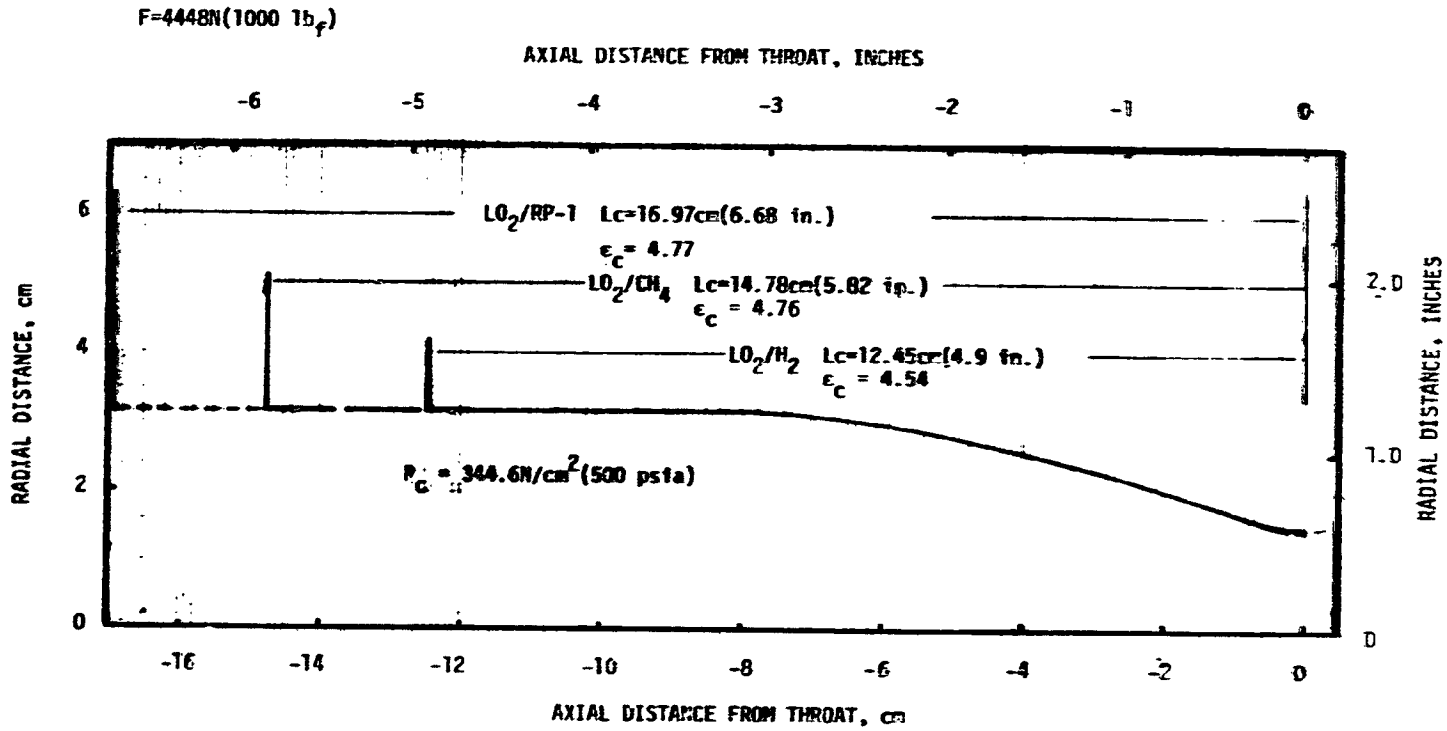

Figure 5 . Typical Combustion Chamber Contour Comparison
[F =4448 N (1000 lbf)]

from 0.392 to 2.0. Therefore, the conventional downstream radius ratio value of 0.392 was used in the design of the 400-to-1 area ratio (90% length) nozzle used in this study. The resulting aerodynamic optimum contour (nondimensional) is shown in Fig. 6 .

Gas-Side Heat Transfer Coefficient Distribution

The gas-side heat transfer coefficient distribution for the thrust chambers was determined using existing test data for regions near the injector and the analytical results of the Rocketdyne boundary layer computer program. This program incorporates an integral solution to the momentum and energy equations.

This program utilizes an integral method to solve the momentum and energy equations. Solution of these equations is accomplished using a semiempirical relation between the Stanton number and the energy thickness and between the skin friction coefficient and momentum thickness. The resulting equation for turbulent flow is of the form:

$$N_{ST_\infty} = \frac{0.0122}{(Re_\phi)^{0.25}} \left(\frac{\rho_\infty}{\rho_r}\right)^{1/2} \left(\frac{\mu_r}{\mu_\infty}\right)^{1/4} \frac{1}{N_{Pr}^{2/3}} \qquad (1)$$

The convective film coefficient (hg) is then found from the relation:

$$hg = \rho_\infty U_\infty C_p N_{ST_\infty} \qquad (2)$$

The Eckert reference temperature is used to evaluate the film properties.

Injector region test data obtained from a LO_2/H_2 water-cooled combustor was used to develop the distribution for LO_2/H_2 thrust chambers. For LO_2/CH_4 and LO_2/RP-1, the injector region distributions are determined by applying an analytical property correction to the LO_2/H_2 test data.

For example for LO_2/CH_4,

$$\left(h_g\right)_{LO_2/CH_4} = \left(h_g\right)_{LO_2/H_2} \frac{\left(C_p\right)_{LO_2/CH_4}}{\left(C_p\right)_{LO_2/H_2}} \left(\frac{\mu_{LO_2/CH_4}}{\mu_{LO_2/H_2}}\right)^{0.2} \left(\frac{Pr_{LO_2/H_2}}{Pr_{LO_2/CH_4}}\right)^{0.6} \qquad (3)$$

$$\left(\frac{C^*_{LO_2/H_2}}{C^*_{LO_2/CH_4}}\right)^{0.8}$$

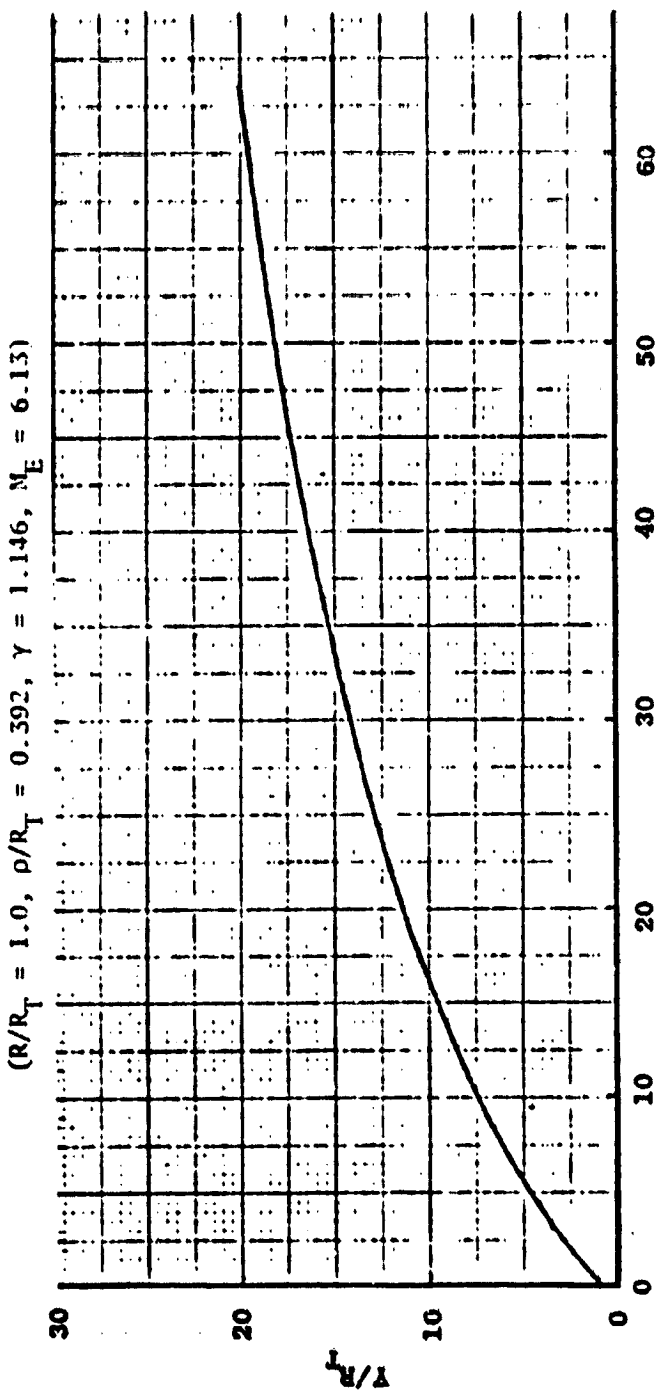

Figure 6. Nondimensional Nozzle Wall Contour (ϵ = 400, 90% L)

Gas-side heat transfer coefficient distributions for the individual thrust chamber designs are presented in the Regenerative Cooling Analysis Section.

Radiation Cooling Analysis

Radiation cooling utilizes a high-temperature, high-emissivity material. At high thrust chamber wall temperatures, the wall material radiates heat to the surroundings through the external surface and from the internal nozzle surface. Conventional high-temperature materials, L-605 alloy (for use up to 1367 K or 2000 F maximum termperature) and molybdenum or columbium (for use up to 1644 K or 2500 F maximum temperature) were evaluated. L605 and molybdenum were hot-fired successfully in a 111 N (25 lbf) thrust $LO2/H_2$ chamber (Ref. 2). Molybdenum and columbium would have to incorporate an oxidation protection coating.

Using the Rocketdyne integral boundary layer computer program, the axial variation in the radiation-cooled wall temperature with chamber pressure and thrust for the LO_2/H_2, LO_2/CH_4, and LO_2/RP-1 thrust chambers were determined. The gas-side wall temperature variation with local nozzle area ratio is shown in Fig. 7 for LO_2/H_2 at a thrust level of 4448 N (1000 lbf). The influence of thrust level on wall temperature is shown in Fig. 8 for LO_2/H_2 at a chamber pressure of 344.7 N/cm^2 (500 psia).

Due to the higher heat fluxes encountered at the higher chamber pressures, the wall temperatures increase with increase in chamber pressure at a fixed area ratio. For a fixed maximum wall temperature limit, this trend results in an increase in the radiation nozzle attach area ratio with chamber pressure. Also, higher heat fluxes are experienced at lower thrust levels, and result in higher wall temperatures.

Using a maximum allowable material temperature limit, the radiation-cooled nozzle attach area ratio for the three propellants can be determined directly from Fig.9 through 11. For two representative maximum wall temperature limits (1367 K or 2000 F and 1644 K or 2500 F) the LO_2/H_2 thrust chambers resulted in the highest heat fluxes of the three propellants and, therefore, the highest radiation nozzle attach area ratio.

The application of these low-thrust engines in the low earth orbit (LEO) to geosynchronous equatorial orbit (GEO) missions will most likely mean that these spacecraft will be launched from the Space Shuttle. As a result, engine length will be important. Since a retractable nozzle would reduce the engine length approximately 50%, the incorporation of the retractable nozzle must be seriously considered even though it increases the engine configuration complexity. Preliminary engine design evaluations of 400-to-1 area ratio engines indicated that the cutoff area ratio for the retractable nozzle should be approximately 200-to-1.

For a regenerative/radiation-cooled thrust chamber, the retractable portion of the nozzle would be ideally radiation cooled. This greatly simplifies thrust chamber coolant plumbing. For a film/radiation-cooled thrust chamber, the retractable nozzle cutoff area ratio will not influence the thrust chamber cooling. These thrust chambers utilize radiation cooling from low supersonic area ratios to the nozzle exit.

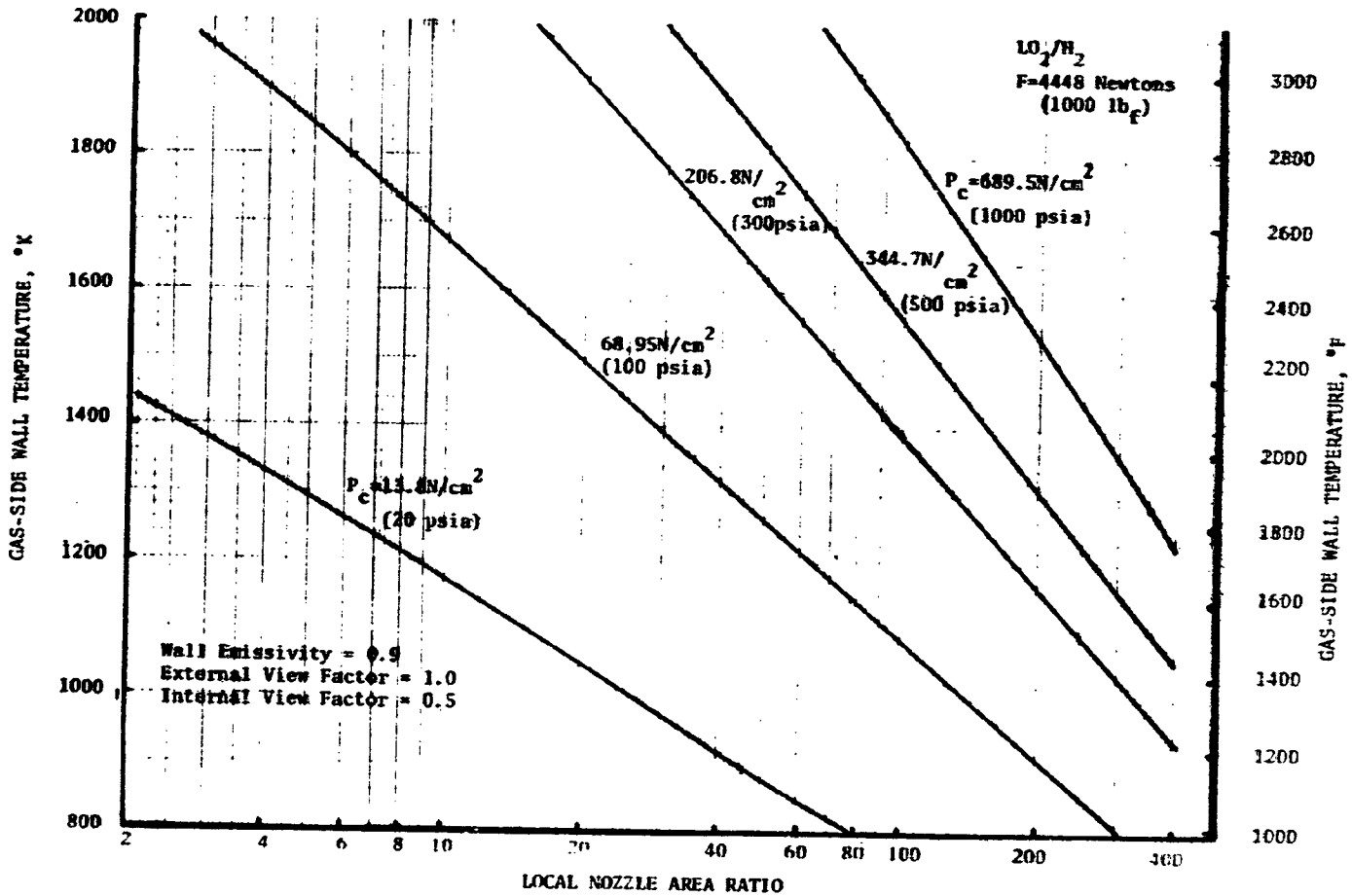

Figure 7 . Axial Variation in Wall Temperature With Chamber Pressure for LO_2/H_2 at 4448 N (1000 lb) Thrust

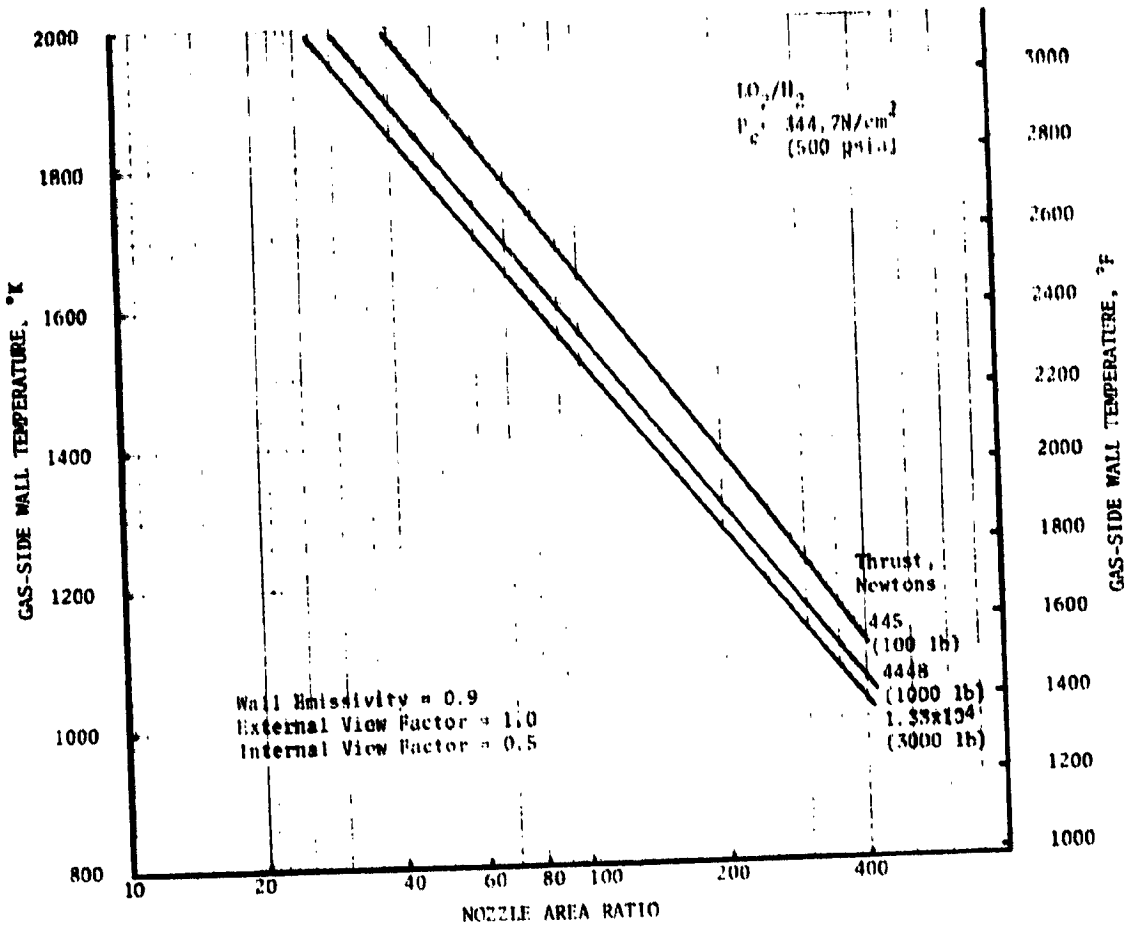

Figure 8 . Axial Variation of Wall Temperature With Thrust for LO_2/H_2 at 344.7 N/cm^2 (500 psia) Chamber Pressure

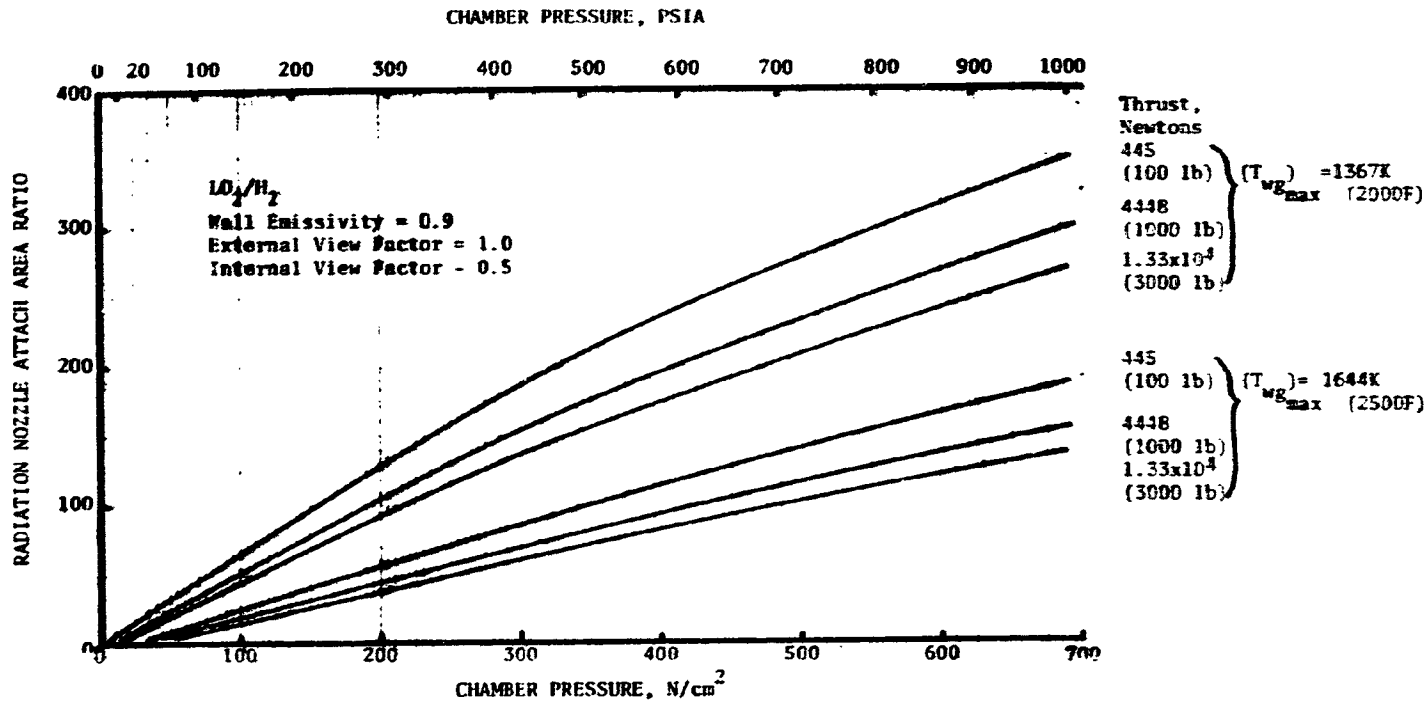

Figure 9. Radiation Nozzle Attach Area Ratio Variation With Chamber Pressure and Thrust for LO_2/H_2

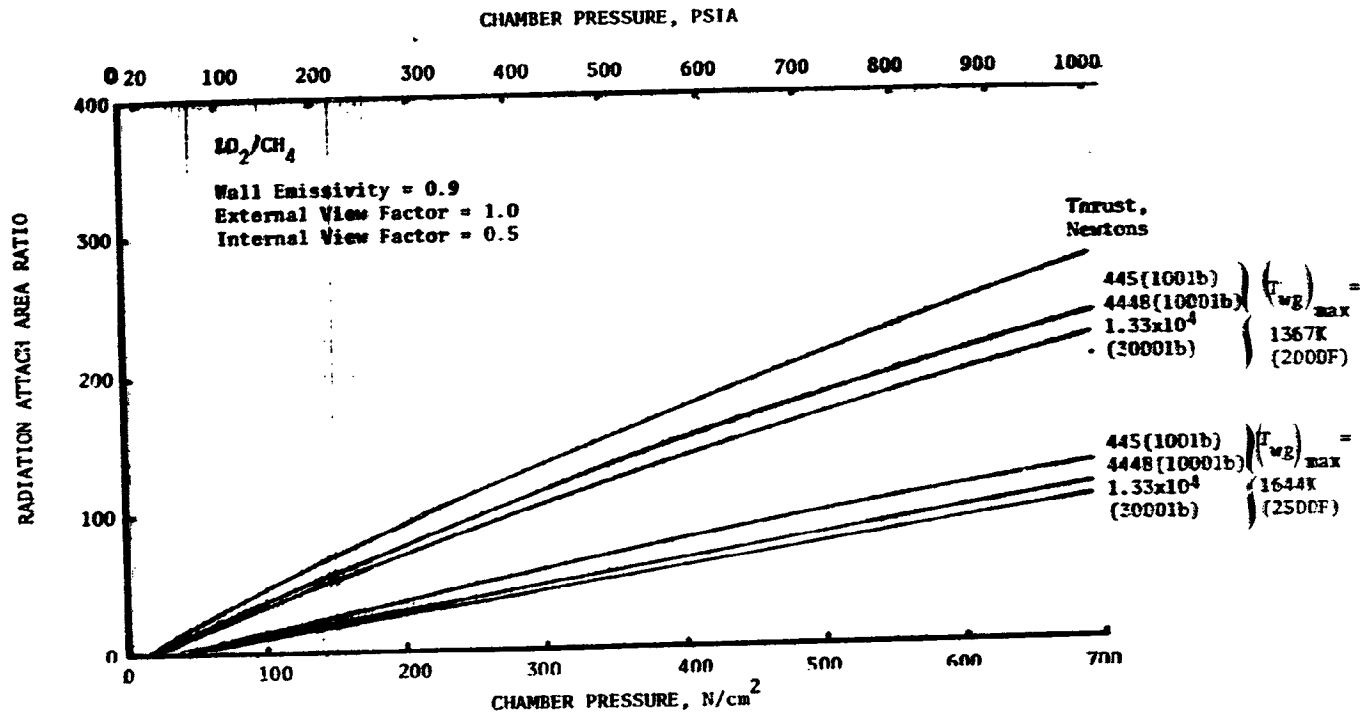

Figure 10 . Radiation Nozzle Attach Area Ratio Variation With Chamber Pressure and Thrust for LO_2/CH_4

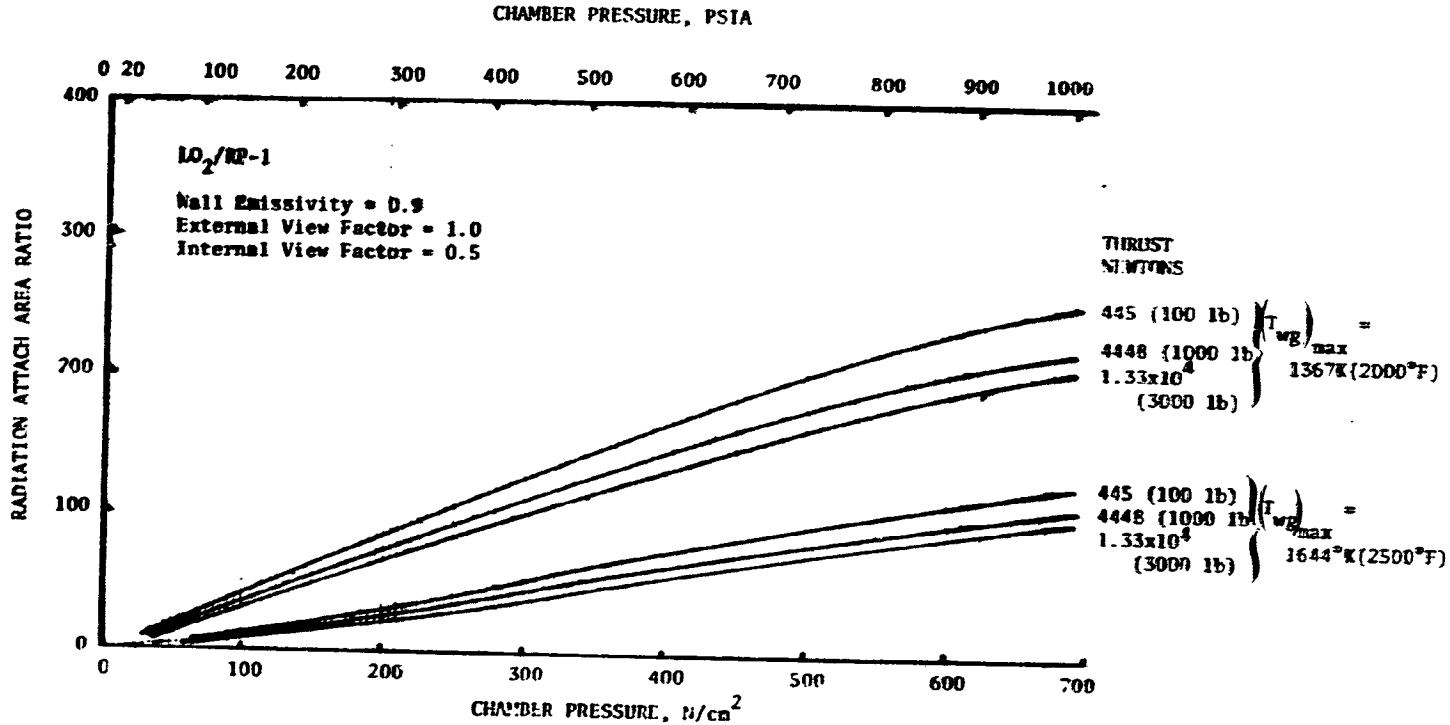

Figure 11. Radiation Nozzle Attach Area Ratio Variation With Chamber Pressure and Thrust for LO_2/RP-1

Since the heat flux profile is highest for LO_2/H_2, LO_2/H_2 has the highest attach area ratio for a given chamber pressure. Assuming a wall temperature limit of 1644 K (2500 F), all the radiation nozzle attach area ratios are less than 200-to-1 (Fig. 9), which would enable a retractable radiation-cooled nozzle design using a 200-to-1 attach area ratio for specified ranges of thrusts and chamber pressures.

A comparison of the radiation nozzle attach area ratio for the three propellants is presented in Fig. 12 for 4448 N (1000 lbf) thrust. The LO_2/H_2 thrust chambers would have the highest attach area ratio for a fixed chamber pressure. Attach area ratio for LO_2/CH_4 and LO_2/RP-1 thrust chambers were similar, with the values for LO_2/RP-1 being slightly lower at the higher chamber pressures.

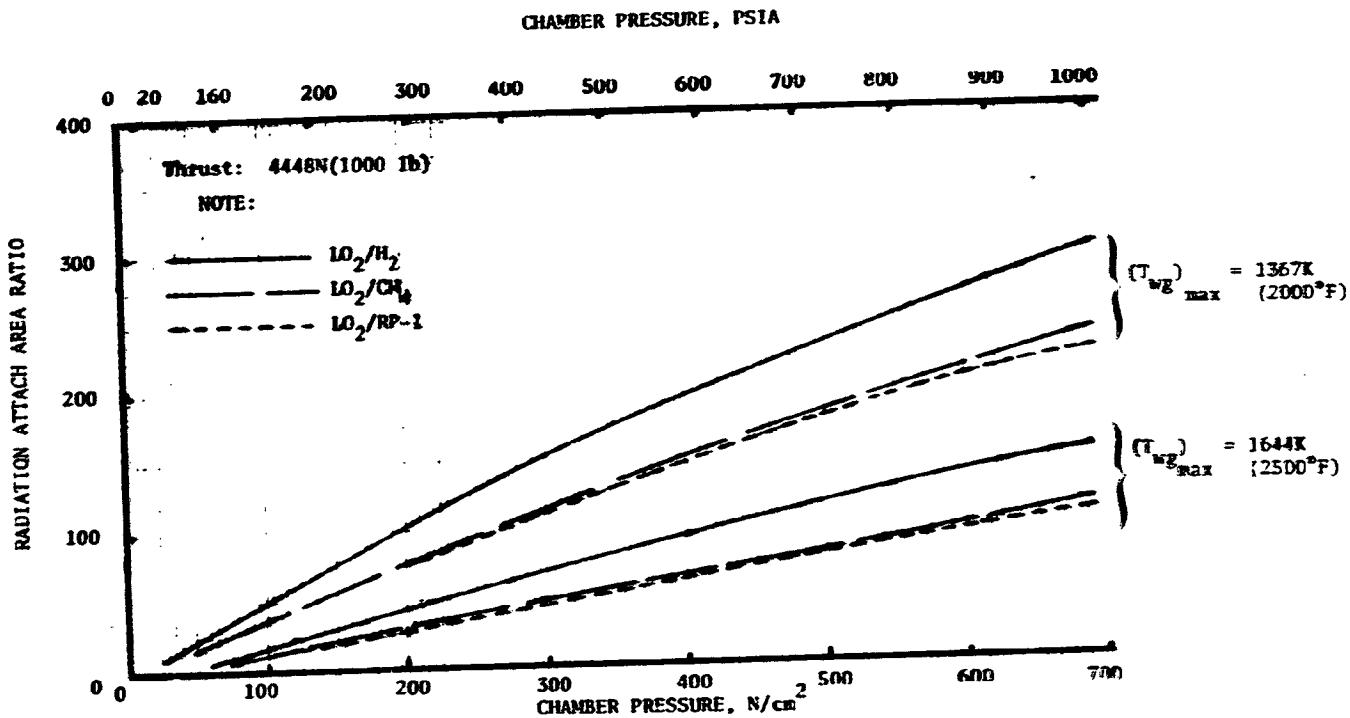

Figure 12. Radiation Nozzle Attach Area Ratio Variation With Propellant [Thrust = 4448 N (1000 lb)]

Regenerative Cooling Analysis

Combining the thrust chamber contour, the gas-side heat transfer coefficient distribution, thrust chamber material properties (thermal conductivity, yield strength, ultimate strength, fatigue, and stress rupture data), and the thrust chamber design conditions (propellant, thrust, chamber pressure, mixture ratio, coolant flowrate), regenerative cooling analyses were performed for a number of cases using the Rocketdyne Regenerative-Cooling Design/Analysis Computer Program. This computer program is capable of either designing or analyzing channel-wall or tubular-wall coolant passages. Program output includes coolant heat input, coolant pressure distribution, two-dimensional wall temperature distributions, structural safety factors, and cycle life.

These detailed analyses were used to more accurately determine the regenerative cooling limits and to provide realistic reference data in the generation of parametric coolant heat input and coolant pressure drop required to perform the engine cycle balances.

Coolant-side Heat Transfer Coefficient. To provide a realistic heat transfer evaluation of the three propellants, the most recent coolant correlation for each of the three fuels was used in the analysis. For hydrogen bulk temperatures below 83.3 K (150 R), the Miller, Seader, and Trebes correlation (Ref.3) was used.

$$Nu_r = 0.0204\ Re_r^{0.8}\ Pr_r^{0.4}\ (1 + 0.00983\ \frac{\nu_w}{\nu_B} \tag{4}$$

where

$$T_r = T_B + 0.4\ (T_w - T_B)$$

And where ν_w and ν_B are the kinematic viscosity evaluated at the wall and fluid bulk temperatures, respectively.

Above 83.3 K (150 R), the hydrogen coolant-side film coefficient was determined using a form of the Dipprey and Sabersky equation modified specifically for hydrogen, although it should be applicable to other coolants with similar Prandtl numbers.

$$C_h = \frac{C_f/2}{0.92 + (C_f/2)^{0.5}\ [g(\varepsilon^*, Pr) - 8.48]} \tag{5}$$

where

$$g(\epsilon^*, Pr) = 4.7(\epsilon^*)^{0.2} \text{ for } \epsilon^* > 7$$

$$g(\epsilon^*, Pr) = 4.5 + 0.57(\epsilon^*)^{0.75} \text{ for } \epsilon^* \leq 7$$

$$\epsilon^* = Re(\epsilon/D)(C_f/2)^{0.5}$$

Roughness enhancements are a function of relative roughness and Reynolds number. Typical enhancements of 1.2 are readily achieved, while values as high as 1.6 are possible at high Reynolds numbers.

For methane, the standard Nusselt number correlation with the curvature and entrance enhancement factors was used.

$$Nu = 0.023\ Re^{0.8}\ Pr^{0.4}\ \phi_c\ \phi_e \tag{6}$$

For RP-1, the Rocketdyne correlation developed from the Atlas, Thor, H-1, and F-1 engine programs was used.

$$Nu = 0.0056\ Re^{0.95}\ Pr^{0.4}\ \phi_c\ \phi_e \tag{7}$$

As presented in the analysis guidelines, the coolant curvature enhancement factor (ϕ_c), was limited to a maximum of 1.4 (same limitation as for the Space Shuttle main engine and the Advanced Space Engine). For the two-dimensional channel wall temperature distribution analyses, the full curvature enhancement value is used on the coolant side fo the hot-gas wall. The value is linearly varied along the side walls (channel height) of the coolant channel to a value of 1.0 at the channel closeout surface.

Influence of Combustion Chamber Length and Contraction Ratio. Using the analysis guidelines of Table 2 and a series cooling circuit, the influence of combustion chamber length and contraction ratio was determined for use in the engine cycle balance evaluation. The analysis was performed for a 4448 N (1000-pound thrust O_2/H_2 NARloy-Z channel wall combustor at a chamber pressure of 344.7 N/cm^2 (500 psia) with a radiation nozzle attach area ratio of 80-to-1. Coolant channel designs were altered for each chamber length and contraction ratio to achieve the same gas-side wall temperature distribution. The results of this analysis are shown in Fig. 13 and Fig. 14. As shown in Fig. 13, the heat input varied approximately linearly with combustion chamber length, but did not vary significantly with chamber contraction ratio. The coolant pressure drop (Fig.14) increased with chamber length and decreased with increase in contraction ratio. The pressure drop increase is merely the result of the increased length. The pressure drop decrease with increase in contraction ratio is the result of the decrease in heat flux which reduces the coolant mass velocity required to achieve the same wall temperature.

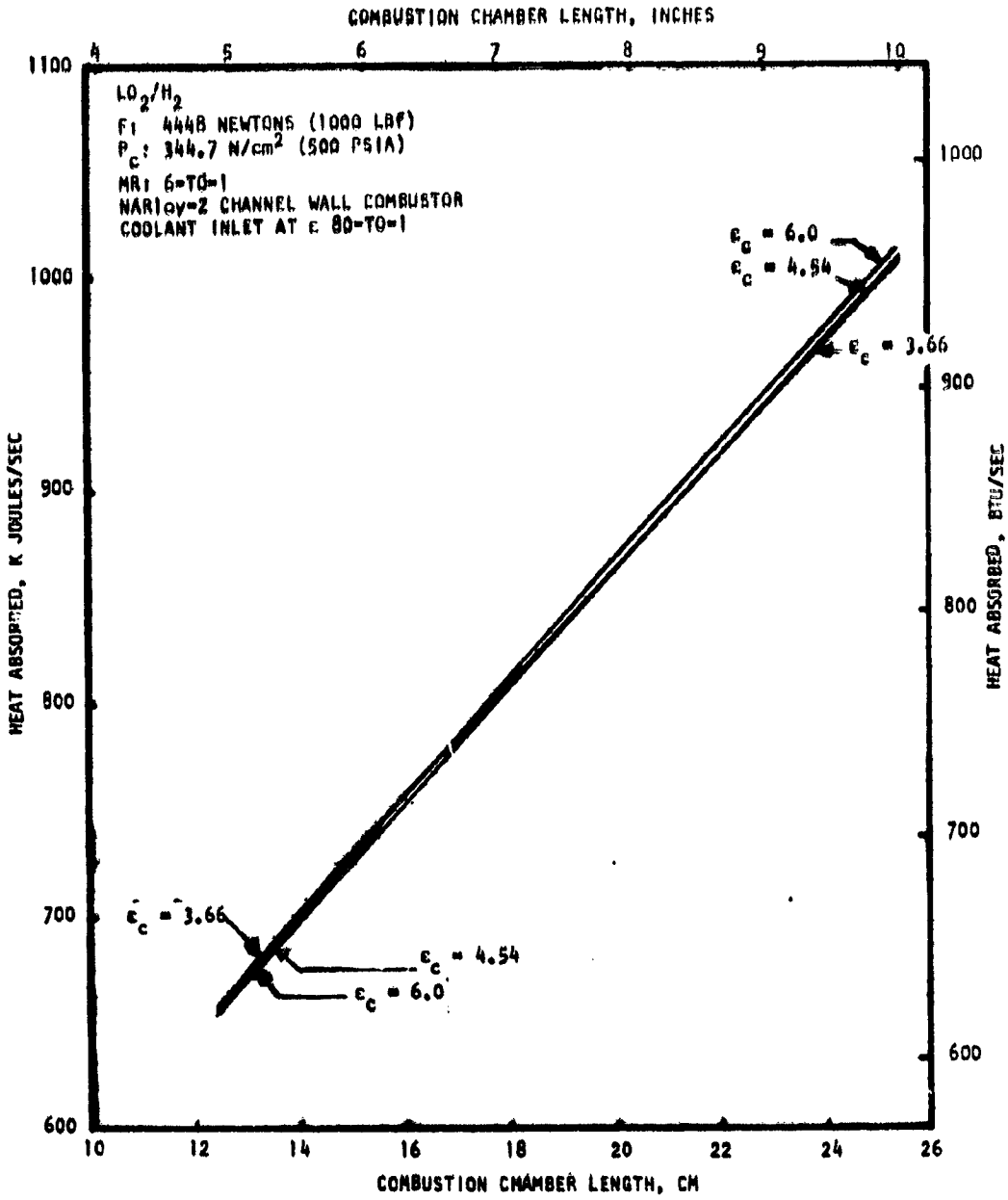

Figure 13. Variation of Heat Absorbed With Combustion Chamber Length and Contraction Ratio

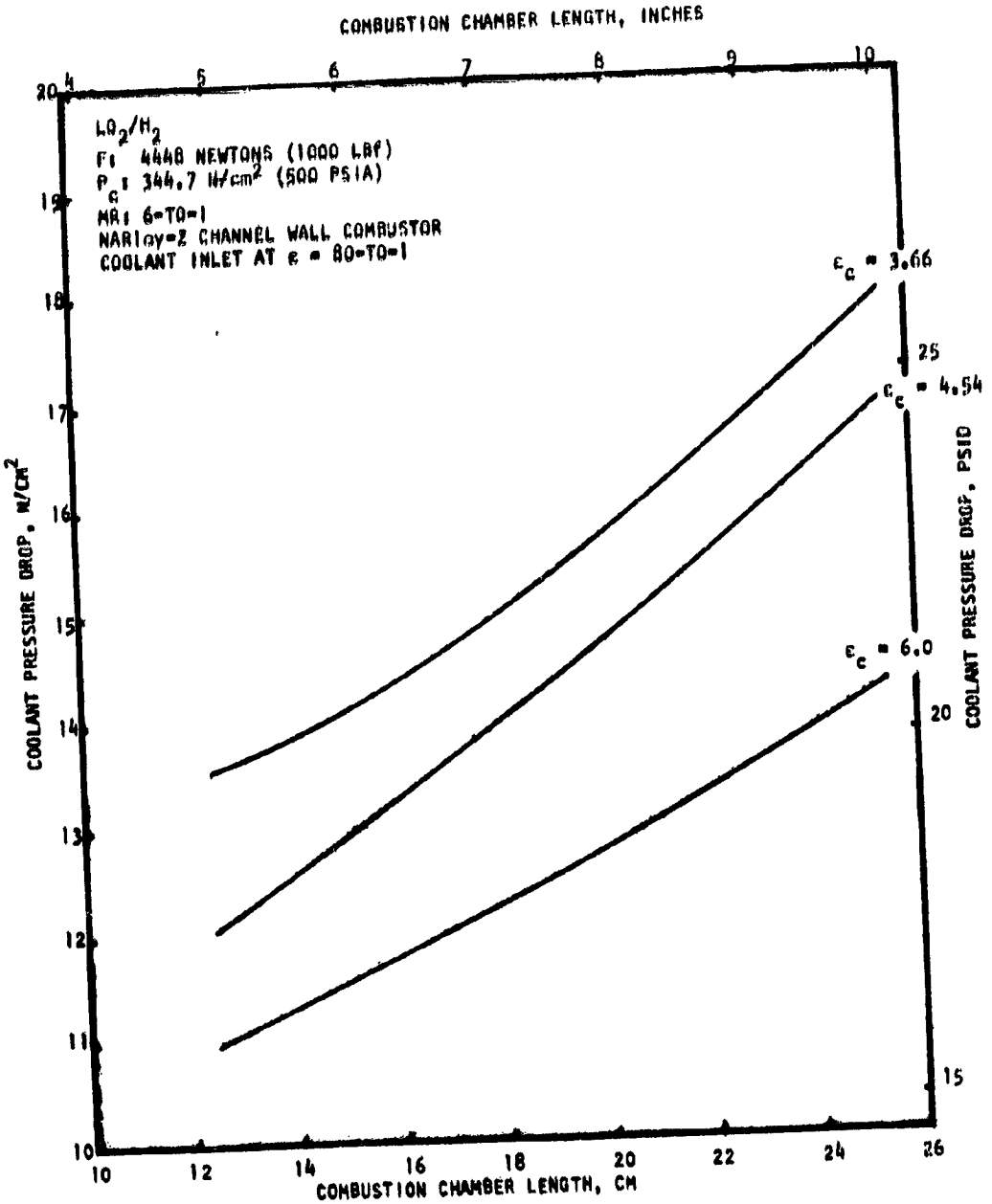

Figure 14 . Variation of Coolant Pressure Drop With Combustion Chamber Length and Contraction Ratio

Coolant Circuit Selection. One of the major goals in regenerative cooling is to minimize the coolant pressure drop for a desired wall temperature distribution. This is particularly important for the pressure-fed engine concepts due to the limited available pressure. Therefore, the selection of the thrust chamber coolant circuit and the design of the coolant passages are important in defining cooling limits. Typical regenerative cooling circuits are illustrated schematically in Fig. 15. The simplest circuit is the single uppass cooling circuit (A and B) with the inlet at the nozzle end. The uppass combustor circuit takes advantage of the coolant curvature enhancement to aid in cooling the high heat flux throat region. However, at the low-thrust conditions of interest, the coolant bulk temperature rise is higher than at high thrusts and, as a result, this circuit would result in higher coolant pressure drops.

In the split-flow cooling circuit, the combustor and nozzle are cooled in parallel. This is the cooling circuit of the 88964 N (20000 pound) thrust Advanced Engine (ASE) thrust chamber.

The fourth cooling circuit shown in Fig.15 consists of a series uppass combustor (channel wall) and a downpass nozzle (tubes). The nozzle also could incorporate a two-pass cooling circuit. This cooling circuit utilizes the highest coolant temperature fluid to cool the lower heat fluxes (nozzle) using a higher-temperature-limit material (steel).

Depending on the resulting coolant passage size and coolant bulk temperature rise, all of these coolant circuits could bypass a portion of the coolant flow. If the thrust chamber coolant passage design is not bulk temperature-limited (high coolant bulk temperature near exit), and the channel sizes are so large that the channel height is being restricted by the channel height limitation, bypassing coolant can reduce the coolant channel sizes to a reasonable value and provide satisfactory cooling.

Typically for the high heat flux applications such as the SSME and ASE thrust chamber, the copper-base alloy such as NARloy-Z or Zr-Cu are the natural choice in material. However for lower heat flux, lower thrust and chamber pressure applications, the thrust chamber designs will, in some cases, be bulk temperature limited. For this type of design case, the peak heat flux location will not be the critical design location. The coolant bulk temperature at the coolant exit will approach the temperature limit of the wall material, and cooling will become difficult. The copper-base alloys should be limited to a maximum gas-side temperature of approximately 811 K (1000 F) to ensure a durable design. Above this temperature, cases of localized wall erosions have been experimentally encountered. A logical solution to this problem is to use a material having a higher wall temperature limit such as nickel. For nickel, the durable design temperature limit is 978K (1300 F). Nickel has a moderate thermal conductivity, but has a hydrogen embrittlement problem. Therefore, nickel was evaluated for methane cooling but not for hydrogen cooling.

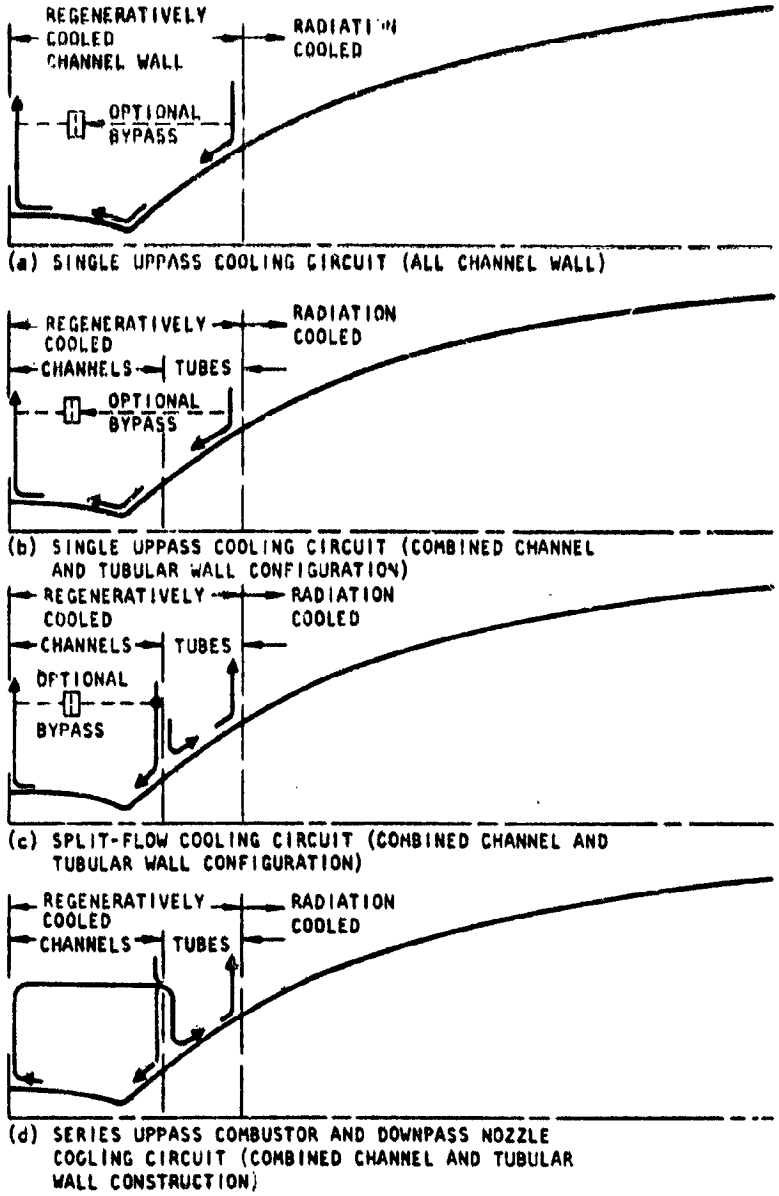

Figure 15. Typical Regenerative Cooling Circuits

Due to their adaptability to low-thrust conditions, the split-flow cooling circuit (Circuit C) and the series cooling circuit (Circuit D) were evaluated. For a nominal LO_2/H_2 case with a thrust of (1000 lbf) and a chamber pressure of 344.7 N/cm^2 (500 psia), thrust chamber analysis was performed for both cooling circuits with NARloy-Z channel wall combustor and a stainless steel tubular nozzle (to ε = 200). The results of the analysis are presented in Table 3 . Both coolant circuits resulted in feasible designs, but the series cooling circuit resulted in a larger total heat input and a lower coolant pressure drop and, therefore, was selected as the baseline regenerative cooling circuit.

Detailed Regenerative-Cooling Analysis. Detailed regenerative-cooling analyses were performed at discrete thrust chamber design points to realistically define the regenerative-cooling limits. The detailed analysis cases performed for the three candidate propellants are presented in Table 4 .

For LO_2/H_2 at a thrust of 4448 N(1000 lbf), the maximum regenerative-cooling chamber pressure, based on the study guidelines, was 689.5 N/cm^2(1000 psia). The detailed coolant passage geometry and other heat transfer parameters are presented for the combustor and nozzle in Fig.16 and 17, respectively. The limiting criterion, was the maximum coolant Mach number of 0.3 (Fig. 16). As shown in Fig. 16, the maximum combustor gas-side wall temperature was less than 811 K(1000 F). These temperatures are the result of two-dimensional thermal anlayses of a discrete number of axial stations. The resulting cycle life exceeded the cycle requirement of five cycles with a safety factor of 4. For thrust levels greater than 4448 N(1000 pounds), the maximum chamber pressure will exceed the maximum chamber pressure of the study of 689.5 N/cm^2(1000 psia) and, therefore, was not defined.

The LO_2/CH_4 regenerative-cooled thrust chamber cooling was also limited by the maximum coolant Mach number criterion. At 4448 N(1000 pounds) thrust, the LO_2/CH_4 thrust chamber maximum chamber pressure was 344.7 N/cm^2(500 psia). Details for the single uppass cooled nickel channel wall combuster is shown in Fig.18 and for the two-pass tubular nozzle in Fig.19 . As shown in Fig. 18, the limiting criterion was the maximum coolant Mach number limit of 0.3. For the LO_2/CH_4 thrust chamber with CH_4 regenerative cooling, a nickel channel wall combustor offered a cooling advantage over a copper alloy combustor. The higher material durability temperature limit for nickel of 978 K (1300 F) as compared to 811 K (1000 R) increased the maximum regenerative-cooling chamber pressure limit for LO_2/CH_4. As shown in Fig.18 , the maximum nickel combustor wall temperature was close to the 978 K (1300 F) maximum allowable temperature.

In determining the regenerative cooling limit for the LO_2/RP-1 thrust chambers, the easiest regenerative-cooling conditions were first evaluated. These conditions were the highest thrust, 13345 N (3000 pounds), and a mid-range chamber pressure of 348 N/cm^2 (500 psia). As shown in Fig.20 , although the gas-side wall temperatures were below the maximum durability

TABLE 3 . REGENERATIVE-COOLING CIRCUIT COMPARISON

Propellant: LO_2/H_2
F: 4448N($10001b_f$)
P_c: 344.7N/cm^2(500 psia)
MR: 6-to-1
Nozzle Area Ratio: 400-to-1
Percent Length: 90
Radiation-cooled Nozzle: ε=200 to ε=400

	SPLIT-FLOW COOLING CIRCUIT		SERIES COOLING CIRCUIT	
NARloy-Z Channel Wall Combustor: (Injector to ε=8)				
Number of Channels	55		55	
Minimum Channel Dimensions, cm(in.)	0.1016x0.0711	(0.04x0.028)	0.1016x0.1651	(0.04x0.065)
Maximum wall temperature, °K(°F)	821	(1018)	802	(983)
Maximum Cooling Mach No.	0.256		0.178	
Heat Input, KW (BTU/sec)	439.5	(416.6)	493.9	(469.1)
Coolant Pressure Drop, N/cm^2(psi)	37.7	(54.7)	9.5	(13.8)
Coolant Flow Split, percent of total fuel	60		-	
STEEL TUBULAR NOZZLE: (ε=8 to ε=200)				
Number of Tubes (2-pass)	90/90		50/50	
Minimum Tube (I.D.) Diameter, cm(in.)	0.1092	(0.043)	0.231	(0.091)
Maximum Wall Temperature, °K(°F)	788	(958)	767	(921)
Maximum Coolant Mach No.	0.189		0.191	
Heat Input, KW (BTU/sec)	356.7	(33[illegible])	356.2	(337.6)
Coolant Pressure Drop, N/cm^2(psi)	13.9	(20[illegible])	12.6	(18.3)
TOTAL HEAT INPUT, KW (BTU/sec)	796.2	(754.7)	851.1	(806.7)
TOTAL COOLANT PRESSURE DROP, N/cm^2(psi)	37.7*	(54.7)*	22.1	(32.1)

NOTE: *FOR SPLIT FLOW CIRCUIT, COMBUSTOR COOLANT PRESSURE DROP

TABLE 4. SUMMARY OF DETAILED REGENERATIVE-COOLING ANALYSIS CASES

PROPELLANT	THRUST, N (lbf)	CHAMBER PRESSURE, N/cm^2 (PSIA)	COMMENTS
LO_2/H_2	13345 (3000)	689.5 (1000)	
LO_2/H_2	13345 (3000)	344.7 (500)	
LO_2/H_2	13345 (3000)	68.95 (100)	2-PHASE H_2
LO_2/H_2	4448.2 (1000)	689.5 (1000)	ON COOLING LIMIT
LO_2/H_2	4448.2 (1000)	344.7 (500)	
LO_2/H_2	4448.2 (1000)	68.95 (100)	2-PHASE H_2
LO_2/H_2	2224.1 (500)	448.2 (650)	ON COOLING LIMIT
LO_2/H_2	444.8 (100)	275.8 (400)	EXCEEDED STUDY GUIDELINES
		137.9 (200)	ON COOLING LIMIT
LO_2/H_2	444.8 (100)	68.95(100)	
LO_2/CH_4	13345 (3000)	689.5 (1000)	ON COOLING LIMIT
LO_2/CH_4	13345 (3000)	344.7 (500)	
LO_2/CH_4	13345 (3000)	68.95 (100)	EXCEEDED STUDY GUIDELINES
LO_2/CH_4	4448.2 (1000)	344.7 (500)	ON COOLING LIMIT
LO_2/CH_4	4448.2 (1000)	275.8 (400)	EXCEEDED STUDY GUIDELINES
LO_2/CH_4	4448.2 (1000)	206.8 (300)	EXCEEDED STUDY GUIDELINES
LO_2/CH_4	4448.2 (1000)	68.95 (100)	EXCEEDED STUDY GUIDELINES
LO_2/RP-1	13345 (3000)	344.7 (500)	EXCEEDED STUDY GUIDELINES
LO_2/RP-1	13345 (3000)	68.95 (100)	EXCEEDED STUDY GUIDELINES

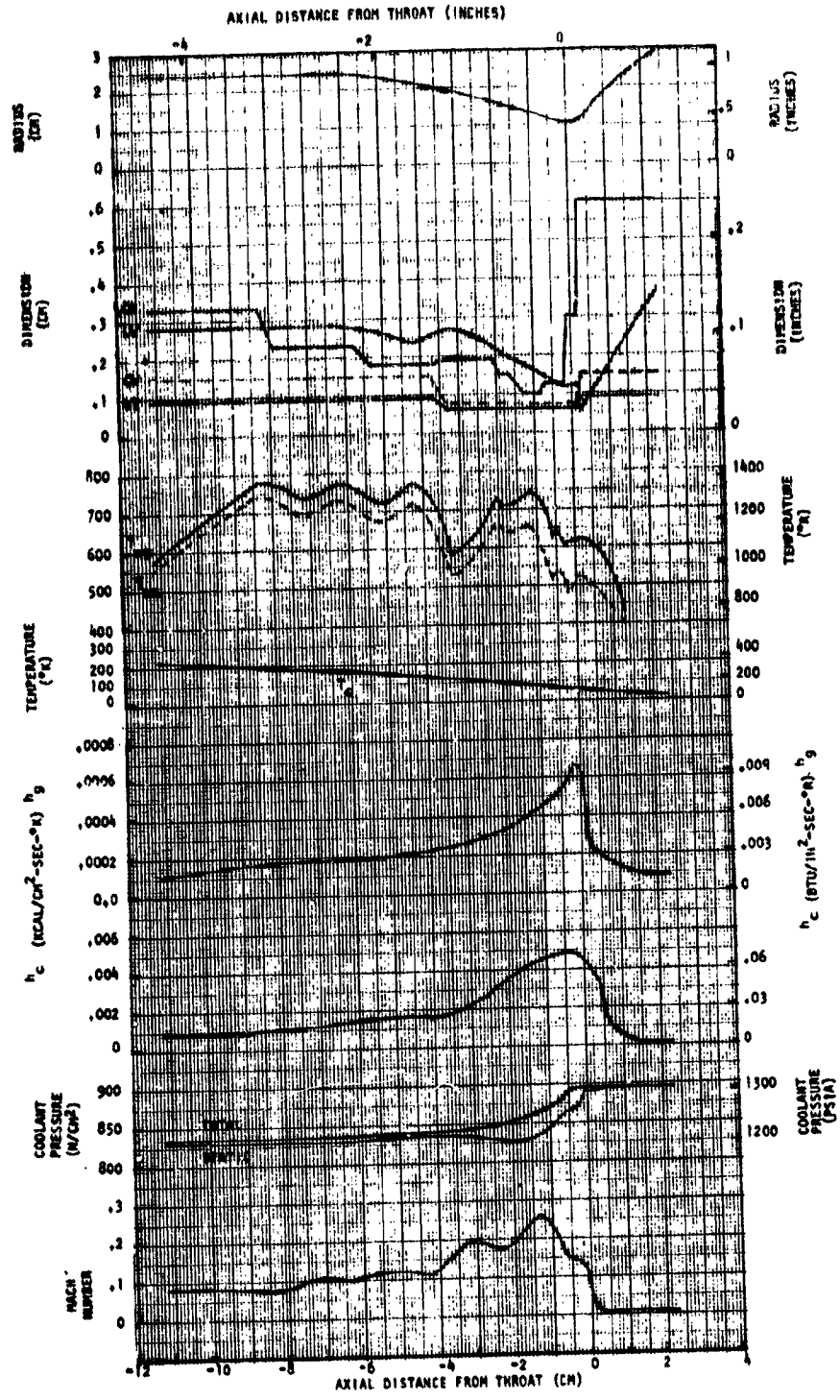

Figure 16. Parameters for the O_2/H_2 Low Thrust Combustor MR = 6.0, F = 4448 N (1000 lbf), P_c = 689.5 N/cm^2 (1000 psia)

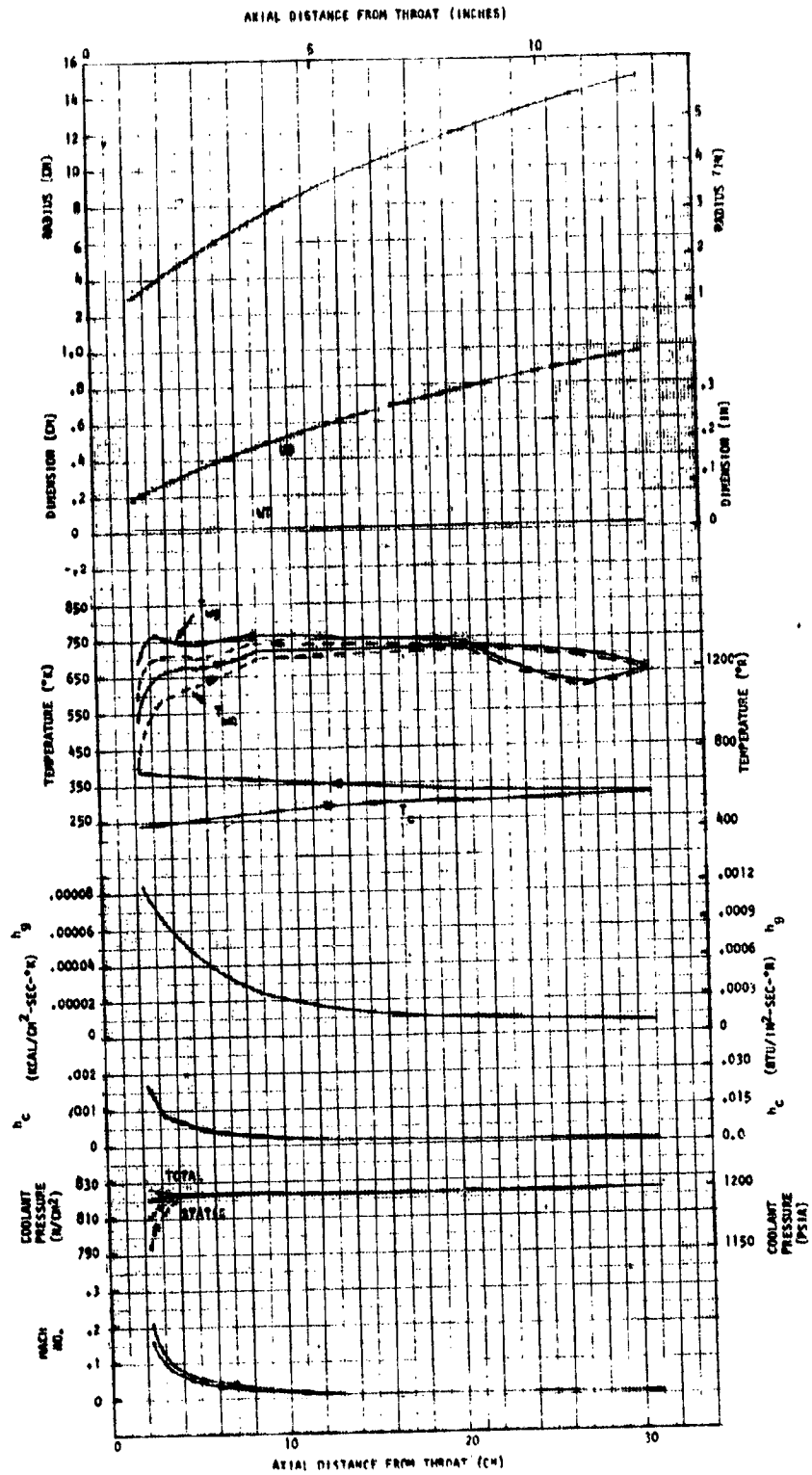

Figure 17. Parameters for the O_2/H_2 Low Thrust Two-Pass Nozzle, MR = 6.0, F = 4448 N (1000 lbf), P_c = 689.5 N/cm^2 (1000 psia), ε = 8 to 200

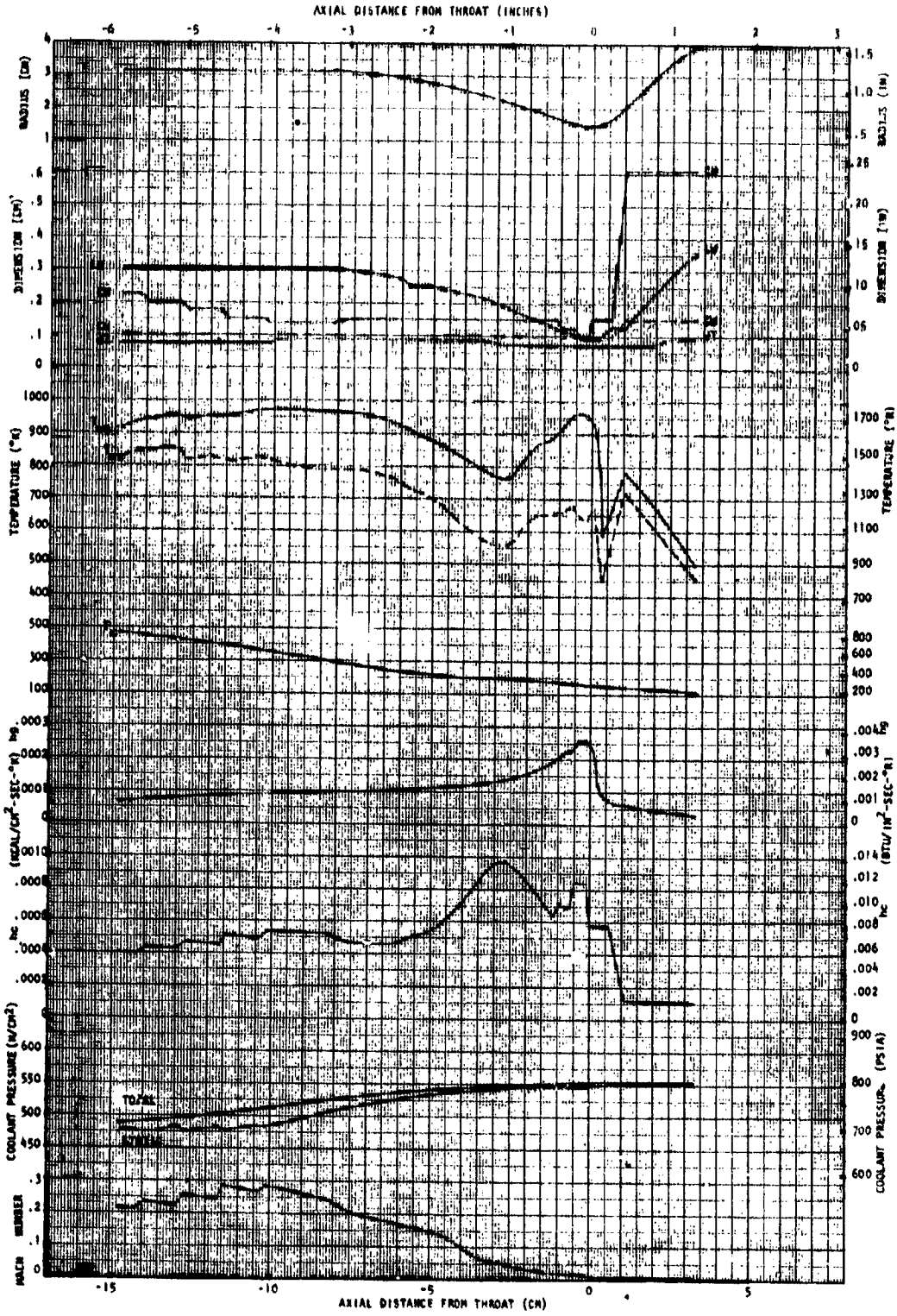

Figure 18. Parameters for the O_2/CH_4 Low Thrust Combustor, MR = 3.7, F = 4448 N (1000 lbf), P_c = 344.75 cm^2 (500 psia)

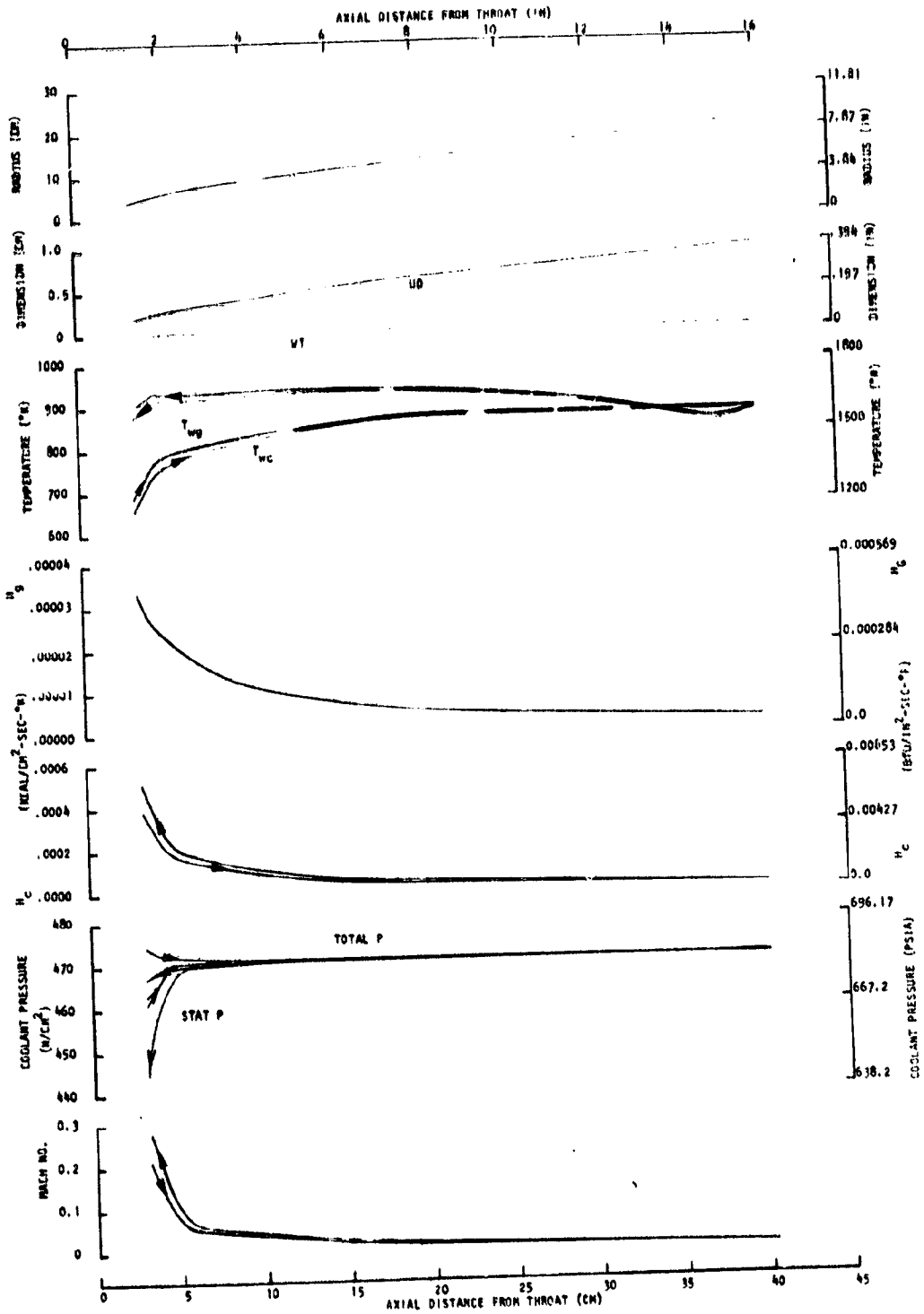

Figure 19. Parameters for the O_2/CH_4 Low Thrust Two-Pass Nozzle-Series Flow, F = 4448 N (1000 lbf), P_c = 344.7 N/cm^2, ε = 8 to 200

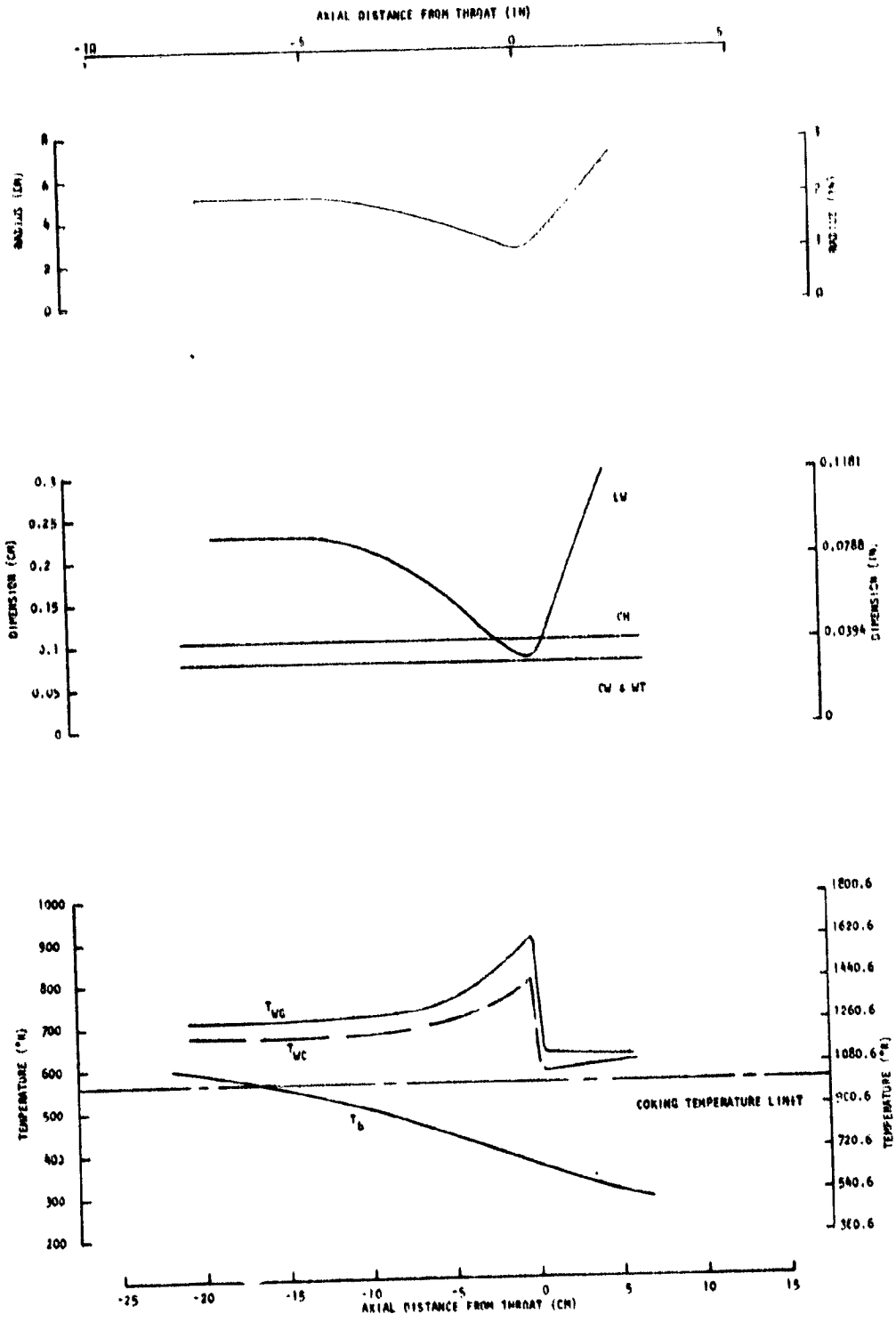

Figure 20. Parameters for O_2/RP-1 Low Thrust Combustor, F = 13344.6 N (3000 lbf), P_{c_o} = 344.74 N/cm^2 (500 psia), ε = Inj to 8

temperature limit of 811 K (1000 F) for NARloy-Z, the coolant-side wall temperature exceeded the RP-1 coking limit of 561 K (1010 R). More important, even the combustor outlet coolant bulk temperature exceeded the RP-1 coking limit. A lower chamber pressure (68.95 N/cm^2 or 100 psia) thrust chamber was analyzed at this thrust level and the same results occurred. In both the midrange chamber pressure and the low chamber pressure cases, the RP-1 coolant bulk temperature exceeded the 561 K (1010 R) coking limit even without considering the nozzle cooling. Therefore, regenerative cooling of LO_2/RP-1 thrust chambers could not be accomplished within the analysis guidelines (neglected the existance of a gas-side carbon layer).

In an extended thrust chamber cooling analysis, the benefit of a gas-side carbon layer for LO_2/RP-1 regenerative cooled thrust chambers was evaluated and found feasible.[2] These analysis results will be presented in a following discussion.

In establishing the minimum regenerative-cooling chamber pressure limit for the LO_2/H_2 and LO_2/CH_4 thrust chambers, two-phase heat transfer analyses were conducted.[2] For the LO_2/CH_4 thrust chamber analysis, a curve-fit of available methane burnout heat flux test data was developed. Since the test data range was limited, the assumption was made that the developed relationship applied for the heat fluxes, pressures, and coolant velocities which were evaluated. Assuming a minimum cooling jacket discharge pressure of 1.087 times chamber pressure methane subcritical pressures are encountered at chamber pressures below 344.7 N/cm^2 (500 psia). An analysis was performed for a 275.8 N/cm^2 (400 psia) chamber pressure and indicated that the coolant velocities required to just cool the burnout heat flux (safety factor equal to 1.0) resulted in coolant Mach numbers exceeding the allowable 0.3 maximum limit.

Another cooling approach to subcritical LO_2/CH_4 chamber pressure thrust chambers was evaluated briefly. This approach was to vaporize the methane at low heat flux (in the nozzle), then cool the combustor with gaseous methane. The two-pass nozzle regenerative cooling circuit to an area ratio of 200-to-1 was analyzed. To cool the burnout heat flux values, the maximum coolant Mach number (nozzle outlet) exceeded the maximum allowable 0.3. Also the coolant bulk temperature exiting the regenerative-cooled nozzle portion was 478 K (860 R). This coolant bulk temperature would make the cooling of the combustor with coolant Mach numbers less than 0.3 extremely difficult if not impossible. Therefore, it was concluded that within study guidelines, regenerative cooling at subcritical pressures with methane was not feasible, and the minimum chamber pressure was set at 344.7 N/cm^2 (500 psia). For subcritical chamber pressure LO_2/H_2 thrust chambers, the heat flux versus ($T_w - T_{sat}$) curves shown in Fig. 21 were used to determine the wall temperatures in the two-phase region. The 68.95 N/cm^2 (100 psia) thrust chambers at 4448 N (1000 pounds) and 13345 N (3000 pounds) thrust were analyzed using Fig. 21 and the regenerative cooling program. As shown by the typical results presented in Fig. 22, satisfactory cooled combustor designs were achieved with maximum coolant Mach numbers and maximum wall temperatures within analysis guidelines.

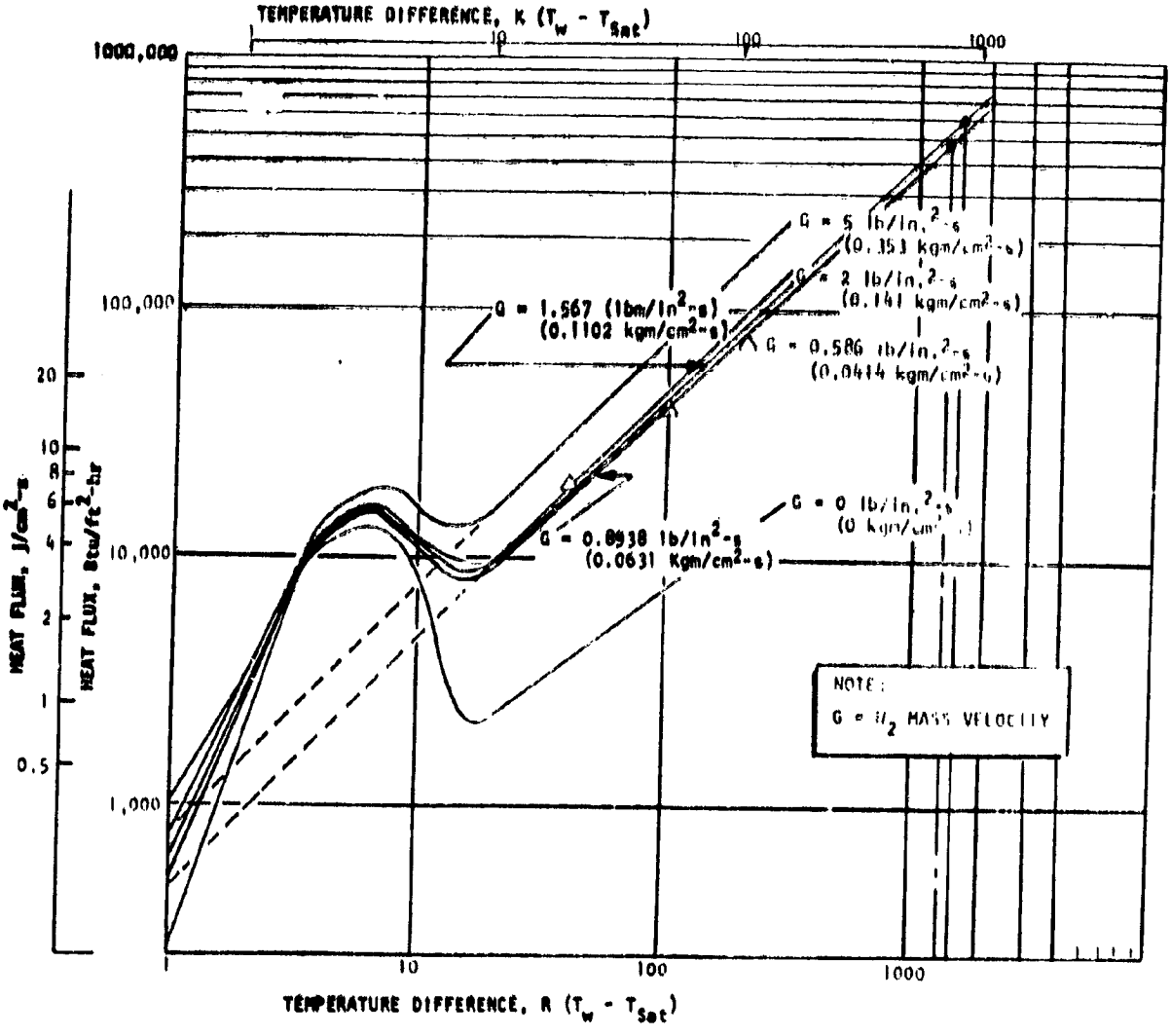

Figure 21. Hydrogen Heat Flux vs ($T_w - T_{sat}$)

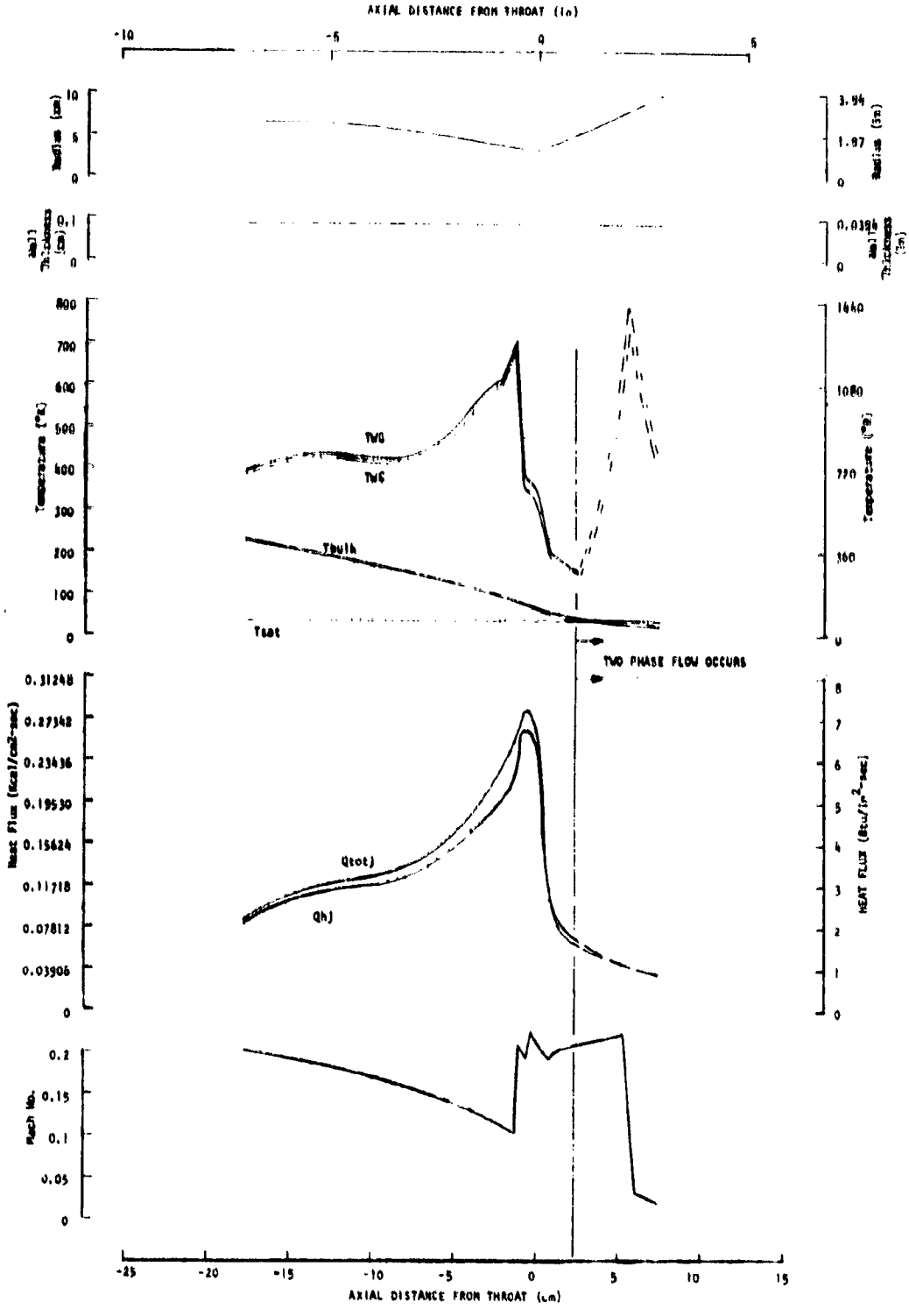

Figure 22. O_2/H_2 Low Thrust Combustor, F = 1K lbf = 4,4482 N, P_c = 68 948 N/cm^2, MR = 6, E(W) = 8, Lcz = 6.97 in = 17.704 cm, E(c) = 3.62

However in applying the Thurston/Rogers flow stability criterion to assess the flow stability of these subcritical chamber pressure LO_2/H_2 thrust chambers, the coolant flow in the combustor designs was found to be unstable. Therefore, the maximum chamber pressure for a regenerative-cooled LO_2/H_2 thrust chamber was limited to chamber pressures having supercritical pressure, which was 103.4 N/cm^2 (150 psia) for thrust levels of 4448 N (1000 pounds) to 13345 N (3000 pounds) and 68.95 N/cm^2 (100 psia) at 445 N (100 pounds) thrust.

Creep Analysis. With the requirement of long engine total firing durations at low thrust levels, the existence of material creep could create detrimental effects on the thrust chambers. With a regenerative-cooled portion, coolant passages could distort and enlarge, resulting in higher-than-design wall temperatures. For film- and radiation-cooled portions, significant creep could result in thrust chamber contour distortion, local hot spots, and additional performance loss.

For the regenerative-cooled channel wall combustors, the maximum fixed end-beam bending stress was computed for thrust chambers on the maximum chamber pressue cooling limit. The maximum creep stress range for both the LO_2/H_2 (NARloy-Z) and LO_2/CH_4 (nickel) combustors and extrapolated wall material[2] creep data are presented in Fig. 23. For NARloy-Z the creep rate was less than 10^{-9} in./in./hr. The creep rate for nickel was approximately 10^{-7} in./in..hr and assuming a 50-hour total engine firing duration and a safety factor of 2, the creep was 0.001%.

The maximum stress on the radiation-cooled nozzle extension was computed at the maximum temperature location (attach area ratio of 200-to-1). Molybdenum was assumed to be used for extensions having maximum wall temperatures of 1644 K (2500 F) or less and L605 alloy for maximum wall temperatures less than 1367 K (2000 F). The maximum creep for molybdenum was less than 0.007% and less than 0.002% for L605 alloy using a safety factor of 4.

Using the same materials for the same temperature ranges for the film-cooled thrust chambers, the maximum creep for the molybdenum was less than 0.7% using a safety factor of 4.

Parametric Data. From the detailed regenerative-cooled analysis, parametric plots of coolant heat input and coolant pressure drop for the LO_2/H_2 and LO_2/CH_4 thrust chambers were developed for the channel wall combustor and tubular nozzle (Fig.24 through 27). The relatively constant combustor coolant heat input is the result of the less-than-linear inverse relationship of combustor gas-side surface area with chamber pressure. The combustion chamber length varies approximately as

$$L_c \propto P_c^{-0.24} \qquad (8)$$

and, as a result, the area decreases almost as much as the average heat flux increases with increase in chamber pressure (fixed thrust) and the heat input remains essentially constant as shown in Fig. and for LO_2/H_2 and LO_2/CH_4 combustors, respectively.

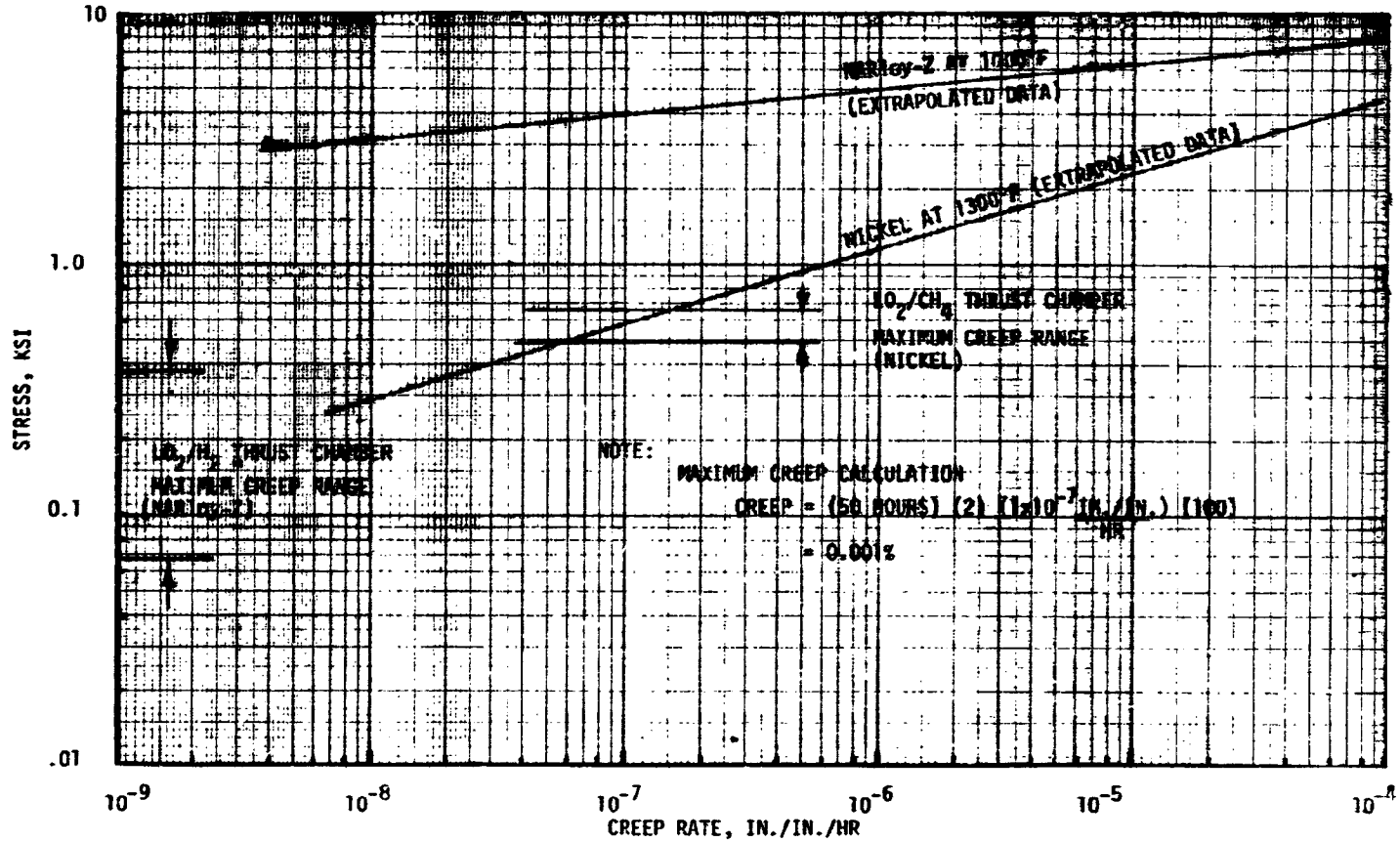

Figure 23. Regenerative-Cooled Thrust Chamber - Combustor Maximum Creep (Maximum Chamber Pressure Limit)

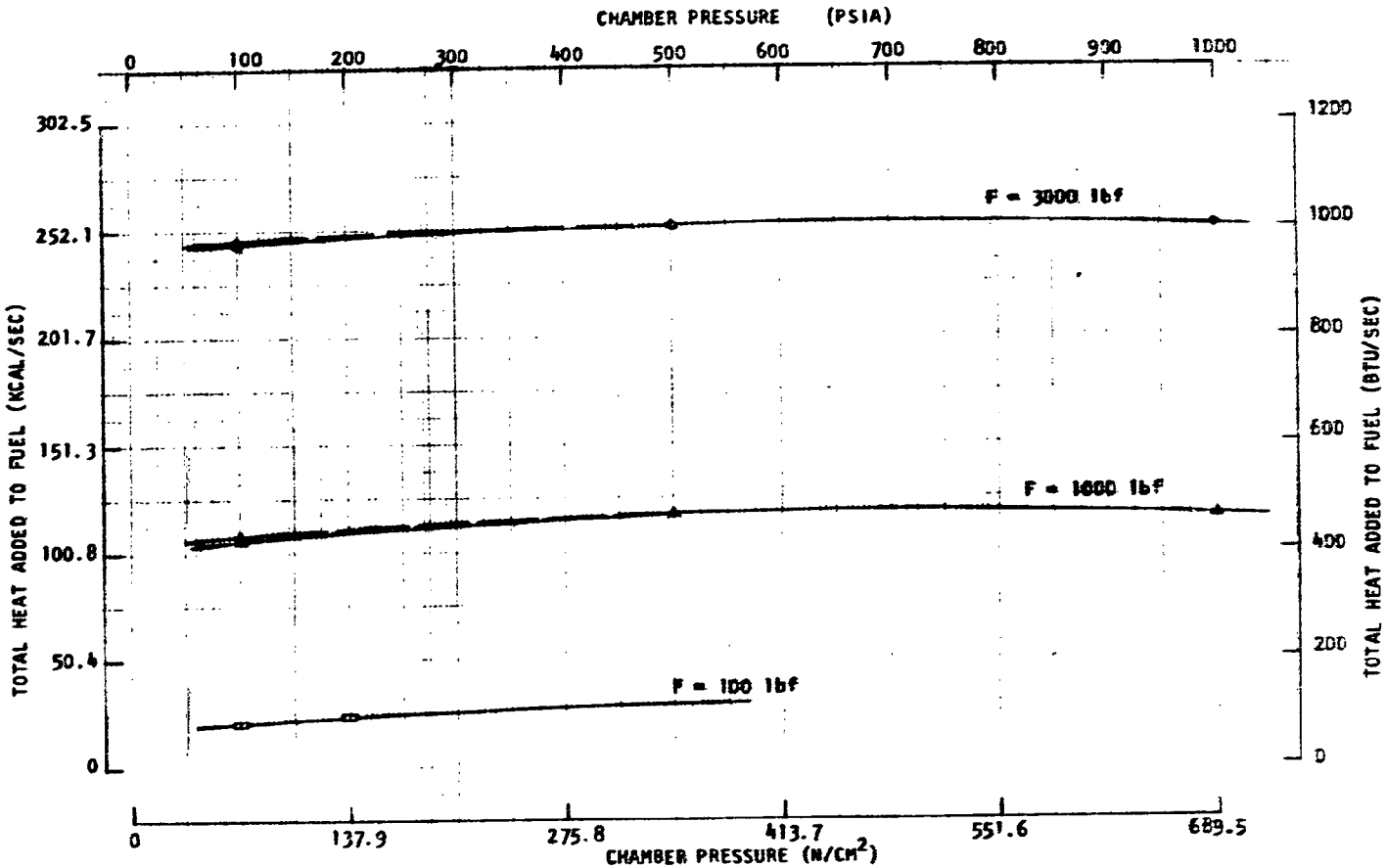

Figure 24. LO_2/H_2 Combustor Coolant Heat Input

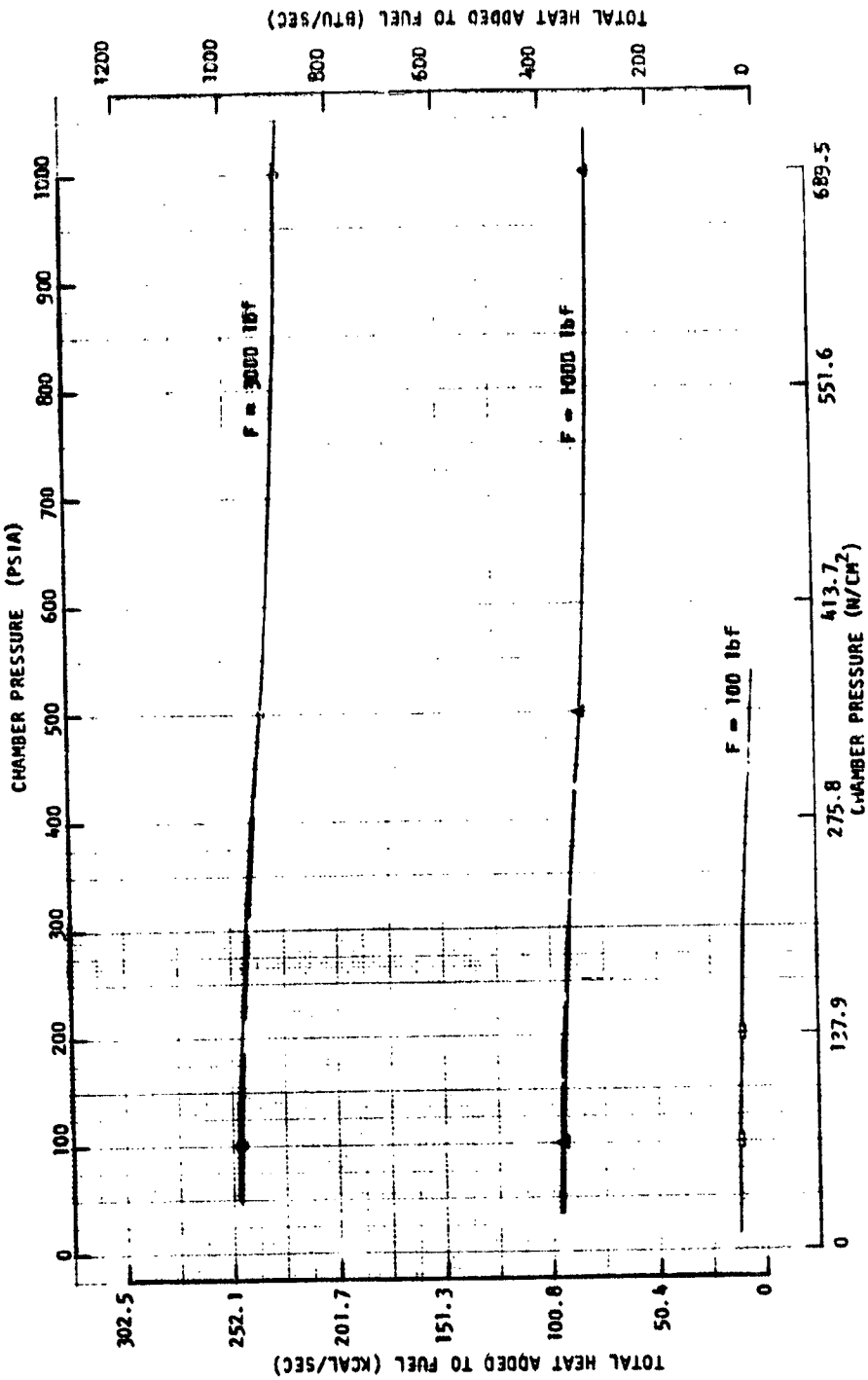

Figure 25. LO_2/H_2 Nozzle Heat Input

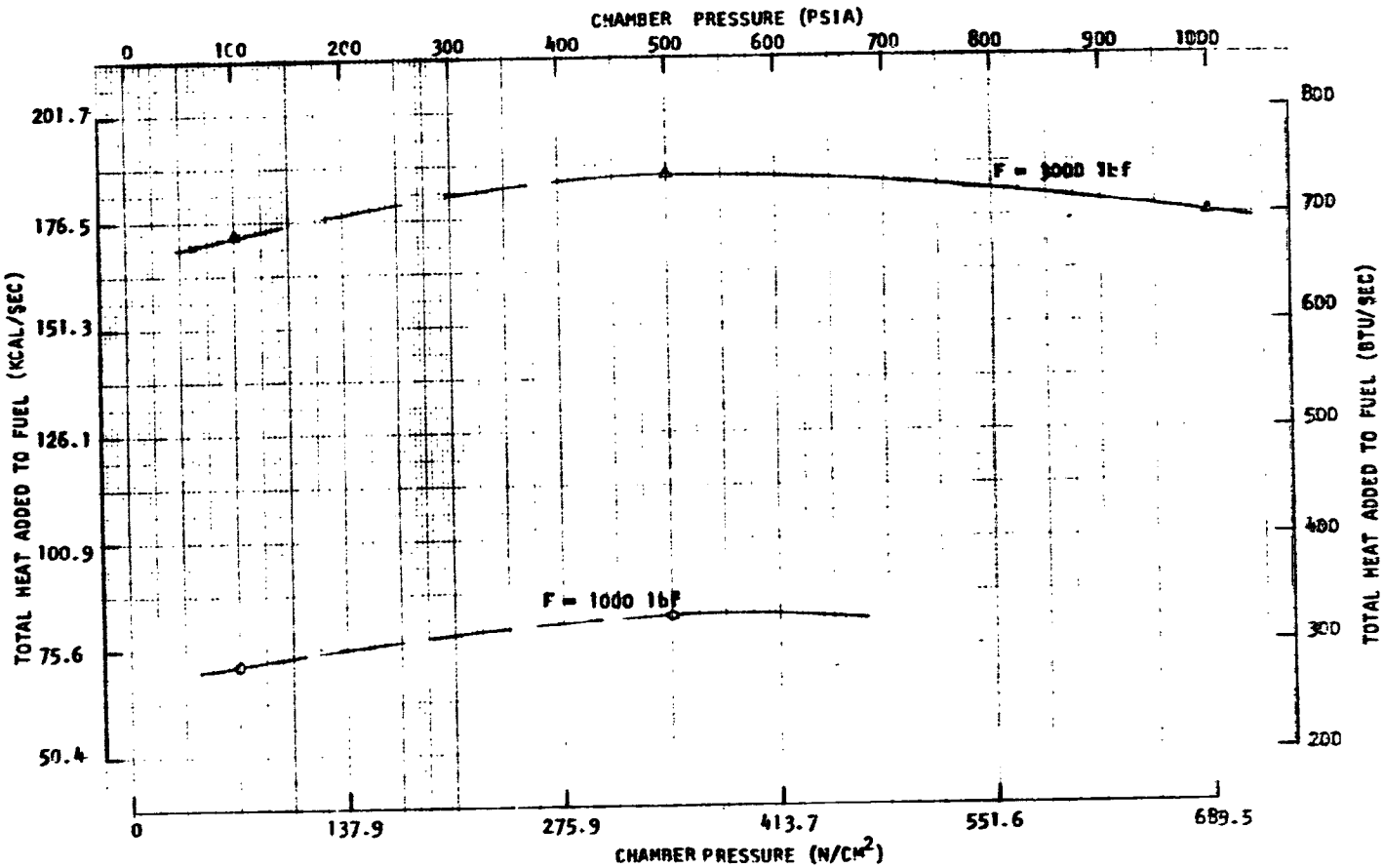

Figure 26. LO_2/CH_4 Combustor Coolant Heat Input

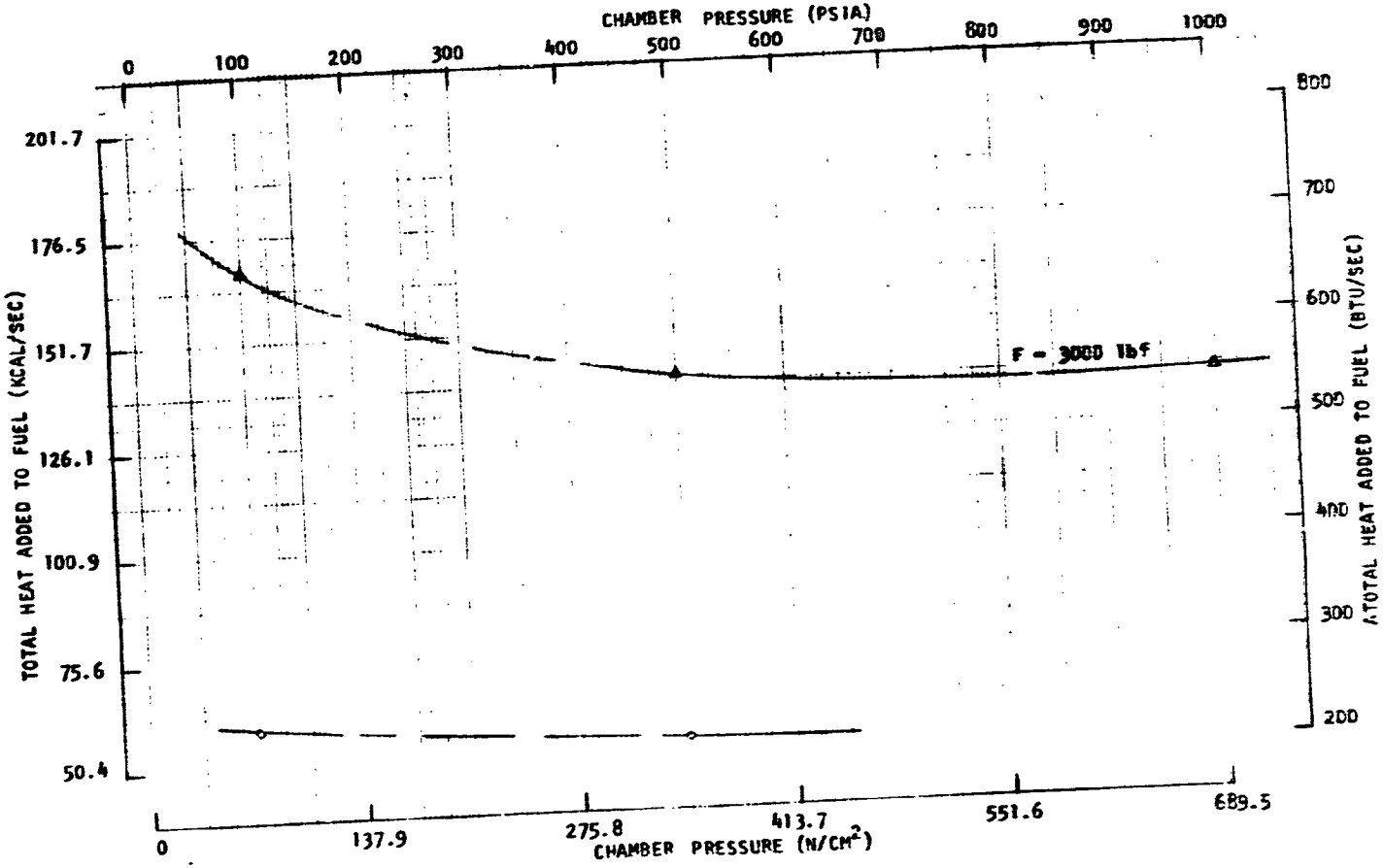

Figure 27. LO_2/CH_4 Nozzle Heat Input

The nozzle coolant heat input decreased with increase in chamber pressure at a constant thrust (Fig. 25 and 27). This trend is the result of the fixed nondimensional nozzle contour so that approximately

$$Q \alpha P_c^{-0.2} \tag{9}$$

The coolant pressure drop for the combustor and nozzle of the LO_2/H_2 and LO_2/CH_4 regenerative-cooled thrust chambers are presented in Fig. 28 through 31. The coolant pressure drop increased with chamber pressure at a fixed thrust level as a result of higher heat fluxes. The influence of thrust on coolant pressure drop at a fixed chamber pressure was almost negligible for the regeneratively cooled LO_2/CH_4 thrust chambers as shown in Fig. 30 and 31. However, with the LO_2/H_2 thrust chambers (Fig. 28 and 29), the coolant pressure drop at high chamber pressures was higher for the lower thrust. At lower chamber pressure, this trend reverses. For LO_2/H_2 chamber pressures below 103.4 N/cm^2 (150 psia), the increased coolant pressure drop was the result of two-phase heat transfer cooling requirements.

Cooling Limits. The regenerative-cooling limits were established for LO_2/H_2 and LO_2/CH_4 thrust chambers through the use of the detailed regenerative-cooling analyses, and are presented in Fig. 32. LO_2/RP-1 thrust chambers could not be regeneratively cooled within the analysis guidelines, but were found feasible in the extended thrust chamber cooling analysis (one of the sections to follow).

For LO_2/H_2 thrust chambers, the study specified maximum chamber pressure of 689.5 N/cm^2 (1000 psia) limited the chamber pressure for thrust levels from 13345 N (3000 lbf) to 4448 N (1000 lbf). Below 4448 N (1000 lbf) thrust, the maximum coolant Mach number limit of 0.3 and the durability limit of the wall temperature limited the LO_2/H_2 regenerative cooling to 448.2 N/cm^2 (650 psia) at 2224 N (500 lbf) thrust and 138 N/cm^2 (200 psia) at 444.8 N (100 lbf) thrust.

For LO_2/CH_4 thrust chambers, the maximum chamber pressure (cooling limit) decreased from 689.5 N/cm^2 (1000 psia) at 13345 N (3000 lbf) thrust to 344.7 N/cm^2 (500 psia) at 4448 N (1000 lbf) thrust.

The LO_2/H_2 thrust chambers offered a larger operational envelope (thrust and chamber pressure) due to the better cooling capability of hydrogen and its lower critical pressure.

The minimum chamber pressure limit was set by the critical pressure of the coolant (fuel) for each propellant combination. However, subsequent engine cycle balances (discussed later) revealed supercritical thrust chamber coolant discharge pressures at subcritical chamber pressures due to the turbine pressure ratios required. Therefore, the minimum chamber pressure limits shown in Fig. 32 were lowered as discussed in the Extended Thrust Chamber Cooling Analysis section.

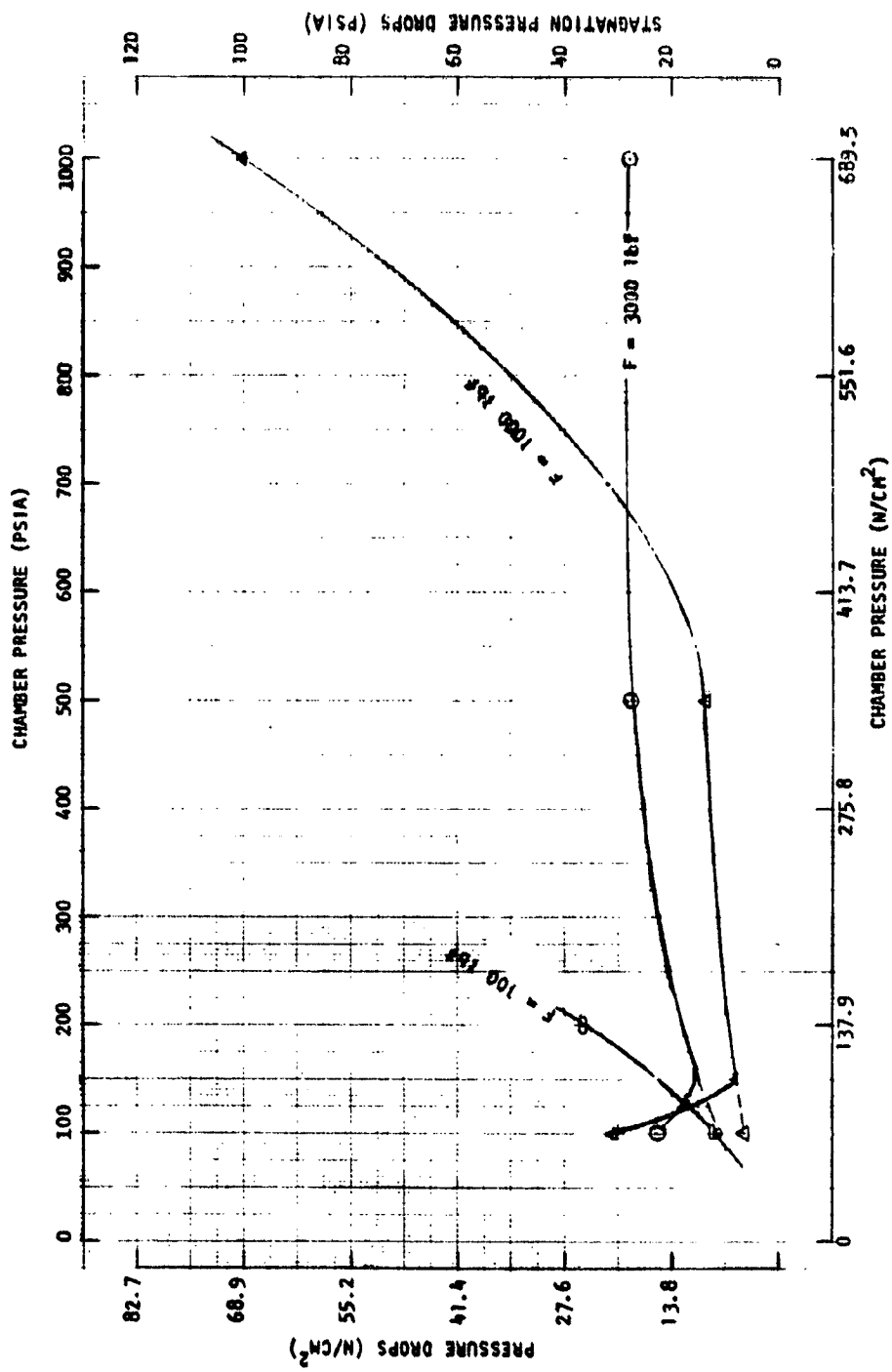

Figure 28. LO_2/H_2 Combustor Coolant Pressure Drop

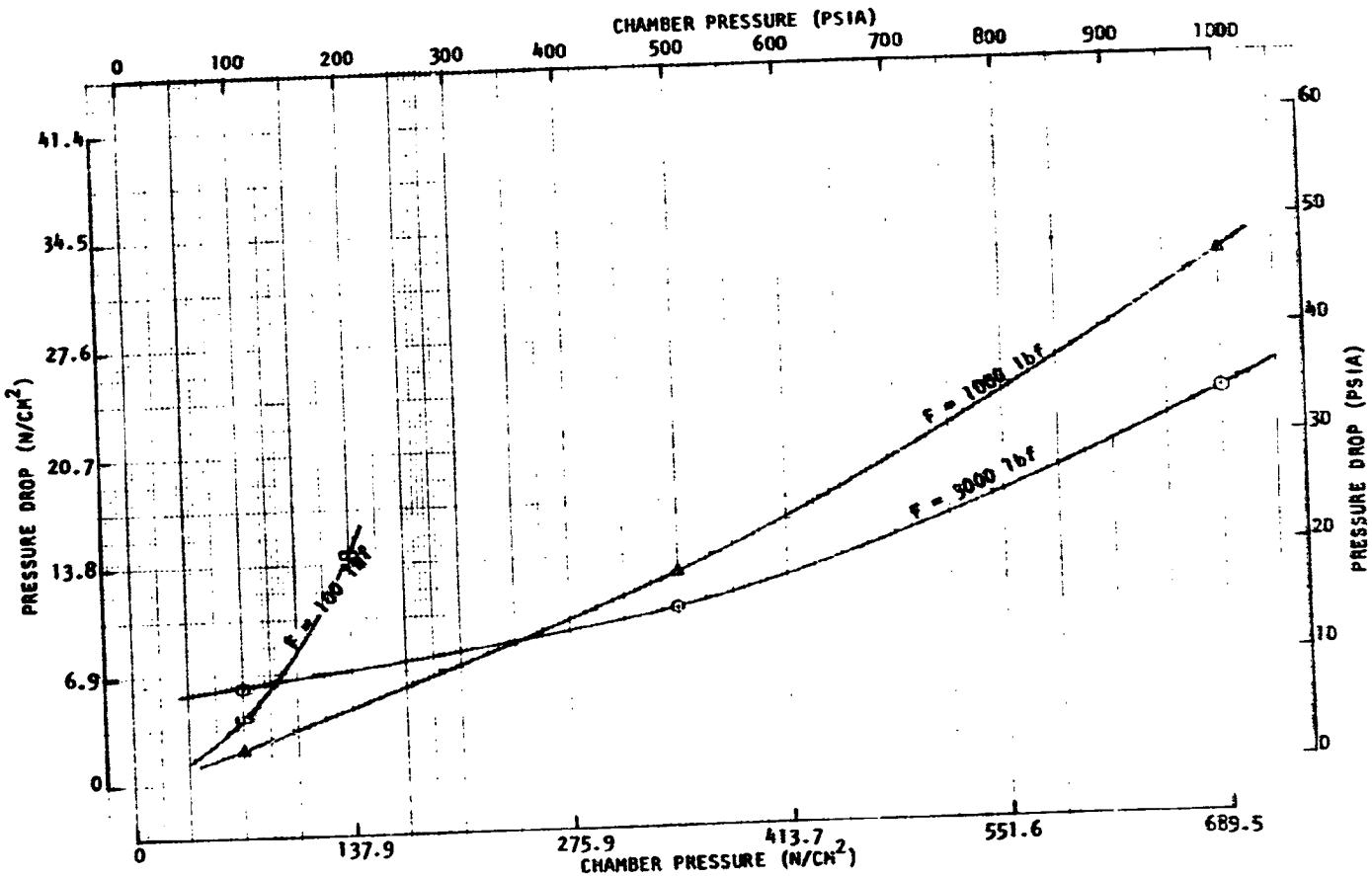

Figure 29. LO_2/H_2 Nozzle Coolant Pressure Drop

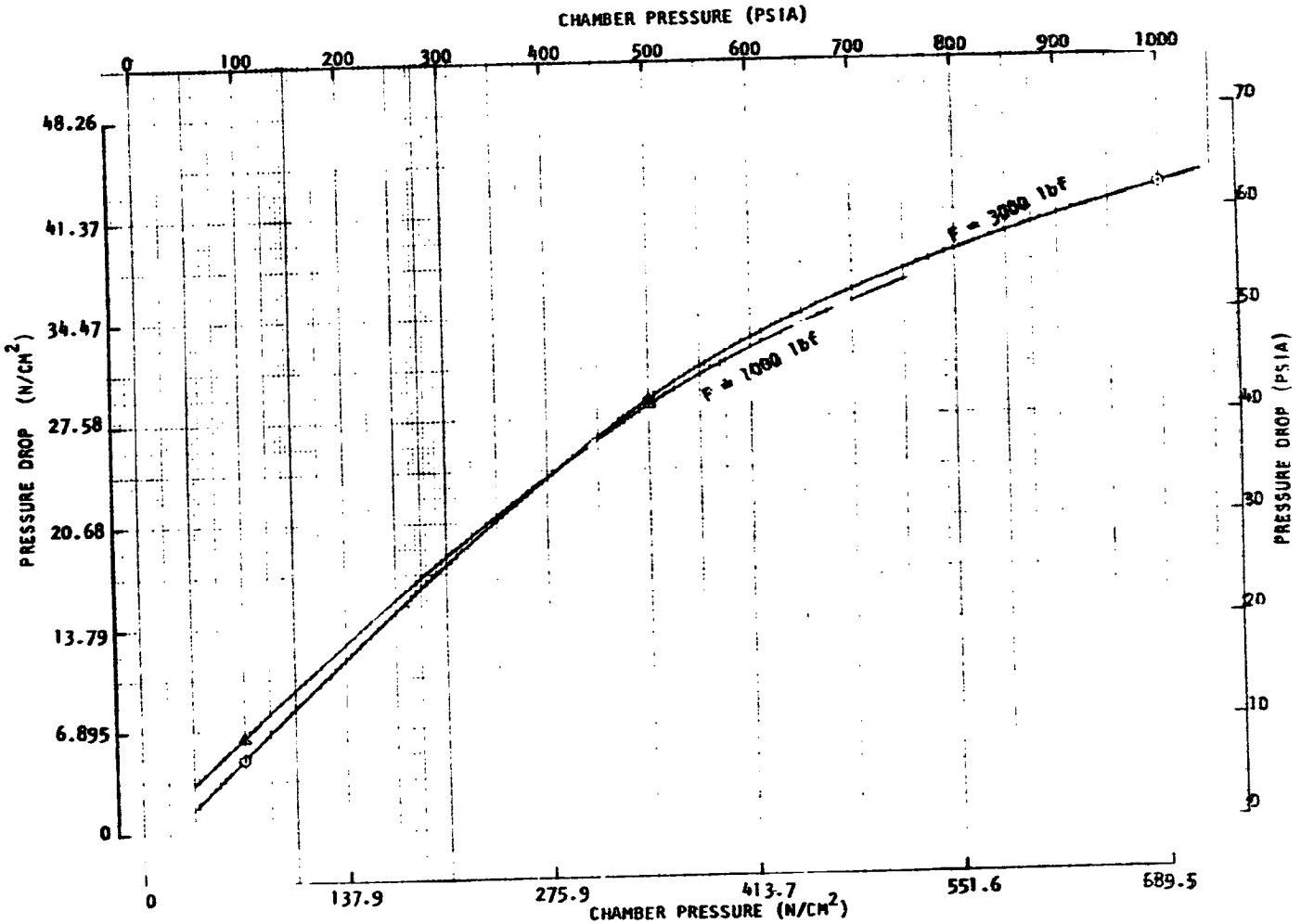

Figure 30 . LO_2/CH_4 Combustor Coolant Pressure Drop

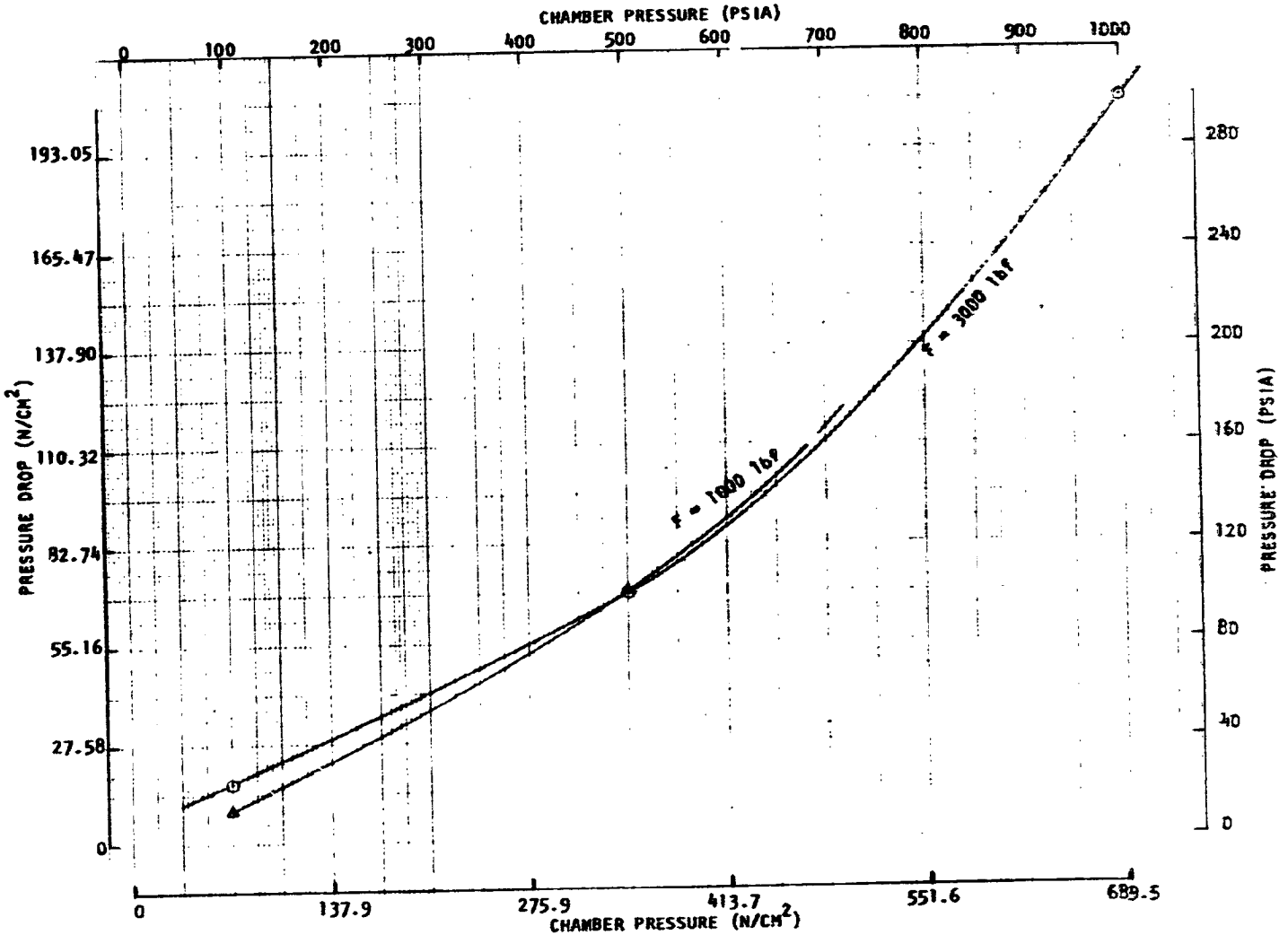

Figure 31. LO_2/CH_4 Nozzle Coolant Pressure Drop

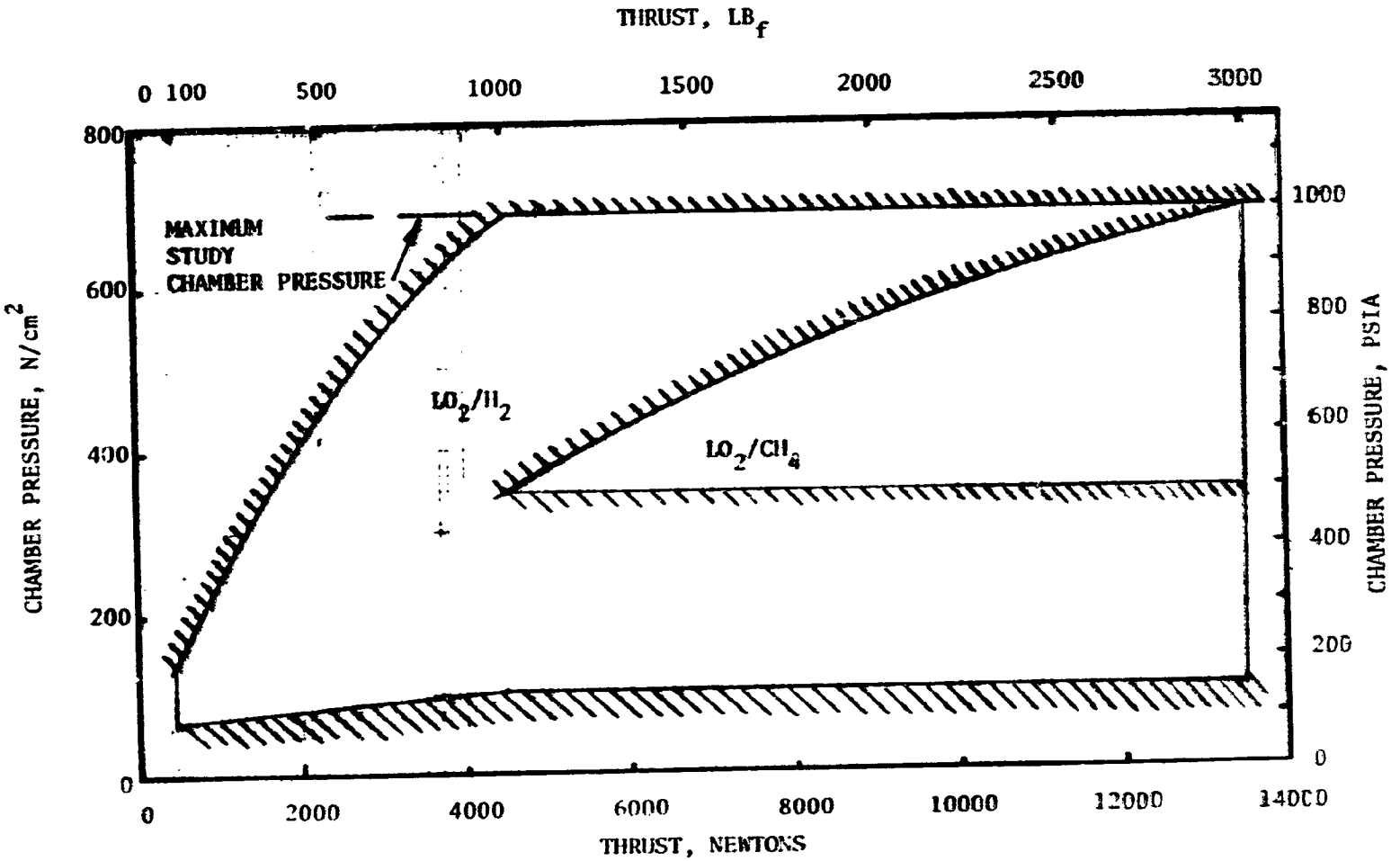

Figure 32 . Regenerative-Cooled Thrust Chamber Cooling Limits Using Table 2 Guidelines

Film Cooling Analysis

From the cooling analysis guidelines (Table 2), a maximum performance loss allowed due to film cooling is 10%. The amount of film coolant (fuel) which results in this performance loss is the maximum allowable film coolant flow, and would achieve the maximum chamber pressure at a given thrust level. Therefore, the film-cooling analysis approach used was to determine the specific impulse loss variation with film coolant flow and define the maximum allowable film coolant flow for a given thrust and chamber pressure. Using this film coolant flow and the gas-side heat transfer coefficient distribution, the thrust chamber wall temperature distribution is determined and compared to the maximum allowable wall material temperature. If the wall temperature is less than the allowable material temperature, the thrust chamber represents a feasible design. This analysis procedure is repeated for different design conditions to define the film-cooling limit.

Performance Loss. The film cooling performance loss was computed using the simplified JANNAF method. The method consists of prescribing a linear mixture ratio distribution from the film-cooled wall (low mixture ratio) to the inner core, and considers the film-cooled region to be divided into several zones. The mixture ratio profile variation and pertinent equations are shown in Fig. 33 For this type of analysis, the following assumptions were used:

1. For fuel injection, the mixture ratio at the wall is low, approaching zero, since the gas is in contact with the pure injected fuel.
2. The mixture ratio of the core gas stream is unaffected by the coolant (i.e., the coolant is completely entrained in the primary gas stream before any of it reaches the center of the chamber).
3. Mixture ratio between these limits is linear (as has already been stated).
4. The variable mixture ratio region is divided into zones and the coolant is assumed to react with the main flow at the local mixture ratio.
5. The flow in each zone is then integrated to determine the mixture ratio and specific impulse, and a mass-weighted average specific impulse is calculated.
6. This value is then compared to the specific impulse at the same overall thrust chamber mixture to determine the loss due to the coolant flow.

The results of this method correlate quite well with experimental results (O_2/H_2) and other propellant combinations).

The film cooling performance results for the three propellant combinations are presented in Fig. 34 through 36 . The specific impulse loss curves which are independent of thrust are presented for chamber pressures of 13.8 N/cm^2 (20 psia), 69 N/cm^2 (100 psia), 344.7 N/cm^2 (500 psia), and 689.5 N/cm^2 (1000 psia) for a 400-to-1 area ratio nozzle. For a given percent film

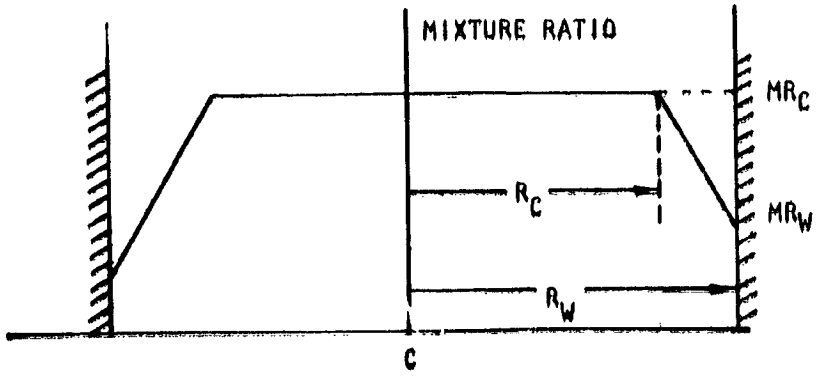

The ratio of (R_C/R_W) is found by solving the quadratic equation:

$$\left[\left(\frac{2}{MR_W-MR_C}\right) - \frac{2\,MR_W \ln\left(\frac{MR_W}{MR_C}\right)}{(MR_C-MR_W)^2} + \frac{1}{MR_C}\right]\left(\frac{R_C}{R_W}\right)^2 -$$

$$\left[\left(\frac{4}{MR_W-MR_C}\right) - \frac{2\,(MR_W+MR_C)\ln\left(\frac{MR_W}{MR_C}\right)}{(MR_C-MR_W)^2}\right]\left(\frac{R_C}{R_W}\right) +$$

$$\left[\left(\frac{2}{MR_W-MR_C}\right) - \frac{2\,MR_C \ln\left(\frac{MR_W}{MR_C}\right)}{(MR_C-MR_W)^2} - \frac{1}{MR_C} - \frac{\dot{M}_{FILM}}{\dot{M}_{OXIDIZER}}\right] = 0$$

where

$$\frac{\dot{M}_{FILM}}{\dot{M}_{OXIDIZER}} = \left[\frac{\dot{M}_{FILM}/\dot{M}_{INJ}}{1 - \dot{M}_{FILM}/\dot{M}_{INJ}}\right]\left[\frac{MR_C+1}{MR_C}\right]$$

The mixture ratio as a function of radius is then given by:

$$MR = MR_C - (MR_C-MR_W)\left(\frac{\frac{R}{R_W} - \frac{R_C}{R_W}}{1 - \frac{R_C}{R_W}}\right)$$

Figure 33. Equations for Computing Maldistribution and Transpiration Cooling Performance Loss

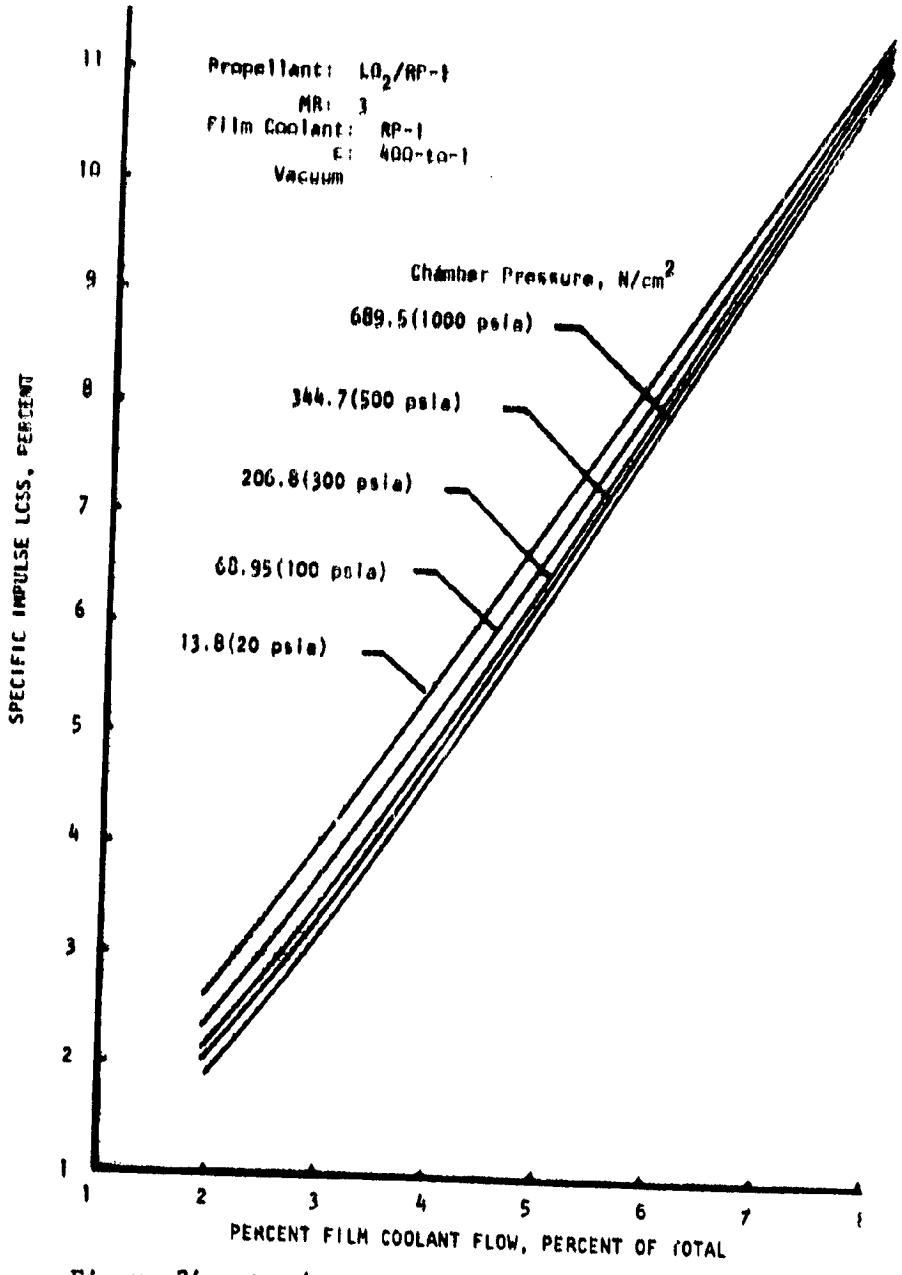

Figure 34. LO_2/RP-1 Film Coolant Performance Loss

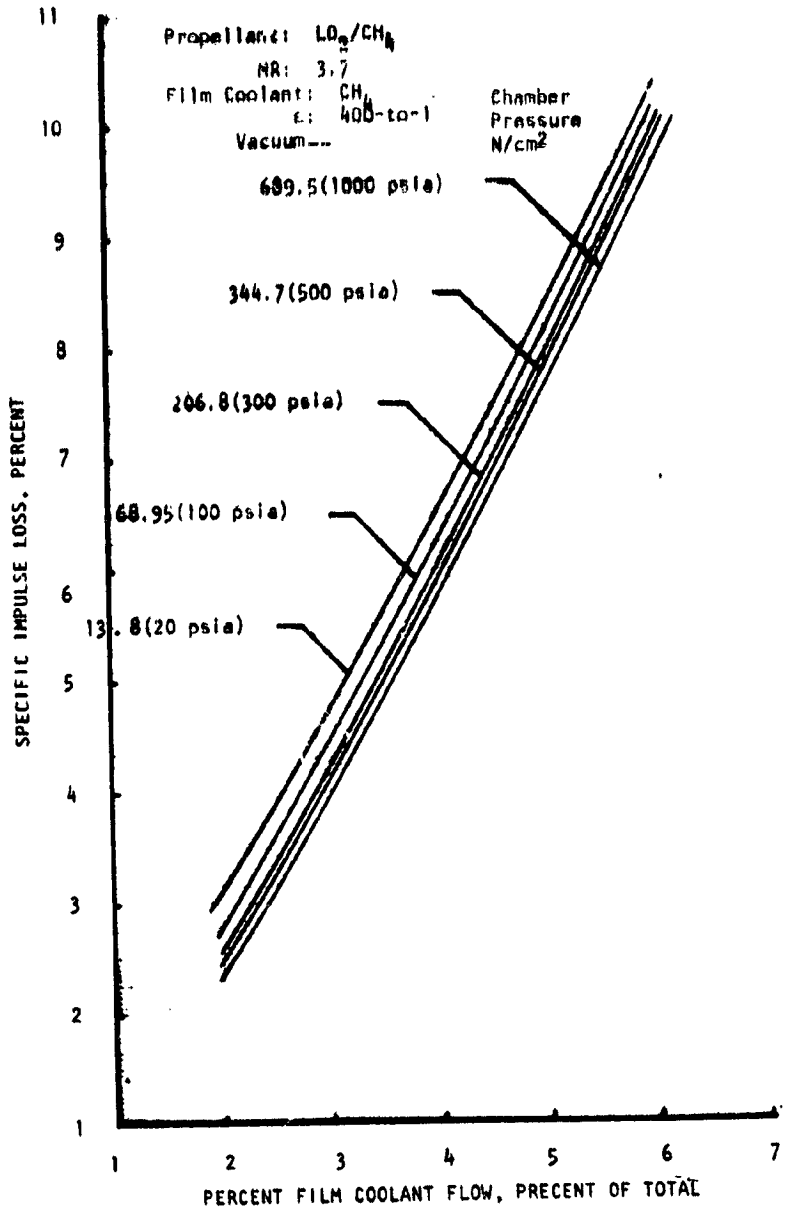

Figure 35. LO_2/CH_4 Film Cooling Performance Loss

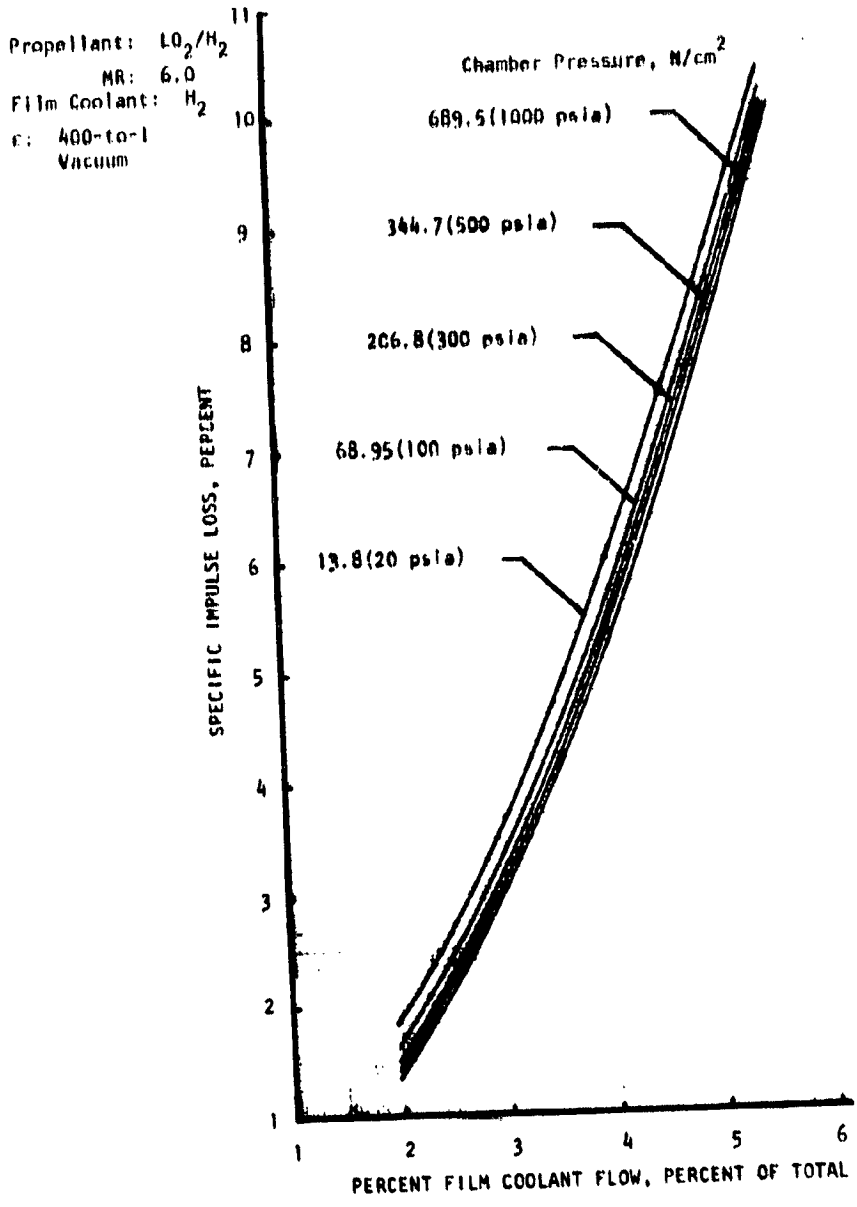

Figure 36. LO_2/H_2 Film Cooling Performance Loss

coolant flowrate, the higher chamber pressures resulted in a lower film cooling loss. The 10% performance loss resulted in approximately 7.2% film coolant for $LO_2/RP\text{-}1$ (Fig.34), 6% for LO_2/CH_4 (Fig.35), and 5.5% for LO_2/H_2 (Fig. 36). For a fixed specific impulse loss, only minor variations in percent film coolant resulted for the chamber pressure of interest.

Analysis Results. In performing the film cooling heat transfer analysis, the Rocketdyne gaseous film cooling model was employed for chamber pressure at supercritical film-coolant pressures, and the Rocketdyne liquid film cooling model was used for thrust chambers with subcritical coolant pressures. The liquid model included the influence of the film coolant heat of vaporization.

The combustion chamber geometries of the regenerative-cooled thrust chambers were used for the film-cooled thrust chambers. Also, the film coolant was assumed to be injected at the injector face plane.

The film cooling heat transfer results for the LO_2/CH_4 thrust chambers with CH_4 film cooling is shown in Fig. 37 . For each design condition (thrust and chamber pressure) analyzed, the maximum chamber wall temperature was plotted to obtain the curves presented in Fig. 37 . Assuming maximum allowable wall temperatures of 1644 K (2500 F) and 1367 K (2000 F), the maximum chamber pressure limit would be below the minimum study chamber pressure of 20 psia and, therefore, film-cooled LO_2/CH_4 thrust chambers were not feasible. The difference in the maximum wall temperature achieved with the 3 and 10% specific impulse loss flowrate (percent of total flowrate) was small due to the fact that the film cooling influenced only a small portion of the combustion chamber length, as shown in Fig. 38. The film temperature increases rapidly within 3.8 cm (1.5 inches) for the 3% film, and within 10.2 cm (4.0 inches) for the 10% film. By the time the flow reached the throat, the film temperature had essentially leveled off and the film cooling had a minimal cooling influence.

Heat transfer analyses of 11 film-cooled LO_2/H_2 thrust chambers were performed assuming core mixture ratio combustion gas properties for film coolant flows resulting in 10 and 3% specific impulse loss. The thrust chambers having a chamber pressure greater than 130 N/cm^2 (188 psia - H_2 critical pressure) were analyzed using the gaseous film cooling analysis model, and below 130 N/cm^2 (188 psia) chamber pressure, the liquid film-cooling model was used. As for the film-cooled LO_2/CH_4 thrust chambers, the maximum chamber wall temperature for each case was plotted to result in the curves presented in Fig. 39 and 40. As shown in Fig. 39 , the 10% specific impulse loss film coolant flow (approximately 5.5% of total flow) resulted in feasible thrust chamber designs for 4448 N (1000 pounds) and 13345 N (3000 pounds) thrust with a maximum chamber pressure of 105 N/cm^2 (152 psia) for a maximum wall temperature of 1644 K (2500 F). For a maximum wall temperature of 1367 K (2000 F), the maximum chamber pressure at 13345 N (3000 pounds) thrust decreased to 78 N/cm^2 (113 psia). Reducing the film coolant flow to that resulting in 3% specific impulse loss, approximately 2.8% of total flow, the region of feasibility decreased significantly as shown in Fig. 40 . The gas-side wall temperature and the film temperature

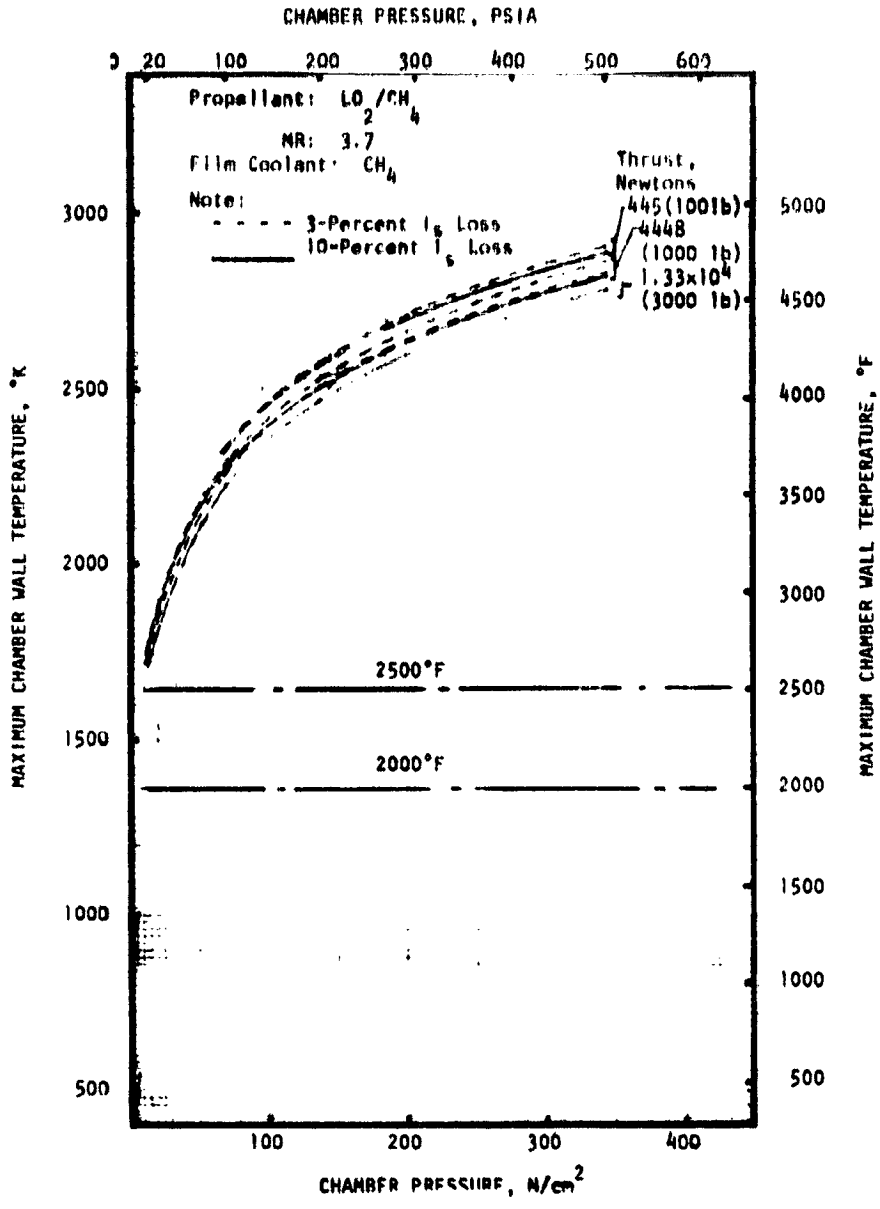

Figure 37 . LO_2/CH_4 Film Cooled Thrust Chamber Maximum Wall Temperature Variation with Chamber Pressure and Thrust

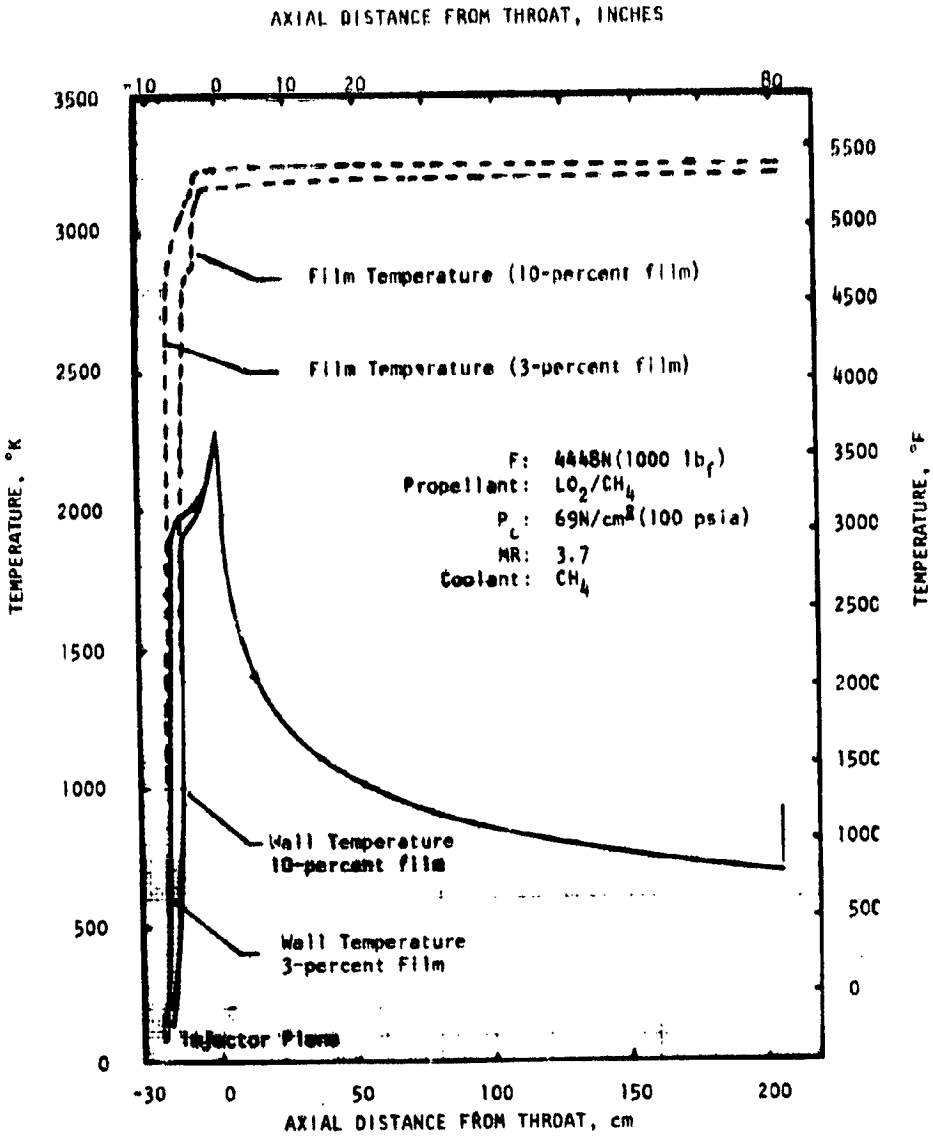

Figure 38 . LO_2/CH_4 Film-cooled Thrust Chamber Wall and Film Temperature Axial Distribution - 4448N (1000 lb_f) Thrust and 69N/cm^2 (100 psia) Chamber Pressure

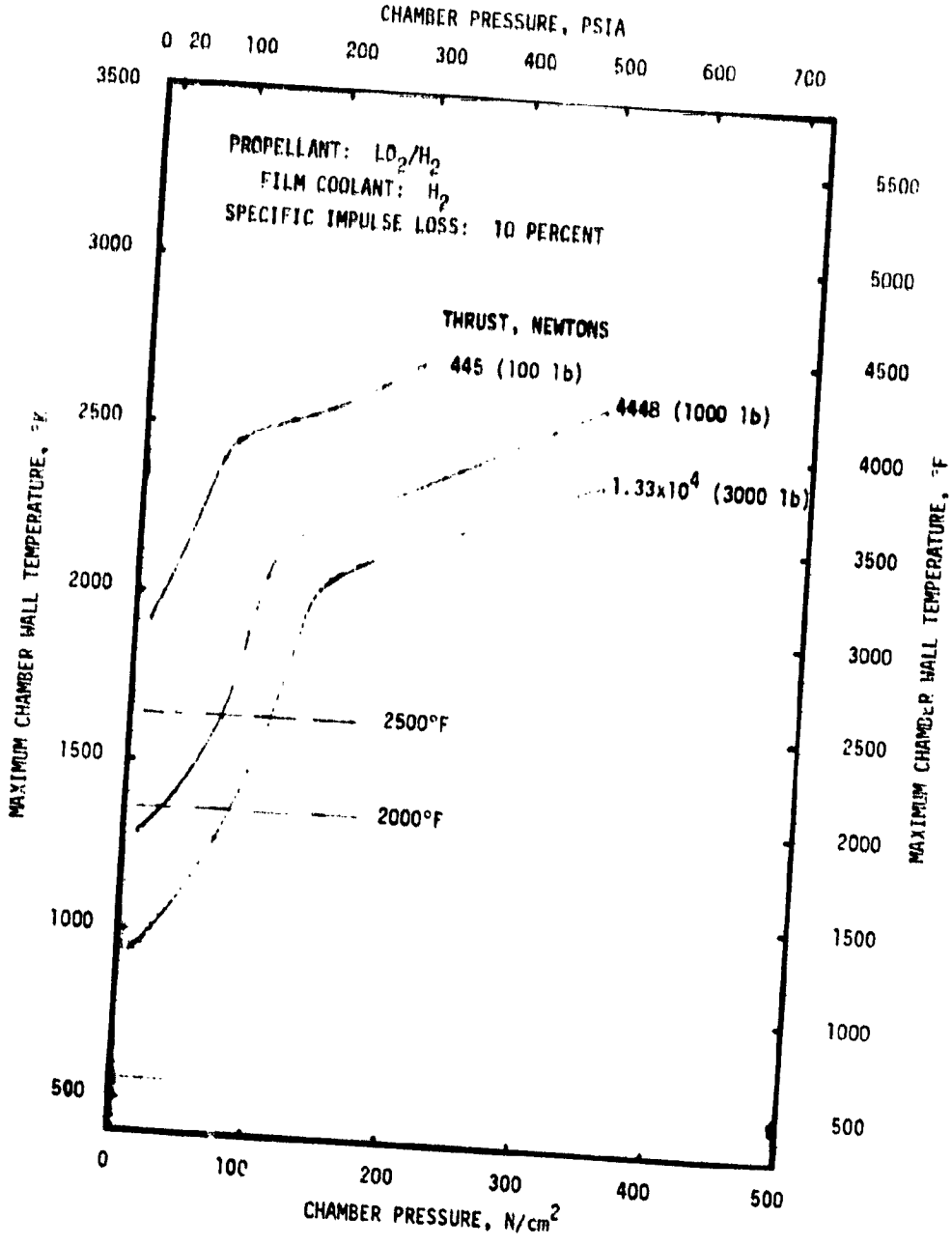

Figure 39 . LO_2/H_2 Film-cooled Thrust Chamber Maximum Wall Temperature Variation with Chamber Pressure and Thrust (10 percent I_s Loss

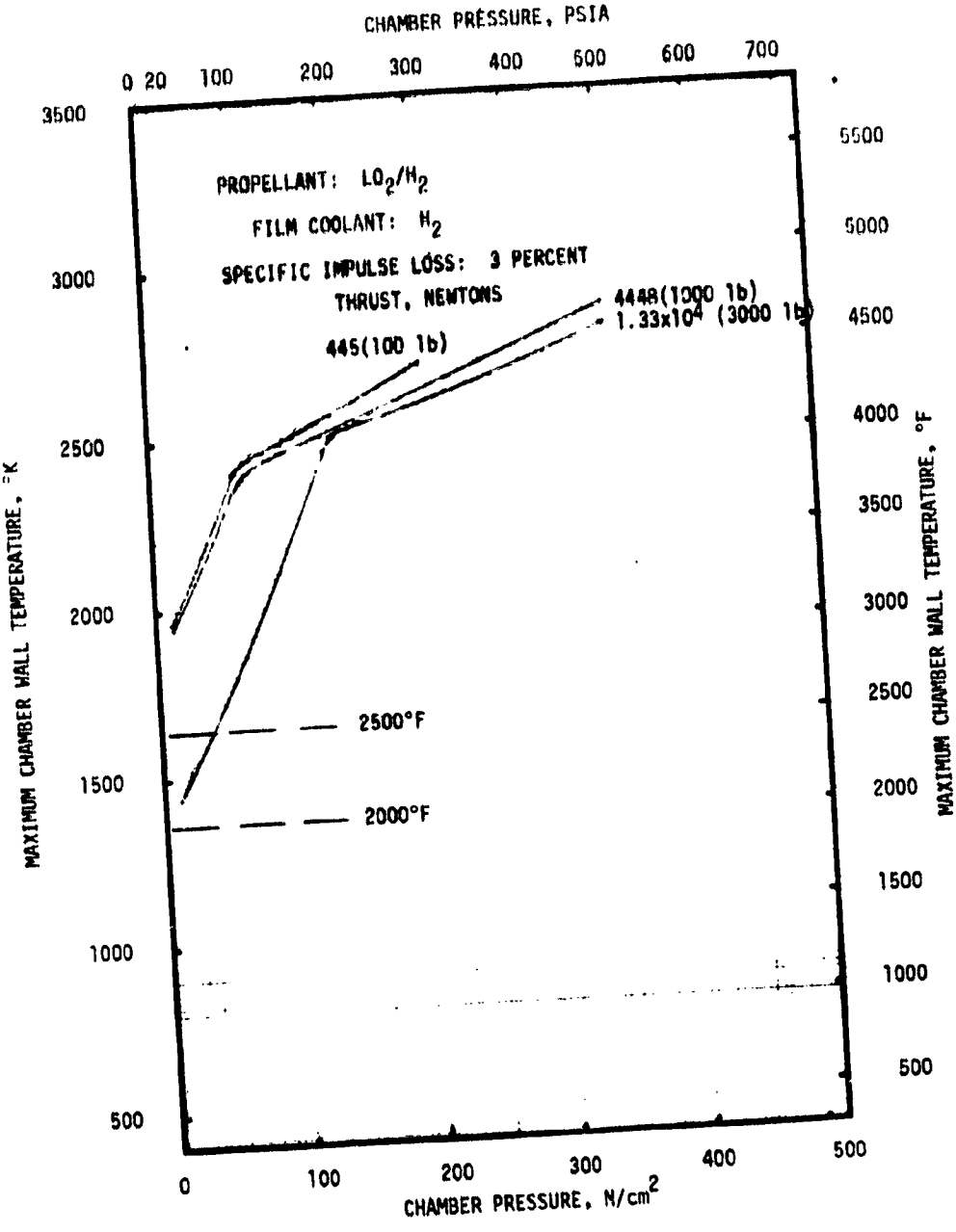

Figure 40. LO_2/H_2 Film-cooled Thrust Chamber Maximum Wall Temperature Variation with Chamber Pressure and Thrust (3 Percent I_s Loss)

distributions for two typical film-cooled thrust chamber designs (10% specific impulse loss) are shown in Fig. 41. The 4448 N (1000 pounds) thrust, 68.95 N/cm^2 (100 psia) chamber pressure design resulted in a maximum wall temperature of 1636 K (2484 F) at the nozzle throat. The 13345 N (3000 pounds) thrust design (68.95 N/cm^2 or 100 psia) had a maximum wall temperature of 1276 K (1836 F) which occurred downstream of the nozzle throat.

The film cooling analysis of 12 film-cooled LO_2/RP-1 thrust chambers were performed using the gaseous film-cooling analysis model for chamber pressures above 234 N/cm^2 (340-psia RP-1 critical pressure), and the liquid film-cooling analysis model was used below this pressure. The resulting maximum chamber wall temperatures versus chamber pressure curves for constant thrust are presented in Fig. 42. For the 10% specific impulse loss film coolant flow (approximately 7.2% of total flow) and a 1644 K (2500 F) maximum wall temperature, a small region of feasibility resulted.

Cooling Limits. For all three propellants, a maximum wall temperature limit of 1644 K (2500 F) was selected as the material temperature limit. Thrust chamber film cooling analysis revealed that LO_2/CH_4 film-cooled thrust chambers were not feasible, and the LO_2/H_2 and LO_2/RP-1 film-cooled thrust chambers were limited to low chamber pressures. As for regenerative-cooled thrust chambers, the LO_2/H_2 thrust chambers offered the largest operational thrust and chamber pressure range.

The maximum film-cooled thrust chamber cooling limits for LO_2/H_2 and LO_2/RP-1 are presented in Fig.43 for the 10% specific impulse loss film-coolant flows. For LO_2/H_2, the maximum chamber pressure at 13345 N (3000 pounds) thrust was 105 N/cm^2 (152 psia) and, as the thrust level was decreased, the maximum chamber pressure decreased to 13.8 N/cm^2 (20 psia) at 1081 N (243 lbf) thrust. For LO_2/RP-1 film-cooled thrust chambers, the region of feasibility was extremely limited. This region, as shown in Fig. 43, extended from a chamber pressure of 13.8 N/cm^2 (20 psia) at 5849 N (1315 lbf) thrust to 17.9 N/cm^2 (26 psia) maximum chamber pressure at 13445 N (3000 lbf) thrust. As for LO_2/RP-1 regenerative cooling, the influence of a gas-side carbon layer was neglected.

The maximum and minimum chamber pressure cooling limits for film-cooled LO_2/H_2 thrust chambers are presented in Fig. 44. Maximum chamber pressure curves (10% specific impulse loss) for maximum wall temperatures of 1644 K (2500 F) and 1367 K (2000 F) are shown. Thrust chamber designs within the maximum and minimum cooling limits have film cooling specific impulse losses varying from 3 to 10%.

Extended Thrust Chamber Cooling

The regenerative/radiation-cooled thrust chamber cooling limits previously defined were extended by altering the cooling criteria and adding a physical thermal barrier for added cooling enhancement. The original cooling criteria (Table 2) were changed by:

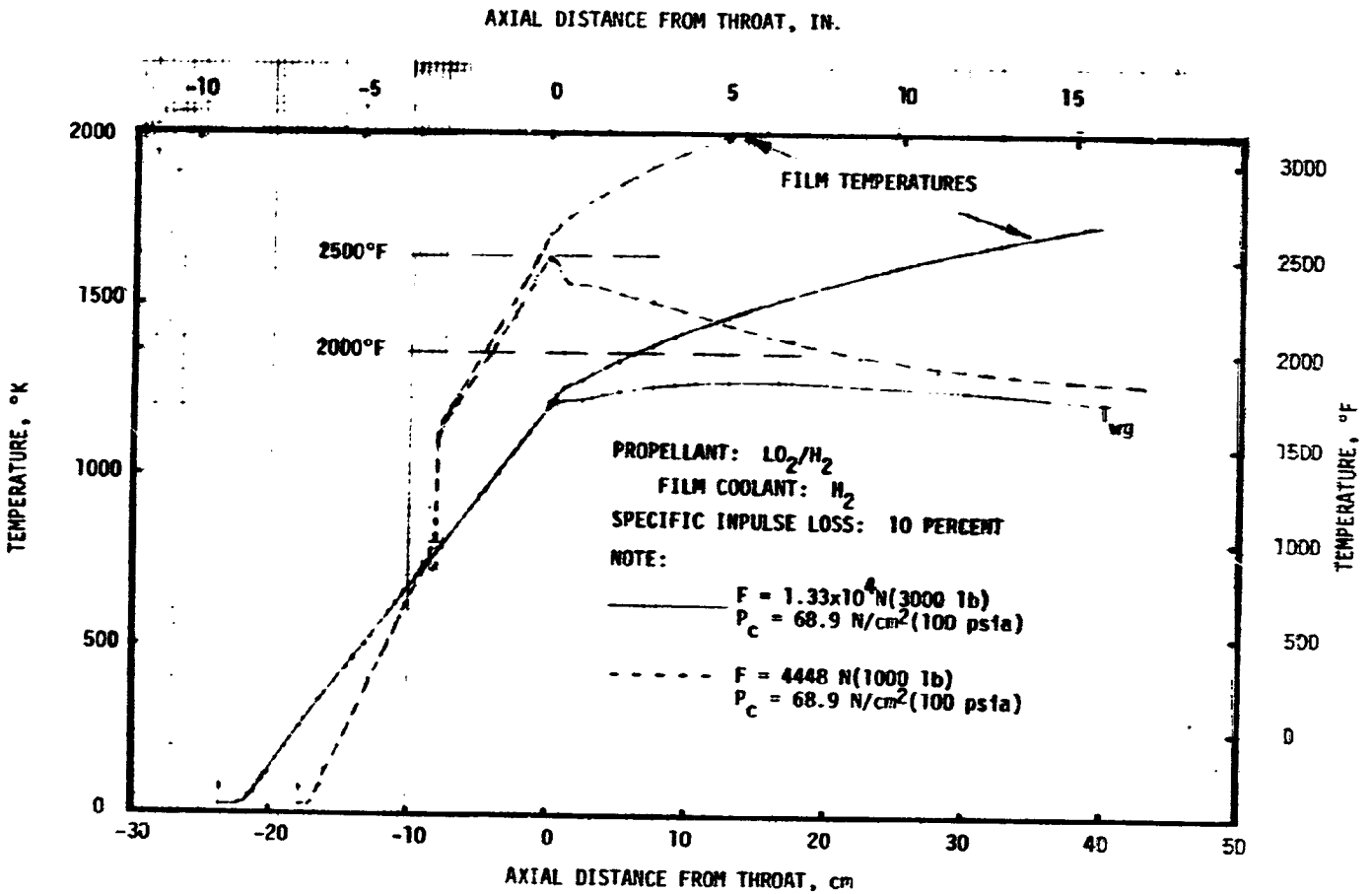

Figure 41 . LO_2/H_2 Film-cooled Thrust Chamber Results

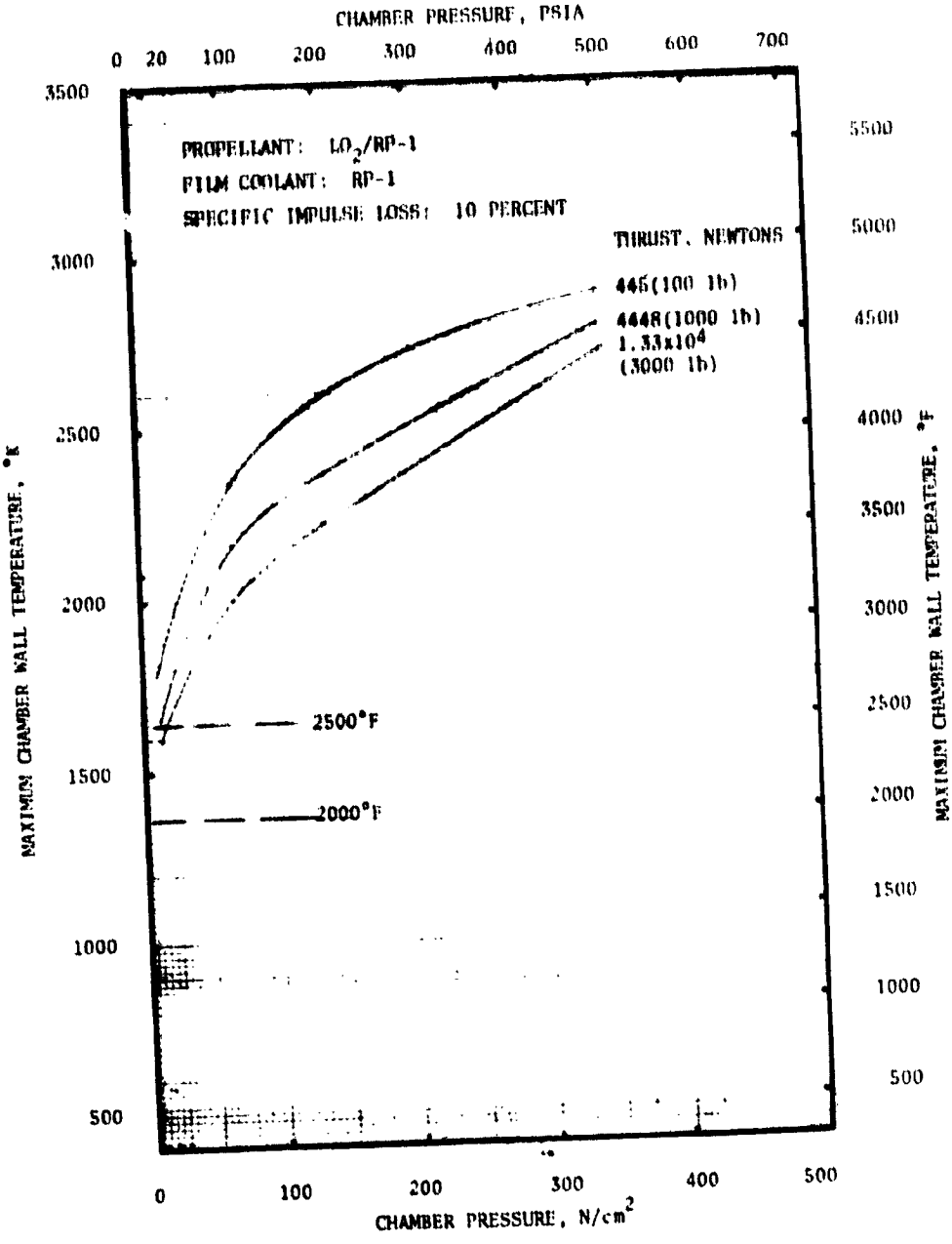

Figure 42. LO_2/RP-1 Film-cooled Thrust Chamber Maximum Wall Temperature Variation with Chamber Pressure and Thrust (10-percent I_s Loss)

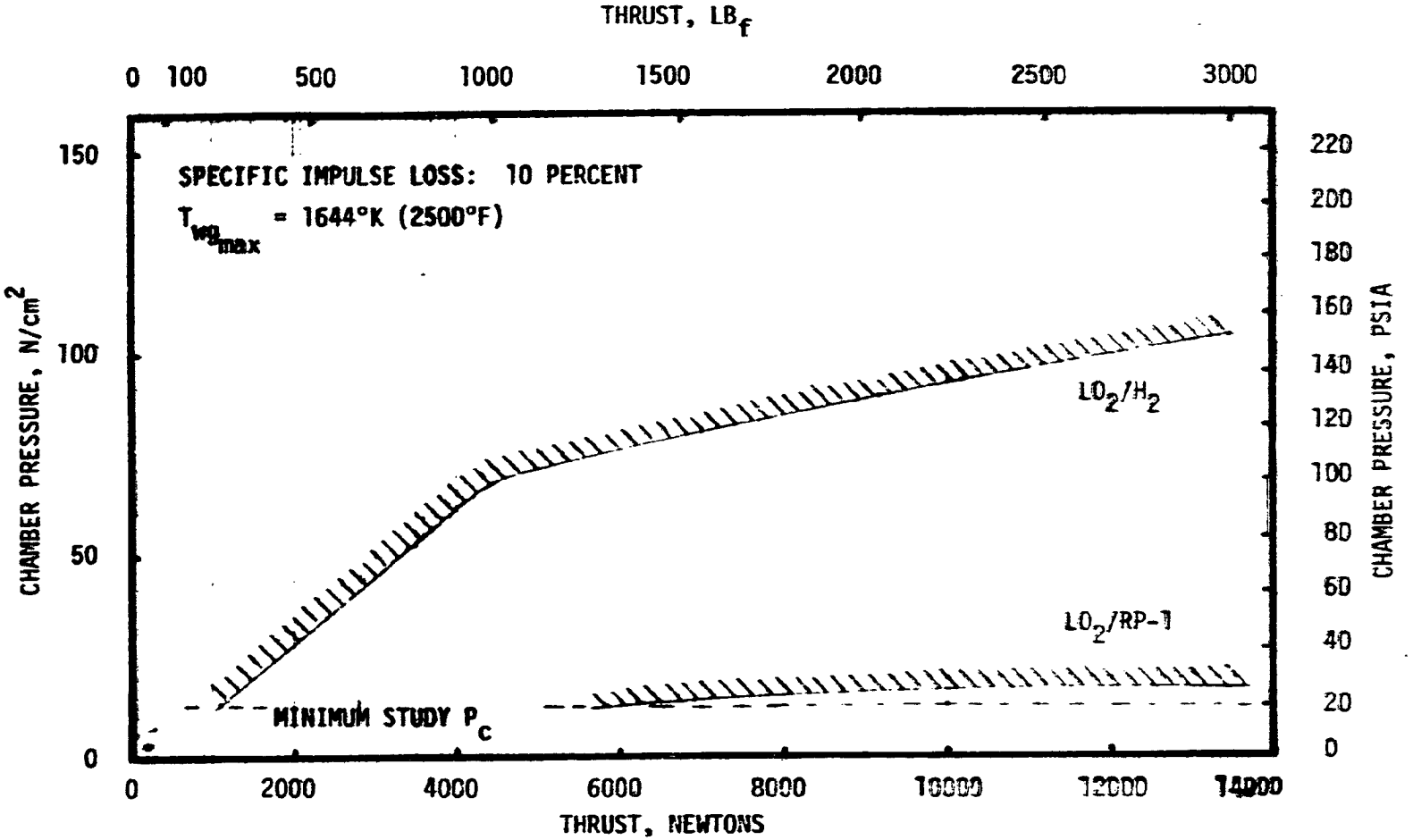

Figure 43 . Film-cooled Thrust Chamber Cooling Limits for LO_2/H_2 and LO_2/RP-1 (1644°K (2500°F) Maximum Wall Temperature)

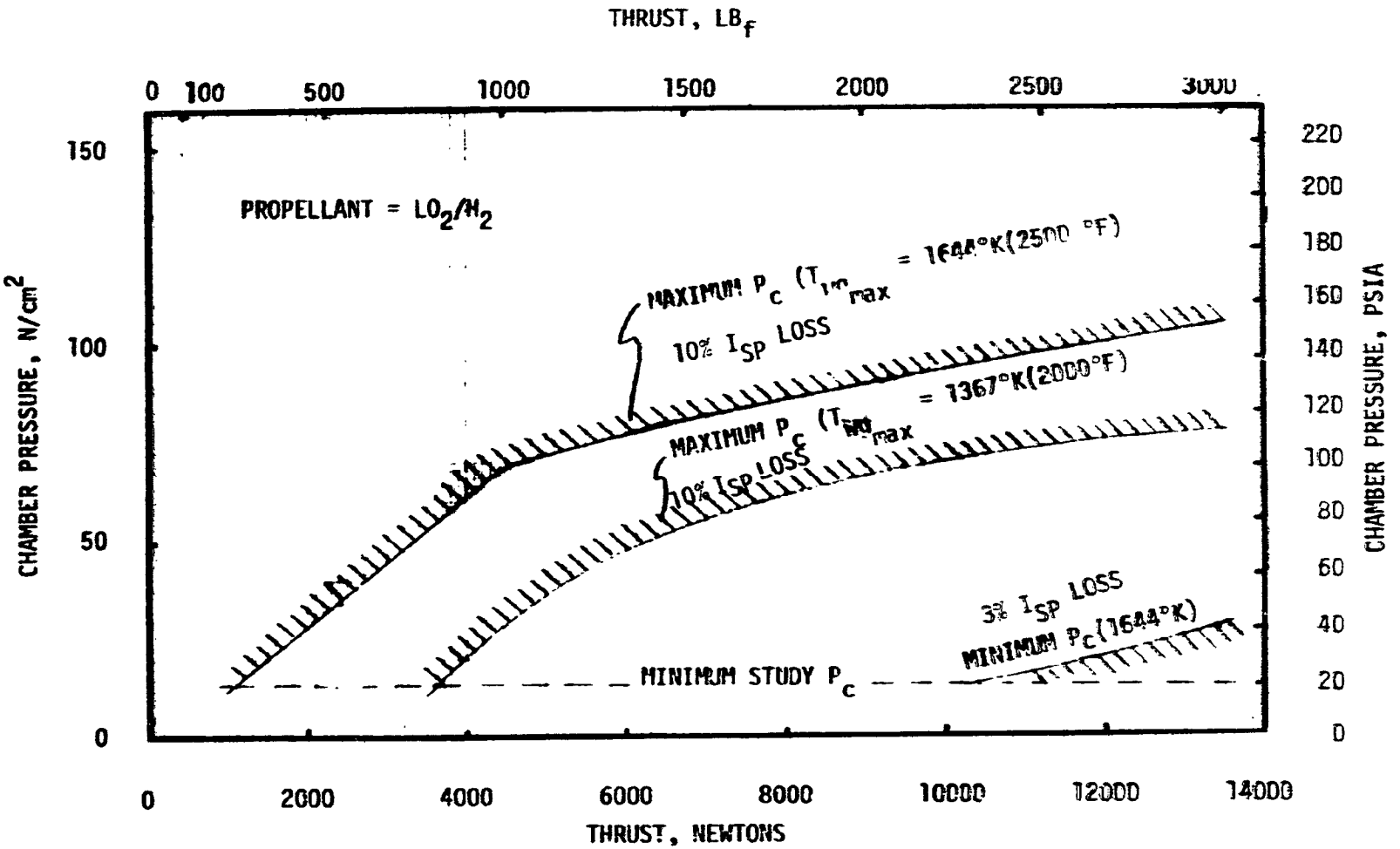

Figure 44 . LO_2/H_2 Film-cooled Thrust Chamber Cooling Limits

1. Increasing the maximum coolant (gas) Mach number from 0.3 to 0.5
2. Increasing the maximum allowable RP-1 coking temperature limit from 561.1 K (550 F) to 644 K (700 F)
3. Adding a carbon layer maximum allowable temperature limit of 3311 K (5500 F) or other physical thermal barrier

The first two changes are increases from conservative values to the upper bounds of feasibility. The third limit was added for designs permitting the added benefit of a gas-side carbon layer. Back calculations from available test data have indicated carbon layer temperatures close to this value.

The physical thermal barriers were selected for each propellant based on previous study analyses and experimental results (Table 5). Physical thermal barriers were chosen over fluid thermal barriers since fluid barriers can result in significant cooling performance losses, and physical barriers do not incur any performance penalty. For both LO_2/CH_4 and LO_2/H_2, a gas-side ceramic coating was added to the regenerative/radiation cooling of these propellants. Experimental results from LO_2/RP-1 rocket engine programs such as the F-1 and Atlas showed the existence of a hot gas-side carbon layer which reduced the local heat flux and heat input to the coolant. In contrast, thermal data from recent LO_2/RP-1 thrust chamber tests over a thrust range from approximately 44482 N (10,000 lbf) to 88964 N (20,000 lbf) and a chamber pressure range from 689.5 N/cm^2 (1000 psia) gave no evidence of carbon deposition creating a thermal barrier on the chamber wall (Ref. 4). In the extended cooling analysis of the LO_2/RP-1 low-thrust chambers, it was assumed that a carbon layer will exist in accordance with the equation in Table 5. Should this not be the case, a gas-side ceramic coating similar to that assumed for the LO_2/CH_4 and LO_2/H_2 chambers could be applied.

TABLE 5 . PHYSICAL THERMAL BARRIERS

PROPELLANTS	BARRIER
LO_2/RP-1	CARBON LAYER $\left[x/k = e^{(9.0-0.51G} \right]$
LO_2/CH_4	CERAMIC COATING
LO_2/H_4	CERAMIC COATING

With LO_2/RP-1 thrust chambers, the extended regenerative/radiation-cooling analysis for thrust levels of 4448.2 N (1000 lbf) to 13345 N (3000 lbf) resulted in a maximum chamber pressure of 344.7 N/cm^2 (500 psia) with the current LO_2/RP-1 carbon layer resistance relationship of $x/k=e^{(9-0.51G)}$. The parameter G is the local hot-gas mass velocity. The resulting constant chamber pressure cooling limit (Fig. 45) can be explained by this relationship and conventional heat flux trends. As thrust is increased, the heat flux level decreases slightly (hydraulic diameter influence) and, since the hot-gas mass flow increases (G) with thrust, the carbon layer thickness decreases. Therefore, these two influences tend to cancel each other and result in an essentially constant maximum regenerative/radiation-cooling chamber pressure for this thrust range. The maximum allowable carbon layer temperature limited both of these designs.

Below 4448.2 N (1000 lbf) thrust, the RP-1 coolant bulk temperature increased in the nozzle section to a value which created a coking problem. Therefore, the maximum coolable chamber pressure decreases as thrust decreases (Fig. 45). The minimum chamber was set by the RP-1 critical pressure.

The results of the detailed LO_2/RP-1 thrust chamber cooling analysis are presented in Fig. 46 through 49. The combustor and nozzle heat inputs (Fig. 46 and 48) decreased with increase in chamber pressure and decrease in thrust. The coolant pressure drop variation with thrust and chamber pressure for the LO_2/RP-1 regenerative/radiation-cooled combustor and nozzle are shown in Fig. 47 and 49. These heat input and coolant pressure drop data were input to the engine cycle balance computer program to perform the LO_2/RP-1 engine balances.

The extended cooling capability evaluation of the LO_2/CH_4 regenerative/radiation-cooled thrust chambers with a ZrO_2 ceramic coating (t = 0.0127 cm or 0.005 inch) resulted in higher maximum chamber pressures over the entire thrust range. As shown in Fig. 50, the maximum study chamber pressure can be cooled for thrust levels down to 4448.2 N (1000 lbf), and cooling is feasible at the low thrust level of 444.8 N (100 lbf).

In performing the engine cycle balances of LO_2/CH_4 engines, supercritical thrust chamber coolant discharge pressures were obtained for subcritical chamber pressures. This trend is due to the turbine pressure ratio requirements of the engine cycle. In fact, for the direct expander cycle, a chamber pressure approximately a factor of 2 below the coolant critical pressure was achieved. Therefore, the minimum chamber pressure limits were lowered.

The extended cooling capability evaluation of the LO_2/H_2 regenerative/radiation-cooled thrust chamber with a ZrO_2 ceramic coating (Fig. 51) achieved higher maximum chamber pressures for the 444.8 N (100 lbf) to 4448.2 N (1000 lbf) thrust range and a lower minimum chamber pressure. The lower minimum chamber pressure limit was established in the same manner as for the LO_2/CH_4 thrust chambers, i.e., by keeping the coolant pressure at the jacket discharge above the critical pressure of hydrogen.

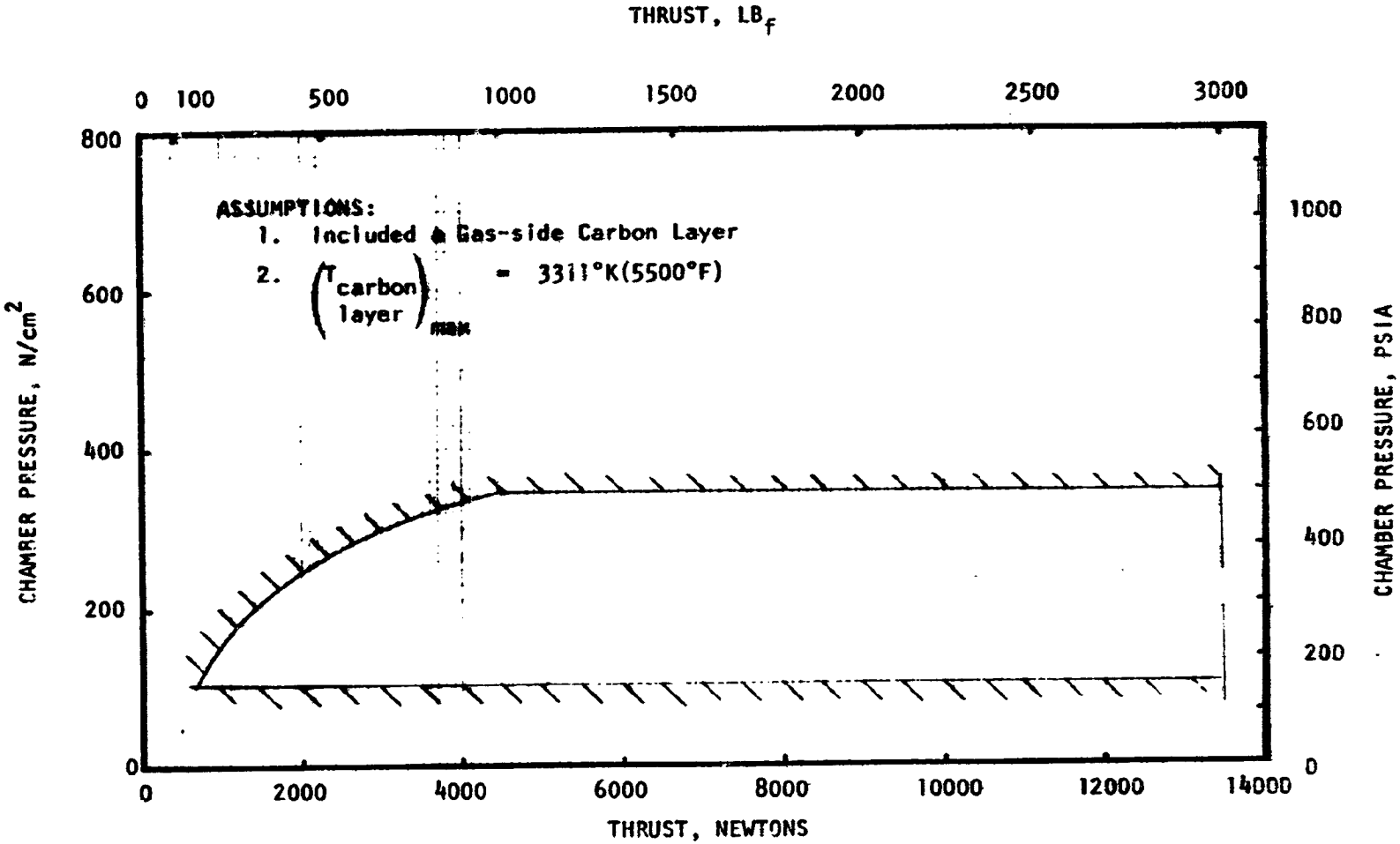

Figure 45. LO_2/RP-1 Regenerative-cooled Thrust Chamber Cooling Limits

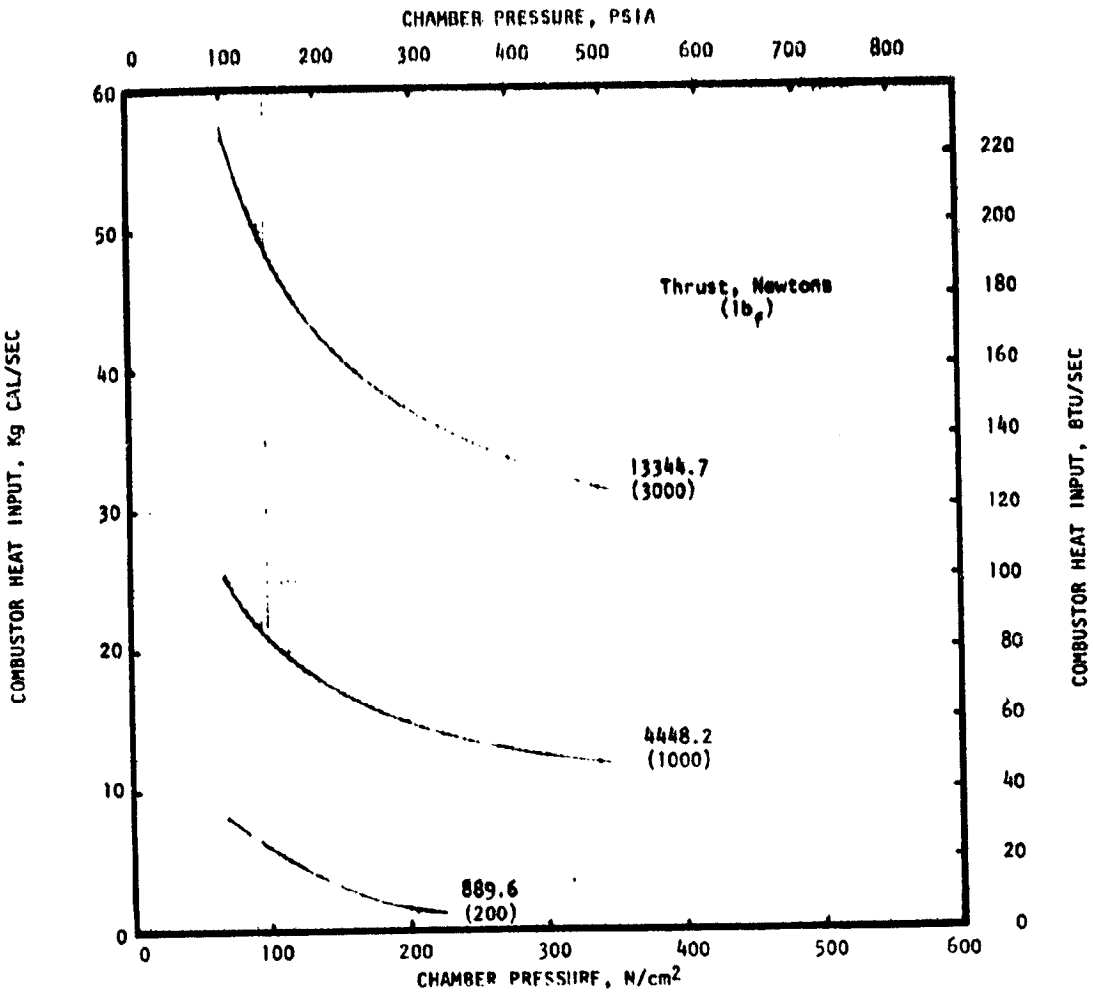

Figure 46 . LO_2/RP-1 Combustor Heat Input
(with Gas-side Carbon Layer)

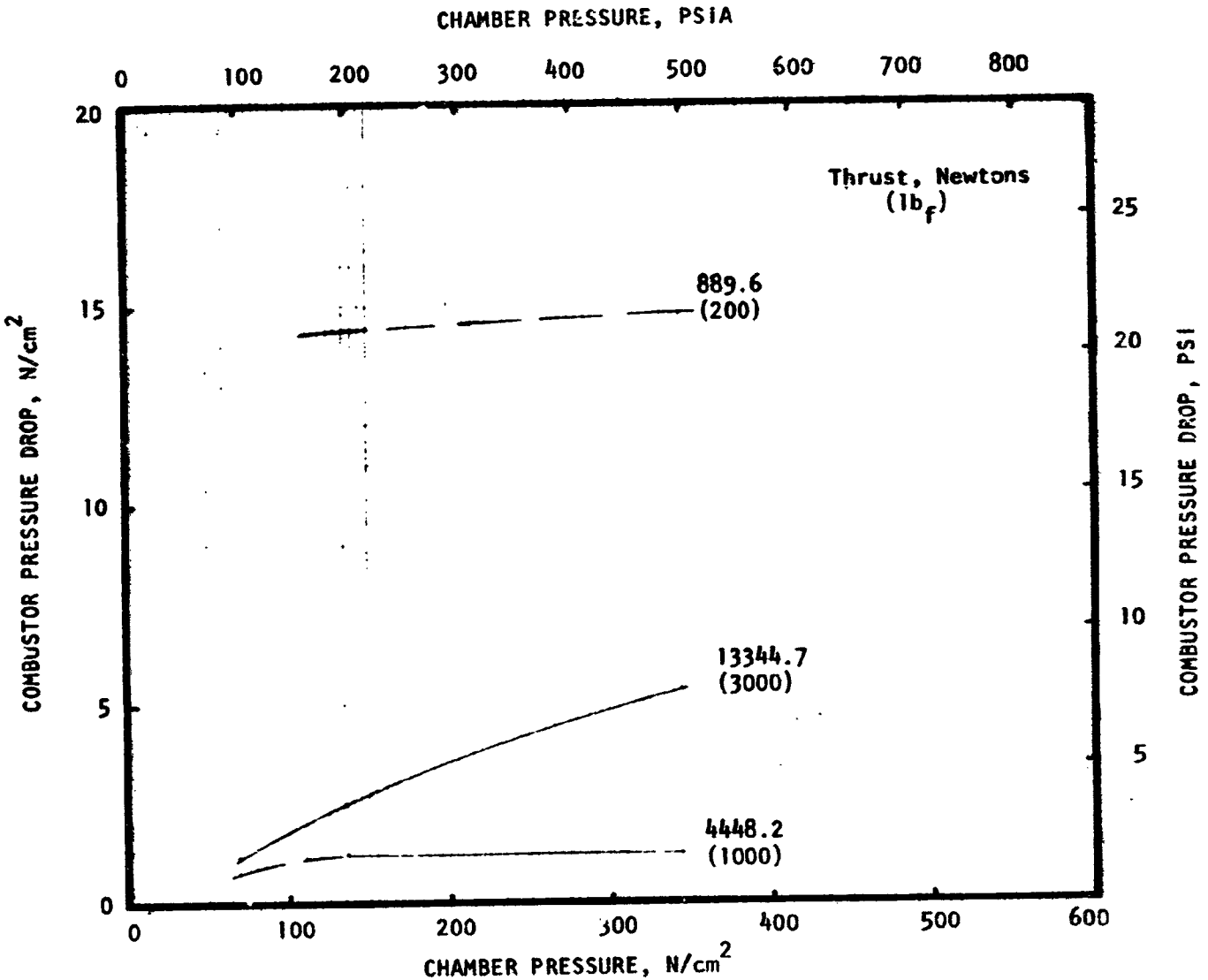

Figure 47 . LO_2/RP-1 Combustor Coolant Pressure Drop
(with Gas-side Carbon Layer)

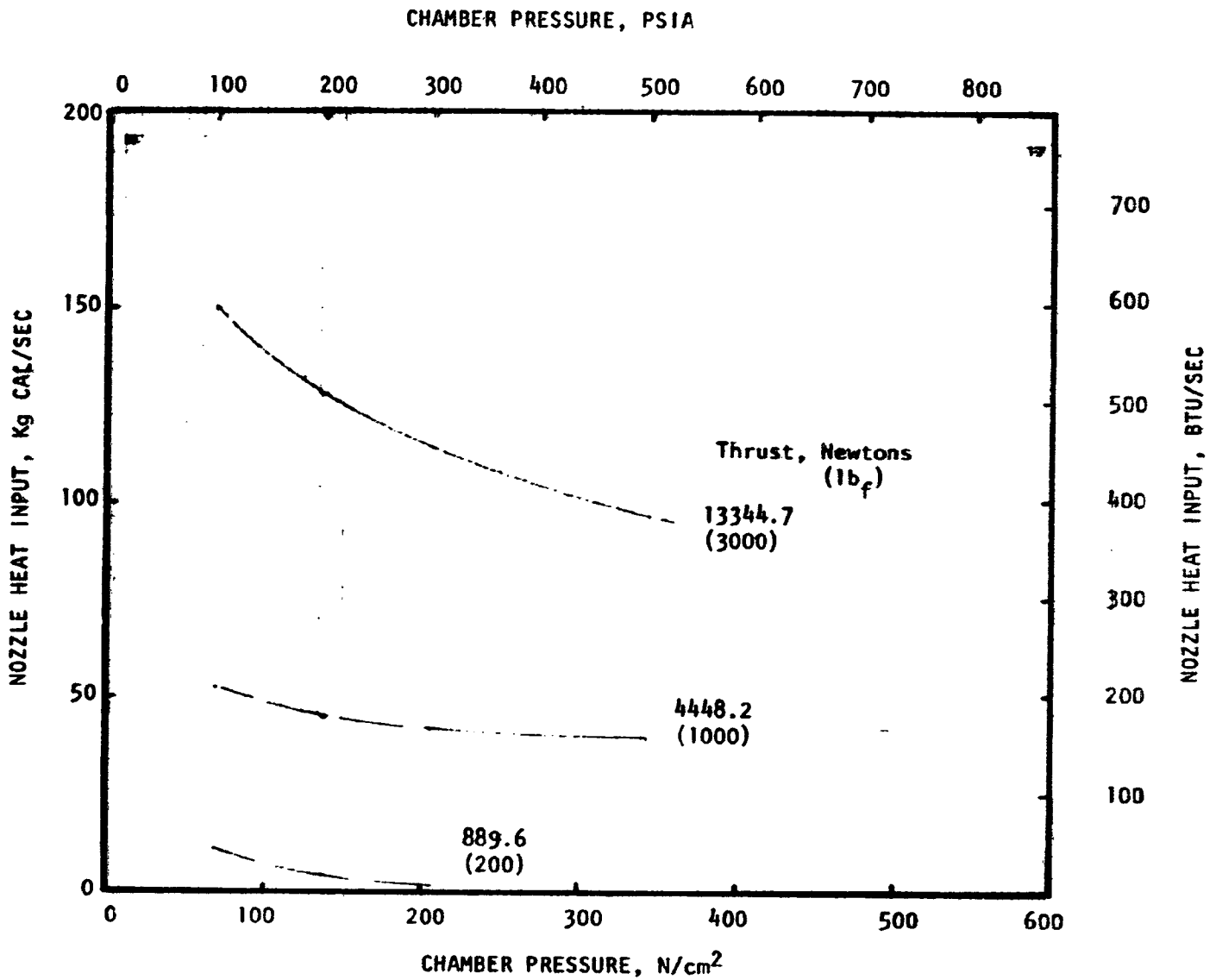

Figure 48 . LO_2/RP-1 Nozzle Heat INput
(with Gas-side Carbon Layer)

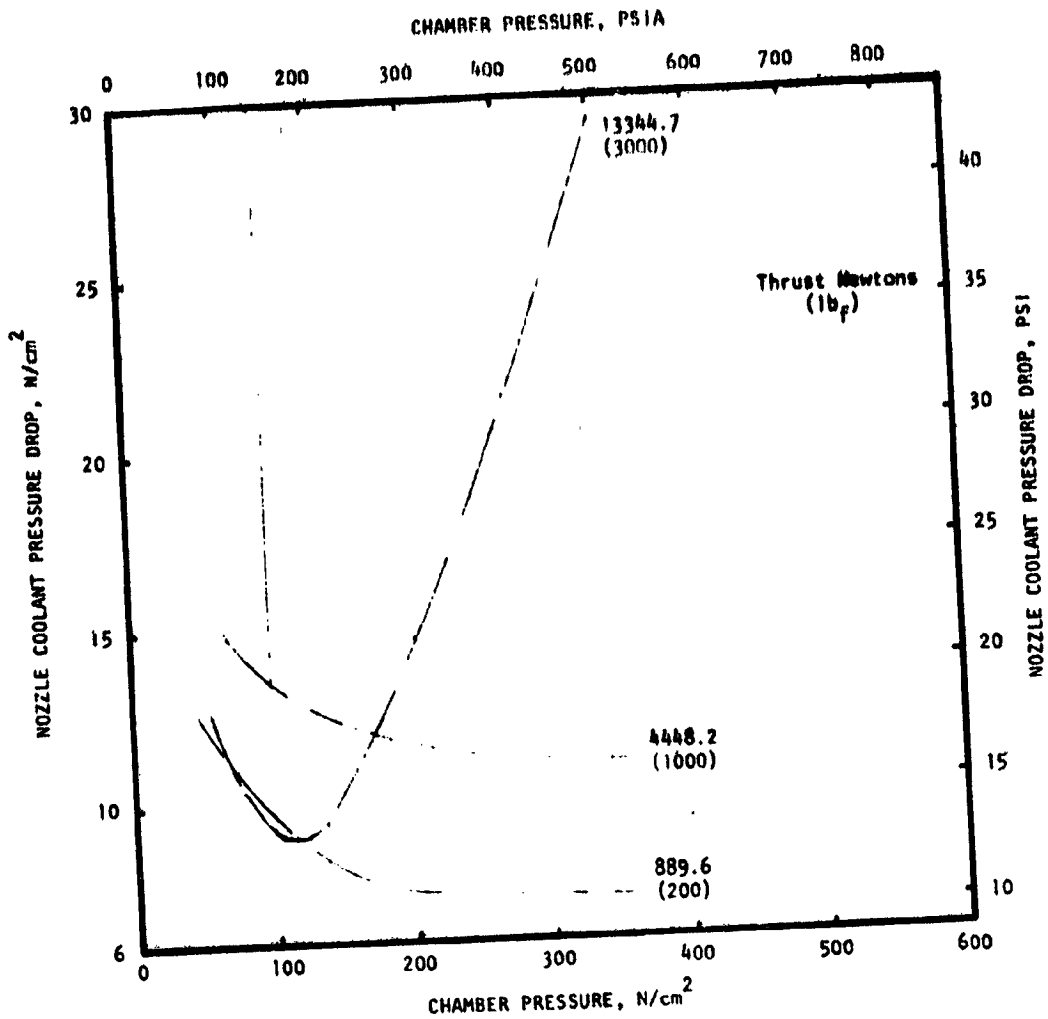

Figure 49 . LO_2/RP-1 Nozzle Coolant Pressure Drop (with Gas-side Carbon Layer)

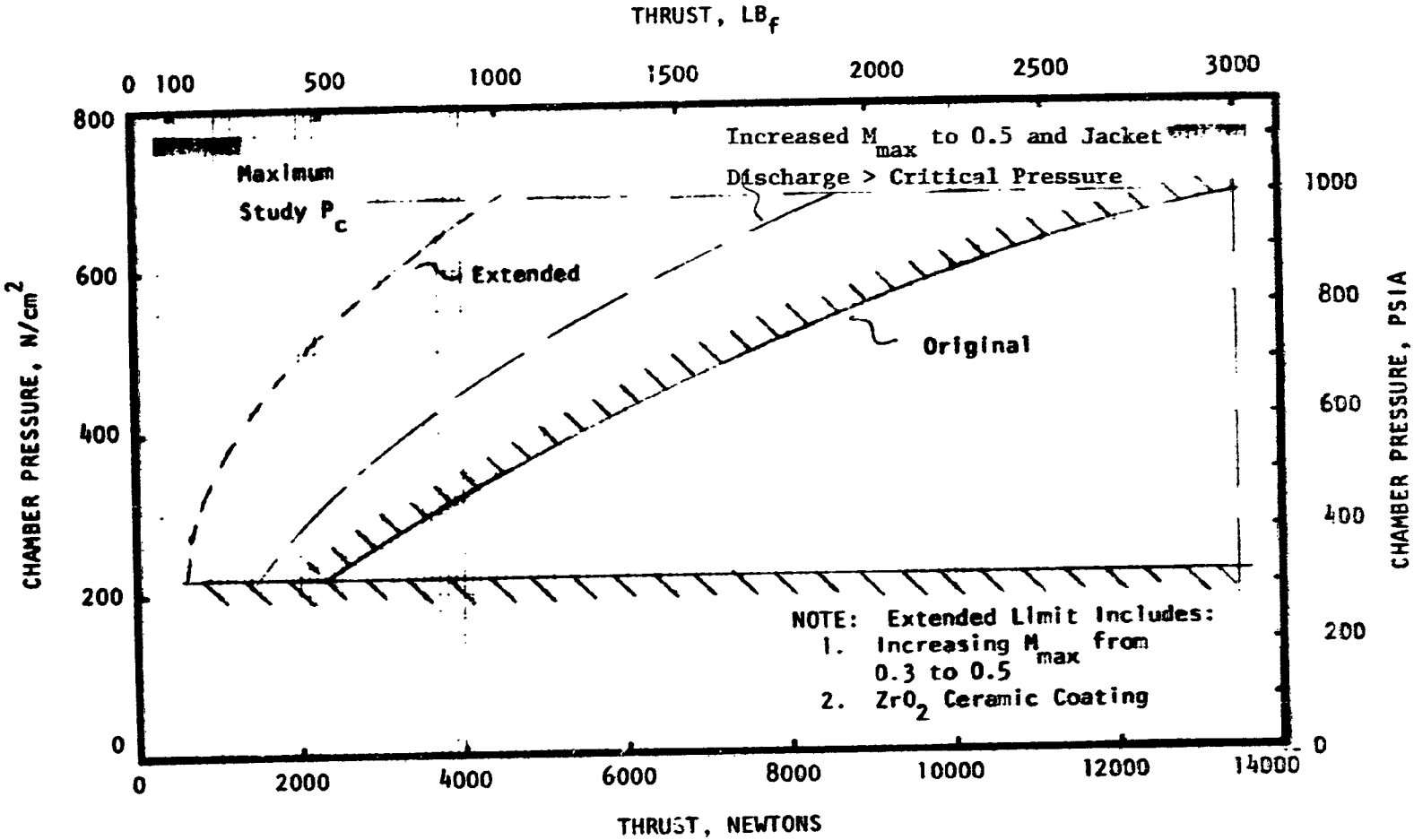

Figure 50 . LO_2/CH_4 Regenerative-cooled Thrust Chamber Cooling Limits -- Original and Extended

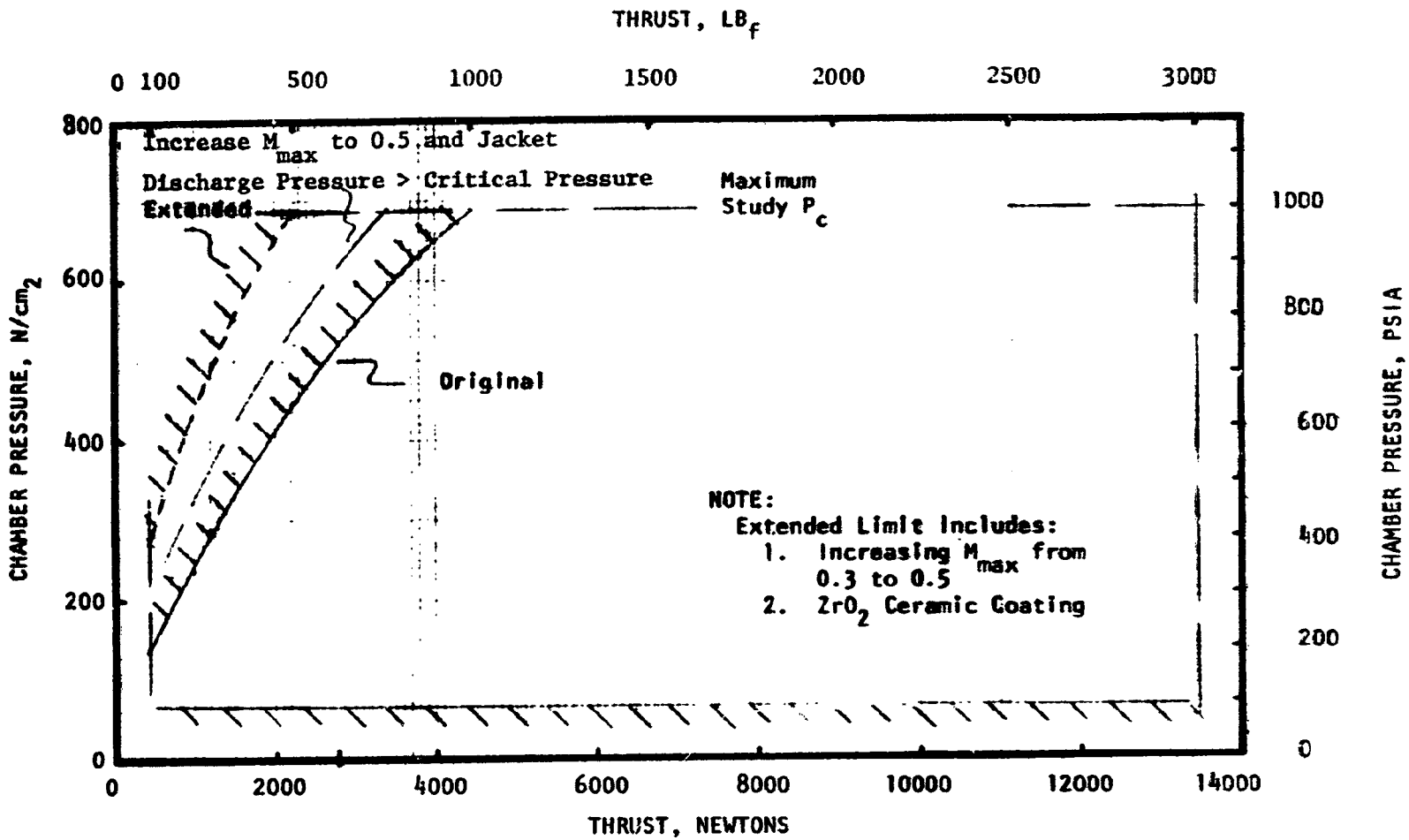

Figure 51 . LO_2/H_2 Regenerative-cooled Thrust Chamber Cooling Limits -- Original and Extended

ENGINE SYSTEM CONCEPTUAL AND PARAMETRIC ANALYSIS

In the engine system analysis, the engine cycle/configuration matrix was first defined by incorporating the thrust chamber cooling analysis for each of the three propellants. The engine schematics of the candidate engine cycle/configuration were established to aid in the cycle analysis and the engine complexity rating determination. Analyses were conducted to determine achievable and/or optimum chamber pressures for each of the candidate systems. Parametric engine performance and preliminary engine weights were generated. The candidate engine cycles were screened and evaluated and concluded in the recommendation of one LO_2/H_2 and one LO_2/ hydrocarbon fuel engine cycle/configuration for preliminary engine design.

Engine Configuration Matrix

Table 6 defines the engine systems on which parametric analyses were conducted. In view of the significant performance losses and limited design range associated with film cooling, it was assumed that all systems would be regeneratively cooled. Simplified schematics of the candidate systems are shown in Fig. 52. These included both pump and pressure-fed engine and the hot-gas turbine/pump-fed cycles such as the expander, gas generator, and staged-combustion cycles with engine-mounted pumps. Variations of these pump-fed engines include locating the pumps at the tank. Also with tank-mounted pumps, the pumps can be driven by electric motors that are supplied electric power through a turboalternator or fuel cells. An additional option is the incorporation of an accumulator that permits the design of a larger capacity pump (higher pump efficiency), which would operate intermittently during the engine firing. A variation of the conventional pressure-fed engine utilizes two, small, parallel, pressurized feed tanks to achieve a potential weight savings. Instead of pressurizing the larger main tank, two small tanks are alternately pressurized, filled, and used during the firing.

TABLE 6. ENGINE CONFIGURATION MATRIX

CONFIGURATION	PROPELLANT	COOLING METHOD
Direct Expander	H_2/O_2	Regenerative
Direct Expander	CH_4/O_2	
Turboalternator Expander	H_2/O_2	
Turboalternator Exapnder	CH_4/O_2	
Fuel Cell Powered	H_2/O_2	
Fuel Cell Powered	CH_4/O_2	
TAnk Mounted Pump Expander	H_2/O_2	
Tank Mounted Pump Expander	CH_4/O_2	
Turboalt. Expander with Accumulator	H_2/O_2	
Turboalt. Expander with Accumulator	CH_4/O_2	
Staged Combustion	H_2/O_2	
Staged Combustion	CH_4/O_2	
Gas Generator	H_2/O_2	
Gas Generator	CH_4/O_2	
Gas Generator	RP-1/O	
Pressure Fed - Conventional	H_2/O_2	
Parallel Pressurized Tank	H_2/O_2	

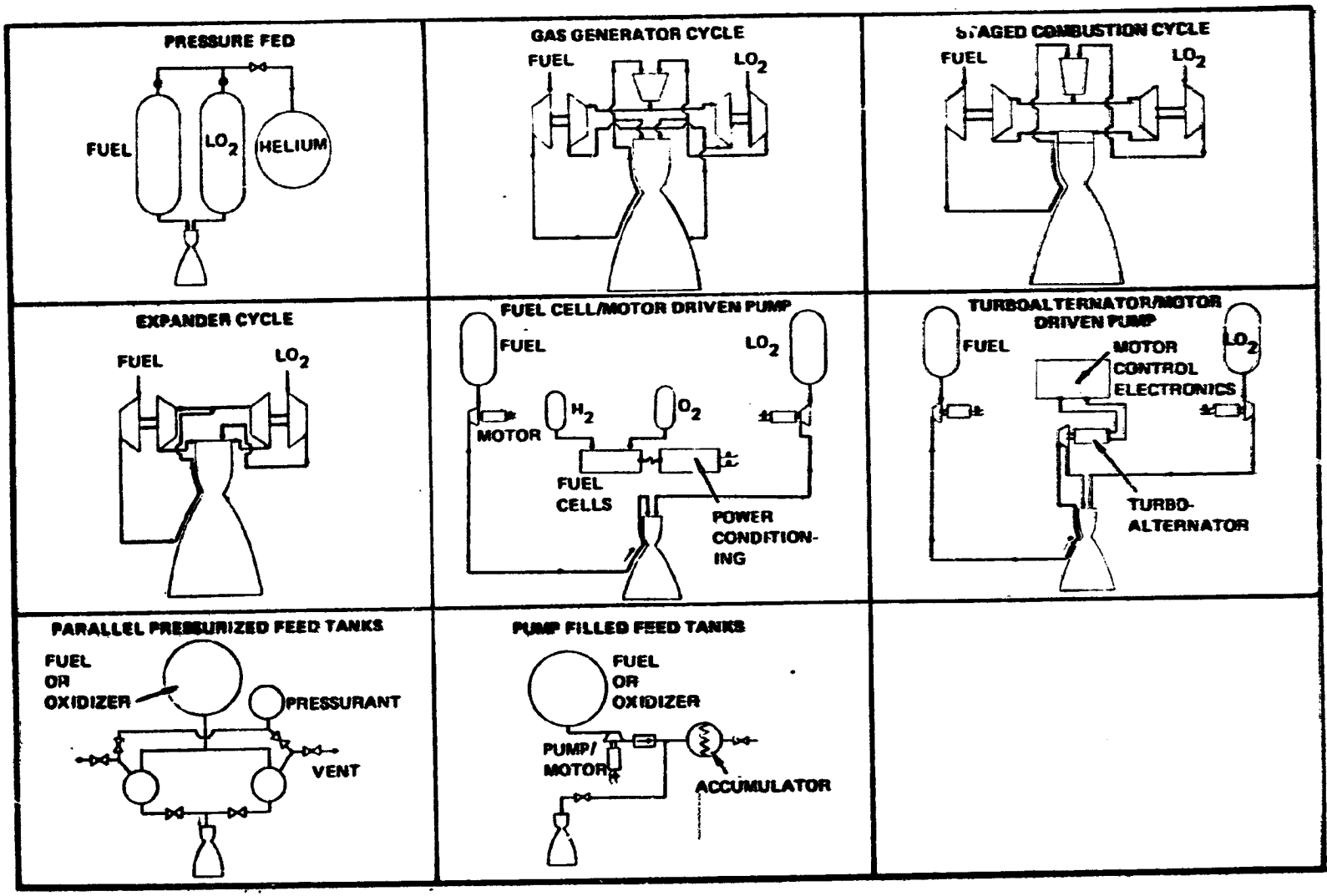

FIGURE 52. ENGINE SYSTEM CONCEPTS TO BE STUDIED

(O_2/H_2, O_2/RP-1, O_2/CH_4 Propellants)

Pump and Pump Drive Analysis

Pump Type. An evaluation of positive displacement pumps (vane, gear, and multilobe) and centrifugal (full and partial emission) pumps was conducted to define the pump type to be used in the engine cycle evaluation. Using a minimum pump clearance of 0.001 inch for the positive-displacement pumps, the partial-emission centrifugal pumps achieved higher pump efficiencies than the positive-displacement pumps at the low flowrates. Therefore, the centrifugal pumps were chosen as the pump type to be used in the engine cycle/configuration. LO_2/H_2 and LO_2/CH_4 engines utilized a three-stage fuel pump and a single stage oxidizer pump. LO_2/RP-1 engines utilized single-stage fuel and oxidizer pumps.

Pump and Turbine Limits. The geometric, hydraulic, and speed limits assumed for the centrifugal pumps and axial turbines in the engine cycle evaluation are presented in Tables 7 and 8, respectively. These limits were imposed on the pump-fed engine configurations evaluated.

In addition to the full-emission centrifugal pump, design relationships for partial-emission centrifugal pumps were incorporated into the engine cycle balance computer program. In the engine cycle balance analysis as the engine thrust was decreased, the full-emission centrifugal pump impeller tip width became less than the assumed minimum of 0.076 cm (0.03 inch) shown in Table 7. When the tip width became less that this minimum, the pump emission was decreased until the minimum tip width value was satisfied.

Electrical Component Data. For engine cycle/configurations incorporating electric-motor-driven pumps and turbine-drive alternators, data were compiled on current component capabilities and component weights as part of a company-funded effort. Parametric data on alternating-current (a-c) generators or alternators are shown in Fig. 53 f[illegible] wound-rotor and permanent magnet (PM) alternators. The maximum speed and corresponding weight as a function of the output power are presented. The PM alternators were typically lighter in weight. Similar data on electric induction motors are shown in Fig. 54. The efficiency of the alternator and the motor were individually assumed to be 85%, which was a representative value.

TABLE 7. ASSUMED CENTRIFUGAL PUMP LIMITS AND GUIDELINES

PARAMETER	FUEL	OXIDIZER
Minimum Limits		
Impeller Tip Width, cm (in)	0.076 (0.03)	0.076 (0.03)
Inducer Diameter, cm (in)	1.143 (0.45)	1.143 (0.45)
Impeller Tip Diameter, cm (in)	1.778 (0.70)	1.778 (0.70)
Head Coefficient	0.1	
Flow Coefficient	0.06	
Bearing Size, mm	8	8
Maximum Limits		
Bearing DN	1.9×10^6 (H_2) 1.5×10^6 (CH_4)	1.5×10^6
Inlet/Outlet Diameter Ratio	0.8	0.8
Impeller Tip Speed, m/sec (ft/sec)	609.6 (2000)	365.76 (1200)
Inducer Tip Speed, m/sec (ft/sec)	457.2 (1500)	304.8 (1000)
Impeller Stage Specific Speed	2000	2000
Head Coefficient	0.5	
Suction Specific Speed	61000 (H_2) 51000 (CH_4)	51000
NPSH, m(ft)	4.57m or 15 ft (H_2) 1.68m or 5.5 ft (CH_4) 13.72m or 45 ft (RP-1)	0.61m or 2 ft

TABLE 8. ASSUMED TURBINE LIMITS AND GUIDELINES

PARAMETER	FUEL OR OXIDIZER
Minimum Limits	
Turbine Admission	0.10
Turbine Pressure Ratio	1.16
Turbine Blade Height, cm (in)	0.635 (0.25)
Turbine Pitch Diameter, cm (in)	5.08 (2.0)
Turbine Blade Hub/Tip Ratio	0.6
Maximum Limits	
Turbine Admission	1.0
Turbine Pressure Ratio	4.0
Turbine Tip Speed, m/sec (ft/sec)	518.16 (1700)
Turbine AN^2 $cm^2(RPM)^2$ or in^2 $(RPM)^2$	2.742×10^{11} (4.25×10^{10})
Turbine Blade Hub/Tip Ratio	0.9
Turbine Inlet Temperature, °K (°R)	1033 (1860)

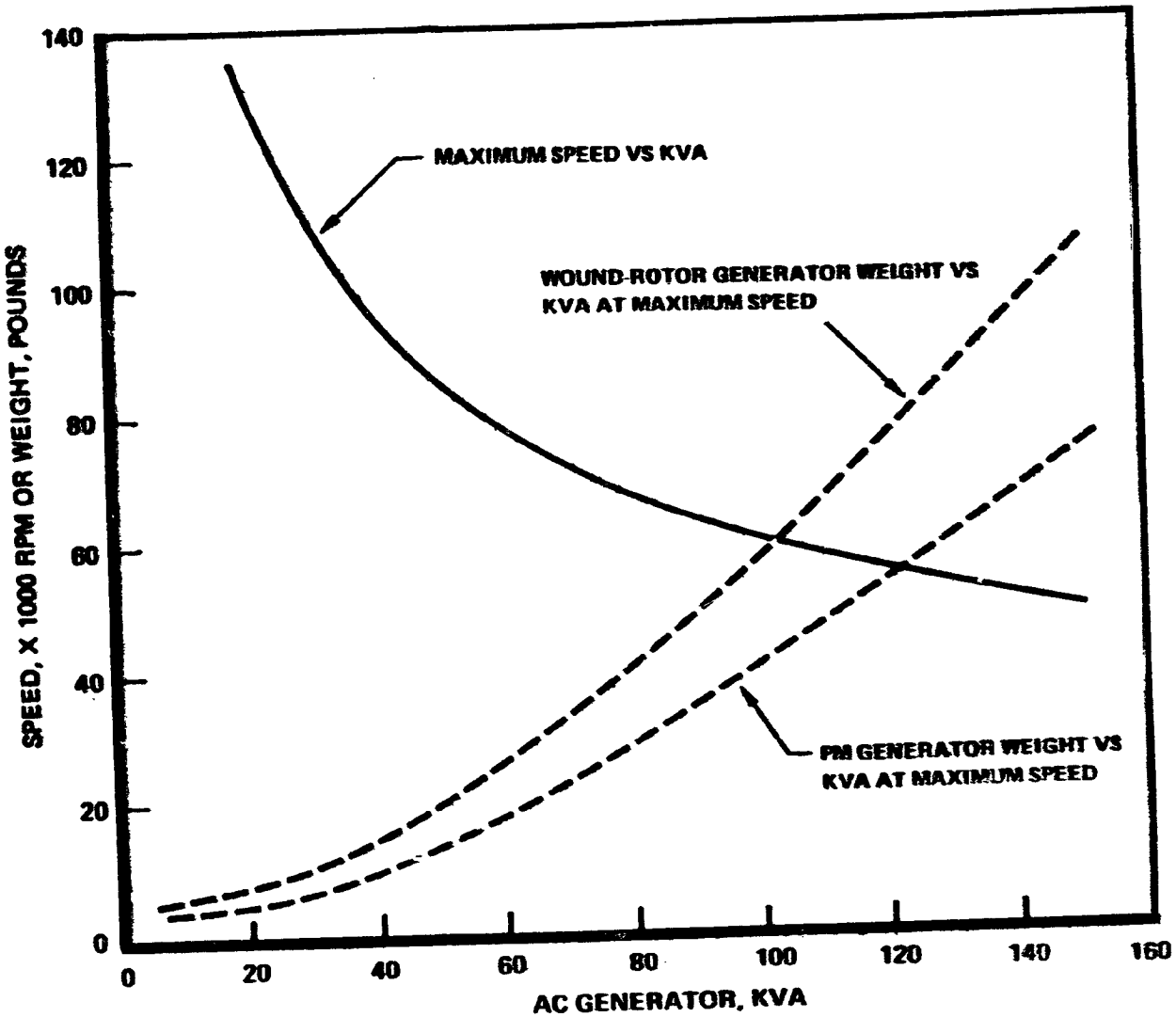

Figure 53 . AC Generator Weight and Maximum Speed Variation with Output Power

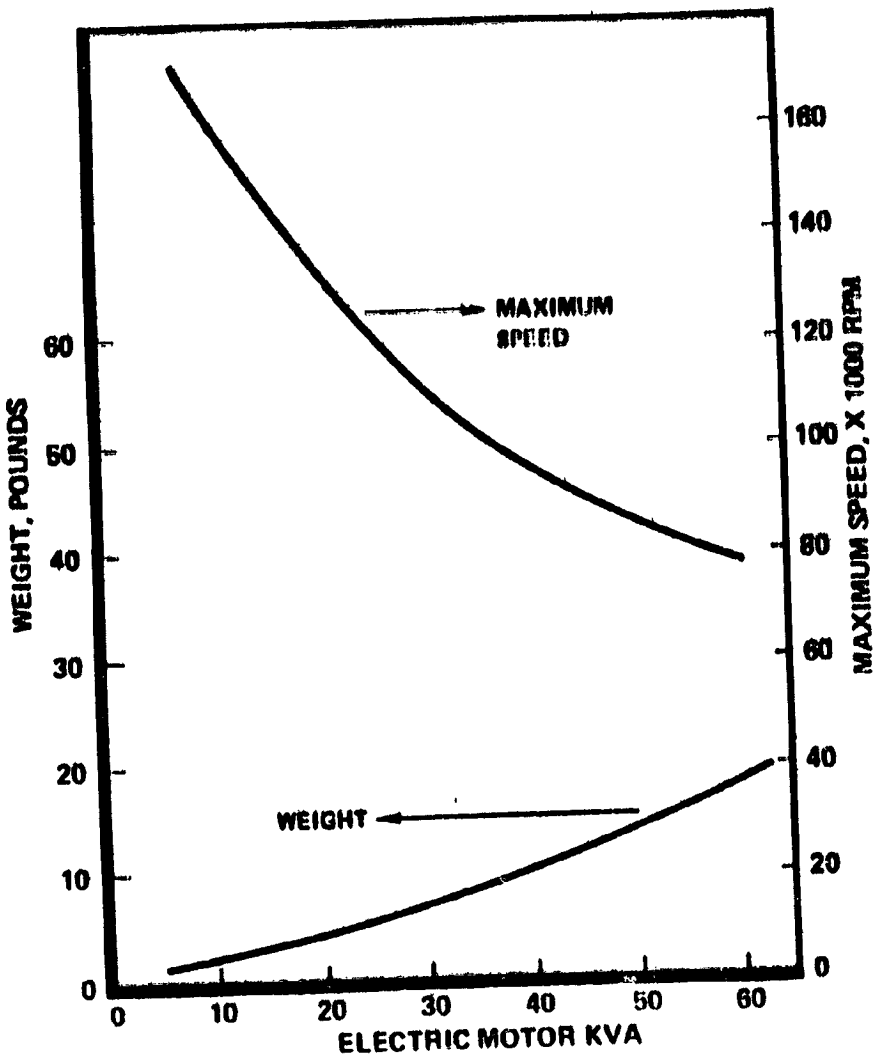

Figure 54 . Induction Motor Weight and Maximum Speed Variation with Power

For the turboalternator cycle the a-c alternator speed can be adjusted to change the electric motor speeds, but the relationship between the alternator and motor speeds is fixed by the ratio of poles in the motor and alternator:

$$\text{Motor Speed, rpm} = \frac{\text{(No. Poles in Alternator)}}{\text{(No. Poles in Motor)}} \times \text{(Alternator Speed)} \times (1\text{-SLIP}) \qquad (10)$$

Typically, the slip is approximately 0.04 (4%). The PM alternator is always excited at the same level by magnets and produces a voltage directly proportionate to speed. The induction motor is a volts/rps device, which should be supplied with a voltage that is proportional to the speed so the alternator and motor can be controlled without sophisticated electronic controls.

Fuel Cell Data. For the O_2/H_2 fuel cell-powered cycle engines, the variation of fuel cell system weight with required power output was determined and formed an input to the engine balance computer program. The currently available data (Ref. 5) indicated that the weight of an O_2/H_2 fuel cell is substantial. United Technology has been developing and testing a fuel cell. It weighed about 9.07 kg/kW (20 lb/kW), although the supporting equipment weight per kW decreased as the fuel cell becomes larger. The General Electric fuel cell (Fig. 55) currently under development is lighter in weight and was the fuel cell assumed for this analysis. As noted in Fig. 55 , the fuel-cell system weight was a strong function of the power output and therefore the required pump horsepower should be minimized to reduce fuel-cell system weight.

A fuel-cell power conditioning (converter) efficiency of 90-percent was assumed in this evaluation.

Tank-mounted Pump-fed Directly-powered Pumps. In the evaluation of the tank mounted pump-fed engines with directly-powered pumps, the heat loss through insulated heated fuel lines to and from the turbines as well as the added fluid pressure drops were determined. Line lengths for the tank-mounted configuration were determined from the NASA-LeRC specified tank configurations and are shown in Fig. 56.

The heat loss from the heated fuel lines to and from the turbine was computed for a range of fluid temperatures, line diameters, and insulation thickness. However, the total heat losses were found to be less than 0.1% of the total enthalpy and, therefore, were neglected in the analysis.

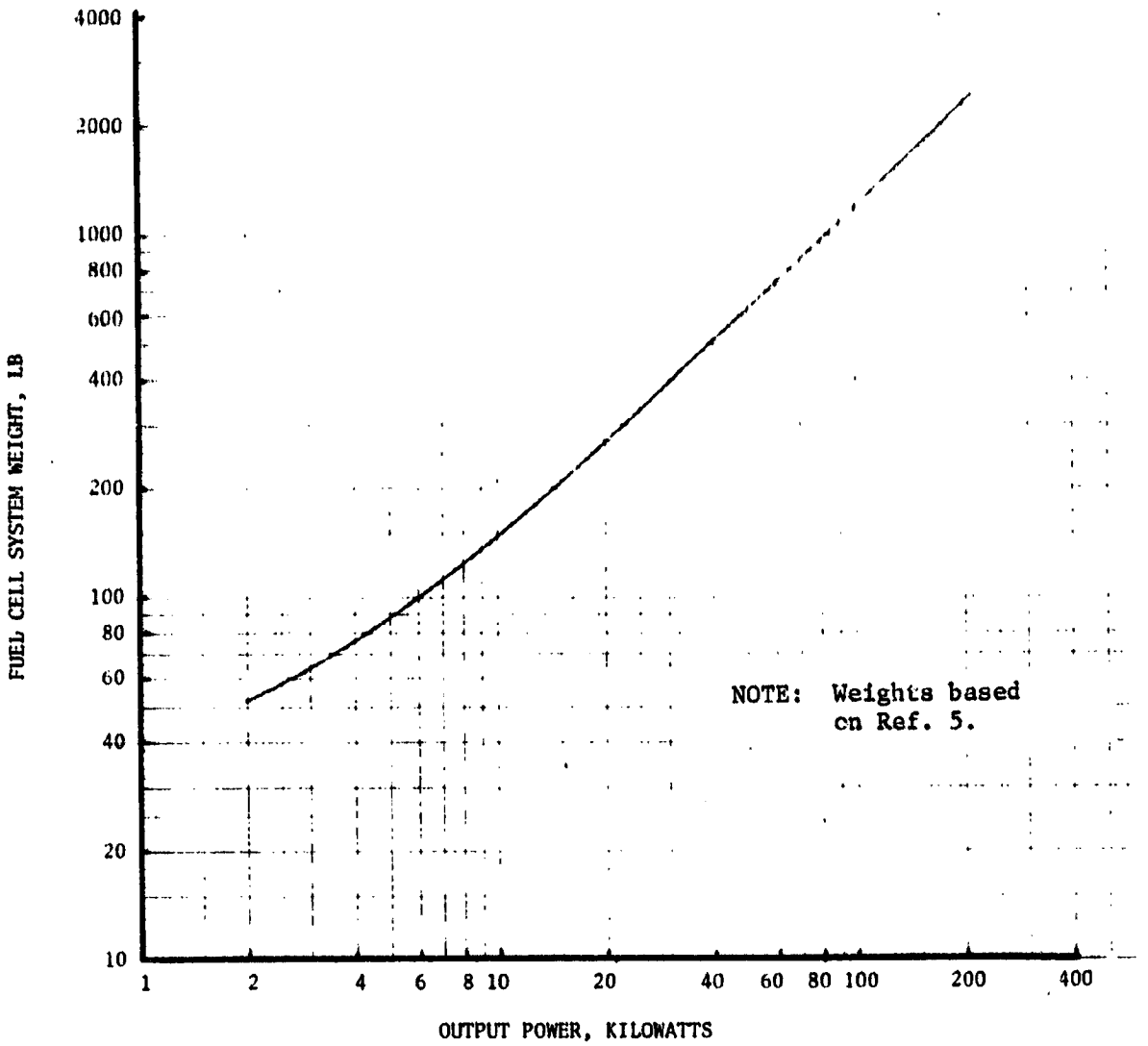

Figure 55 . Fuel Cell System Weight Variation with Output Power

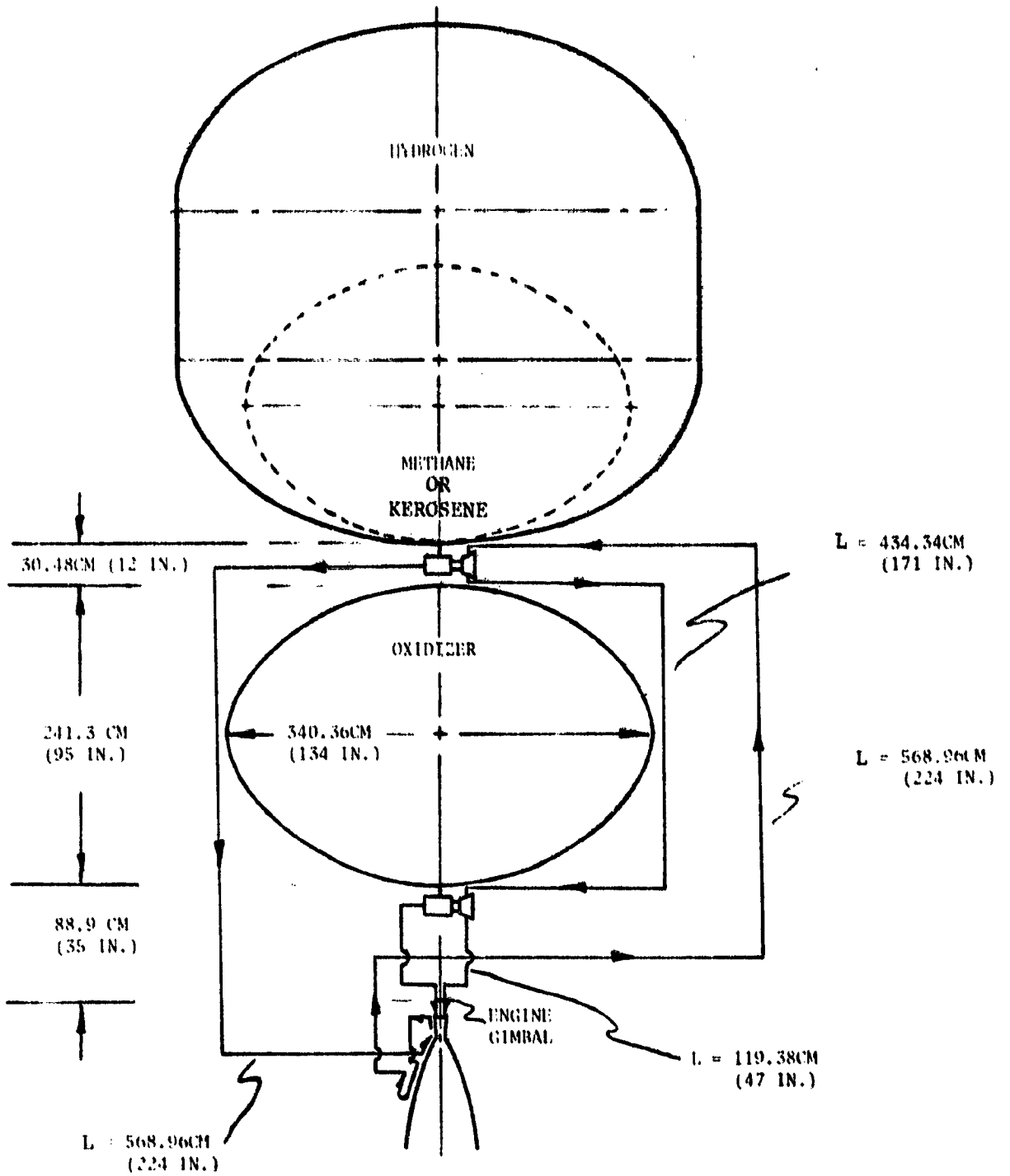

Figure 56 Propellant Line Configuration for Tank-Mounted Pump-Fed Directly Powered-Pumps

Engine Cycle/Configuration Parametrics

Engine Cycle/Configuration Schematics. Schematics of the candidate engine cycle/configurations are presented in Figs. 57 through 63. Major components, propellant valves, and number of functions required by the controller are shown as well as the engine/vehicle interface for both engine and tank-mounted pumps. Autogenous pressurization and boost pumps which are identified as optional on the schematics were not included in the analysis of the various systems.

Delivered Engine Performance. Based on past experimental data, the combustion efficiency for the LO_2/H_2 engines was expected to be 99.5% for chamber pressures of 344.7 N/cm^2 (500 psia) or greater and decrease to 99% at 13.79 N/cm^2 (20 psia). For the LO_2/CH_4 and LO_2/RP-1 engines, a combustion efficiency of 98% was expected to provide a realistic value for the thrust and chamber range of interest.

The thrust chamber performance losses included in the analysis were the nozzle geometric (divergence), reaction kinetic, and boundary layer losses. For regenerative-/radiation-cooled thrust chambers, the net enthalpy gained through thrust chamber cooling is included. For film-/radiation-cooled thrust chambers, the film cooling loss (10% maximum) is added.

Regenerative-/Radiation-Cooled Engines. Using the previously discussed trend of combustion efficiency and the parametric coolant heat input determined in the thrust chamber cooling analysis, parametric delivered thrust chamber performance data were generated for regenerative-/radiation-cooled LO_2/H_2 and LO_2/CH_4 engines with a nozzle area ratio of 400:1 (90% length). The resulting parametric data are presented in Figs. 64 through 66. For LO_2/H_2 (Fig. 64), the delivered thrust chamber specific impulse increases approximately 2.5% from 444.8 N (100 lbf) to 2224.1 N (500 lbf) thrust but increased less than 1% from 2224.1 N (500 lbf) to 1.33×10^4 N (3000 lbf) thrust. Similar trends occurred for the LO_2/CH_4 engines (Fig. 65). As expected, the LO_2/H_2 engines achieved significantly higher delivered specific impulse (approximately 28%) than the LO_2/CH_4 engines for the same thrust and chamber pressure. For both propellants, the specific impulse dropped rapidly below 206.8 N/cm^2 (300 psia) chamber pressure due to a decrease in theoretical specific impulse and an increase in kinetic and boundary layer losses.

For the gas generator engine cycle, a higher chamber pressure does not necessarily result in a higher delivered specific impulse. As chamber pressure increases, the pump required horsepower also increases and more gas generator flow is required to power the turbines. This gas generator flow, which is injected into the nozzle gas flow, has a significantly lower specific impulse than that of the primary thrust chamber flow. As the design chamber pressure increases, the primary thrust chamber delivered specific impulse increases due to the theoretical value increasing and the reaction kinetic and boundary layer losses decreasing with increase in chamber pressure. However, as more gas generator flow is required (higher chamber pressure), the overall engine delivered specific impulse will eventually decrease as the gas generator flow becomes a more significant part of the total flow.

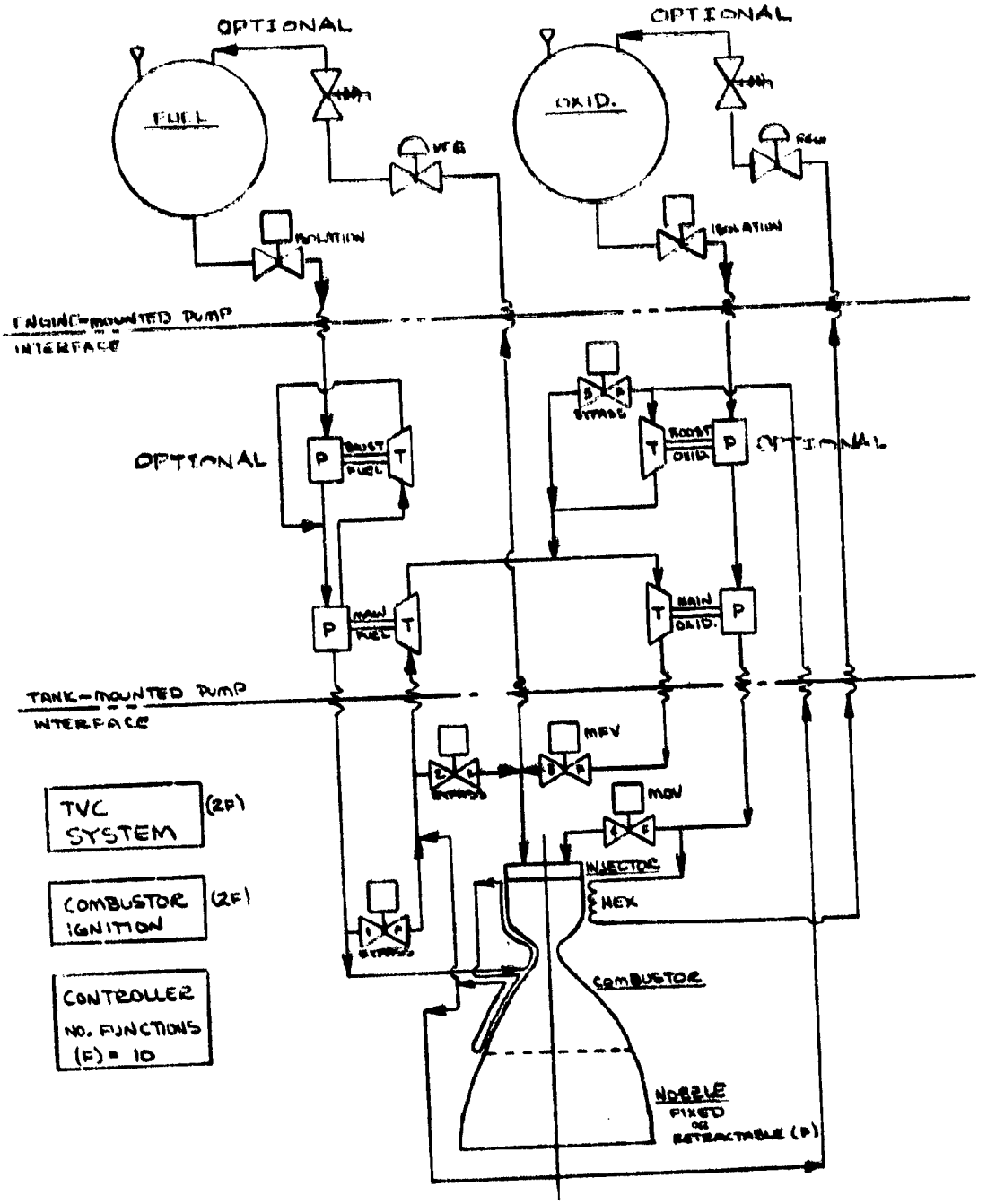

Figure 57 . Expander-Cycle Engine Schematic

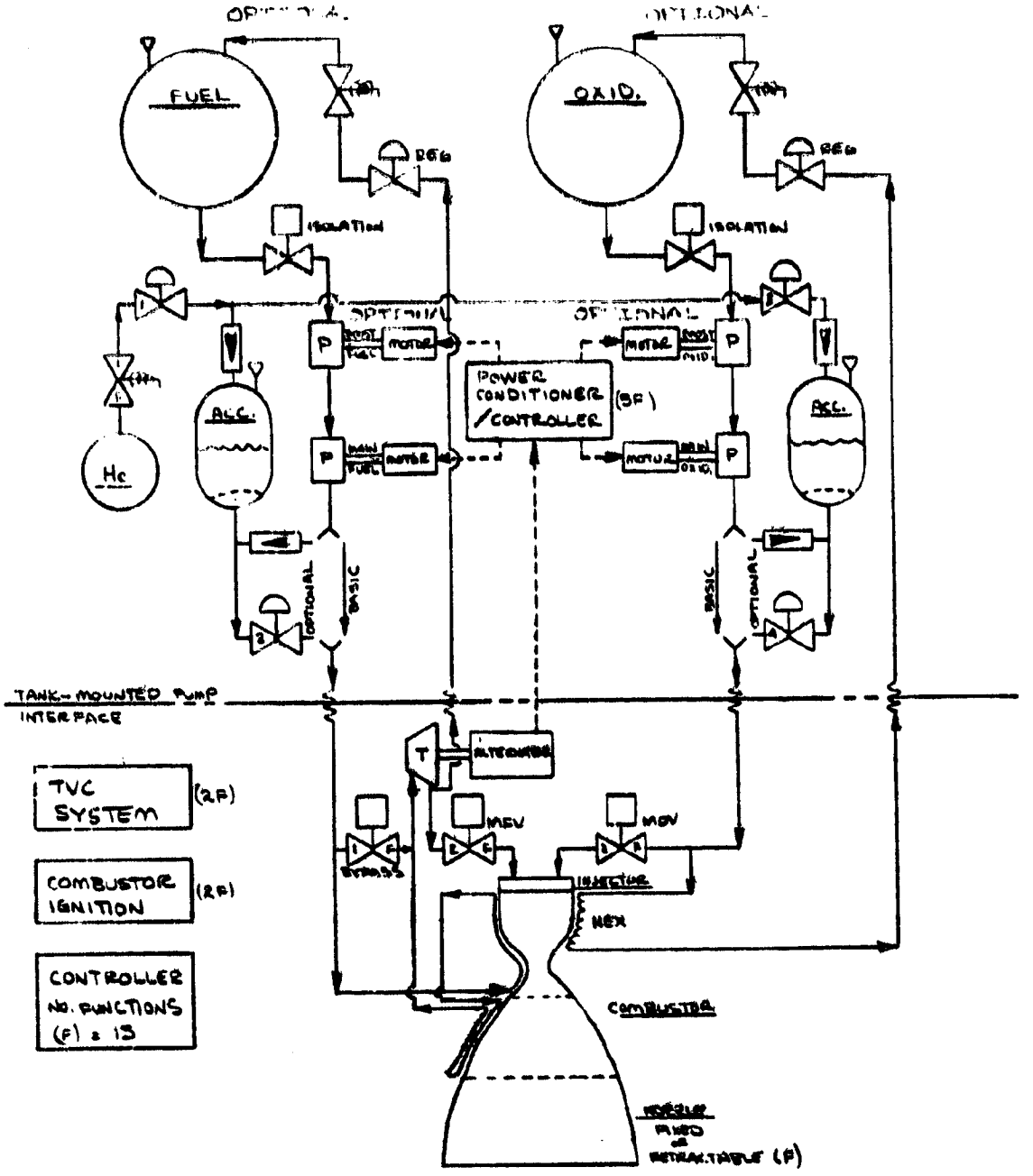

Figure 58 . Turboalternator - Expander Schematic

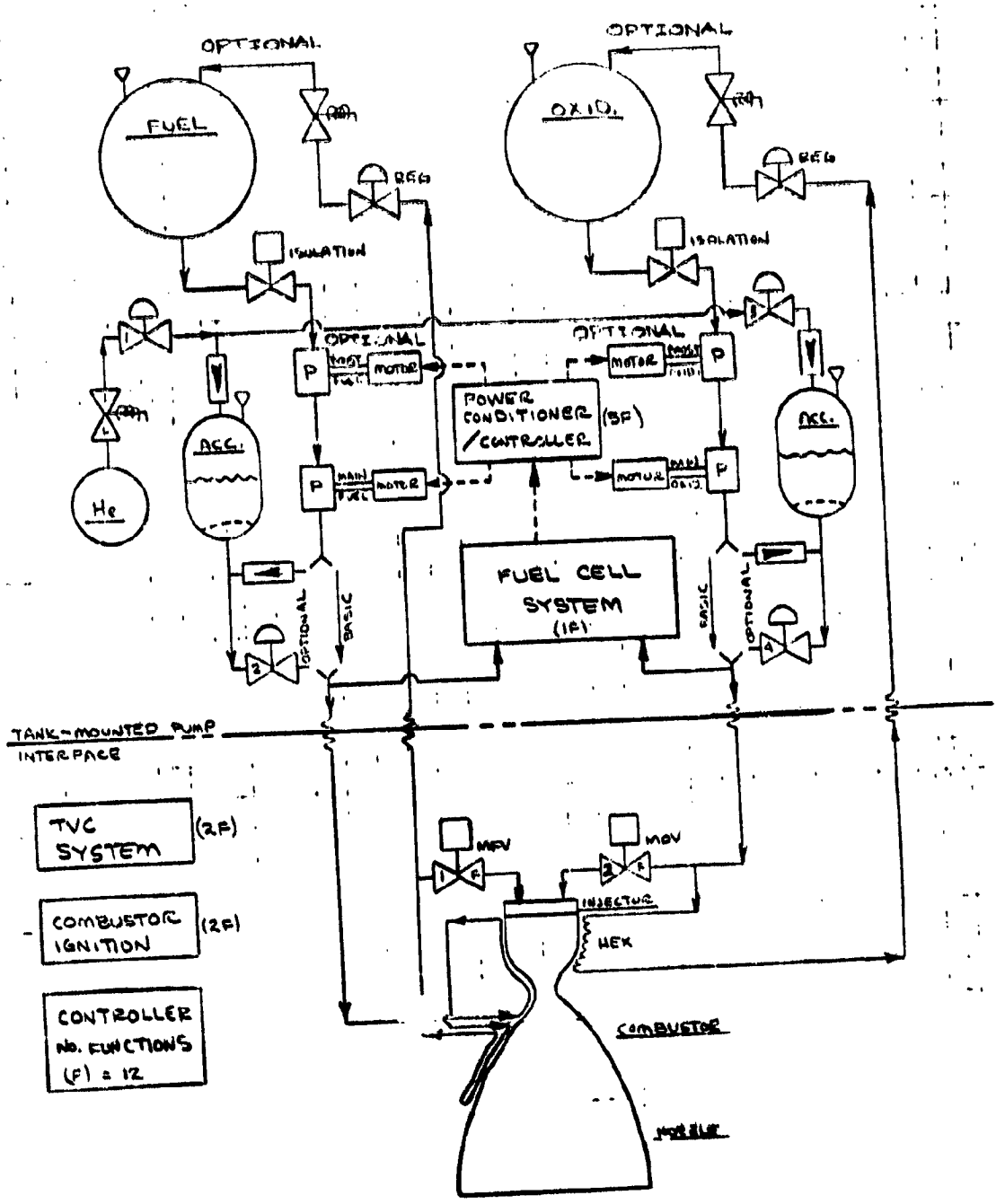

Figure 59 . O_2/H_2 Fuel Cell/Motor-Driven Pumps

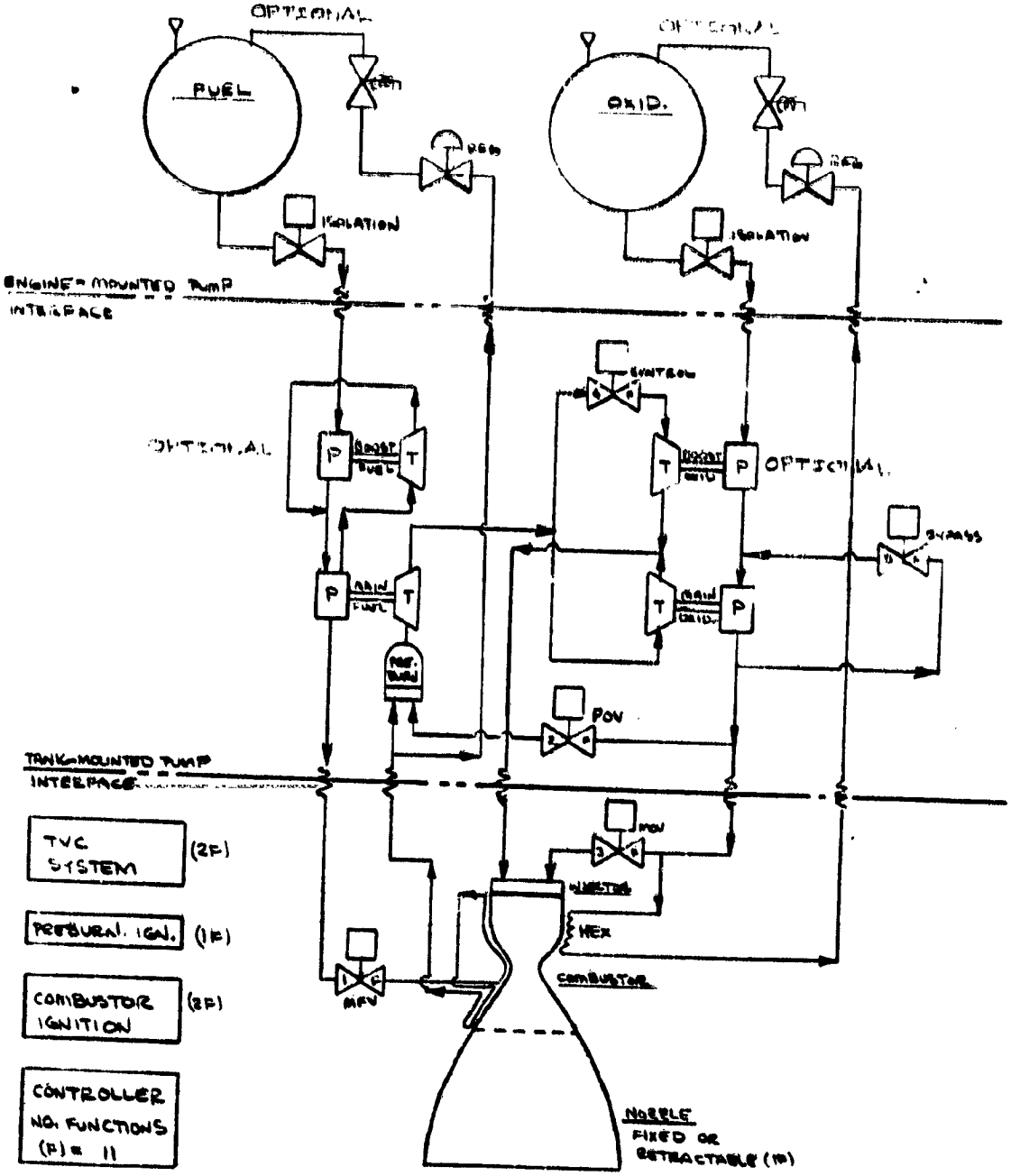

Figure 60. Staged-Combustion Engine Schematic

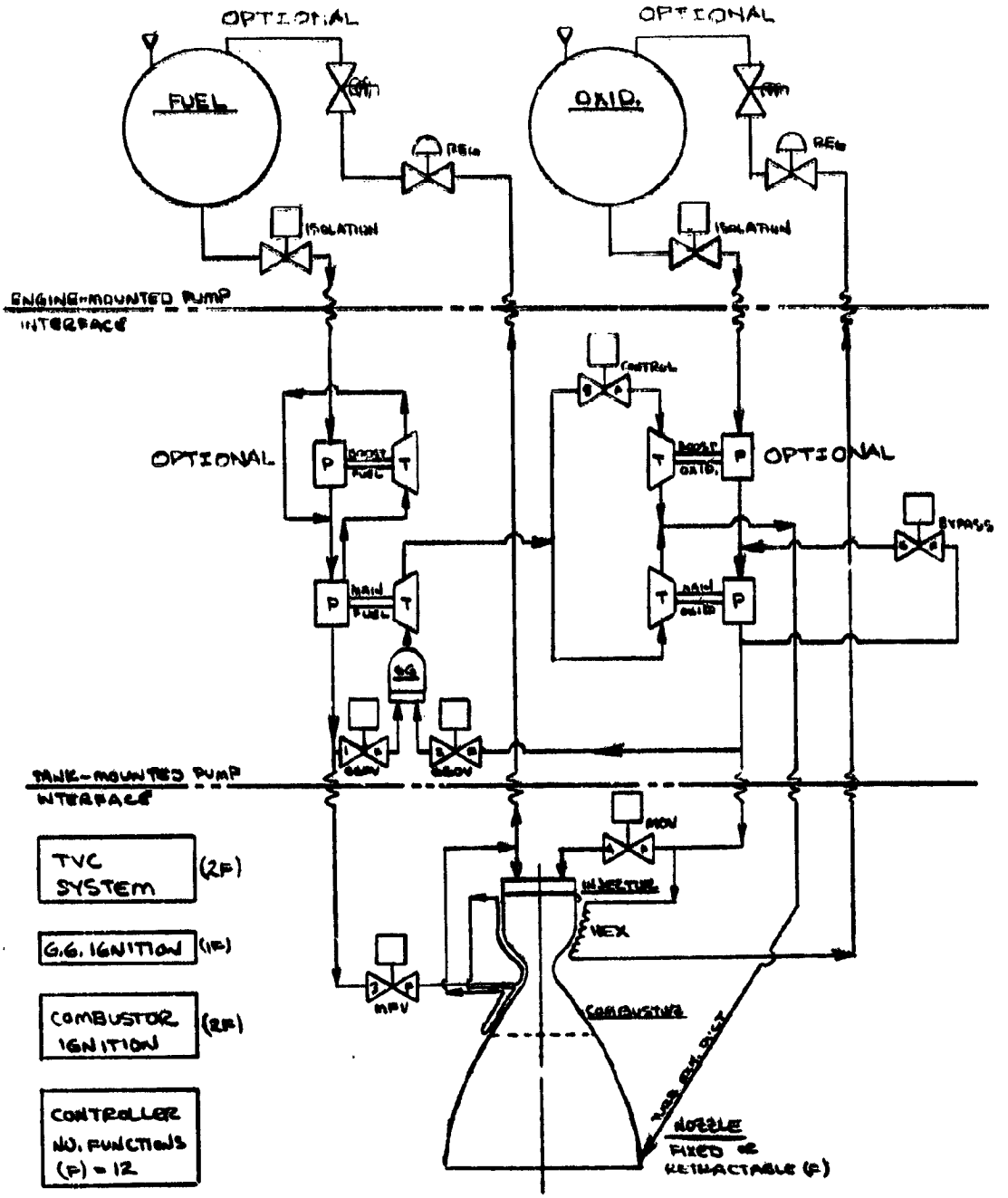

Figure 61. Gas Generator Cycle Engine Schematic

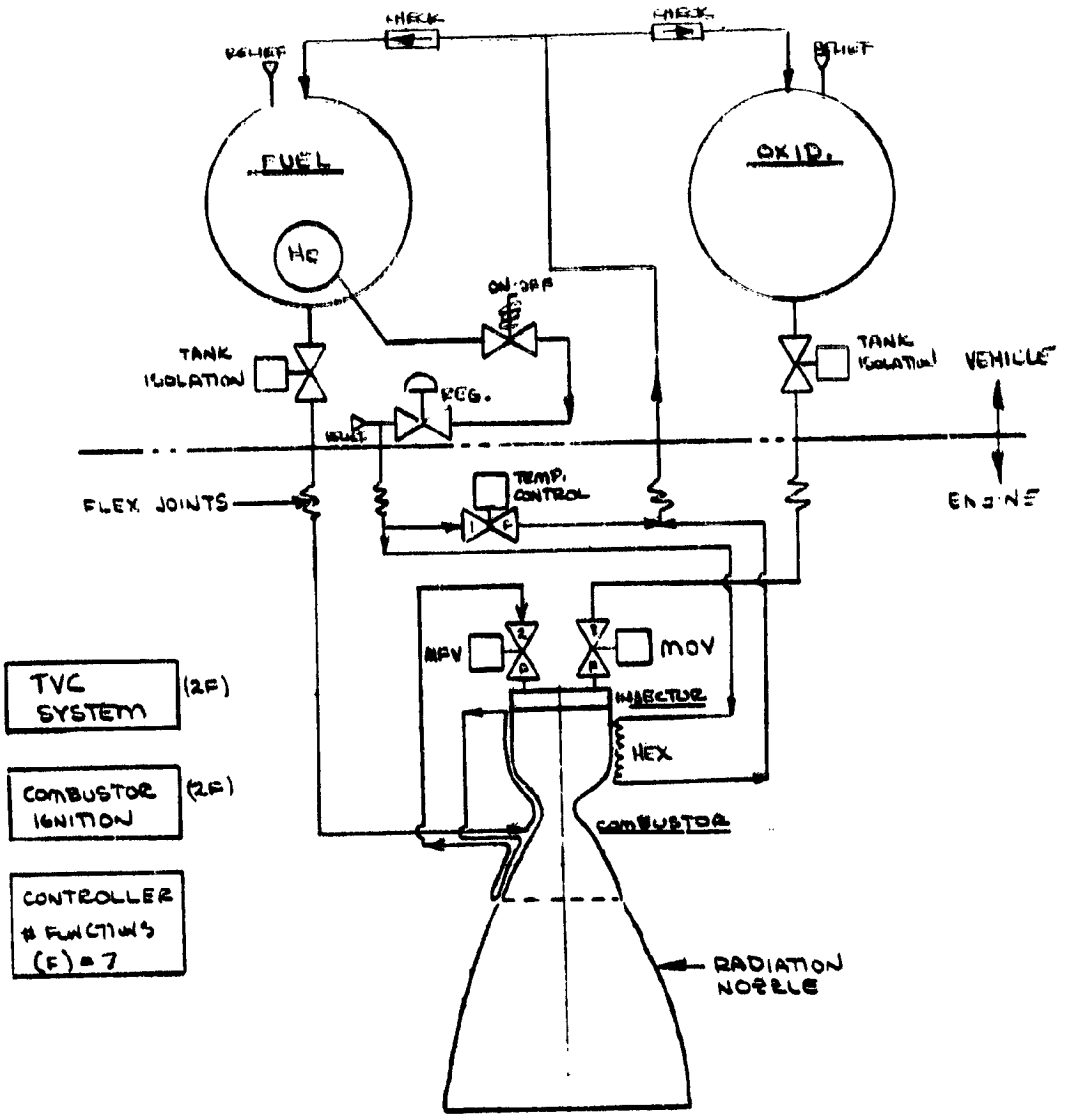

Figure 62 . CONVENTIONAL PRESSURE FED ENGINE SCHEMATIC

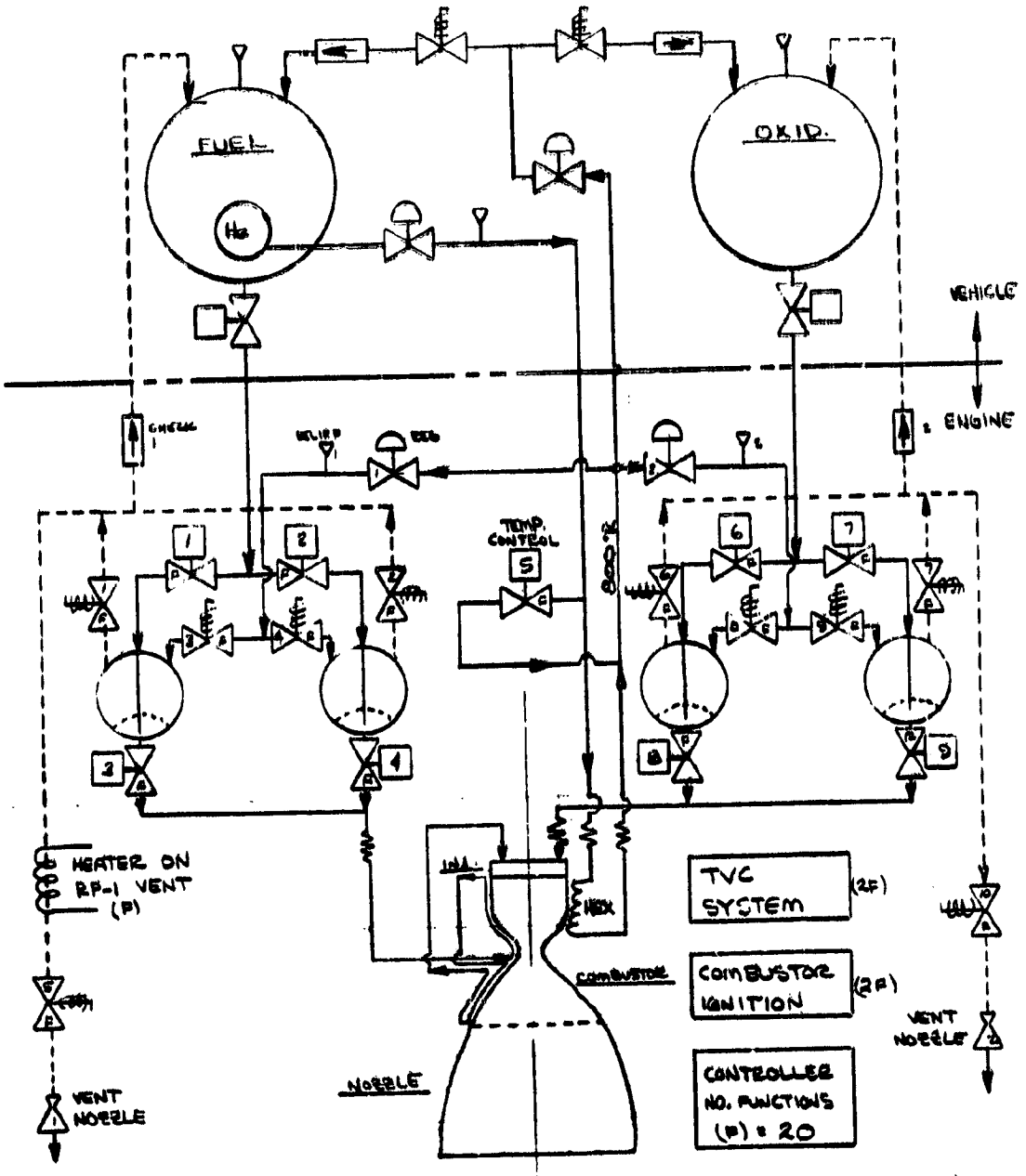

Figure 63 . Parallel Pressurized Feed Tank Schematic

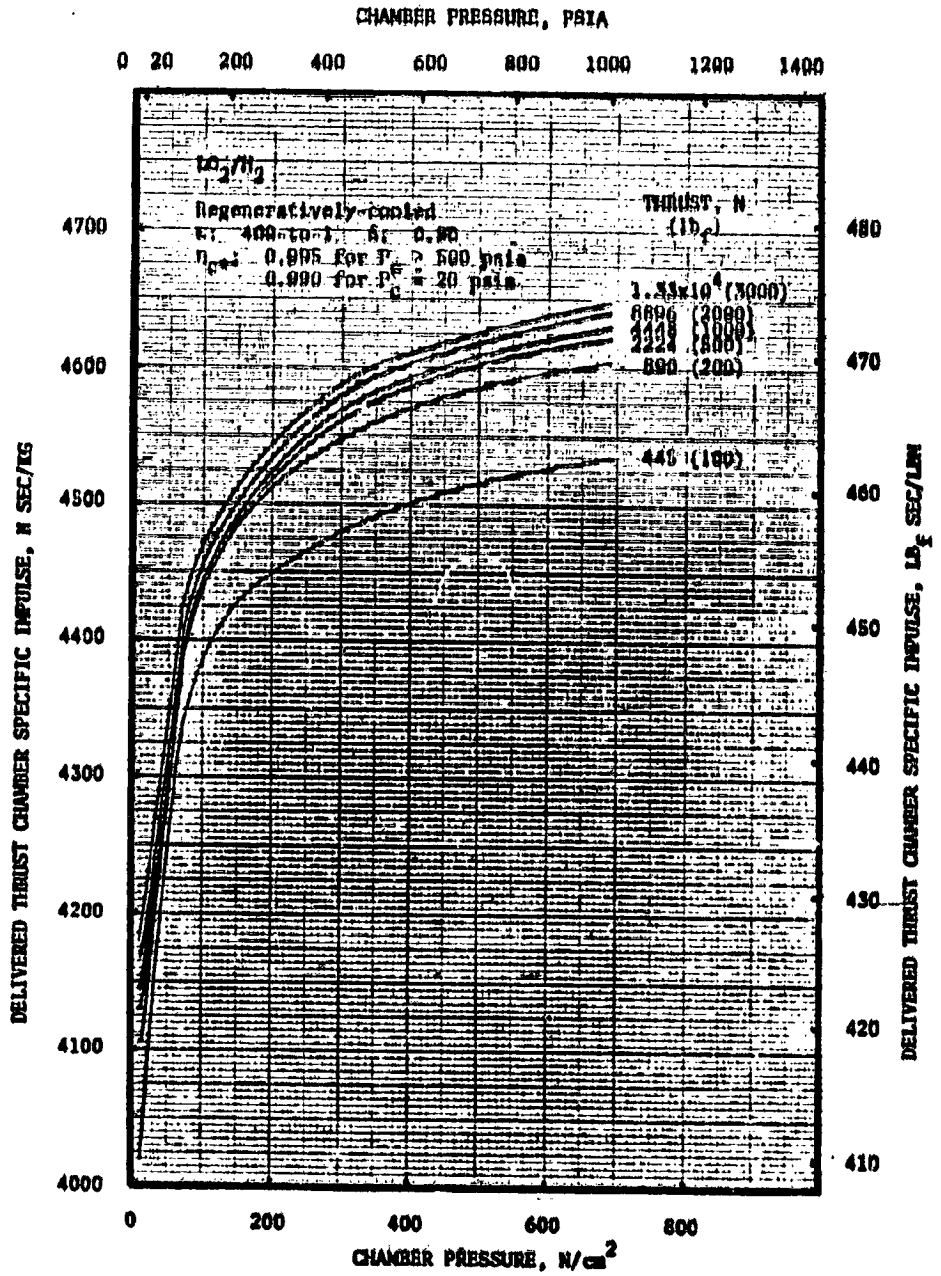

Figure 64. LO_2/H_2 Regeneratively-cooled Thrust Chamber Delivered Specific Impulse Variation with Chamber Pressure and Thrust

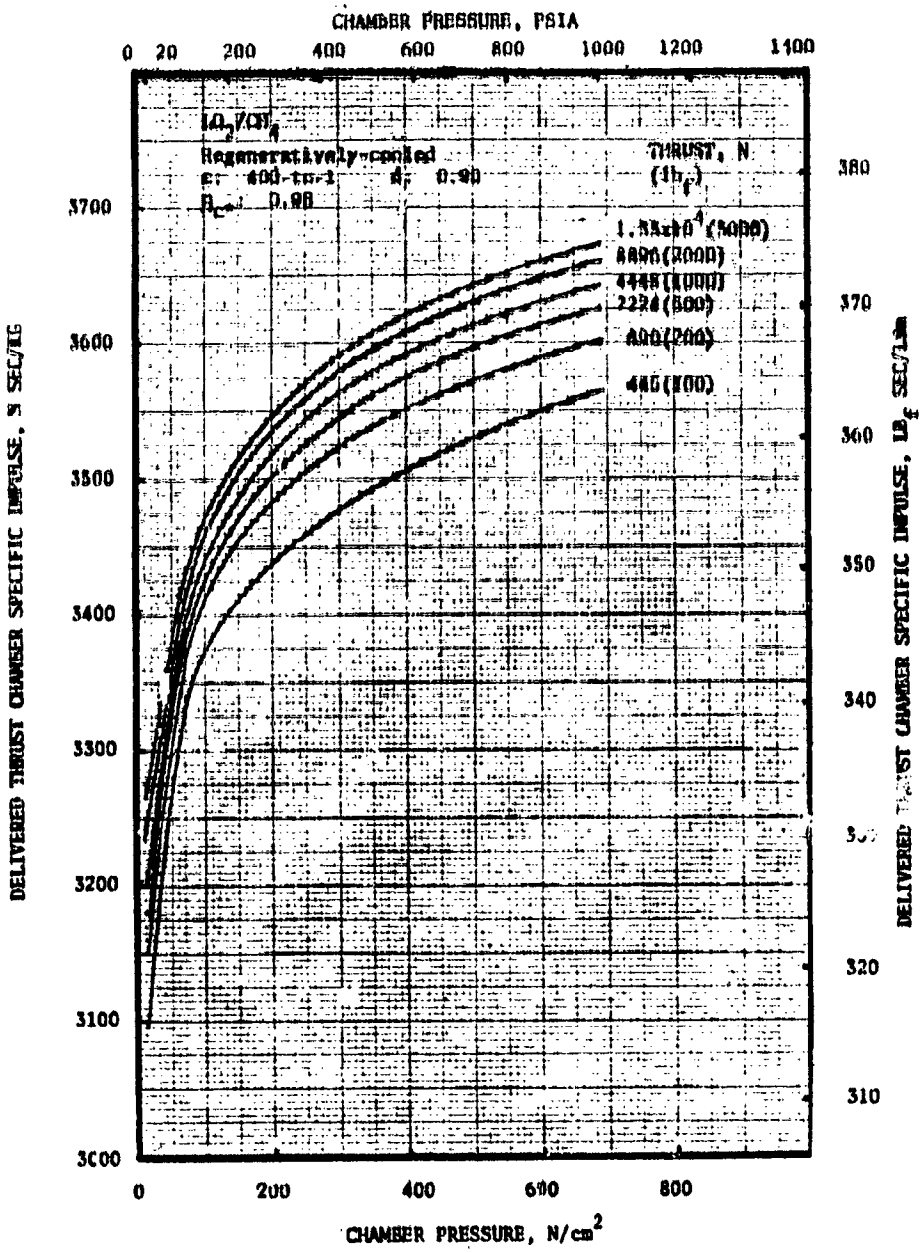

Figure 65. LO_2/CH_4 Regeneratively-cooled Thrust Chamber Delivered Specific Impulse Variation with Chamber Pressure and Thrust

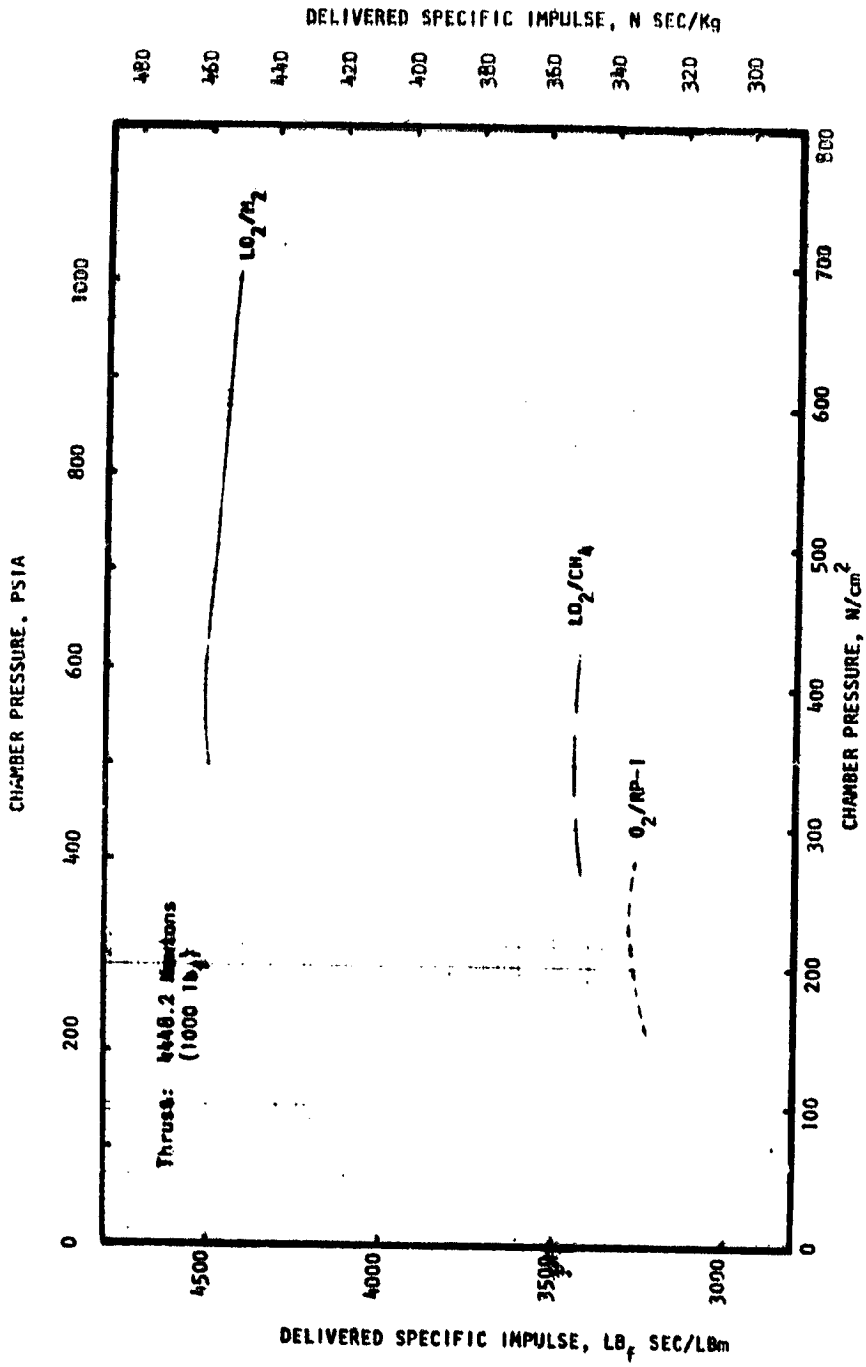

Figure 66. Regeneratively-Cooled Gas Generator Cycle Engine Performance
(Thrust = 4448.2 Newtons or 1000 lb_f)

Film-/Radiation-Cooled Engines. The delivered thrust chamber specific impulse for the film-/radiation-cooled LO_2/H_2 and LO_2/RP-1 thrust chambers are shown in Figs. 67 and 68 with the cooling limit superimposed. For a fixed thrust as the chamber pressure is decreased, the film-cooling loss and the theoretical specific impulse decreases and the reaction kinetic loss increases. Therefore, as the chamber pressure was decreased, the delivered specific impulse increased until the increase in kinetic loss and the decrease in the theoretical specific impulse dominated and then the delivered specific impulse decreased. For the LO_2/H_2 film-/radiation-cooled thrust chambers, a maximum delivered specific impulse occurred for 4448.2 N (1000 pounds) and 13345 N (3000 pounds) thrust at 41.37 N/cm^2 (60 psia) and 68.95 N/cm^2 (100 psia) chamber pressures, respectively. For the LO_2/RP-1 film-/radiation-cooled thrust chambers, the minimum study chamber pressure of 13.79 N/cm^2 (20 psia) was reached before a maximum specific impulse value was achieved.

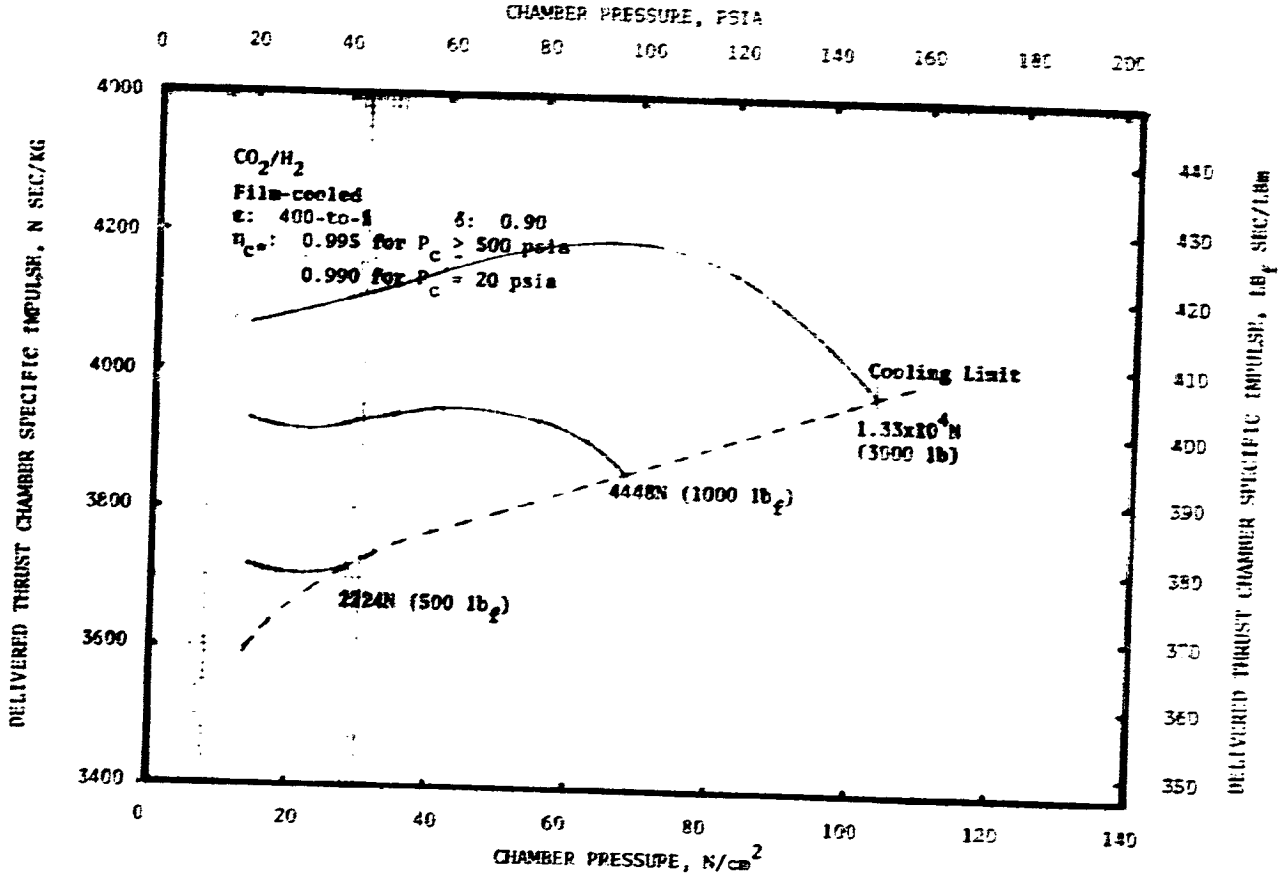

Figure 67 . LO_2/H_2 Film-cooled Thrust Chamber Delivered Specific Impulse Variation with Chamber Pressures and Thrust

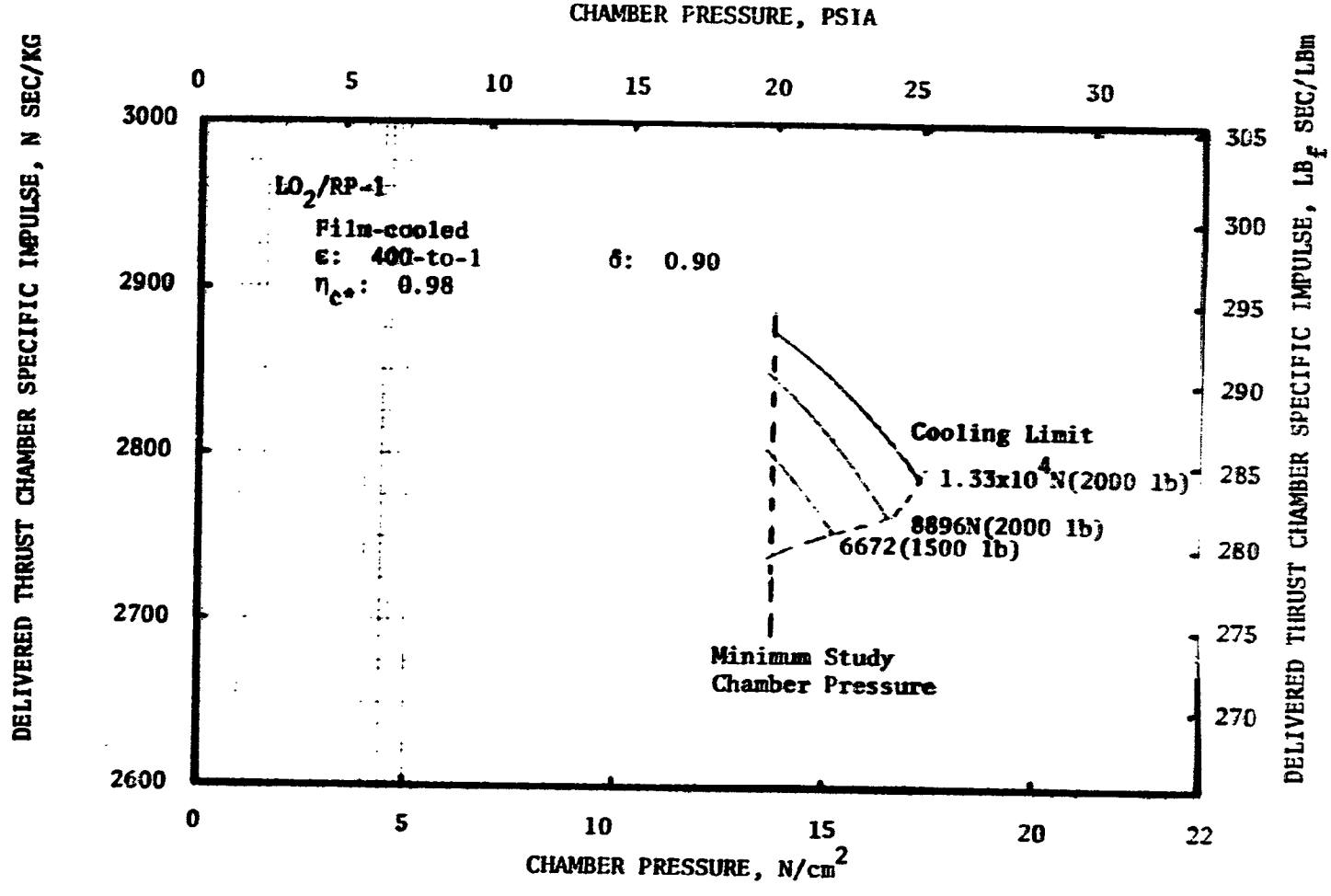

Figure 68. LO_2/RP-1 Film-cooled Thrust Chamber Delivered Specific Impulse Variation with Chamber Pressure and Thrust

Pump-Fed Engine Cycle Analysis. Engine cycle analyses were performed for each of the candidate pump-fed expander and staged combustion engine cycle/configurations to determine chamber pressure limits and delivered performance over the low thrust range of interest. Cycle analysis of the gas generator engines was limited to specific thrust levels of 2224.1 N and 4448.2 N (500 lbf and 1000 lbf). As indicated previously, all thrust chambers were regeneratively cooled with fuel. Also, boost pumps and autogenuous pressurization systems were not incorporated in the cycles. For the expander cycles, a number of balances were conducted assuming 4% and 10% turbine bypass flow as power margins. However, the majority of the effort was conducted assuming 20% turbine bypass flow and the results reported herein are based on the more conservative value of 20%.

Results of the cycle balances which show achievable chamber pressure as a function of thrust are given in Figs. 69 and 70 for LO_2/H_2 and LO_2/CH_4 engines, respectively, and are discussed in the following paragraphs.

Direct Expander Cycle Limits. As shown in Fig. 69, the direct expander power limits for LO_2/H_2 engines were less than the cooling limits from 13345 N (3000 pounds) to approximately 1400 N (314.7 pounds) thrust. From approximately 1400 N (314.7 pounds) to 44.8 N (100 pounds) thrust, the cooling limit was slightly lower than the cycle limit. The maximum chamber pressure 453.2 N/cm^2 (657.3 psia) was achieved at 13345 N (3000 pounds). For the LO_2/CH_4 engines, the direct expander power limits (Fig. 70) were lower than the cooling limits from 13345 N (3000 pounds) thrust to 4448.2 N (1000 pounds). The maximum LO_2/CH_4 chamber pressure at 13344.7 N (3000 pounds) thrust of 398.5 N/cm^2 (378 psia) was less than the 453.2 N/cm^2 (657.3 psia) achieved with LO_2/H_2.

The LO_2/CH_4 engine cycle balances for thrust levels greater than 2224.1 N (500 lbf) had a thrust chamber coolant discharge pressure greater than the methane critical pressure due to turbine pressure ratio requirements of the cycle. The LO_2/CH_4 direct expander cycle resulted in the lowest allowable coolant discharge pressure at 2224.1 N (500 lbf) thrust and a chamber pressure of 327 psia. Therefore, for this cycle configuration, the minimum coolable chamber pressure is approximately a factor of 2 below the coolant critical pressure.

Below 2224.1 N (500 lbf) thrust, the LO_2/CH_4 direct expander cycle encountered subcritical pressures and the two-phase heat transfer problem. Therefore, the lower thrust levels were evaluated by adding coolant pressure drop (an orifice) between the thrust chamber coolant discharge and the turbine inlet to maintain supercritical methane pressures. Using this approach, engine cycle balances were successfully performed down to a thrust level of 667.2 N (150 lbf) and a chamber pressure of 75.8 N/cm^2 (110 psia). A total of 193.1 N/cm^2 (280 psi) was added for this condition.

Turboalternator Expander Cycle Limits. Analysis of the turbo-alternator cycle engine was performed using an option of the expander cycle engine balance code. This option permits incorporation of the electric pump drive and the turbine-driven alternator. The pumps were driven by the electric motors which, in turn, were powered by the fuel turbine through the alternator.

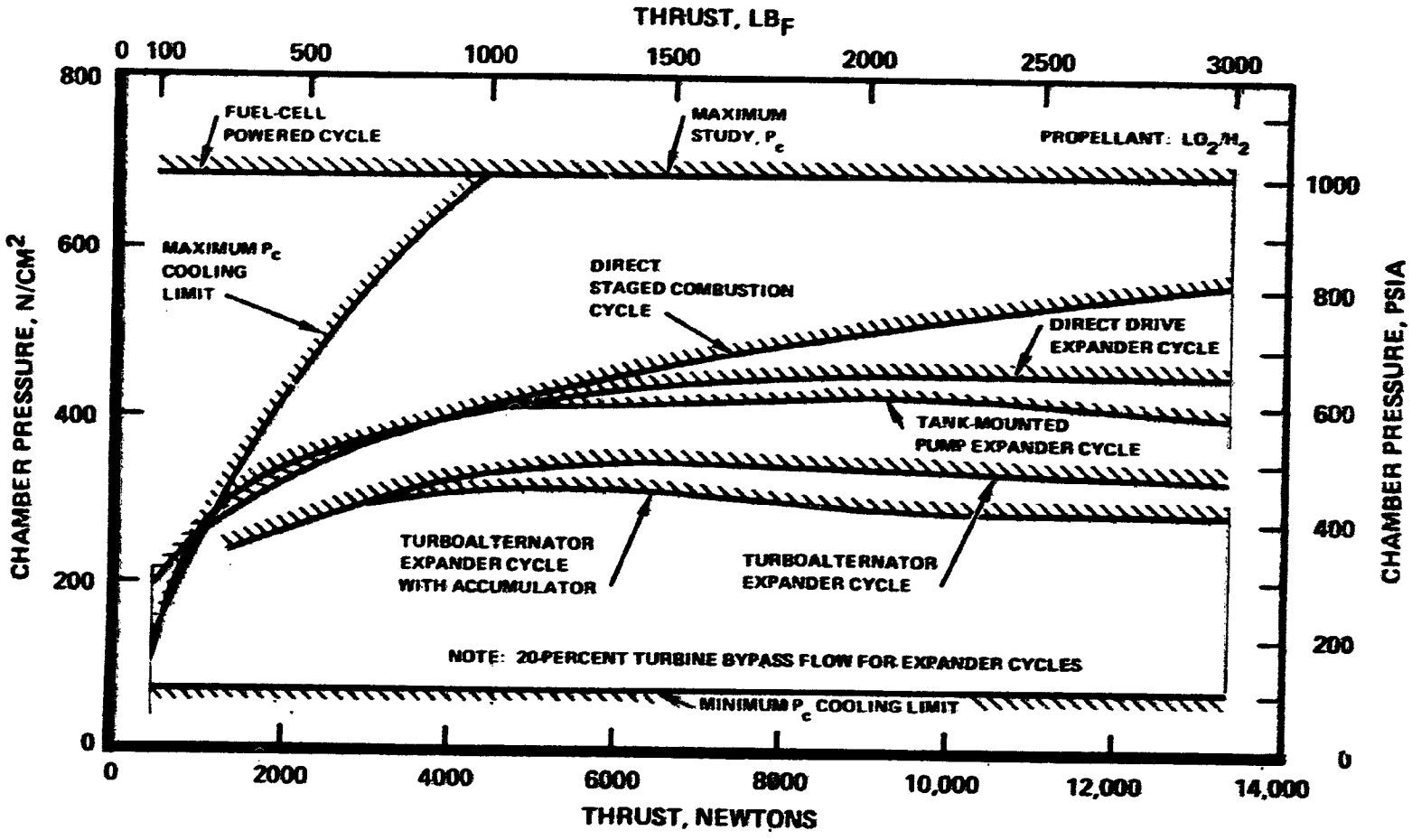

FIGURE 69. Regenerative - Cooling and Cycle Limits for LO_2/H_2 Engines

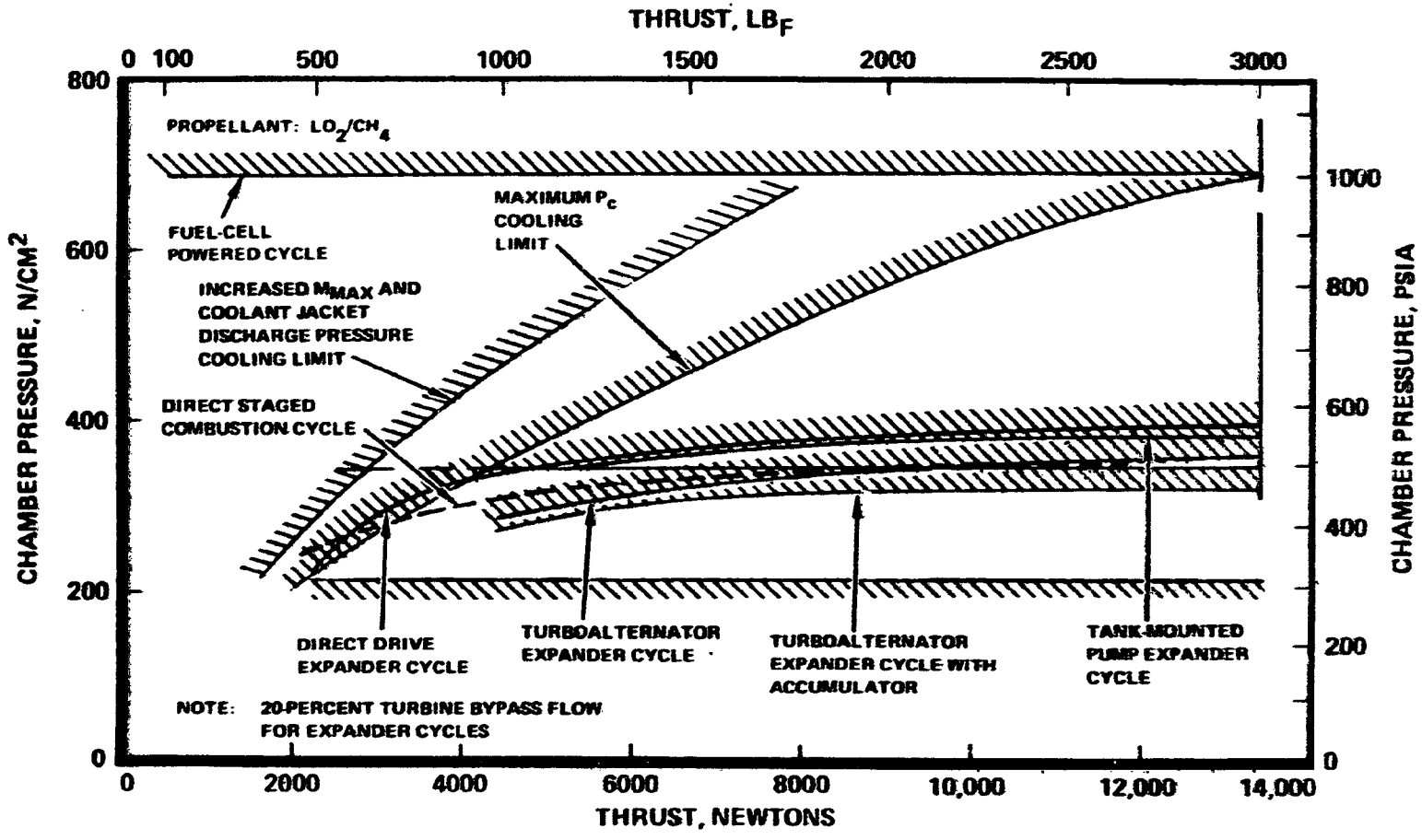

Figure 70. Regenerative - Cooling and Cycle Limits for LO_2/CH_4 Engines

The turboalternator expander cycle limits for LO_2/H_2 and LO_2/CH_4 are presented in Figs. 69 and 70. As shown, the added inefficiencies of the alternator and the electric motors resulted in a lower maximum chamber pressure than for the direct expander cycle. The maximum chamber pressure for the LO_2/H_2 engine was 340 N/cm^2 (493 psia) at 6672.4 N (1500 pounds) thrust. At thrust levels above 6672.4 N (1500 pounds) thrust it was necessary to operate the turbine at increasingly higher pressure ratios to develop the required power. As a result, chamber pressure decreased. The maximum chamber pressure for the LO_2/CH_4 engine was 355 N/cm^2 (515 psia) at 13344.7 N (3000 pounds) thrust. The trend of decreasing achievable chamber pressure as thrust increased was not observed in the LO_2/CH_4 turboalternator cycle.

Fuel-Cell Powered Cycle Limits. In the O_2/H_2 fuel cell-powered engine cycle, the pumps were driven by electric motors that were powered by the fuel cell through electric converters. Converters are used to change the direct current obtained from the fuel cell to alternating current and to avoid the speed matching requirement of the fuel and oxidizer motors.

In analyzing this engine cycle, the thrust chamber performance parameters for a given thrust level and chamber pressure are first calculated. Then the system pressure drops and the pump discharge pressures are obtained. Based on the engine flowrates and the pump discharge pressures, the fuel pump and the oxidizer pump designs can be determined. Once the pump efficiencies and required horsepowers were calculated, the fuel cell output power was obtained assuming the efficiencies of the converter and the motors to be 90 and 85%, respectively.

To reduce the fuel cell weight, the performance calculation is conducted at or near the pump limiting speed through an optimization procedure. In the fuel cell system, the engine cycle balance program was written to minimize the cell weight. Since the O_2/H_2 fuel cell has its own separate feed system that is different from the engine, theoretically if the cooling limit is not considered, the fuel cell-powered engine can perform at any desired chamber pressure for a given thrust level as shown on Figs. 69 and 70. The maximum study chamber pressure of 689.5 N/cm^2 (1000 psia) chamber pressure was obtained at thrust levels between 444.8 N (100 pounds) and 13345 N (3000 pounds) for both the LO_2/H_2 and LO_2/CH_4 engine systems.

Tank-Mounted Pump Expander Cycle. In the analysis of expander cycle engine configuration utilizing tank-mounted pumps, the fluid line pressure drops due to the long line lengths added to the engine system.

Based on NASA-LeRC propellant tankage configuraion previously shown in Fig. 56, 569 cm (224 inches) of line were added between fuel pump discharge to combustor coolant jacket inlet and between nozzle coolant jacket outlet to turbine inlet 434.3 cm (171 inches) of hot-gas duct was added. The extra duct length added between oxidizer turbine and thrust chamber was 113.4 cm (47 inches). Also, a number of elbows and losses for inlet and outlet pressure drop losses were included.

As shown in Figs. 69 and 70, this cycle/configuration suffered some reduction in maximum attainable chamber pressure when compared with that of the engine-mounted expander cycle. The maximum chamber pressure for the LO_2/H_2 engine was 420 N/cm^2 (610 psia) at 8896.4 N/cm^2 (2000 pounds) thrust. Above the thrust level, the volumetric flow rate of the turbine drive gas was large enough to cause substantial pressure drop in the turbine feed and return lines and resulted in lower chamber pressures. The maximum chamber pressure for the LO_2/CH_4 engine was 385 N/cm^2 (558 psia) at the maximum study thrust level of 13345 N (3000 lbf). The trend of decreasing achievable chamber pressure above 8896.4 N/cm^2 (2000 pounds) thrust did not occur in the LO_2/CH_4 engine because of the increased density of the CH_4 turbine drive gas compared to the H_2.

Turboalternator Expander with Accumulator Cycle Limits. The use of pump-filled feed tanks (accumulators) permits the design of higher flow pumps and enables higher pump efficiencies. The pumps would be designed for a higher-than-nominal engine flow. During the pumping operation, the flow is divided between the engine and the accumulators. When the accumulators reach their capacity, the pump would be shut off and the engine would be supplied propellants from the accumulators.

The engine cycle balance computer program option used to analyze this cycle is the same as the turboalternator expander cycle, except in the pump design routine, the pump flowrate is the sum of the thrust chamber flowrate and the accumulator flowrate.

The analysis results indicated that the addition of the accumulators in the system did improve the pump efficiency but the pump required horsepower increased. The volumetric flowrate increased faster than the efficiency resulting in a decrease in the maximum attainable chamber pressure.

Figure 69 shows that the LO_2/H_2 engine achieved a maximum chamber pressure of 310 N/cm^2 (450 psia) at 4448.2 N (1000 pounds) thrust. Above this thrust level, there was a trend of decreasing chamber pressure similar to that experienced on the LO_2/H_2 turboalternator expander cycle engine. For the LO_2/CH_4 engine (Fig. 70), maximum chamber pressure was 320 n/cm^2 (464 psia) at 13345 N (3000 pounds) thrust with a trend of increasing chamber pressure with increasing thrust similar to the LO_2/CH_4 turboalternator expanded engine.

Staged Combustion Cycle Limits. The direct-drive, staged-combustion cycle/configuration engine balances were generated using the staged combustion analysis option of the engine balance computer program. The computer program generates an engine, combustor, and nozzle design at the highest attainable chamber pressure for a given thrust; engine and preburner mixture ratio; nozzle expansion area ratio; and a given set of turbopump assembly parameter limits. Four turbopump parameters (fuel and oxidizer turbopump speeds and both turbine's pressure ratios) are used as independent variables of an optimization routine that searches for the highest value of the chamber pressure.

As shown in Fig. 69, the maximum chamber pressure for the LO_2/H_2 engine was 560 N/cm^2 (812 psia) at 13345 N (3000 pounds) thrust. Also, note that below 4448.2 N (1000 pounds) thrust, the LO_2/H_2 staged combustion cycle power balanced at chamber pressures below those achieved for the direct expander cycle. For the LO_2/CH_4 engine (Fig. 70), a maximum chamber pressure of 355 N/cm^2 (515 psia) was achieved at the maximum study thrust level of 13345 N (3000 lbf). Note that the LO_2/CH_4 staged combustion cycle power balanced at chamber pressures below the expander cycle over almost the entire thrust range. Examination of the detail cycle balance results verified that the increased pump power required by the LO_2/CH_4 staged combustion cycle could not be supplied at the assumed turbine inlet temperature of 1033K (1860R) without increasing turbine pressure ratio to magnitudes which resulted in the chamber pressures shown in Fig. 70.

Gas Generator Cycle Limits. The methodology for the gas generator engine cycle was based on optimizing engine performance at a chosen thrust and chamber pressure. The engine cycle balance computer program first calculated thrust chamber performance parameters such as engine flowrate, thrust chamber flowrate, engine specific impulse, and thrust chamber specific impulse for a given thrust level and chamber pressure. The program then calculated the system pressure drops and the pump discharge pressures. Based on the engine flowrates and the pump discharge pressures, the fuel pump and the oxidizer pump designs were determined. The turbine required horsepowers were then set equal to those of the pumps. The gas generator design was based on a combustion temperature of 1033K (1860R), and its mixture ratio and hence flowrate can then be calculated. With this new gas generator flowrate, the thrust chamber performance parameters were recalculated, and new engine delivered specific impulse obtained. A multi-dimensional optimization routine was then used to find the maximum performance by changing four selected key independent variables that included the oxidizer and fuel pump rpm and oxidizer and fuel turbine pressure ratio. This optimization was performed within the constraints of the pump and turbine design limits and consistent with the available turbine drive energy.

Design points for the gas generator cycle engines are shown in Table 9. Design points were selected to provide maximum performance based on the performance curves shown in Fig. 66.

TABLE 9. GAS GENERATOR CYCLE DESIGN POINTS (ϵ = 400:1)

PROPELLANT	MIXTURE RATIO	THRUST N (LBF)	CHAMBER PRESSURE N/CM^2 (PSIA)	DELIVERED SPECIFIC IMPULSE N-SEC/KG (LBF-SEC/LBM)
LO_2/H_2	6.0	4448.2 (1000)	413.7 (600)	4512.8 (460.2)
LO_2/H_2	6.0	2224.1 (500)	275.8 (400)	4448.6 (453.6)
LO_2/CH_4	3.7	4448.2 (1000)	344.7 (500)	3443.5 (351.1)
LO_2/RP-1	3.0	4448.2 (1000)	227.5 (330)	3286.7 (335.2)

Pressure-Fed Engine Cycle Analysis. In order to establish optimum chamber pressure for the conventional and the parallel pressurized tank pressure-fed engine systems, analyses were conducted to provide vehicle payload trends as a function of chamber pressure. In general, both of the pressure-fed configurations utilize a pressurant (assumed to be helium) to expel liquid propellants from the main tanks. The conventional pressure-fed engine chamber pressure is obtained directly from the main propellant tanks. The parallel-pressurized feed tank engine configuration utilizes a high-pressure pressurant tank to feed and alternately pressurize two, small, propellant tanks that supply the chamber pressure.

Propellant is fed from a main tank to one of its small pressurized tanks and then to the rocket engine. Pressurizing gas is also supplied to the small tanks through a pressure regulator and a heat exchanger. To draw propellants from the main tank, the small tanks are reduced in pressure by venting. Initial ventant goes to the main tank to maintain its pressure and the remainder is dumped overboard through thrust producing nozzles.

Starting with a small tank full (except for ullage) of propellant, at main tank pressure, the sequence of operations is listed in Table 10 and described as follows:

1. The pressurization valve and then the engine feed valve are opened on a signal from the liquid level sensor near the top of the small tank. Pressurant gas fills the ullage space after passing through a pressure regulator and heat exchanger. The pressurant storage tank is immersed in the colder propellant to provide maximum density pressurant.

TABLE 10. VALVE SEQUENCE OPERATIONS FOR PARALLEL SMALL TANK CONCEPT

Tank 1	Tank 2
OPEN PRESSURIZATION	
OPEN ENGINE FEED	
	CLOSE ENGINE FEED
	CLOSE PRESSURIZATION
	OPEN TANK VENT
	OPEN OVERBOARD VENT
	OPEN FILL
	CLOSE OVERBOARD VENT
	CLOSE TANK VENT
	CLOSE FILL
	OPEN PRESSURIZATION
	OPEN ENGINE FEED
CLOSE ENGINE FEED	
CLOSE PRESSURIZATION	
OPEN TANK VENT	
OPEN OVERBOARD VENT	
OPEN FILL	
CLOSE OVERBOARD VENT	
CLOSE TANK VENT	
CLOSE FILL	

2. Pressurization and engine feed valves are closed on a signal from the liquid level sensor in the engine feed line. The same signal then opens the tank vent valve. Pressurant and propellant vapor flow to the main propellant tank until the pressure lost by propellant withdrawal is regained. The latter condition is sensed by a pressure transducer, which signals the overboard vent valve to open.

   The remainder of the vented material is released through a rearward facing nozzle to provide additional thrust. A check valve prevents any flow from the main tank.

3. Another pressure controlled valve allows filling of the small tank, from the main tank, when its pressure is below that in the main tank. The overboard vent valve would be closed, by a signal from the liquid level sensor near the top of the small tank, when the tank has been filled. The same signal will cause closing of the tank vent valve and the fill valve.

To ensure a continuous propellant feed during an engine burn, an override signal would be sent to open the engine feed line valve on either small tank when the other small tank feed line valve is closed. This acts as a safety factor above the margin allowed in line sizing and pressure differences. Pressure relief valves on the main tanks and downstream of the pressure regulator protect the system from overpressure.

The assumptions of this analysis are presented in Table 11. To determine the delivered payload to a GEO orbit, the NASA-LeRC specified vehicle gross weight of 27216 kg (6000 pounds) was used. A representative engine thrust of 4448.2 N (1000 lbf) was selected for the comparative analysis with LO_2/H_2 as the propellant. The assumed velocity increment was 5410 m/sec (17750 ft/sec).

To simplify this comparative analysis, spherical propellant tanks were assumed and the pressurant bottle was assumed to be located within the hydrogen tank. The main tanks and pressurant bottle were composed of an aluminum liner with Kevlar overwrap. Titanium was used for the small tanks of the parallel-pressurized feed tank engine configuration. Minimum material thicknesses selected for the aluminum tanks was 0.1524 cm (0.060 inch) and 0.0889 cm (0.035 inch) for titanium. The minimum Kevlar thickness was 0.03048 cm (0.012 inch), which coincides to a single minimum strand wrap. A tank wall stress safety factor of 2 to 1 was assumed for this analysis.

Payload trends between the engine configurations are shown in Figs. 72 and 73. For the analysis results shown in Fig. 72, the helium pressurant temperature for all main tanks was assumed to be the stored hydrogen temperature of 37.8 R. As shown in Fig. 72, the parallel-pressurized feed tank configuration resulted in a 13% higher payload than the conventional pressure-fed engine due to reduction in tank and pressurant weight. The maximum payload for the engines was extremely sensitive to chamber pressure and initially increased due to the increase in specific impulse, but as chamber pressure increased, the increase in tank weights dominated and payload decreased. A comparison was also made using heated helium at 530 R as a pressurant (Fig. 73). Results showed an increase

TABLE 11 . PRESSURE-FED ENGINE ANALYSIS

ASSUMPTIONS

Vehicle Gross Weight = 27216 Kg (60,000 lbs)

Engine Delivered Specific Impulse = From Fig. 64

Engine Weight = from Fig. 71

Engine Thrust = 4448.2 Newtons (1000 lb_f)

Propellant Tanks:

Tank Configuration: Spherical

$P_{main\ tank}$ = 20.7 N/cm^2 (30 psia) (For parallel pressurized feed tanks)

$\left(P_{He_{storage}}\right)_{initial}$ = 2068.4 N/cm^2 (3000 psia) (located in H_2 tank)

Main tank ullage volume fraction = 2%

Small tank ullage volume = 5%

Small tank size = 20-second fill and 20-second drain time

Total System Weight = 2*(tank weight + engine weight + misc. weight)

NOTES:

1. For the parallel pressurized-feed tank engine configuration, an average engine specific impulse was computed from the thrust chamber and helium nozzle contributions.
2. * Factor accounts for tank structure and plumbing weights.

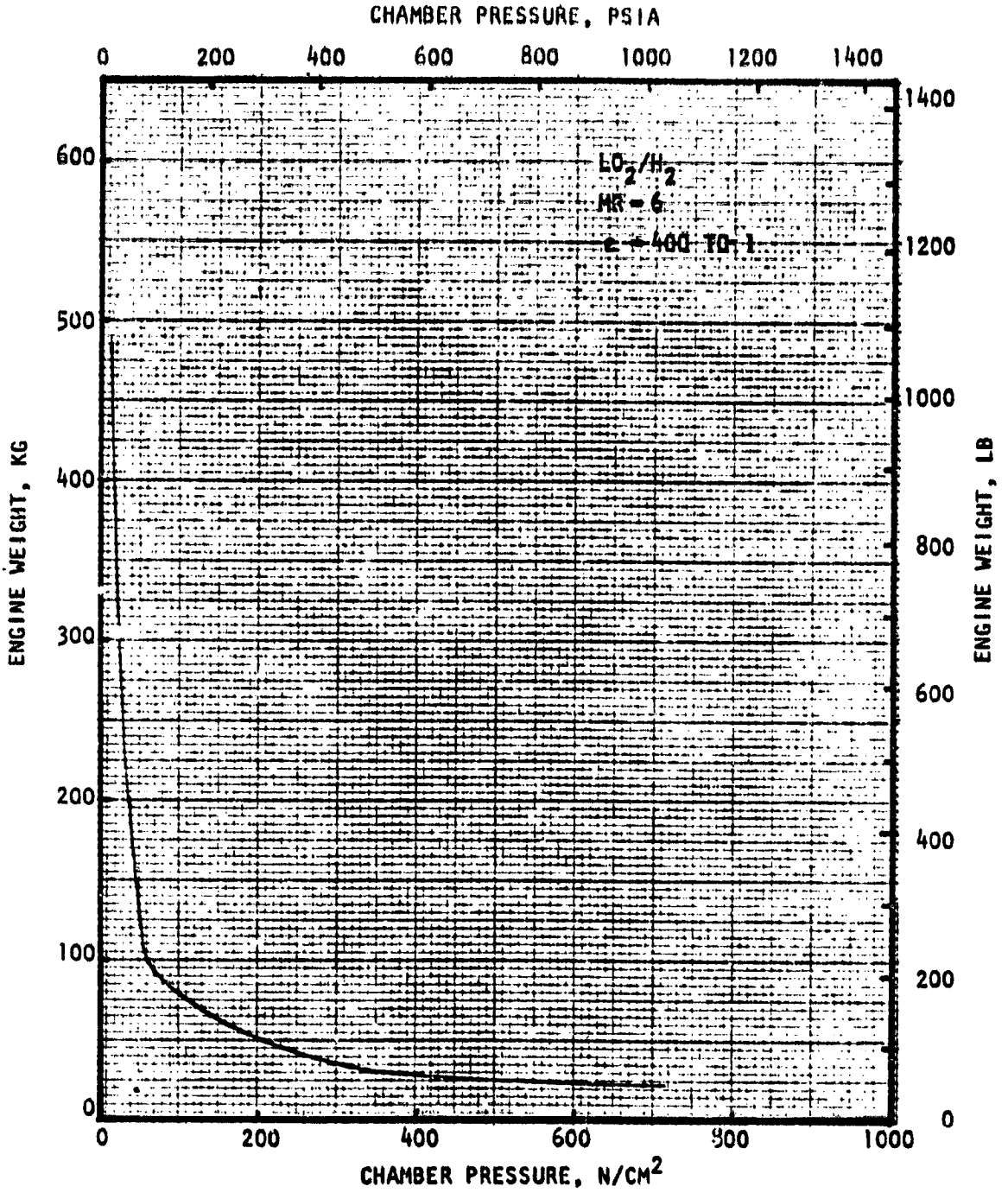

Figure 71. Pressure-Fed LO_2/H_2 Engine Weight
(Thrust = 4448.2 N or 1000 lbf)

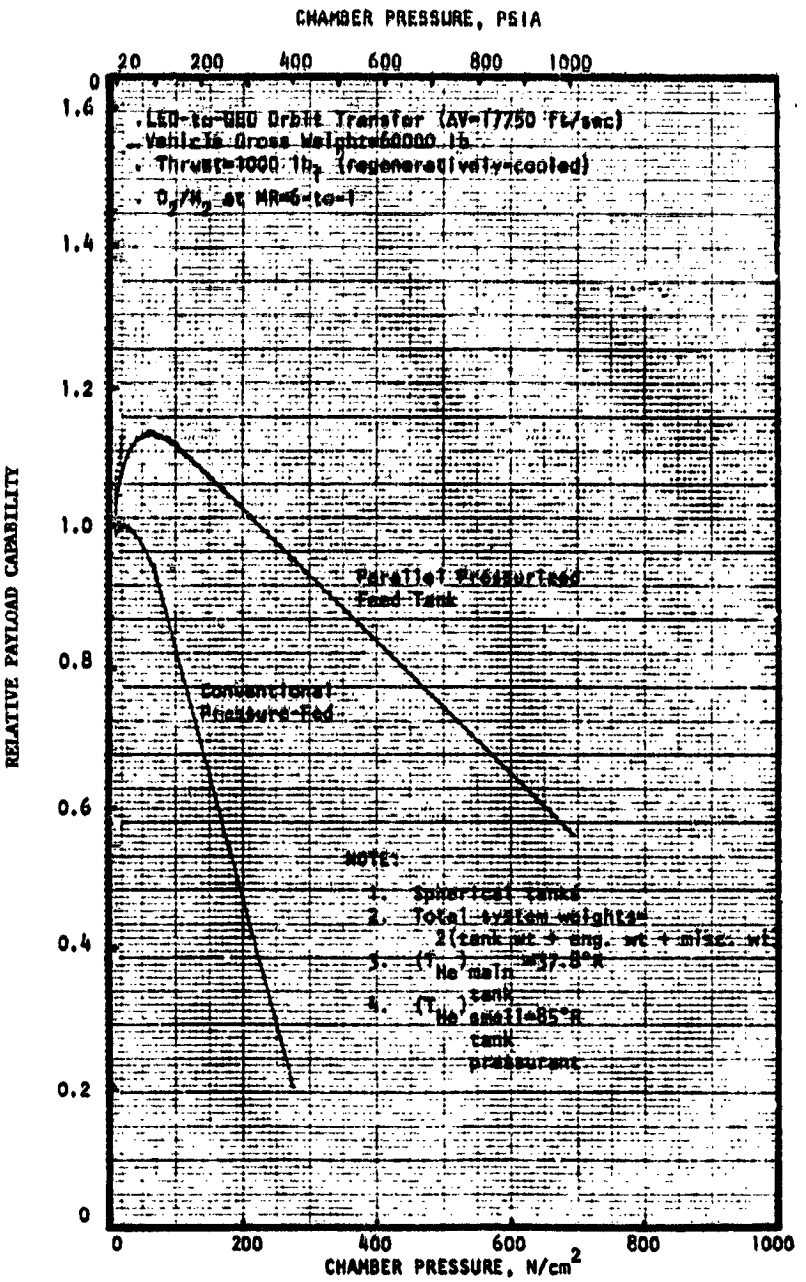

Figure 72. Relative Payload Capability - Low Temperature Pressurant (LO_2/H_2 at 4448.2 N or 1000 lbf)

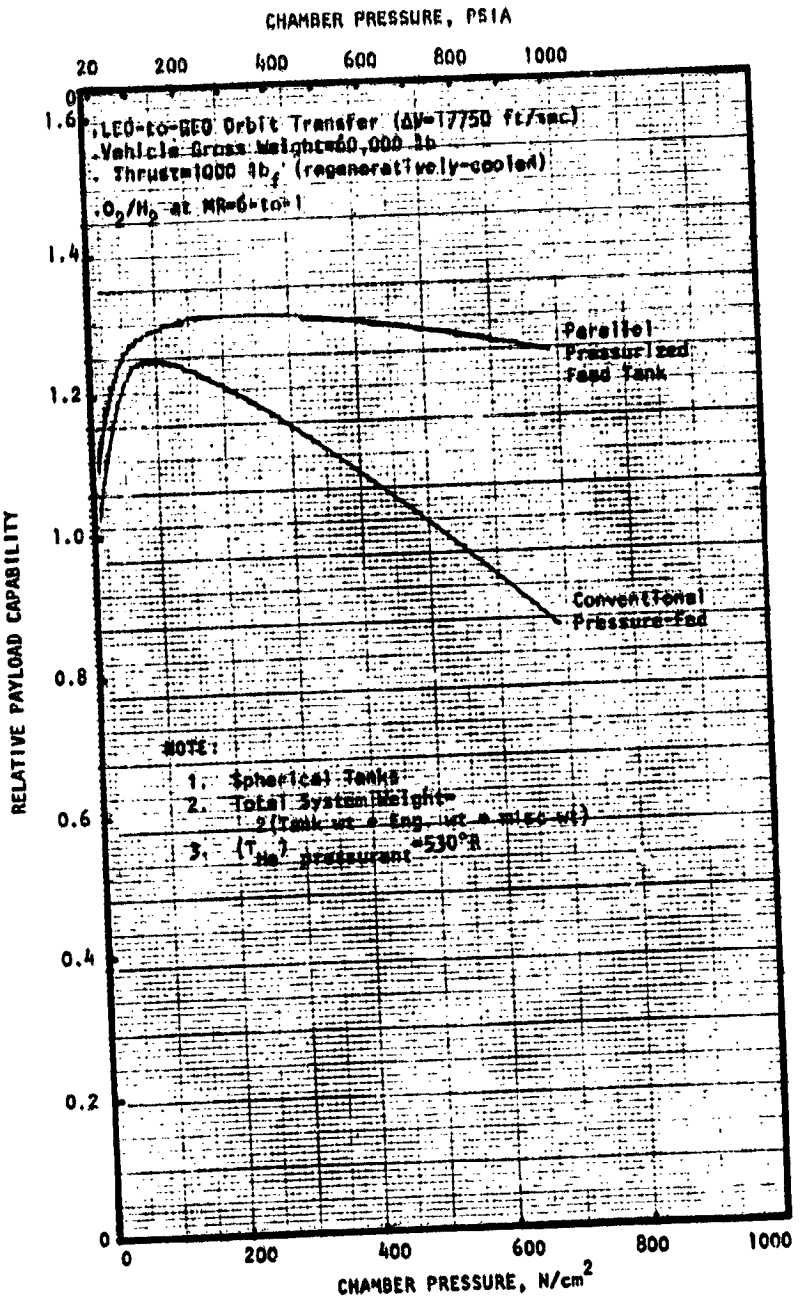

Figure 73. Relative Payload Capability - Heated Pressurant (LO_2/H_2 at 4448.2 N or 1000 lbf)

in payload and a shift of optimum chamber pressure to higher values than for the low temperature pressurant case. In view of the higher payload capability, the optimum chamber pressures shown in Fig. 73 were utilized as design points in the evaluation of candidate engine systems.

Pump-Fed Engine Cycle/Performance Summary. Results from the pump-fed engine cycle analyses were superimposed on performance curves as shown in Figs. 74 and 75. The resulting curves show the delivered specific impulse potential for the various engine configurations over the permissible design range of thrust and chamber pressure. As indicated in the figures, the highest delivered specific impulse for each of the engine systems occurs at the maximum study thrust level of 13345 N (3000 lbf).

For the LO_2/H_2 engines, the fuel-cell powered cycle achieved the highest specific impulse followed by the staged combustion cycle and the direct expander cycle (Fig. 74). Also, for the LO_2/CH_4 engines, the fuel-cell powered cycle achieved the highest specific impulse followed by the direct expander cycle and the tank mounted pump expander cycle (Fig. 75).

The curves also show a decrease in delivered specific impulse as thrust is reduced along the power limit line for each of the engine systems. This trend is due to an increase in the reaction kinetic and boundary layer losses at the low thrust levels. For the LO_2/H_2 direct expander cycle engine, this specific impulse decrease was approximately 1% from 13345 N (3000 lbf) to 2224.1 N (500 lbf) thrust and almost 3% for LO_2/CH_4 over this same thrust range. It can also be observed that engine power (as opposed to cooling) limits the maximum achievable delivered impulse except at very low thrust levels. This is due primarily to the low pump efficiencies at the moderate required pump discharge pressure and the low propellant flowrates. At extremely low thrusts, the thrust chamber cooling may limit the engine design.

Engine Cycle/Configuration Evaluation

In evaluating and comparing the candidate engine cycle/configurations, six parameters were compared at a selected thrust level. These parameters included:

1. "Design" chamber pressure
2. Delivered specific impulse
3. Engine length
4. Cooling margin
5. Engine weight
6. Engine cycle/configuration complexity

The design chamber pressure was based on different criteria for each engine cycle/configuration. For expander-type cycles, the maximum achievable chamber pressure for the particular cycle was used. The chamber pressure resulting in the maximum delivered specific impulse at the chosen thrust level was selected for the gas generator cycle engine. For the pressure-fed engine configurations, the chamber pressure achieving the maximum payload was used.

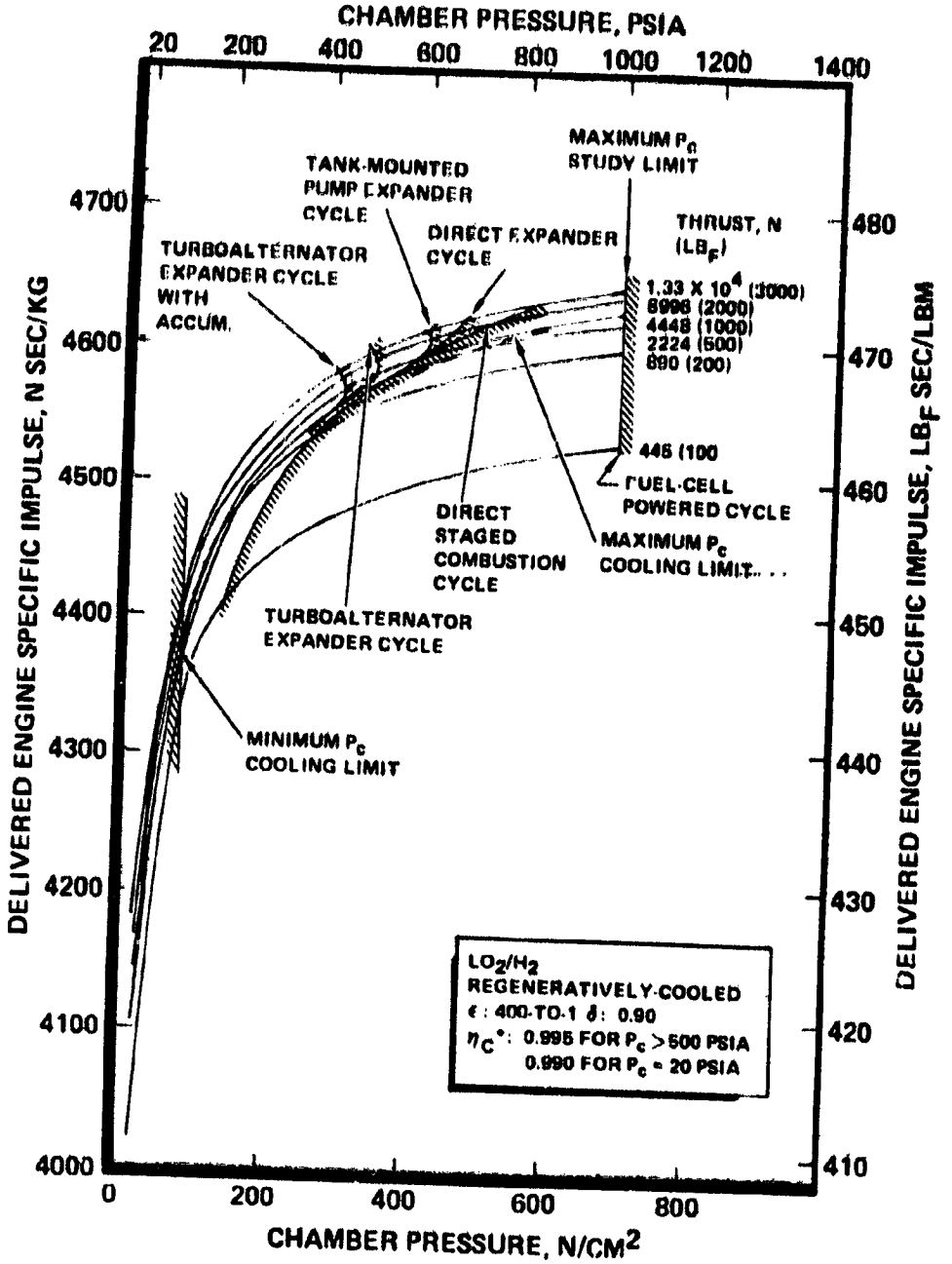

FIGURE 74. LO_2/H_2 REGENERATIVELY - COOLED PUMP-FED ENGINE DELIVERED SPECIFIC IMPULSE (COOLING AND CYCLE LIMITS SUPERIMPOSED)

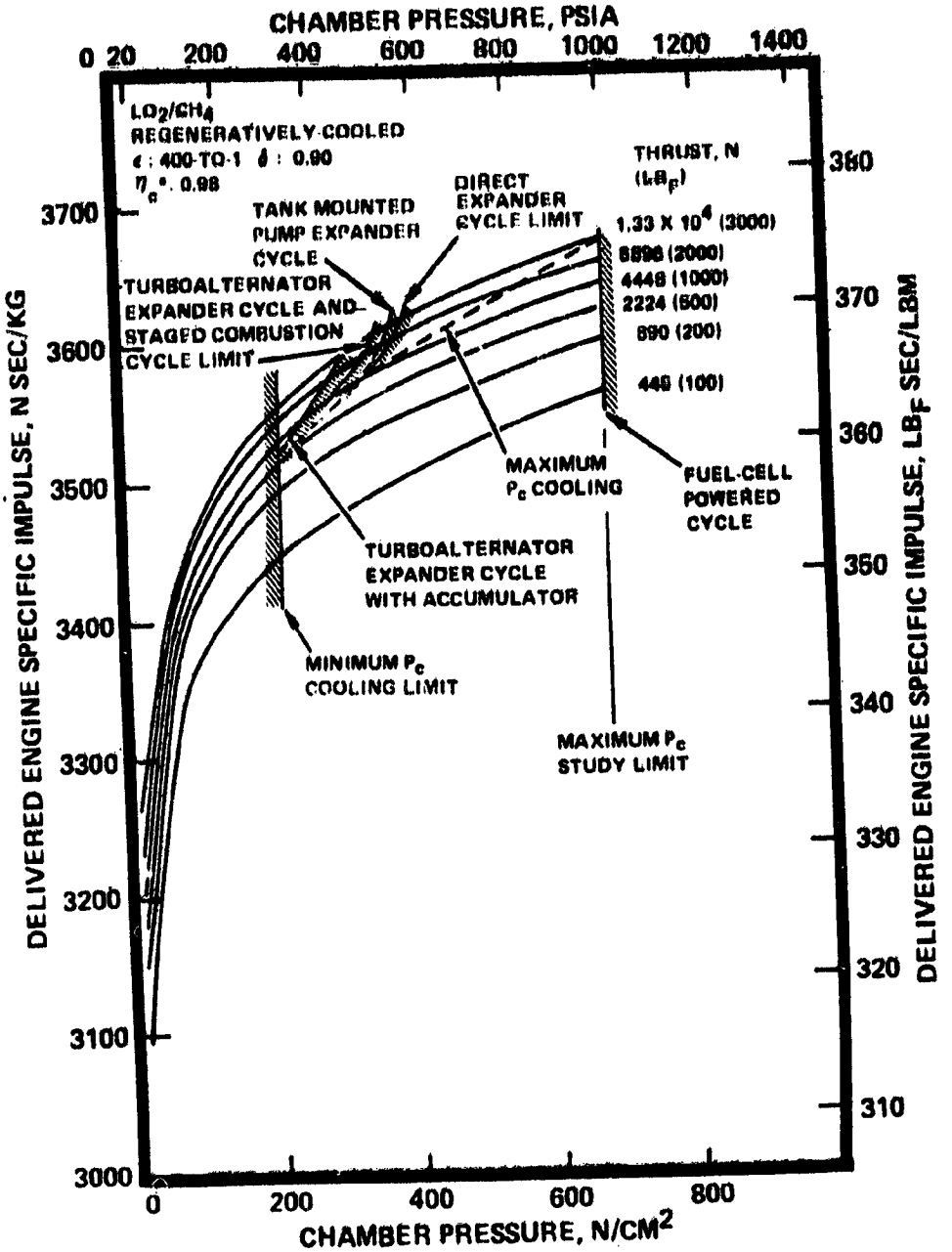

FIGURE 75. LO_2/CH_4 REGENERATIVELY - COOLED PUMP-FED ENGINE DELIVERED SPECIFIC IMPULSE (COOLING AND CYCLE LIMITS SUPERIMPOSED)

To determine a quantitative indication of the complexity of each engine cycle/configuration, the number of components and the component's relative complexity for each engine were determined as shown in Table 12. These individual component complexity factors were used in combination with the respective engine cycle schematic to determine the complexity of each engine cycle/configuration.

In selecting the engine cycle/configurations to be recommended for the engine system preliminary design effort, a relative comparison was performed. The four parameters selected for this relative comparison were:

1. Design chamber pressure
2. Delivered specific impulse
3. Engine weight
4. Engine complexity

The engine length and the cooling margin were not included since the chamber pressure determines the engine length (fixed thrust) and since the thrust chamber cooling margin factors were all less than 1.0 (no cooling problems envisioned).

The value of each of these four parameters were transformed into normalized factors using as references the highest chamber pressure, the highest delivered specific impulse, the lowest engine weight, and the lowest complexity rating. These normalized factors were weighted equally and summed to obtain a total engine cycle/configuration rating. A high total rating is desirable.

LO_2/H_2 Engine Cycle/Configuration. The engine cycle/configuration comparison of the nine candidates for the LO_2/H_2 engine are shown in Table 13 for a thrust level of 4448.2 N (1000 lbf). The fuel cell-powered cycle achieved the highest chamber pressure [689.5 N/cm^2 (1000 psia)] and the highest specific impulse [4631.6 N sec/kg (472.29 lbs sec/lbm)] but also was the heaviest engine (by at least an order of magnitude) and the most complex. As expected, the conventional pressure-fed engine configuration was the simplest cycle (lowest complexity rating), but also had the lowest design chamber pressure and the lowest specific impulse.

These parameters are presented in a composite bar graph in Fig. 76 . The configuration variations of the direct expander cycle resulted in lower design chamber pressures (lower specific impulses) and the additional components required increased engine weight. The parallel pressurized feed tank configuation achieved a higher specific impulse (higher chamber pressure for maximum payload weight) and a lower engine weight than the conventional pressure fed but a significantly more complex engine.

The relative engine cycle/configuration comparison for the 4448.2 N (1000 lbf) thrust LO_2/H_2 engine is presented in Table 14. These results indicated that the direct expander cycle/configuration achieved the highest total rating. The expander cycle achieved the second highest specific impulse factor, the third highest engine weight factor, the fourth highest chamber pressure factor, and the second highest complexity factor to result in the highest total rating.

TABLE 12. INDIVIDUAL COMPONENT COMPLEXITY

COMPONENT			COMPLEXITY
1. Injector - regular	H_2	(Coax)	.6
	CH_4	(Coax)	.6
	RP-1	(Doublet)	.5
2. Injector - Staged Comb.	H_2	(Coax)	.7
	CH_4	(Coax)	.7
	RP-1		.6
3. Chamber - regen	H_2		1
	CH_4		1
4. Chamber - Film cool (Single inj. ring)	H_2		.3
	RP-1		.3
5. Nozzle-radiation-fixed			.3
6. Nozzle-radiation-retractable			5.0
7. Gas generator	H_2		.3
	CH_4		.3
	RP-1		.3
8. Preburner	H_2		.3
	CH_4		.3
	RP-1		.3
9. Ignition System-main inj.			1.3
10. Ignition system-GG or Preburner			.6
11. Tank Pressurization	HEX		.3

TABLE 12. (Continued)

COMPONENT		COMPLEXITY
12. Turbine - Self contained		1
- Integral with pump		.5
13. Gearbox nozzle extention		.5
14. Main fuel pump-centrifugal	H_2	1.2
	CH_4	1.1
	RP-1	1
15. Main fuel pump-positive disp.	H_2	1.2
	CH_4	1.1
	RP-1	.5
16. Fuel boost pump	H_2	1
	CH_4	1
	RP-1	1
17. Main oxid. pump-centrifugal		1
18. Oxid. boost pump		1
19. Alternator		1
20. Electric motor		1
21. Power conditioner/controller		1
22. Fuel cell system		25.0
23. Additional H_2 feed system for fuel cell system (use with CH_4 or RP-1 eng.)		4.6
24. Fuel parallel press. tanks Assume: NO positive expulsion Devices required	H_2	.3
	CH_4	.3
	RP-1	.1
25. Oxid. parallel press. tanks		.3
Valve-Relief		.2
Accumulator - O_2, H_2 or CH_4		.3

TABLE 12 . (Concluded)

COMPONENT			COMPLEXITY	
26. Valve - control/on-off	Electric motor or pneumatic		1	
27. Valve - solenoid			.2	
28. Valve - check			.1	
29. Valave - pressure reg.			.3	
			Short Eng. Mount	Long Tank Mount
30. Main Duct - rigid	H_2		.1	.3
	CH_4		.1	.3
	RP-1		.1	.3
	O_2		.1	.3
	Hot gas		.2	.6
31. Main duct - gimbaled	H_2		.3	.5
	CH_4		.3	.5
	RP-1		.3	.5
	O_2		.3	.5
	Hot gas		.4	.8
32. Small duct - gimbaled			.1	
33. Power transmission circuit			.1	
34. TVC System			2.8	
35. Engine controller and instrumentation and wiring harnesses function=any component that requires A control input Valve Ignition Igniter Motor controller TVC actuators	1+.2x(#functions)			
	3 function		1.6	
	5		2.0	
	10		3.0	
	15		4.0	
	20		5.0	
	25		6.0	
	30		7.0	

TABLE 13. LO_2/H_2 ENGINE CYCLE/CONFIGURATION COMPARISON AT 4448.2 NEWTONS (1000 lb_f) THRUST

PROPELLANT LO_2/H_2
MR = 6
ϵ = 400
F = 4448.2 N (1000 lb_f)

ENGINE CYCLE / CONFIGURATION / PARAMETER	DIRECT EXPANDER	TANK-MOUNTED PUMP EXPANDER	TURBOALTERNATOR EXPANDER	TURBOALTERNATOR EXPANDER WITH ACCUM.	FUEL-CELL POWERED	DIRECT STAGED COMBUSTION	GAS GENERATOR	CONVENTIONAL PRESSURE FED	PARALLEL PRESSURIZED FEED TANK
MAXIMUM P_c N/cm^2 (PSIA)	404.6 (586.8)	404.0 (586.88)	327.4 (474.78)	311.7 (452.09)	689.5 (1000)	415.4 (602.43)	413.7[1] (600)	89.5[2] (130)	241.3[2] (350)
$I_{s_{DEL}}$ N-sec/Kg (lb_f-sec/lb_m)	4597.6 (468.82)	4597.6 (468.82)	4576.3 (466.65)	4569.6 (465.97)	4631.6 (472.29)	4599.2 (468.98)	4612.8 (470.28)	4432.6 (452)	4548.3 (463.8)
TOTAL ENGINE LENGTH, cm (in)	110.0 (43.32)	110.1 (43.36)	119.9 (47.21)	122.4 (48.18)	89.6 (35.28)	108.9 (42.87)	107.7 (42.40)	211.6 (83.3)	135.6 (53.4)
COOLING MARGIN, $P_c/(P_{c_{max}} - \Delta P_{COOL})$	0.587	0.586	0.475	0.452	1.0	0.602	0.600	0.130	0.350
ENGINE WEIGHT, Kg (lb)	31.8 (69.8)	35.3 (77.8)	44.0 (97.1)	44.2 (97.4)	934.1 (2059.4)	31.3 (69.0)	31.3 (69)	74.8 (165)	38.3 (84.5)
COMPLEXITY RATING	24.6[3]	26.8[3]	33.4[3]	36.7[3]	50.4[3]	27.7[3]	28.7[3]	12.7	25.5

NOTES
(1) MAXIMUM I_{sp} CONDITION
(2) MAXIMUM PAYLOAD CONDITION
(3) WITH RETRACTABLE NOZZLE
(SUBTRACT 4.7 FOR FIXED NOZZLE)

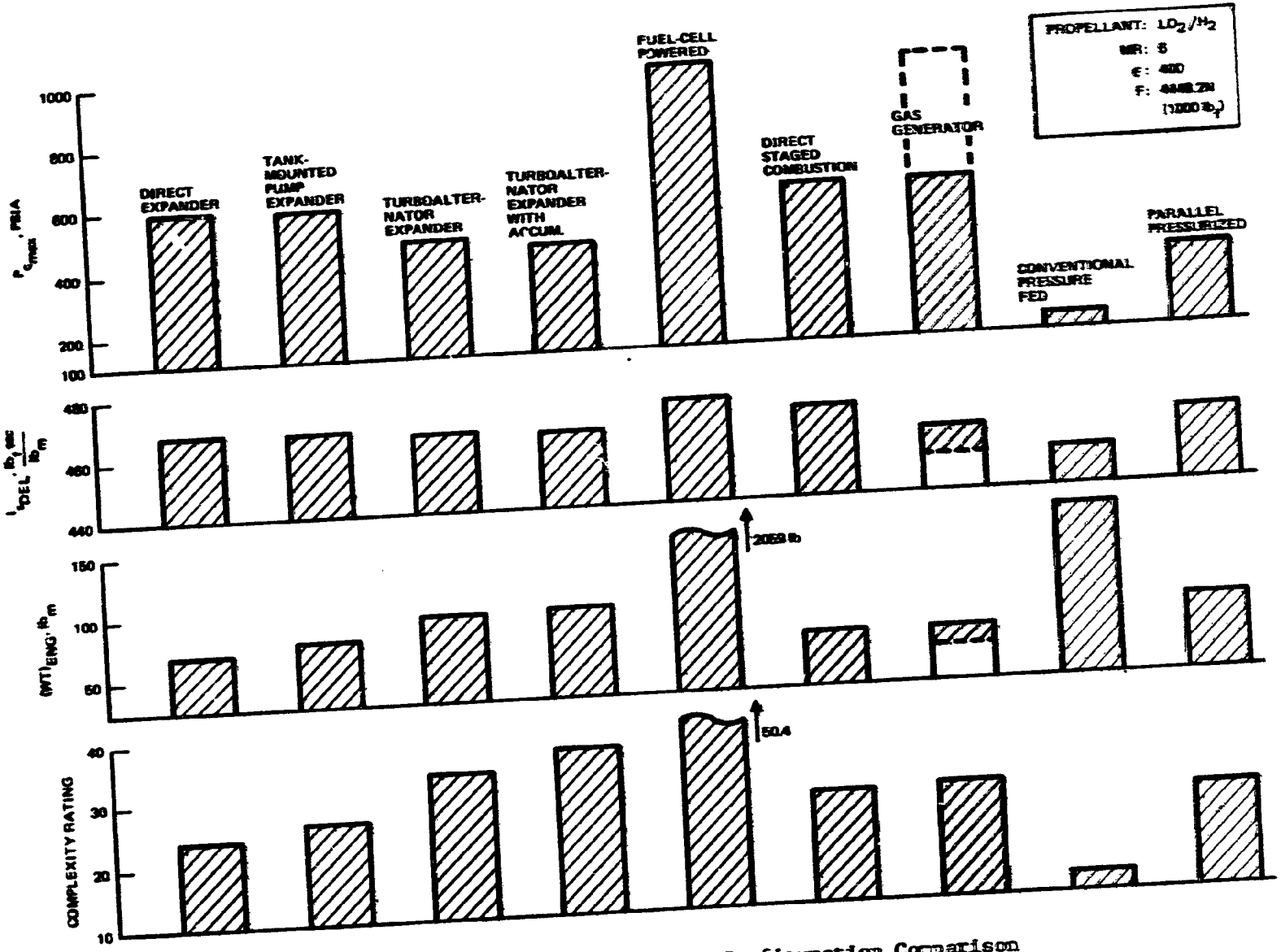

Figure 76 . LO_2/H_2 Engine Cycle Configuration Comparison At 4448.2 Newtons (1000 lb_f Thrust

TABLE 14. LO_2/H_2 ENGINE CYCLE/CONFIGURATION RATING COMPARISON AT 4448.2 NEWTONS (1000 lb_f) THRUST

PROPELLANT: LO_2 H_2
MR: 6
ϵ: 400
F: 4448.2N (1000 lb_f)

FACTOR \ ENGINE CYCLE / CONFIGURATION	DIRECT EXPANDER	TANK-MOUNTED PUMP EXPANDER	TURBO-ALTERNATOR EXPANDER	TURBO-ALTERNATOR EXPANDER WITH ACCUM.	FUEL-CELL POWERED	DIRECT STAGED COMBUSTION	GAS GENERATOR	CONVENTIONAL PRESSURE-FED	PARALLEL PRESSURIZED FEED TANK
$P_{c_{max}}$ FACTOR	0.596	0.586	0.475	0.452	1.0	0.602	0.600	0.130	0.350
$I_{s_{DEL.}}$ FACTOR	0.993	0.993	0.988	0.987	1.0	0.993	0.974	0.957	0.982
ENGINE WEIGHT FACTOR	0.990	0.886	0.709	0.708	0.034	1.0	0.999	0.418	0.815
COMPLEXITY FACTOR	0.516	0.474	0.380	0.346	0.252	0.458	0.443	1.0	0.479
TOTAL RATING FACTOR (ASSUMED EQUAL WEIGHTING)	3.085	2.939	2.552	2.493	2.286	3.054	3.016	2.505	2.626

The LO_2/H_2 engine cycle/configuration comparison for a design thrust of 2224.1 N (500 lbf) is summarized in Table 15 and 16. Again the direct expander cycle achieved the highest overall rating. Therefore, the direct expander cycle/configuration was selected as the LO_2/H_2 engine to be recommended for preliminary engine design evaluation.

LO_2/Hydrocarbon Engine Cycle/Configuration. The parameter comparison for the LO_2/hydrocarbon engines is presented in Table 17 and Fig. 77 for a thrust of 4448.2 N (1000 lbf). Both LO_2/CH_4 and LO_2/RP-1 engines were evaluated. Pressure-fed engines were not evaluated since low chamber pressure operation for both of these propellants was extremely limited due to thrust chamber cooling difficulties. The only LO_2/RP-1 engine cycle/configuration evaluated was the gas generator cycle. This configuration was made feasible (thrust chamber cooling) by assuming the existence of a gas-side carbon layer.

Overall engine cycle/configuration rating results were similar to those previously presented for LO_2/H_2. As shown in Table 18, the LO_2/CH_4 direct expander cycle engine achieved the highest total rating. Also noted in Table 18 was that the LO_2/CH_4 gas generator cycle engine resulted in a higher total rating than the LO_2/RP-1 gas generator cycle engine due to higher rating factors in all categories except engine complexity. Based on these comparison results, the LO_2/CH_4 direct expander cycle/configuration was selected as the LO_2/hydrocarbon engine to be recommended for preliminary engine design evaluation.

Design Point Thrust. In selecting the design thrust for the preliminary design of the two engine cycle/configurations, the delivered specific impulse variation with thrust on the engine cycle limit was evaluated. The data of Figs. 74 and 75 were replotted in Figs. 78 and 79 for the LO_2/H_2 and LO_2/CH_4 expander cycle engines. As previously discussed, the design thrust specific impulse decreased with decrease in thrust due to increases in the reaction kinetic and boundary layer losses and the decrease in the theoretical specific impulse due to the decrease in design chamber pressure. This specific impulse trend is amplified if the engine is required to throttle. Although at the time of this study the need and benefit of engine throttling was not clear, the delivered specific impulse at a 4:1 throttled condition was determined for two throttling approaches: (1) constant chamber pressure (variable chamber throat area), and (2) constant throat area (variable chamber pressure). The obvious advantage of constant pressure throttling is clearly shown. The high chamber pressure and high nozzle area ratio ($\varepsilon = 1600$) result in increasing the delivered specific impulse to values higher than those at the design thrust condition. The specific impulse for the 4:1 throttled condition is plotted at the design thrust so that each engine is described by reading values on a vertical line (design thrust). As shown in Figs. 78 and 79, the throttled condition specific impulse values for both the LO_2/H_2 and LO_2/CH_4 engines start to sharply decrease below a design thrust of 448.2 N (1000 lbf).

TABLE 15 . LO_2/H_2 ENGINE CYCLE/CONFIGURATION COMPARISON AT 2224.1 NEWTONS (500 lb_f) THRUST

PROPELLANT: LO_2/H_2

MR: 6

ϵ: 400

F: 2224.1 N (500 lb_f)

ENGINE CYCLE / CONFIGURATION / PARAMETER	DIRECT EXPANDER	TANK-MOUNTED PUMP EXPANDER	TURBOALTERNATOR EXPANDER	TURBOALTERNATOR EXPANDER WITH ACCUM.	FUEL-CELL POWERED	DIRECT STAGED COMBUSTION	GAS GENERATOR	CONVENTIONAL PRESSURE FED	PARALLEL PRESSURIZED FEED TANK
MAXIMUM P_c N/cm^2 (PSIA)	342.8 (497.17)	342.8 (497.17)	268.6 (389.58)	267.5 (388.03)	689.5 (1000)	330.3 (479.04)	275.8[1] (400)	89.6[2] (130)	241.3[2] (350)
$I_{s_{DEL}}$ · $\frac{N\text{sec}}{Kg}$ (lb_f sec/lb_m)	4575.7 (466.60)	4575.7 (466.59)	4545.9 (463.55)	4545.4 (463.50)	4623.8 (471.5)	4570.7 (466.08)	4448.6 (453.63)	4427.7 (451.5)	4542.4 (463.2)
TOTAL ENGINE LENGTH, cm (in)	89.3 (35.17)	89.3 (35.17)	98.3 (38.71)	98.5 (38.77)	68.6 (27.0)	90.6 (35.68)	96.1 (37.85)	157.0 (61.8)	102.9 (40.5)
COOLING MARGIN, $P_c/P_{c_{max}}$ COOL	0.765	0.765	0.569	0.597	1.538 (1.0)[3]	0.765	0.615	0.200	0.539
ENGINE WEIGHT, Kg (lb)	24.4 (53.8)	28.1 (62.97)	32.9 (72.62)	33.1 (72.91)	1392.0 (3068.8)	24.7 (54.50)	27.1 (59.7)	51.0 (112.5)	29.4 (64.7)
COMPLEXITY RATING	24.6[4]	26.0[4]	33.4[4]	36.7[4]	50.4[4]	27.2[4]	28.7[4]	12.7	28.5

NOTES:

(1) MAXIMUM I_{sp} CONDITION

(2) ASSUMED SAME P_c AS FOR 1000 lb_f THRUST

(3) FOR EXTENDED COOLING LIMIT

(4) WITH RETRACTABLE NOZZLE
(SUBTRACT 4.7 FOR FIXED NOZZLE)

TABLE 16 . LO_2/H_2 ENGINE CYCLE/CONFIGURATION RATING COMPARISON AT 2224.1 NEWTONS (500 lb_f) THRUST

PROPELLANT: LO_2 H_2
MR: 6
ϵ: 400
F: 2224.1 N (500 lb_f)

ENGINE CYCLE/ CONFIGURATION / FACTOR	DIRECT EXPANDER	TANK-MOUNTED PUMP EXPANDER	TURBO-ALTERNATOR EXPANDER	TURBO-ALTERNATOR EXPANDER WITH ACCUM.	FUEL-CELL POWERED	DIRECT STAGED COMBUSTION	GAS GENERATOR	CONVENTIONAL PRESSURE-FED	PARALLEL PRESSURIZED FEED TANK
$P_{c_{max}}$ FACTOR	0.497	0.497	0.390	0.388	1.0	0.479	0.400	0.130	0.35
$I_{s_{DEL.}}$ FACTOR	0.990	0.990	0.983	0.983	1.0	0.989	0.982	0.958	0.982
ENGINE WEIGHT FACTOR	1.0	0.868	0.741	0.738	0.018	0.987	0.900	0.478	0.832
COMPLEXITY FACTOR	0.516	0.474	0.380	0.348	0.252	0.459	0.443	1.0	0.479
TOTAL RATING FACTOR (ASSUMED EQUAL WEIGHTING)	3.003	2.829	2.494	2.455	2.27	2.914	2.705	2.566	2.643

TABLE 17 . LO_2/HYDROCARBON ENGINE CYCLE/CONFIGURATION COMPARISON AT 4448.2 NEWTONS (1000 lb_f) THRUST

PROPELLANT: LO_2/CH_4 AND LO_2/RP-1
MR: 3.7 AND 3.0
ϵ: 400
F: 4448.2 N (1000 lb_f) ——— LO_2/CH_4 ——— LO_2/RP-1

ENGINE CYCLE / CONFIGURATION / PARAMETER	DIRECT EXPANDER	TANK-MOUNTED PUMP EXPANDER	TURBOALTER-NATOR EXPANDER	TURBOALTER-NATOR EXPANDER WITH ACCUM.	FUEL-CELL POWERED	DIRECT STAGED COMBUSTION	GAS GENERATOR	GAS GENERATOR
MAXIMUM P_c, N/cm^2 (PSIA)	337.8 (489.84)	337.5 (489.51)	288.2 (418.43)	273.4 (396.48)	689.5 (1000)	313.3 (454.41)	344.7[1] (500)	227.5[1] (330)
$I_{sDEL.}$. $\frac{Nsec\ (lb_f\ sec/lb_m)}{Kg}$	3674.1 (364.48)	3671.1 (364.48)	3653.1 (362.31)	3648.1 (361.8)	3843.4 (371.52)	3683.6 (363.38)	3663.5 (361.14)	3386.7 (335.15)
TOTAL ENGINE LENGTH, cm (in)	120.0 (47.28)	120.0 (47.28)	128.0 (50.39)	131.0 (51.58)	81.0 (38.82)	123.8 (48.74)	117.3 (46.19)	104 (40.6)
COOLING MARGIN, $P_c/(P_{c_{max}})_{COOL}$	0.979	0.979	0.839	0.783	2.0 (1.0)[2]	0.909	1.0	0.880
ENGINE WEIGHT, Kg (lb)	33.7 (74)	37.3 (82.2)	41.5 (91.4)	43.1 (94.9)	612.1 (1349.5)	34.7 (76.4)	33.3 (73.4)	41.3 (91.0)
COMPLEXITY RATING	24.5[3]	26.7[3]	33.3[3]	36.6[3]	60.3[3]	27.6[3]	28.6[3]	28.4[3]

NOTES:
(1) MAXIMUM I_{sp} CONDITION
(2) FOR EXTENDED COOLING LIMIT
(3) WITH RETRACTABLE NOZZLE
(SUBTRACT 4.7 FOR FIXED NOZZLE)

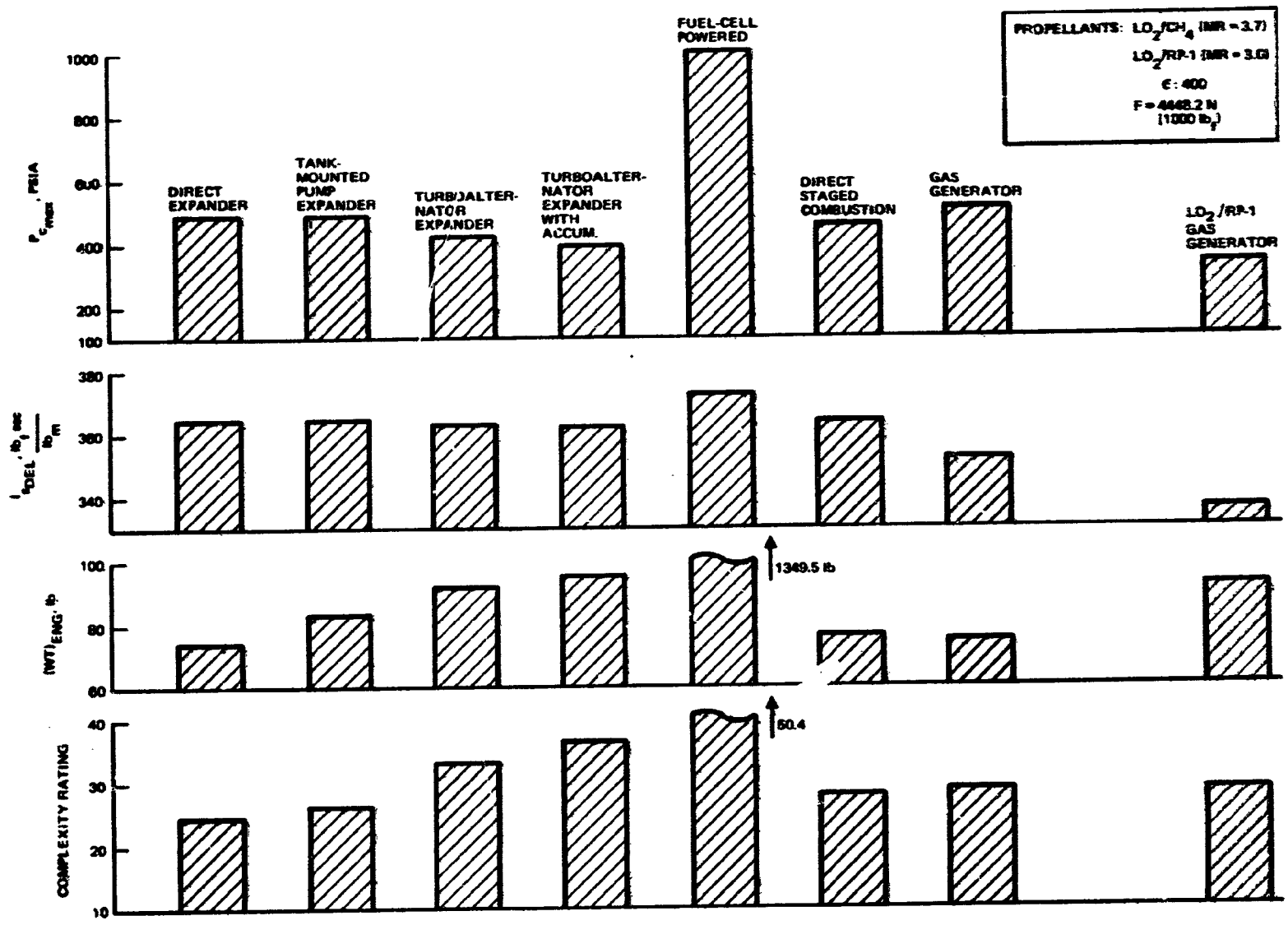

Figure 77. LO_2/Hydrocarbon Engine Cycle/Configuration Comparison at 4448.2 Newtons (1000 lb_f) Thrust

TABLE 18 . LO_2/HYDROCARBON ENGINE CYCLE/CONFIGURATION RATING COMPARISON AT 4448.2 NEWTONS (1000 lb_f) THRUST

PROPELLANT: LO_2/CH_4 AND LO_2/RP-1
MR: 3.7 AND 3.0
: 400
F: 4448.2 N(1000 lb_f)

ENGINE CYCLE/ CONFIGURATION / FACTOR	LO_2/CH_4 DIRECT EXPANDER	LO_2/CH_4 TANK-MOUNTED PUMP EXPANDER	LO_2/CH_4 TURBO-ALTERNATOR EXPANDER	LO_2/CH_4 TURBO-ALTERNATOR EXPANDER WITH ACCUM.	LO_2/CH_4 FUEL-CELL POWERED	LO_2/CH_4 DIRECT STAGED COMBUSTION	LO_2/CH_4 GAS GENERATOR	LO_2/RP-1 GAS GENERATOR
$P_{c_{max}}$ FACTOR	0.490	0.490	0.419	0.397	1.0	0.454	0.500	0.330
$I_{sDEL.}$ FACTOR	0.981	0.981	0.975	0.973	1.0	0.978	0.945	0.902
ENGINE WEIGHT FACTOR	0.992	0.893	0.803	0.774	0.054	0.961	1.0	0.807
COMPLEXITY FACTOR	1.0	0.918	0.736	0.669	0.487	0.888	0.857	0.863
TOTAL RATING FACTOR (ASSUMED EQUAL WEIGHTING)	3.463	3.282	2.933	2.813	2.541	3.281	3.302	2.902

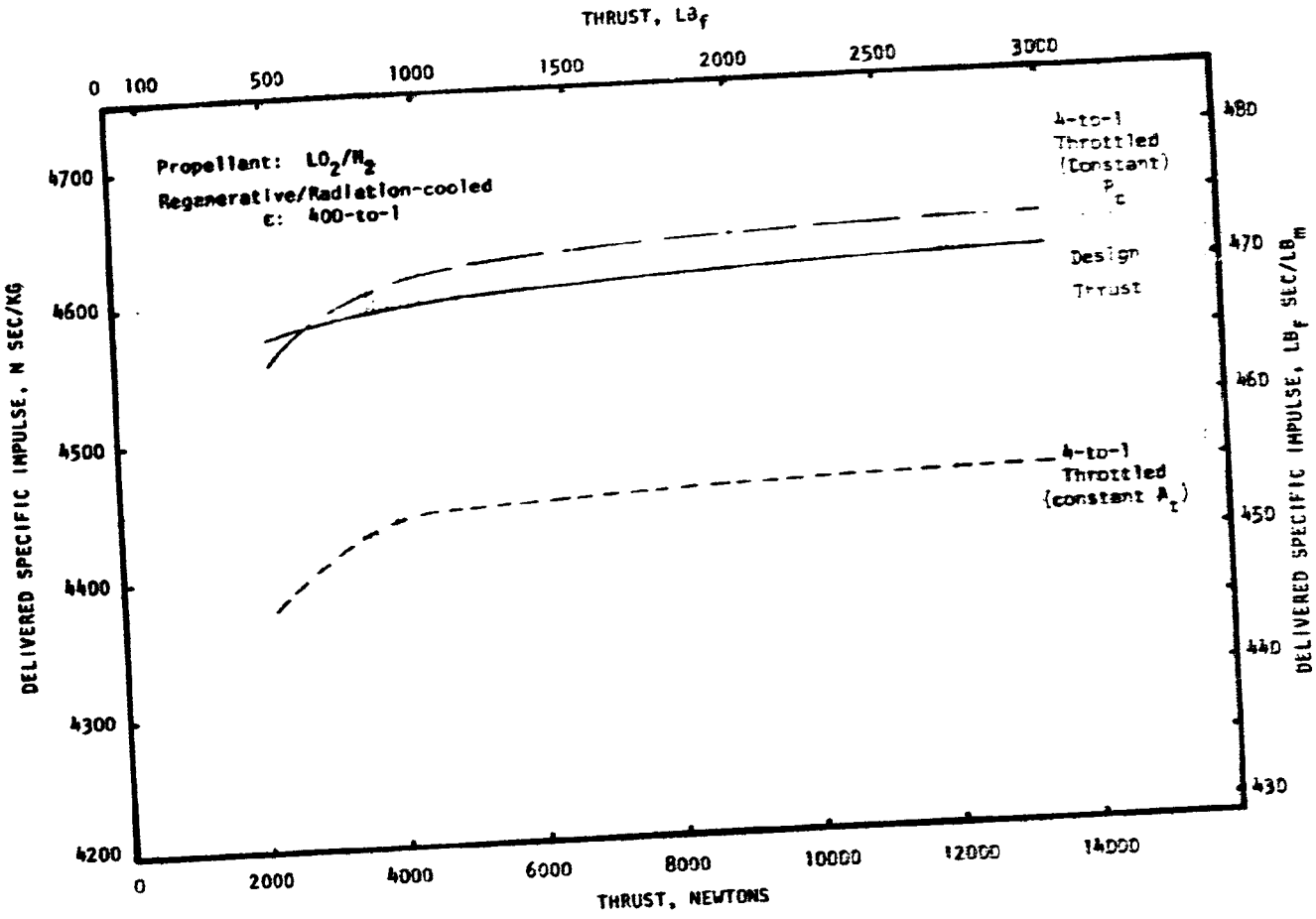

Figure 78. LO_2/H_2 Direct Expander Cycle Delivered Specific Impulse --Design Thrust (on cycle limit) and 4-to-1 Throttled Condition

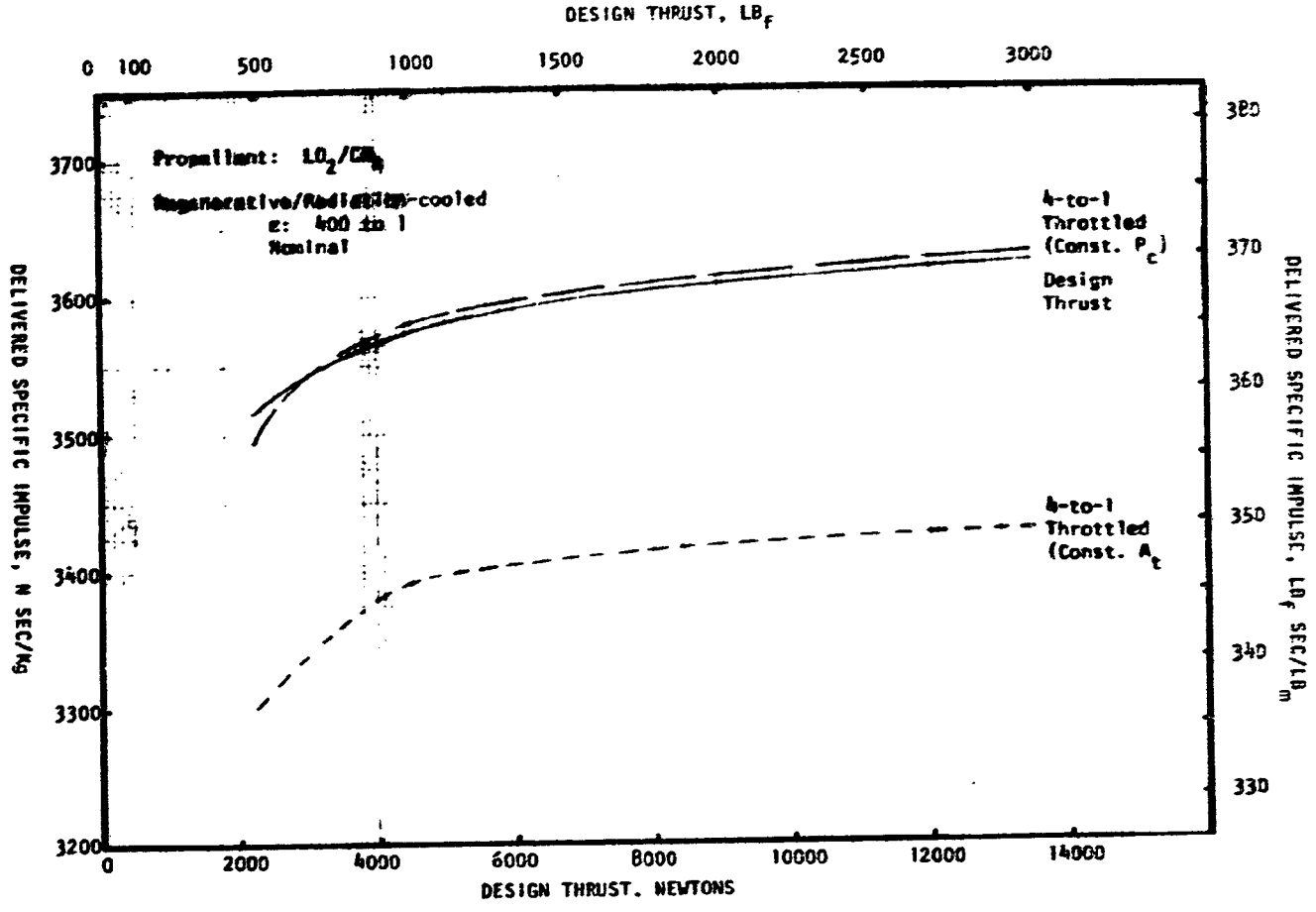

Figure 79. LO_2/CH_4 Direct Expander Cycle Delivered Specific Impulse --Design Thrust (on cycle limit) and 4-to-1 Throttled Condition

The engine cycle/configuration comparisons previously presented and the performance variation with thrust were reviewed by NASA-LeRC personnel and the two recommended engine cycle/configruations were approved for preliminary design. A design thrust of 2224.1 N (500 lbf) was selected by NASA-LeRC for the two engines.

ENGINE SYSTEM PRELIMINARY DESIGN

The approach taken in the preliminary design of the 2224.1 N (500 lbf) thrust LO_2/H_2 and LO_2/CH_4 engines was first to define engine systems which would operate at maximum chamber pressure within the design constraints of the engine system components. This was accomplished through iterations of cycle balances and engine component preliminary designs. Initial balances were used to establish component operating requirements. Component preliminary designs (e.g. pumps, turbines, thrust chamber) were generated for these requirements and their performance characteristics were defined. This information was then used in the cycle balance with iterations performed until the cycle balance output matched the performance characteristics of the component preliminary designs. Final engine cycle balances were performed at the nominal design condition and the $\pm$10% mixture ratio off-design conditions. The balances determined the delivered engine specific impulse, the conditions of each major component, and the required turbine bypass flows.

Layout drawings and/or sketches showing principle dimensions of the major components were prepared. An engine layout drawing was prepared for each engine incorporating a retractable nozzle extension to minimize engine length. Mass properties of the engines, consisting of engine weight breakdown, gimballed moments of inertia and center of gravity location, were determined. Using updated thrust chamber heat transfer data, parametric engine performance (delivered specific impulse) and engine dimension (engine length and diameter) data were gathered over a range of thrust, chamber pressure, and area ratio. In addition, parametric engine weights were generated over this same parameter range.

Guidelines and Assumptions

The major guidelines utilized in the preliminary design effort were the same as those previously presented in Table 2 (Thrust Chamber), Table 7 (Pump Stages), and Table 8 (Turbine Stages).

Since the pump and turbine efficiencies directly influence the achievable design chamber pressure for an expander cycle engine, the number of pump and turbine stages which had been utilized in the conceptual design effort was re-evaluated in an attempt to maximize chamber pressure for the preliminary designs. Results of the study indicated that an increase in the number of pump stages (one to two for the oxygen pumps and three to four for the hydrogen and methane pumps) resulted in a 15% improvement in oxygen pump efficiency and a 4% improvement in the hydrogen and methane pump efficiencies. Since no mechanical or hydrodynamic design problems were foreseen with an increase in the number of stages, two-stage oxygen pumps and four-stage fuel pumps were selected for the preliminary design configurations.

A similar study which compared two-stage, partial-admission fuel turbines with the single-stage partial-admission turbines utilized in the conceptual designs resulted in a 2% efficiency increase. However, due to the lack of previous experience with two-stage partial-admission turbines, the predicted increase was somewhat questionable and the single-stage configurations were retained.

Engine System Design

LO_2/H_2 Expander Cycle Engine.

Design Point Operating Characteristics. Performance and operating characteristics of the LO_2/H_2 engine system at the nominal design point of 2224.1 N (500 pounds) thrust and a mixture ratio of 6.0 are summarized in Table 19 and Fig. 80. The achieved design chamber pressure was 328.9 N/cm^2 (477 psia) for the nominal mixture ratio of 6. The delivered specific impulse was 4564.5 N-sec/kg (465.45 lbf-sec/lbm) for the 400-to-1 area ratio nozzle. The breakdown of the thrust chamber performance losses for this engine is presented in Fig. 81 obtained using simplified JANNAF methodology. The heat loss term is included in the one-dimensional equilibrium (ODE) specific impulse. The major performance losses were associated with the reaction kinetic loss (2.3%) and the boundary layer loss (3.3%).

Off-Design Operating Characteristics. Off-design operating characteristics for the LO_2/H_2 engine system and components at 2224.1 N (500 pounds) thrust and mixture ratios of 5.4 and 6.6 are given in Appendix C.

Engine Operation and Control. Control valves for the LO_2/H_2 engine are identified in the schematic presented in Fig. 80. Six primary engine control valves are provided. Three of these valves are modulated while the other three are on-off valves. The inlet oxidizer valve (IOV, Valve Number 2) and the inlet fuel valve (IFV, Valve Number 1) provide propellant isolation functions by isolating the engine system from the propellant feed system between firings. Propellant leakage at the pump seals determined the location of these valves just upstream of the pumps. The main oxidizer valve (MOV, Valve Number 4) and the main fuel valve (MFV, Valve Number 3) provide engine start and shutdown functions. The main oxidizer valve (MOV, Valve Number 4) and the turbine bypass valve (TBV, Valve Number 5) provide mixture ratio and thrust control. The oxidizer turbine bypass valve (OTBV, Valve Number 6) extends the mixture ratio control of the MOV at off-design thrust and mixture ratio conditions. These three valves (MOV, TBV, OTVB) are modualted valves.

Engine Layout. The component arrangement for the LO_2/H_2 engine is shown in Fig. 82. The overall engine length was 91.9 cm (36.19 inches), and the retracted engine length was 56.2 (22.13 inches). The engine diameter (nozzle exit) was 42.29 cm (16.65 inches) and with the $\pm$7 degree gimbaling requirement, the gimbal envelope diameter was 63.86 cm (25.14 inches).

As shown in Fig. 82, the turbopumps were trunnion mounted to the injector flange with a pivoting link located on the combustor outer wall to stabilize and allow some relative movement between the pump housing and the thrust chamber.

Engine Mass Properties. Using the engine component drawings and the engine design drawing, the engine weight of the LO_2/H_2 engine was 28.1 kg (62 pounds). An engine weight breakdown for this engine is presented in Table 20. The major weight contributors were the fixed nozzle, oxidizer turbopump, and the extendible nozzle. The engine center of gravity was determined to be 25.2 cm (9.92 inches) from the gimbal point with the nozzle exteded (Table 21). The component package arrangement close to the gimbal resulted in a forward center of gravity and minimized the gimbaled mass. The center of gravity moved approximately 5 cm (2 inches) closer to the gimbal point with the nozzle extension retracted. In addition, the moment of inertia of the engine about the three axes was determined as shown in Table 21.

TABLE 19. LO_2/H_2 ENGINE PERFORMANCE CHARACTERISTICS
DESIGN POINT, O/F = 6.0

Thrust, N, (lbf)	2224.1	500
Chamber Pressure, N/cm^2 (psia)	328.9	477
Engine Mixture Ratio, O/F	6.0	
Area Ratio	400	
ODE Specific Impulse, N-sec/kg (lbf-sec/lbm)	4882.7	497.9
ODE Characteristic Velocity, M/sec (ft/sec)	2334.2	7658
Specific Impulse Energy Release Efficiency, Fraction	.9950	
Specific Impulse Reaction Kinetic Efficiency, Fraction	.9774	
Specific Impulse Divergence Efficiency, Fraction	.9957	
Specific Impulse Non-Boundary Layer Heat Loss Efficiency, Fraction (1)	.9912	
Specific Impulse Boundary Layer Efficiency, Fraction	.9666	
Delivered Specific Impulse N-sec/kg (lbf-sec/lbm)	4565.0	465.5

(1) Non-Boundary Layer Heat Loss Included in ODE Specific Impulse

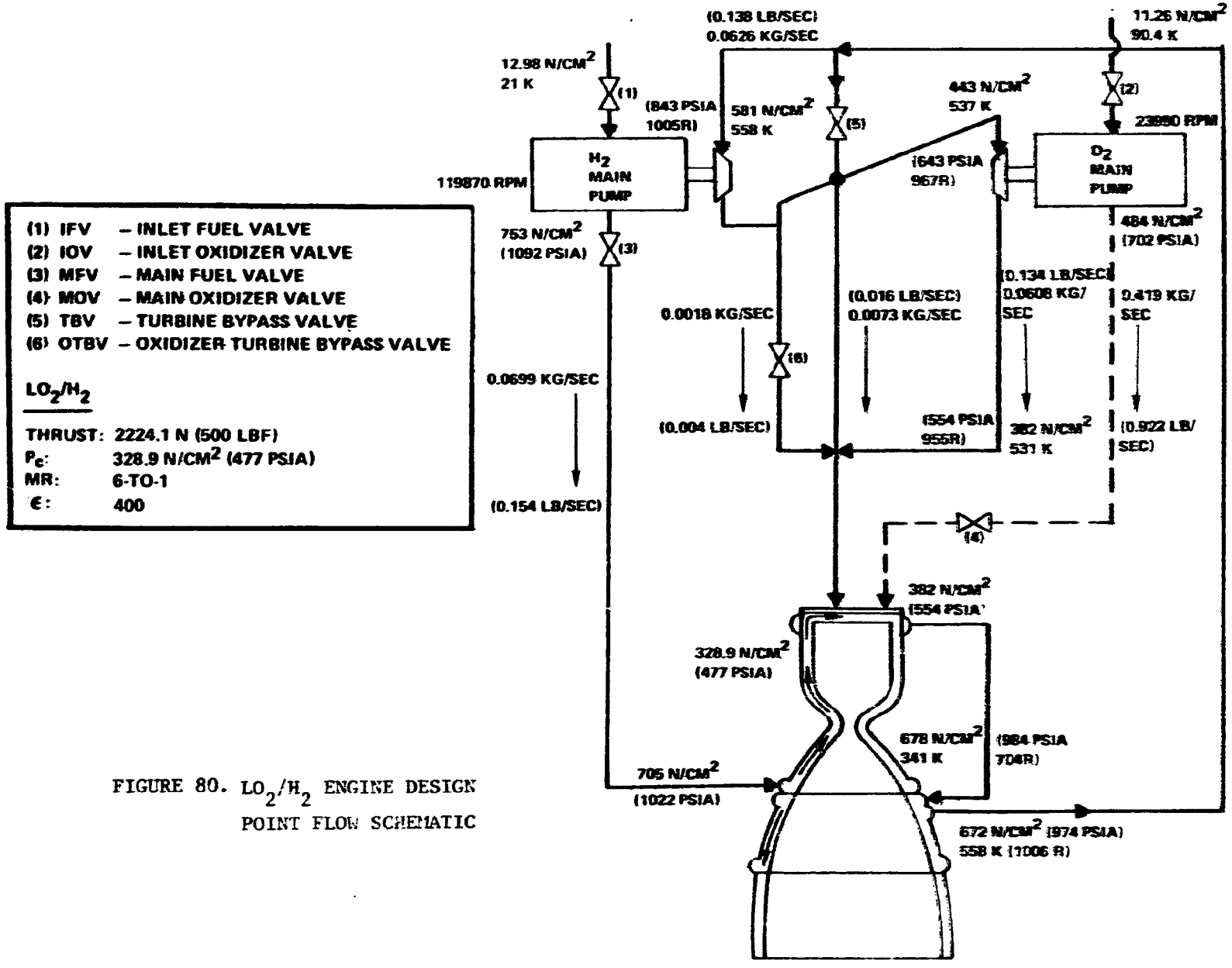

FIGURE 80. LO_2/H_2 ENGINE DESIGN POINT FLOW SCHEMATIC

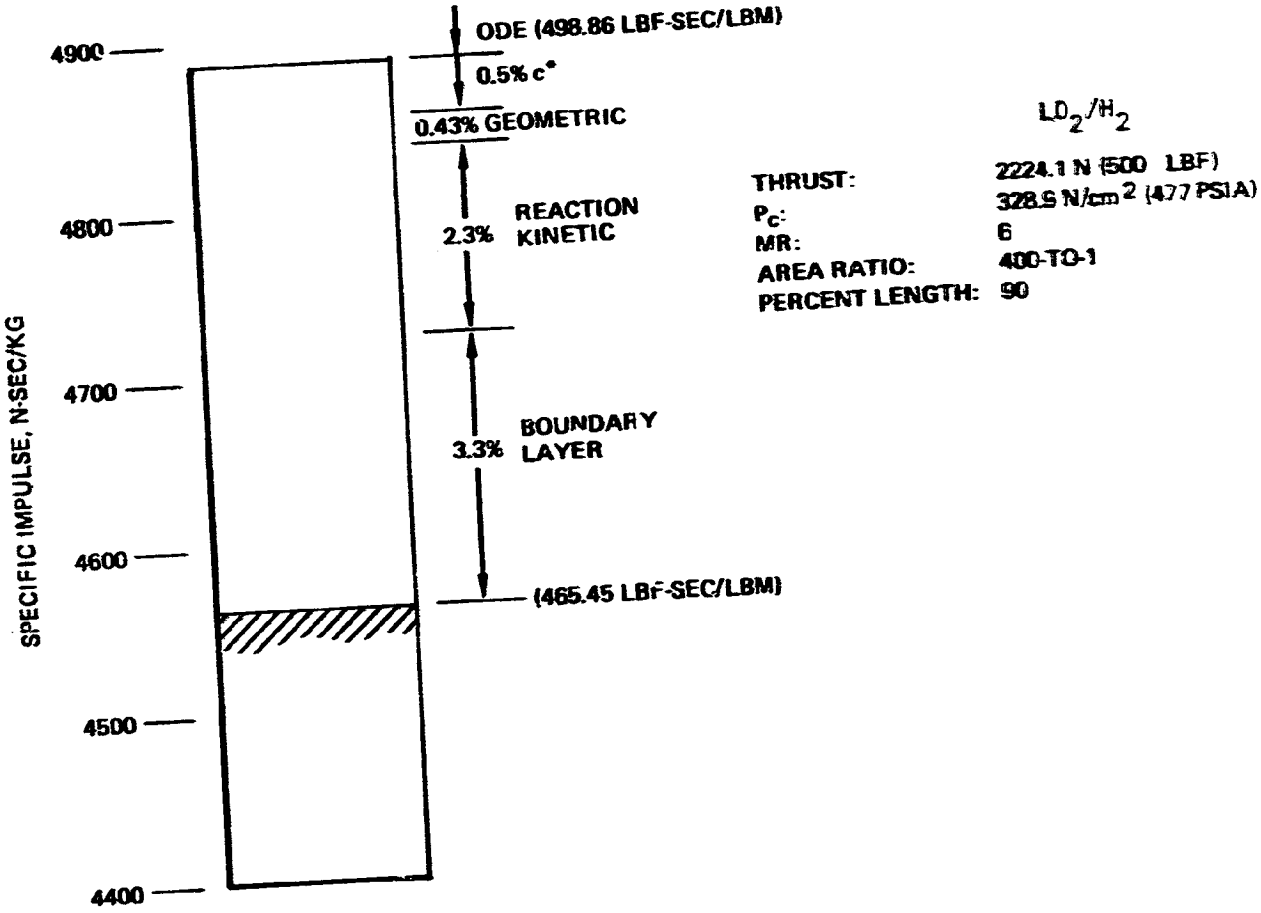

Figure 81. Performance Loss Breakdown for 2224.1 N (500 lbf) Thrust, LO_2/H_2 Expander Cycle Engine

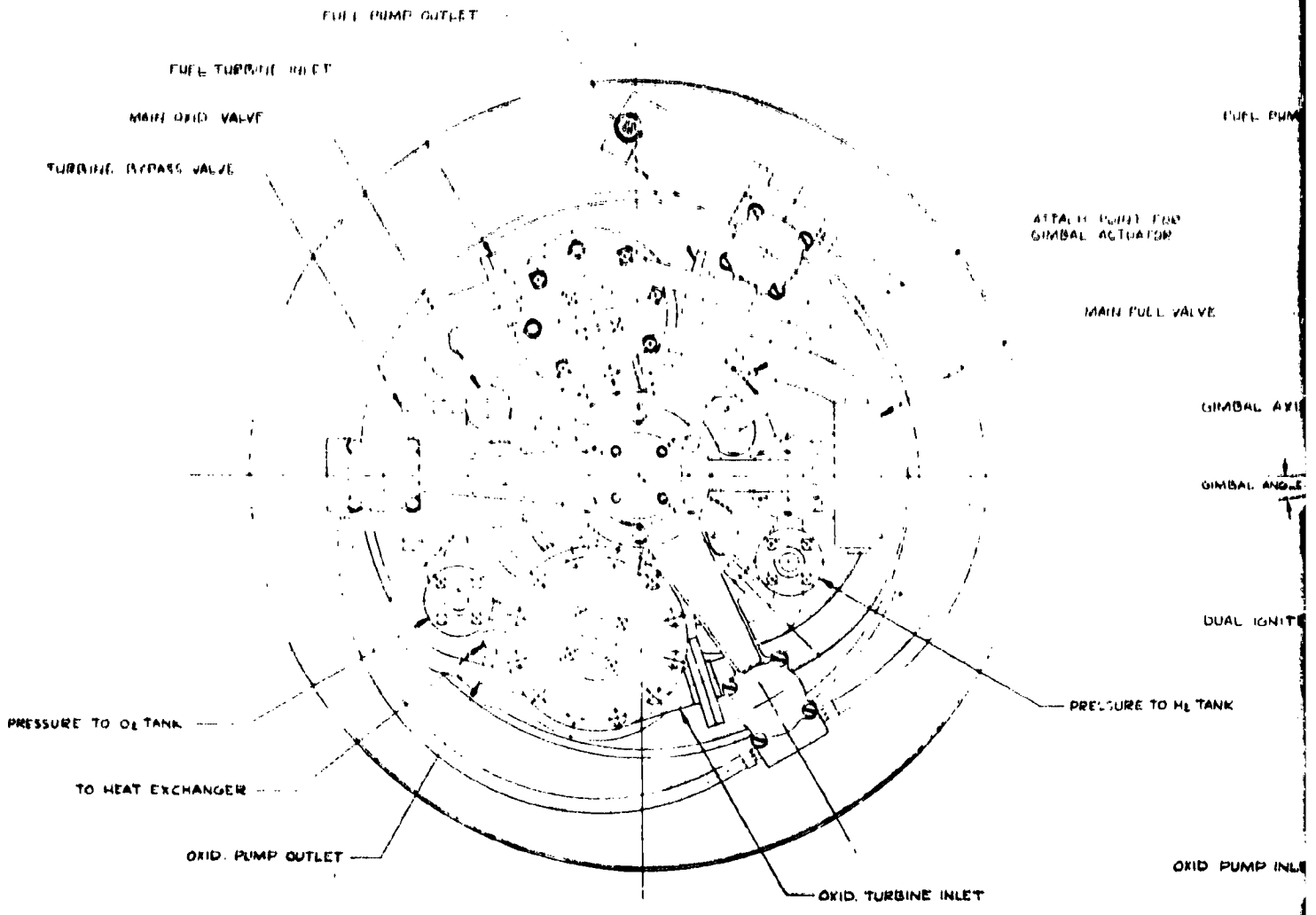

FOLDOUT FRAME

PRECEDING PAGE BLANK NOT FILMED

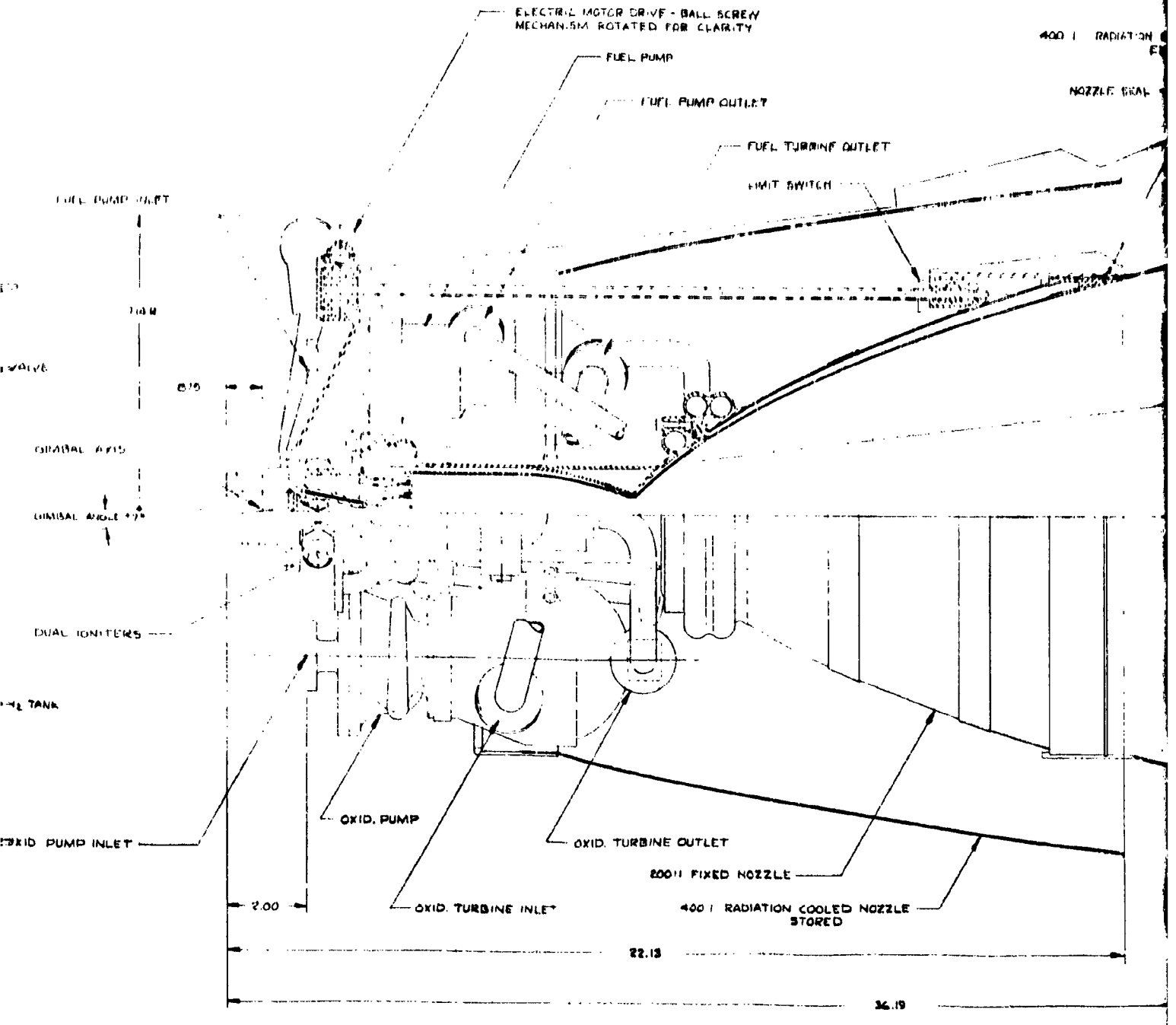

FOLDOUT FRAME 2

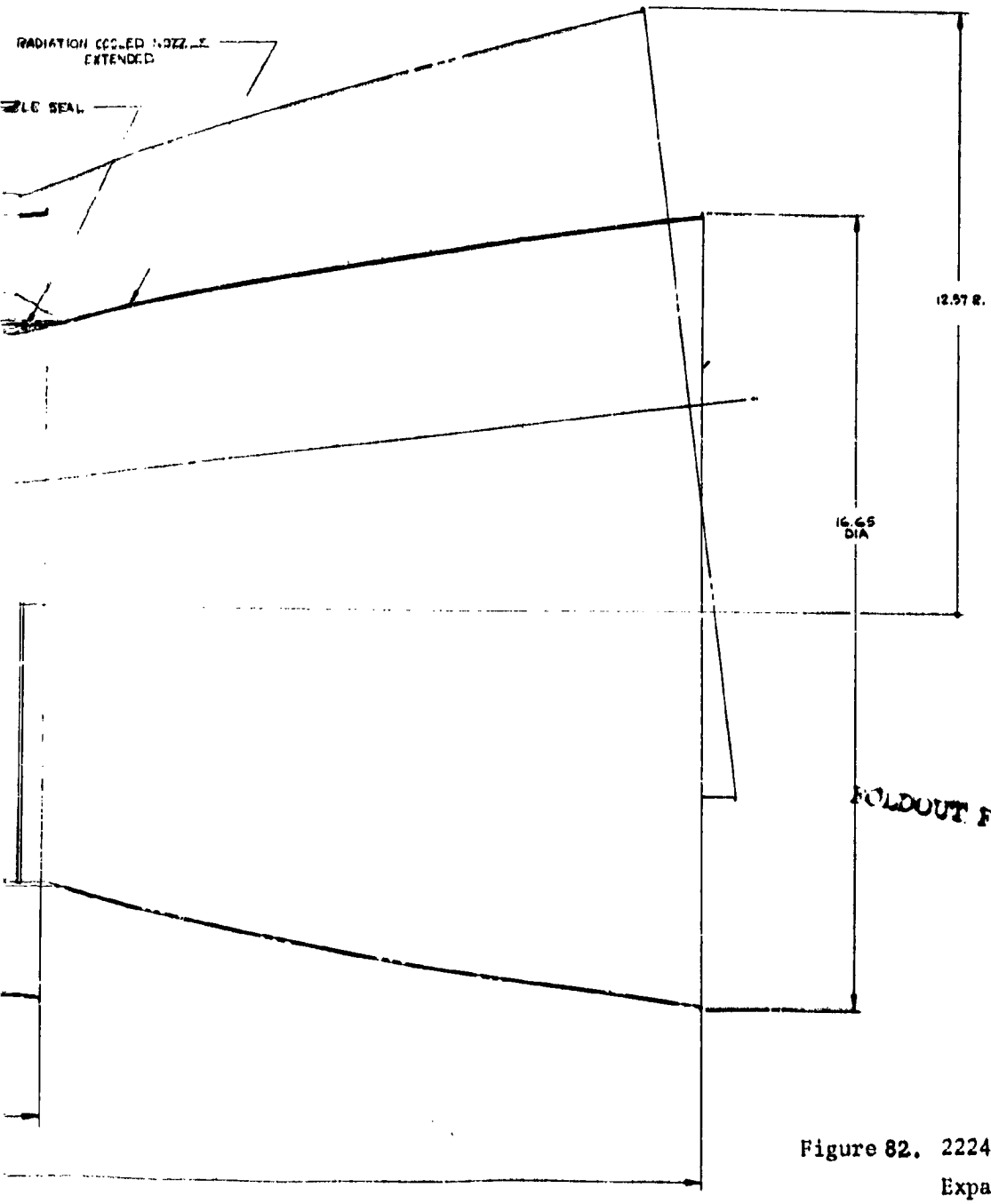

Figure 82. 2224.1 N (500 lbf) LO_2/H_2 Expander Cycle Engine

LOW THRUST CHEMICAL ROCKET ENGINE LO_2/H_2

J 02602 AP80-180

TABLE 20. LO_2/H_2 ENGINE MASS PROPERTIES

LO_2/H_2

THRUST: 2224.1 N (500 lbf)

P_c: 328.9 N/cm^2 (477 psia)

MR: 6-TO-1

AREA RATIO: 400

ITEM	WEIGHT, kg	WEIGHT, POUNDS
GIMBAL BEARING	0.20	0.45
INJECTOR	0.45	1.00
MAIN COMBUSTOR	2.59	5.70
FIXED NOZZLE	5.07	11.17
EXTENDIBLE NOZZLE (t-0.018 IN.)	4.00	8.82
EXTENDIBLE MECHANISM	2.35	5.17
H_2 TURBOPUMP	2.72	6.00
LO_2 TURBOPUMP	4.99	11.00
MAIN FUEL VALVE	0.68	1.50
MAIN OXIDIZER VALVE	0.54	1.20
BYPASS VALVES	1.36	3.00
PROPELLANT DUCTS	1.24	2.73
TURBINE EXHAUST COLLECTORS	0.34	0.76
CONTROLS (EST)	0.91	2.00
IGNITER AND EXCITERS	1.02	2.25
TOTAL WEIGHT	28.46	62.75

TABLE 21. MOMENT OF INERTIA AND CENTER OF GRAVITY ABOUT GIMBAL AXIS (LO_2/H_2 ENGINE)

NOZZLE EXTENDED

WEIGHT, kg (POUNDS)	cg, cm (INCHES)			kg-cm^2 MOMENT OF INERTIA, (LB-IN.^{2})		
	X	Y	Z	I_{xx}	I_{yy}	I_{zz}
28.46 (62.75)	25.20 (9.92)	-1.04 (-0.41)	0.15 (0.06)	8957 (1296)	32787 (11204)	32916 (11248)

CENTER OF GRAVITY
NOZZLE RETRACTED

WEIGHT, kg POUND	cg, cm (INCHES)		
	X	Y	Z
28.46 (62.75)	19.69 (7.75)	-1.04 (-0.41)	0.15 (0.06)

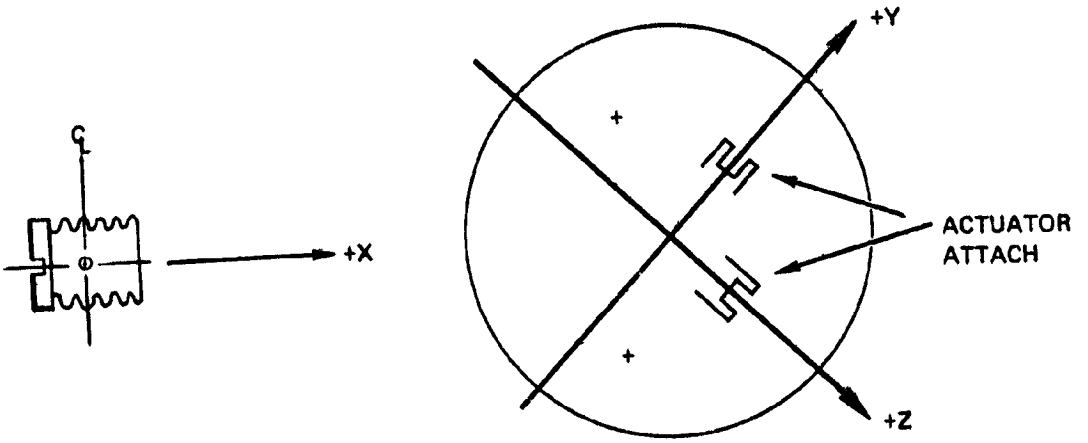

LO_2/CH_4 Expander Cycle Engine.

Design Point Operating Characteristics. Performance and operating characteristics for the LO_2/CH_4 engine system at the nominal design point of 2224.1 N (500 pounds) thrust and a mixture ratio of 3.7 are summarized in Table 22 and Fig. 83.

The achieved design chamber pressure was 307.5 N/cm^2 (446 psia) for the nominal mixture ratio of 3.7. This engine delivered a specific impulse of 354.3 N-sec/kg (361.29 lbf-sec/lbm) for the 400-to-1 area ratio nozzle. The thrust chamber performance loss breakdown presented in Fig. 84 indicates that the major loss factors are the reaction kinetic loss (6.1%) and the boundary layer loss (3.4%).

Off-Design Operating Characteristics. Off-design operating characteristics for the LO_2/CH_4 engine system and components at 2224.1 N (500 pound) thrust and mixture ratios of 3.33 and 4.07 are given in Appendix C.

Engine Operation and Control. Operation and control of the LO_2/CH_4 engine are the same as previously described for the LO_2/H_2 engine.

Engine Layout. The component arrangement for the LO_2/CH_4 engine is shown in Fig. 85. The layout of the LO_2/CH_4 engine is similar to the LO_2/H_2 layout (Fig. 82). The primary differences are the smaller turbopumps and slightly larger envelope for the LO_2/CH_4 configuration. The overall engine length was 94.1 cm (37.06 inches) and the retracted length was 56.6 cm (22.28 inches). The engine diameter was 43.7 cm (17.22 inches) at the nozzle exit.

Engine Mass Properties. The calculated weight for the LO_2/CH_4 engine was 25.8 kg (56.87 pounds), and the engine weight breakdown is shown in Table 23. The major differences from the LO_2/H_2 engine are in the turbopump weights. As for the LO_2/H_2 engine, the major engine weight contributors were the fixed nozzle, extendible nozzle, and the oxygen turbopump.

The engine center of gravity trends and the moments of inertia of the LO_2/CH_4 engine would be similar to those of the LO_2/H_2 engine.

TABLE 22. LO_2/CH_4 ENGINE PERFORMANCE CHARACTERISTICS
DESIGN POINT, O/F = 3.7

Thrust, N, (lbf)	2224.1	500
Chamber Pressure, N/cm^2 (psia)	307.5	446
Engine Mixture Ratio, O/F	3.7	
Area Ratio	400	
ODE Specific Impulse, N-sec/kg (lbf-sec/lbm)	4016.8	409.6
ODE Characteristic Velocity, M/sec (ft/sec)	1823.9	5984
Specific Impulse Energy Release Efficiency, Fraction	.9800	
Specific Impulse Reaction Kinetic Efficiency, Fraction	.9386	
Specific Impulse Divergence Efficiency, Fraction	.9957	
Specific Impulse Non-Boundary Layer Heat Loss Efficiency, Fraction (1)	.9945	
Specific Impulse Boundary Layer Efficiency, Fraction	.9964	
Delivered Specific Impulse N-sec/kg (lbf-sec/lbm)	3543.1	361.3

(1) Non-Boundary Layer Heat Loss
Included in ODE Specific Impulse

TABLE 23. LO_2/CH_4 ENGINE MASS PROPERTIES

LO_2/CH_4
THRUST: 2224.1 N (500 lbf)
Pc: 307.5 N/cm^2 (446 psia)
MR: 3.7-TO-1
AREA RATIO: 400

ITEM	WEIGHT, kg	WEIGHT, POUNDS
GIMBAL BEARING	0.20	0.45
INJECTOR	0.58	1.28
MAIN COMBUSTOR	2.11	4.65
FIXED NOZZLE	5.17	11.39
EXTENDIBLE NOZZLE (t=0.018 IN.)	4.08	9.00
EXTENDIBLE MECHANISM	2.35	5.17
CH_4 TURBOPUMP	2.27	5.00
LO_2 TURBOPUMP	3.18	7.00
MAIN FUEL VALVE	0.68	1.50
MAIN OXIDIZER VALVE	0.54	1.20
BYPASS VALVES	1.36	3.00
PROPELLANT DUCTS	1.10	2.43
TURBINE EXHAUST COLLECTORS	0.25	0.55
CONTROLS	0.91	2.00
IGNITER AND EXCITER	1.02	2.25
TOTAL WEIGHT	25.80	56.87

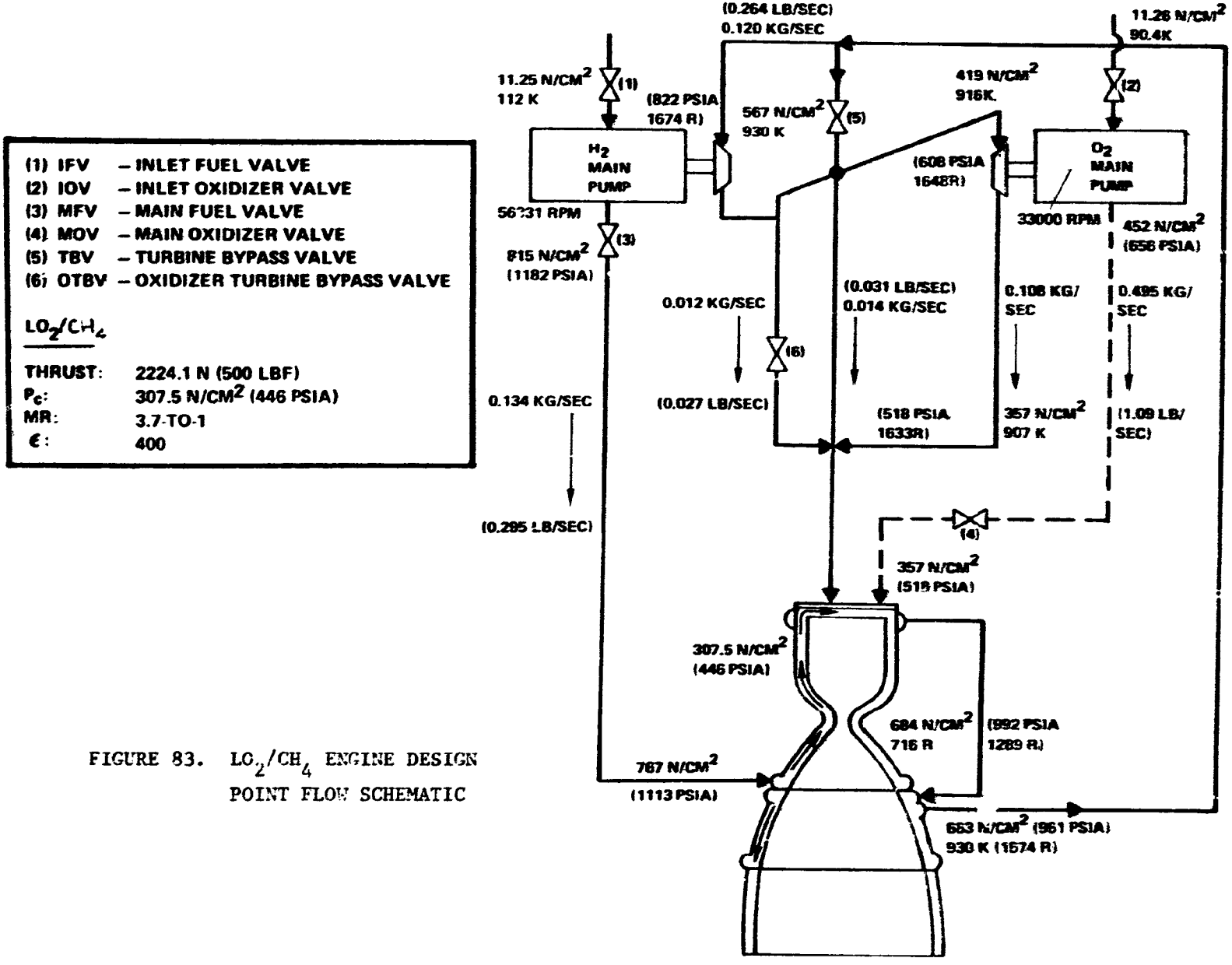

FIGURE 83. LO_2/CH_4 ENGINE DESIGN POINT FLOW SCHEMATIC

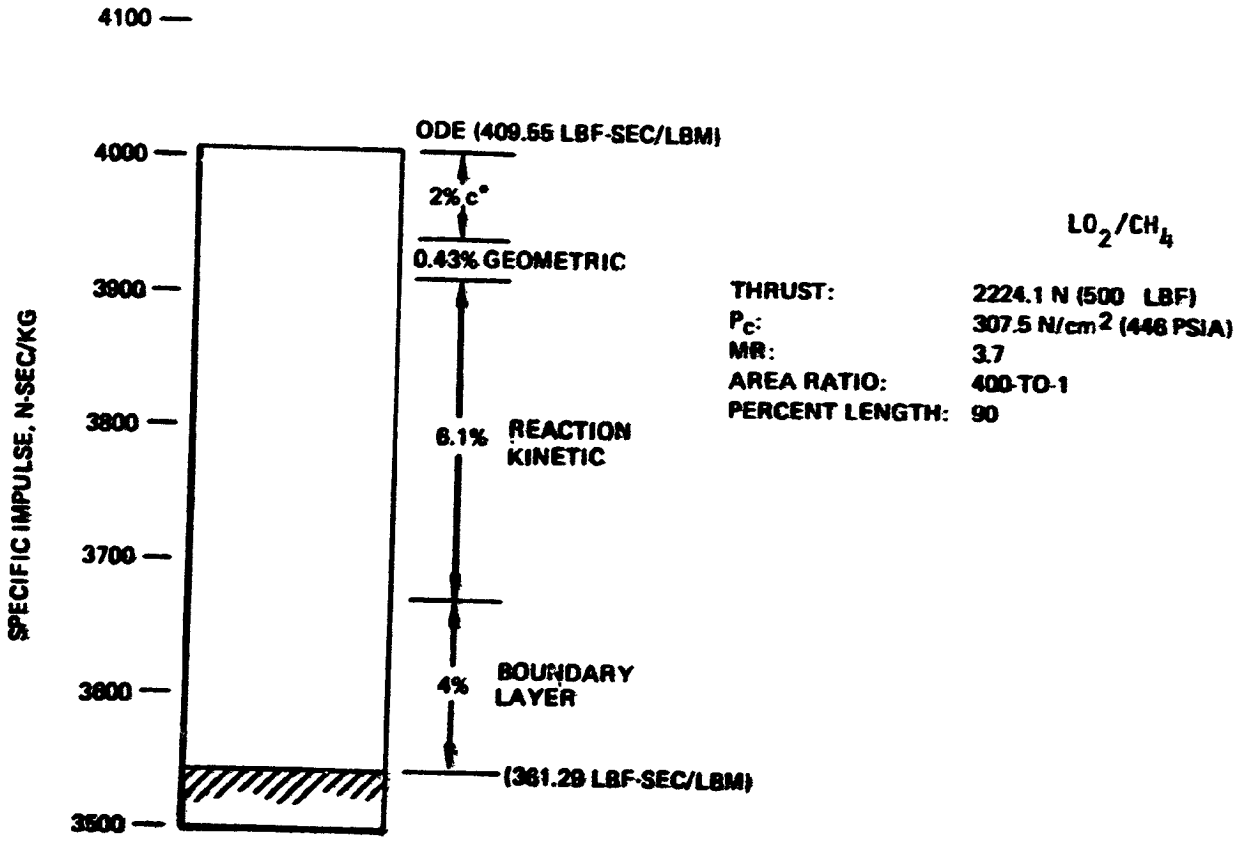

Figure 84 . Performance Loss Breakdown for 2224.1N (500 lb_f) Thrust, LO_2/CH_4 Expander Cycle Engine

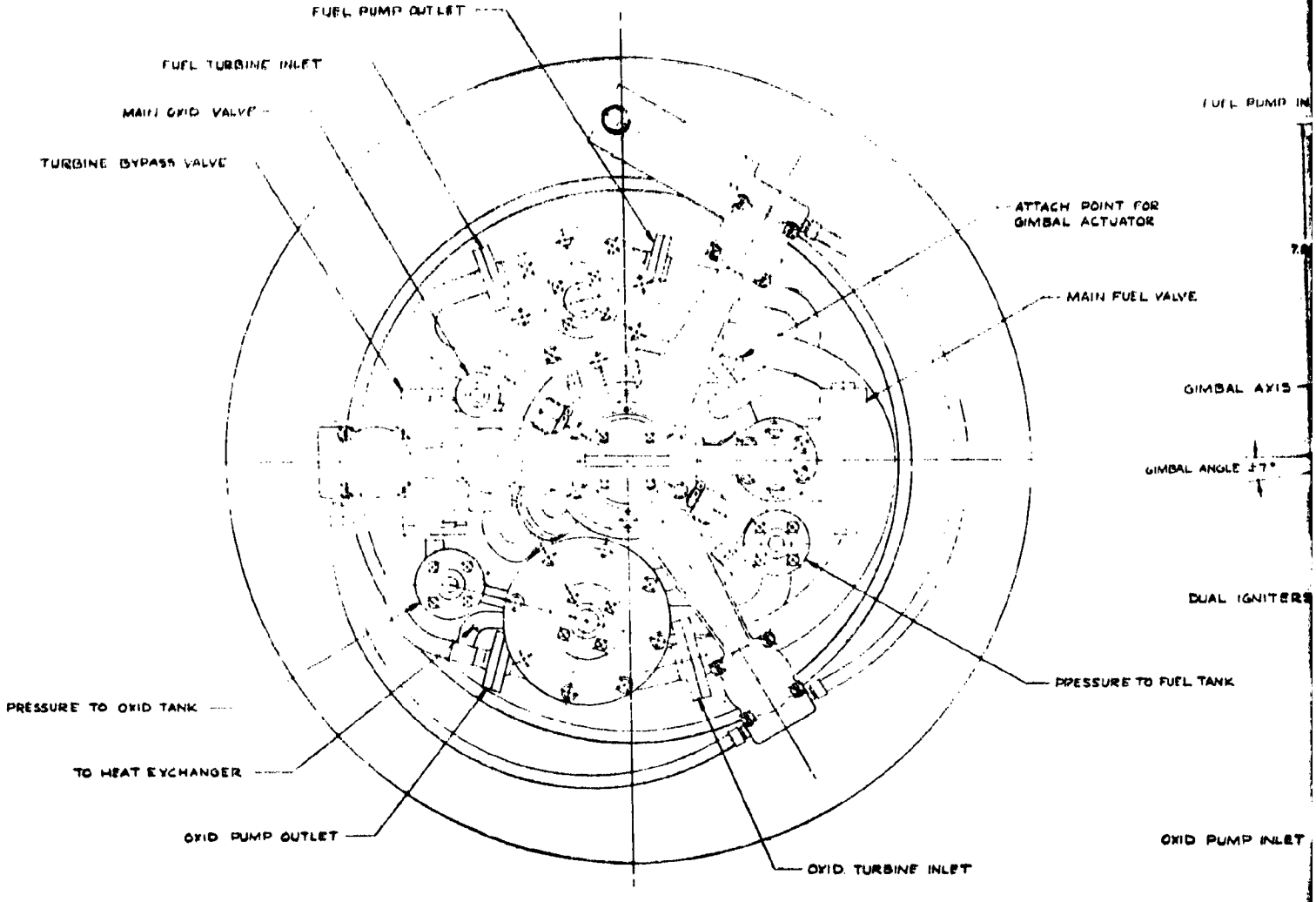

FOLDOUT FRAME

PRECEDING PAGE BLANK NOT FILMED

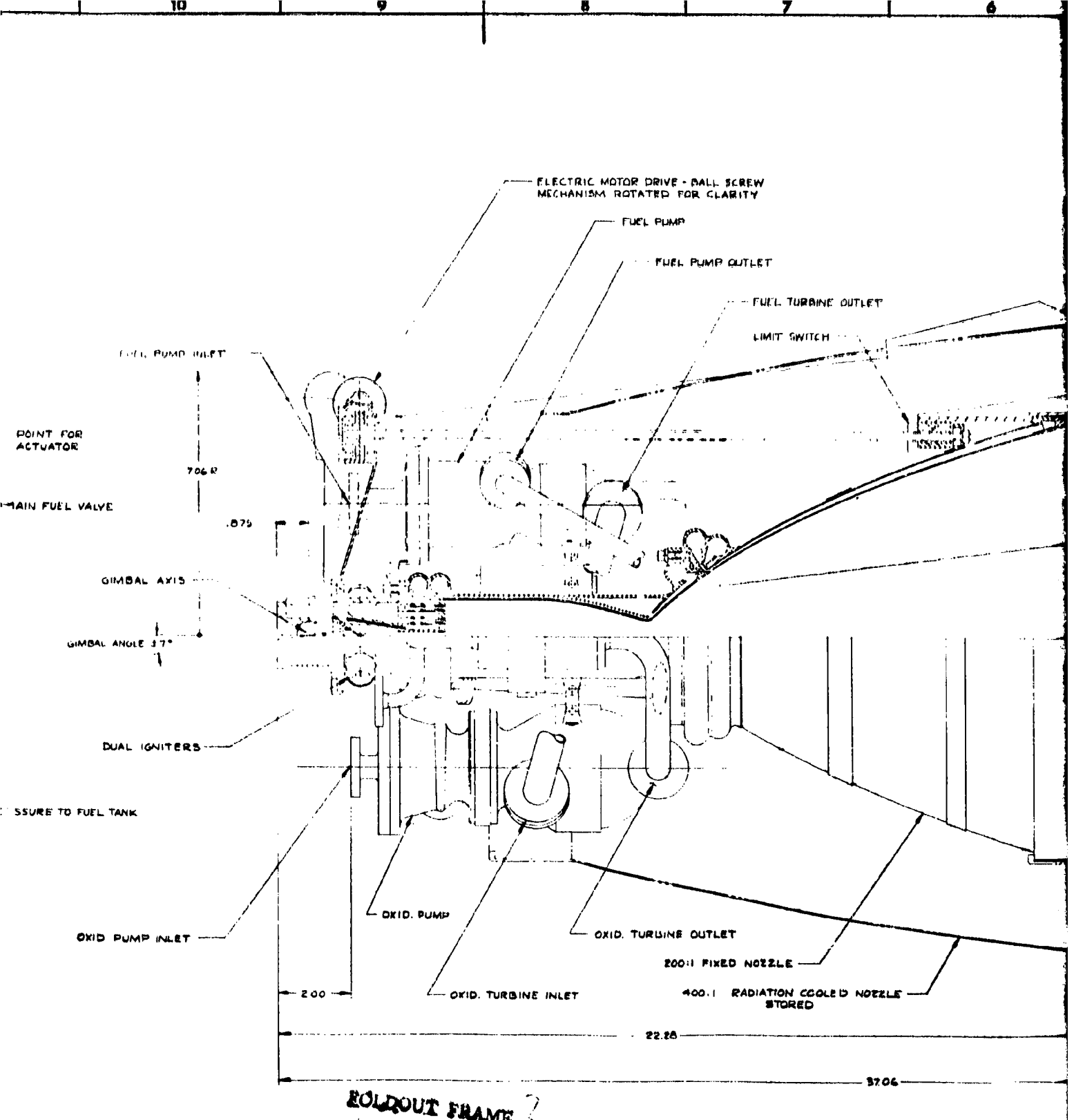

FOLDOUT FRAME 2

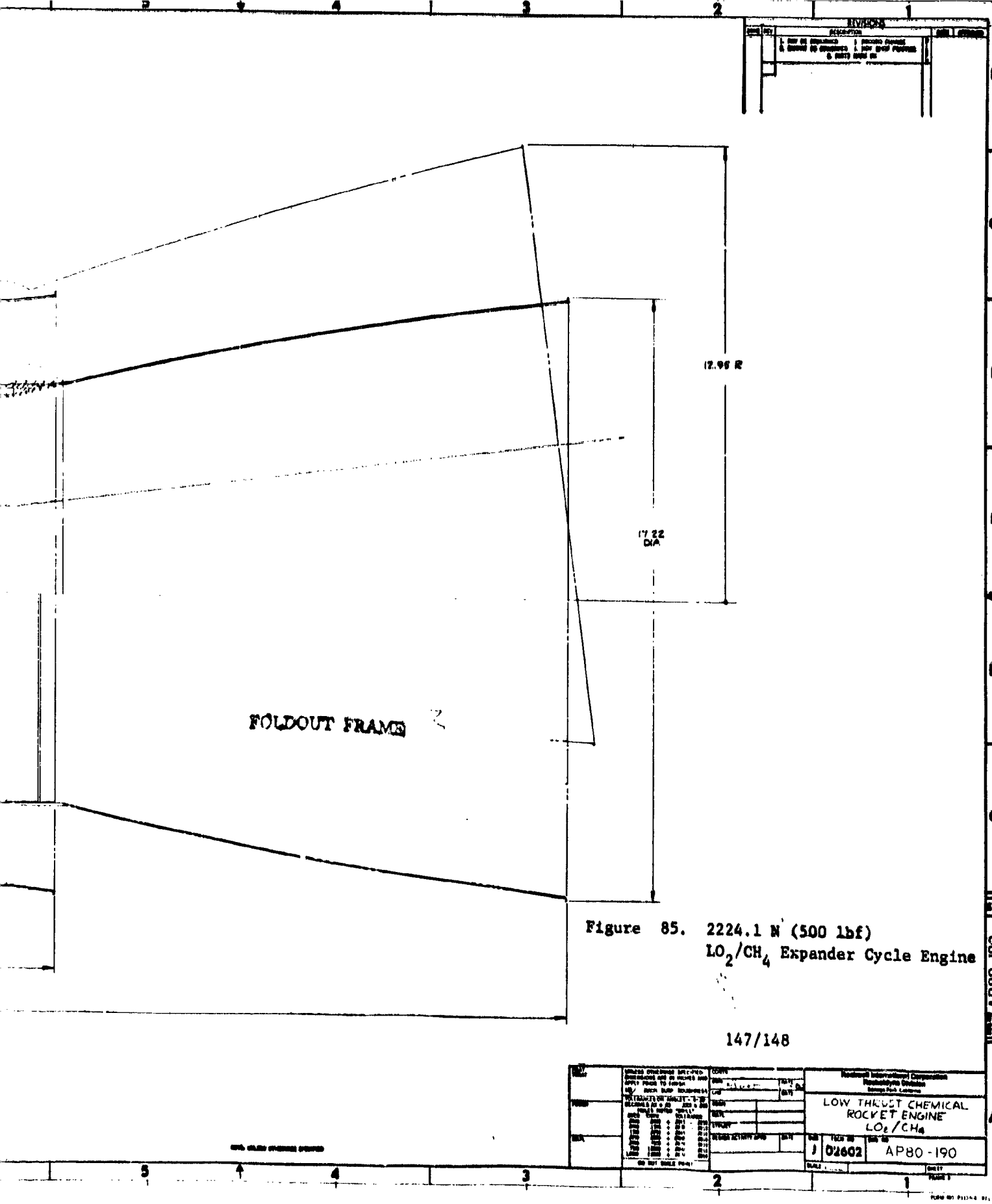

Figure 85. 2224.1 N (500 lbf) LO_2/CH_4 Expander Cycle Engine

LOW THRUST CHEMICAL ROCKET ENGINE LO_2/CH_4

AP80-190

This subsection describes the design point operating characteristics and mechanical designs of the major LO_2/H_2 and LO_2/CH_4 engine components. Both engines utilize the same basic type of component configurations (e.g. two-stage oxidizer pump, four-stage fuel pump). With the exception of the thrust chambers, basic materials are also the same.

Thrust Chamber Design. For the 224.1 N (500 lbf) thrust LO_2/H_2 engine with a design chamber pressure of 328.9 N/cm^2 (477 psia) a combustion chamber length of 11.3 cm (4.45 inches) and a contraction ratio of 5.2 were determined from the previously presented combustion chamber geometry curves for LO_2/H_2. In the process of performing the combustor heat transfer analysis, the combustor heat input was approximately 10% lower than the engine cycle balance value, and therefore the combustor chamber length was increased to 13.97 cm (5.5 inches). This increased length should further ensure high combustion efficiency. As shown in Fig. 86, the combustor chamber contour selected for the LO_2/H_2 engine has approximately a 7.62 cm (3 inch) long cylindrical section followed by a gentle (~20 degree maximum wall angle) convergence section. The cylindrical section provides a vaporization, mixing, and combustion region and the gentle convergence section will prevent any boundary layer separation which could increase throat region heat transfer rates. The throat diameter was 2.093 cm (0.824 inch) and the injector face diameter was 4.773 cm (1.879 inches).

The complete thrust chamber contour for the LO_2/H_2 engine with a 400-to-1 area ratio nozzle is presented in Fig. 87. The length from the injector face to the nozzle exit (not overall engine length) is 80.5 cm (31.7 inches) and the nozzle exit diameter is 42.29 cm (16.65 inches).

For the 2224.1 N (500 lbf) thrust LO_2/CH_4 engine with a design chamber pressure of 307.5 N/cm^2 (446 psia), a combustion chamber length of 13.39 cm (5.27 inches) and a cortraction ratio of 5.4 were obtained from the LO_2/CH_4 combustion chamber geometry data previously discussed. To ensure an adequate coolant heat input, the combustion chamber length was increased to 13.97 cm (5.5 inches). A gradual convergence chamber contour similar to that defined for the LO_2/H_2 engine was chosen for the LO_2/CH_4 engine. The throat diameter was 2.16 cm (.850 inch) and the injector face diameter was 5.03 cm (1.975 inch). The 400-to-1 area ratio nozzle was scaled to obtain the rest of the thrust chamber contour. Combustion chamber and nozzle contours for the LO_2/CH_4 engine are shown in Figs. 88 and 89.

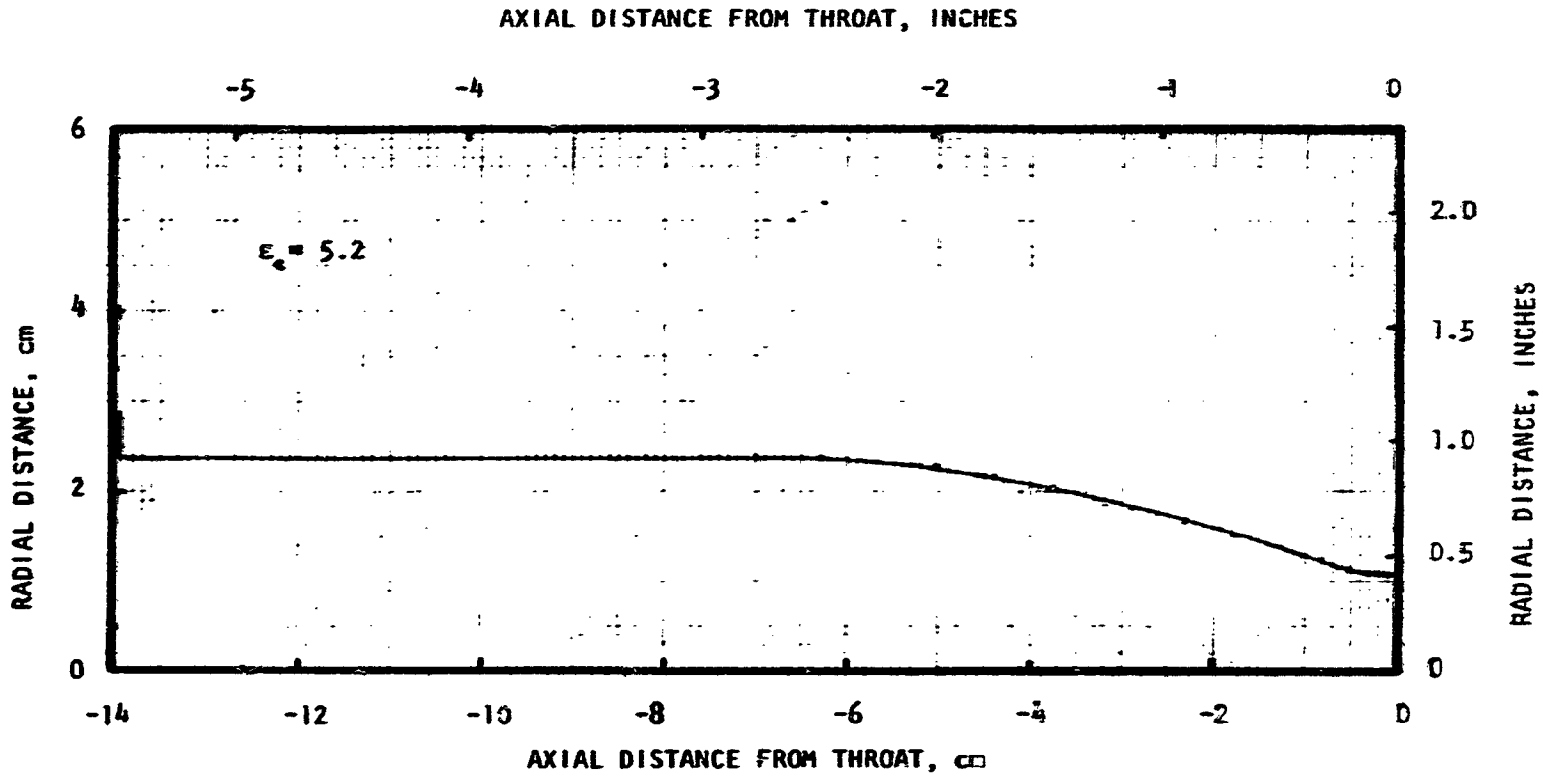

Figure 86. 2224.1 N (500 lb_f) Thrust LO_2/H_2 Engine Combustion Chamber

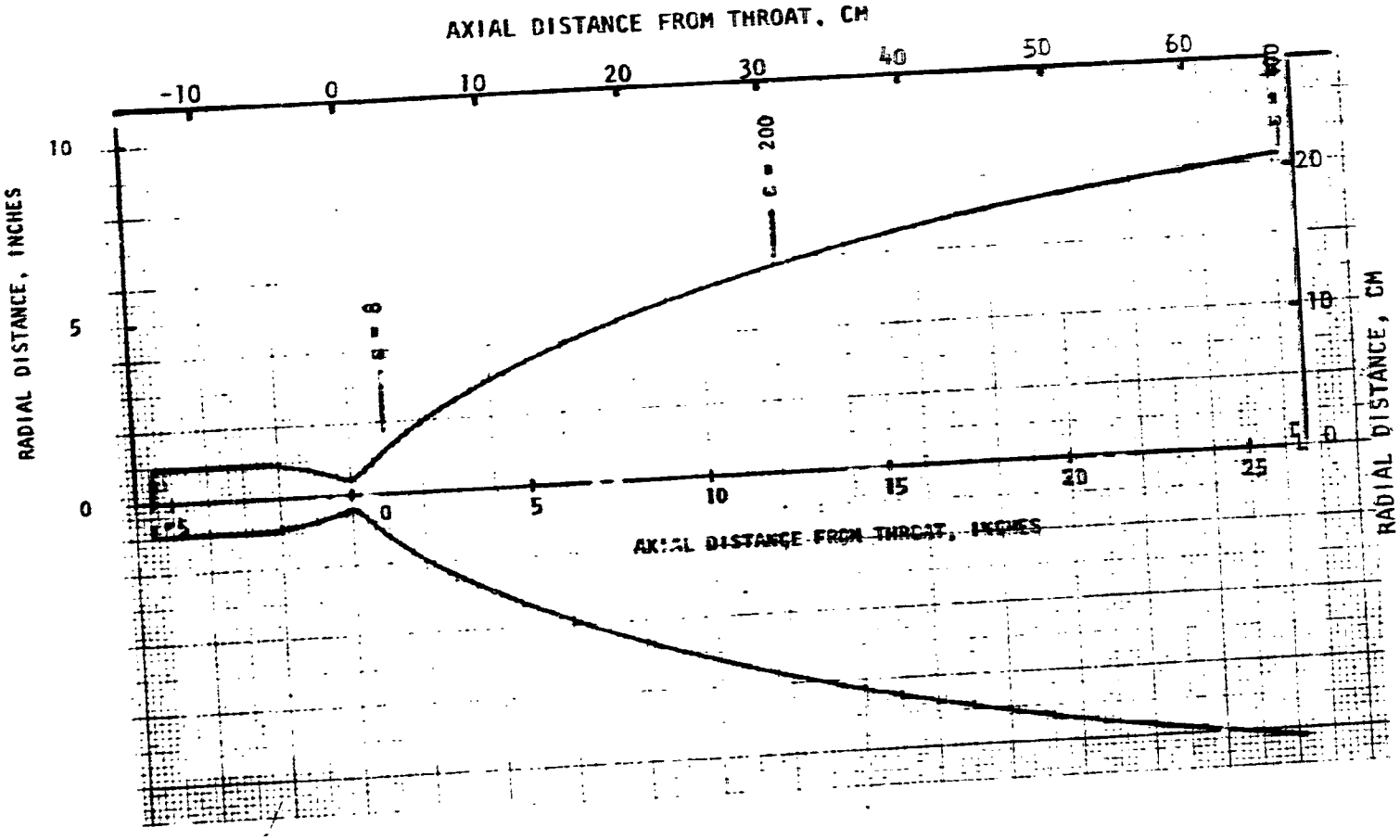

Figure 87. 2224.1 N (500 lbf) Thrust LO_2/H_2 Thrust Chamber

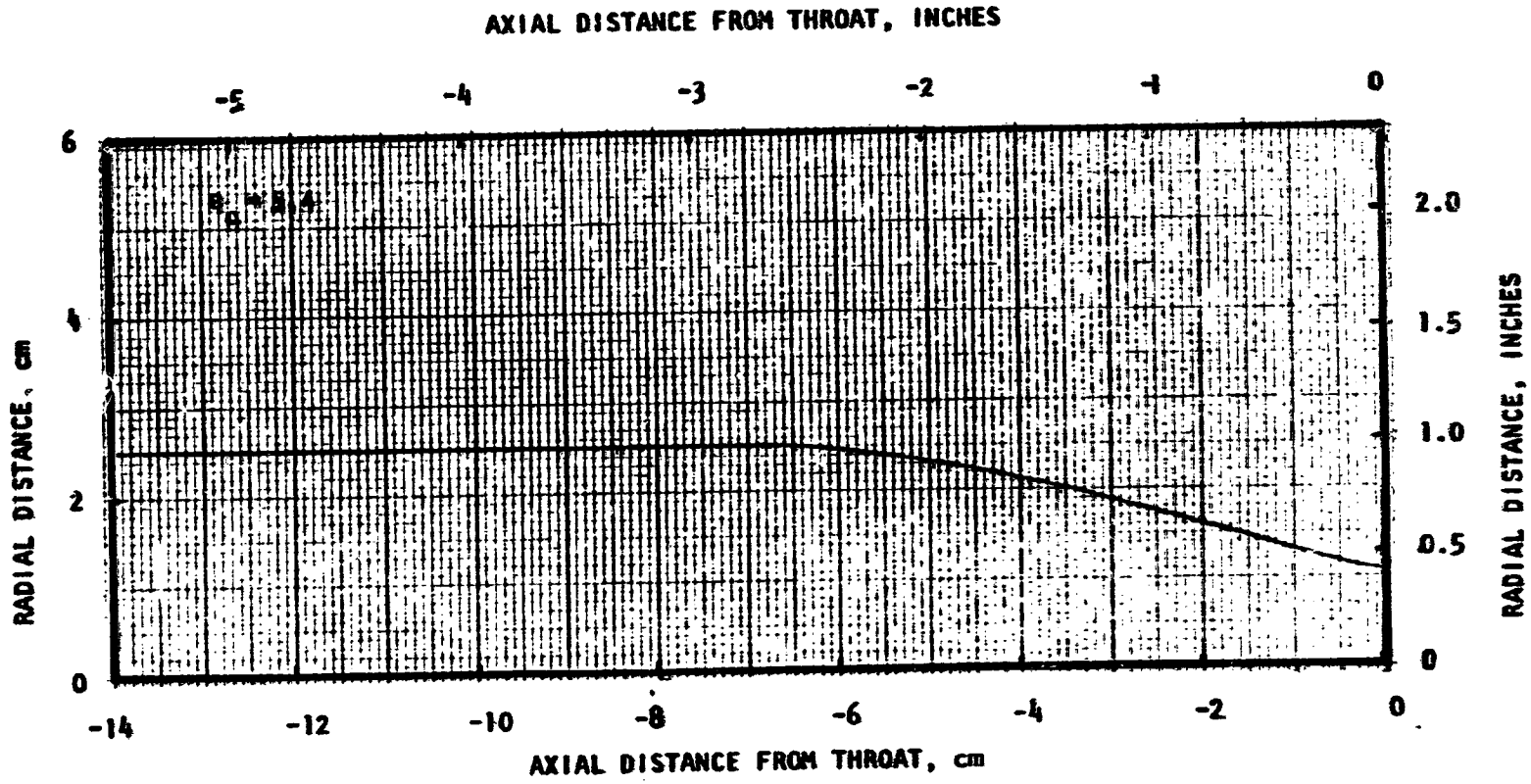

Figure 88. 2224.1 N (500 lb_f) Thrust LO_2/GH_4 Engine Combustion Chamber

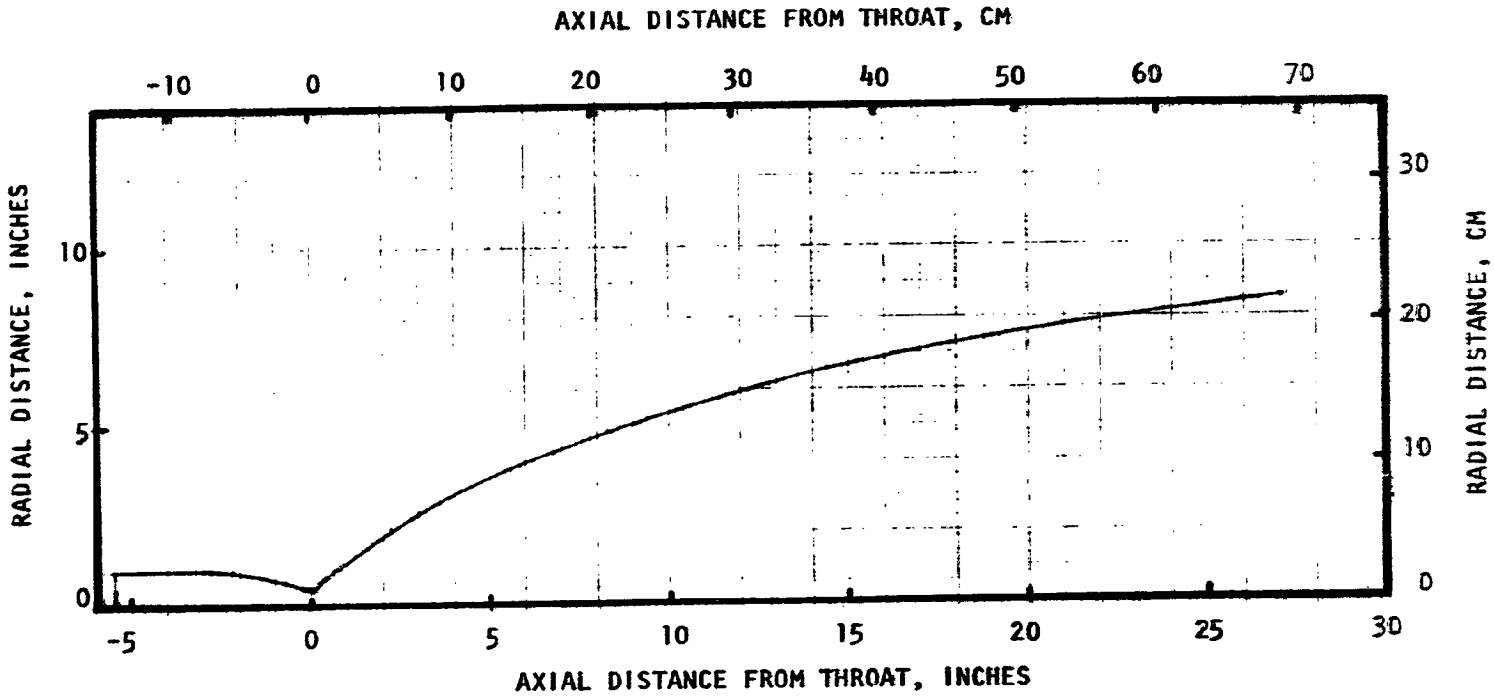

Figure 89. 2224.1 N (500 lb_f) Thrust LO_2/CH_4 Thrust Chamber

Coolant Passage Design. Using the series coolant circuit previously described, the thrust chamber coolant passage design was determined using the Rocketdyne regenerative-cooling design/analysis computer program. The thrust chamber series coolant circuit consisted of a single uppass combustor cooling circuit followed in series by a two-pass nozzle circuit. The coolant inlet and outlet for the nozzle were located at the low area ratio and to permit clearance for the extendible nozzle. A radiation-cooled nozzle extension was attached at an area ratio of 200-to-1 for both engines.

LO_2/H_2 Thrust Chamber. The resulting NARloy-Z channel wall combustor coolant passage design for the LO_2/H_2 engine is presented in Fig. 90. The design consisted of 39 channels with minimum channel dimensions of:

Channel Width:	0.0762 cm (0.03 in)
Channel Depth:	0.0813 cm (0.032 in)
Channel Land:	0.0836 cm (0.0329 in)
Wall Thickness:	0.0635 cm (0.025 in)

The maximum channel depth-to-width ratio was 3.5 which is lower than the limit of 4.0 set in the heat transfer analysis. In fact, all the minimum channel dimensions are within current fabrication limits.

The resulting two-dimensional wall temperatures are presented in Fig. 91. The maximum gas-side wall (T_{wg}), the coolant-side wall (T_{wc}), the back-side wall (T_{back}), and the coolant bulk (T_{bulk}) temperatures are presented. The maximum gas-side wall temperature was 750.6 K (891 F) located approximately 2.5 cm (1 inch) upstream of the geometric throat. This value is lower than the 811 K (1000 F) durability limit previoulsy set.

The maximum coolant Mach number in the combustor was 0.154 and a coolant heat input of 349.4 KW (331.2 BTU/sec) was achieved. The combustor coolant pressure drop was 26.5 N/cm^2 (38.4 psi) including exit manifold losses. The minimum yield safety factor was 8 and the minimum cycle life section occurred near the throat but exceeded 2000 cycles times a safety factor of four.

The coolant tube design of the two-pass stainless tube nozzle to an area ratio of 200-to-1 is shown in Fig. 92. A constant tube wall thickness of 0.0245 cm (0.01 inch) was used. To minimize weight a round tube design was selected. The resulting design consisted of 480 tubes (240 up and 240 down) with the outside diameter variation shown in Fig. 92.

The maximum fixed nozzle wall temperature was 778 K (940 F). The complete temperature distributions are presented in Fig. 93. The arrows indicate the direction of coolant flow. Maximum coolant Mach number was 0.105. The coolant heat input from the fixed nozzle was 170.8 KW (161.9 BTU/sec) with a 6.7 N/cm^2 (9.7 psi) coolant pressure drop. The minimum yield safety factor exceeded four and a cycle life exeeding 700 cycles times a safety factor of four was achieved.

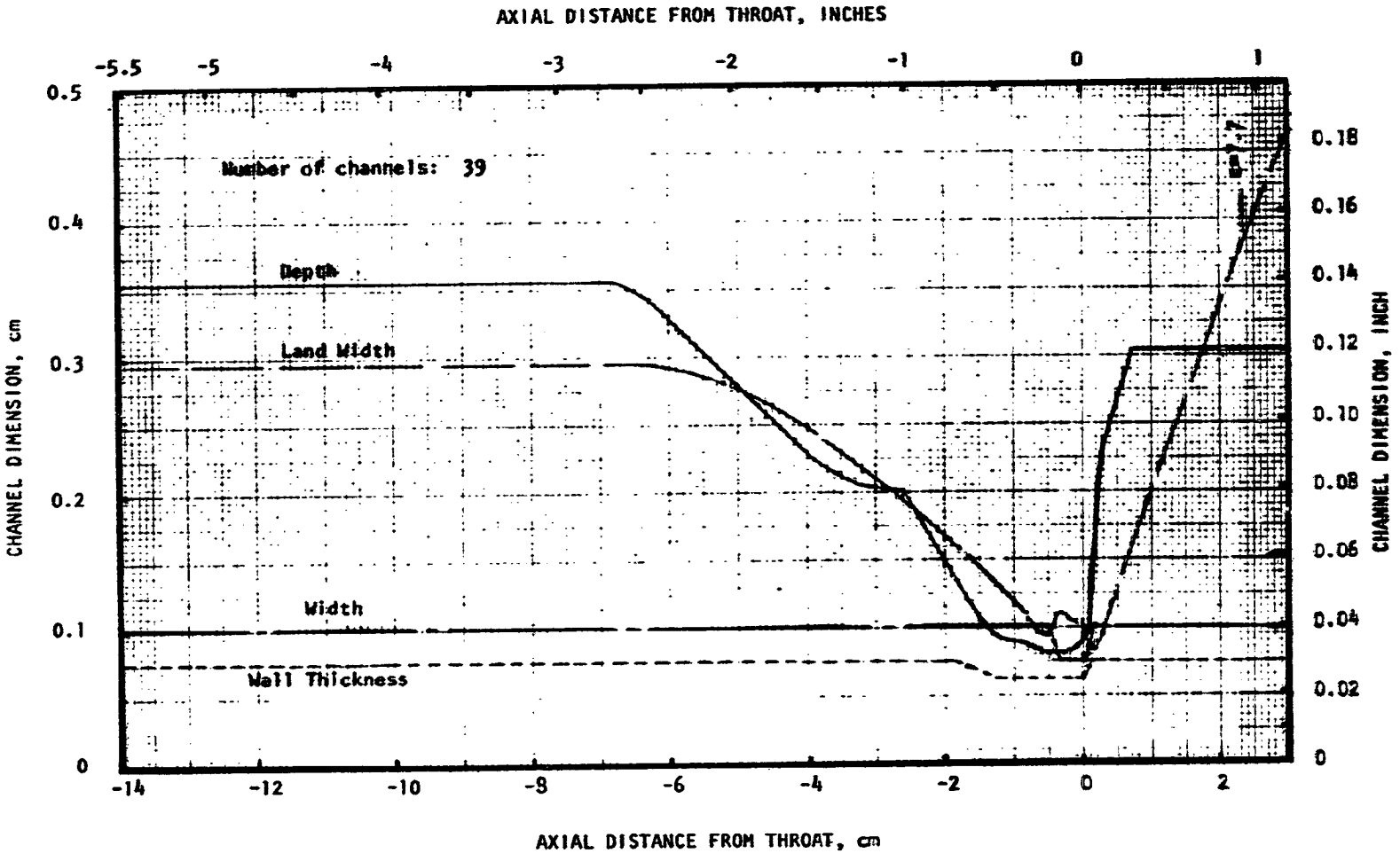

Figure 90 . LO_2/H_2 Engine - Combustor Coolant Channel Dimensions

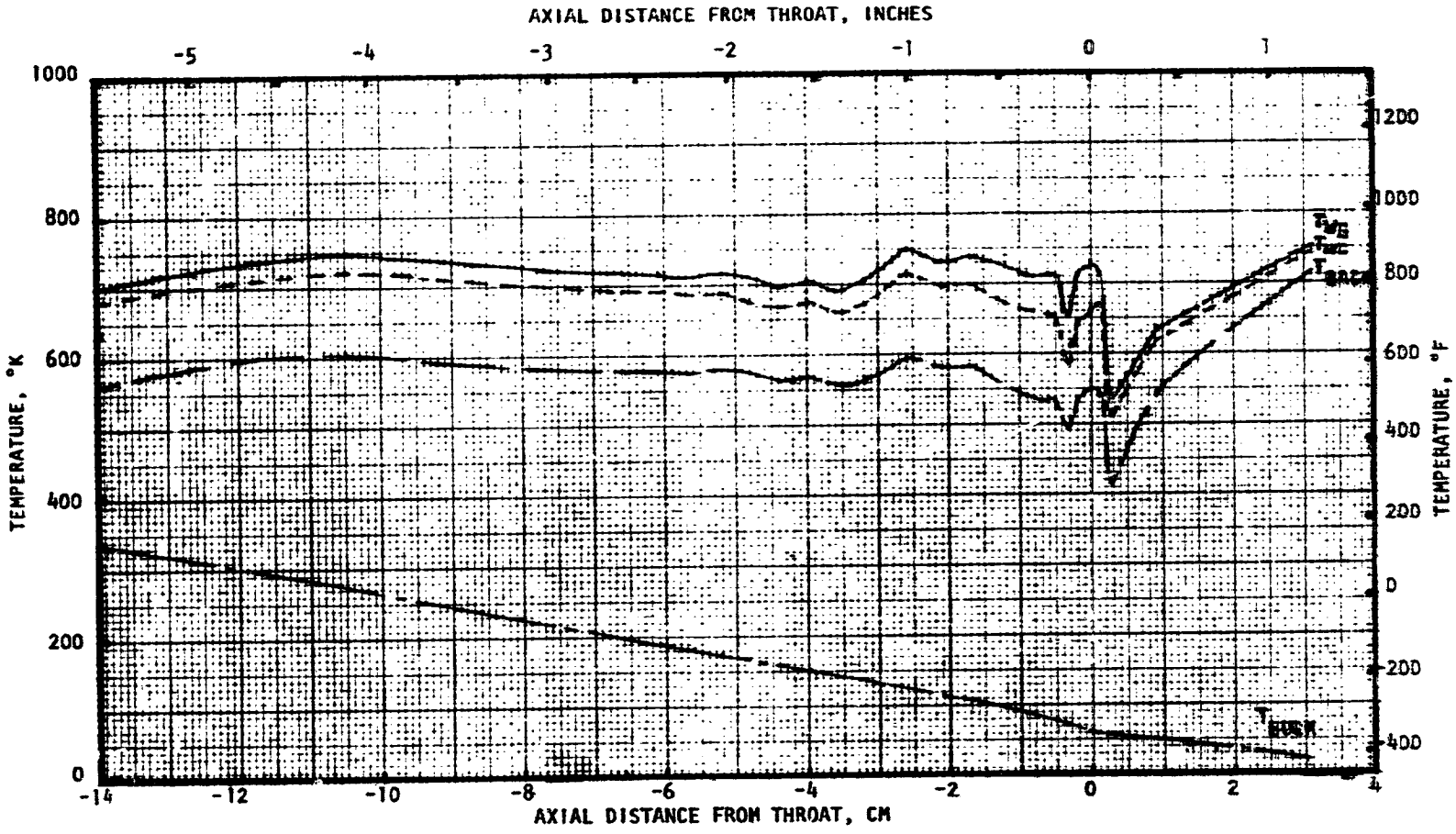

Figure 91. LO_2/H_2 Engine - Combustor Temperature Distributions

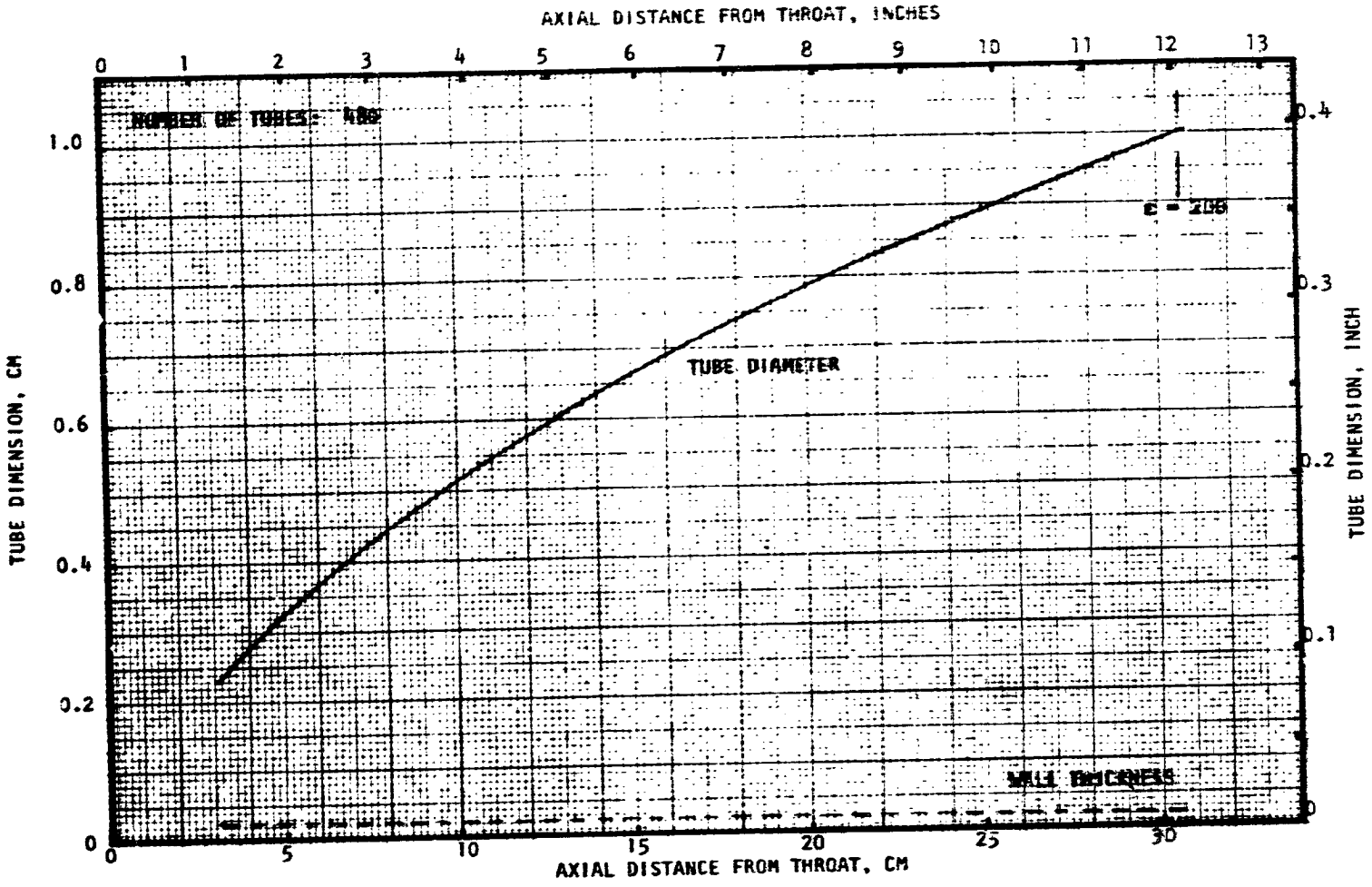

Figure 92. LO_2/H_2 Engine - Fixed Nozzle Tube Dimensions

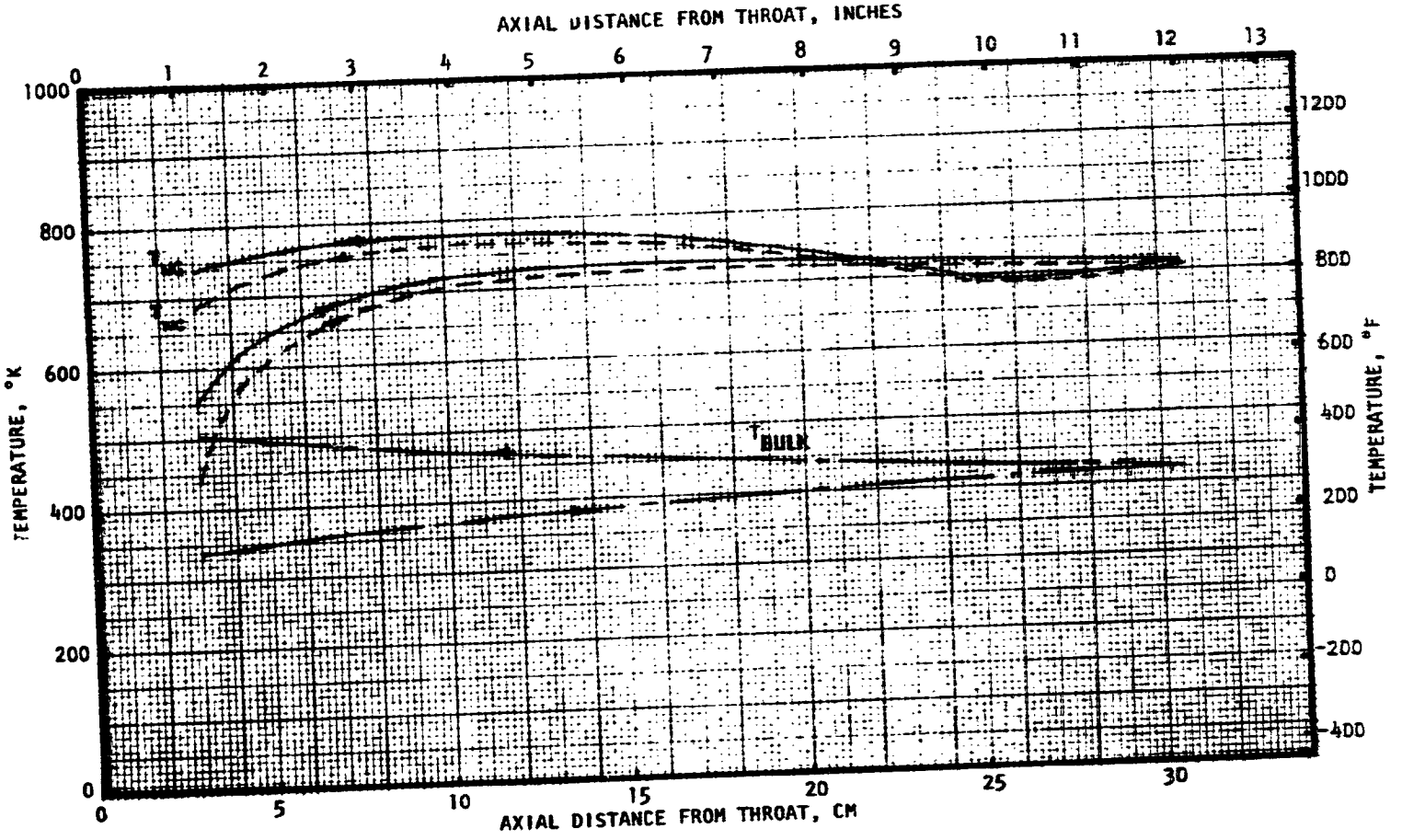

Figure 93. LO_2/H_2 Engine - Fixed Nozzle Temperature Distributions

LO_2/CH_4 Thrust Chamber. The coolant passage design for the nickel channel wall combustor of the LO_2/CH_4 engine is presented in Fig. 94. The design consisted of 43 channels with minimum channel dimensions of:

Channel Width:	0.0889 cm (0.035 inch)
Channel Depth:	0.1143 cm (0.045 inch)
Channel Land:	0.0796 cm (0.0313 inch)
Wall Thickness:	0.0711 cm (0.028 inch)

As for the LO_2/H_2 combustor, the channel dimensions of the LO_2/CH_4 combustor are all within current fabrication limits.

The two-dimensional wall temperature distributions for the LO_2/CH_4 combustor are shown in Fig. 95. A maximum wall temperature of 977.8 K (1300 F) was obtained, which is equal to the nickel durability limit temperature. A coolant heat input of 237.4 KW (234.5 BTU/sec) and a coolant pressure drop of 83.8 N/cm^2 (121.6 psi) resulted. As for the LO_2/H_2 combustor, the structural and cyclic life far exceed the specified requirements.

The fixed nozzle coolant tube design is presented in Fig. 96. A total of 700 round stainless steel tubes were used. The maximum nozzle wall temperature was 979 K (1302 F) as shown in Fig. 97; however, the maximum coolant-side temperature was 971 K (1288 F) which is only 7 K (12 F) less than the methane coking limit temperature. Therefore, this thrust chamber design is close to the cooling limit for LO_2/CH_4 regenerative/radiation-cooled thrust chambers. The fixed nozzle coolant heat input was 113.4 KW (106.5 BTU/sec) and a coolant pressure drop of 21.4 N/cm^2 (31 psi) was obtained.

Mechanical Design. The combustors for the LO_2/H_2 and LO_2/CH_4 engines are similar in construction and consist of milled channel wall liners with electro-deposited (ED) nickel closeouts. Material for the LO_2/H_2 liner is NARloy-Z copper alloy. Material for the LO_2/CH_4 liner is nickel . The manifolds are machined from stainless steel bonded to the liner and closeoust welded. A cylindrical ED nickel stiffener was incorporated to strengthen the chamber throat region. A flanged manifold is located at the combustor-to-fixed nozzle joint. This manifold joint could be welded once developmental testing of the thrust chamber was completed and would result in a weight saving.

The fixed nozzle was a conventional tubular brazed nozzle section. The two-pass coolant circuit design permits the unobstructed extension of the radiation-cooled nozzle extension. The design of the fixed nozzle coolant inlet and outlet manifolds enables identical up and down tube designs. At the 200-to-1 area ratio location, a CRES turnaround manifold closes off the fixed nozzle and provides a terminal and seal junction for the nozzle extension.

The radiation-cooled nozzle extension is a 0.046 cm (0.018 inch) thick L605 contour which would be extended by a ball screw mechanism powered by an electric motor equipped with an internal overruning clutch. A limit switch located at the

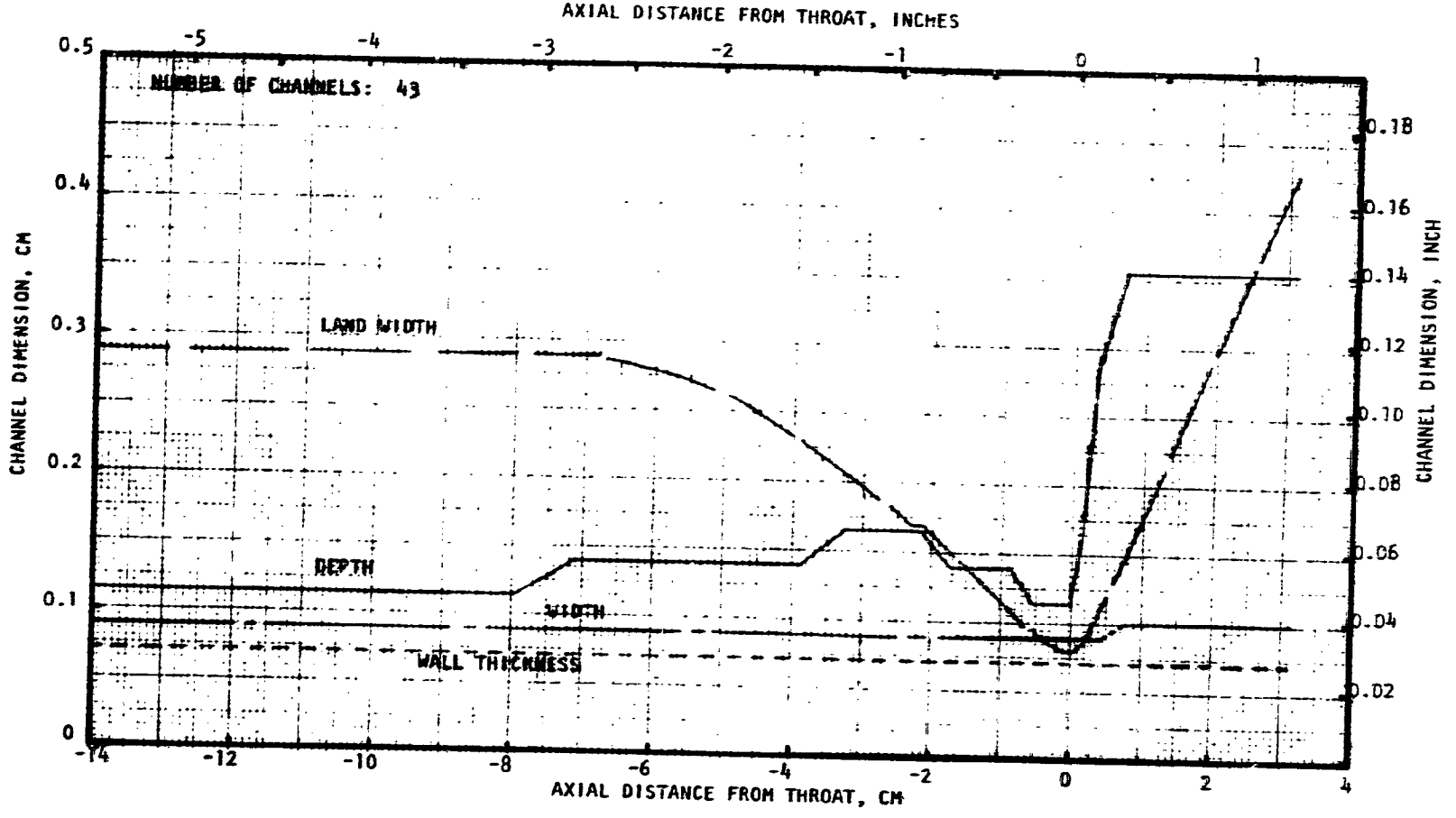

Figure 94. LO_2/CH_4 Engine - Combustor Coolant Channel Dimensions

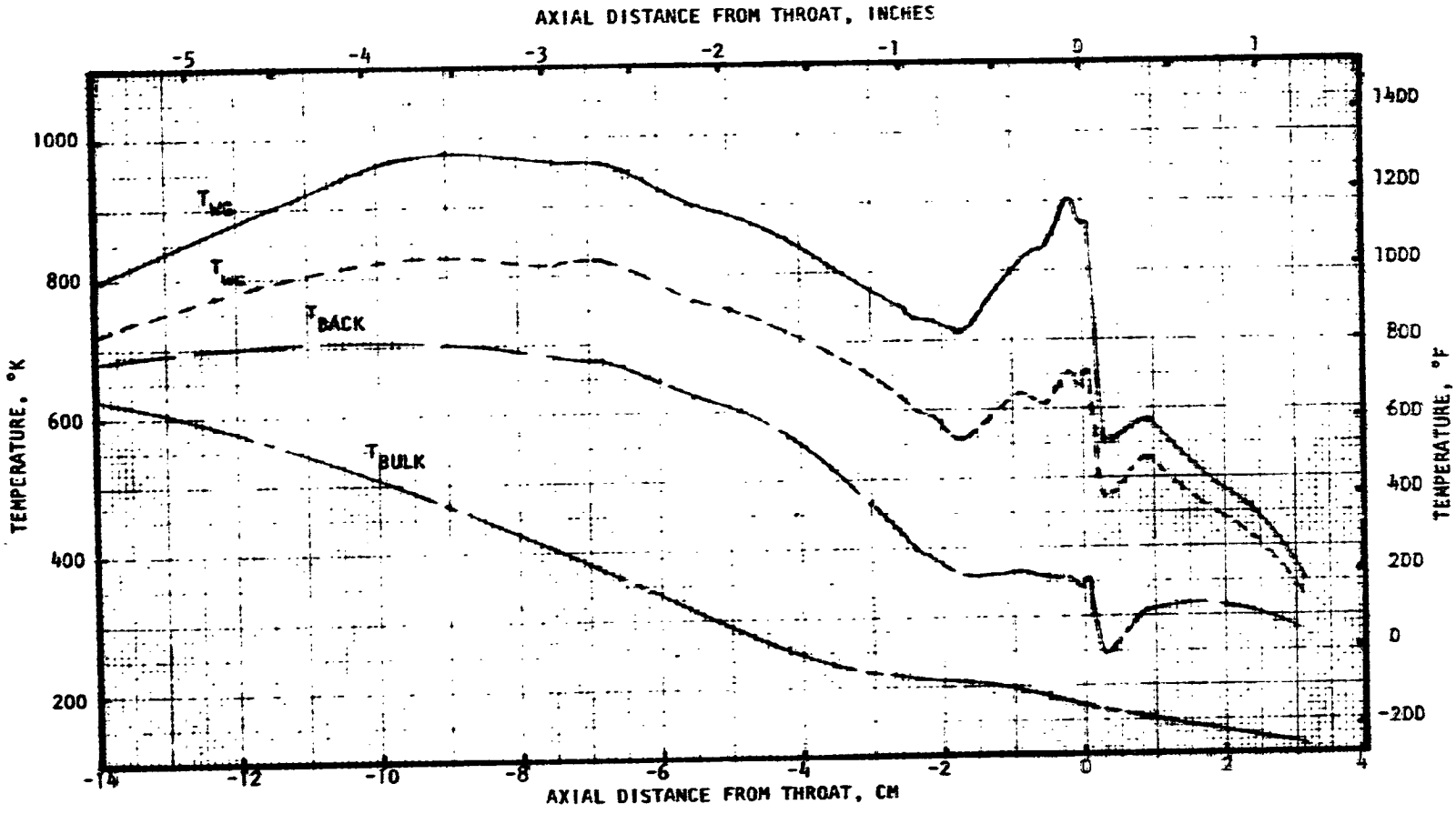

Figure 95 . LO_2/CH_4 Engine - Combustor Temperature Distributions

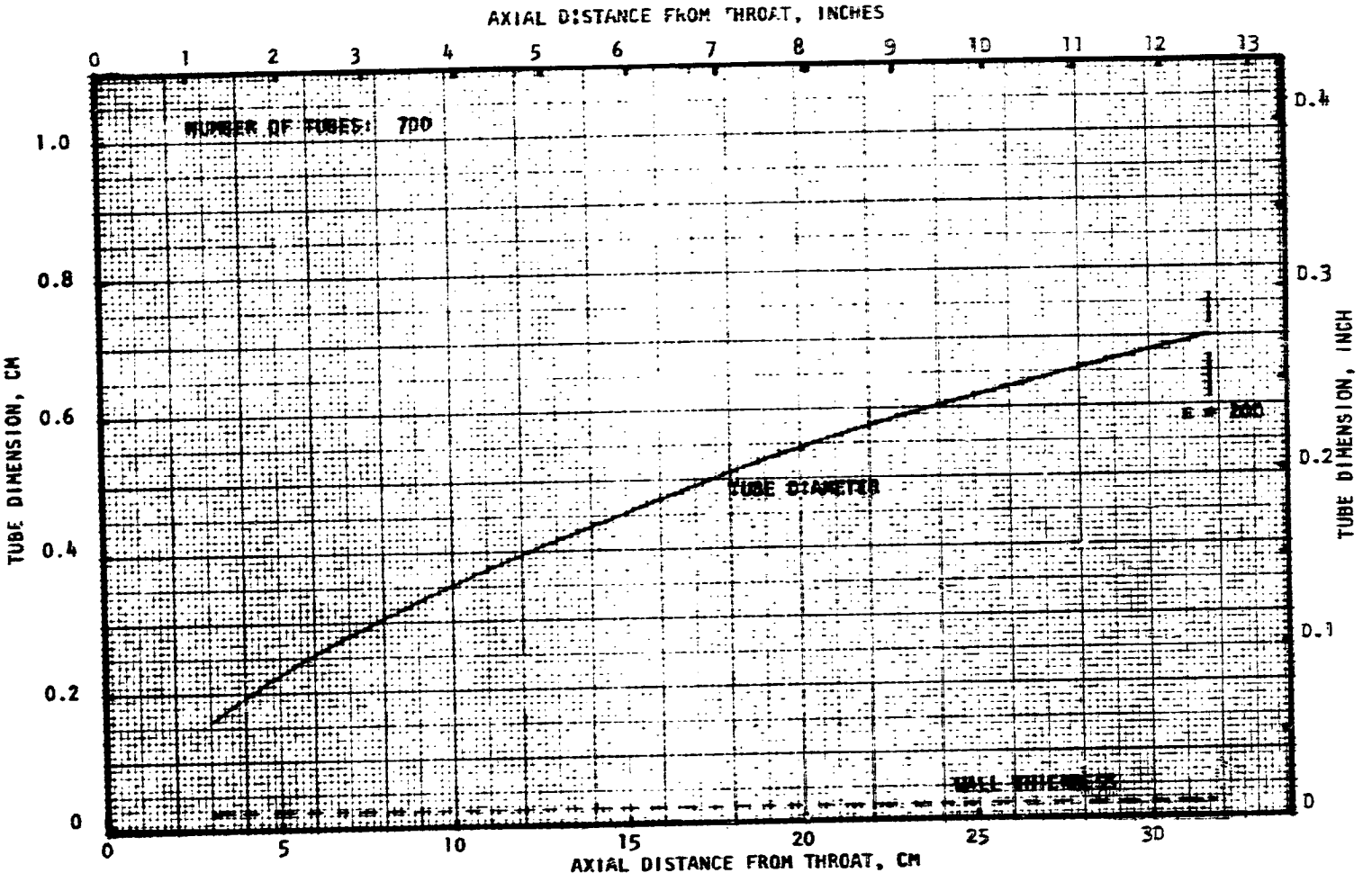

Figure 96. LO_2/CH_4 Engine - Fixed Nozzle Tube Dimensions

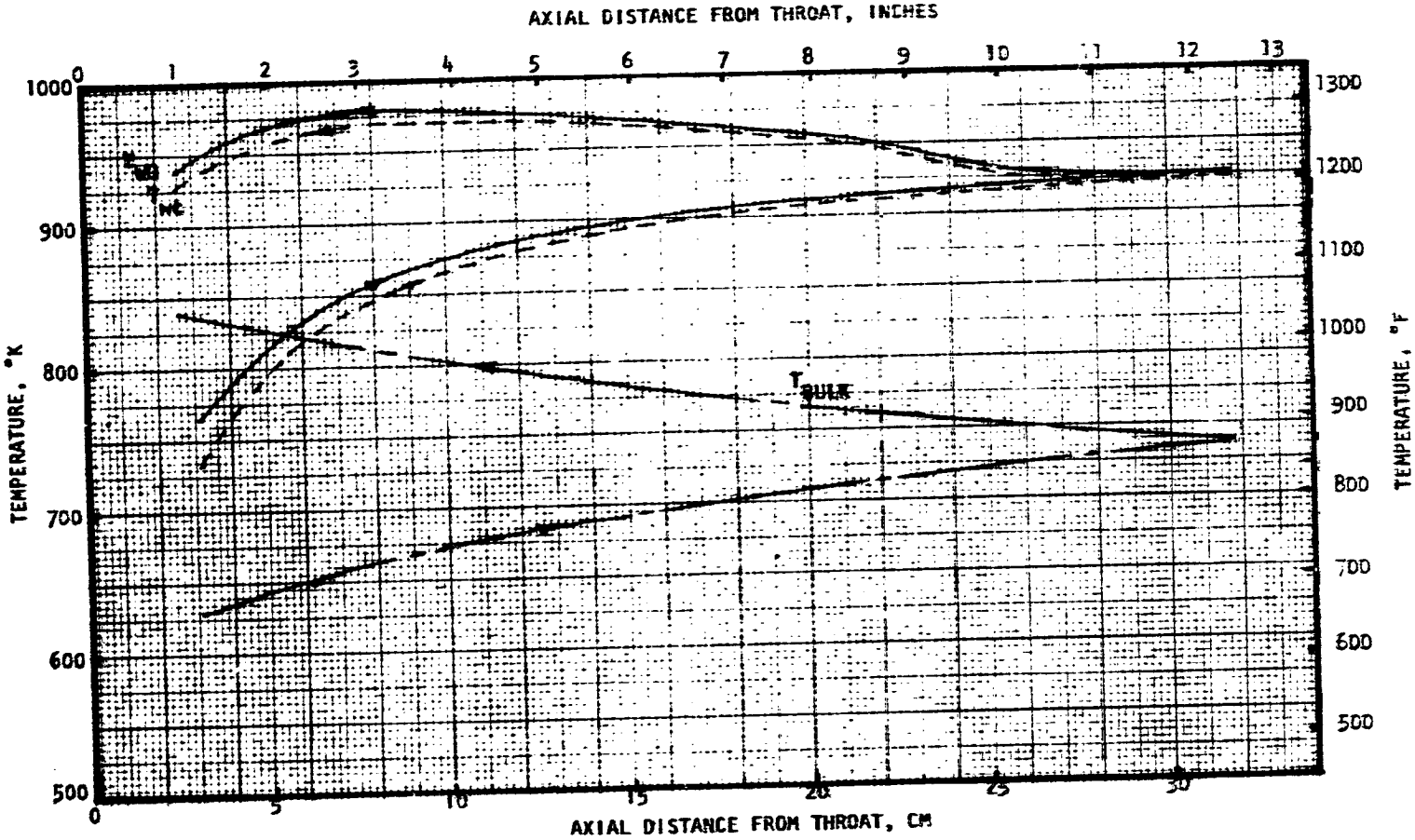

Figure 97. LO_2/CH_4 Engine - Fixed Nozzle Temperature Distributions

extreme end of the nozzle extension's travel provides a shutoff for the motor drive. A worm gear and flexible shafts to the three ball screws complete the nozzle extending mechanism Provisions for the gimbal actuators were provided by incorporating two clevis attachments to the structure housing the ball screw mechanism for the extendible nozzle.

Injector Design.

Element Design. Based on the propellants and the engine design conditions, the concentric element injector was selected for both engines. The pertinent parameters for the two injector designs are presented in Table 24. Both injectors consisted of 18 elements with 12 elements in the outer ring and 6 in the inner ring.

The LO_2/H_2 injector resulted in an expanded hydrogen velocity of 484 m/sec (1589 ft/sec) and an oxygen velocity of 16 m/sec (53 ft/sec). An oxidizer post recess of 0.1016 cm (0.04 inch) was selected.

The higher oxygen flowrate of the LO_2/CH_4 injector required a slightly larger oxidizer post diameter. The expanded methane velocity was 263 m/sec (862 ft/sec) and the oxygen velocity was 13 m/sec (43 ft/sec). Due to the larger oxidizer post diameter, the post recess of the LO_2/CH_4 injector was increased to 0.152 cm (0.06 inch).

Mechanical Design. The preliminary injector designs for the LO_2/H_2 and LO_2/CH_4 engines are presented in Fig. 98. The injectors contain 18 concentric tube elements previously described. The fuel manifold is formed by the injector face and a back plate. Due to the lower heat fluxes at the low-thrust engine conditions, the injector face would employ conduction/regenerative cooling. A high thermal conductivity material such as a copper alloy could be used as the injector face plate. This plate would be cooled by the fuel flowing through the face plate and the fuel flowing in the manifold. The body would be fabricated from stainless steel with a copper alloy injector face.

The fuel enters each element through a series of holes or slots in each fuel sleeve. The oxidizer manifold is behind the fuel manifold, and the oxygen is fed through the individual element tubes.

One approach to an ignitor design is shown in Fig. 98. Two igniters are installed 90 degrees to the thrust chamber centerline, and the ignitor gas flows into the combustion chamber through a center tube. Although this approach has been used in the past on larger chambers, this system will require further evaluation for this low-thrust application.

Turbomachinery Design. The hydrogen and methane turbopumps for the LO_2/H_2 and LO_2/CH_4 engines are similar in construction and consist of four partial-emission centrifugal pump stages with an inducer preceding the first-stage impeller; power is supplied by a partial-admission, single-stage axial-flow turbine. The mechanical arrangement and overall dimensions of the fuel turbopumps are shown in Fig. 99.

TABLE 24. LOW THRUST ENGINE INJECTOR SUMMARY

THRUST: 2224.1 N (500 lbf)	LO_2/H_2	LO_2/CH_4
CHAMBER PRESSURE, N/cm^2 (psia)	328.9 (477)	307.6 (446)
MIXTURE RATIO	6	3.7
ELEMENT TYPE	CONCENTRIC	CONCENTRIC
NUMBER OF ELEMENTS	18	18
OXIDIZER:		
"POST" INSIDE DIAMETER, cm (IN.)	0.127 (0.05)	0.1524 (0.06)
"POST" OUTSIDE DIAMETER, cm (IN.)	0.1778 (0.07)	0.2032 (0.08)
METERING ORIFICE DIAMETER, cm (IN.)	0.0864 (0.034)	0.0914 (0.036)
LO_2 FLOWRATE, kg/sec (lb/sec)	0.419 (0.923)	0.4944 (1.09)
EXIT VELOCITY, m/sec (ft/sec)	16.2 (53)	13.1 (43)
PRESSURE DROP, N/cm^2 (psi)	51.0 (74)	49.6 (72)
FUEL:		
CUP OUTSIDE DIAMETER., cm (IN.)	0.2921 (0.115)	0.2794 (0.110)
CUP GAP, cm (IN.)	0.0572 (0.0225)	0.0381 (0.015)
FUEL FLOWRATE, kg/sec (lb/sec)	0.0699 (0.154)	0.1338 (0.295)
GAP VELOCITY, m/sec (ft/sec)	615.7 (2020)	385.9 (1266)
EXPANDED VELOCITY, m/sec (ft/sec)	484.3 (1589)	262.7 (862)
PRESSURE DROP, N/cm2 (psia)	49.6 (72)	68.95 (100)
ELEMENT:		
RECESS, cm (IN.)	0.1016 (0.04)	0.1524 (0.06)
EXPANDED VELOCITY RATIO	30	20

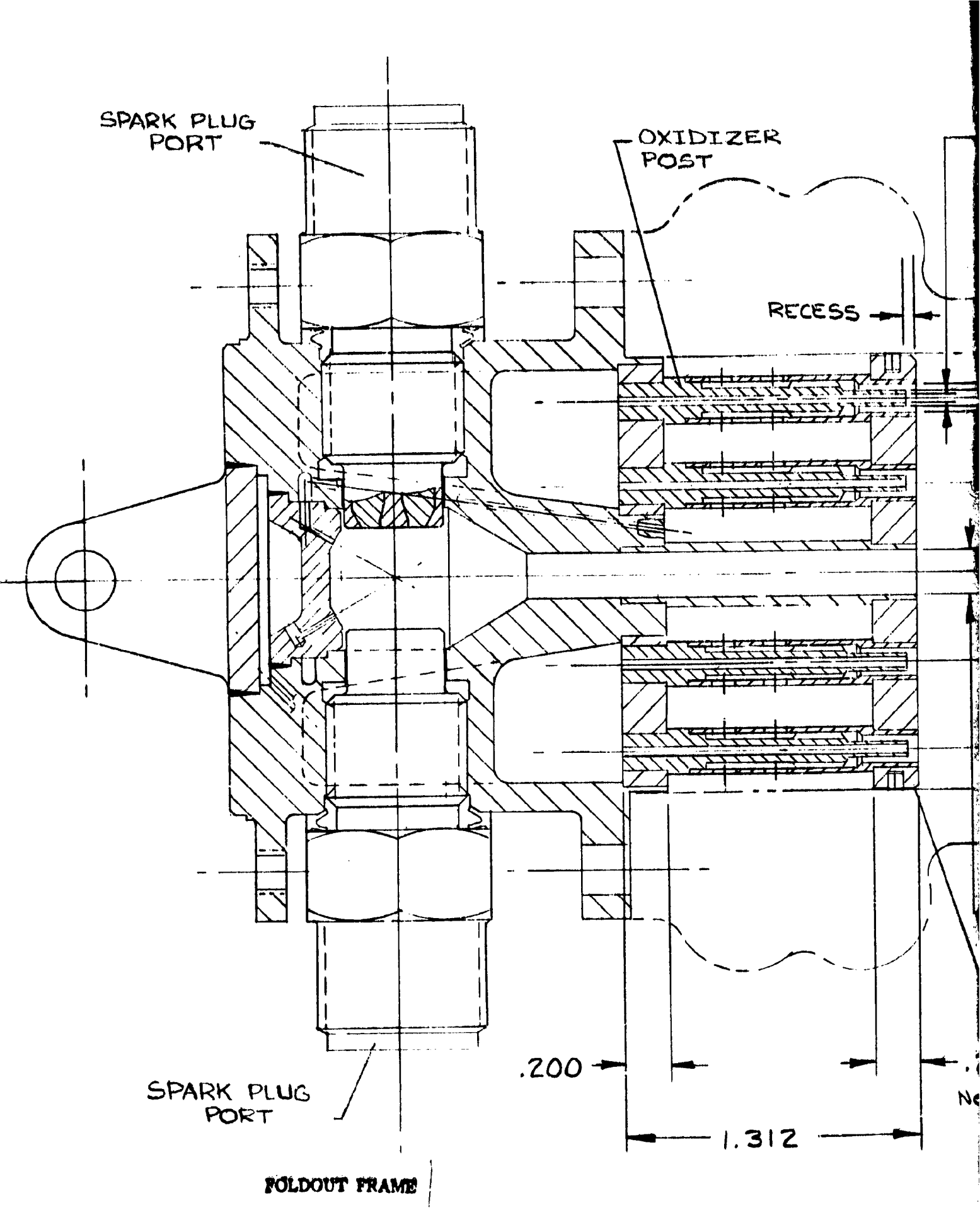

FOLDOUT FRAME

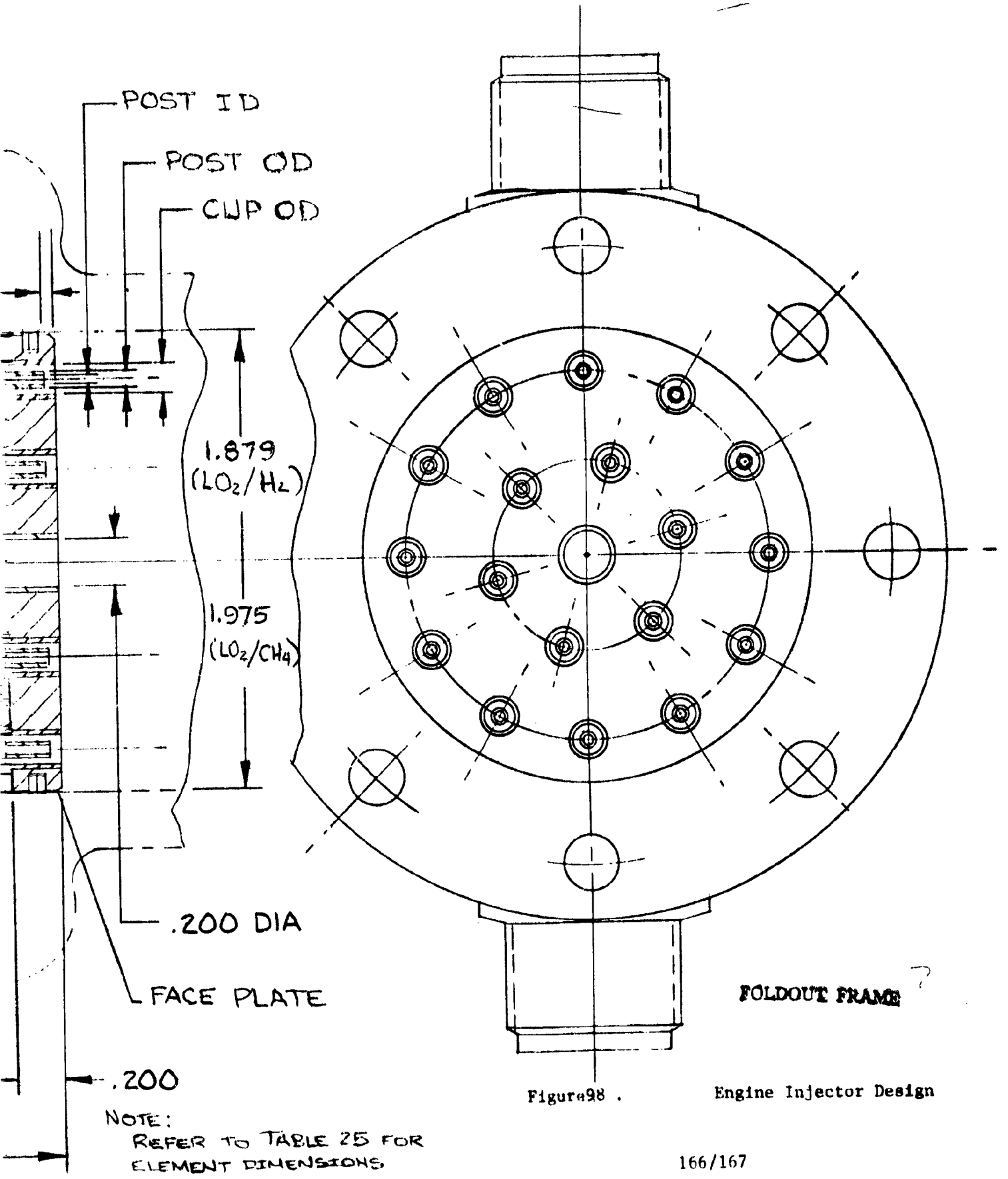

FOLDOUT FRAME

Figure98 . Engine Injector Design

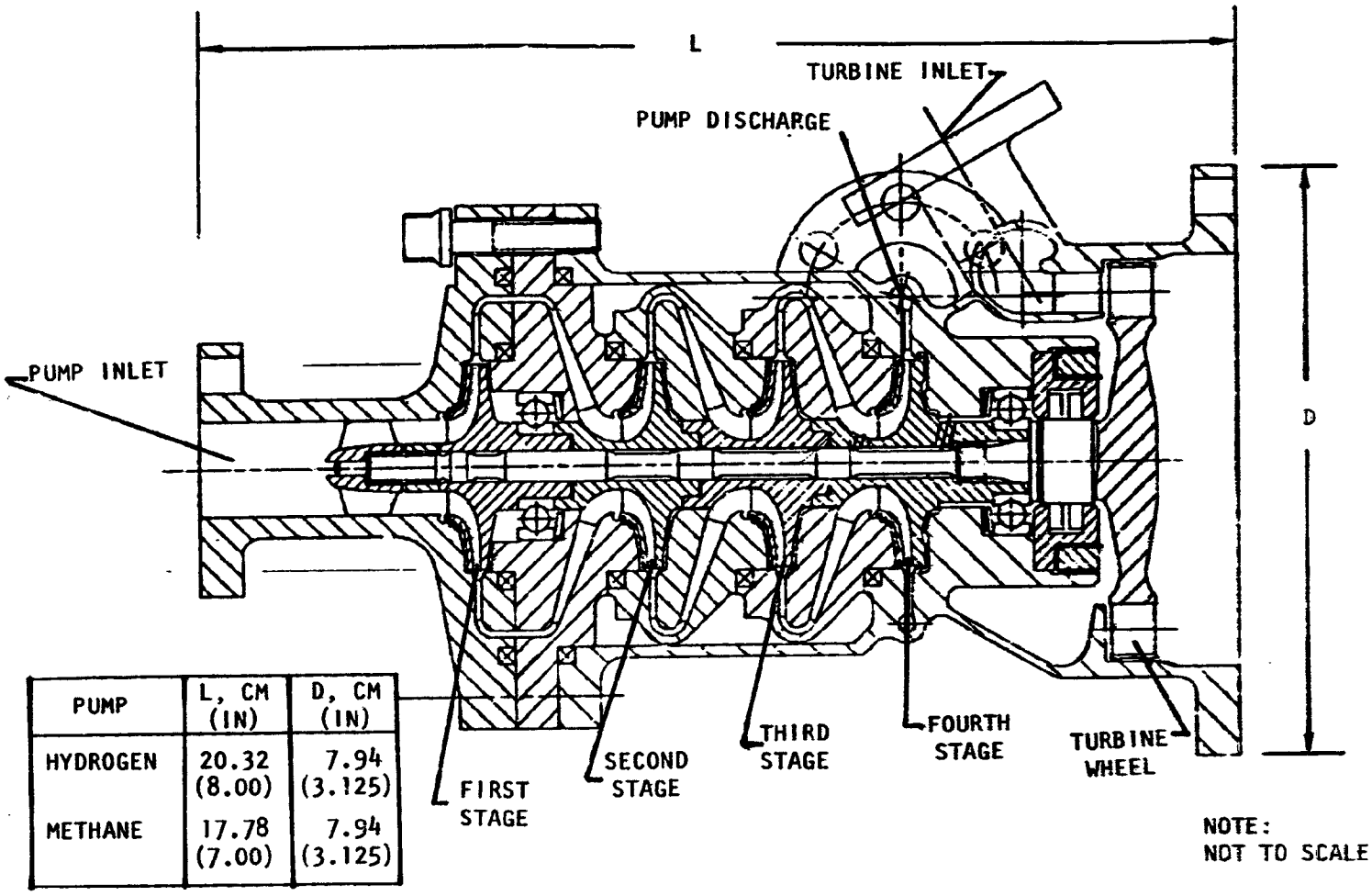

PUMP	L, CM (IN)	D, CM (IN)
HYDROGEN	20.32 (8.00)	7.94 (3.125)
METHANE	17.78 (7.00)	7.94 (3.125)

Figure 99. Hydrogen and Methane Turbopump Design

The oxygen turbopumps for the LO_2/H_2 and LO_2/CH_4 engines are also similar in construction and consist of two partial-emission centrifugal pump stages with an inducer preceding the first stage impeller; power is supplied by a partial-admission, single-stage axial-flow turbine similar to the fuel pump drive turbines. The mechanical arrangement and overall dimensions of the oxidizer turbopumps are shown in Fig. 100.

Design Point Operating Characteristics.

Hydrogen Turbopump - LO_2/H_2 Engine. Major design point hydrodynamic and aerodynamic parameters for the hydrogen pump and drive turbine are given in Tables 25 and 26. At the design speed of 12553 rad/sec (119870 rpm), the pump develops a head rise of 10921 M (35830 ft) with a delivered hydrogen flow rate of .000984 M^3/sec (15.59 gpm) and an efficiency of 37.9 percent. The turbine provides the required power of 19.67 Kw (26.38 HP) using .0628 kg/sec (.138 lb/sec) at an inlet temperature and pressure of 558 K (1005 R) and 581 N/cm^2 (843 psia) respectively and a pressure ratio of 1.31. A turbine efficiency of 51.1 percent is predicted.

Oxygen Turbopump - LO_2/H_2 Engine. Major design point hydrodynamic parameters for the oxygen pump and drive turbine are given in Tables 27 and 28. At the design speed of 2512 rad/sec (23990 rpm), the pump develops a head rise of 424 M (1392 ft) with an oxygen delivered flowrate of .000366 M^3/sec (5.80 gpm) and an efficiency of 28.2 percent. The turbine provides the required power of 6.16 Kw (8.26 HP) using .0608 kg/sec (.134 lb/sec) of hydrogen gas as the working fluid at an inlet temperature and pressure of 537 K (967 R) and 443 N/cm^2 (643 psia) respectively, and a pressure ratio of 1.16. A turbine efficiency of 30.7 percent is predicted.

Methane Turbopump - LO_2/CH_4 Engine. Major design point hydrodynamic and aerodynamic parameters for the methane pump and drive turbine are given in Tables 29 and 30. At the design speed of 4899 rad/sec (56330 rpm) the pump develops a head rise of 194 M (8358 ft) with a methane delivered flowrate of .000315 M^3/sec (4.0 gpm) and an efficiency of 34.9 percent. The turbine provides the required power of 7.27 Kw (9.75 HP) using .120 kg/sec (.265 lb/sec) of methane gas as the working fluid at an inlet temperature and pressure of 930 K (1674 R) and 567 N/cm^2 (823 psia) respectively and a pressure ratio of 1.35. A turbine efficiency of 42.5 percent is predicted.

Oxygen Turbopump - LO_2/CH_4 Engine. Major design point hydrodynamic and aerodynamic parameters for the oxygen pump and drive turbine are given in Tables 31 and 32. At the design speed of 3456 rad/sec (33000 rpm) the pump develops a head rise of 396 M (1299 ft) with an oxygen delivered flowrate of .000433 M^3/sec (6.86 gpm) and an efficiency of 49.5 percent. The turbine provides the required power fo 3.87 Kw (5.19 HP) using .108 kg/sec (.238 lb/sec) of methane gas as the working fluid at an inlet temperature and pressure of 916 K (1648 R) and 419 N/cm^2 (608 psia) respectively, and a a pressure ratio of 1.17. A turbine efficiency of 50 percent is predicted.

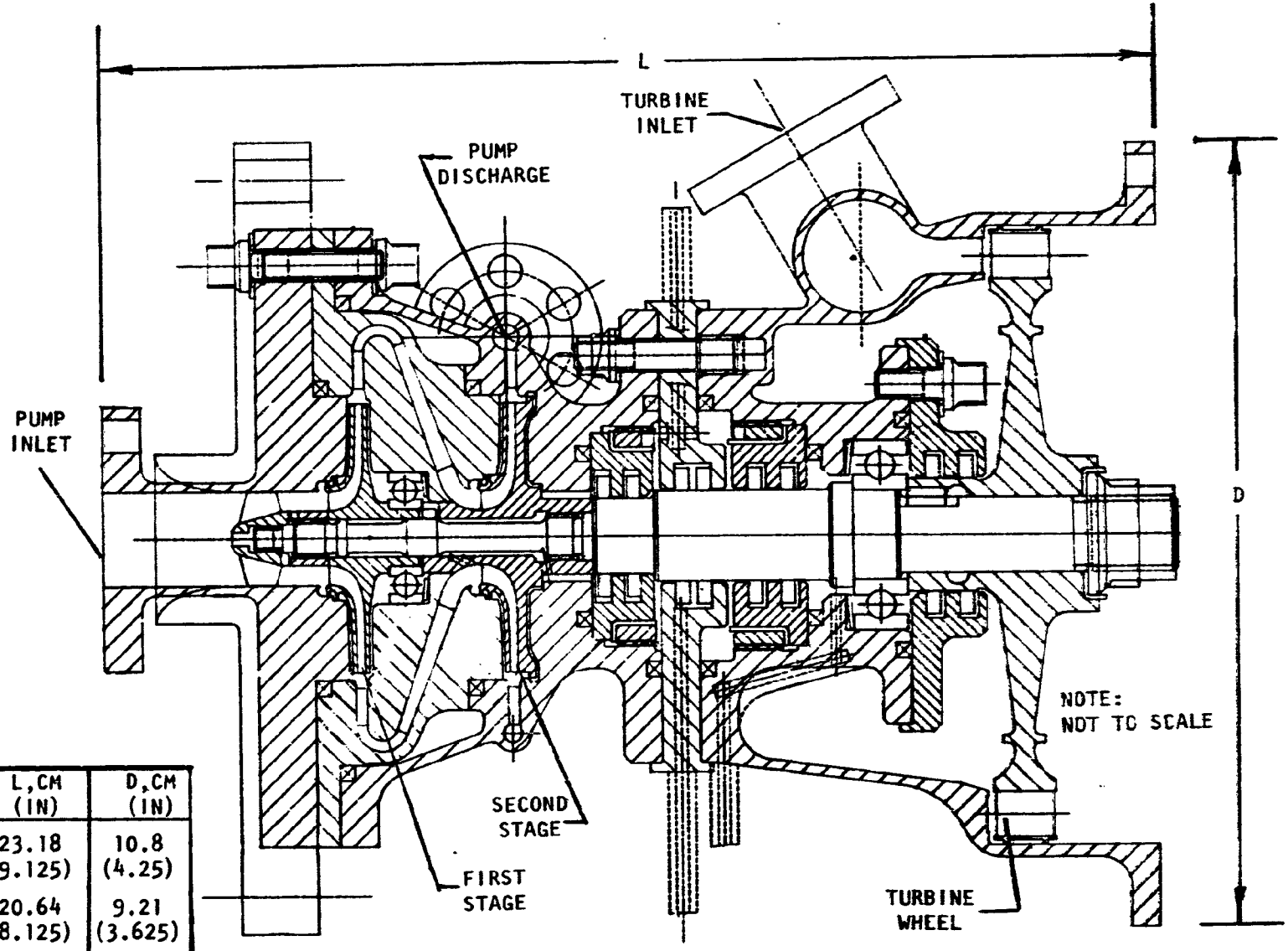

PROPELLANT	L, CM (IN)	D, CM (IN)
LO_2/H_2	23.18 (9.125)	10.8 (4.25)
LO_2/CH_4	20.64 (8.125)	9.21 (3.625)

Figure 100. Oxygen Turbopump Design

Type	INDUCER + 4 CENT.	
Speed, rad/sec (rpm)	12553	119870
Flowrate, M^3/sec (gpm)	.000984	15.59
NPSH, M (ft)	4.57	15.0
Inducer Headrise, M (ft)	66.5	218
Stage Headrise, M (ft)	2652.7	8703
Overall Headrise, M (ft)	10921	35830
Suction Specific Speed, rpm-gpm$^{.5}$/ft$^{.75}$	-	62100
Stage Specific Speed, rpm-gpm$^{.5}$/ft$^{.75}$	-	525
Power, Kw (HP)	19.67	26.38
Overall Efficiency, %		37.9
Inducer Inlet Tip Diameter, cm (in)	1.288	.507
Impeller Inlet Tip Diameter, cm (in)	1.288	.507
Impeller Discharge Tip Diameter, cm (in)	3.658	1.440
Impeller Discharge Tip Width, cm (in)	0.130	.051
Emission, %		42

TABLE 26. TURBINE DESIGN POINT HYDROGEN TURBOPUMP - LO_2/H_2 ENGINE

Type	PARTIAL ADMISSION SINGLE STAGE AXIAL	
Working Fluid	HYDROGEN	GAS
Speed, rad/sec (rpm)	12553	119870
Flowrage, Kg/sec (lb/sec)	.0628	.138
Total Inlet Temperature, K (R)	558	1005
Total Inlet Pressure, N/cm^2 (psia)	581	843
Total Exit Pressure, N/cm^2 (psia)	443	643
Pressure Ratio (total/total)		1.31
Power, Kw (HP)	19.67	26.38
Efficiency (total/total) %		51.1
Mean Diameter, cm (in)	5.97	2.35
Blade Height, cm (in)	.76	.30
Admission, %		7.4
Velocity Ratio		.35

Type	INDUCER	+ 2 CENT.
Speed, rad/sec (rpm)	2512	23990
Flowrate, M^3/sec (gpm)	0.000366	5.80
NPSH, M (ft)	0.610	2
Inducer Headrise, M (ft)	3.66	12
Stage Headrise, M (ft)	210	690
Overall Headrise, M (ft)	424	1392
Suction Specific Speed, rpm-gpm$^{.5}$/ft$^{.75}$	-	34350
Stage Specific Speed, rpm-gpm$^{.5}$/ft$^{.75}$	-	429
Power, Kw (HP)	6.16	8.26
Overall Efficiency, %		28.2
Inducer Inlet Tip Diameter, cm (in)	1.501	.591
Impeller Inlet Tip Diameter, cm (in)	1.501	.591
Impeller Discharge Tip Diameter, cm (in)	5.105	2.010
Impeller Discharge Tip Width, cm (in)	0.076	.03
Emission, %		33

TABLE 28. TURBINE DESIGN POINT OXYGEN TURBOPUMP - LO_2/H_2 ENGINE

Type	PARTIAL ADMISSION SINGLE STAGE AXIAL	
Working Fluid	HYDROGEN	GAS
Speed, rad/sec (rpm)	2512	23990
Flowrage, Kg/sec (lb/sec)	.0608	.134
Total Inlet Temperature, K (R)	537	967
Total Inlet Pressure, N/cm^2 (psia)	443	643
Total Exit Pressure, N/cm^2 (psia)	382	554
Pressure Ratio (total/total)		1.16
Power, Kw (HP)	6.16	8.26
Efficiency (total/total) %		30.7
Mean Diameter, cm (in)	9.4	3.7
Blade Height, cm (in)	.76	.30
Admission, %		9.6
Velocity Ratio		.15

TABLE 29
PUMP DESIGN POINT
METHANE TURBOPUMP - LO_2/CH_4 ENGINE

Type	INDUCER + 4 CENT.	
Speed, rad/sec (rpm)	5899	56330
Flowrate, M^3/sec (gpm)	.000315	5.00
NPSH, M (ft)	1.68	5.5
Inducer Headrise, M (ft)	11.6	38
Stage Headrise, M (ft)	482	1580
Overall Headrise, M (ft)	1938	6358
Suction Specific Speed, rpm-gpm$^{.5}$/ft$^{.75}$	-	35070
Stage Specific Speed, rpm-gpm$^{.5}$/ft$^{.75}$	-	503
Power, Kw (HP)	7.27	9.75
Overall Efficiency, %		34.9
Inducer Inlet Tip Diameter, cm (in)	1.143	.450
Impeller Inlet Tip Diameter, cm (in)	1.143	.450
Impeller Discharge Tip Diameter, cm (in)	3.302	1.300
Impeller Discharge Tip Width, cm (in)	0.076	.030
Emission, %		37

TABLE 30
TURBINE DESIGN POINT
METHANE TURBOPUMP - LO_2/CH_4 ENGINE

Type	PARTIAL ADMISSION SINGLE STAGE AXIAL	
Working Fluid		METHANE GAS
Speed, rad/sec (rpm)	5899	56330
Flowrage, Kg/sec (lb/sec)	.120	.265
Total Inlet Temperature, K (R)	530	1674
Total Inlet Pressure, N/cm^2 (psia)	567	823
Total Exit Pressure, N/cm^2 (psia)	419.2	608
Pressure Ratio (total/total)		1.35
Power, Kw (HP)	7.27	9.75
Efficiency (total/total) %		42.5
Mean Diameter, cm (in)	5.84	2.3
Blade Height, cm (in)	0.762	.30
Admission, %		7.6
Velocity Ratio		.32

TABLE 31
PUMP DESIGN POINT
OXYGEN TURBOPUMP - LO_2/CH_4 ENGINE

	INDUCER + 2 CENT.	
Type		
Speed, rad/sec (rpm)	3456	33000
Flowrate, M^3/sec (gpm)	.000433	6.86
NPSH, M (ft)	0.61	2.0
Inducer Headrise, M (ft)	8.23	27
Stage Headrise, M (ft)	194	636
Overall Headrise, M (ft)	396	1299
Suction Specific Speed, rpm-gpm$^{.5}$/ft$^{.75}$		51400
Stage Specific Speed, rpm-gpm$^{.5}$/ft$^{.75}$		682
Power, Kw (HP)	3.87	5.19
Overall Efficiency, %		49.5
Inducer Inlet Tip Diameter, cm (in)	1.633	.643
Impeller Inlet Tip Diameter, cm (in)	1.633	.643
Impeller Discharge Tip Diameter, cm (in)	3.556	1.400
Impeller Discharge Tip Width, cm (in)	0.076	.03
Emission, %		92

TABLE 32
TURBINE DESIGN POINT
OXYGEN TURBOPUMP - LO_2/CH_4 ENGINE

Type	PARTIAL ADMISSION SINGLE STAGE AXIAL	
Working Fluid —		METHANE GAS
Speed, rad/sec (rpm)	3456	33000
Flowrage, Kg/sec (lb/sec)	.108	.238
Total Inlet Temperature, K (R)	916	1648
Total Inlet Pressure, N/cm^2 (psia)	419	608
Total Exit Pressure, N/cm^2 (psia)	357	518
Pressure Ratio (total/total)		1.17
Power, Kw (HP)	3.87	5.19
Efficiency (total/total) %		50
Mean Diameter, cm (in)	7.37	2.9
Blade Height, cm (in)	0.838	.33
Admission, %		7.8
Velocity Ratio		.34

OFF-DESIGN OPERATING CHARACTERISTICS

The off-design characteristics of the pumps were developed utilizing available experimental data. In general the off-design pump characteristics are of a function of design flow coefficient, design head coefficient, number of blades, discharge blade angle, and impeller inlet to discharge tip diameter ratio. These influences essentially reduce to a variation of normalized head coefficient with inlet flow coefficient and specific speed since typically small discharge blade angles are used and the other parameters are a function of specific speed.

The non-cavitating off-design normalized head coefficient and efficiency curves which were generated and used to perform the off-design cycle balances are shown in Figure 101. Because of similarity in thermophysical fluid properties and pump head coefficient, the off-design characteristics of the oxygen pumps and methane pumps were assumed to be the same.

Typical off-design cavitating performance curves for the pumps are shown in Fig. 102. At flow coefficients higher than the design value, the suction performance deteriorates rapidly. A slight reduction in supplied NSPH (slight increase in suction specific speed) causes a large drop in head rise, which means that there is little margin when operating at flow coefficients greater than design. Section characteristics are much more forgiving at lower than design flow coefficients where a slight decrease in NPSH causes a slight decrease in head rise.

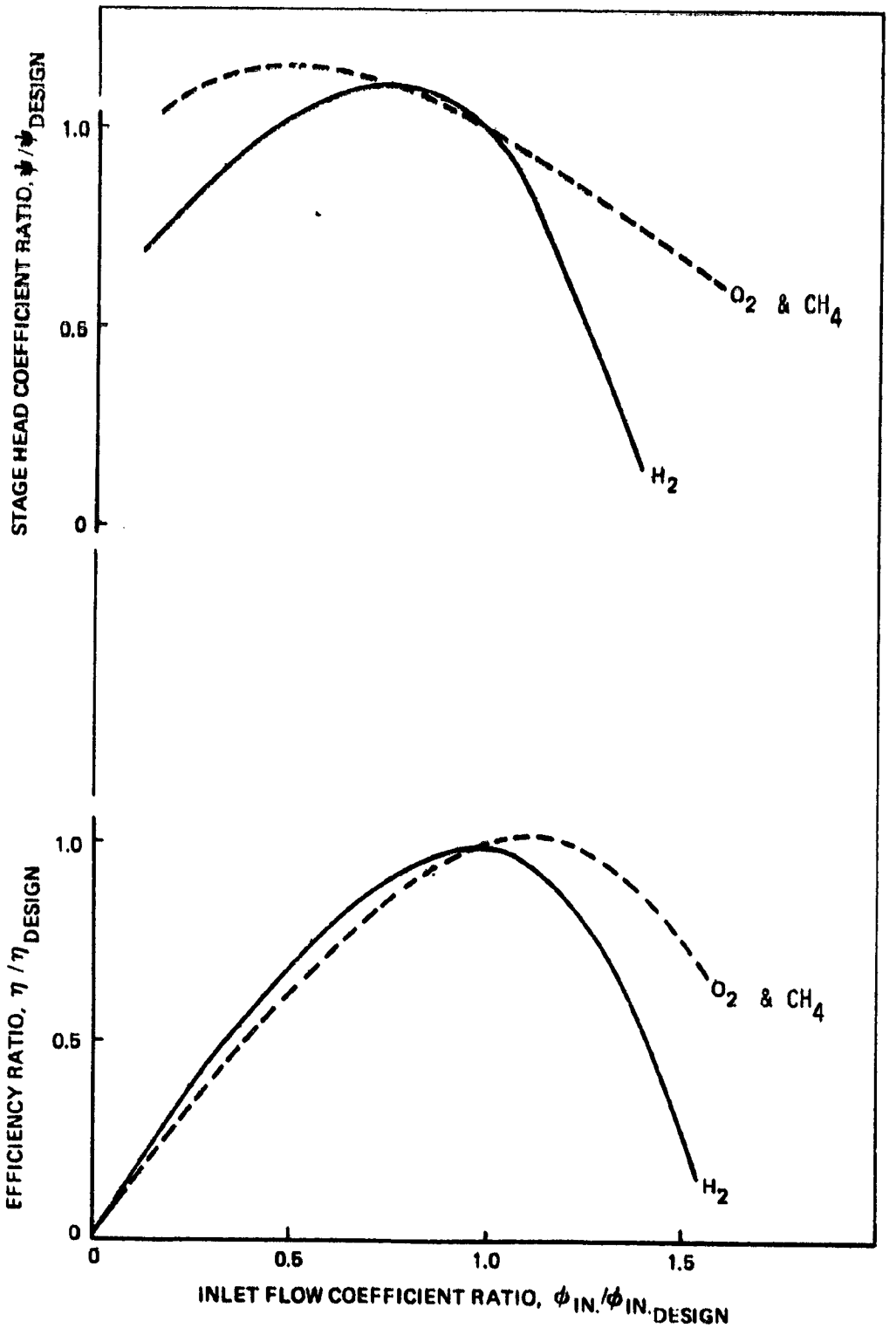

Figure 101. NON-CAVITATING OFF-DESIGN PUMP CHARACTERISTICS

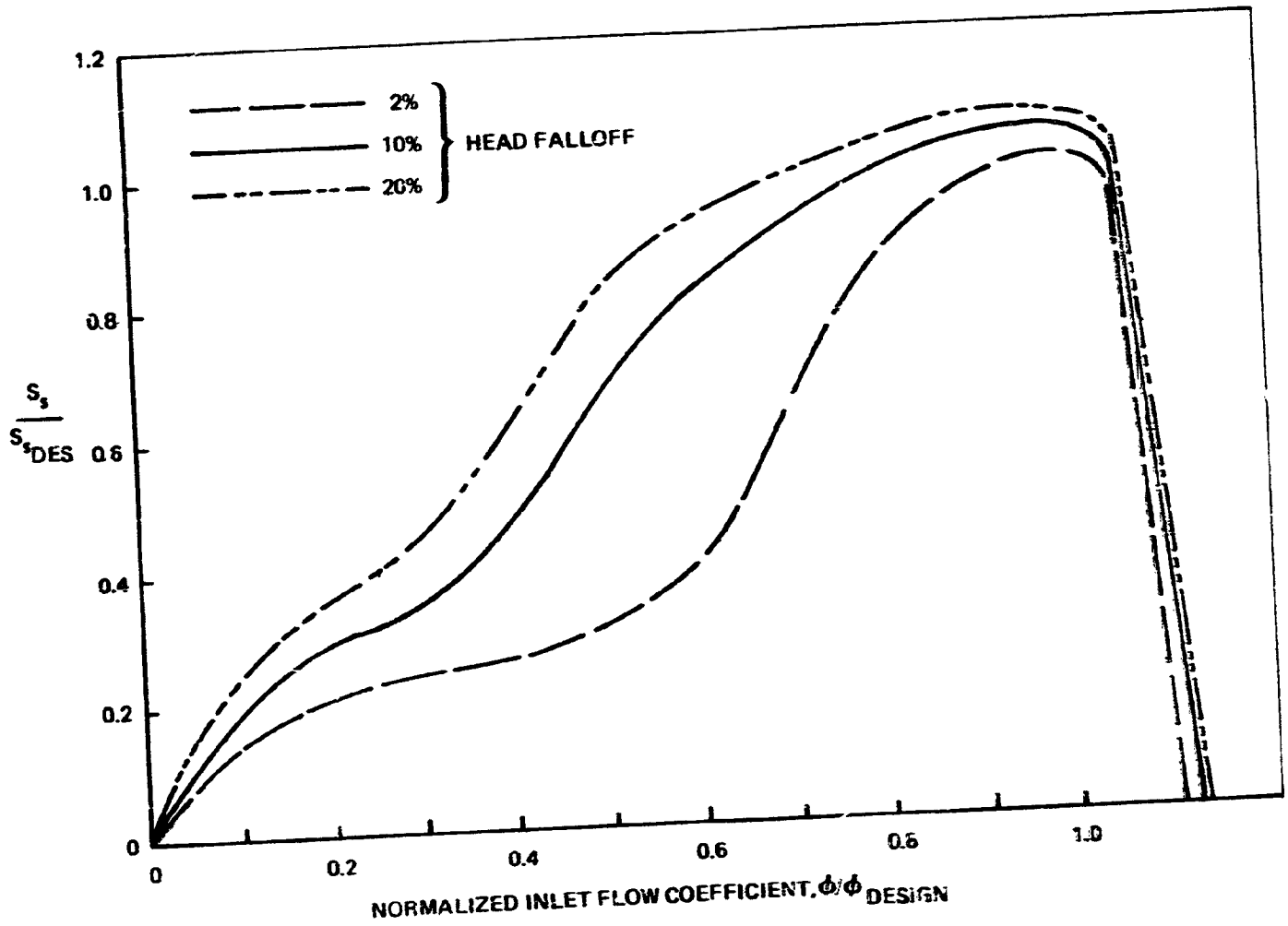

Figure 102 . OFF-DESIGN CAVITATING PERFORMANCE

Turbine off-design losses are characterized by a loss coefficient that is a function of the angle of attack on the rotor blade leading edge. When operating at the turbine design point, the angle of attack is zero, and as a result, no incidences losses are encountered. The losses increases as the approach angle is greater or less than the design angle.

The turbine off-design performance was determined using a turbine stage efficiency versus velocity ratio (blade mean velocity-to-isentropic velocity) curve for the single stage stage partial admission turbine of the design pitch diameter.

For the LO_2/H_2 engine, the fuel turbine efficiency varied $\pm$ 3 - percent and the oxidizer turbine efficiency varied $\pm$ 1 - percent from the design point value for the $\pm$ 10 - percent engine mixture ratio variation. The turbine efficiencies increased with decrease in mixture ratio. The LO_2/CH_4 engine fuel turbine efficiency varied $\pm$ 1 - percent and the oxidizer turbine efficiency varied $\pm$ 2 - percent for the $\pm$ 10 - percent mixture ratio variation

MECHANICAL DESIGN

Hydrogen and Methane Turbopumps

The hydrogen and methane turbopumps are four-stage, partial emmission centrifugal pumps with an inducer preceeding the first impeller, and powered by a partial-admission, single-stage, axial-flow turbine (Fig. 99). The pumps have an axial inlet and a radial discharge. The turbines have a radial inlet and an axial discharge.

The rotating assembly for both turbopumps consists of the turbine wheel with an integrally fabricated draw bar on which are mounted the four impellers and two bearings. Tension in the draw bar is applied by a nut in front of the first-stage impeller. The bearings are mounted on the first- and fourth-stage impellers, and the compressive load from the draw bar passes through the bearing inner races. The torque applied by the turbine is transmitted to the fourth-stage impeller by a spline. The torque is then transferred between the impellers by tanks and slots machined integrally in each impeller. The use of a through-hole in the impellers is possible because of the low tip speed of the impellers. The inducer is threaded on to the draw bar. The tab lock between the inducer and the impeller retaining nut allows the nut to be locked in an infinite number of positions when tensioning the draw bar. The torque required to drive the inducer will be transmitted by the lock tab washer.

Positioning of the impellers is provided by a pilot diameter and a normal bearing surface on each end. Repositioning error when the rotor is disassembled and reassembled is reduced by allowing the impellers to be assembled in only one angular rotation position.

The pump housing assembly contains of three major components. The pump inlet contains a cast diffuser passage for the first-stage impeller and provides a tunnel for the inducer. The pump bearing carrier contains the cast "down comer" which completes the crossover for the first-stage impeller. It also provides a precision diameter for accepting the forward pump bearing. The main pump housing contains the cast fourth-stage impeller diffuser, the volute collector and discharge diffuser plus the turbine inlet manifold and nozzle blades. The second- and third-stage impeller crossovers are cast and are buried in the assembly (i.e., no external flanges). They are slotted fore and aft and are pinned for angular radial positioning. The pins also carry the reaction torque from the crossovers. The turbine end bearing and seal are located in the turbine end of the housing.

The bearings are preloaded against each other at assembly by tension in the draw bars. The seal is retained in the main housing by a nut and cup lock washer.

Static seals are provided for all external flanges. An inner row of static seals seal the crossover at the impeller discharge diameter. Leakage past the seals will be vented to the pump inlet aft of the inducer. The result is that the flange seals will experience the inducer discharge pressure, except for the inlet flange static seal which will be subjected to the first-stage impeller diffuser discharge pressure.

The bearings are of the angular contact type designed to run in LH$_2$. The turbine/pump seal is of the "controlled gap" type and is internally pressurized. The pressurizing flow comes from the pump discharge. The leakage flow toward the pump provides the coolant flow for the turbine end bearing. The pump end bearing coolant flow is provided by the pressure rise of the first-stage crossover.

The rotor thrust loads are balanced out by a "balance piston" that is an integral part of the fourth-stage impeller. The high-pressure orifice is provided by a lip on the pump housing and a lip on the impeller OD. The low pressure orifice is provided by a matching surface on the impeller and housing. Balance piston flow is ducted to the ID of the fourth-stage impeller and delivered to the inlet of the same impeller. The flow from the balance piston is mixed with the bearing coolant flow in the balance piston sump prior to returning to the fourth-stage impeller inlet.

The impeller's eyes are sealed by a stepped labyrinth wear rings. The rear shroud leakage is controlled by a close-fitting diameter between the crossovers and the impeller hubs. This close-fitting diameter also forms a "squeeze film damper" for controlling the shaft excursions experienced during times that the pump rpm passes through a critical speed range.

The materials chosen for use in the pump and turbine are those that have been proven in previous turbopump designs. The impellers and crossovers will be fabricated from cast Inconel 718. The pump inlet and main pump housing will be fabricated from cast and wrought Inconel 718. The turbine wheel will have integrally machined blades and be made from Inconel 718. The bearings are 440c corrosion-resistant steel. In the hydrogen turbopump, protection of the structural parts from the hydrogen environment is provided by plating the exposed surfaces with a suitable material.

Oxygen Turbopumps

The oxygen turbopumps are two-stage, partial-emission, centrifugal pumps with an inducer, and are powered by a partial-admission, single-stage, axial-flow turbine (Fig. 100). The basic pump and turbine design approaches used in the oxygen turbopump design were similar to those incorporated in the hydrogen and methane turbopumps. The primary differences are associated with the turbine wheel-to-shaft mounting and the pump-to-turbine seal package. For the oxygen turbopump, the turbine wheel is bolted on the pump shaft and not integral to the shaft as in the fuel turbopumps.

The oxygen turbopump seals that separate the pumped fluid from the turbine bearing coolant fluid are all of the "controlled gap" type. The pump seal has two sealing elements, and leakage past this seal flows into the area between the pump seal and the intermediate seal. The intermediate seal is pressurized internally by an inert gas that forms the high-pressure barrier between the two working fluids. Inert gas that leaks toward the pump is mixed with the pump fluid that leaked past the pump seal and is vented over board. The bearing coolant seal has two bearing elements, and leakage past them mixes with the leakage flow of the inert gas past the intermediate seal that leaked towards the turbines. This mixed gas is then vented over board. The turbine gas seal is of the controlled gap type, and the chamber that contains the turbine end bearing is pressurized to a higher pressure than the turbine nozzle exit pressure so that the bearing coolant leakage flow goes into the turbine.

The materials for the individual components of the oxygen turbopumps are the same as those utilized in the hydrogen and methane turbopumps.

VALVE DESIGN

Design of the four primary control valves (MOV, MFV, TBV, and OTBV) was based on a rotary configuration utilizing a common electric actuator. Fail safe actuator electrical operation is provided by dual electric motors and coils in the linear variable differential transformer (LVDT) position transducer. Fail safe engine shutdown is provided by a pneumatic override piston on the MOV and TBV actuated from separate three-way solenoid valves.

The MOV and MFV employ a common design sector ball valve closure with a positive shutoff seat seal. Minimum friction in the ball suspension is accomplished by two roller bearings at the valve ball shaft and a roller thrust bearing to support shaft seal unbalanced area. Since no metal-to-metal sliding parts exist within the valve, lubrication is not required. A typical MOV configuration is presented in Fig. 103. The valving elements of the MFV and MOV are identical. Line geometry and sizes differ since the MFV would operate full open to minimize pressure drop. For both the LO_2/H_2 and the LO_2/CH_4 engine, the MFV is incorporated on a 1.905 cm (3/4 - IN) line and the MOV in a 0.957 (3/8 - IN) line. The electric actuator on the MFV is identical with the MOV except that the pneumatic override and clutch assemblies are omitted.

The TBV and OTBV both utilize a simple rotary plug configuration. The plug is guided by precision roller bearings similar to the main valves. A typical TBV design is shown in Fig. 104. Assembly and construction features of the shaft seal and actuators of the TBV and OTBV are identical to those of the MOV and MFV, respectively. For both engines, these valves were incorporated in a 0.953 cm (3/8 - IN) line.

PARAMETRIC ENGINE DATA

The parametric engine data generated in this program included delivered specific impulse, engine length and diameter, and engine weight for the following range of conditions for both LO_2/H_2 and LO_2/CH_4 expander cycle engines.

Thrust: 444.8 N (100 lbf) to 13345 N (3000 lbf)

Chamber Pressure: 68.95 N/cm^2 (100 psia) to 689.5 N/cm^2 (1000 psia)

Area Ratio: 200 to 1000

The data were generated for a nominal LO_2/H_2 mixture ratio of 6-to-1 and 3.7-to-1 for LO_2/CH_4.

For the 200-to-1 area ratio engines, the nozzle was completely regeneratively-cooled and for the engines having higher area ratios, the nozzle was regeneratively-cooled to one half the total nozzle area ratio.

The engine dimensions for the LO_2/H_2 and LO_2/CH_4 engines were essentially identical. The LO_2/CH_4 engines are only 0.3 to 2% longer in length. Therefore the LO_2/H_2 engine dimensional data can be used for the LO_2/CH_4 engine.

The engine performance parametric data are presented in Appendix D, the engine dimensional data in Appendix E, and the engine weights in Appendix F.

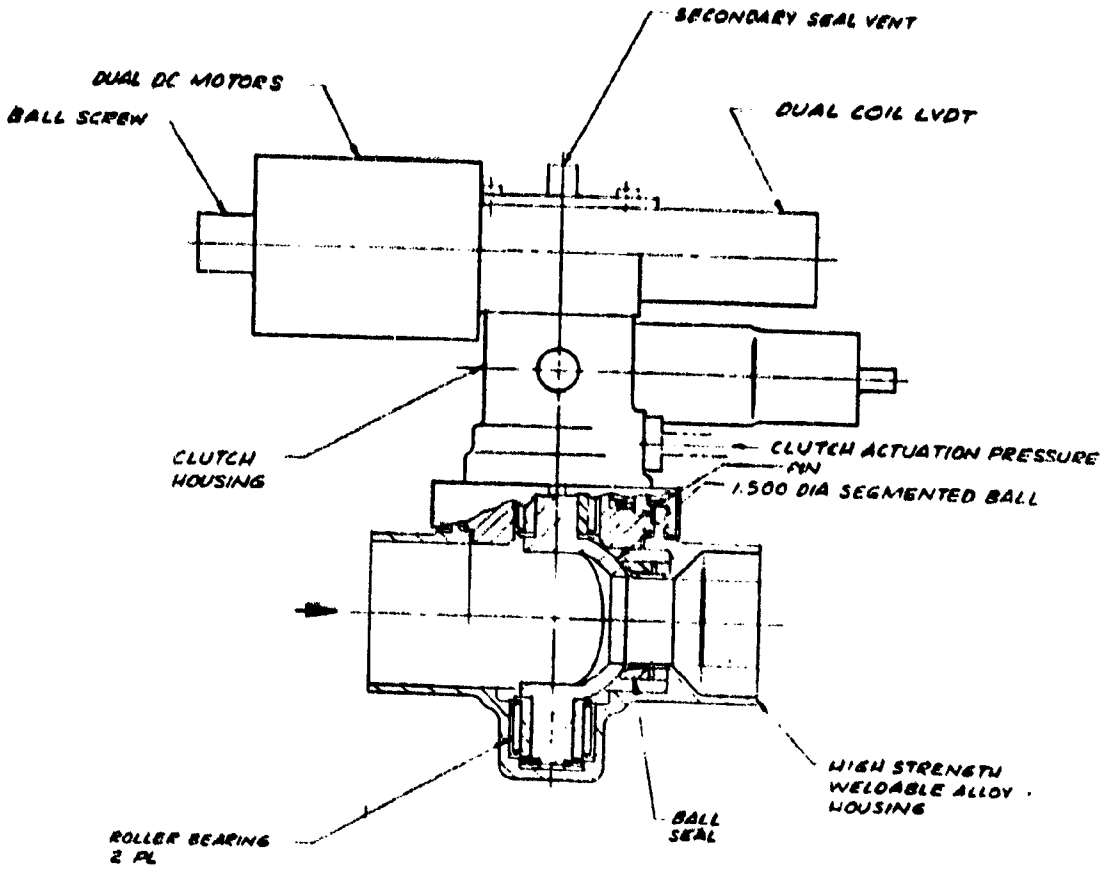

FIGURE 103. TYPICAL MAIN OXIDIZER VALVE (MOV) DESIGN

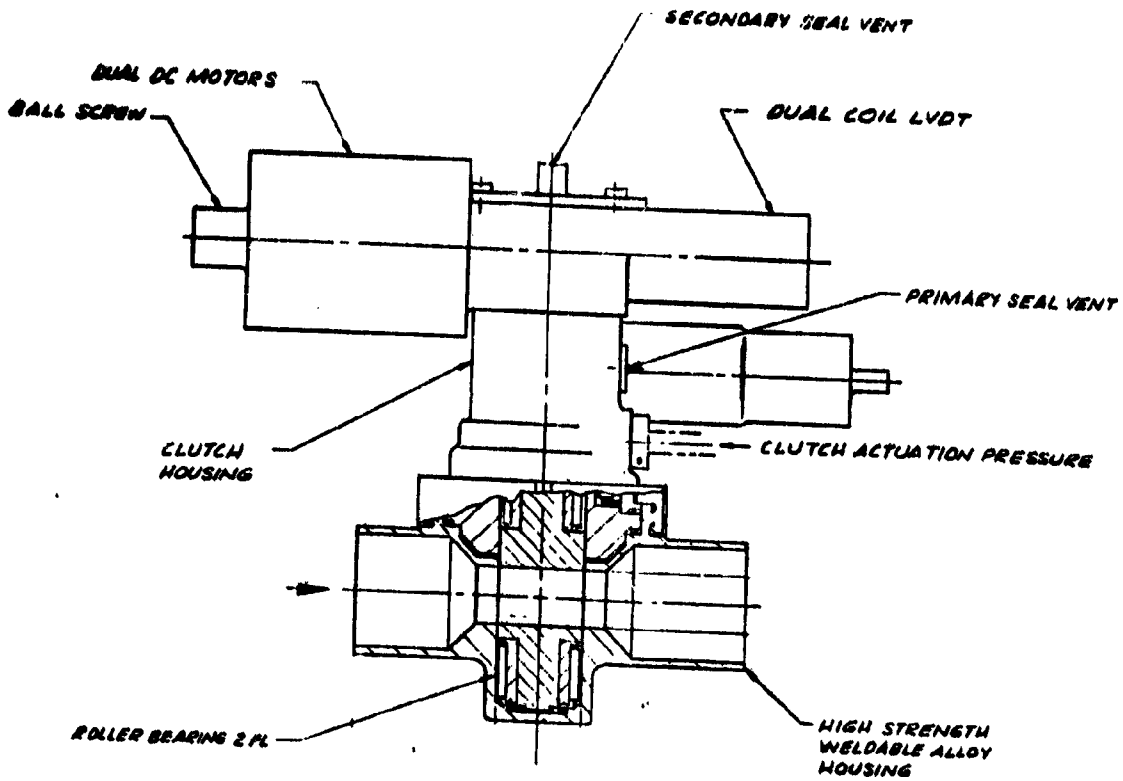

FIGURE 104. TYPICAL TURBINE BYPASS VALVE (TBV) DESIGN

Engine Performance

The delivered engine specific impulse parametric data are presented in Appendix D in a series of three types of plots for each propellant. These included:

1. Delivered engine specific impulse versus nozzle area ratio for parametric chamber pressure at constant thrust.

2. Delivered engine specific impulse versus thrust for parametric chamber pressure at constant nozzle area ratio.

3. Delivered engine specific impulse versus chamber pressure for parametric thrust at constant nozzle area ratio.

An interesting trend is evident from the LO_2/H_2 engine performance data. Increases in nozzle area ratio resulted in significant performance gains. For example, 2224.1 N (500 lbf) thrust and 344.7 N/cm^2 (500 psia) chamber pressure, an increase in nozzle area ratio from the nominal 400 to 1000 resulted in a 1.0% specific impulse gain which is more than if the chamber pressure was doubled with a 400-to-1 area ratio nozzle.

For the LO_2/CH_4 engines, increasing chamber pressure provided more specific impulse gain than increase in the nozzle area ratio.

As previously shown and discussed, the LO_2/H_2 delivered engine specific impulse is not significantly influenced by thrust beyond 1334.5 N (3000 lbf) and this was true for the entire area ratio range of interest.

The influence of thrust was more significant for the LO_2/CH_4 engines although most of the change again occurred below 1334.5 N (300 lbf) thrust.

The delivered specific impulse decreased rapidly as the design chamber pressure decreased, particularly below 206.8 N/cm^2 (300 psia) chamber pressure for the LO_2/H_2 engines. For the LO_2/CH_4 engines, the delivered specific impulse continually decrease with decrease in chamber pressure for all thrust levels. The overall specific impulse decrease from a chamber pressure of 689.5 N/cm^2 (1000 psia) to 68.95 N/cm^2 (100 psia) was 6.3 for the LO_2/H_2 engines and 9.6% for the LO_2/CH_4 engines.

Engine Dimensions

The parametric engine dimensional data generated included the total engine length (nozzle extended) and the engine/diameter (nozzle exit diameter). A series of parametric plots are presented in Appendix E. These included:

Engine Length:

1. Engine length versus nozzle area ratio for parametric chamber pressure at constant thrust.

2. Engine length versus chamber pressure for parametric thrust at constant nozzle area ratio.

3. Engine length versus chamber pressure for parametric area ratio at constant thrust.

Engine Diameter:

1. Engine diameter versus nozzle area ratio for parametric chamber pressure at constant thrust.

2. Engine diameter versus chamber pressure for parametric area ratio at constant thrust.

Because the LO_2/H_2 and LO_2/CH_4 engine dimensional data were essentially identical, only the LO_2/H_2 engine data were plotted.

The parametric engine length and diameter can be used to explore the chamber pressure, thrust, and nozzle area ratio dimensional variations for a specific vehicle application. As discussed previously, the engine cycle limits previously determined for the nominal 400-to-1 area ratio engines can be used to conservatively determine the upper design chamber pressure limit.

Primary engine dimensional trends are that short engine lengths and small engine diameters are achieved by high chamber pressures, low thrusts, and low nozzle area ratios. The total engine length is equal to the sum of the distance from the injector plane to the engine gimbal, the combustion chamber length, and the nozzle length. Although the data presented in Appendix E contain these terms, the nozzle length is the dominant term for high area ratio. Therefore the engine length can be approximated by

$$l_{ENG} \alpha \sqrt{\frac{F\varepsilon}{\delta}}$$

for a constant percent length nozzle and a constant thrust coefficient (C_f).

The engine diameter is exactly proportional to the same term

$$D_{ENG} \propto \sqrt{\frac{F\epsilon}{\delta}}$$

Engine Weight

Due to small size of some low thrust engines, the wall thicknesses of many components become gauge or fabrication limited, particularly at low thrusts and low chamber pressures. Also turbopump weight trends are dependent on the pump design limitation. The limitation can be suction performance, bearing DN or impeller diameter. These influences were estimated and the component weight variations with thrust, chamber pressure and area ratio were developed and the parametric engine weights generated.

The parametric engine weight data for the LO_2/H_2 and the LO_2/CH_4 expander cycle engines are presented in Appendix F. The LO_2/CH_4 engines were 5 to 15% lighter than the LO_2/H_2 engines for the same design conditions. Engine weights decreased with increase in chamber pressure and became less sensitive to chamber pressure at high chamber pressure. Of course, as thrust was increased (engine size increased) for a given chamber pressure and nozzle area ratio, the engine weight increased. The engine weight increase with increase in nozzle area ratio was expected but increased more at low chamber pressures than at high chamber pressures. Therefore increases in nozzle area ratio at high chamber pressures would minimize added engine weight to achieve engine performance increases.

TECHNOLOGY ASSESSMENT

In determining the preliminary design of each component within each engine system, the technology advancements required were assessed in the formulation of the design. The assessment was divided into sections as follows: engine system and the individual engine components (turbopump, thrust chamber, and injector/igniter).

Engine System

In formulating the low thrust propulsion system, the primary goals were high engine performance, decreased engine size and weight and system simplicity. To achieve high engine performance, two areas warrant further investigation: (1) design point evaluation utilizing a high nozzle area ratio, and (2) evaluation of improved turbopump performance and enhanced turbine drive gas heat transfer.

For the most part the current program focused on a 400-to-1 area ratio nozzle, but in the process of generating the parametric engine performance data, it became apparent the significant performance gains could be achieved through increases in area ratio. For example, the delivered specific impulse for a 2224.1 N (500 lbf) thrust LO_2/H_2 expander cycle engine at 344.7 N/cm^2 (500 psia) chamber pressure increased from 4571.5 N sec/kg (466.16 lbf sec/lbm) to 4653 N sec/kg (474.47 lbf sec/lbm) for an area ratio increase from 400 to 1000. Using a payload/specific impulse influence coefficient of 2.54 kg/(N sec/kg) (55 lb/lbf sec/lbm), this specific impulse increase represents a 196 kg (432 lb) payload increase. The additional nozzle weight was approximately 11 kg (25 lb). The 1000-to-1 area ratio engine would add approximately 38 cm (15 inches) to the engine length and 23 cm (9 inches) in the engine diameter.

The second approach to increased engine chamber pressure and specific impulse is through increased pump and turbine efficiencies and enhanced heat transfer to the turbine drive gas. Increases in these parameters will result in increases in design chamber pressure which will decrease engine size. For this study, the best available predictions of the pump efficiencies were utilized; however possibly further efficiency improvements can be achieved. A brief evaluation using the generated parametric LO_2/H_2 engine performance data indicated that increasing the design chamber pressure from 344.7 N/cm^2 (500 psia) to 689.5 (1000 psia) at 2224.1 N (500 lbf) thrust resulted in only a 0.26% increase in delivered specific impulse. Therefore, to achieve a significant performance improvement, the turbine drive gas heat input and turbopump efficiencies must all be increased.

If continuing large space structure vehicle and mission studies indicate engine throttling is beneficial, the feasibility and design of a throttling pump drive system should be evaluated. Also complete engine cycle operation at various throttled conditions should be performed. Since previous discussions in this report revealed that substantial performance gains can be achieved utilizing constant chamber pressure throttling, the thrust chamber design to accomplish this would be of particular interest.

To further improve the low thrust engine cycle, the utilization of an efficient regenerator with the turbine discharge gas should be explored for possible performance gains.

As the design point engine cycle becomes finalized, an analysis of the engine start transient will not only aid in defining the complete engine system but will be of particular interest to the vehicle contractors. The thrust build-up during engine start may influence the design of the large space structure, or perhaps the engine start transient could be tailored to the structure limitations.

Turbopumps

The achievable chamber pressure of the low thrust expander cycle engines below 4448.2 N (1000 lbf) thrust were primarily limited by the turbopump efficiencies. The moderate head and low flowrates required at low thrusts result in low pump efficiencies. The near term pump technology advancement required is the design, fabrication, and demonstration of the predicted performance and life for these small pump turbines. In the design, particular attention must be given to the efficiency goal, pump/turbine thermal management, and light-weight pumps. The design and fabrication of these turbopumps will demonstrate component producibility with regard to the small components and small tolerances. Testing of the fabricated turbopumps would verify the analytical methods of predicting performance of the small multi-stage partial emission centrifugal pump and the small partial admission turbines.

To further advance low thrust engine technology, design approaches to improve current predicted pump performance values with simple, compact pumps will be required. This combined with turbine drive gas heat transfer enhancement and thrust chamber importance will enable higher design chamber pressure and higher engine performance values.

Thrust Chamber

The thrust chamber itself does not appear to represent a major technology advancement, however, the design, fabrication, and hot-fire testing of a thrust chamber is necessary to demonstrate durability and verify the analytically predicted heat transfer and performance for the low thrust application. In particular, the long total burn duration of approximately 10 - hours.

For the actual engine configuration design, further heat transfer analysis of the fixed nozzle-to-radiation cooled extension joint should be performed to prevent localized overheating and to reduce induced thermal gradients. This is especially true for the LO_2/H_2 engine in which the forward portion of the radiation-cooled nozzle extension has wall temperatures approaching 1367°K (2000 F) and the fixed nozzle tube wall temperatures near this location are less than 811°K (1000 F).

The need for an extendable nozzle will require evaluation of the specific vehicle application. In a conventional stacked-tank vehicle configuration, the engine length would be extremely important and an extendable nozzle would be definitely required. However, in current low thrust vehicle studies, a torus liquid oxygen tank has been considered to minimize the stage length. For this tank configuration, a retracted nozzle engine may not be required.

In this study a simple high temperature steel radiation-cooled nozzle extension was employed. A lighter weight nozzle should be evaluated to reduce engine weight. The design approach to accomplish this will be of particular value for high area ratio nozzles. In addition simpler nozzle extension techniques would be worthy of further exploration to simplify the engine system and reduce engine weight.

Injector/Ignitor

A major area requiring technology advancement for the low thrust engine is the miniaturization of the ignitor. Current ignitors tend to be large in relation to the combustion chamber and the conventional in-line installation would significantly influence engine length. This ignitor miniaturization may require new design approaches and concepts, as well as component testing.

In addition to the performance of the injector, the cooling and durability of injector face, and the injector/chamber heat transfer compatibility, especially with regard to injector streaking, will require test demonstration.

CONCLUSIONS

The thrust chamber cooling analysis resulted in the LO_2/H_2 regenerative/radiation-cooled thrust chambers providing the largest chamber pressure versus thrust operational envelope. The film/radiation-cooled thrust chambers were limited to low chamber pressures. Within the original thrust chamber cooling analysis guidelines, LO_2/RP-1 regenerative/radiation-cooled thrust chambers and the LO_2/CH_4 film/radiation-cooled thrust chambers were found not to be feasible. However, the inclusion of the gas-side carbon layer resulted in a feasible operational regime.

Candidate engine cycle/configurations were evaluated with regard to the maximum achievable chamber pressure, delivered specific impulse, engine weight, and system complexity. For both the LO_2/H_2 and LO_2/hydrocarbon fuel engines, the direct expander cycle achieved the highest overall rating and therefore was the cycle recommended for preliminary engine design for the two engines. NASA-LeRC selected the recommended engine cycle/configurations and a design thrust of 2224.1N (500 lb_f).

To achieve the desired high chamber pressures for both of these engines a two-stage partial emission oxidizer pump and a four-stage partial emission fuel pump with single-stage partial admission turbines were required. The turbines were arranged in series with the fuel turbine upstream of the oxidizer turbine. The engine cycle, in particular the turbopump efficiencies, limited the achievable design chamber pressure.

The 2224.1N (500 lb_f) thrust LO_2/H_2 expander cycle engine resulted in a design chamber pressure of 328.9 N/cm^2 (477 psia) with a delivered specific impulse of 4564.5 Nsec/kg (465.45 lb_f sec/lbm) for the 6-to-1 design mixture ratio and 400-to-1 nozzle area ratio. This engine has a total engine length of 91.9cm (36.19in), a retracted engine length of 56.2 cm (22.13in), a maximum engine diameter of 42.29cm (16.65in), and an engine weight of 28.46kg (62.75 lb.).

A design chamber pressure of 307.5 N/cm^2 (446 psia) was selected for the 2224.1 N (500 lb_f) thrust LO_2/CH_4 expander cycle engine. This engine achieved a delivered specific impulse of 3543 N sec/kg (361.29 lb_f sec/lb_m) for the design mixture ratio of 3.7-to-1 and 400-to-1 nozzle area ratio. With the nozzle fully extended, the total engine length was 94.1 cm (37.06in). The total engine weight was 25.8 kg (56.87 lb).

The LO_2/H_2 engine resulted in a higher chamber pressure and, therefore, achieved a smaller engine. However, the LO_2/CH_4 engine achieved a lighter

engine due to its smaller turbopumps. The LO_2/H_2 engine attained a significantly higher delivered specific impulse (approximately 29 percent higher) due to the lighter molecular weight propellant and a higher design chamber pressure.

In terms of technology advancements, the recommended improved performance engine system advancements include the continued analytical and experimental evaluation of high area ratio nozzle performance, improved efficiency pumps and turbines, and techniques to increase the turbine drive gas heat input. Since the design of the large space structure payload can be directly influenced by the engine start and shutdown transient, the analysis of these engine transients is required to evaluate loads imposed on the payload.

Although the thrust chamber itself does not currently appear to represent a major technology advancement, the required long burn duration of approximately 10-hours total will impose a strigent durability limit on the hardware. Experimental testing of a thrust chamber will ensure meeting this requirement. An evaluation of advanced minimum length propulsion stage configurations would enable the assessment of the need of an extendible nozzle on the engine. Also technology advancements in lighter weight nozzles (materials and design concepts) would reduce engine weight. In the area of ignitors, technology advancement is required to miniaturize the thrust chamber ignitor to improve component packaging.

c_p = Specific heat

C_f = Skin friction coefficient

C_h = Stanton number

C^* = Characteristic velocity

D = Diameter

F = Thrust

G = Mass velocity

$g(c^*, P_r)$ = Hydrogen coolant correlation parameter

h_g = Gas-side heat transfer coefficient

I_s = Specific impulse

k = Thermal conductivity

L_c = Combustion chamber length (injector-to-throat)

L_{eng} = Total engine length

$\dot{m}$ = Mass flowrate

MR = Mixture ratio

N_{st} = Stanton number

N_u = Nusselt number

P_c = Chamber pressure

$P_r = N_{pr}$ = Prandtl number

Q = Coolant heat input

R = Radius

R_e = Reynold's number

S_s = Specific speed

T = Temperature

U = Free stream velocity

x = Wall thickness

γ = Specific heat ratio

δ = Nozzle percent length (fraction)

ϵ = Nozzle area ratio

ϵ_c = Contraction ratio

ϵ^* = Hydrogen coolant correlation parameter

η = Efficiency

μ = Viscosity

ν	=	Kinematic viscosity
ρ	=	Density
ϕ	=	Energy thickness
ϕ_{in}	=	Inlet flow coefficient
ϕ_c	=	Coolant curvature enhancement
ϕ_e	=	Coolant entrance enhancement
ψ	=	Stage head coefficient

Subscripts

b	=	Bulk
c	=	Core
r	=	Reference temperature
sat	=	Saturation
w	=	Wall
wc	=	Coolant-side wall
wg	=	Gas-side wall
∞	=	Free stream

REFERENCES

1. Yost, M.C., Pregurner of Staged Combustion Rocket Engine, final report, Contract NASA CR-135356, February 1978.

2. Eberle, E.E. and L. Kusak, Liquid Oxygen/Liquid Hydrogen Auxiliary Power System Thruster Investigation, Final Report, Contract NASA CR-159674, December 1979.

3. Miller, S.S., J.D. Seader, and D.M. Trebes, Forced Convection Heat Transfer to Liquid Hydrogen at Supercritical Pressures, presented at the International Institute of Refrigeration, Commission, Grenoble, France, 9 to 11 June 1965.

4. Labotz, R., Valler, H.W., and Rouster, D., high density fuel combustion and cooling investigation, final report NASA CR 165177, Aerojet Liquid Rocket Company, Sacramento, California, January 1981.

5. SD72-SH-0029, "Electrical Power System for Space Shuttle Program", March 1972.

APPENDIX A

PROPELLANT PERFORMANCE DATA

Theoretical propellant performance data were generated for LO_2/H_2, LO_2/CH_4, and LO_2/RP-1 for a range of chamber pressure from 13.79 N/cm^2 (20 psia) to 689.5 N/cm^2 (1000 psia) and appropriate mixture ratios and fuel injection temperatures. These data were generated using the Rocketdyne Free-Energy Program, which utilizes the latest JANNAF combustion gas species data file and yields results which are in agreement with NASA's TRAN 78 program.

The theoretical characteristic velocity as a function of mixture ratio and chamber pressure for two fuel injection temperatures are shown in Fig. A-1 through A-5 for the three propellant combinations. The theoretical vacuum specific impulse as a function of mixture ratio and nozzle area ratio for five chamber pressures and two fuel injection temperatures are presented in Fig. A-6 through A-35.

The presented data are a part of the data file incorporated in the low-thrust engine cycle balance computer program and were used in this study.

Figure A-1 .

O_2/H_2 EQUILIBRIUM CHARACTERISTIC CHAMBER VELOCITY, C*, as a function of CHAMBER PRESSURE and MIXTURE RATIO

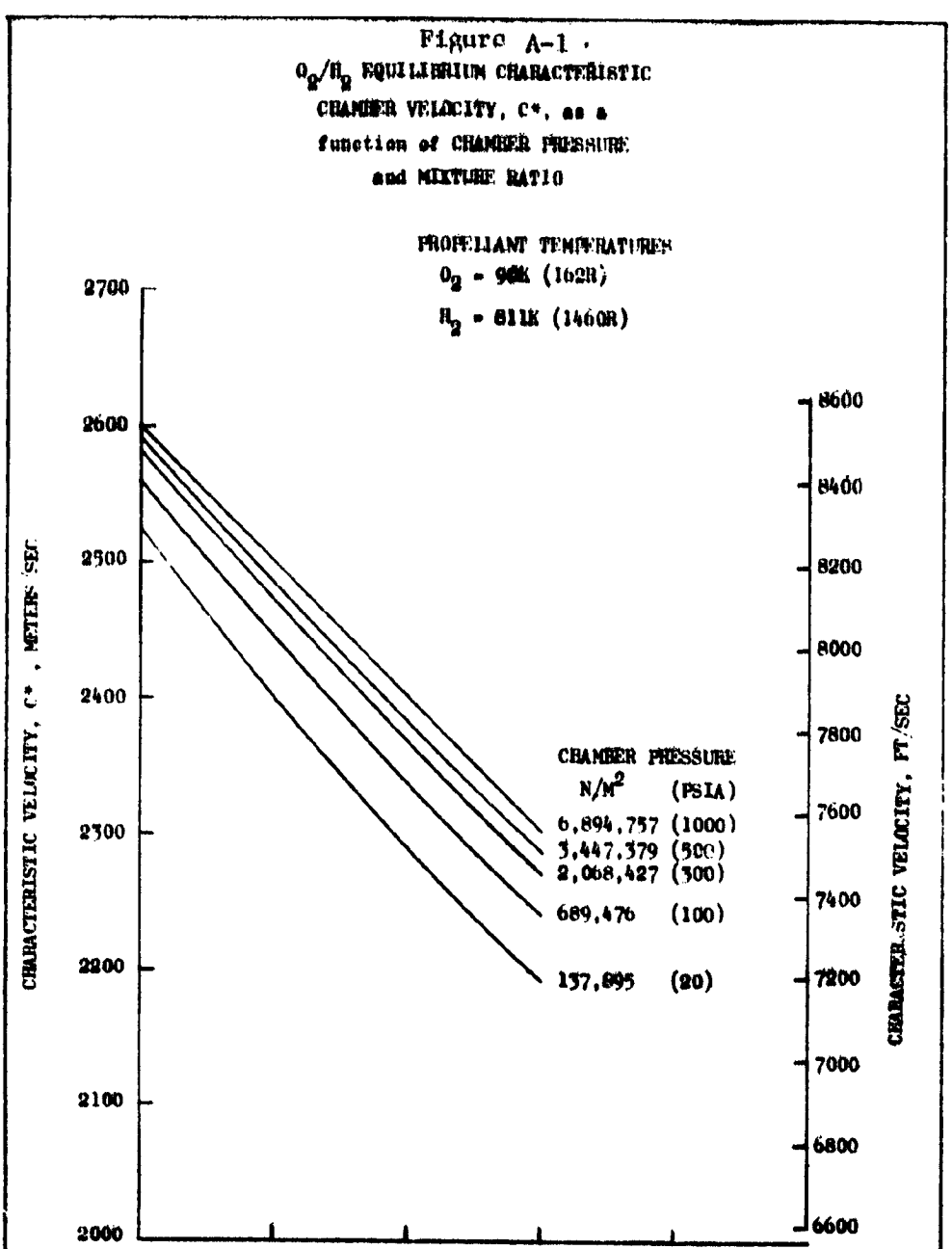

Figure A-2

O_2/CH_4 EQUILIBRIUM CHARACTERISTIC CHAMBER VELOCITY, C* , as a function of CHAMBER PRESSURE and MIXTURE RATIO

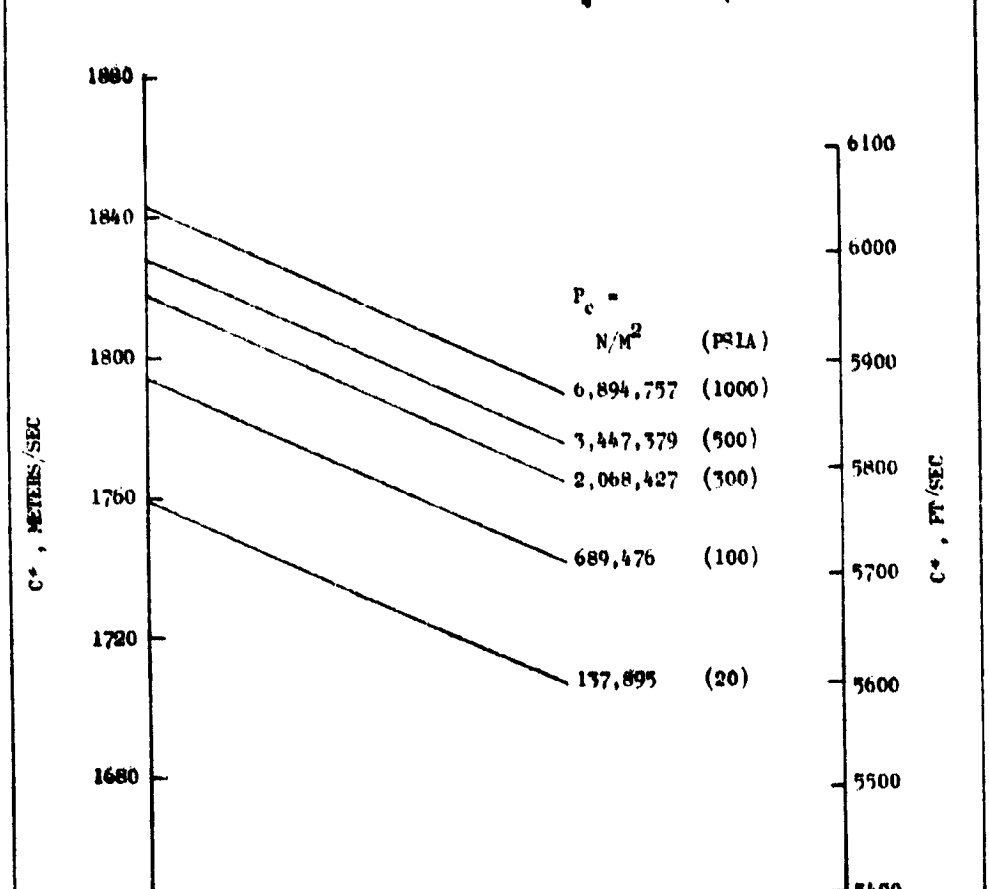

Figure A-3

O_2/CH_4 EQUILIBRIUM CHARACTERISTIC CHAMBER VELOCITY, C* , as a function of CHAMBER PRESSURE and MIXTURE RATIO

PROPELLANT TEMPERATURES
O_2 = 90K (162R)
CH_4 = 811K (1460R)

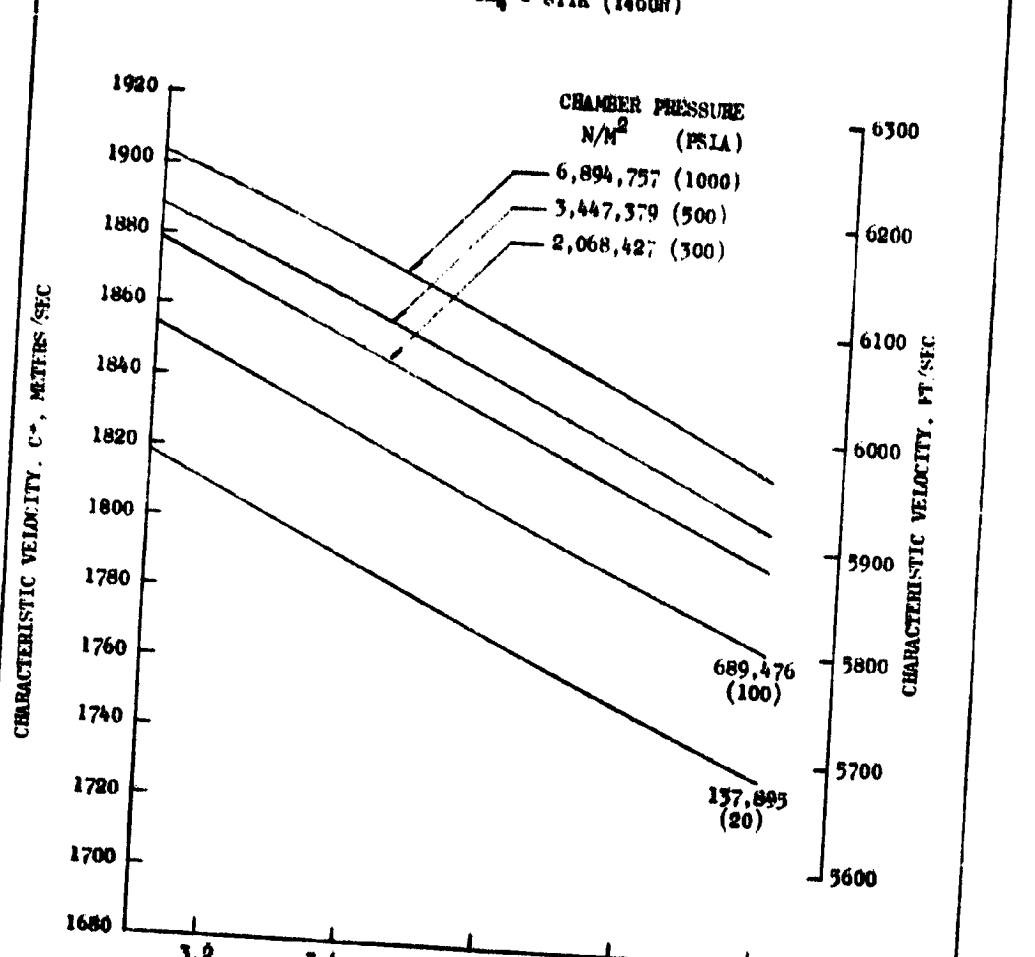

8/79

Figure A-4

O_2/RP-1 EQUILIBRIUM CHARACTERISTIC CHAMBER VELOCITY, C* , as a function of CHAMBER PRESSURE and MIXTURE RATIO

ASR79-84
8-17-79
Page 8

PROPELLANT INLET TEMP.
O_2 = 90.18K (162.32R)
RP-1 = 298.15K (536.67R)

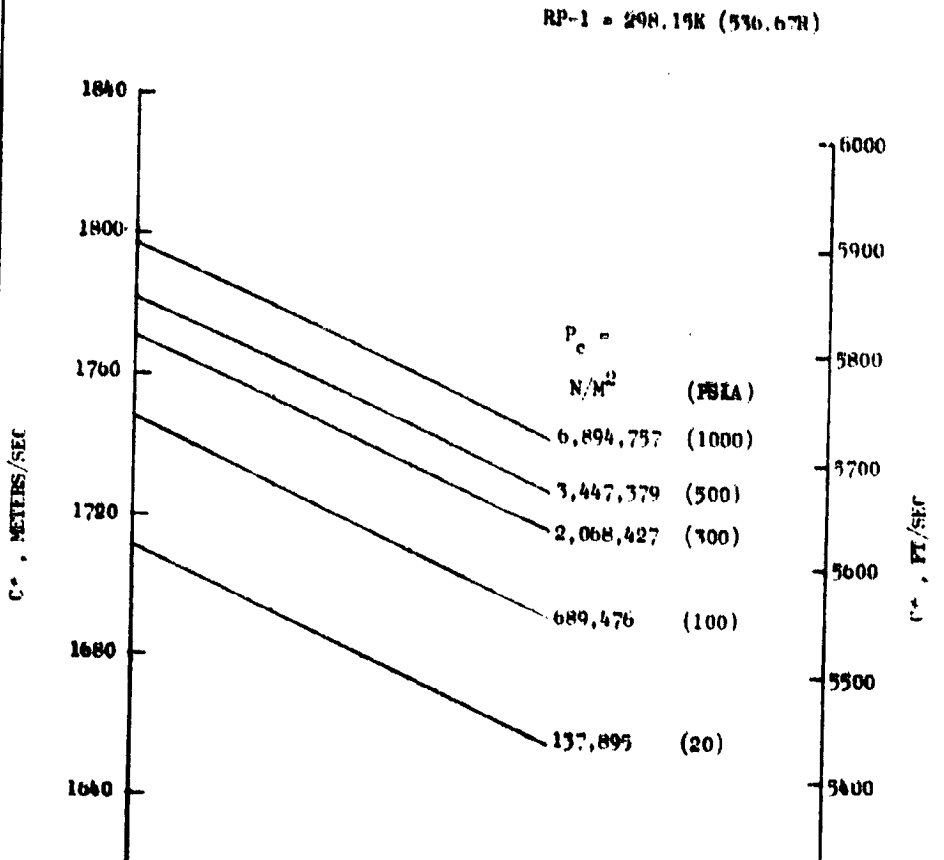

7-79

Figure A-5

O_2/RP-1 EQUILIBRIUM CHARACTERISTIC CHAMBER VELOCITY, C* , as a function of CHAMBER PRESSURE and MIXTURE RATIO

PROPELLANT TEMPERATURES

O_2 = 90K (162R)

RP-1 = 556K (1000R)

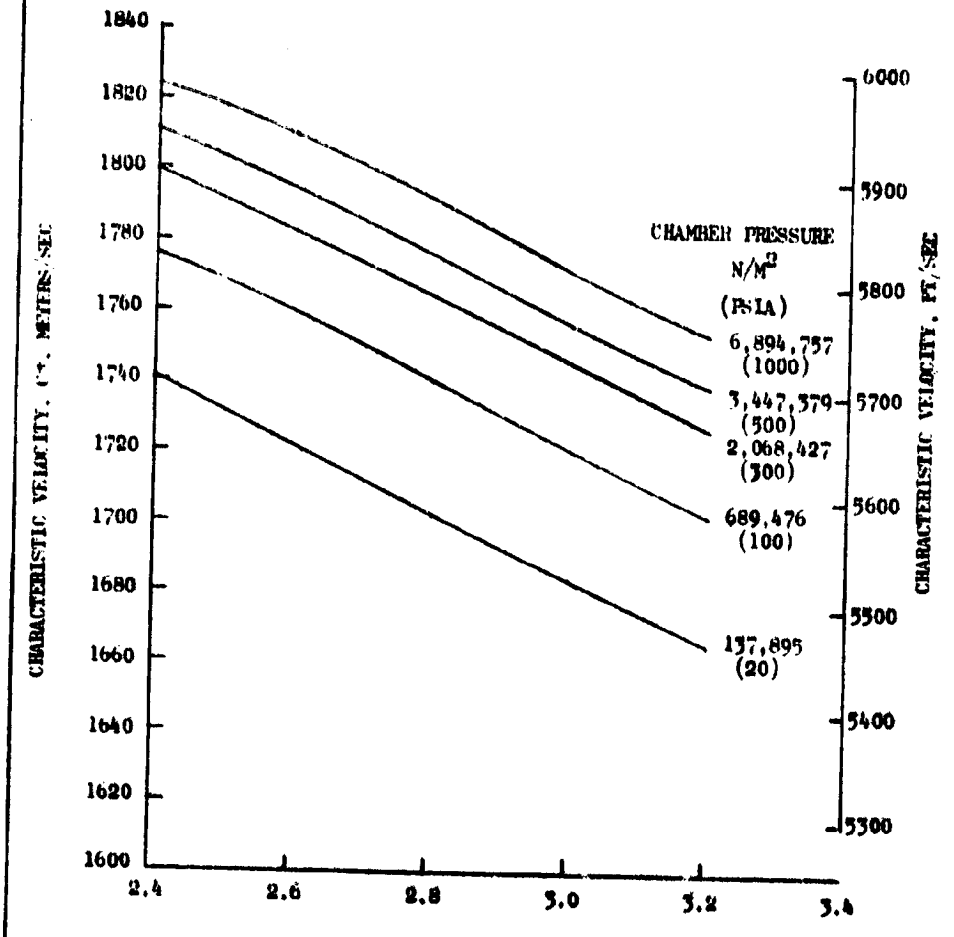

8/79

Figure A-6

THEORETICAL EQUILIBRIUM VACUUM SPECIFIC IMPULSE
for O_2/H_2 as a function of
MIXTURE RATIO and NOZZLE AREA RATIO

PROPELLANT INLET TEMPERATURES
O_2 = 90.18K (162.32R)
H_2 = 20.27K (36.49R)

CHAMBER PRESSURE = 137,809 N/M^2 (20 PSIA)

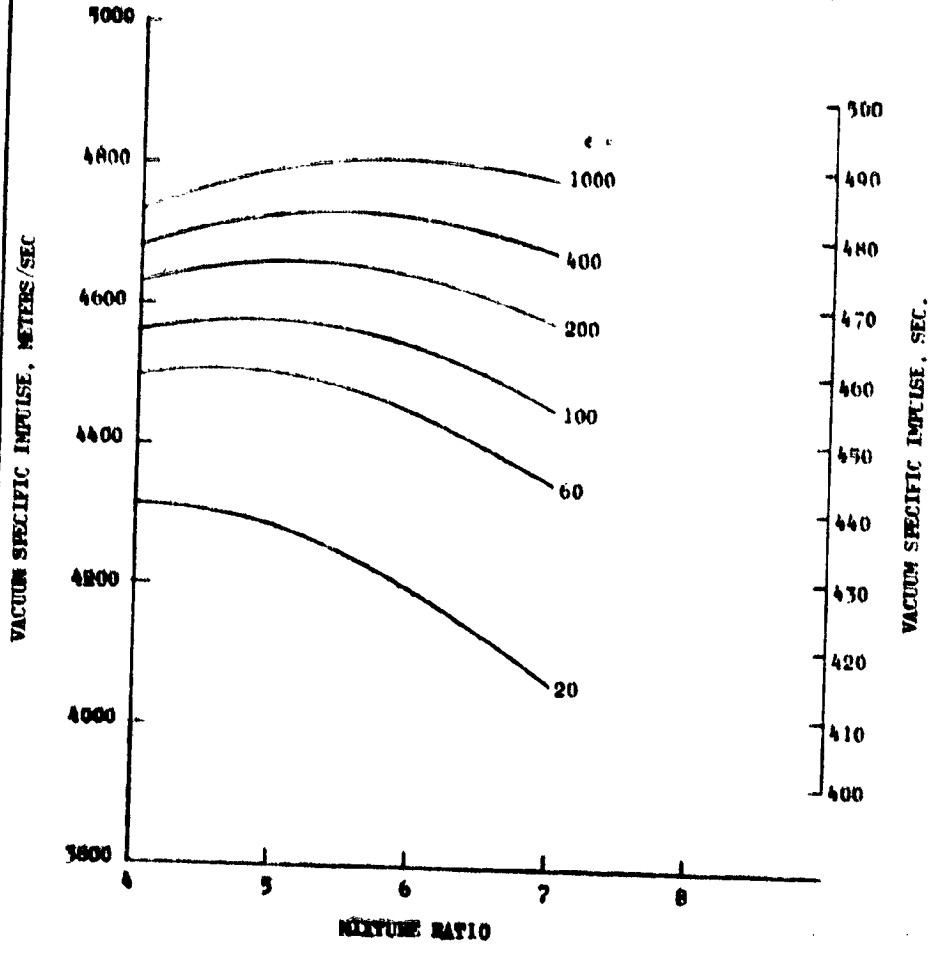

7/79

Figure A-7

THEORETICAL EQUILIBRIUM VACUUM SPECIFIC IMPULSE

for O_2/H_2 as a function of

MIXTURE RATIO and NOZZLE AREA RATIO

PROPELLANT INLET TEMPERATURES

O_2 = 90.18K (162.32R)

H_2 = 20.27K (36.49R)

CHAMBER PRESSURE = 689,476 N/M^2 (100 PSIA)

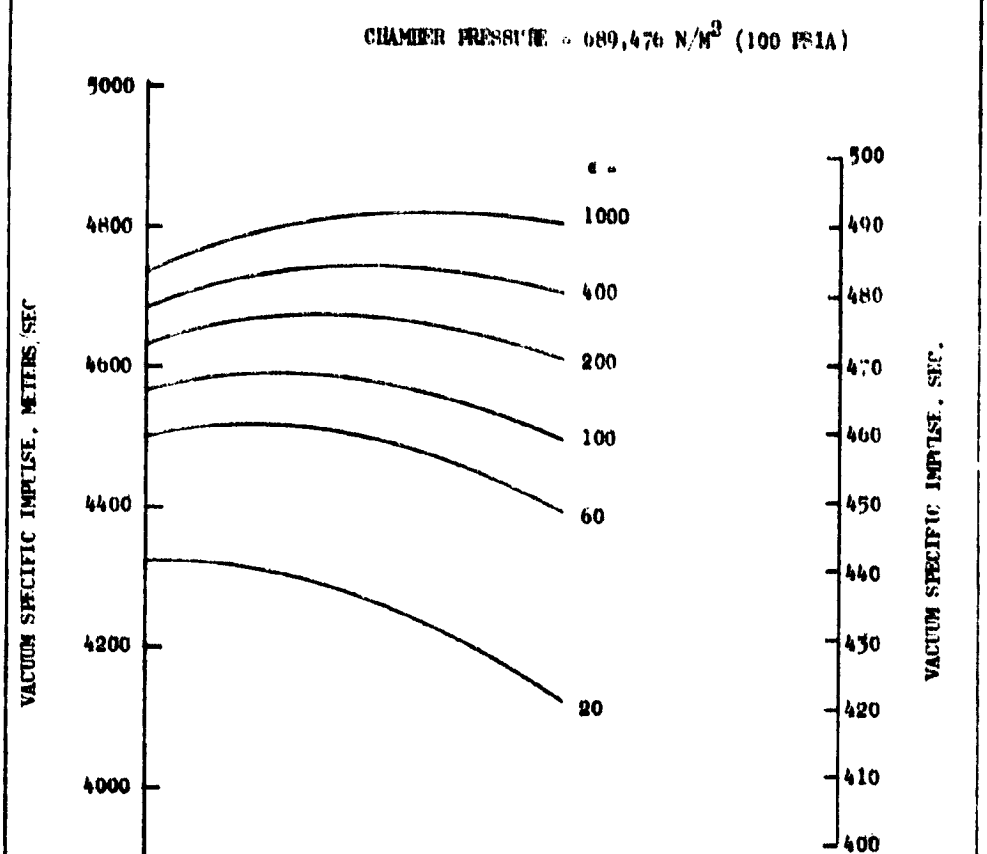

7/79

Figure A-8

THEORETICAL EQUILIBRIUM VACUUM SPECIFIC IMPULSE

for O_2/H_2 as a function of

MIXTURE RATIO and NOZZLE AREA RATIO

PROPELLANT INLET TEMPERATURES

O_2 = 90.18K (162.32R)

H_2 = 20.27K (36.49R)

CHAMBER PRESSURE = 2,068,427 N/M^2 (300 PSIA)

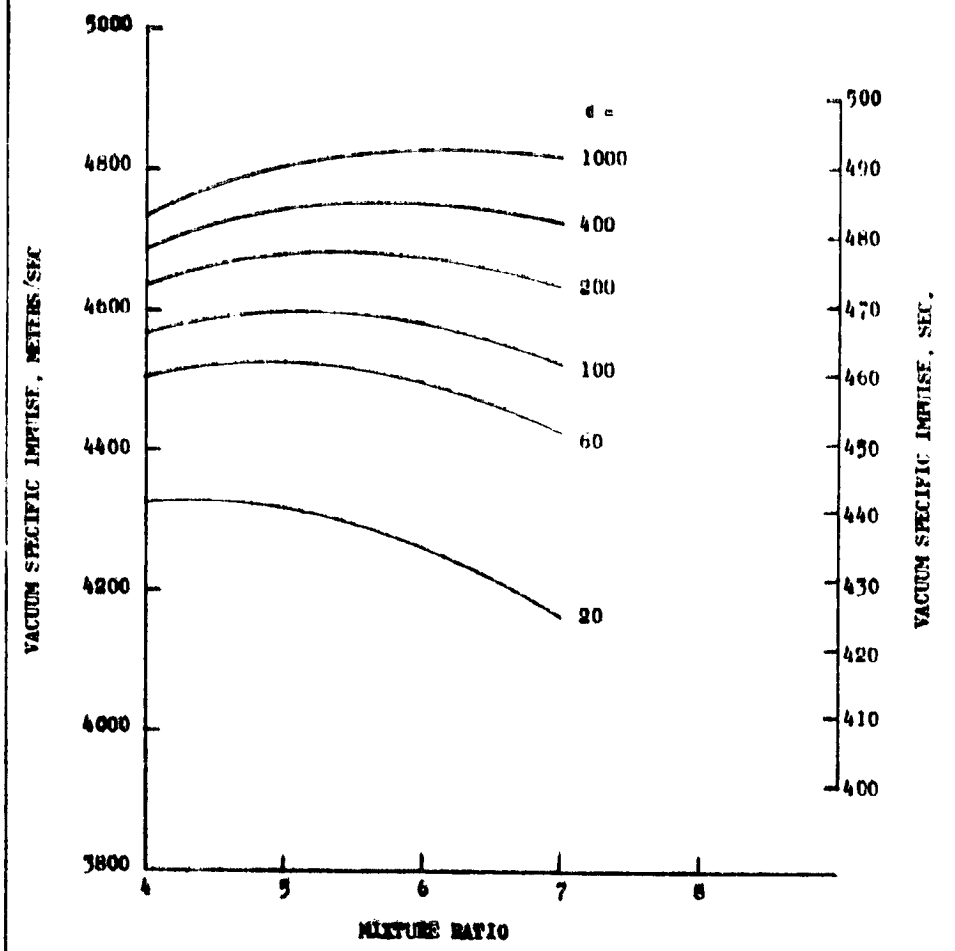

7/79

Figure A-9

THEORETICAL EQUILIBRIUM VACUUM SPECIFIC IMPULSE
for O_2/H_2 as a function of
MIXTURE RATIO and NOZZLE AREA RATIO

PROPELLANT INLET TEMPERATURES
O_2 = 90.18K (162.32R)
H_2 = 20.27K (36.49R)

CHAMBER PRESSURE = 3,447,379 N/M^2 (500 PSIA)

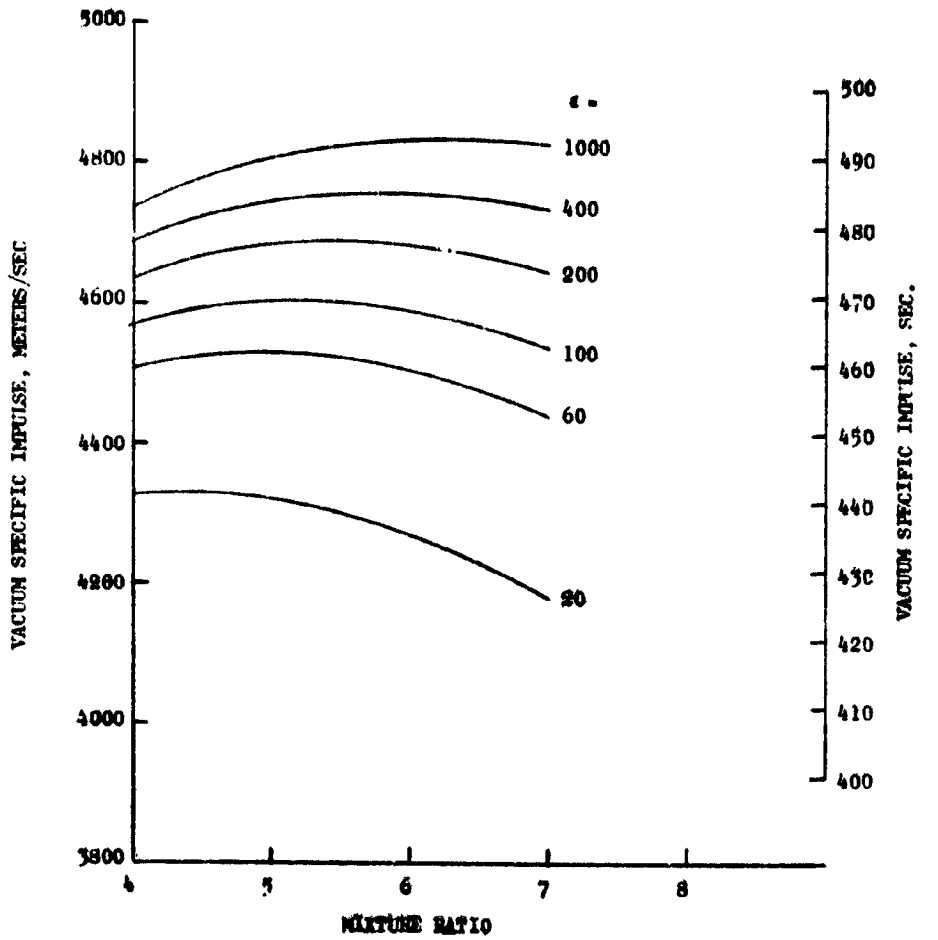

7/79

Figure A-10

THEORETICAL EQUILIBRIUM VACUUM SPECIFIC IMPULSE
for O_2/H_2 as a function of
MIXTURE RATIO and NOZZLE AREA RATIO

PROPELLANT INLET TEMPERATURES
O_2 = 90.18K (162.32R)
H_2 = 20.27K (36.49R)

CHAMBER PRESSURE = 6,894,757 N/M^2 (1000 PSIA)

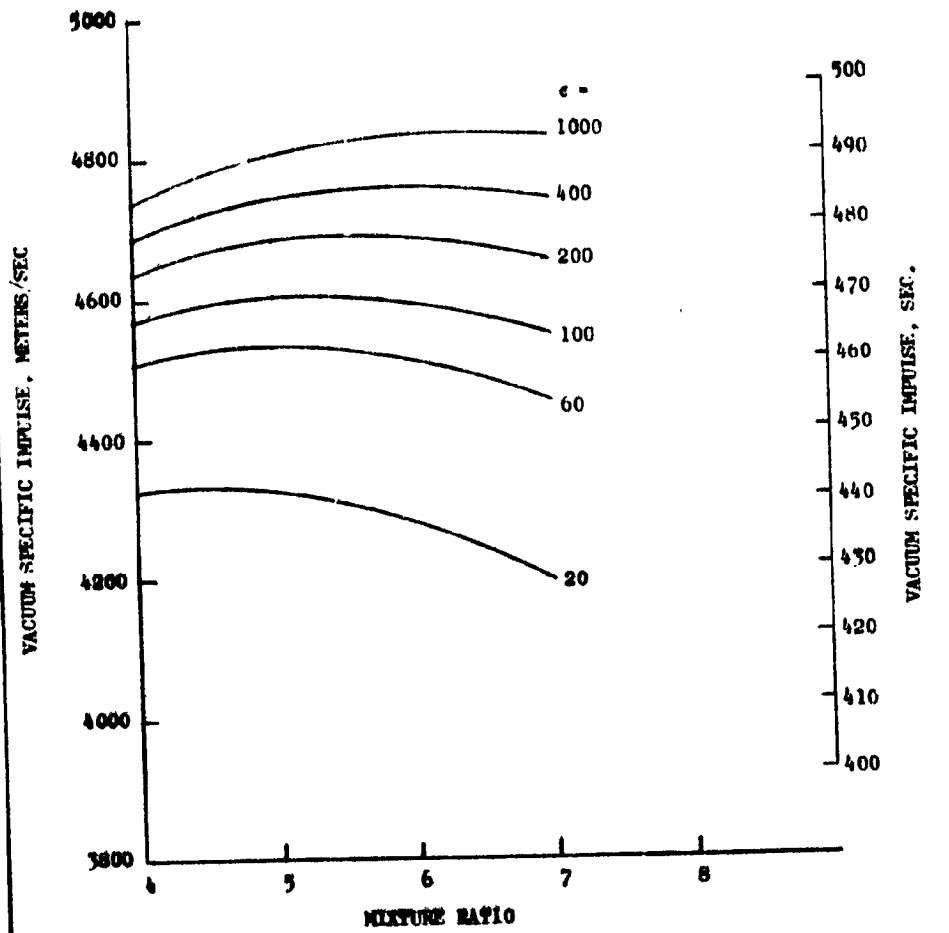

7/79

Figure A-11

THEORETICAL EQUILIBRIUM VACUUM SPECIFIC IMPULSE

for O_2/H_2 as a function of

MIXTURE RATIO and NOZZLE AREA RATIO

PROPELLANT INLET TEMPERATURES

O_2 = 90K (162R)

H_2 = 81IK (146OR)

CHAMBER PRESSURE = 137,895 N/M^2 (20 PSIA)

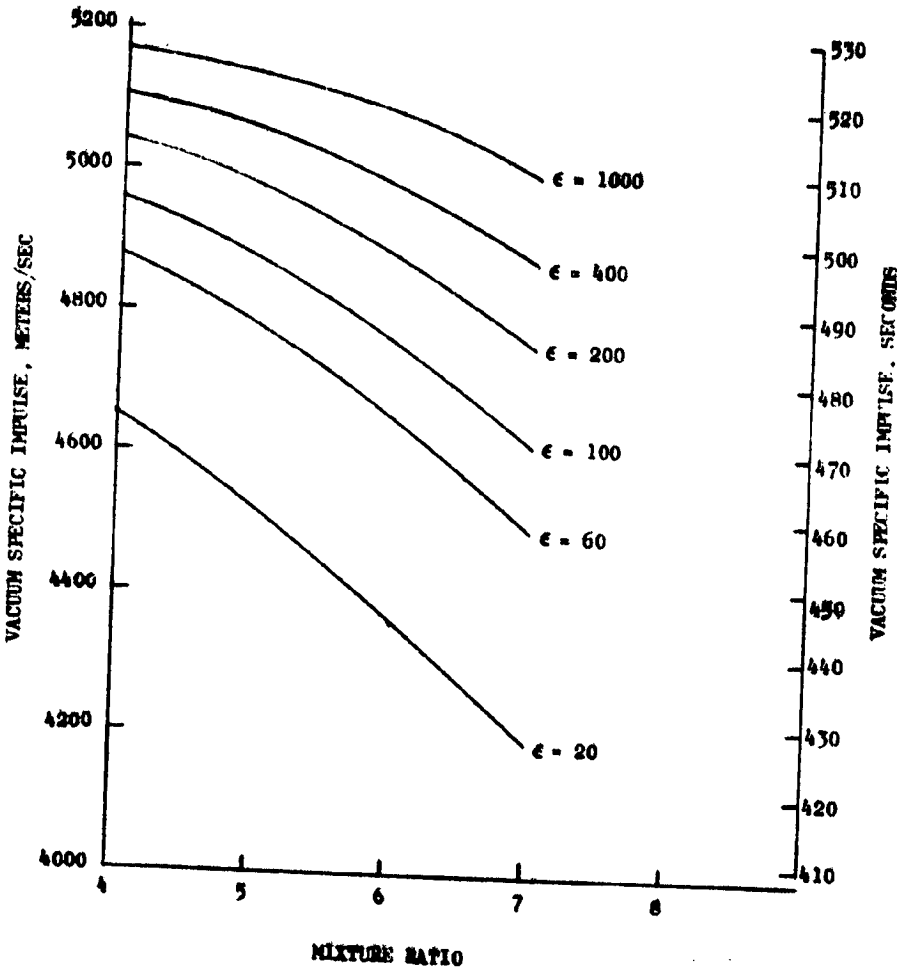

8/79

Figure A-12

THEORETICAL EQUILIBRIUM VACUUM SPECIFIC IMPULSE
for O_2/H_2 as a function of
MIXTURE RATIO and NOZZLE AREA RATIO

PROPELLANT INLET TEMPERATURES
O_2 = 90K (162R)
H_2 = 811K (1460R)

CHAMBER PRESSURE = 689,476 N/M^2 (100 PSIA)

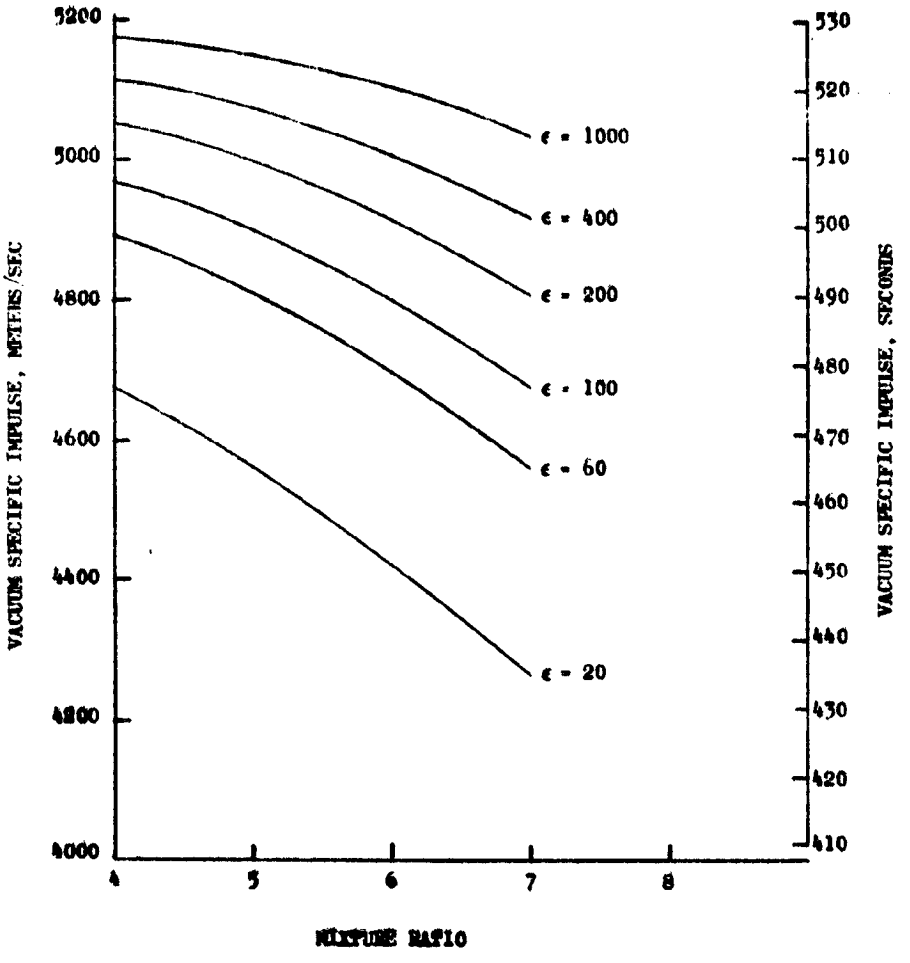

8/79

Figure A-13

THEORETICAL EQUILIBRIUM VACUUM SPECIFIC IMPULSE

For O_2/H_2 as a function of

MIXTURE RATIO and NOZZLE AREA RATIO

PROPELLANT INLET TEMPERATURES

O_2 = 90K (162R)

H_2 = 81IK (1460R)

CHAMBER PRESSURE = 2,068,427 N/M^2 (300 PSIA)

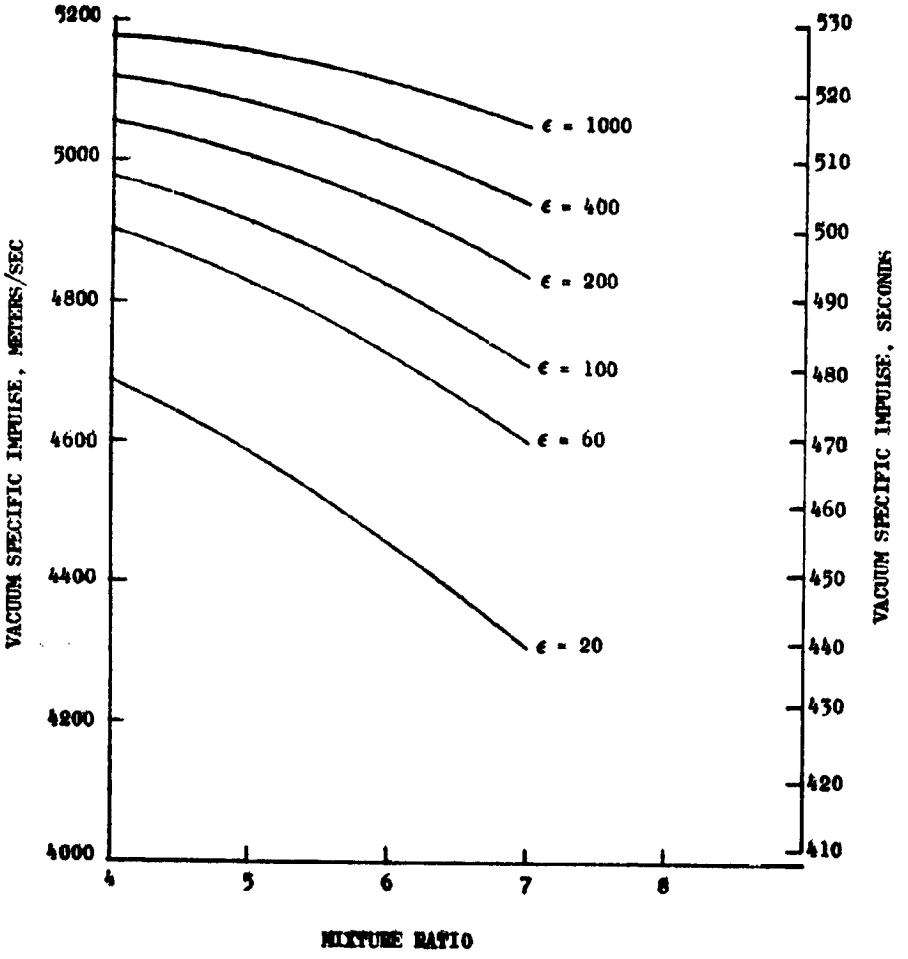

8/79

Figure A-14

THEORETICAL EQUILIBRIUM VACUUM SPECIFIC IMPULSE
for O_2/H_2 as a function of
MIXTURE RATIO and NOZZLE AREA RATIO

PROPELLANT INLET TEMPERATURES
O_2 = 90K (162R)
H_2 = 81IK (146OR)

CHAMBER PRESSURE = 3,447,379 N/M^2 (500 PSIA)

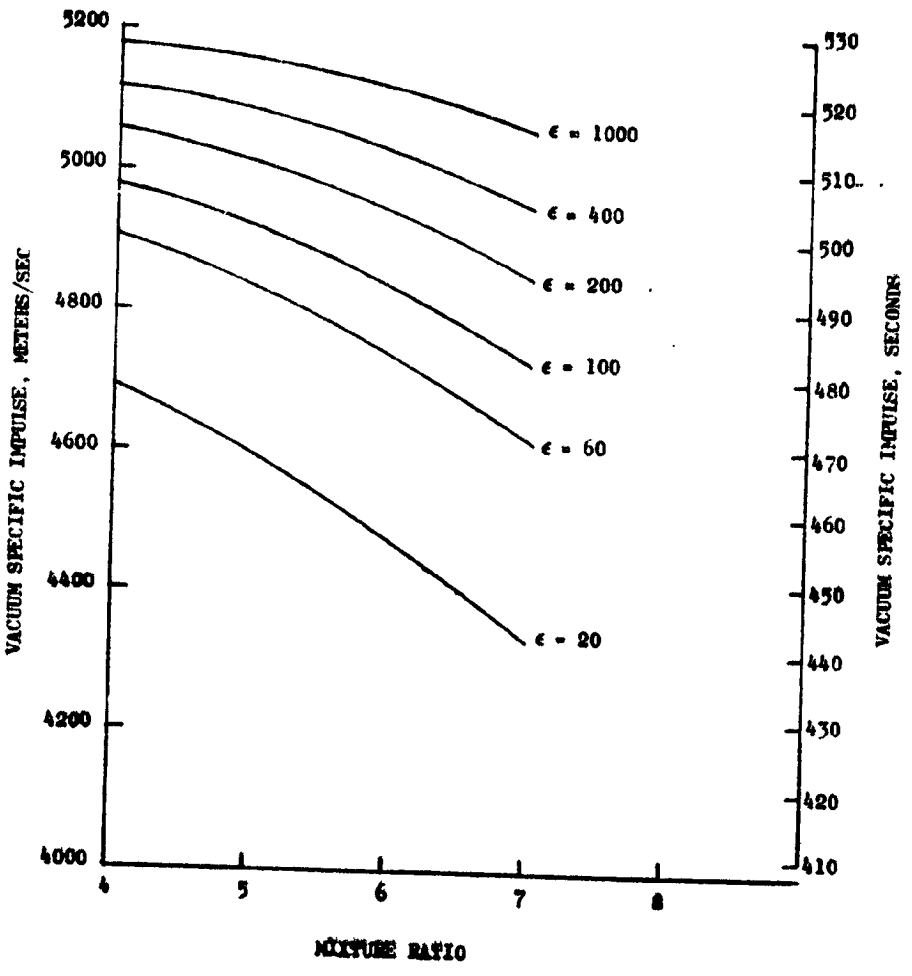

8/79

Figure A-15

THEORETICAL EQUILIBRIUM VACUUM SPECIFIC IMPULSE
for O_2/H_2 as a function of
MIXTURE RATIO and NOZZLE AREA RATIO

PROPELLANT INLET TEMPERATURES
O_2 = 90K (162R)
H_2 = 811K (1460R)

CHAMBER PRESSURE = 6,894,757 N/M^2 (1000 PSIA)

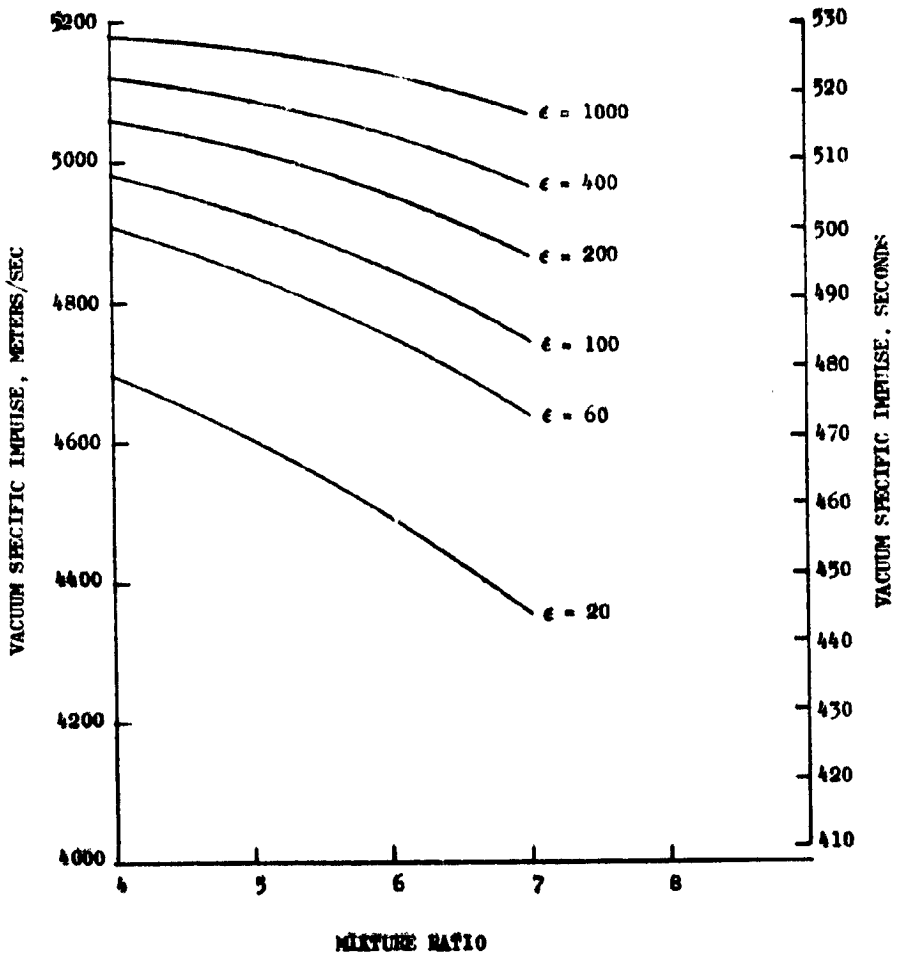

8/79

Figure A-16

THEORETICAL EQUILIBRIUM VACUUM SPECIFIC IMPULSE
for O_2/CH_4 as a function of
MIXTURE RATIO and NOZZLE AREA RATIO

PROPELLANT INLET TEMPERATURES
O_2 = 90.18K (162.32R)
CH_4 = 111.66K (200.99R)

CHAMBER PRESSURE = 137,895 N/M^2 (20 PSIA)

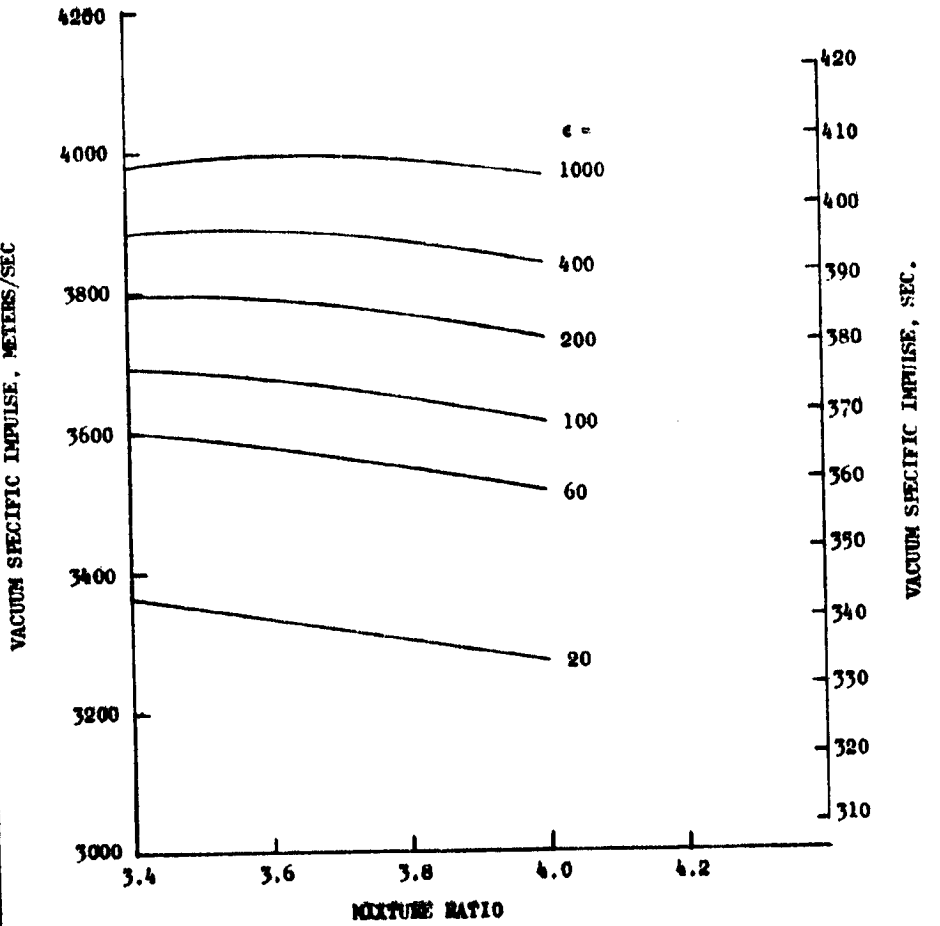

7/79

Figure A-17

THEORETICAL EQUILIBRIUM VACUUM SPECIFIC IMPULSE
for O_2/CH_4 as a function of
MIXTURE RATIO and NOZZLE AREA RATIO

PROPELLANT INLET TEMPERATURES
O_2 = 90.18K (162.32R)
CH_4 = 111.66K (200.99R)

CHAMBER PRESSURE = 689,476 N/M^2 (100 PSIA)

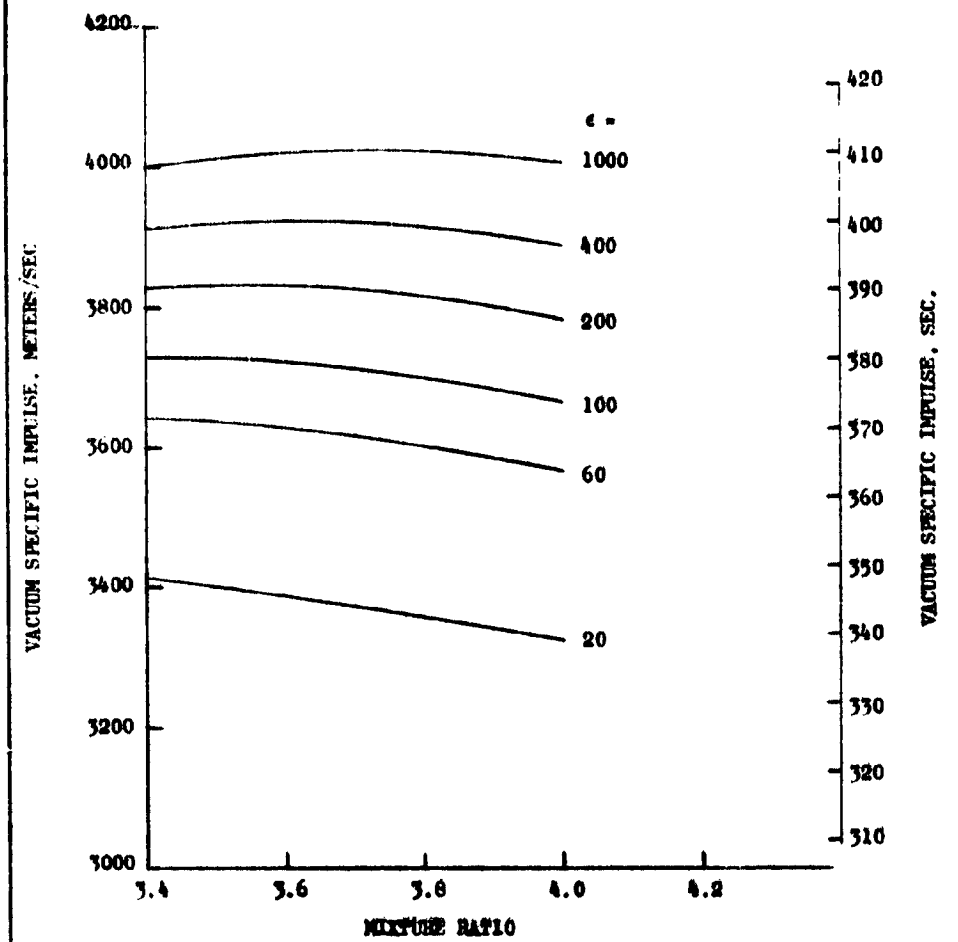

7/79

Figure A-18

THEORETICAL EQUILIBRIUM VACUUM SPECIFIC IMPULSE

for O_2/CH_4 as a function of

MIXTURE RATIO and NOZZLE AREA RATIO

PROPELLANT INLET TEMPERATURES

O_2 = 90.18K (162.32R)

CH_4 = 111.66K (200.99R)

CHAMBER PRESSURE = 2,068.27 N/M^2 (300 PSIA)

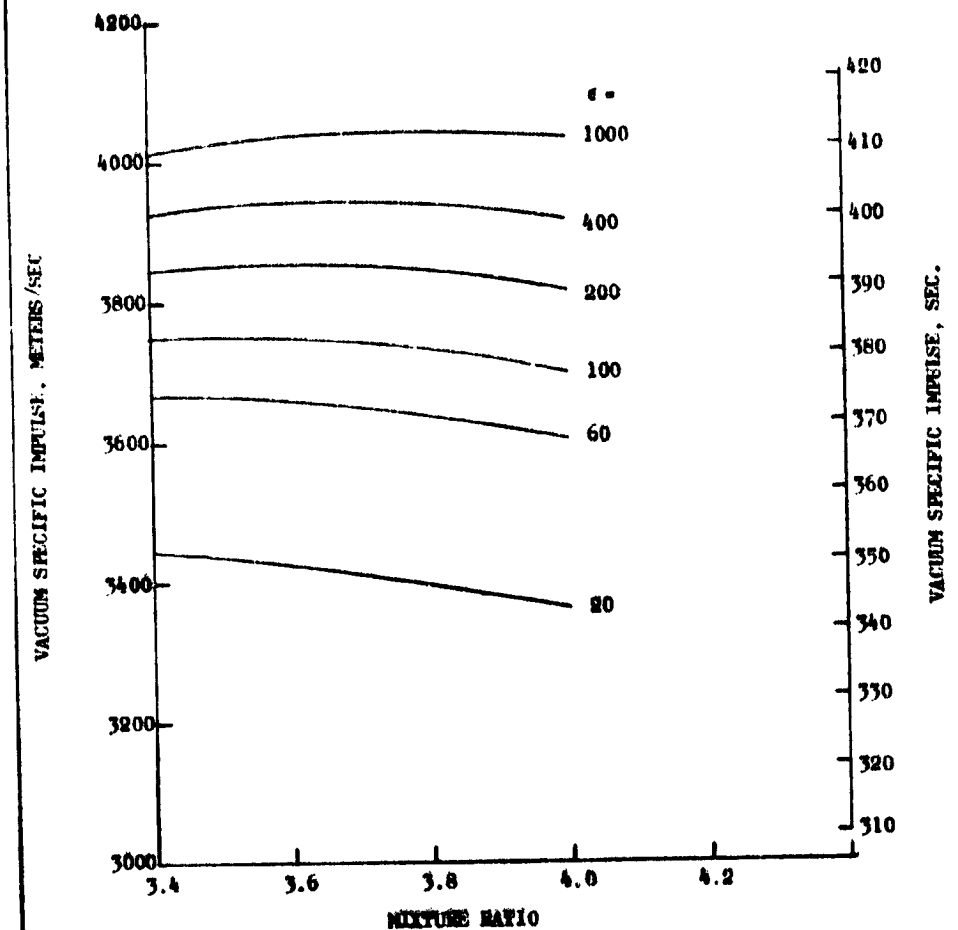

7/79

Figure A-19

ASR79-84
8-17-79
Page 10

THEORETICAL EQUILIBRIUM VACUUM SPECIFIC IMPULSE
for O_2/CH_4 as a function of
MIXTURE RATIO and NOZZLE AREA RATIO

PROPELLANT INLET TEMPERATURES
O_2 = 90.18K (162.32R)
CH_4 = 111.66K (200.99R)

CHAMBER PRESSURE = 3,447,379 N/M^2 (500 PSIA)

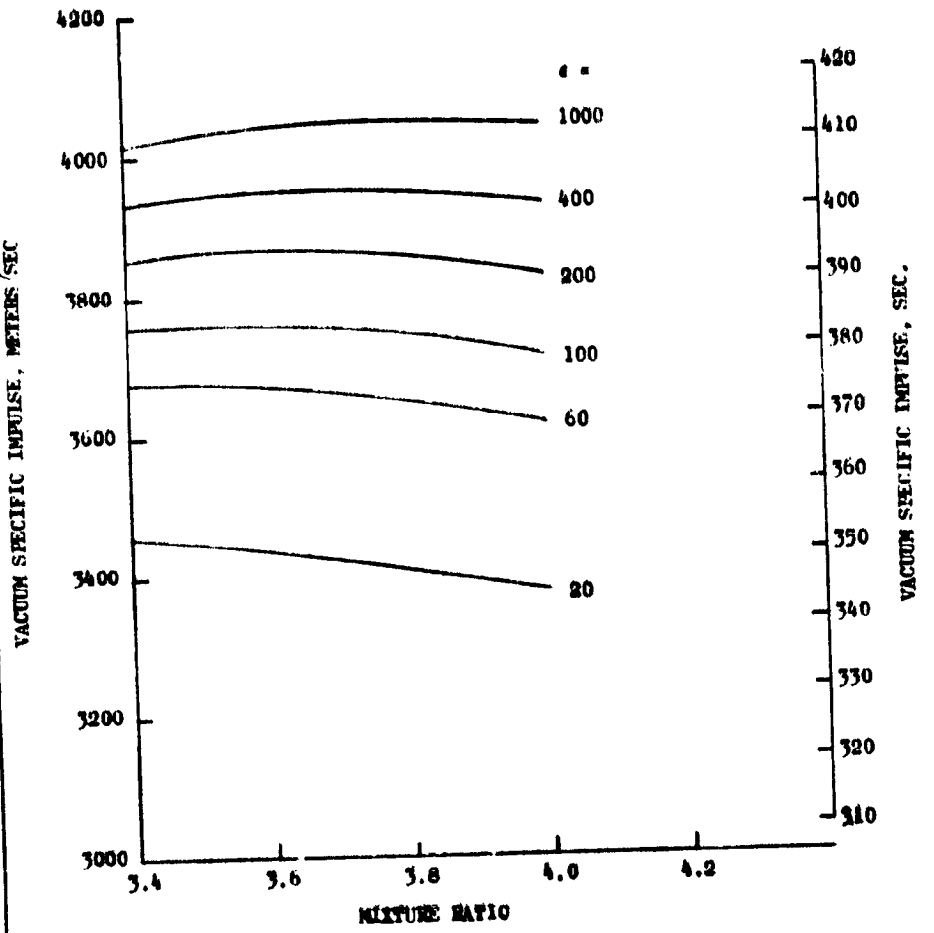

7/79

Figure A-20

THEORETICAL EQUILIBRIUM VACUUM SPECIFIC IMPULSE
for O_2/CH_4 as a function of
MIXTURE RATIO and NOZZLE AREA RATIO

PROPELLANT INLET TEMPERATURES
O_2 = 90.18K (162.32R)
CH_4 = 111.66K (200.99R)

CHAMBER PRESSURE = 6,894,757 N/M^2 (1000 PSIA)

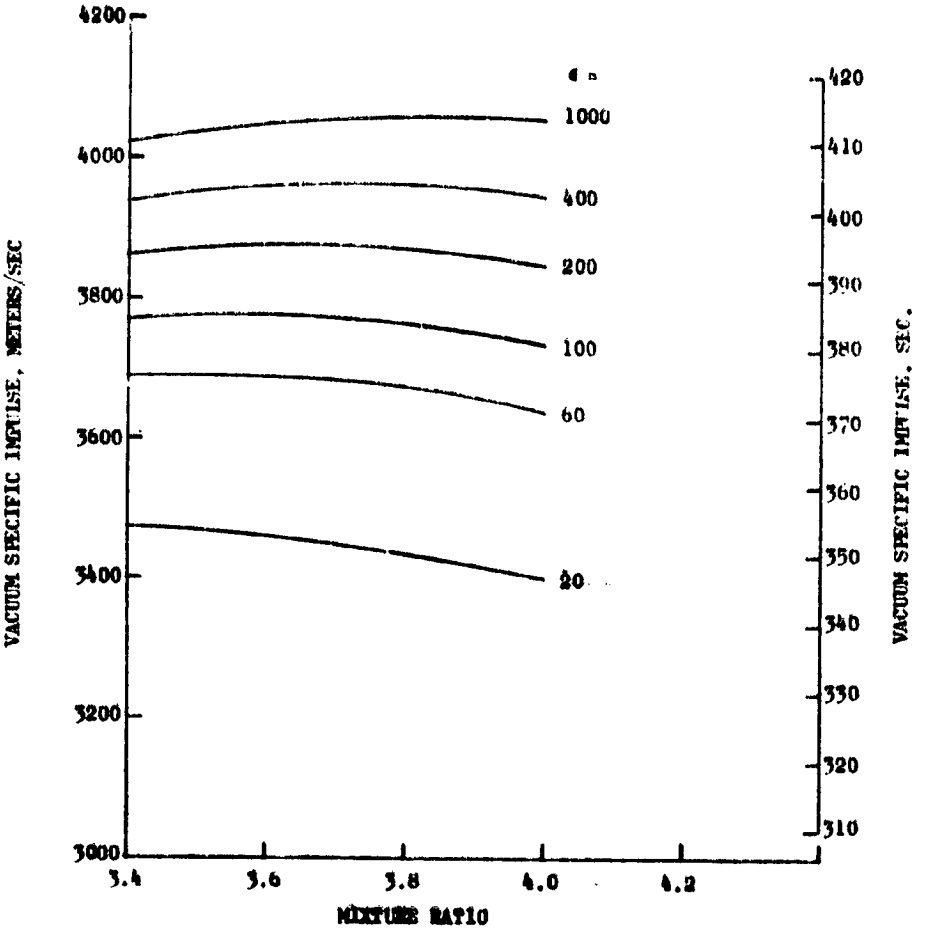

7/79

Figure A-21

THEORETICAL EQUILIBRIUM VACUUM SPECIFIC IMPULSE

for O_2/CH_4 as a function of

MIXTURE RATIO and NOZZLE AREA RATIO

PROPELLANT INLET TEMPERATURES

O_2 = 90K (162R)

CH_4 = 811K (1460R)

CHAMBER PRESSURE = 137,895 N/M^2 (20 PSIA)

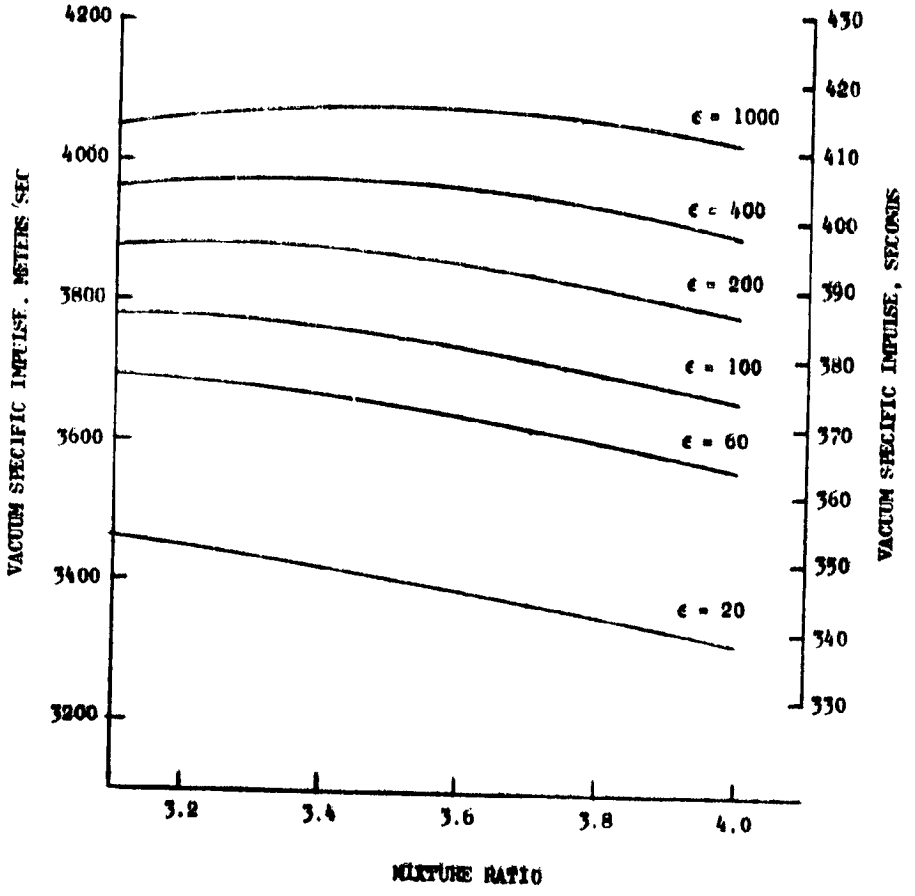

8/79

Figure A-22

THEORETICAL EQUILIBRIUM VACUUM SPECIFIC IMPULSE
for O_2/CH_4 as a function of
MIXTURE RATIO and NOZZLE AREA RATIO

PROPELLANT INLET TEMPERATURES
O_2 = 90K (162R)
CH_4 = 811K (1460R)

CHAMBER PRESSURE = 689,476 N/M^2 (100 PSIA)

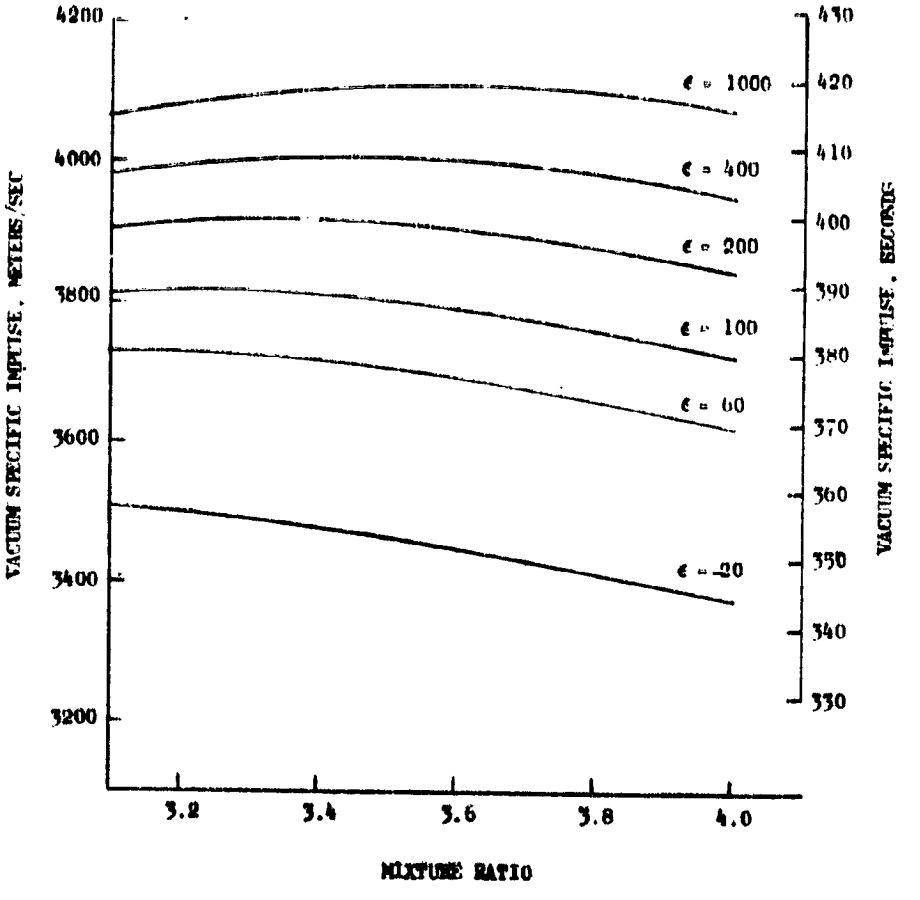

8/79

Figure A-23

THEORETICAL EQUILIBRIUM VACUUM SPECIFIC IMPULSE

for O_2/CH_4 as a function of

MIXTURE RATIO and NOZZLE AREA RATIO

PROPELLANT INLET TEMPERATURES

O_2 = 90K (162R)

CH_4 = 811K (1460R)

CHAMBER PRESSURE = 2,068,427 N/M^2 (300 PSIA)

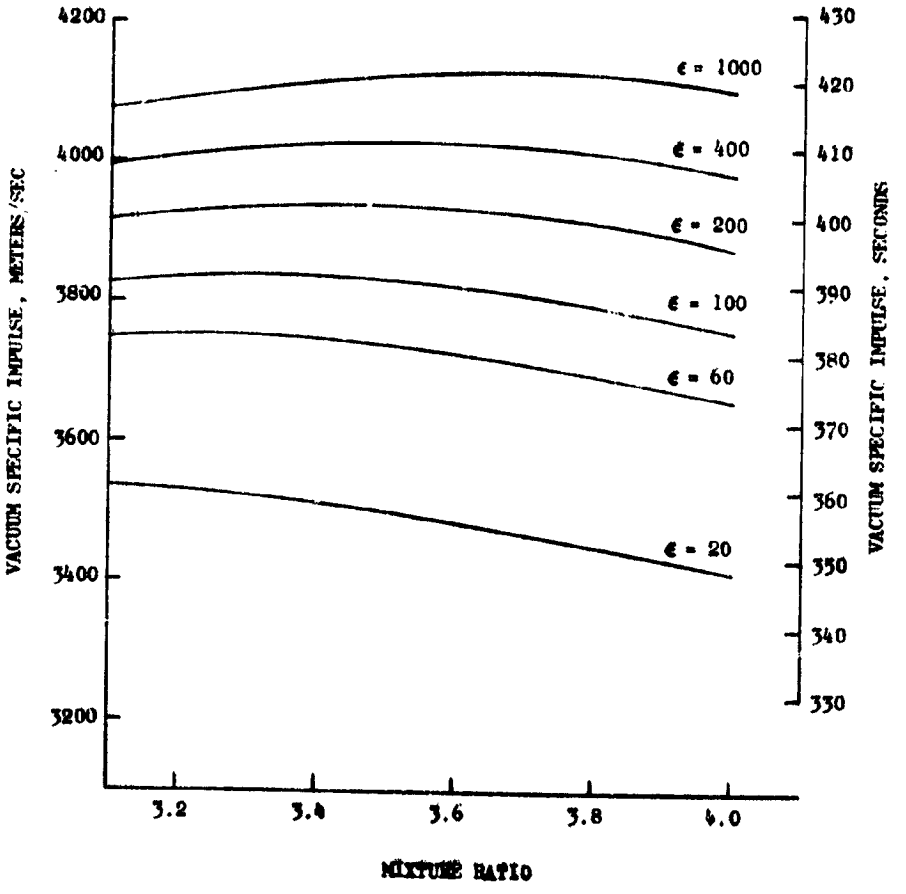

8/79

Figure A-24

THEORETICAL EQUILIBRIUM VACUUM SPECIFIC IMPULSE

For O_2/CH_4 as a function of

MIXTURE RATIO and NOZZLE AREA RATIO

PROPELLANT INLET TEMPERATURES

O_2 = 90K (162R)

CH_4 = 811K (1460R)

CHAMBER PRESSURE = 3,447,379 N/M^2 (500 PSIA)

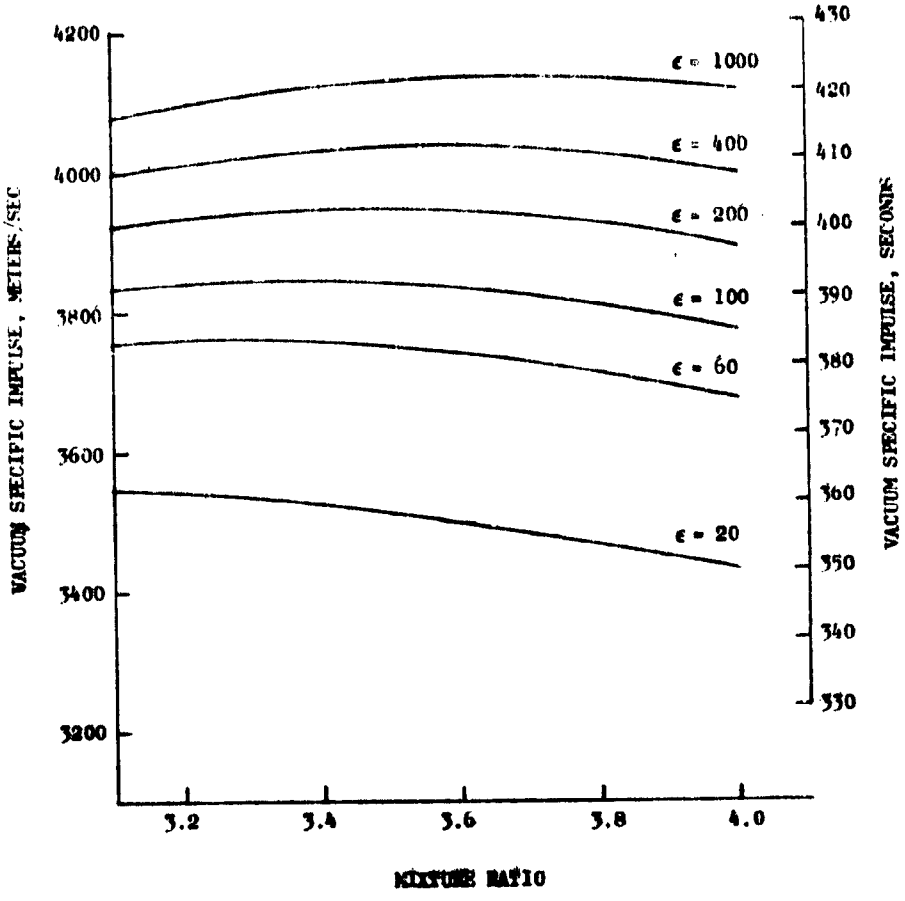

8/79

Figure A-25

THEORETICAL EQUILIBRIUM VACUUM SPECIFIC IMPULSE

for O_2/CH_4 as a function of

MIXTURE RATIO and NOZZLE AREA RATIO

PROPELLANT INLET TEMPERATURES

O_2 = 90K (162R)

CH_4 = 811K (1460R)

CHAMBER PRESSURE = 6,894,757 N/M^2 (1000 PSIA)

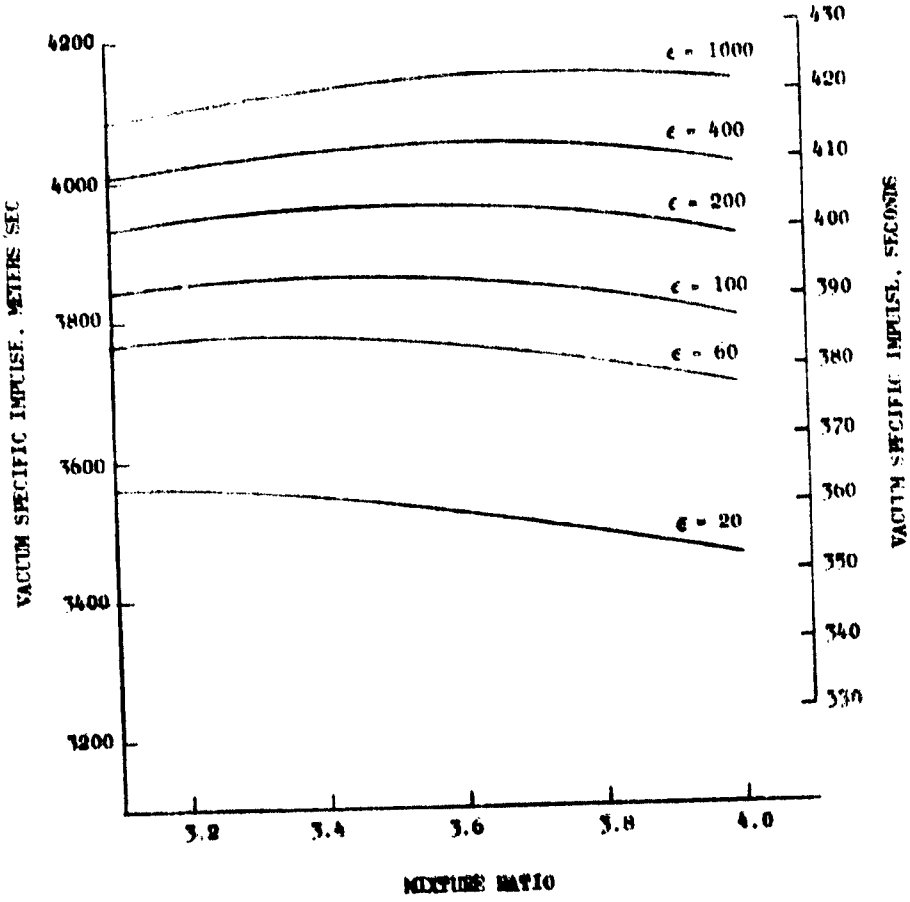

8/79

Figure A-26

THEORETICAL EQUILIBRIUM VACUUM SPECIFIC IMPULSE
for O_2/RP-1 as a function of
MIXTURE RATIO and NOZZLE AREA RATIO

PROPELLANT INLET TEMPERATURES
O_2 = 90.18K (162.32R)
RP-1 = 298.17K (536.67R)

CHAMBER PRESSURE = 137,895 N m^2 (20 PSIA)

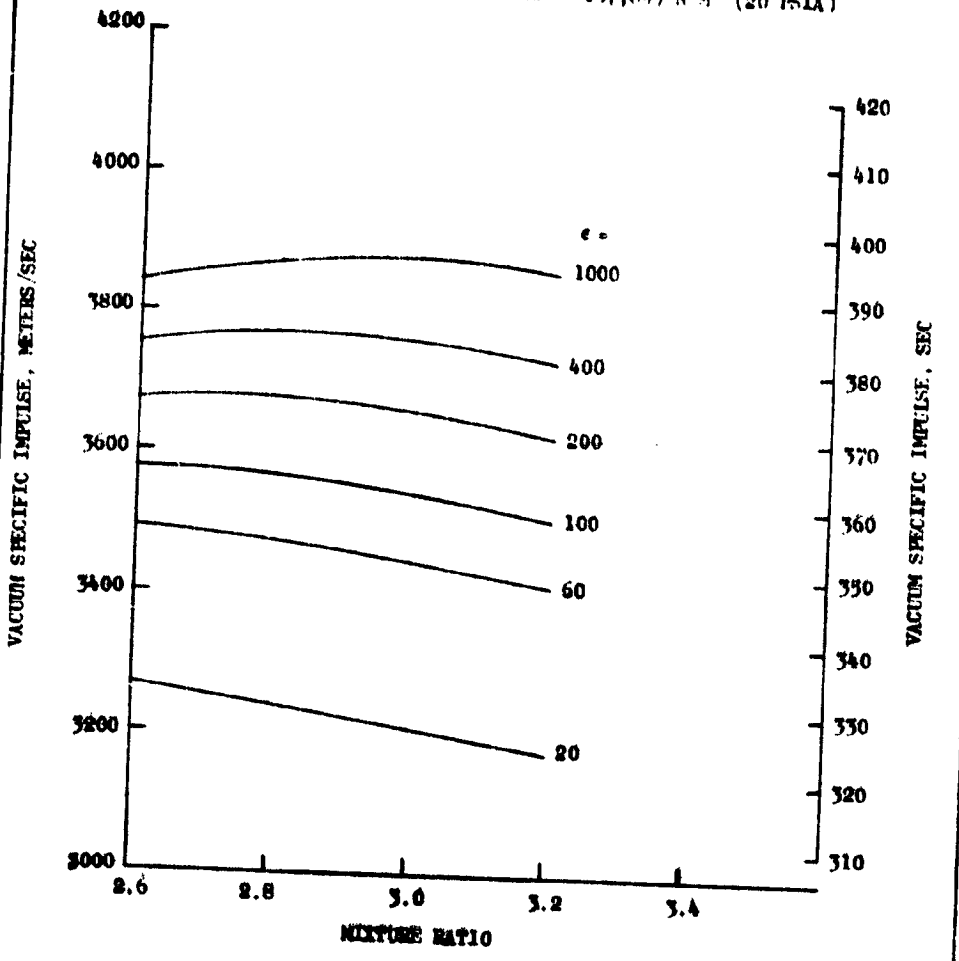

7/79

Figure A-27

THEORETICAL EQUILIBRIUM VACUUM SPECIFIC IMPULSE
for O_2/RP-1 as a function of
MIXTURE RATIO and NOZZLE AREA RATIO

PROPELLANT INLET TEMPERATURES
O_2 = 90.18K (162.32R)
RP-1 = 298.15K (536.67R)

CHAMBER PRESSURE = 689,476 N/M^2 (100 PSIA)

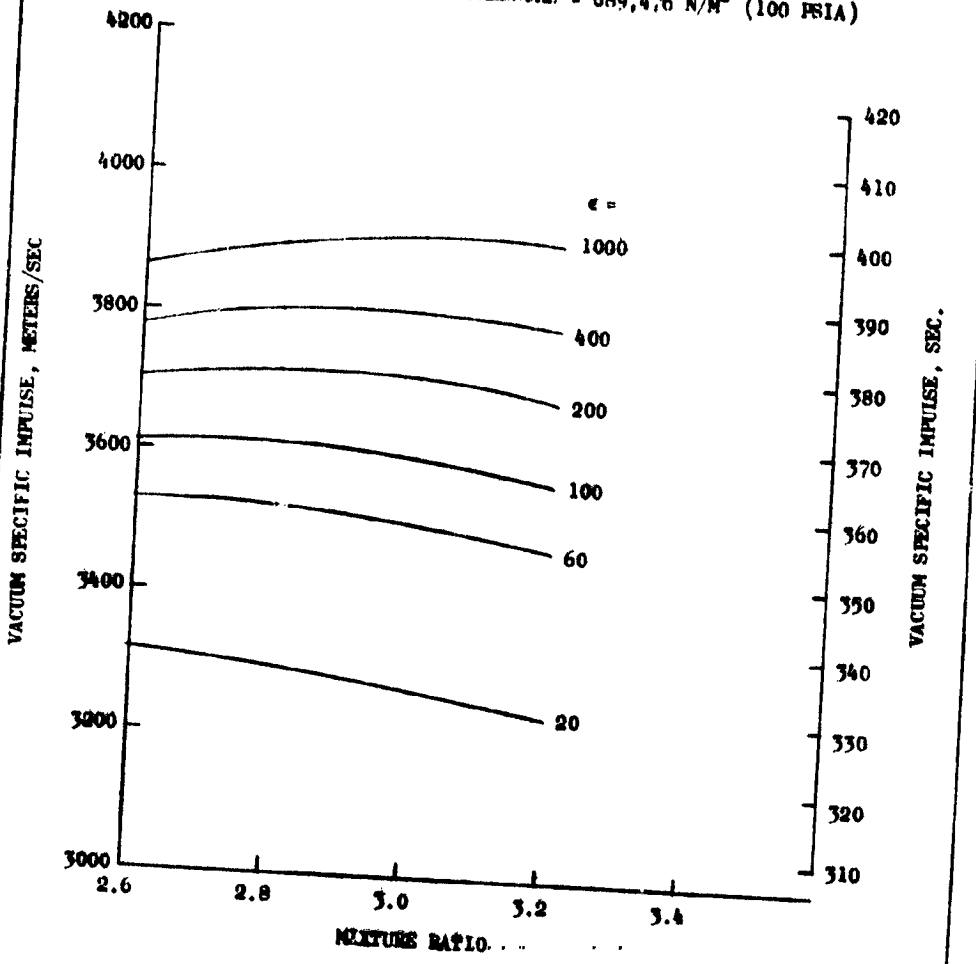

7/79

Figure A-28

THEORETICAL EQUILIBRIUM VACUUM SPECIFIC IMPULSE
for O_2/RP-1 as a function of
MIXTURE RATIO and NOZZLE AREA RATIO

PROPELLANT INLET TEMPERATURES
O_2 = 90.18K (162.32R)
RP-1 = 298.15K (536.67R)

CHAMBER PRESSURE = 2,068,427 N/M^2 (PSIA)

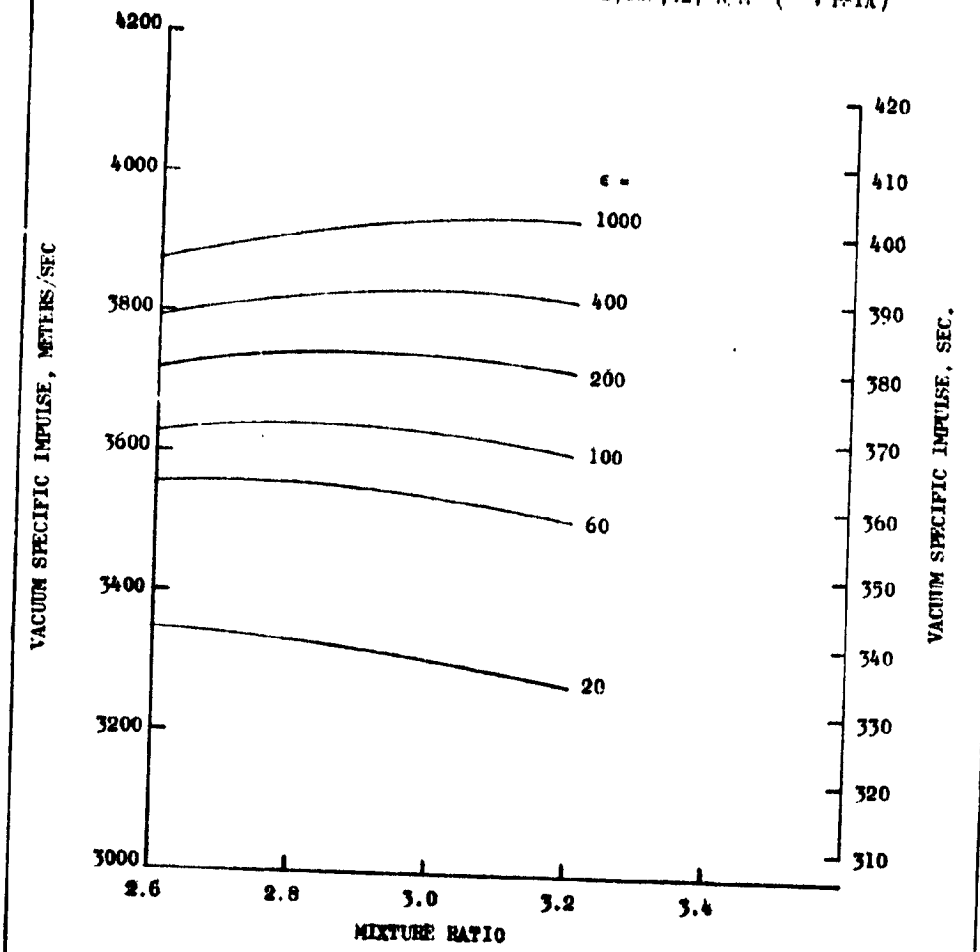

7/79

Figure A-29

THEORETICAL EQUILIBRIUM VACUUM SPECIFIC IMPULSE
for O_2/RP-1 as a function of
MIXTURE RATIO and NOZZLE AREA RATIO

PROPELLANT INLET TEMPERATURES
O_2 = 90.18K (162.32R)
RP-1 = 298.15K (536.67R)

CHAMBER PRESSURE = 3,447,379 N/M^2 (500 PSIA)

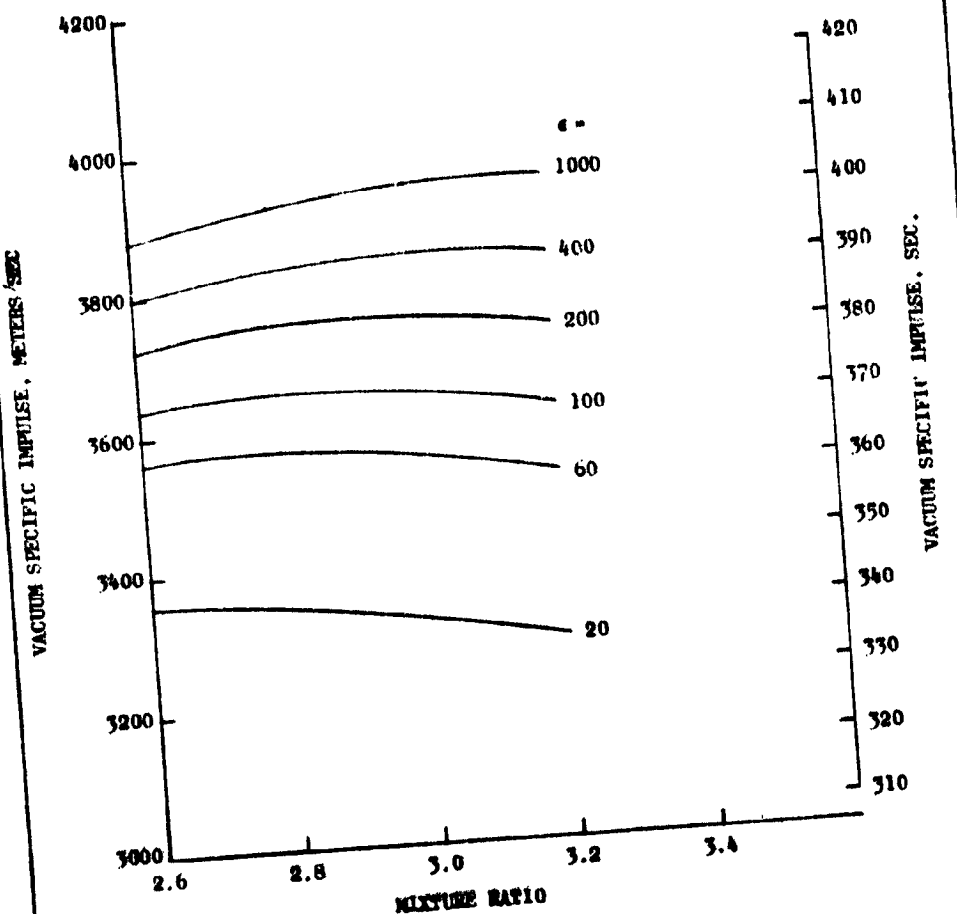

7/79

Figure A-30

THEORETICAL EQUILIBRIUM VACUUM SPECIFIC IMPULSE
for O_2/RP-1 as a function of
MIXTURE RATIO and NOZZLE AREA RATIO

PROPELLANT INLET TEMPERATURES
O_2 = 90.18K (162.32R)
RP-1 = 298.15K (536.67R)

CHAMBER PRESSURE = 6,894,757 N/M^2 (1000 PSIA)

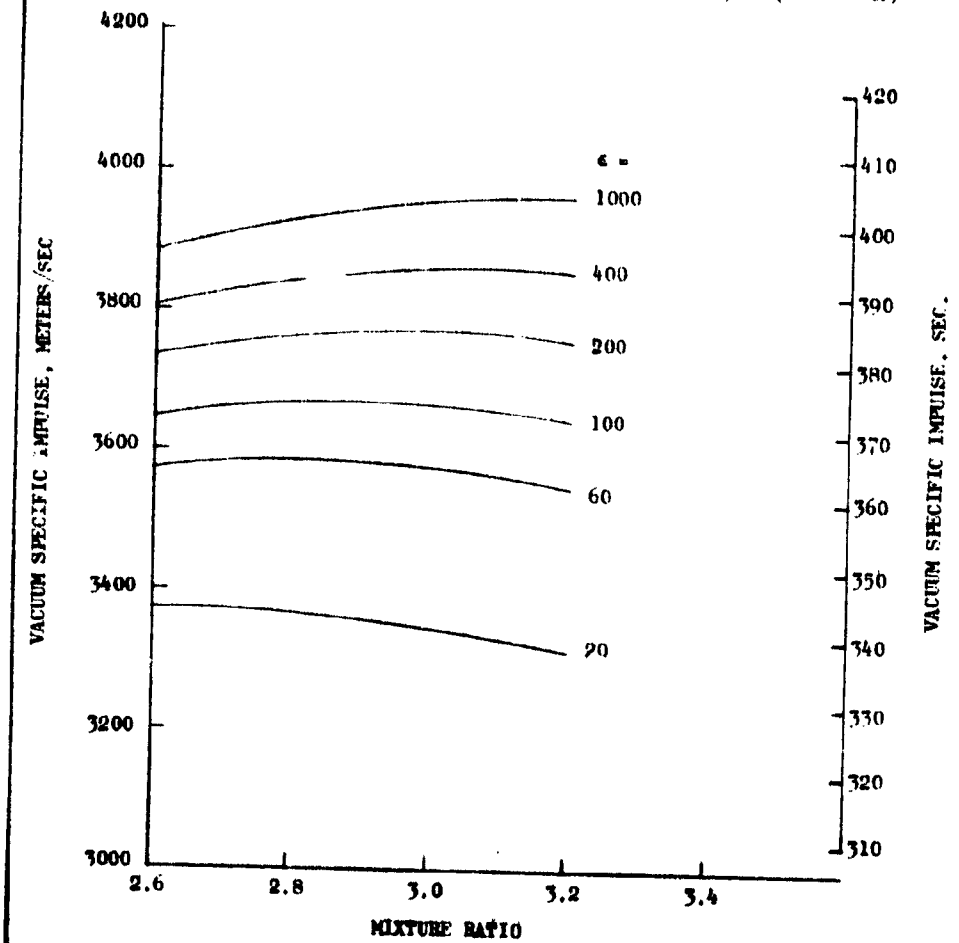

7/79

Figure A-31

THEORETICAL EQUILIBRIUM VACUUM SPECIFIC IMPULSE
for O_2/RP-1 as a function of
MIXTURE RATIO and NOZZLE AREA RATIO

PROPELLANT INLET TEMPERATURES
O_2 = 90K (162R)
RP-1 = 556K (1000R)

CHAMBER PRESSURE = 137,895 N/M^2 (20 PSIA)

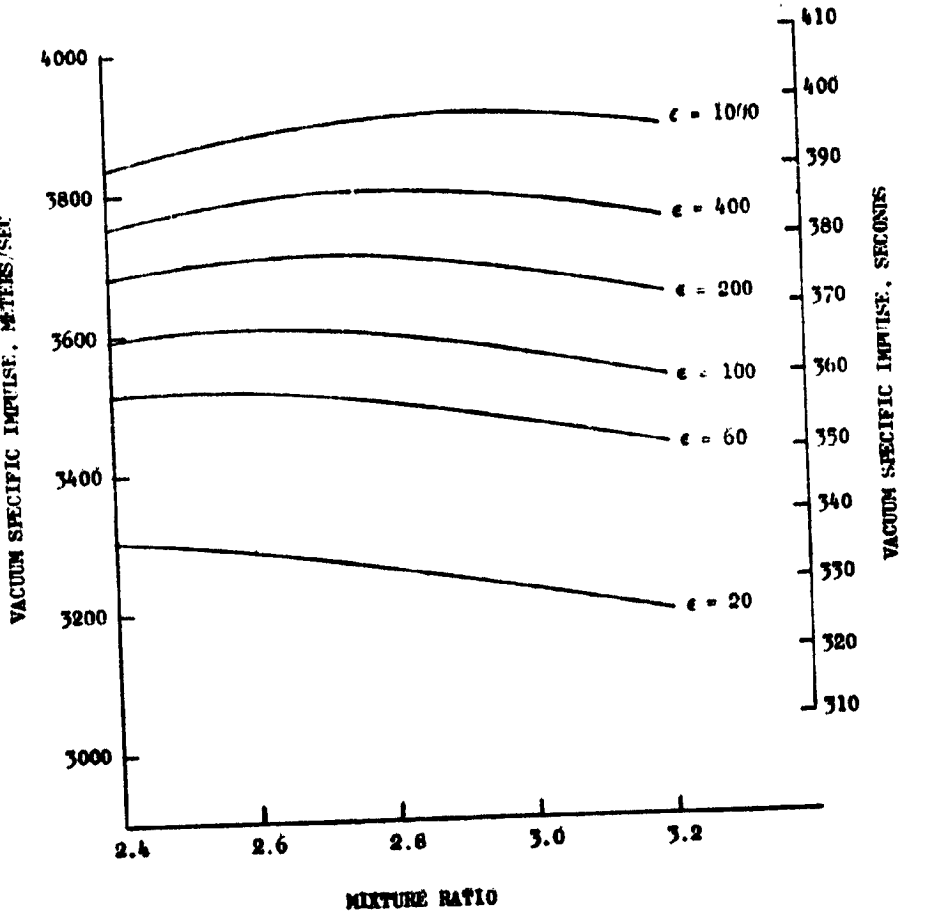

8/79

Figure A-32

THEORETICAL EQUILIBRIUM VACUUM SPECIFIC IMPULSE
for O_2/RP-1 as a function of
MIXTURE RATIO and NOZZLE AREA RATIO

PROPELLANT INLET TEMPERATURES
O_2 = 90K (162R)
RP-1 = 556K (1000R)

CHAMBER PRESSURE = 689,476 N/M^2 (100 PSIA)

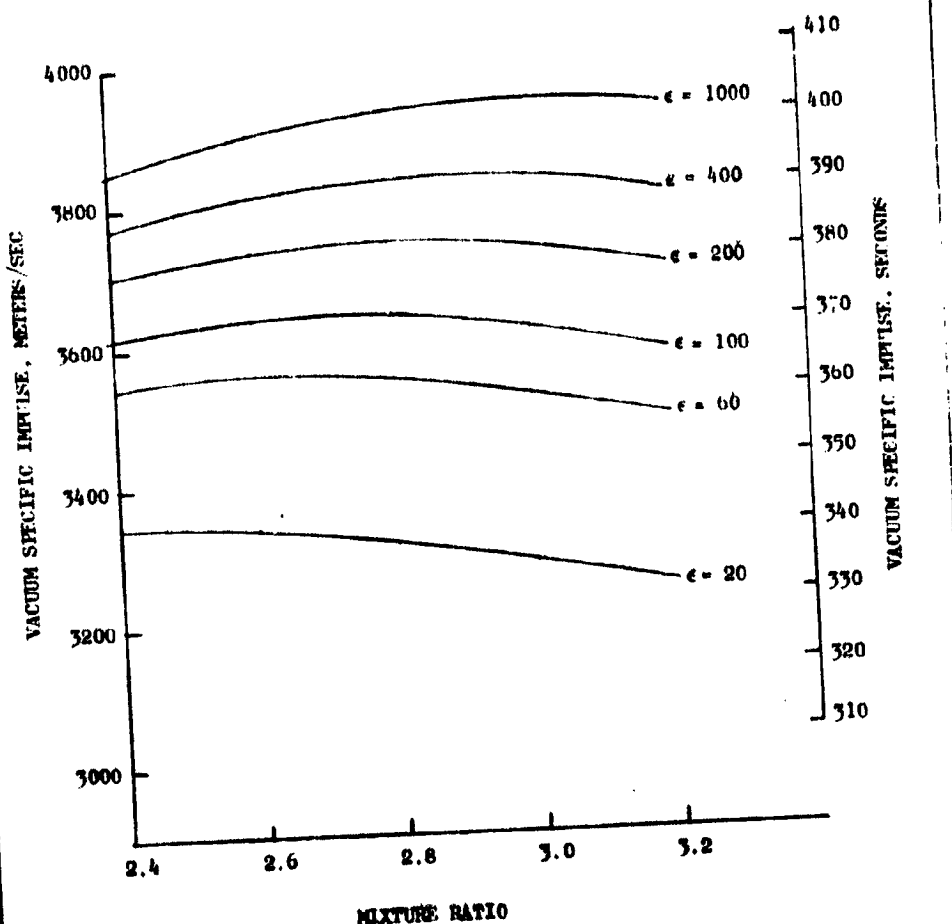

8/79

Figure A-33

THEORETICAL EQUILIBRIUM VACUUM SPECIFIC IMPULSE

for O_2/RP-1 as a function of

MIXTURE RATIO and NOZZLE AREA RATIO

PROPELLANT INLET TEMPERATURES

O_2 = 90K (162R)

RP-1 = 556K (1000R)

CHAMBER PRESSURE = 2,068,427 N/M^2 (300 PSIA)

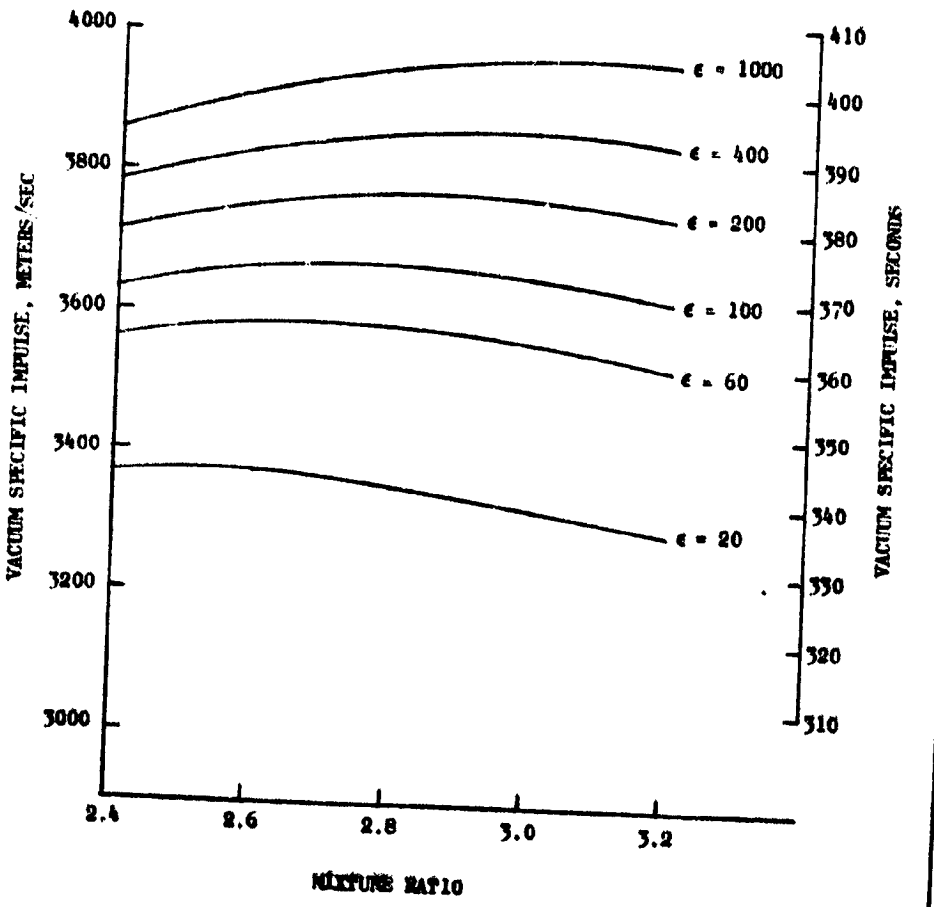

8/79

Figure A-34

THEORETICAL EQUILIBRIUM VACUUM SPECIFIC IMPULSE

for O_2/RP-1 as a function of

MIXTURE RATIO and NOZZLE AREA RATIO

PROPELLANT INLET TEMPERATURES

O_2 = 90K (162R)

RP-1 = 556K (1000R)

CHAMBER PRESSURE = 3,447,379 N/M^2 (500 PSIA)

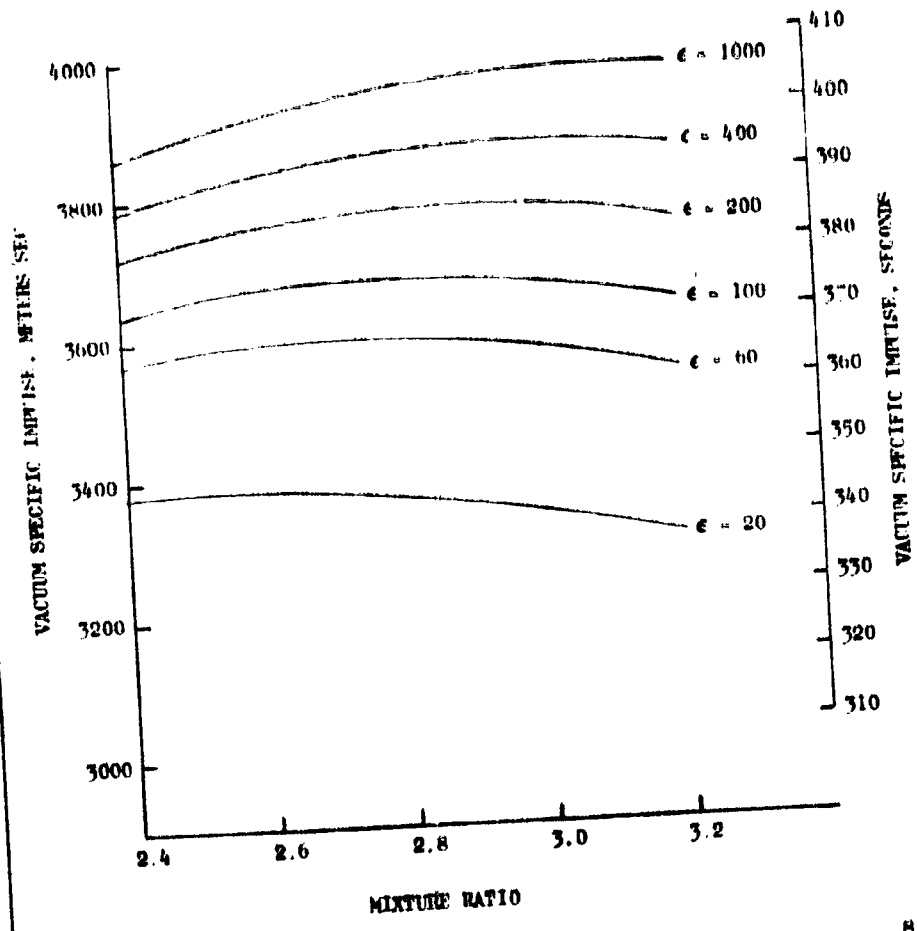

8/79

Figure A-35

THEORETICAL EQUILIBRIUM VACUUM SPECIFIC IMPULSE
for O_2/RP-1 as a function of
MIXTURE RATIO and NOZZLE AREA RATIO

PROPELLANT INLET TEMPERATURES
O_2 = 90K (162R)
RP-1 = 556K (1000R)

CHAMBER PRESSURE = 6,894,757 N/M^2 (1000 PSIA)

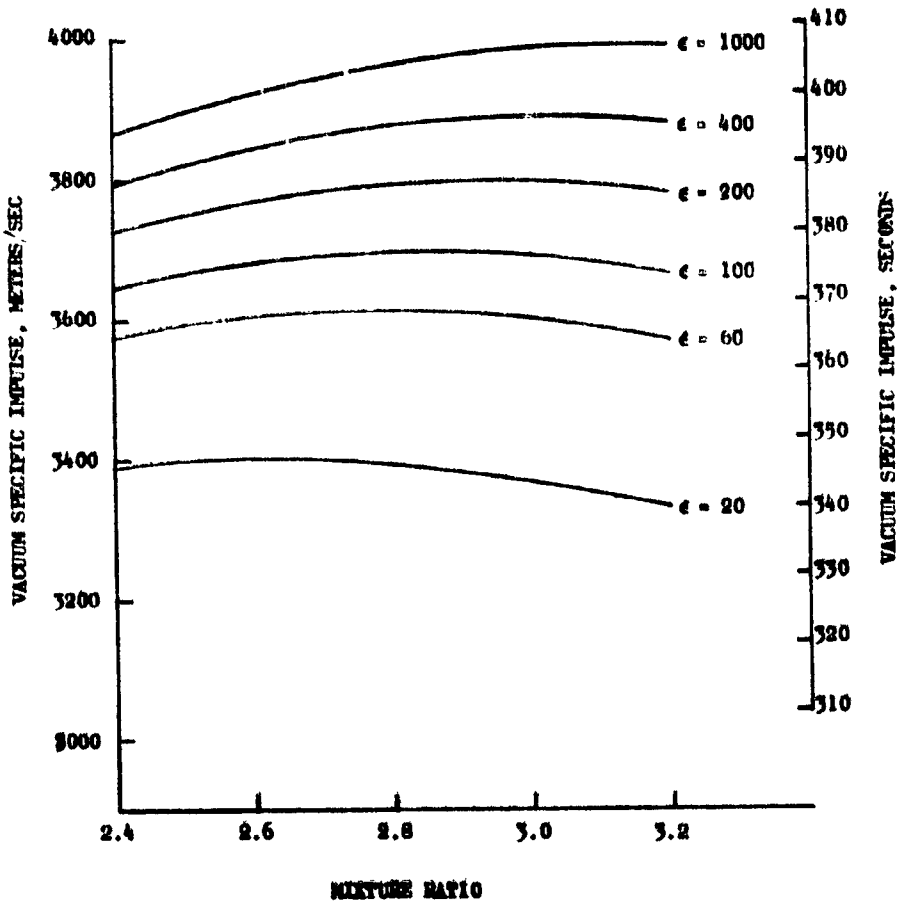

8/79

APPENDIX B

PROPELLANT PROPERTY DATA

The theoretical propellant property data were generated for LO_2/H_2, LO_2/CH_4, and LO_2/RP-1 using the TRAN 78 computer program. The propellant property data are plotted versus chamber pressure for parametric mixture ratio. The data presented included combustion chamber gas temperature, density, molecular weight, specific heat, gamma, viscosity, and thermal conductivity. The LO_2/H_2 data are presented in Fig. B-1 through B-7, and data for LO_2/CH_4 and LO_2/RP-1 are shown in Fig. B-8 through B-14 and B-15 through B-21, respectively.

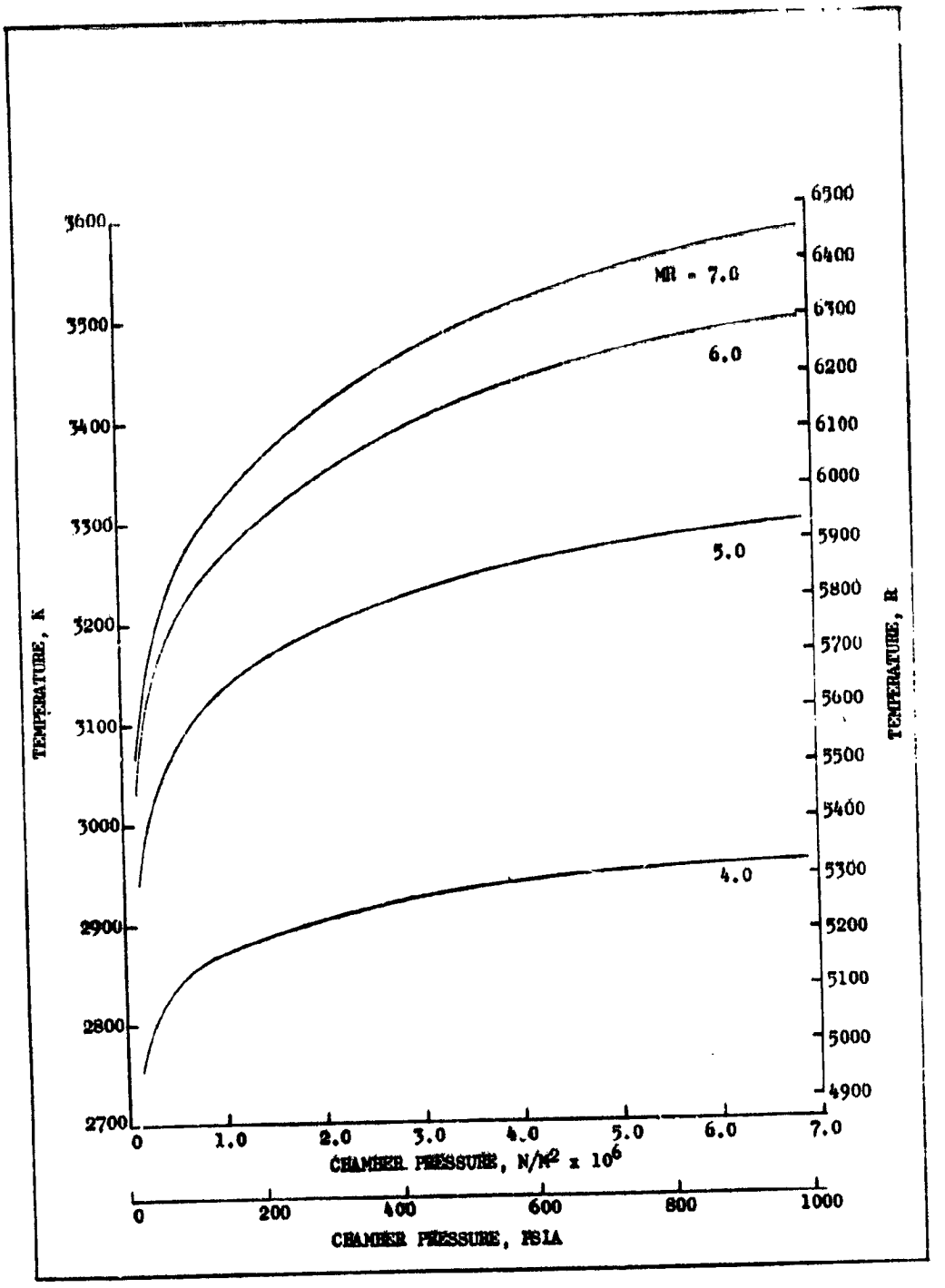

Figure B-1. Combustion Temperature Variation With Chamber Pressure and Mixture Ratio for LO_2/H_2

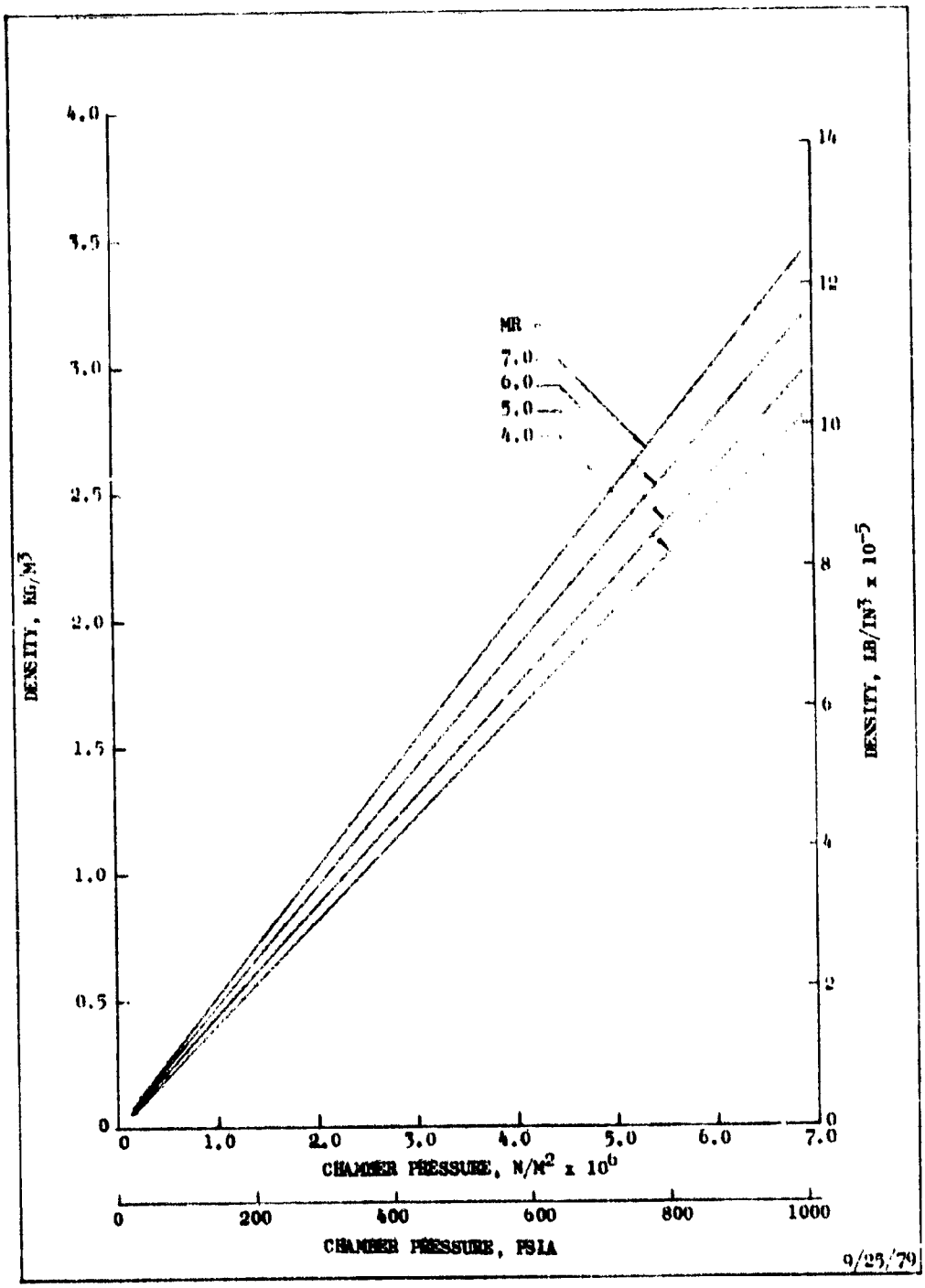

Figure B-2. Combustion Chamber Density Variation With Chamber Pressure and Mixture Ratio for LO_2/H_2

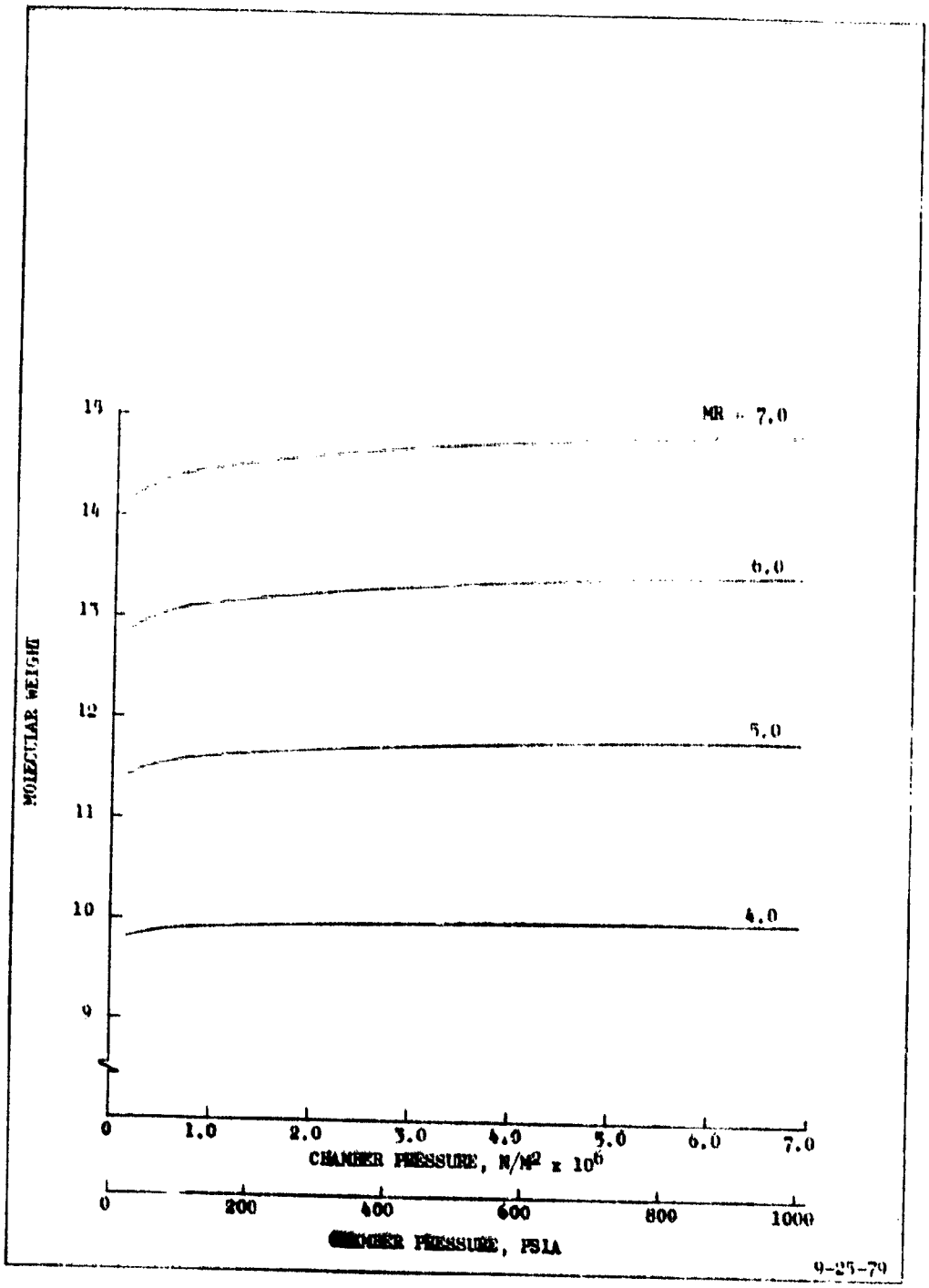

Figure B-3. Combustion Chamber Molecular Weight Variation With Chamber Pressure and Mixture Ratio for LO_2/H_2

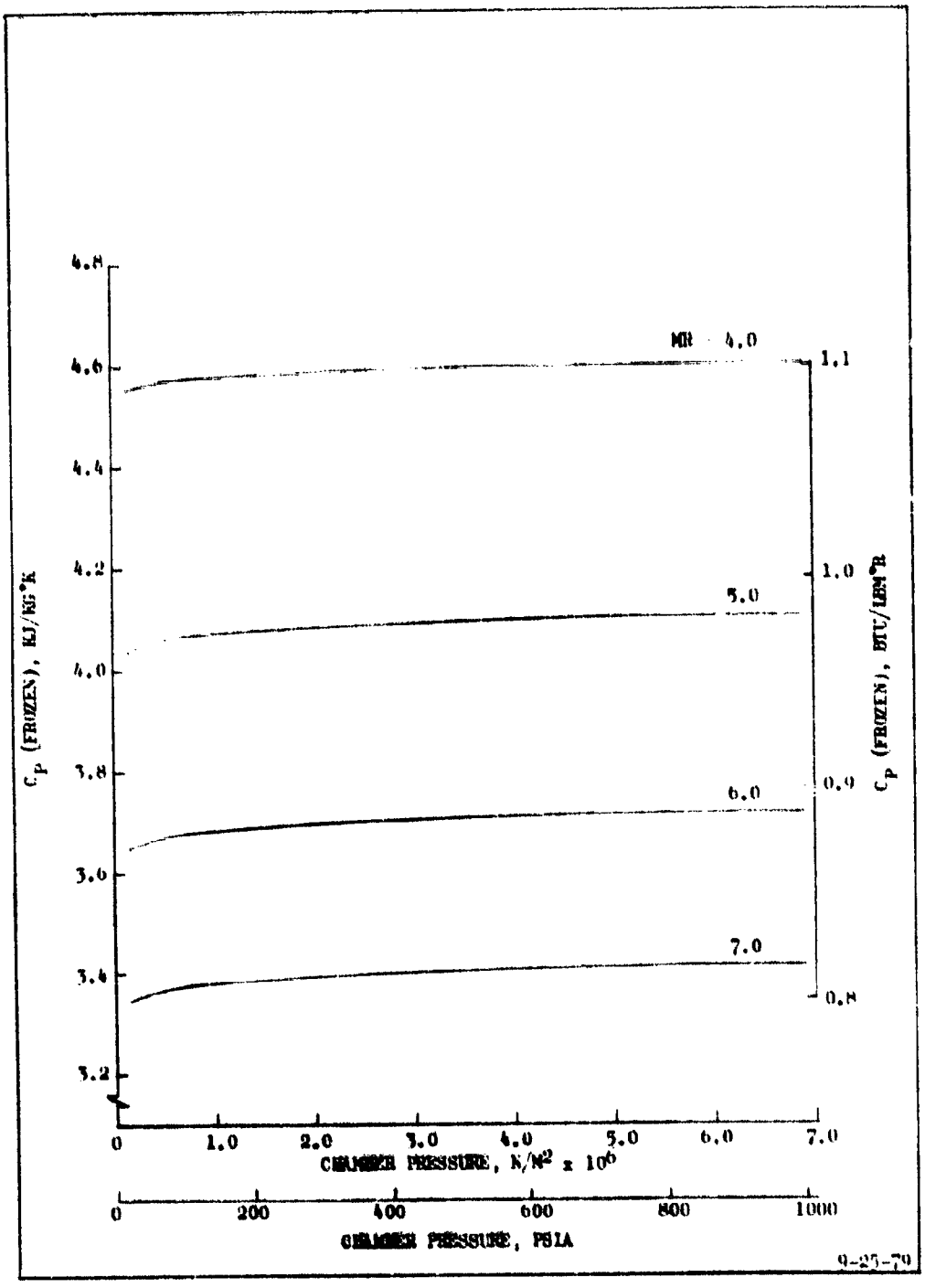

Figure B-4. Combustion Chamber Specific Heat Variation With Chamber Pressure and Mixture Ratio for LO_2/H_2

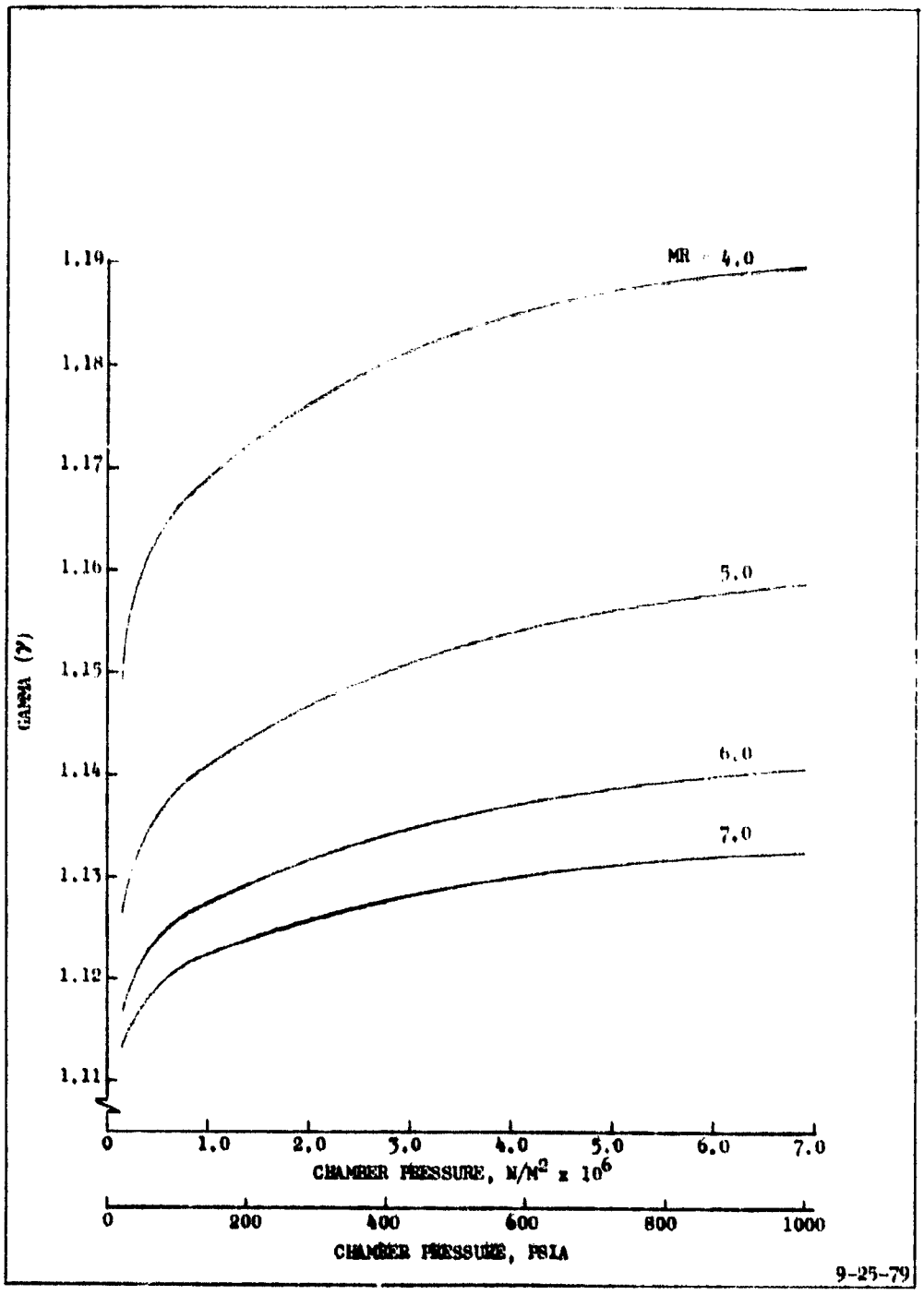

Figure B-5. Combustion Chamber Specific Heat Ratio (γ) Variation With Chamber Pressure and Mixture Ratio for LO_2/H_2

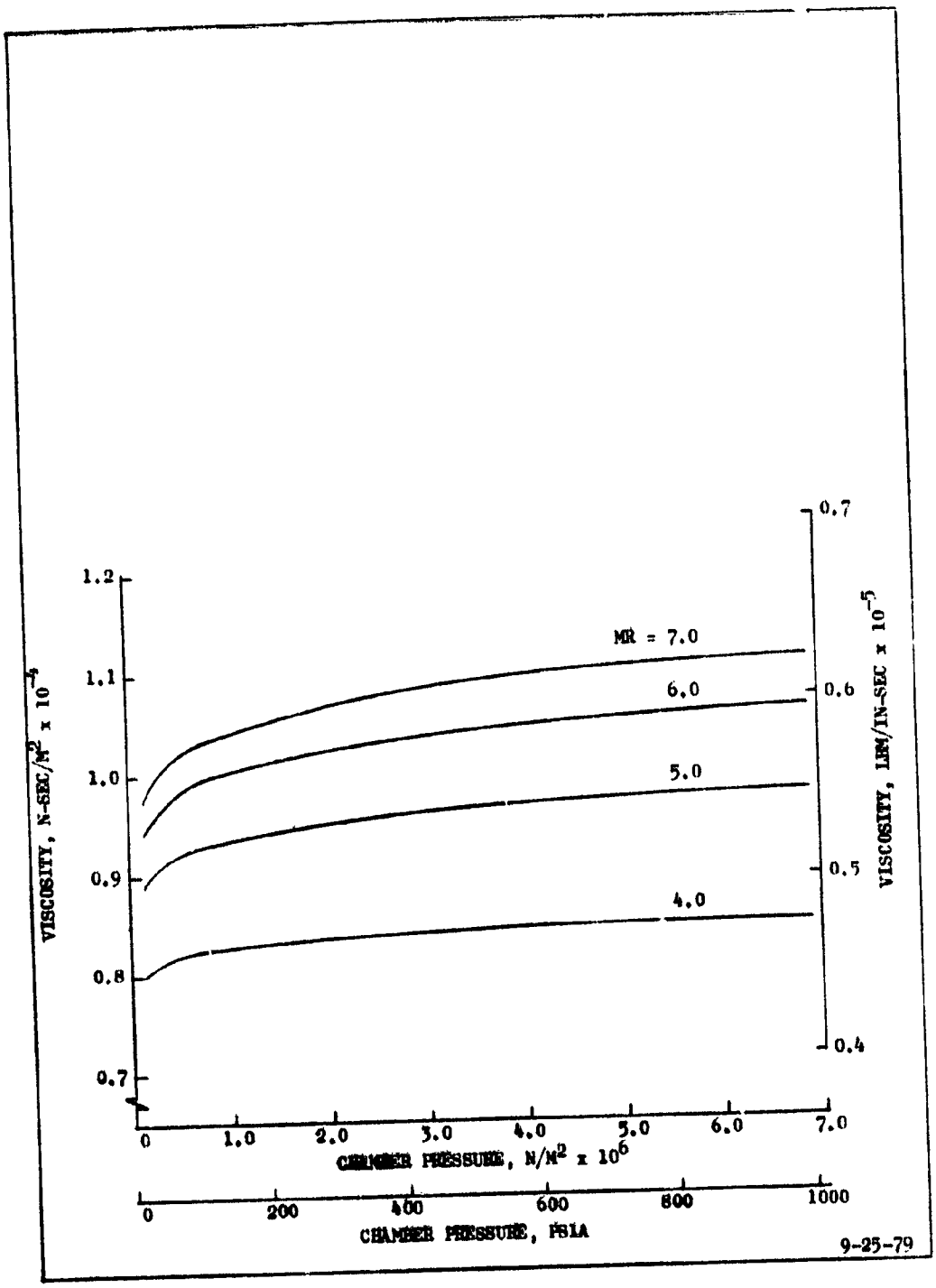

Figure B-6. Combustion Chamber Viscosity Variation With Chamber Pressure and Mixture Ratio for LO_2/H_2

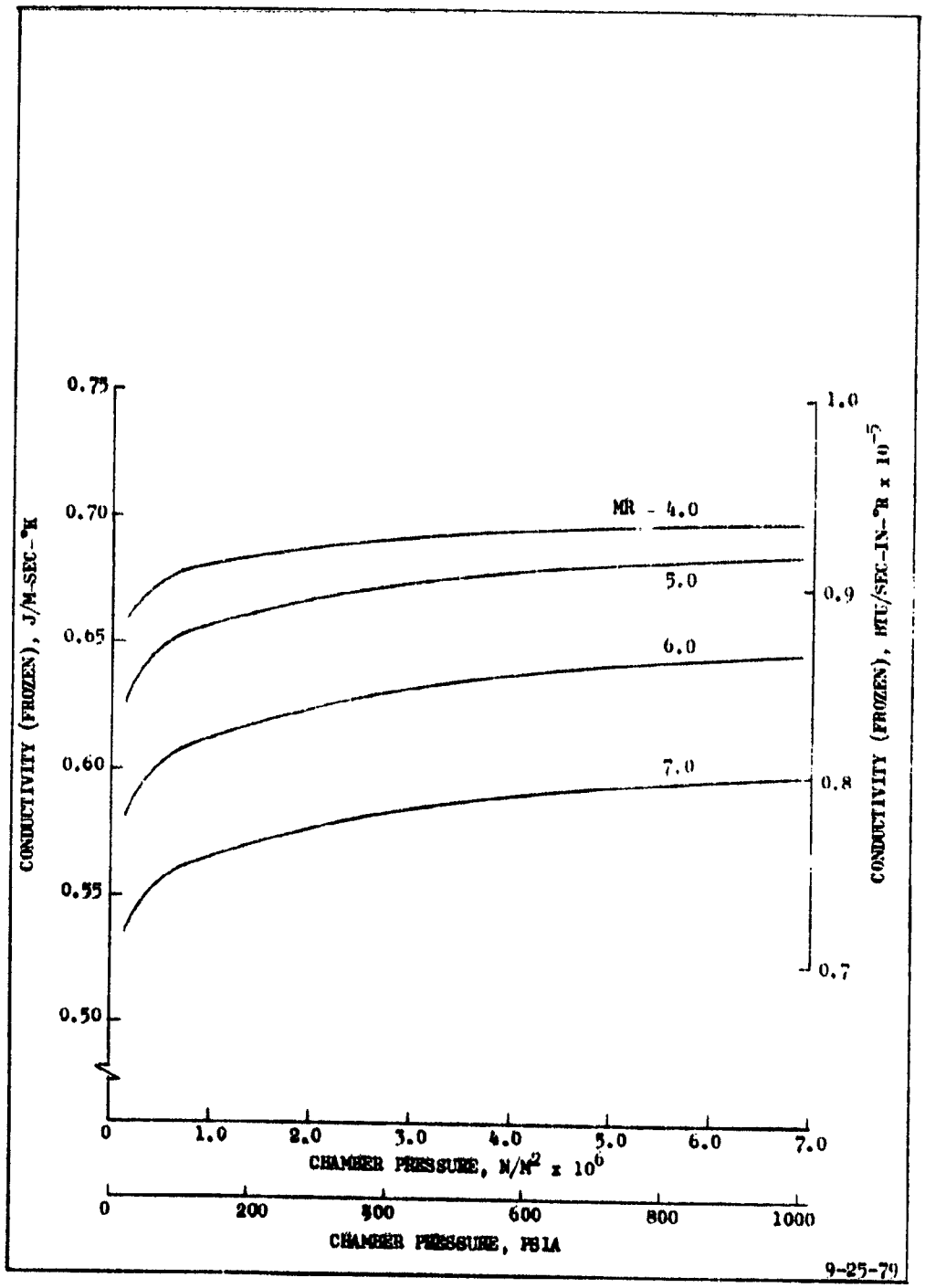

Figure B-7. Combustion Chamber Thermal Conductivity Variation With Chamber Pressure and Mixture Ratio for LO_2/H_2

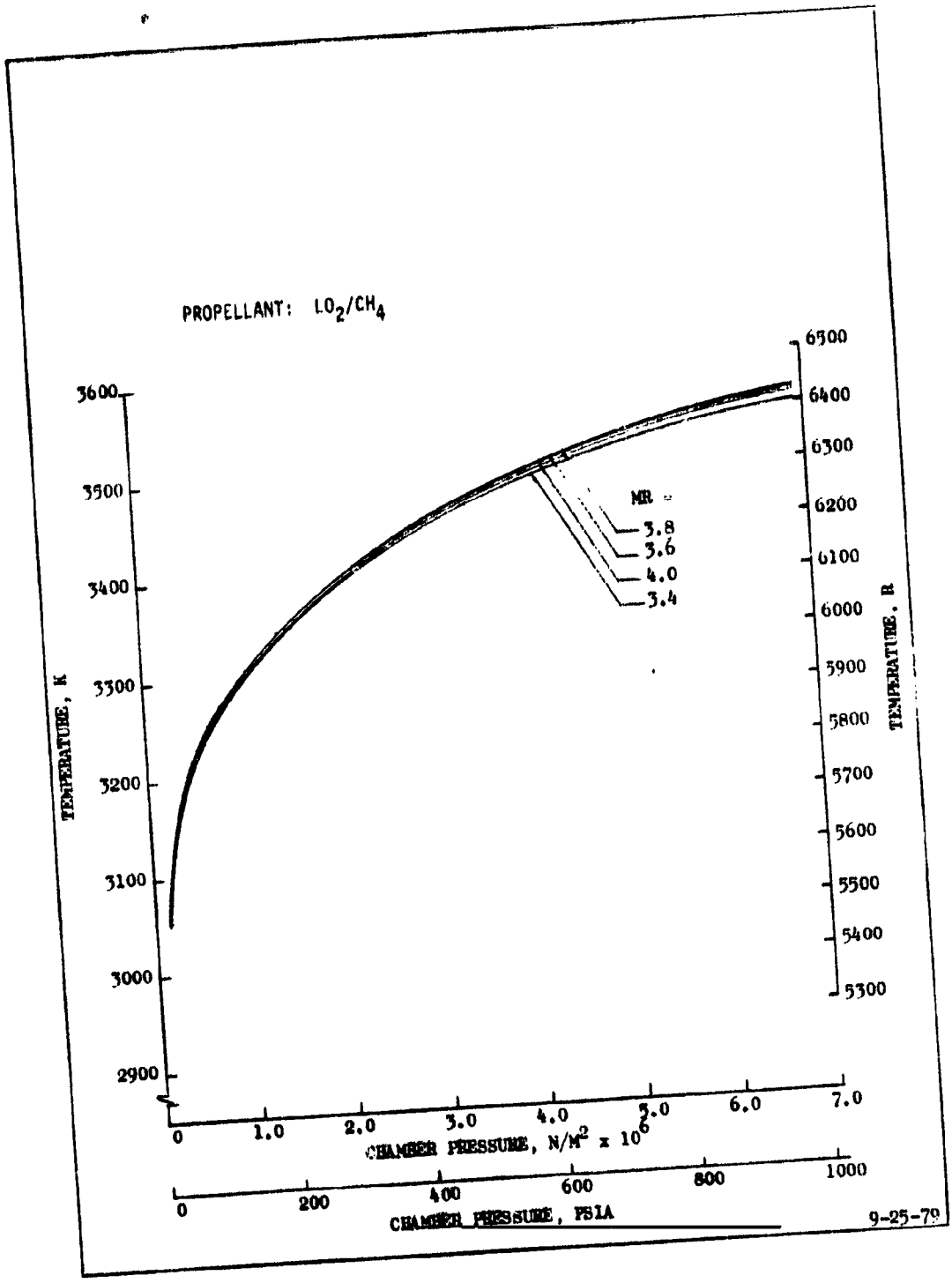
PROPELLANT: LO_2/CH_4
MR
3.8
3.6
4.0
3.4
TEMPERATURE, K
3600
3500
3400
3300
3200
3100
3000
2900
TEMPERATURE, R
6500
6400
6300
6200
6100
6000
5900
5800
5700
5600
5500
5400
5300
0
1.0
2.0
3.0
4.0
5.0
6.0
7.0
CHAMBER PRESSURE, $N/M^2 \times 10^6$
0
200
400
600
800
1000
CHAMBER PRESSURE, PSIA
9-25-79

Figure B-8.

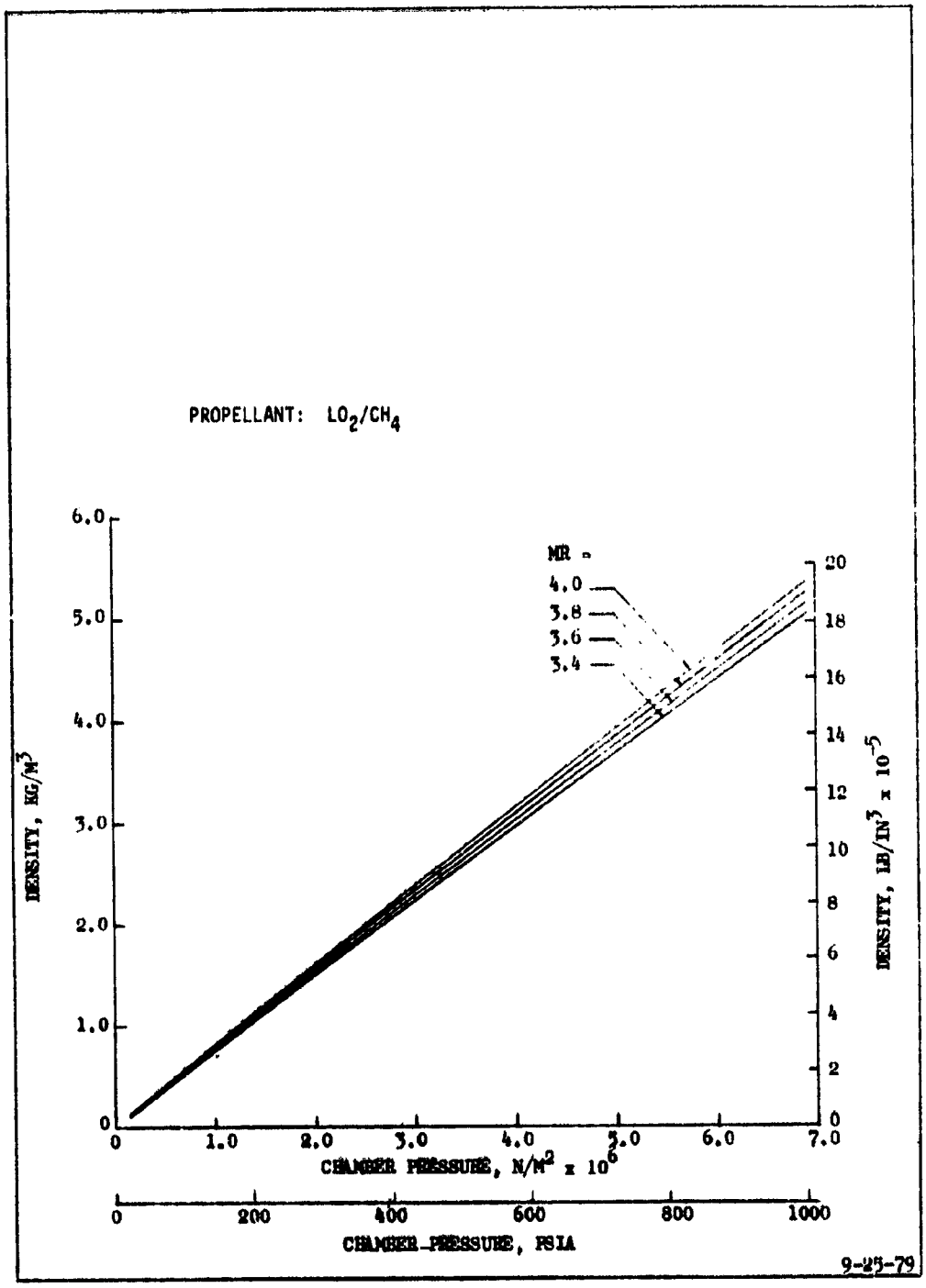
PROPELLANT: LO_2/CH_4
MR =
4.0
3.8
3.6
3.4
DENSITY, KG/M^3
DENSITY, LB/IN^3 x 10^{-5}
CHAMBER PRESSURE, N/M^2 x 10^6
CHAMBER PRESSURE, PSIA
9-25-79

Figure B-9.

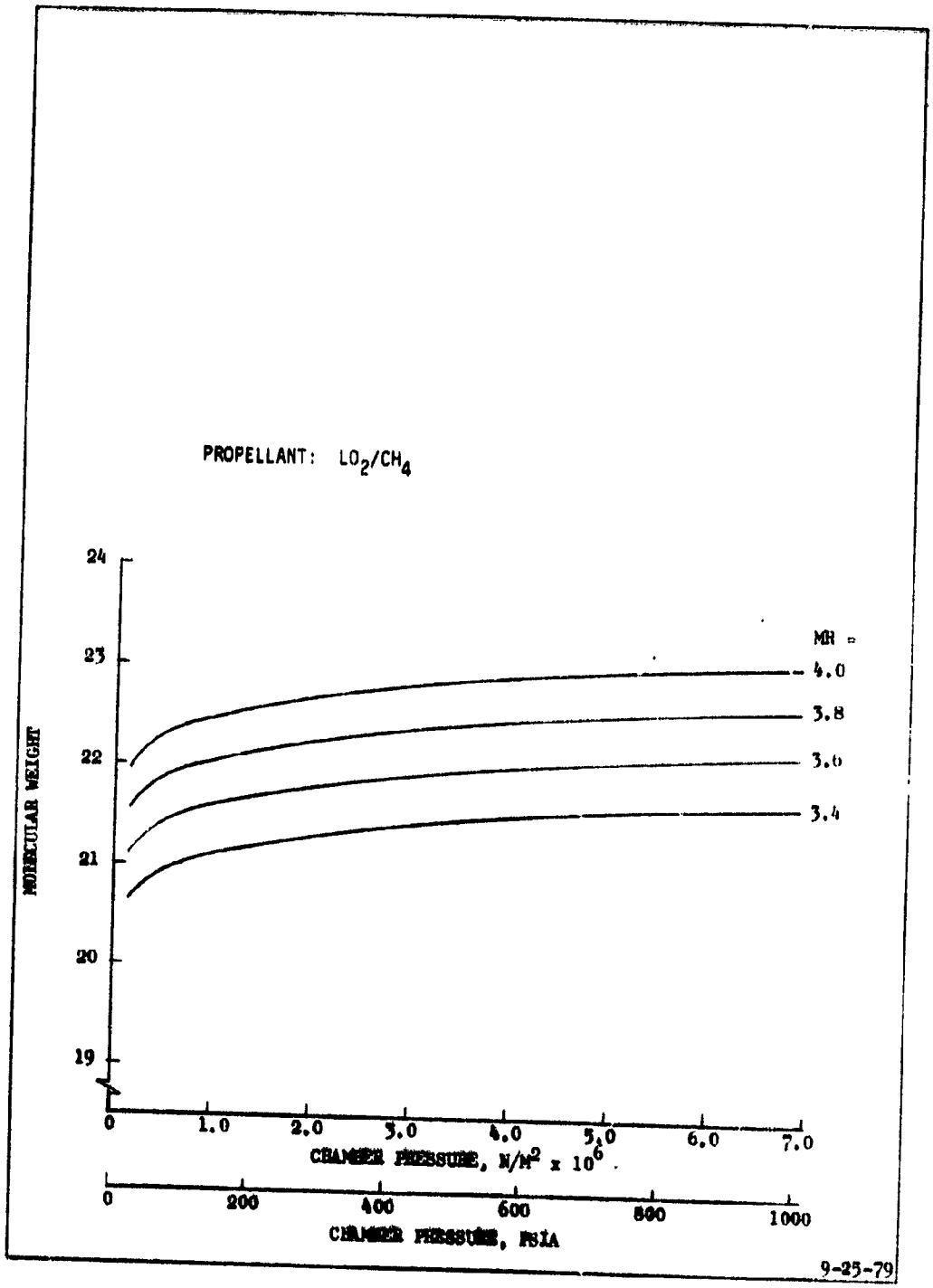
PROPELLANT: LO_2/CH_4
MOLECULAR WEIGHT
24
23
22
21
20
19
MR =
4.0
3.8
3.6
3.4
0
1.0
2.0
3.0
4.0
5.0
6.0
7.0
CHAMBER PRESSURE, $N/M^2 \times 10^6$
0
200
400
600
800
1000
CHAMBER PRESSURE, PSIA
9-25-79

Figure B-10.

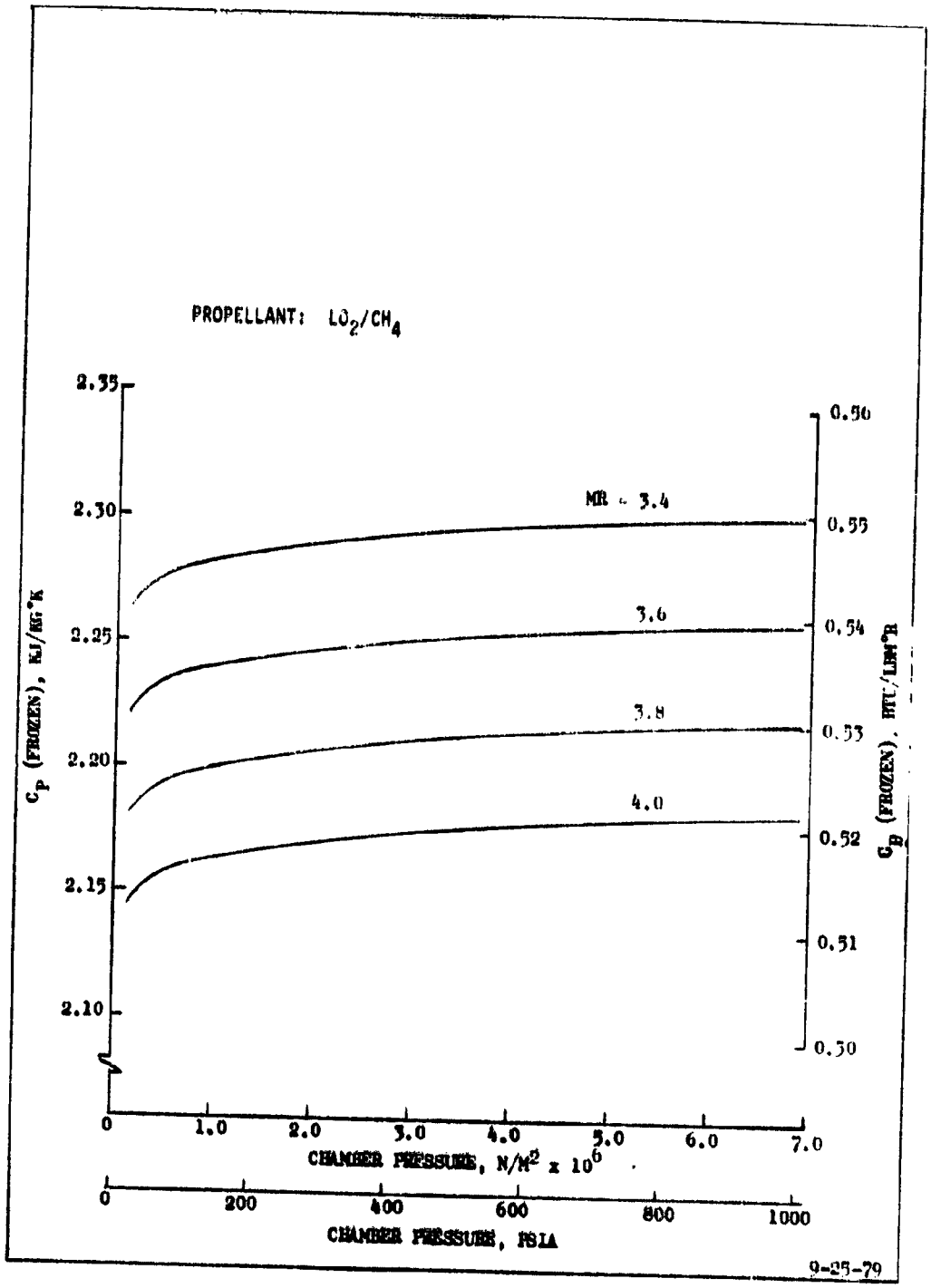
PROPELLANT: LO_2/CH_4
MR = 3.4
3.6
3.8
4.0
C_p (FROZEN), KJ/KG°K
C_p (FROZEN), BTU/LBM°R
2.35
2.30
2.25
2.20
2.15
2.10
0.56
0.55
0.54
0.53
0.52
0.51
0.50
0
1.0
2.0
3.0
4.0
5.0
6.0
7.0
CHAMBER PRESSURE, $N/M^2 \times 10^6$
0
200
400
600
800
1000
CHAMBER PRESSURE, PSIA
9-25-79

Figure B-11.

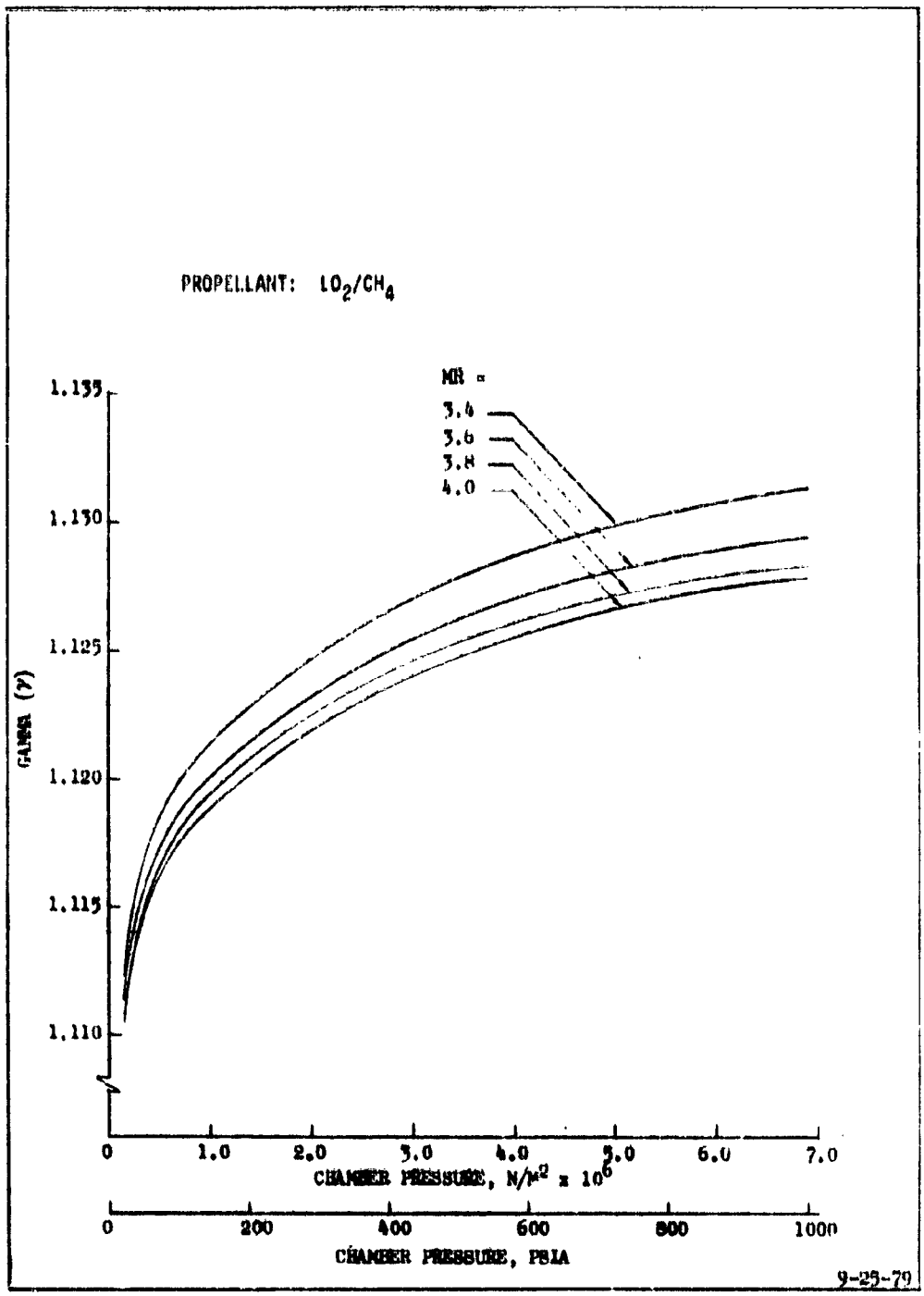
PROPELLANT: LO_2/CH_4
MR =
3.4
3.6
3.8
4.0
1.135
1.130
1.125
1.120
1.115
1.110
GAMMA (γ)
0
1.0
2.0
3.0
4.0
5.0
6.0
7.0
CHAMBER PRESSURE, $N/M^2 \times 10^6$
0
200
400
600
800
1000
CHAMBER PRESSURE, PSIA
9-25-79

Figure B-12.

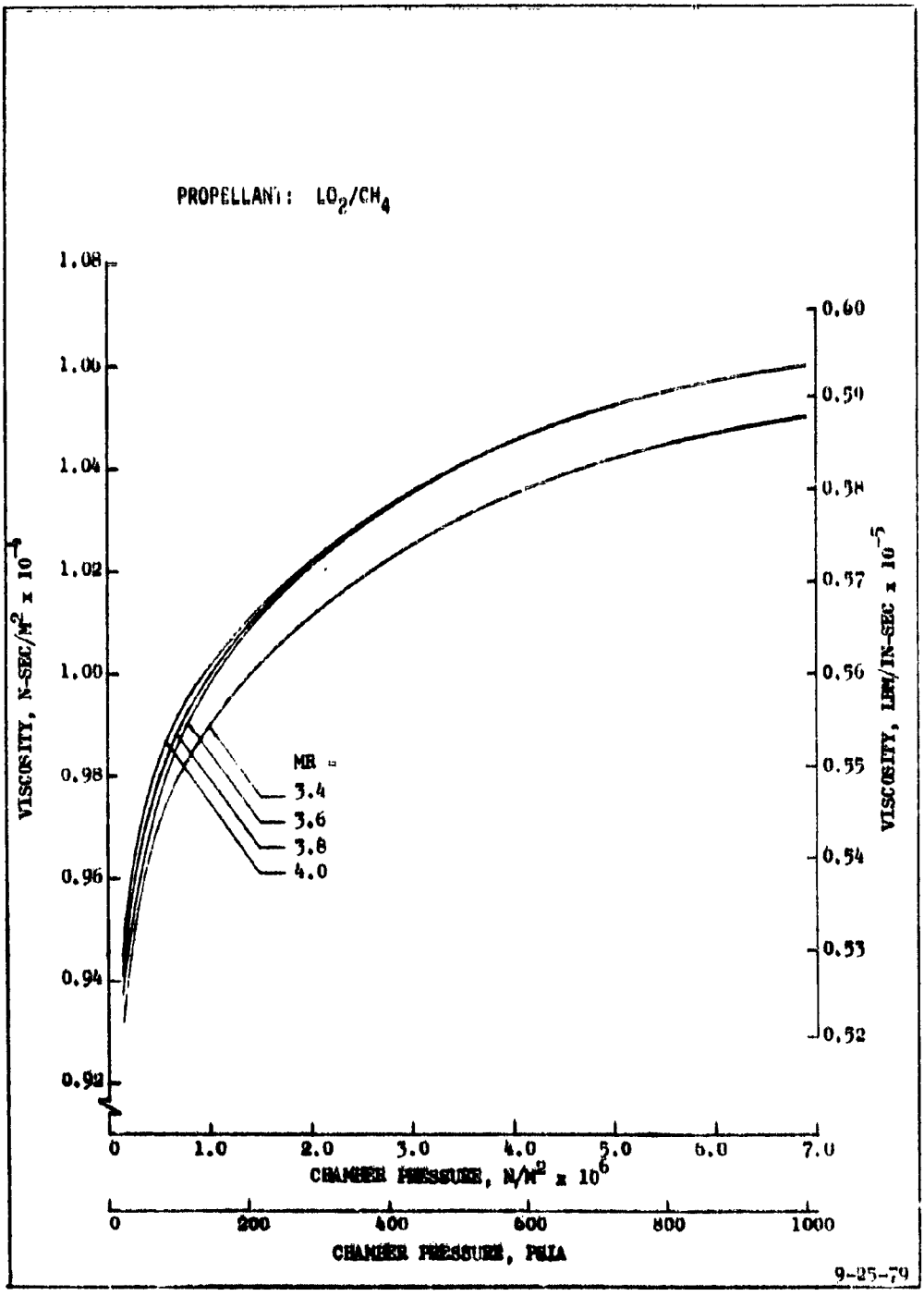
PROPELLANT: LO_2/CH_4
VISCOSITY, N-SEC/M^2 x 10^{-4}
VISCOSITY, LBM/IN-SEC x 10^{-5}
1.08
1.06
1.04
1.02
1.00
0.98
0.96
0.94
0.92
0.60
0.59
0.58
0.57
0.56
0.55
0.54
0.53
0.52
MR =
3.4
3.6
3.8
4.0
0
1.0
2.0
3.0
4.0
5.0
6.0
7.0
CHAMBER PRESSURE, N/M^2 x 10^6
0
200
400
600
800
1000
CHAMBER PRESSURE, PSIA
9-25-79

Figure B-13.

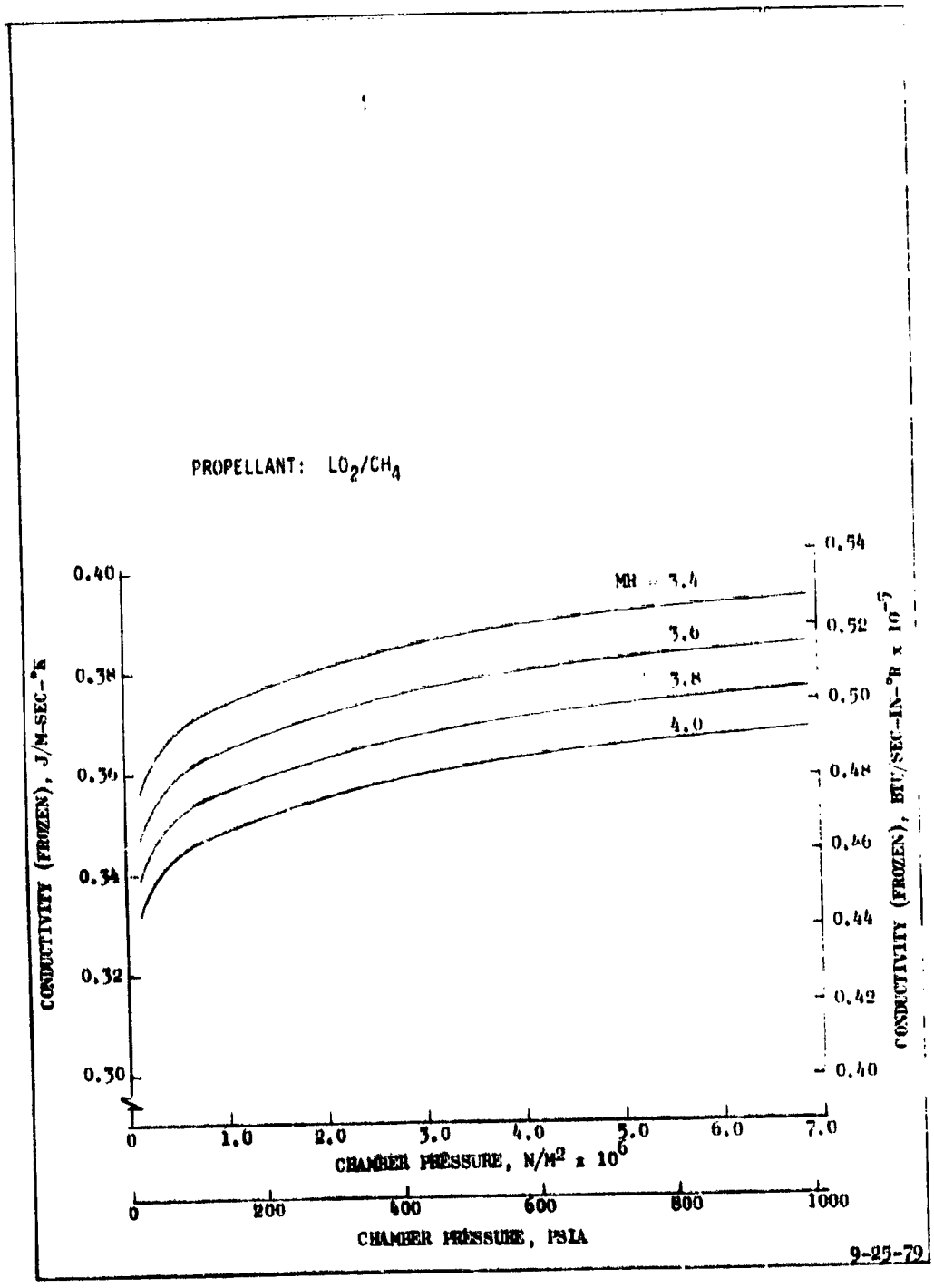
PROPELLANT: LO_2/CH_4
MR = 3.4
3.6
3.8
4.0
CONDUCTIVITY (FROZEN), J/M-SEC-°K
0.40
0.38
0.36
0.34
0.32
0.30
CONDUCTIVITY (FROZEN), BTU/SEC-IN-°R x 10^{-5}
0.54
0.52
0.50
0.48
0.46
0.44
0.42
0.40
0
1.0
2.0
3.0
4.0
5.0
6.0
7.0
CHAMBER PRESSURE, N/M^2 x 10^6
0
200
400
600
800
1000
CHAMBER PRESSURE, PSIA
9-25-79

Figure B-14.

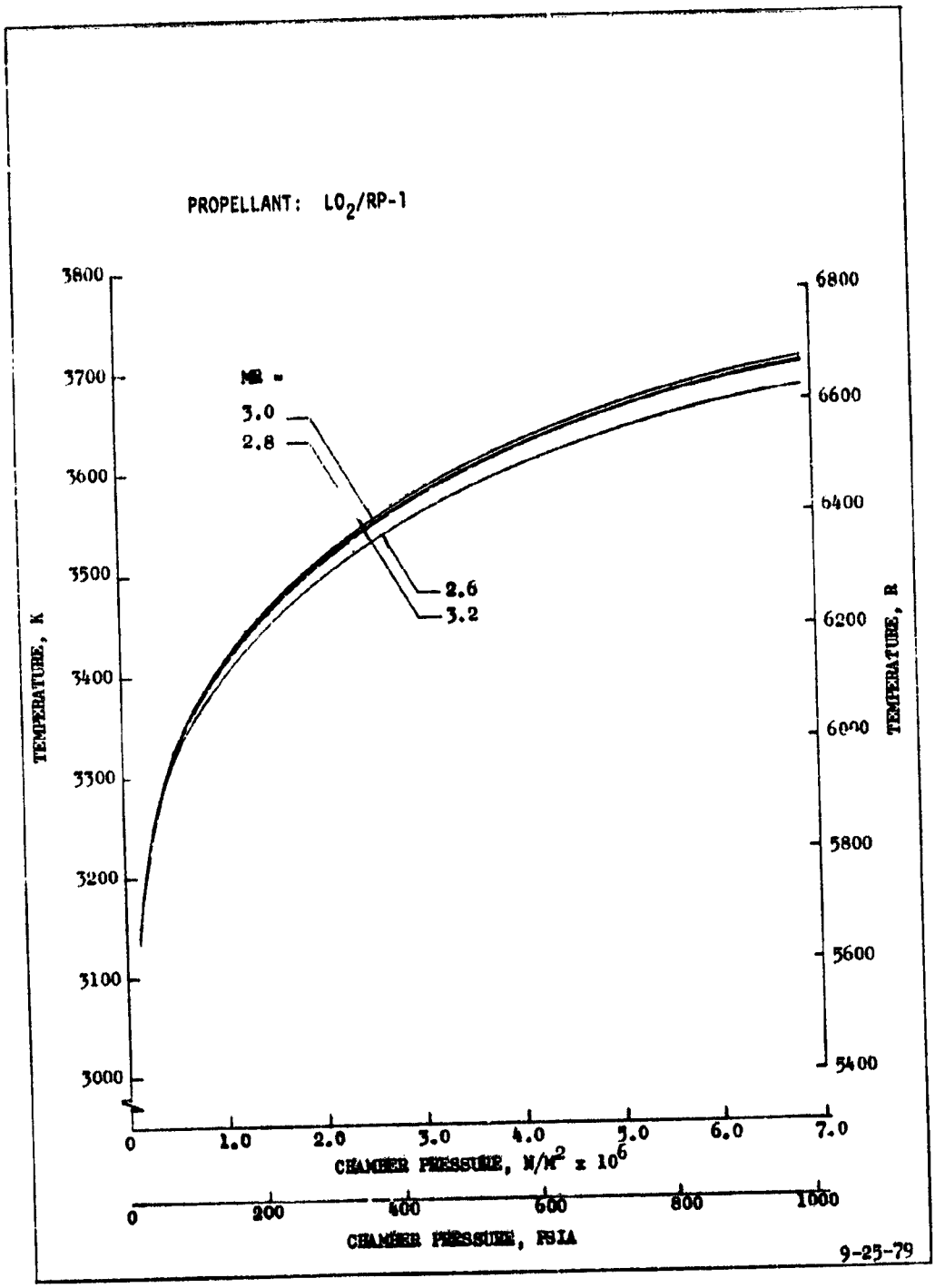
PROPELLANT: LO_2/RP-1
MR =
3.0
2.8
2.6
3.2
TEMPERATURE, K
TEMPERATURE, R
3800
3700
3600
3500
3400
3300
3200
3100
3000
6800
6600
6400
6200
6000
5800
5600
5400
0
1.0
2.0
3.0
4.0
5.0
6.0
7.0
CHAMBER PRESSURE, $N/M^2 \times 10^6$
0
200
400
600
800
1000
CHAMBER PRESSURE, PSIA
9-25-79

Figur. B-15.

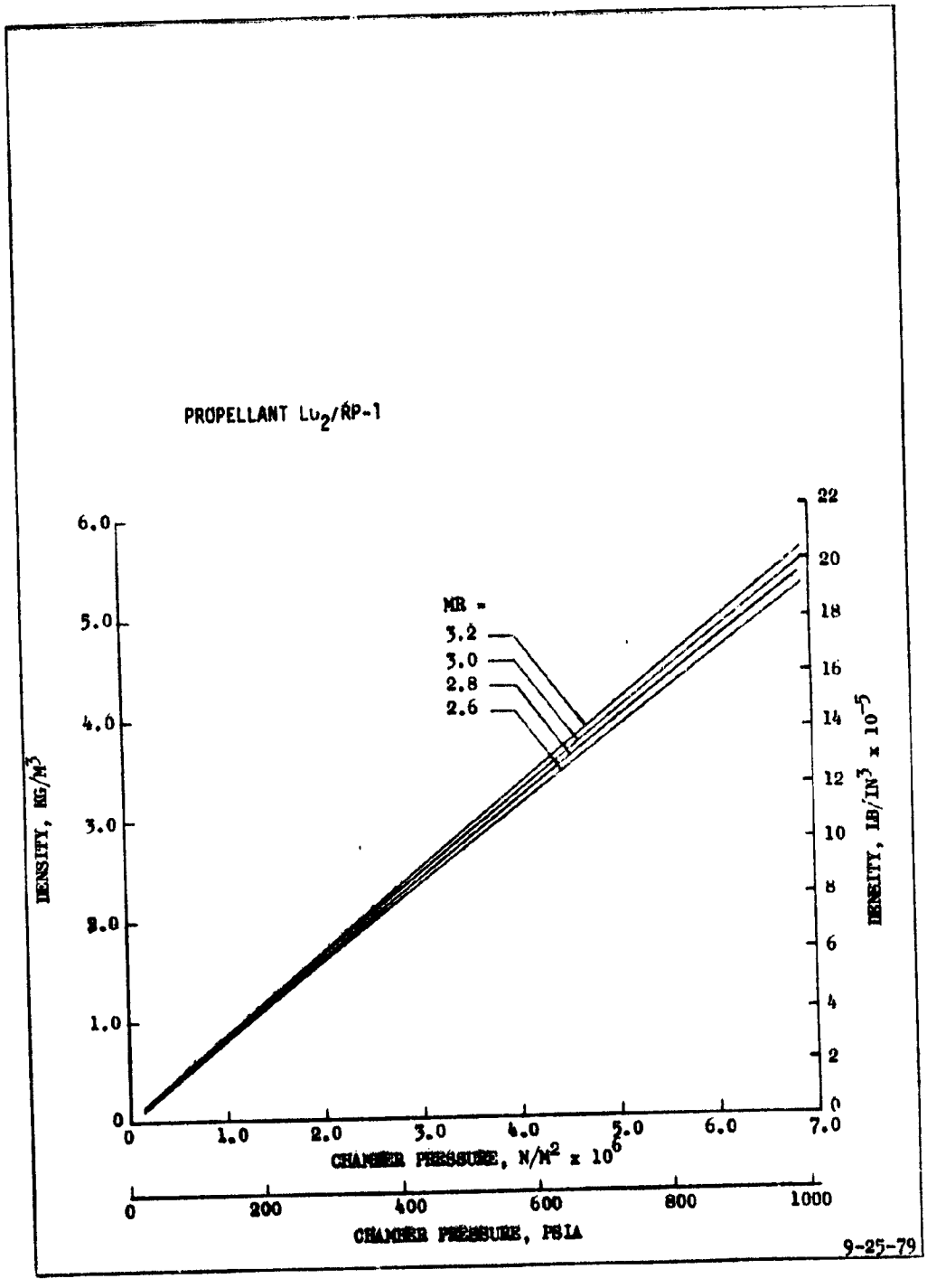
PROPELLANT Lu_2/RP-1
DENSITY, MG/M^3
DENSITY, LB/IN^3 x 10^{-5}
MR =
3.2
3.0
2.8
2.6
CHAMBER PRESSURE, N/M^2 x 10^6
CHAMBER PRESSURE, PSIA
9-25-79

Figure B-16.

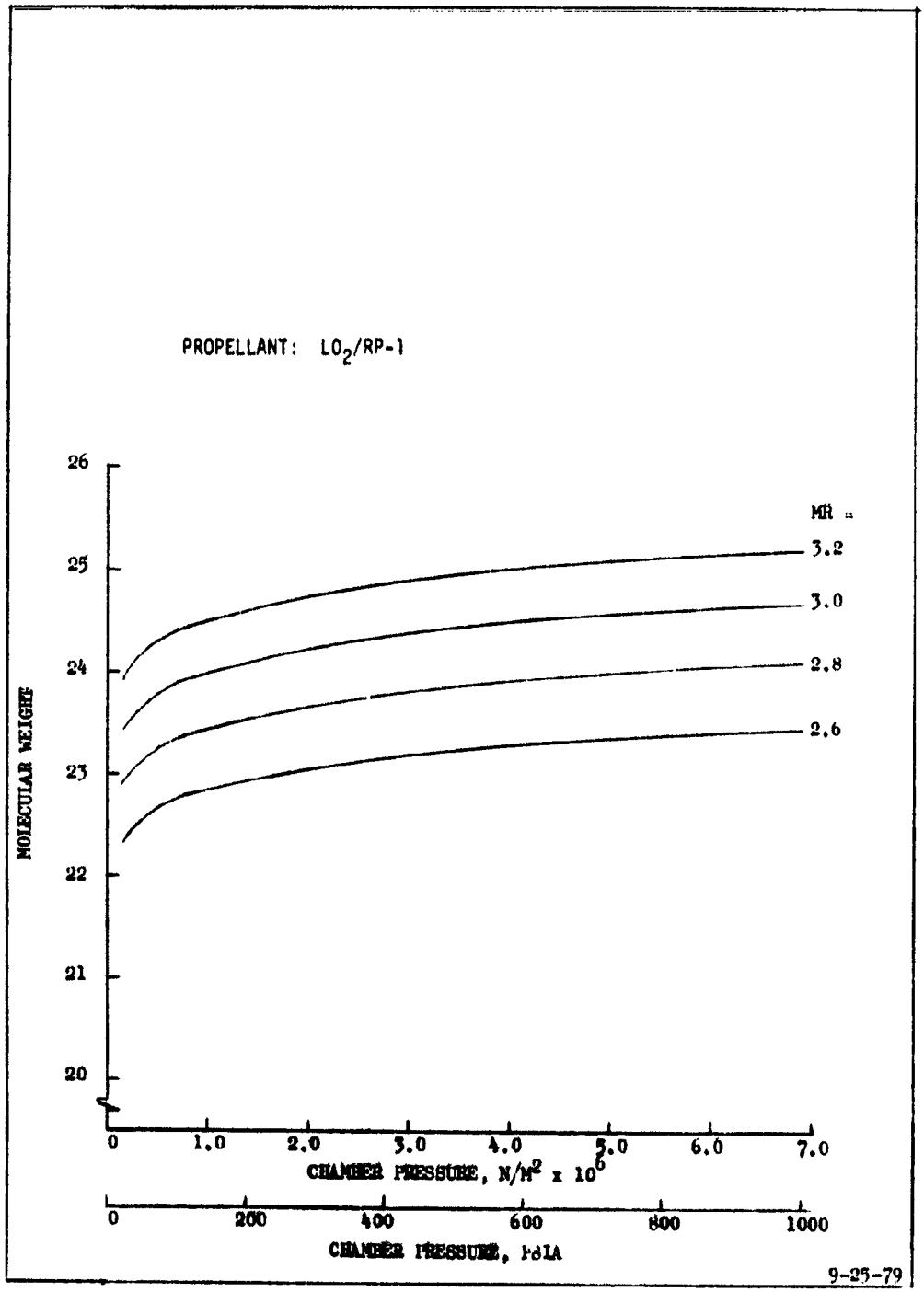
PROPELLANT: LO_2/RP-1
MOLECULAR WEIGHT
26
25
24
23
22
21
20
MR =
3.2
3.0
2.8
2.6
0
1.0
2.0
3.0
4.0
5.0
6.0
7.0
CHAMBER PRESSURE, N/M^2 x 10^6
0
200
400
600
800
1000
CHAMBER PRESSURE, PSIA
9-25-79

Figure B-17

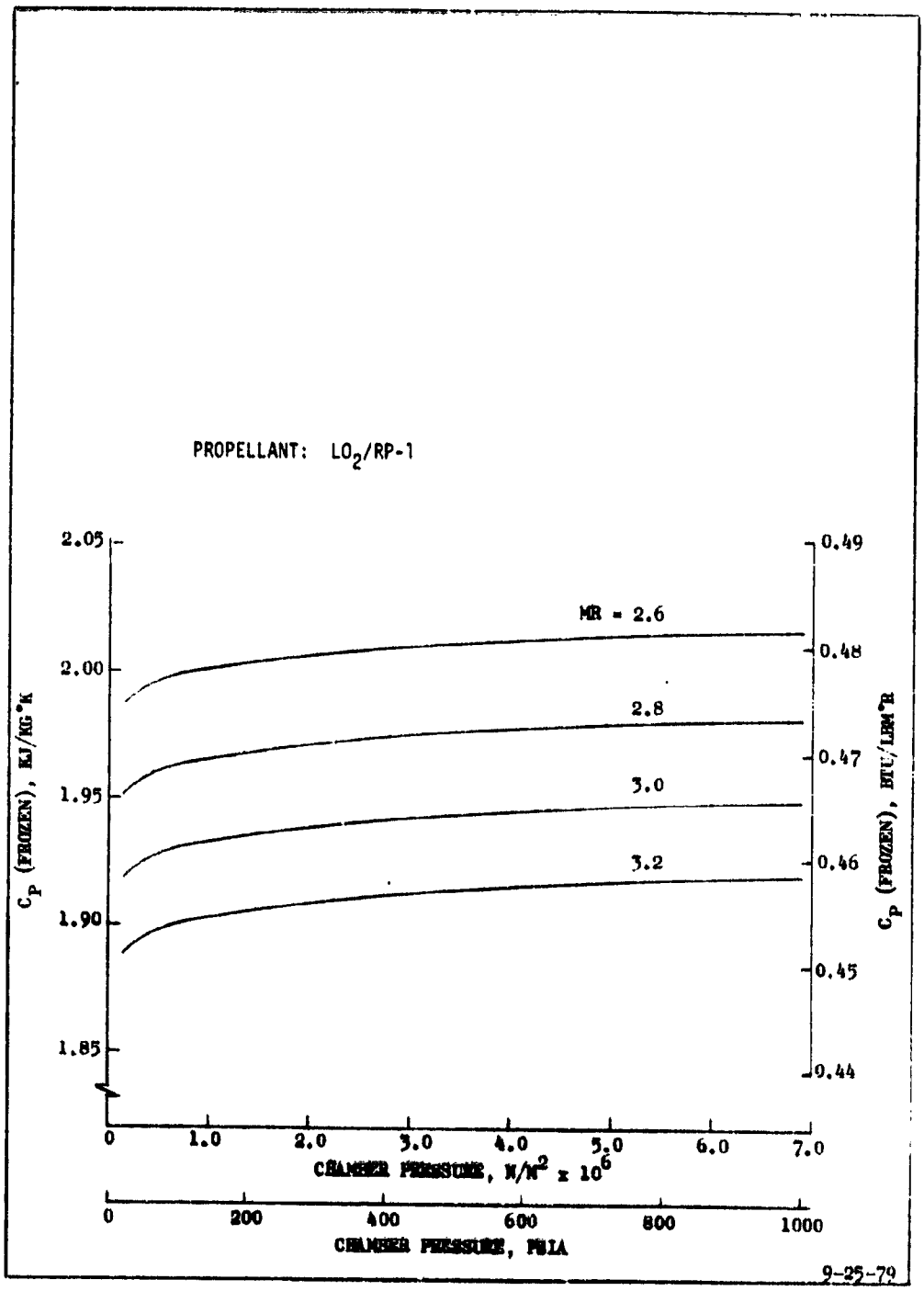
PROPELLANT: LO_2/RP-1
2.05
2.00
1.95
1.90
1.85
C_p (FROZEN), KJ/KG °K
0.49
0.48
0.47
0.46
0.45
0.44
C_p (FROZEN), BTU/LBM °R
MR = 2.6
2.8
3.0
3.2
0
1.0
2.0
3.0
4.0
5.0
6.0
7.0
CHAMBER PRESSURE, $N/M^2 \times 10^6$
0
200
400
600
800
1000
CHAMBER PRESSURE, PSIA
9-25-79

Figure B-18.

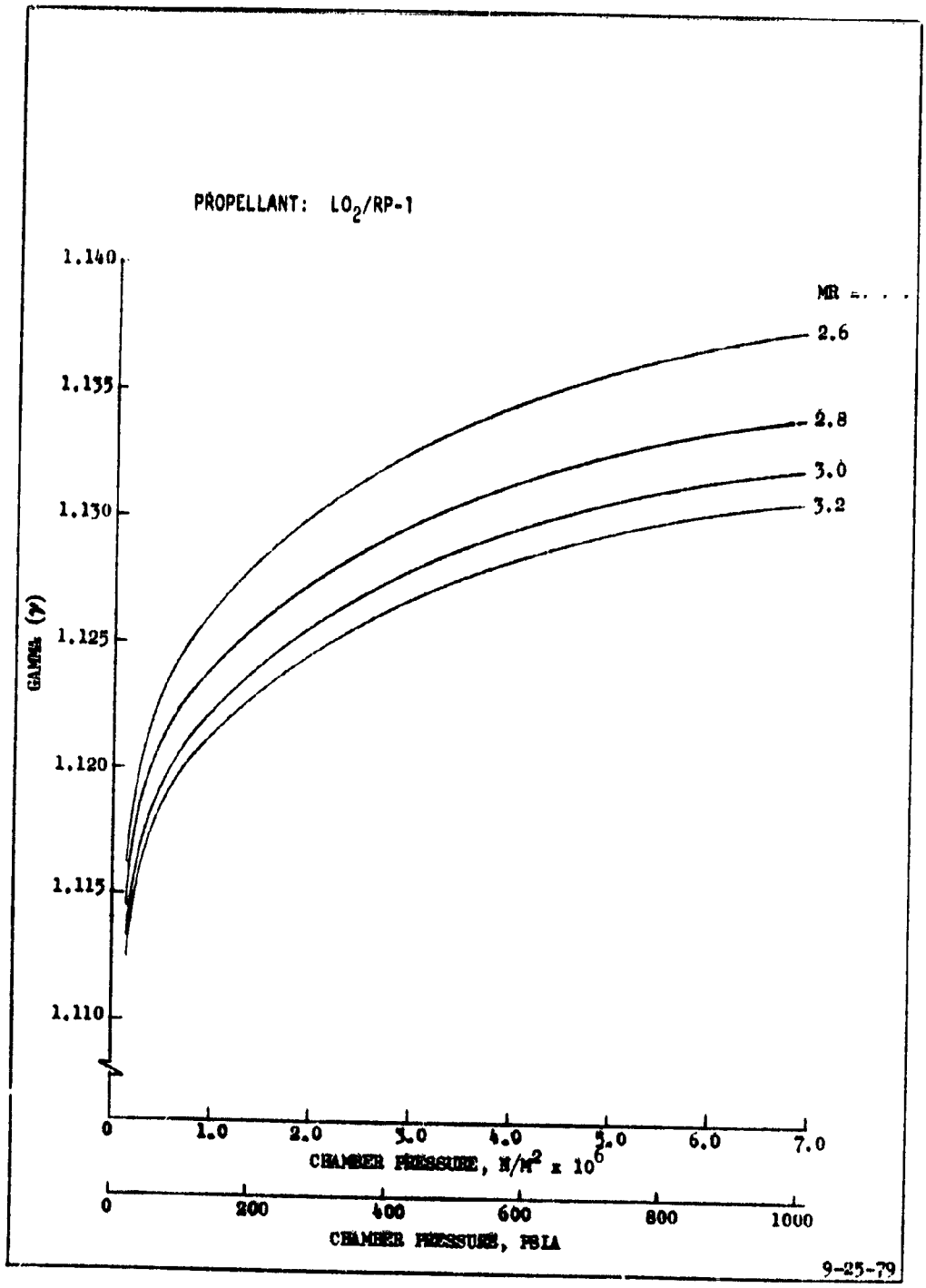
PROPELLANT: LO_2/RP-1
MR = . . .
2.6
2.8
3.0
3.2
1.140
1.135
1.130
1.125
1.120
1.115
1.110
GAMMA (γ)
0
1.0
2.0
3.0
4.0
5.0
6.0
7.0
CHAMBER PRESSURE, N/M^2 x 10^6
0
200
400
600
800
1000
CHAMBER PRESSURE, PSIA
9-25-79

Figure B-19.

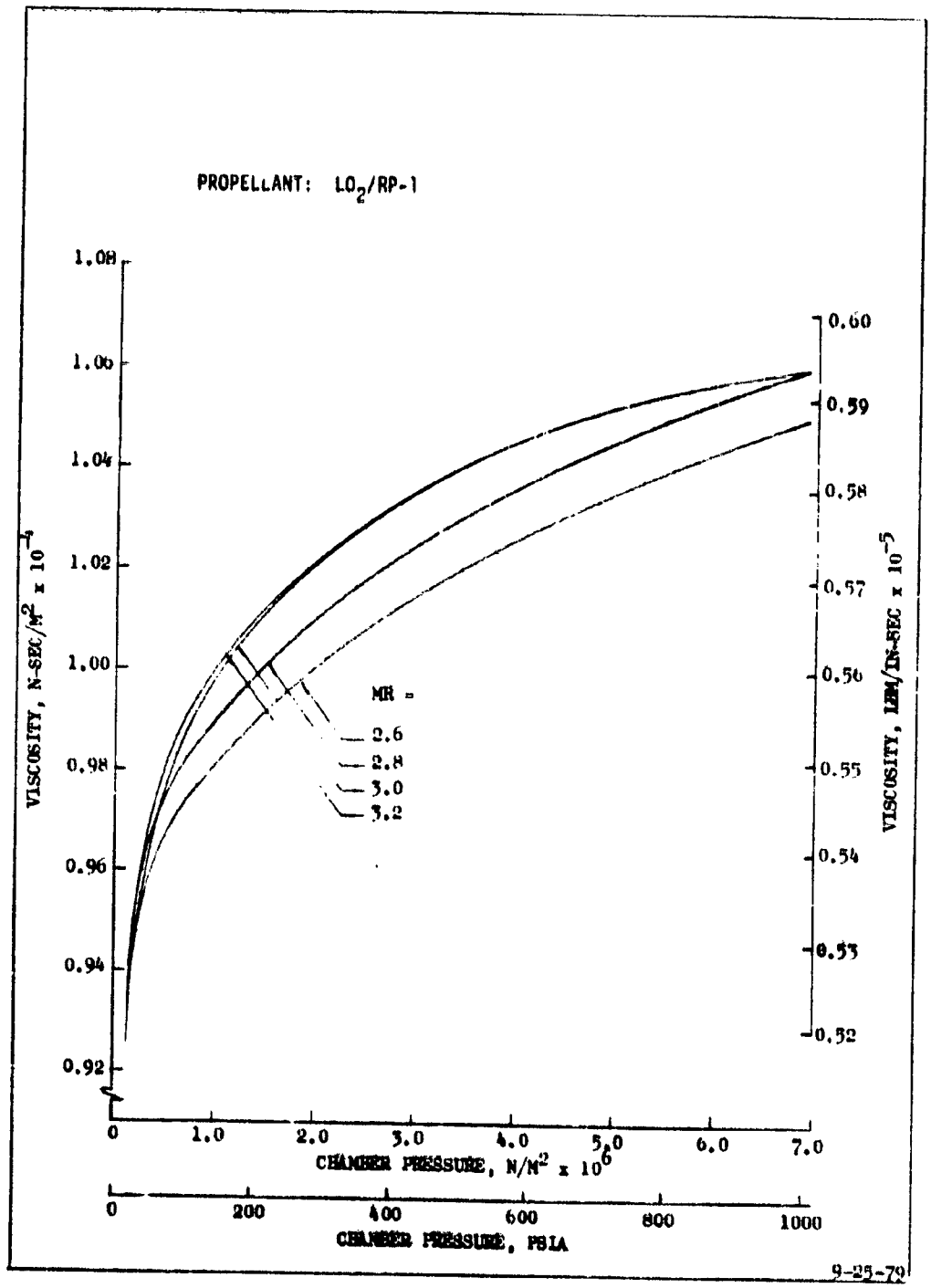
PROPELLANT: LO_2/RP-1
VISCOSITY, N-SEC/M^2 x 10^{-4}
VISCOSITY, LBM/IN-SEC x 10^{-5}
MR =
2.6
2.8
3.0
3.2
1.08
1.06
1.04
1.02
1.00
0.98
0.96
0.94
0.92
0.60
0.59
0.58
0.57
0.56
0.55
0.54
0.53
0.52
0
1.0
2.0
3.0
4.0
5.0
6.0
7.0
CHAMBER PRESSURE, N/M^2 x 10^6
0
200
400
600
800
1000
CHAMBER PRESSURE, PSIA
9-25-79

Figure B-20.

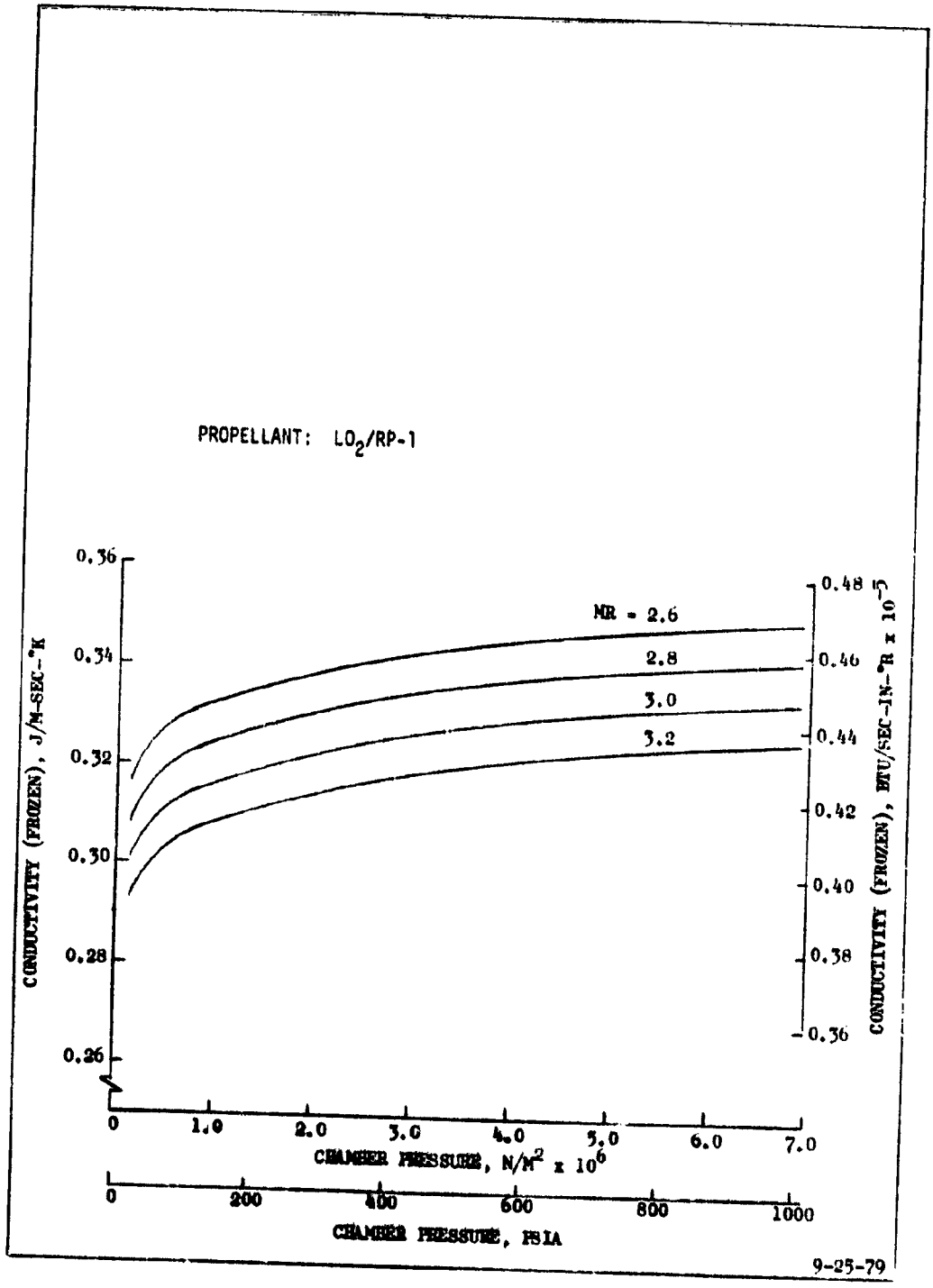
PROPELLANT: LO_2/RP-1
CONDUCTIVITY (FROZEN), J/M-SEC-°K
CONDUCTIVITY (FROZEN), BTU/SEC-IN-°R x 10^{-5}
MR = 2.6
2.8
3.0
3.2
0.36
0.34
0.32
0.30
0.28
0.26
0.48
0.46
0.44
0.42
0.40
0.38
0.36
0
1.0
2.0
3.0
4.0
5.0
6.0
7.0
CHAMBER PRESSURE, N/M^2 x 10^6
0
200
400
600
800
1000
CHAMBER PRESSURE, PSIA
9-25-79

Figure B-21.

APPENDIX C
ENGINE CYCLE BALANCE SUMMARIES

The following figures and tables present engine cycle balance summaries for the LO_2/H_2 and LO_2/CH_4 expander cycle engines at the $\pm$10% design mixture ratio conditions.

A simplified engine cycle balance procedure was developed for the off-design mixture ratio conditions. Maintaining the design condition thrust and constant throat area, the chamber pressure was determined by first assuming a chamber pressure, calculating the engine performance (specific impulse and thrust coefficient) and iterating on the chamber pressure. With the computed propellant flowrates, the engine cycle balance was accomplished by performing a pump/turbine power balance through an iteration of turbine flowrates. The approach taken was to control mixture ratio by varying the turbine bypass flow valves and not changing the main valve positions.

For the LO_2/H_2 engine as the engine mixture ratio was reduced to 90% of the nominal value (5.4 to 1), the hydrogen pump horsepower increased and the oxygen pump horsepower decreased due to propellant flow variations. The chamber pressure increased to 333.7 N/cm^2 (484 psia) due to the decrease in the vacuum thrust coefficient. The delivered specific impulse increased due to the mixture ratio influence to 4601.1 N-sec/kg (469.18 lbf-sec/lbm). The increased hydrogen flow resulted in a slight reduction in the fuel turbine inlet temperature.

To balance the LO_2/H_2 engine at the low mixture point, the pressure drop margin was reduced to zero and the turbine bypass flow reduced to 3.97%. The system pressure and temperatures for this off-design condition are presented in Fig. C-1.

At the high mixture ratio off-design point (6.6-to-1) for the LO_2/H_2 engine, the chamber pressure decreased to 326.1 N/cm^2 (473 psia) due to an increase in thrust coefficient. The increase in mixture ratio caused a decrease in delivered specific impulse to 4505.4 N-sec/kg (459.42 lbf-sec/lbm). As expected, the hydrogen pump horsepower decreased and the oxygen pump horsepower increase.

Although the pump efficiencies remained essentially constant, the turbine efficiencies were slightly lower. To balance the cycle at this condition, the overall turbine bypass was reduced to 7.69% with a total of 21.9% bypassing the fuel turbine and the 10% pressure margin was maintained. Observing the turbine flows in Fig. C-2, a fuel turbine bypass is required since the oxidizer turbine flow is greater than the fuel turbine flow.

Therefore, for the LO_2/H_2 engine, the $\pm$10% mixture ratio change resulted in approximately a $\pm$1% chamber pressure change and a +0.6¢ and a -1.3% specific impulse change.

The off-design engine cycle balance trends for the LO_2/CH_4 engine were similar. Performance and engine system operating conditions are given in Tables C-3 and C-4 and Figures C-3 and C-4.

TABLE C-1
LO_2/H_2 ENGINE PERFORMANCE CHARACTERISTICS
OFF-DESIGN, O/F = 5.4

Thrust, N, (lbf)	2224.	500
Chamber Pressure, N/cm^2 (psia)	333.7	484
Engine Mixture Ratio, O/F	5.4	
Area Ratio	400	
ODE Specific Impulse, N-sec/kg (lbf-sec/lbm)	4890.6	498.7
ODE Characteristic Velocity, M/sec (ft/sec)	2385.4	7826
Specific Impulse Energy Release Efficiency, Fraction	.9950	
Specific Impulse Reaction Kinetic Efficiency, Fraction	.9833	
Specific Impulse Divergence Efficiency, Fraction	.9957	
Specific Impulse Non-Boundary Layer Heat Loss Efficiency, Fraction (1)	.9916	
Specific Impulse Boundary Layer Efficiency, Fraction	.9666	
Delivered Specific Impulse N-sec/kg (lbf-sec/lbm)	4601.3	469.2

(1) Non-Boundary Layer Heat Loss Included in ODE Specific Impulse

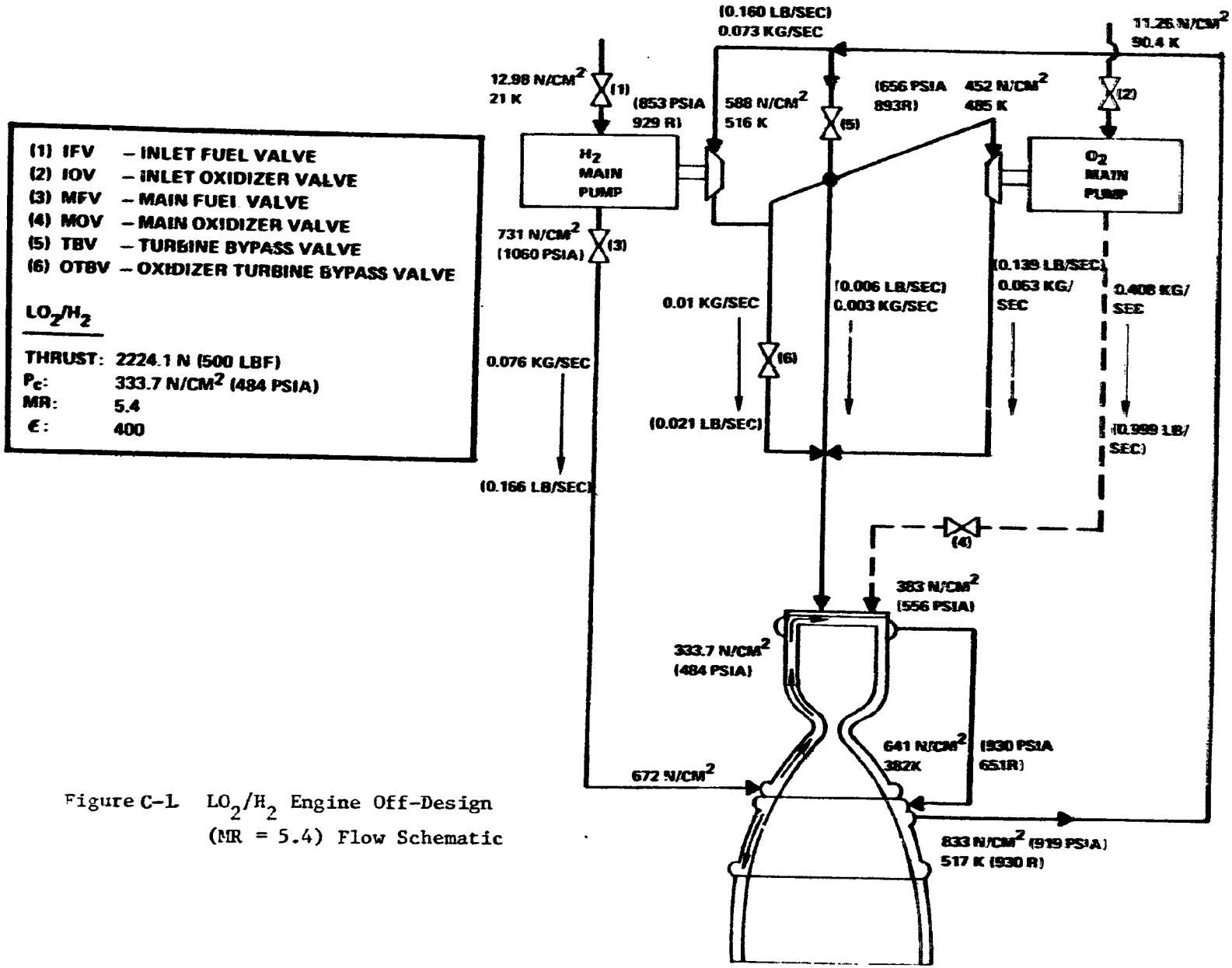

Figure C-1 LO_2/H_2 Engine Off-Design (MR = 5.4) Flow Schematic

TABLE C-2
LO_2/H_2 ENGINE PERFORMANCE CHARACTERISTICS
OFF-DESIGN, O/F = 6.6

Thrust, N, (lbf)	2224.1	500
Chamber Pressure, N/cm^2 (psia)	326.1	473
Engine Mixture Ratio, O/F	6.6	
Area Ratio	400	
ODE Specific Impulse, N-sec/kg (lbf-sec/lbm)	4863.1	495.9
ODE Characteristic Velocity, M/sec (ft/sec)	2283.3	7491
Specific Impulse Energy Release Efficiency, Fraction	.9950	
Specific Impulse Reaction Kinetic Efficiency, Fraction	.9689	
Specific Impulse Divergence Efficiency, Fraction	.9957	
Specific Impulse Non-Boundary Layer Heat Loss Efficiency, Fraction (1)	.9916	
Specific Impulse Boundary Layer Efficiency, Fraction	.9666	
Delivered Specific Impulse N-sec/kg (lbf-sec/lbm)	4505.2	459.4

(1) Non-Boundary Layer Heat Loss
Included in ODE Specific Impulse

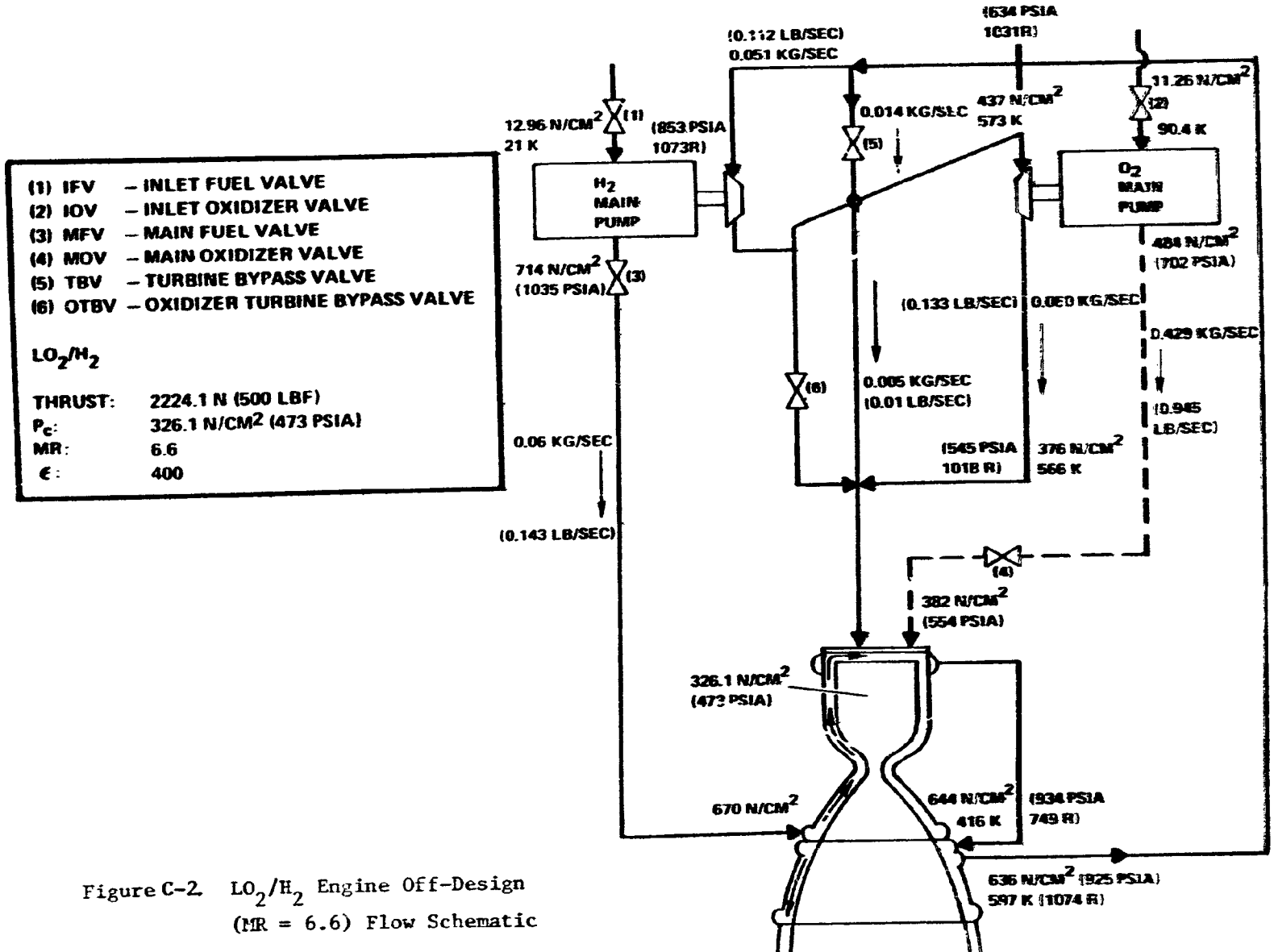

Figure C-2. LO_2/H_2 Engine Off-Design (MR = 6.6) Flow Schematic

TABLE C-3
LO_2/CH_4 ENGINE PERFORMANCE CHARACTERISTICS
OFF-DESIGN, O/F = 3.33

Thrust, N, (lbf)	2224.1	500
Chamber Pressure, N/cm^2 (psia)	308.9	448
Engine Mixture Ratio, O/F	3.3	
Area Ratio	400	
ODE Specific Impulse, N-sec/kg (lbf-sec/lbm)	4003.1	408.2
ODE Characteristic Velocity, M/sec (ft/sec)	1858.4	6097
Specific Impulse Energy Release Efficiency, Fraction	.9800	
Specific Impulse Reaction Kinetic Efficiency, Fraction	.9561	
Specific Impulse Divergence Efficiency, Fraction	.9957	
Specific Impulse Non-Boundary Layer Heat Loss Efficiency, Fraction (1)	.9942	
Specific Impulse Boundary Layer Efficiency, Fraction	.9664	
Delivered Specific Impulse N-sec/kg (lbf-sec/lbm)	3600.0	367.1

(1) Non-Boundary Layer Heat Loss Included in ODE Specific Impulse

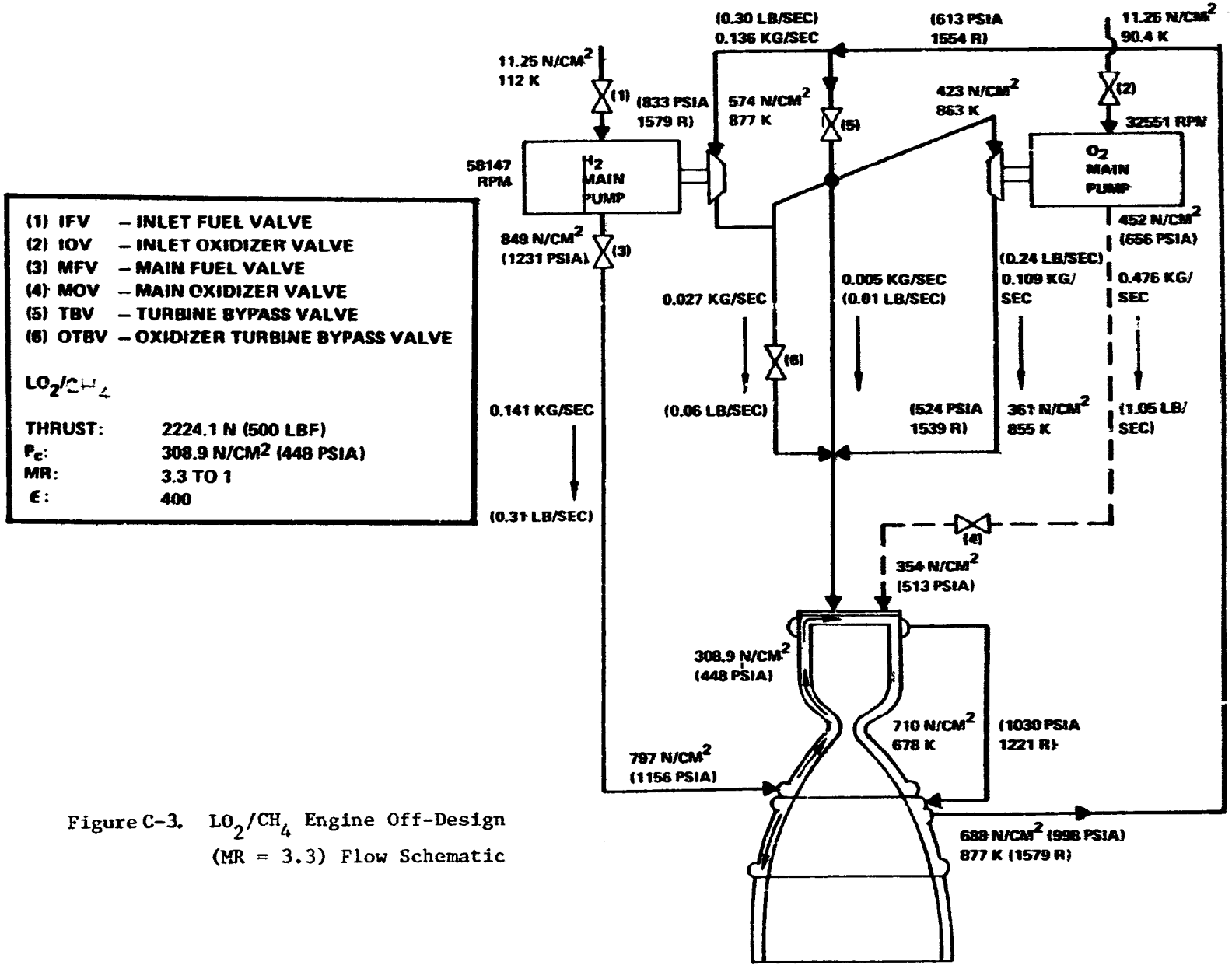

Figure C-3. LO_2/CH_4 Engine Off-Design (MR = 3.3) Flow Schematic

TABLE C-4
LO_2/CH_4 ENGINE PERFORMANCE CHARACTERISTICS
OFF-DESIGN, O/F =

Thrust, N, (lbf)	2224.1	500
Chamber Pressure, N/cm^2 (psia)	307.5	446
Engine Mixture Ratio, O/F	4.07	
Area Ratio	400	
ODE Specific Impulse, N-sec/kg (lbf-sec/lbm)	3978.6	405.7
ODE Characteristic Velocity, M/sec (ft/sec)	1789.5	5871
Specific Impulse Energy Release Efficiency, Fraction	.9800	
Specific Impulse Reaction Kinetic Efficiency, Fraction	.9315	
Specific Impulse Divergence Efficiency, Fraction	.9957	
Specific Impulse Non-Boundary Layer Heat Loss Efficiency, Fraction (1)	.9953	
Specific Impulse Boundary Layer Efficiency, Fraction	.9664	
Delivered Specific Impulse N-sec/kg (lbf-sec/lbm)	3599.0	367.0

(1) Non-Boundary Layer Heat Loss
Included in ODE Specific Impulse

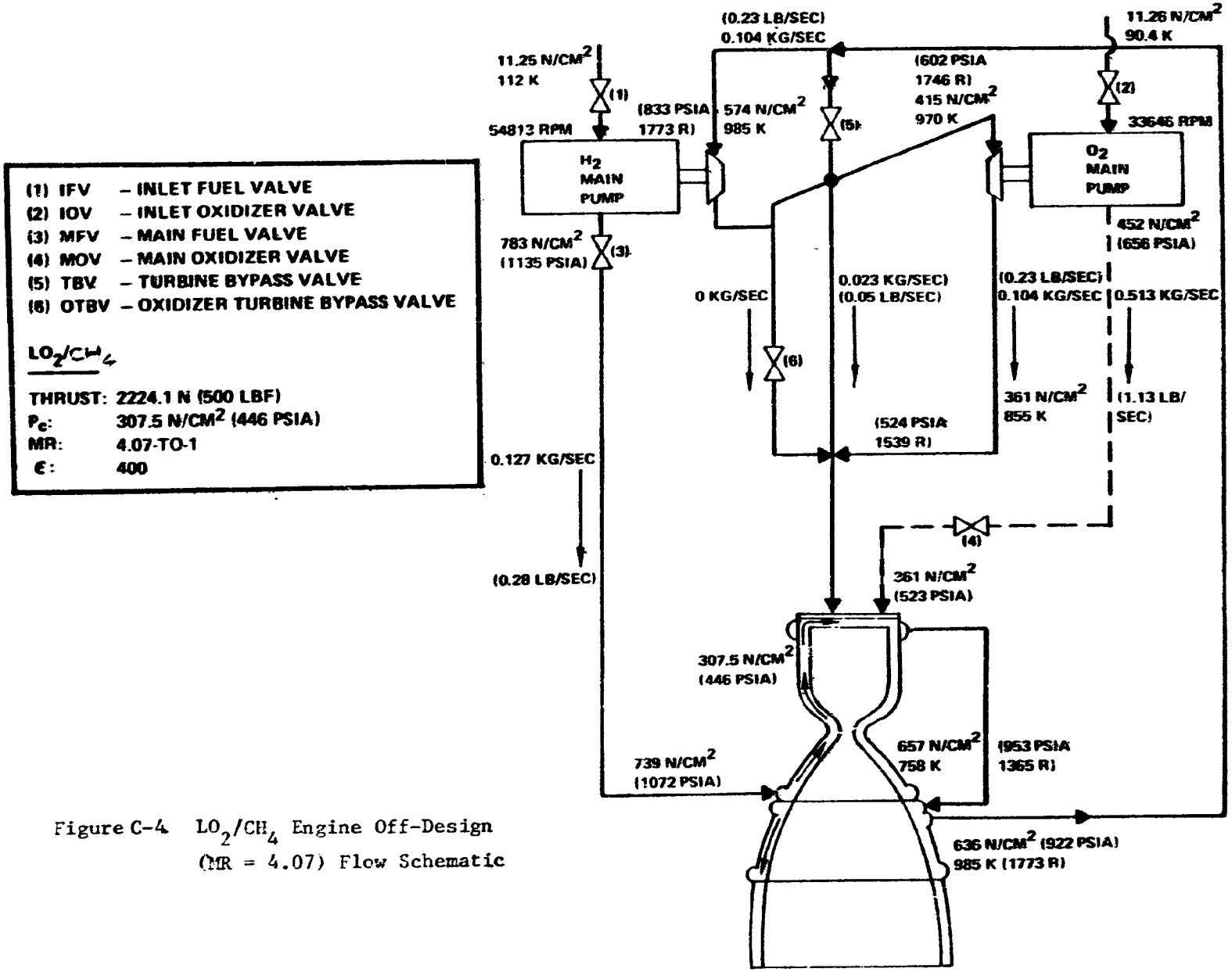

Figure C-4 LO_2/CH_4 Engine Off-Design (MR = 4.07) Flow Schematic

APPENDIX D

PARAMETRIC ENGINE PERFORMANCE

Parametric delivered engine specific impulses were generated using the simplified JANNAF method for LO_2/H_2 and LO_2/CH_4 expander cycle engines. The data included a thrust range from 444.8 N (100 lbf) to 13345 N (3000 lbf) and chamber pressures from 68.95 N/cm^2 (100 psia) to 689.5 N/cm^2 (1000 psia) and nozzle area ratios from 200 to 1000. A series of three types of plots were presented for each propellant. These included:

1. Delivered engine specific impulse versus nozzle area ratio for parametric chamber pressure at constant thrust

2. Delivered engine specific impulse versus thrust for parametric chamber pressure at constant nozzle ratio

3. Delivered engine specific impulse versus chamber pressure for parametric thrust at constant nozzle area ratio

The LO_2/H_2 engine performance data presented in Fig. D-1 through D-14 and the LO_2/CH_4 data is Fig. D-15 through D-28.

Note that the parametric data are presented over the entire study range of thrust (444.8N, 100 lbf to 13345 N, 3000 lbf) and chamber pressure (68.95 N/cm^2, 100 psia to 689.5 N/cm^2, 1000 psia). In using these data for mission studies it is important to consider possible engine system design constraints in order to avoid unrealistic design points. The parametric plots of delivered specific impulse versus thrust for the 400-to-1 area ratio LO_2/H_2 and LO_2/CH_4 engines (Figures D-6 and D-20, Appendix D) show the preliminary design points, thrust chamber cooling constraints, and expander cycle power constraints which resulted from this study. These constraints can be used to conservatively define feasible engine system operating conditions over the range of thrust and chamber pressure.

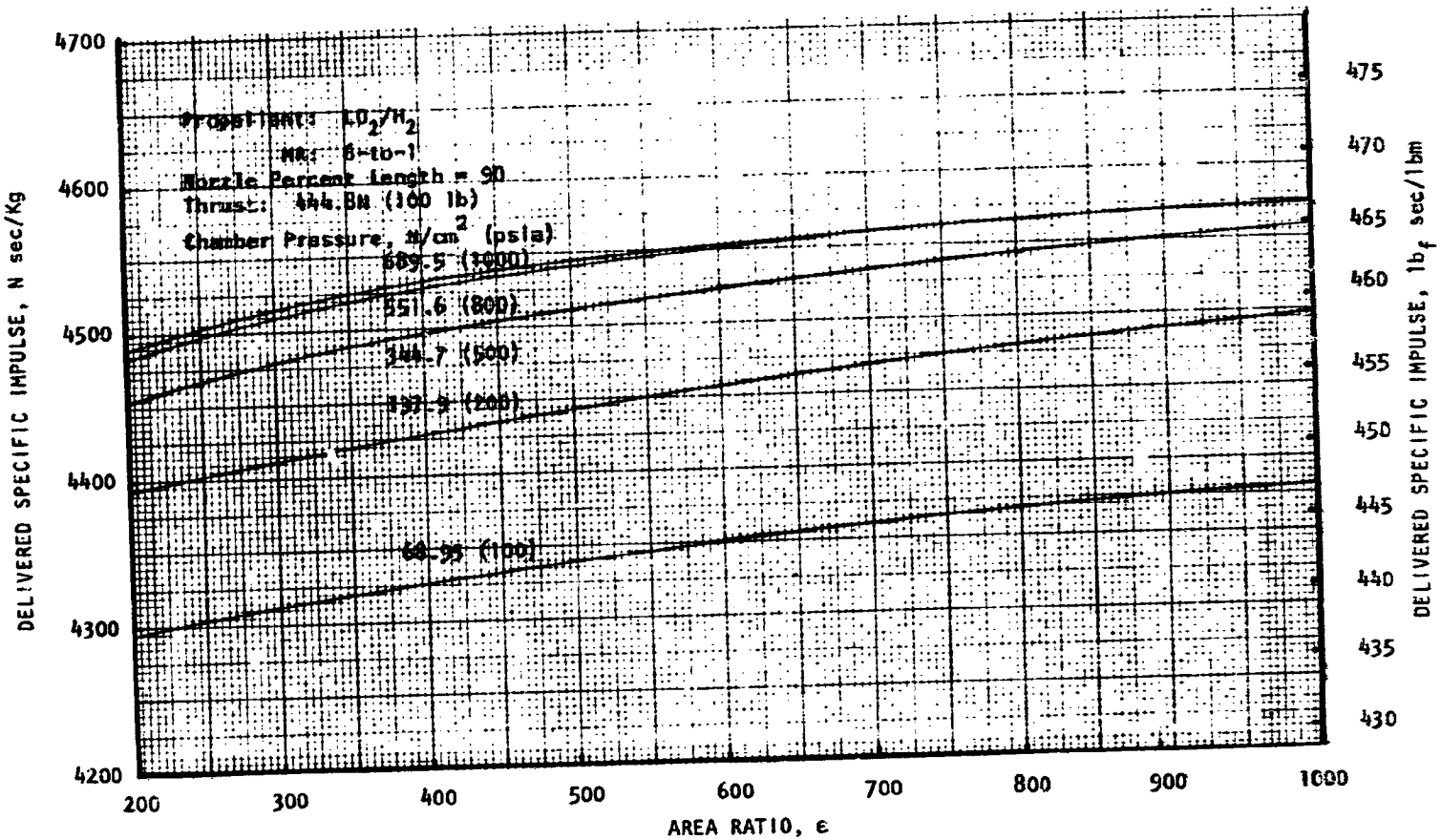

Figure D-1. LO_2/H_2 Expander Cycle Engine Specific Impulse Variation With Nozzle Area Ratio and Chamber Pressure (Thrust = 444.8N (100 lb)

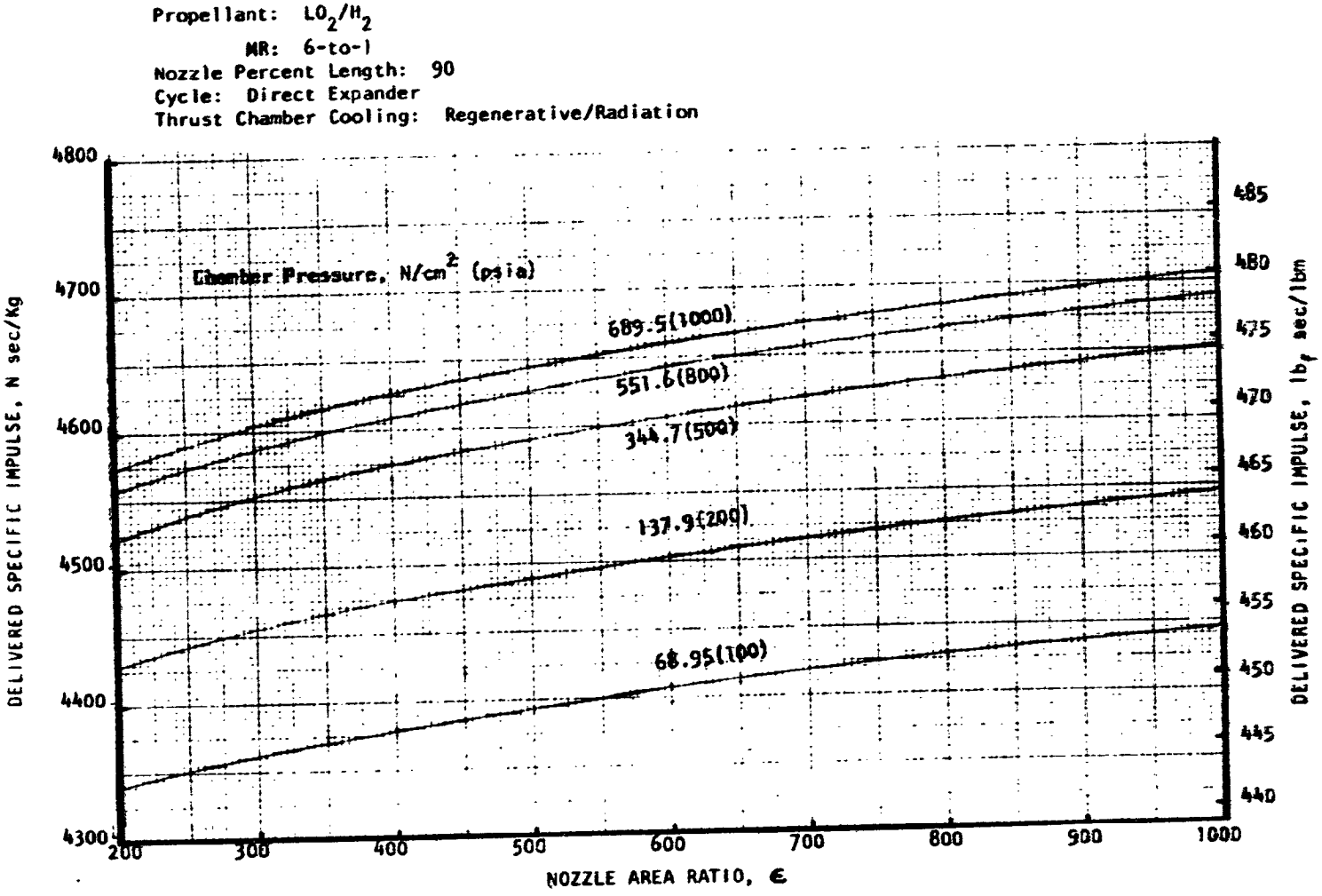

Figure D-2. LO_2/H_2 Expander Cycle Engine Specific Impulse Variation With Area Ratio and Chamber Pressure (Thrust = 2224.1 N (500 lb_f)

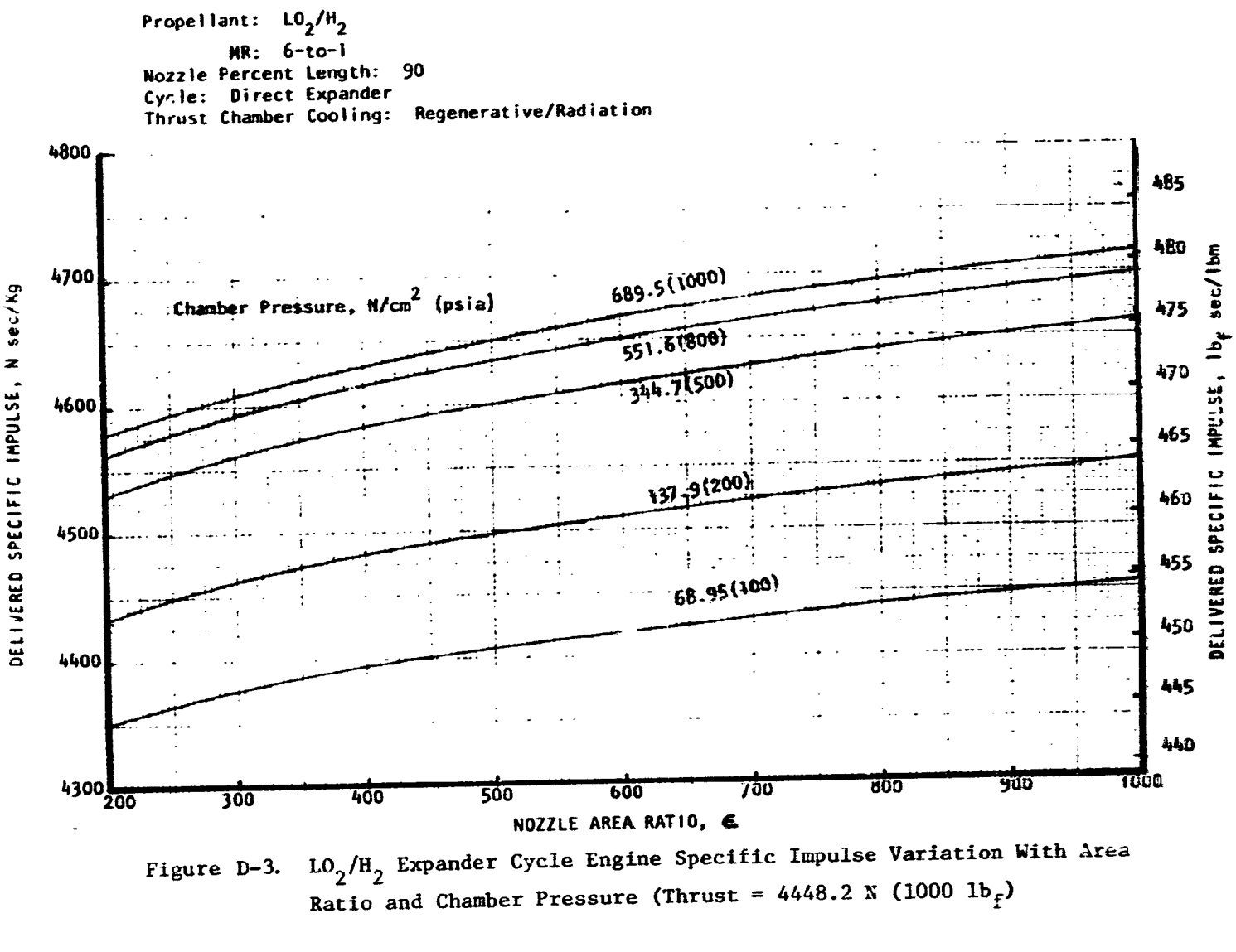

Figure D-3. LO_2/H_2 Expander Cycle Engine Specific Impulse Variation With Area Ratio and Chamber Pressure (Thrust = 4448.2 N (1000 lb_f)

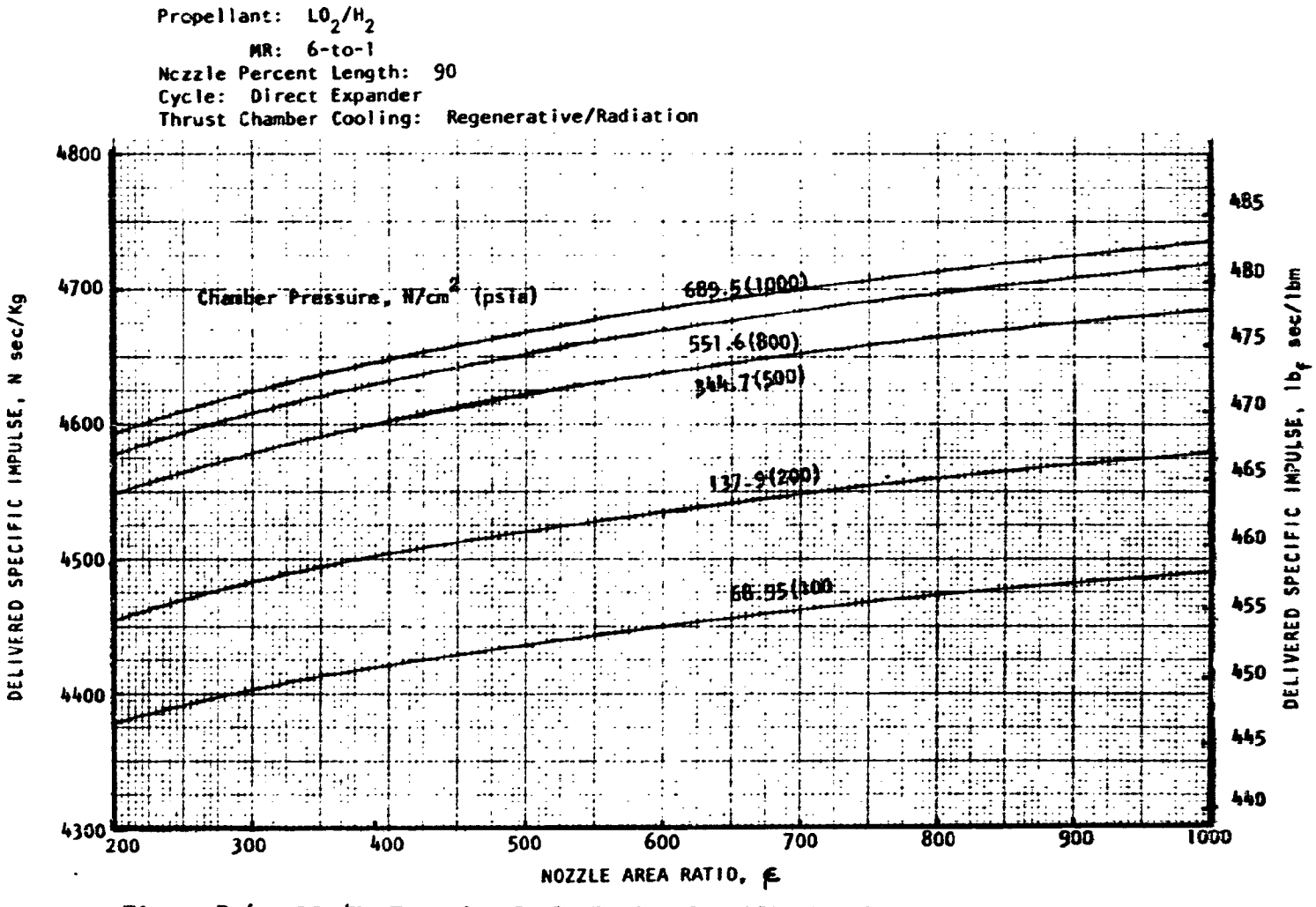

Figure D-4. LO_2/H_2 Expander Cycle Engine Specific Impulse Variation with Area Ratio and Chamber Pressure (Thrust = 3000 lb_f)

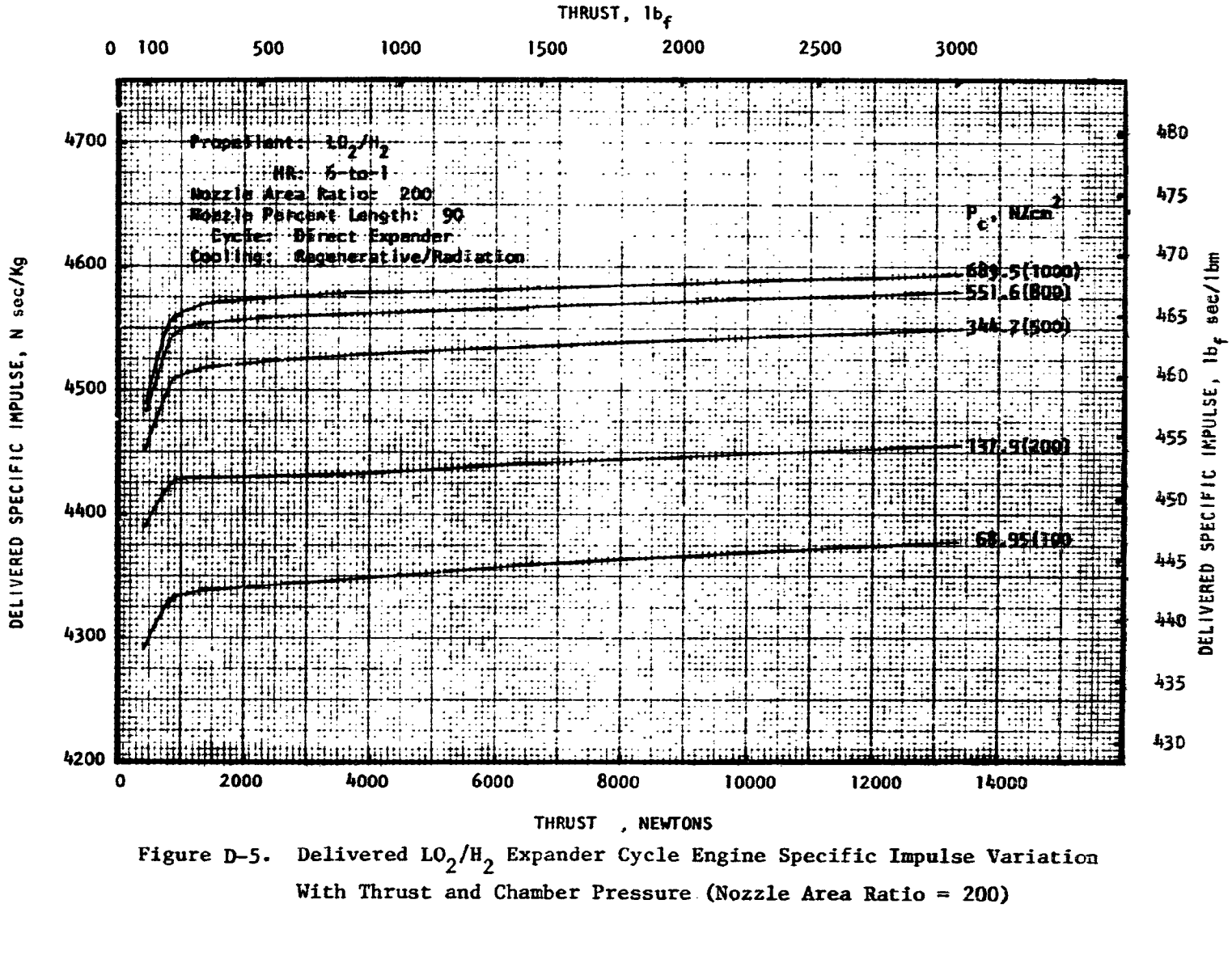

Figure D-5. Delivered LO_2/H_2 Expander Cycle Engine Specific Impulse Variation With Thrust and Chamber Pressure (Nozzle Area Ratio = 200)

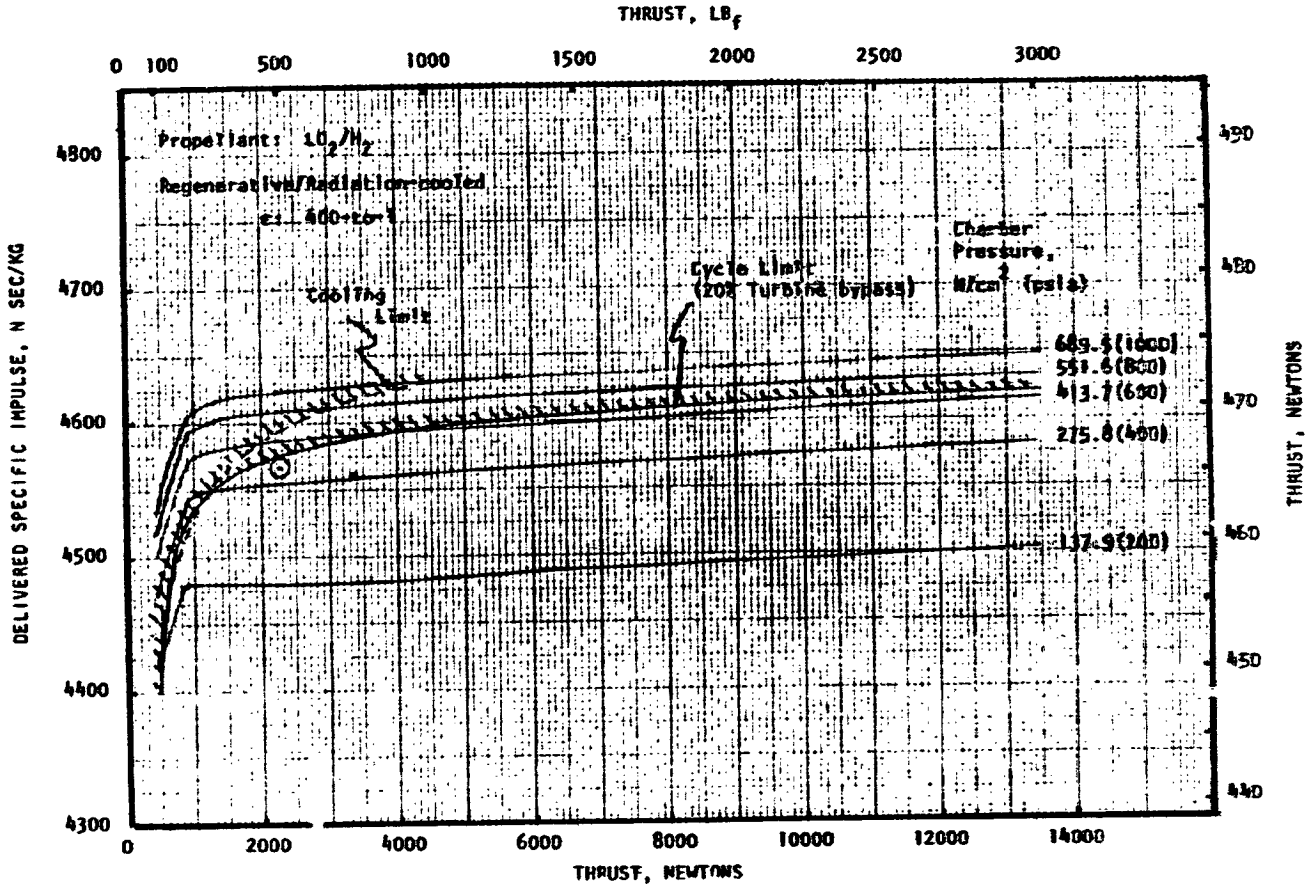

FIGURE D-6. LO_2/H_2 Direct Expander Cycle Delivered Specific Impulse

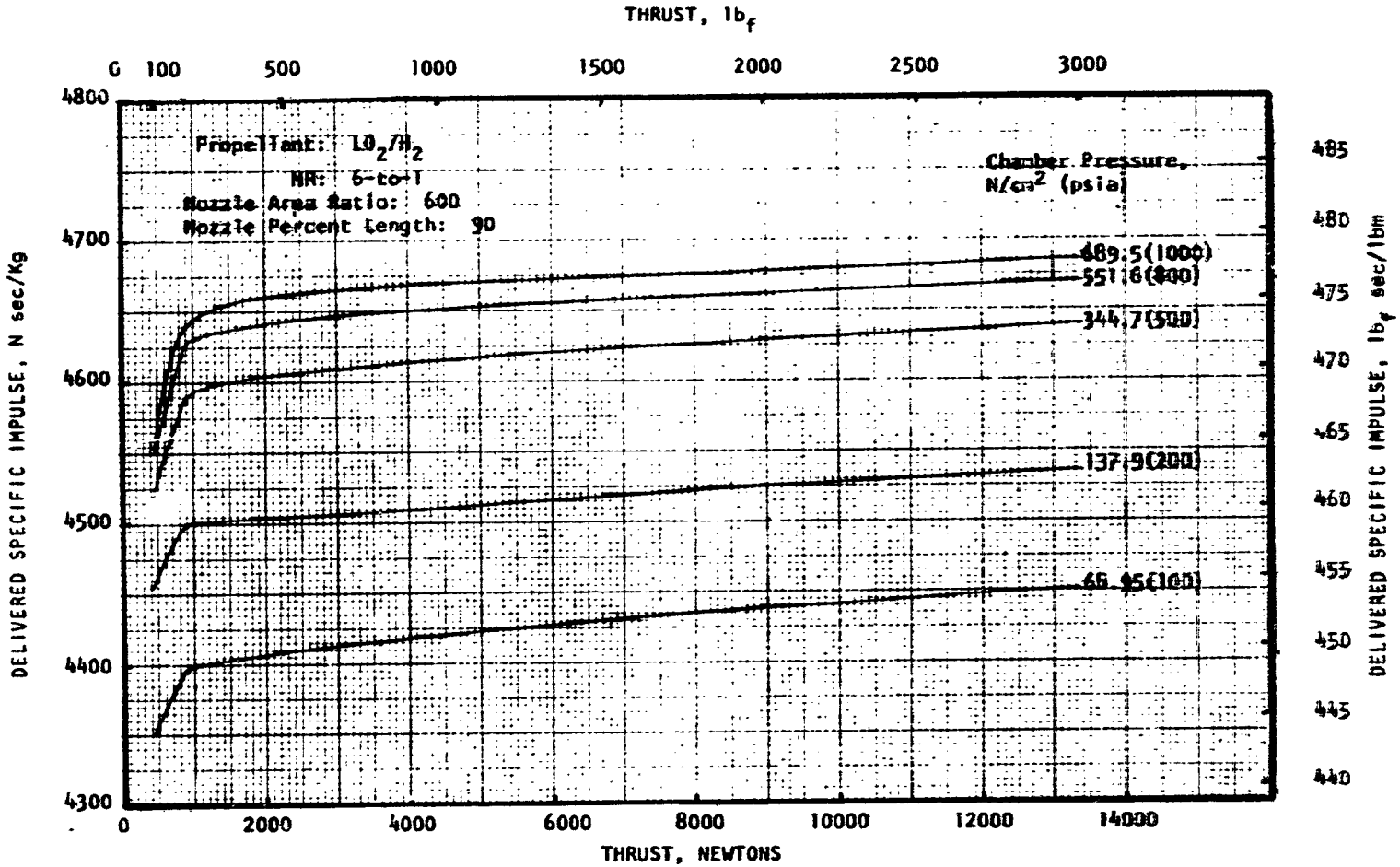

Figure D-7. Delivered LO_2/H_2 Expander Cycle Engine Specific Impulse Variation With Thrust and Chamber Pressure (Nozzle Area = 600)

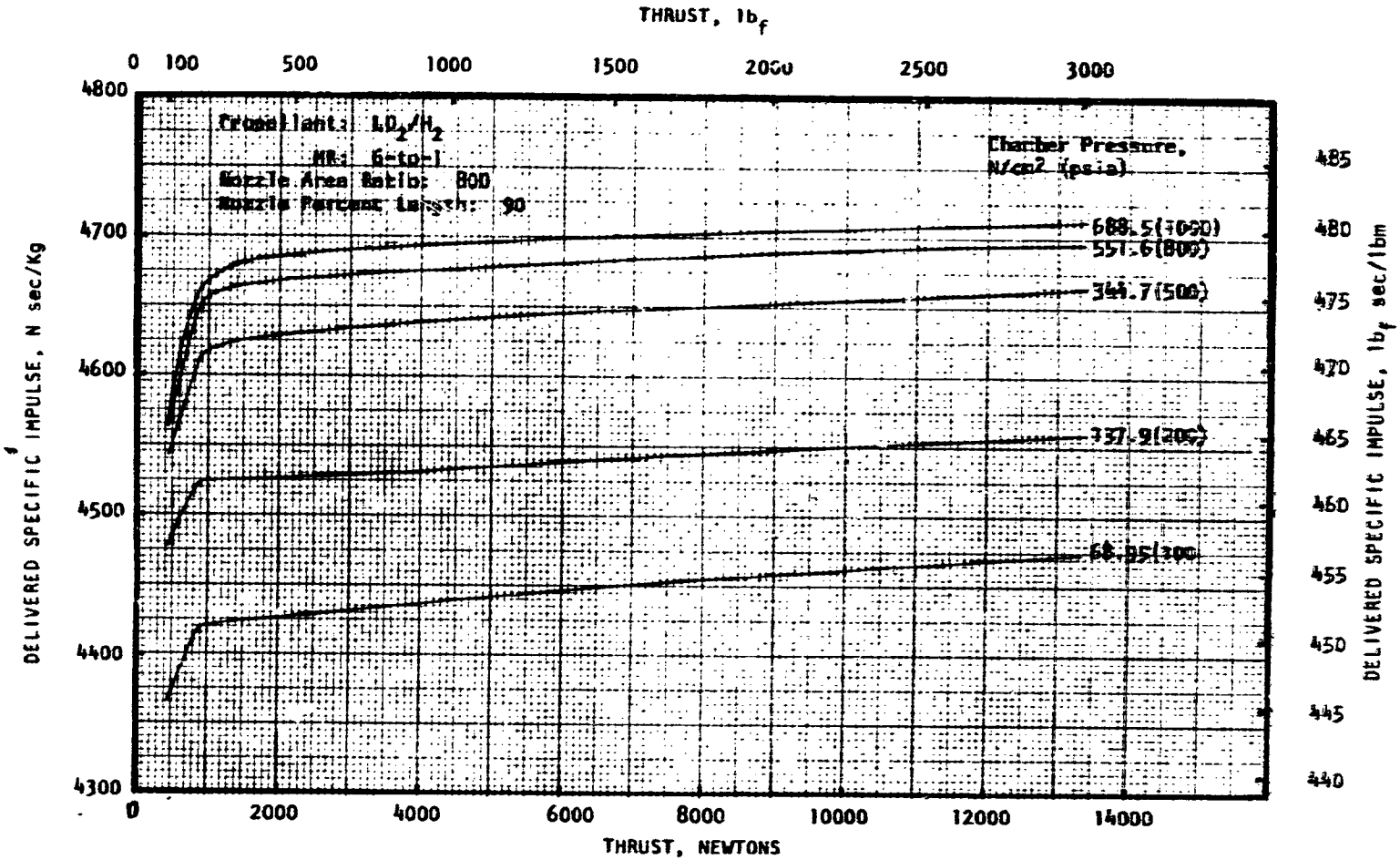

Figure D-8. Delivered LO_2/H_2 Expander Cycle Engine Specific Impulse Variation With Thrust and Chamber Pressure (Nozzle Area = 800)

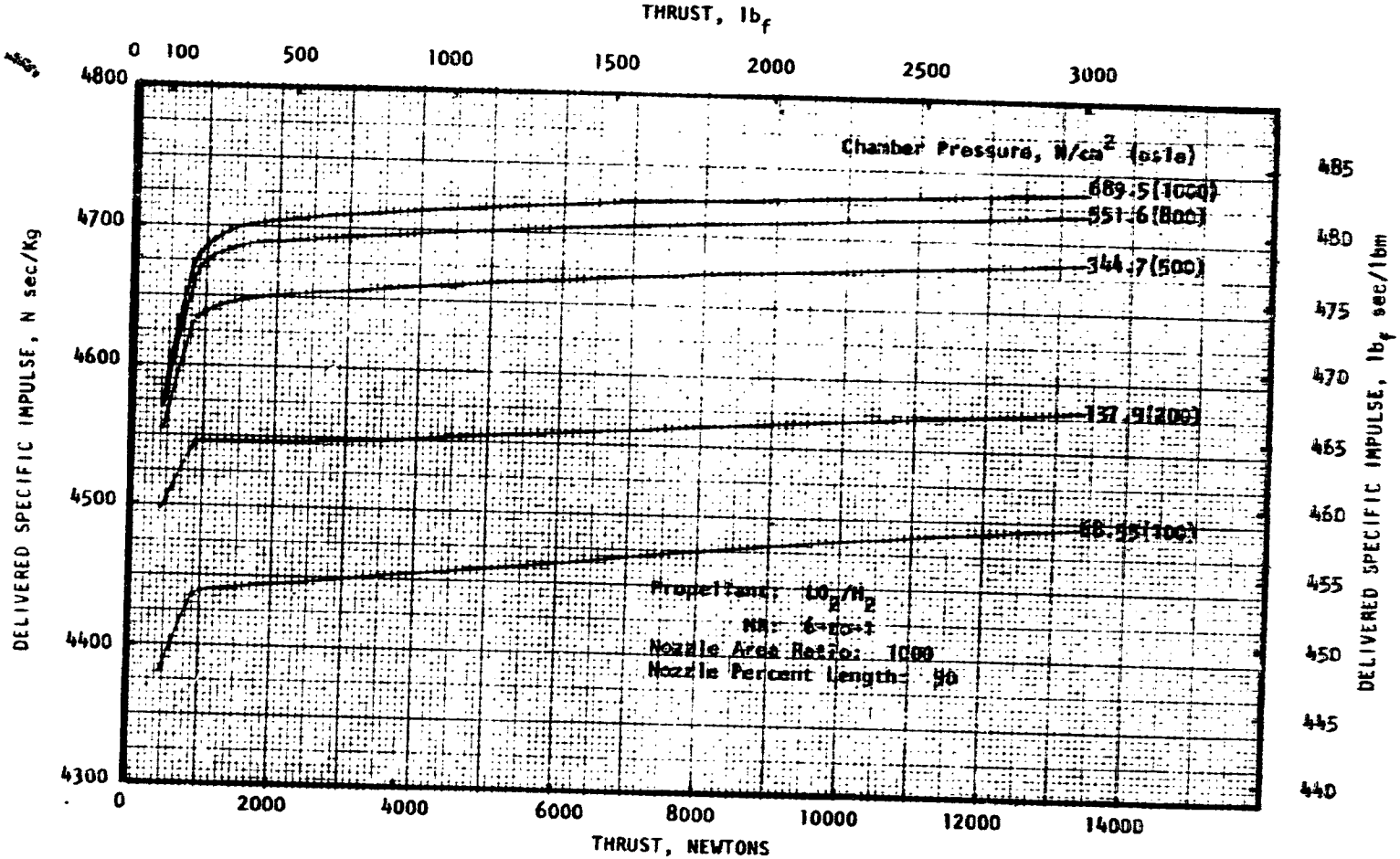

Figure D-9. Delivered LO_2/H_2 Expander Cycle Engine Specific Impulse Variation With Thrust and Chamber Pressure (Nozzle Area = 1000)

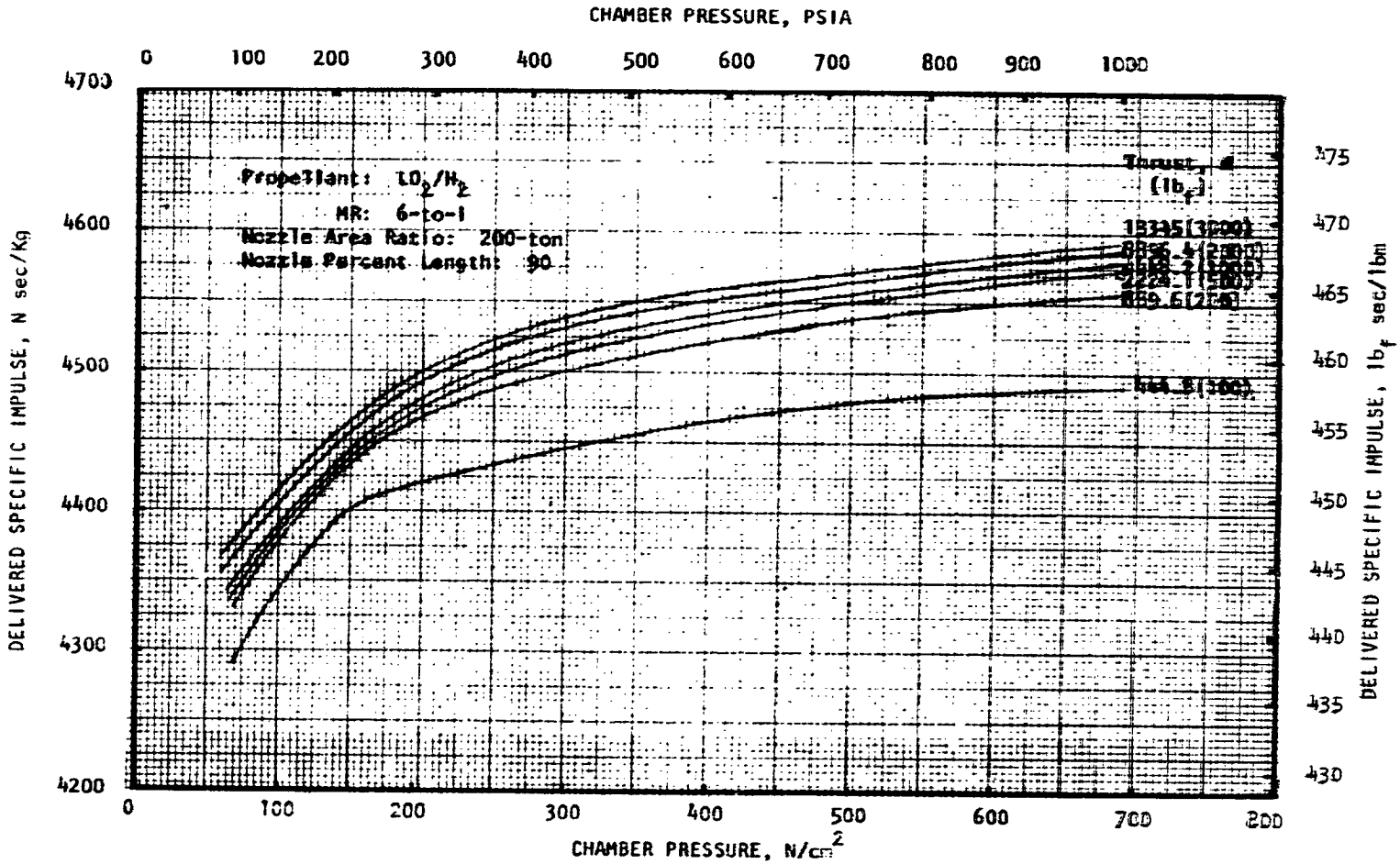

Figure D-10. LO_2/H_2 Expander Cycle Engine Specific Impulse Variation With Chamber Pressure and Thrust (Nozzle Area Ratio = 200)

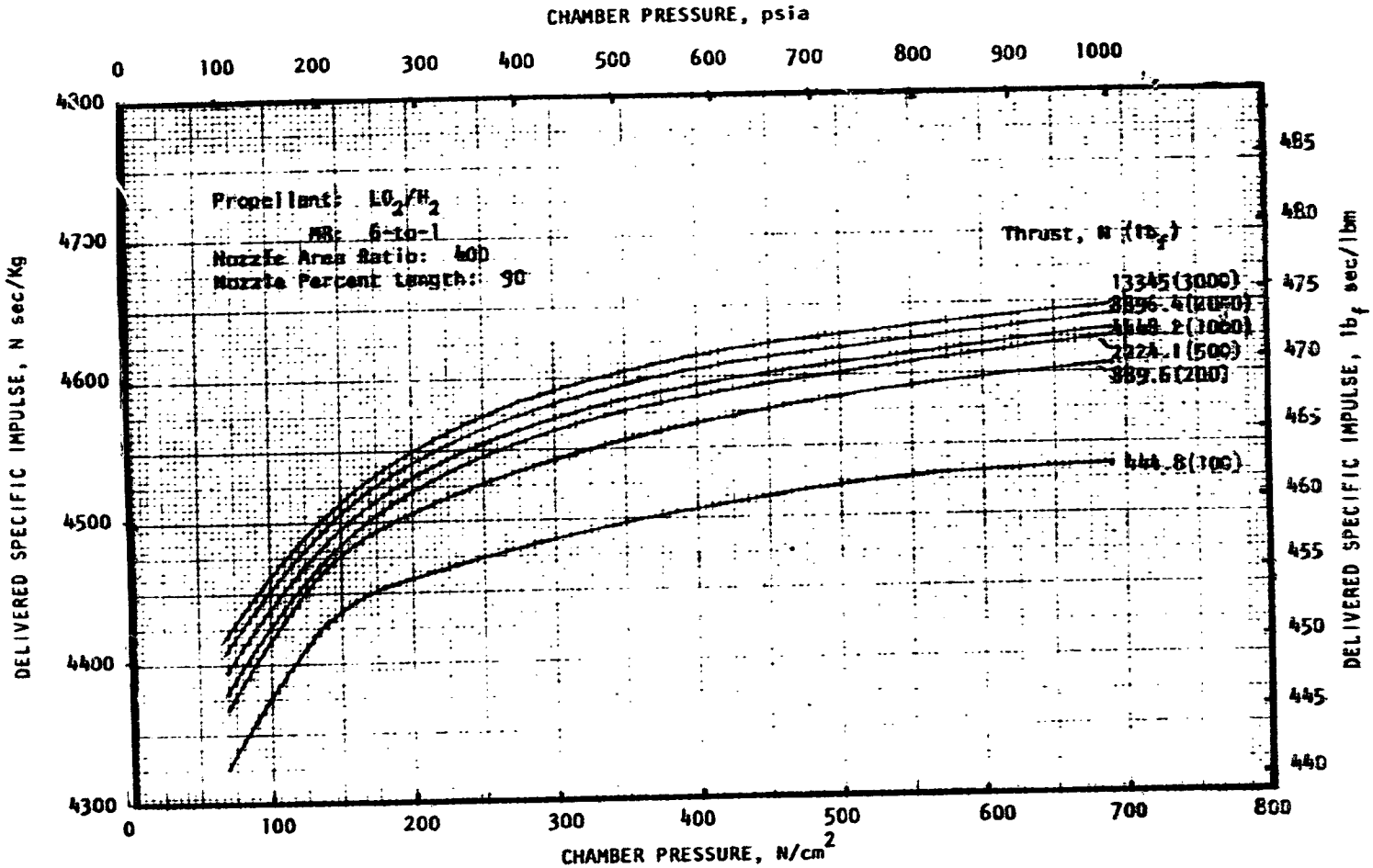

Figure D-11 LO_2/H_2 Expander Cycle Engine Specific Impulse Variation With Chamber Pressure and Thrust (Nozzle Area Ratio = 400)

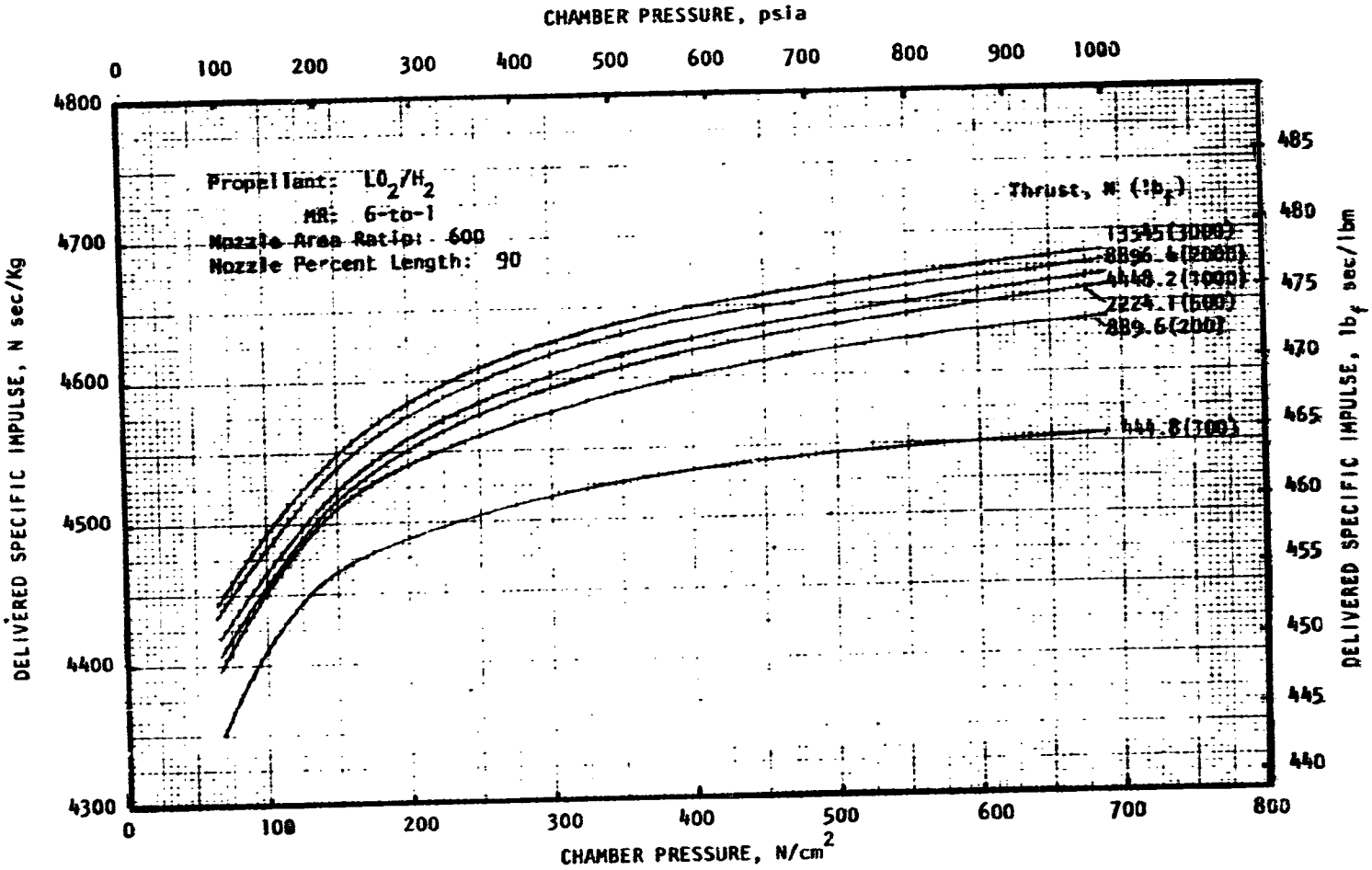

Figure D-12. LO_2/H_2 Expander Cycle Engine Specific Impulse Variation With Chamber Pressure and Thrust (Nozzle Area Ratio = 600)

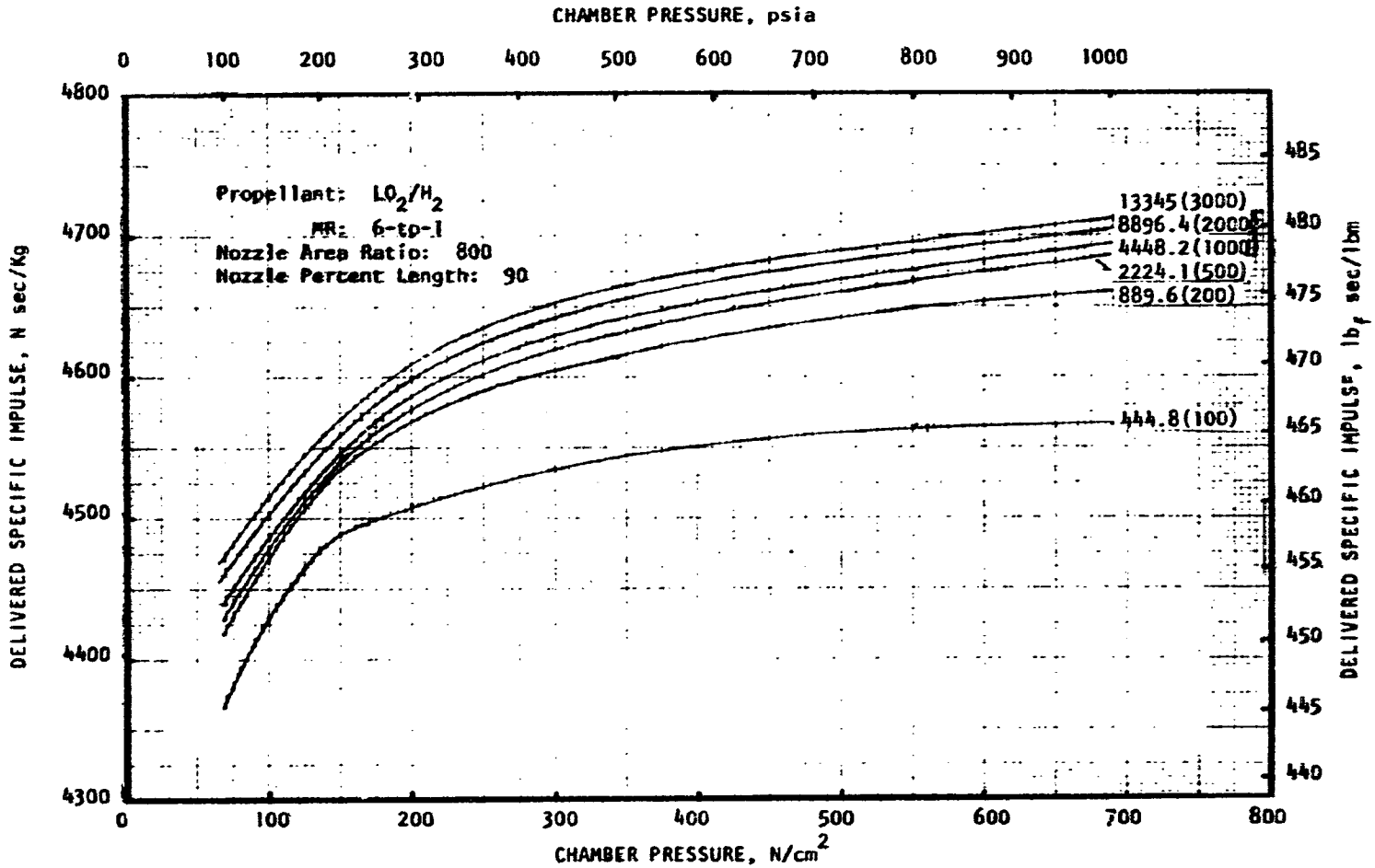

Figure D-13. LO_2/H_2 Expander Cycle Engine Specific Impulse Variation With Chamber Pressure and Thrust (Nozzle Area Ratio = 800)

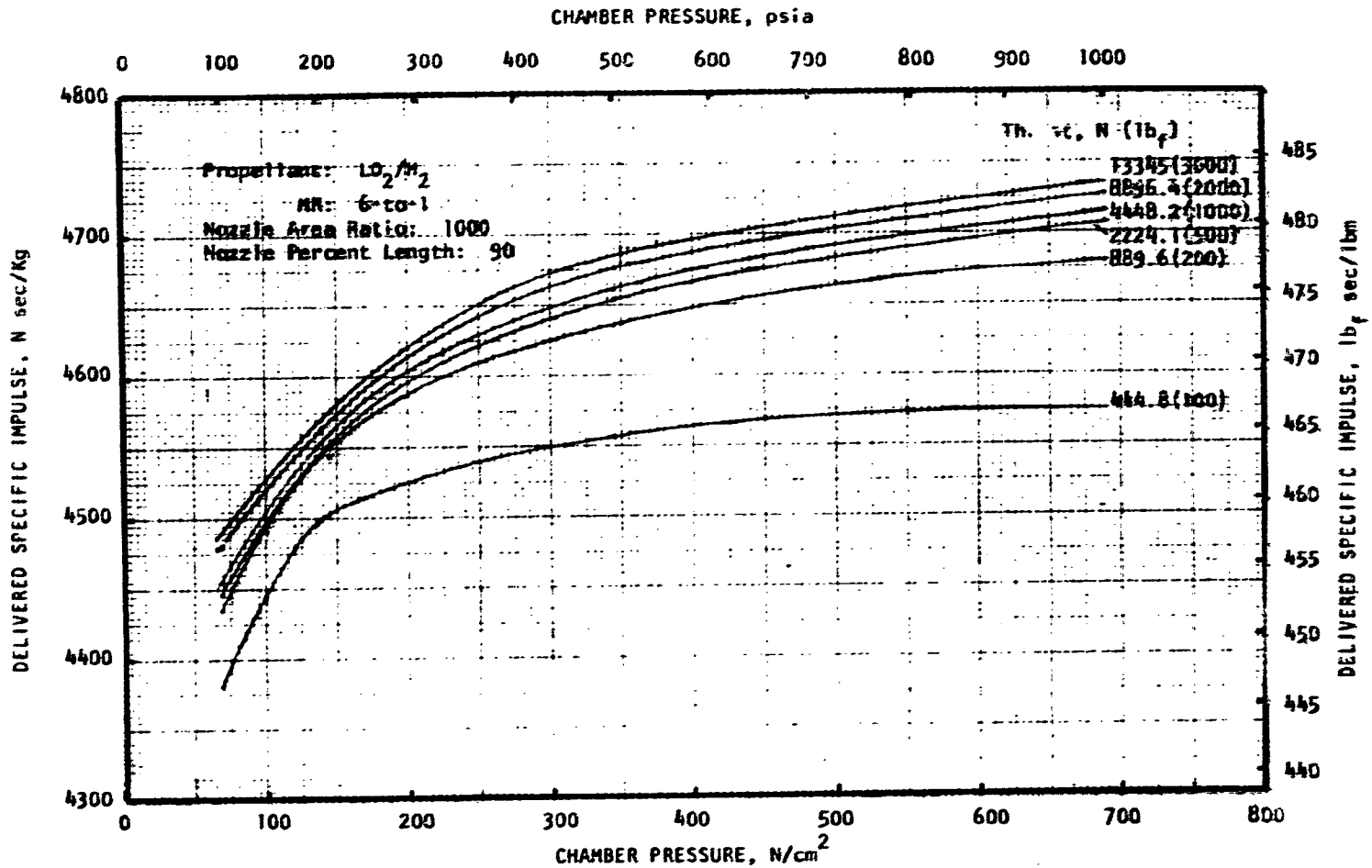

Figure D-14. LO_2/H_2 Expander Cycle Engine Specific Impulse Variation With Chamber Pressure and Thrust (Nozzle Area Ratio = 1000)

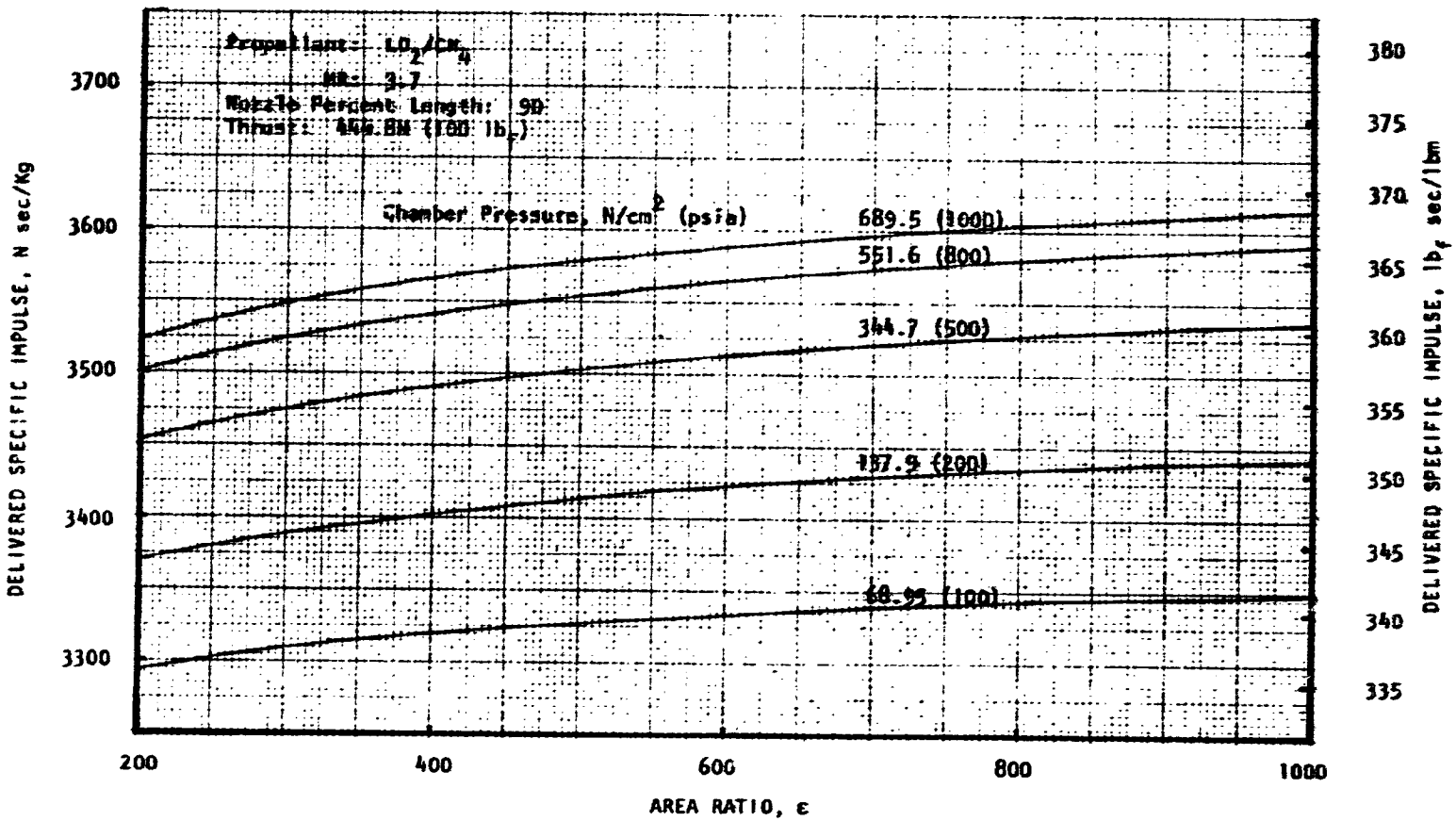

Figure D-15. LO_2/CH_4 Expander Cycle Engine Specific Impulse Variation With Area Ratio and Chamber Pressure (Thrust = 444.8 N (100 lb_f)

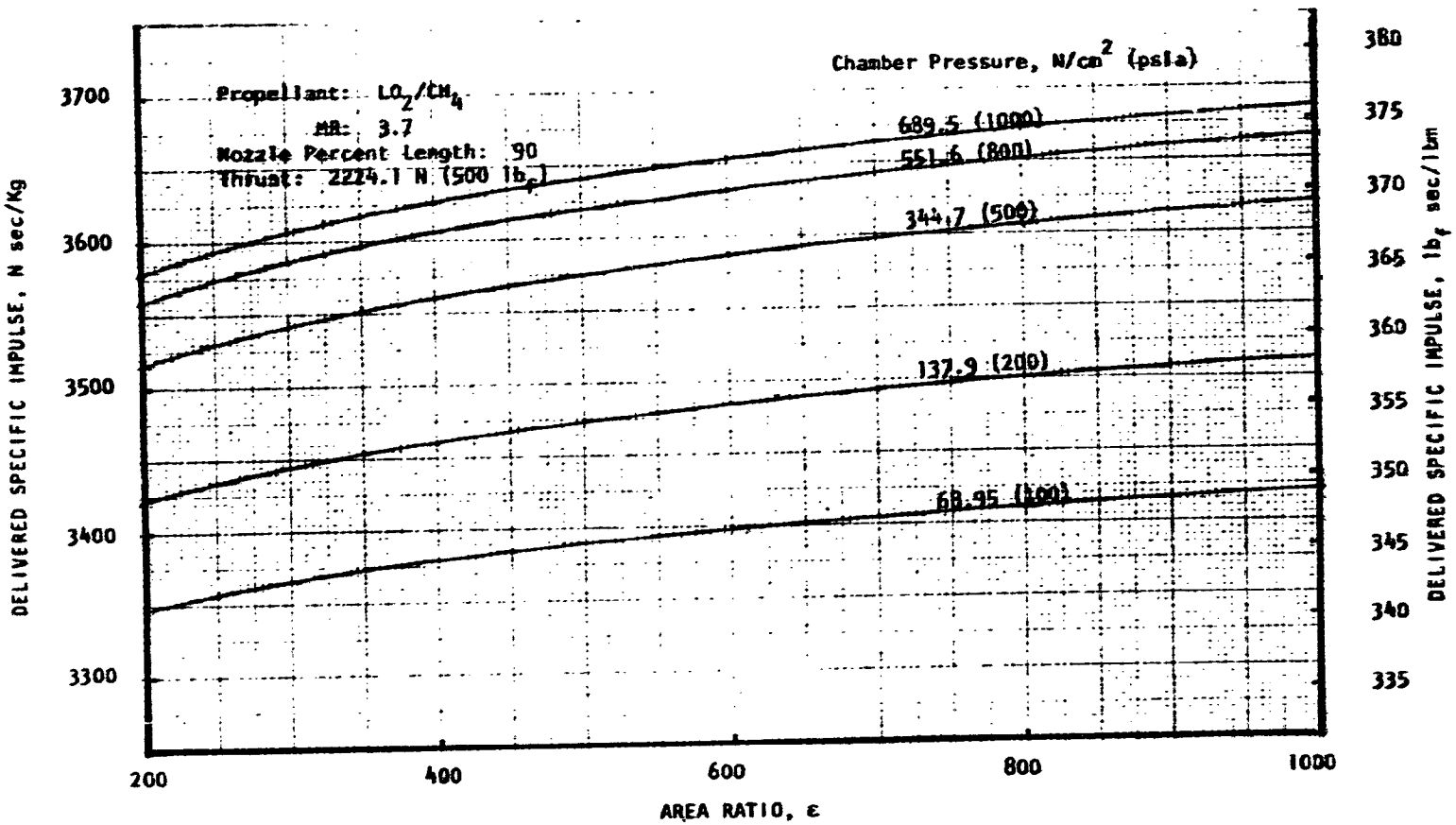

Figure D-16. LO_2/CH_4 Expander Cycle Engine Specific Impulse Variation With Area Ratio and Chamber Pressure (Thrust = 2224.1 N (500 lb_f)

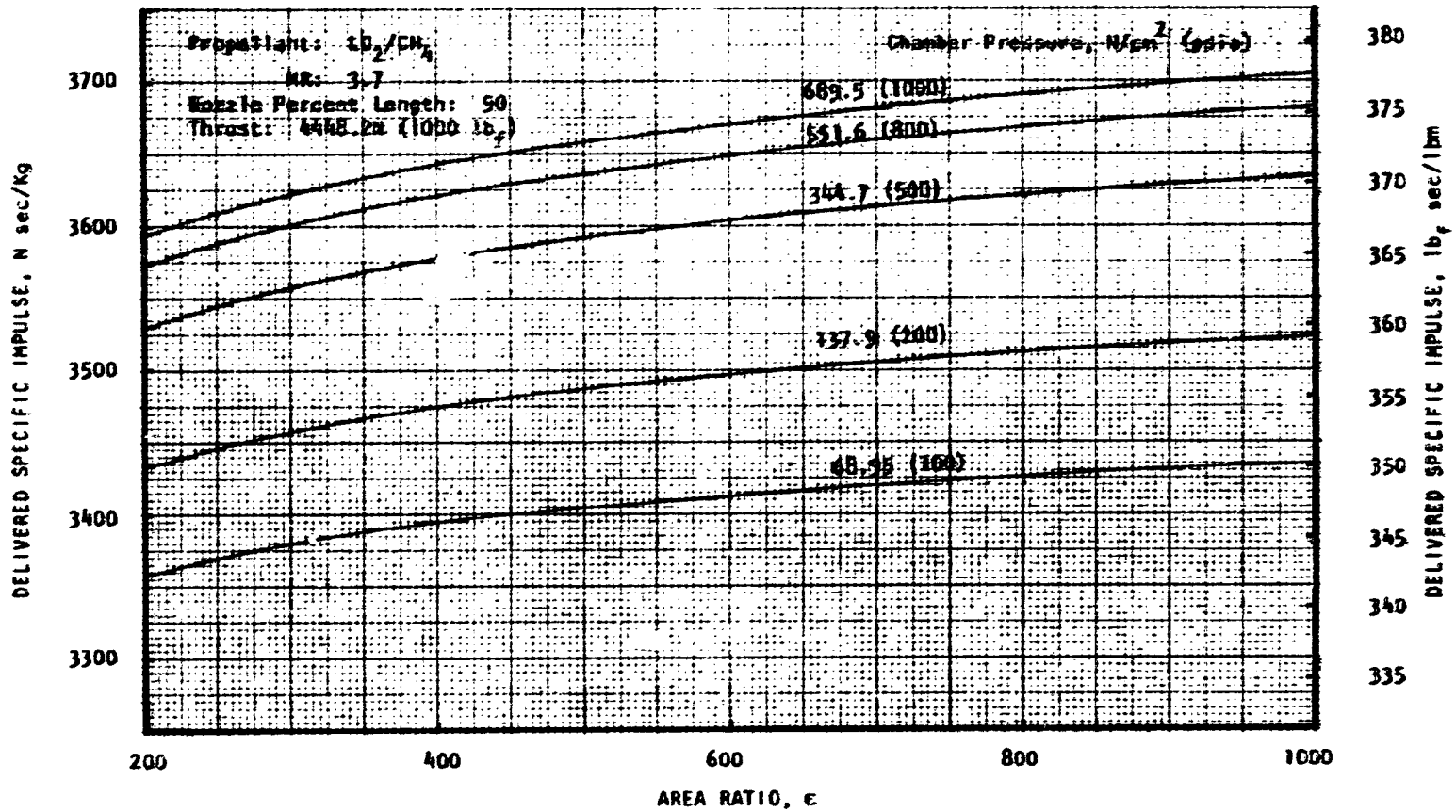

Figure D-17. LO_2/CH_4 Expander Cycle Engine Specific Impulse Variation With Area Ratio and Chamber Pressure (Thrust = 4448.2N(1000 lb_f)

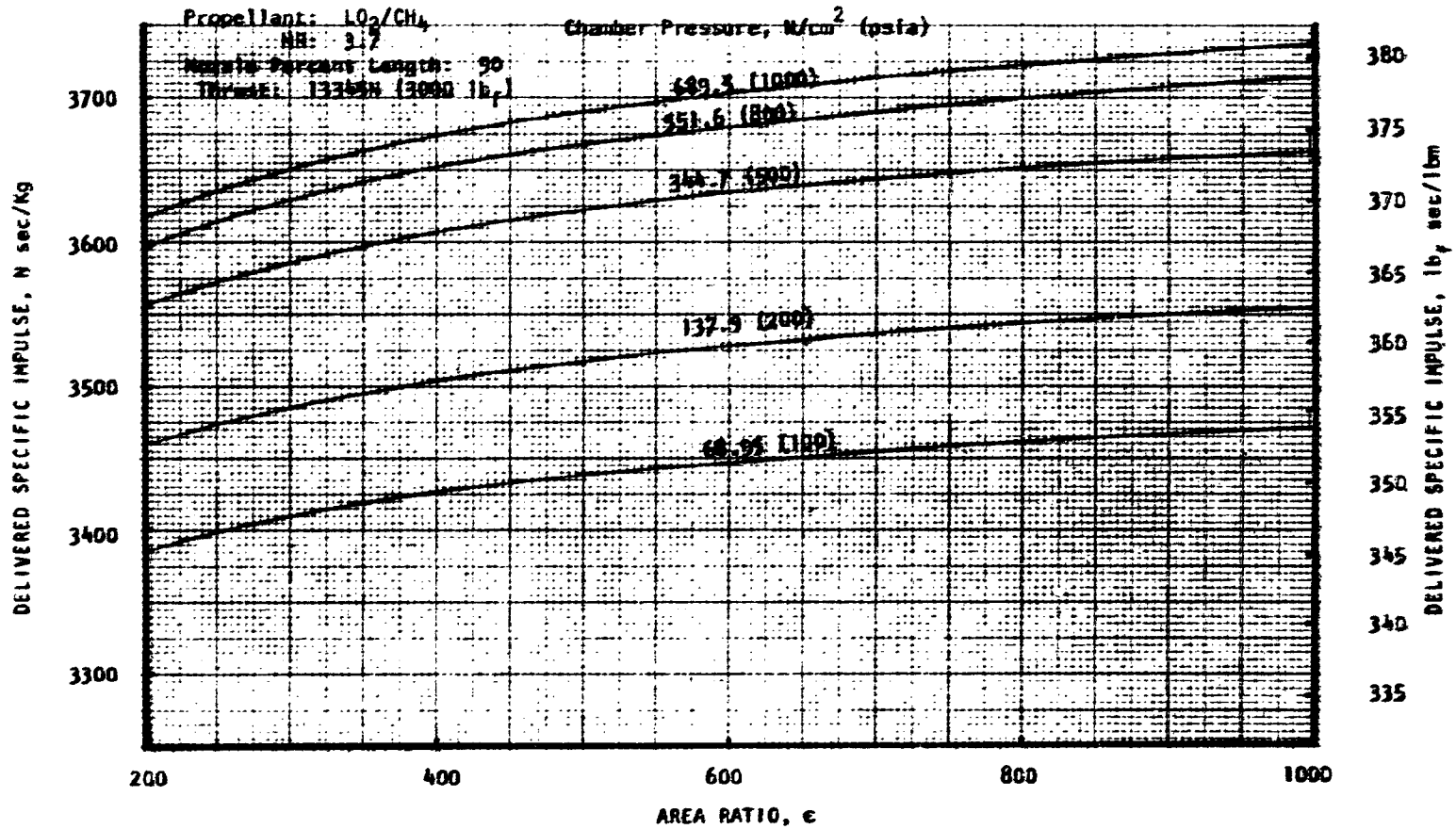

Figure D-18. LO_2/CH_4 Expander Cycle Engine Specific Impulse Variation With Area Ratio and Chamber Pressure (Thrust = 13345N(3000 lb_f)

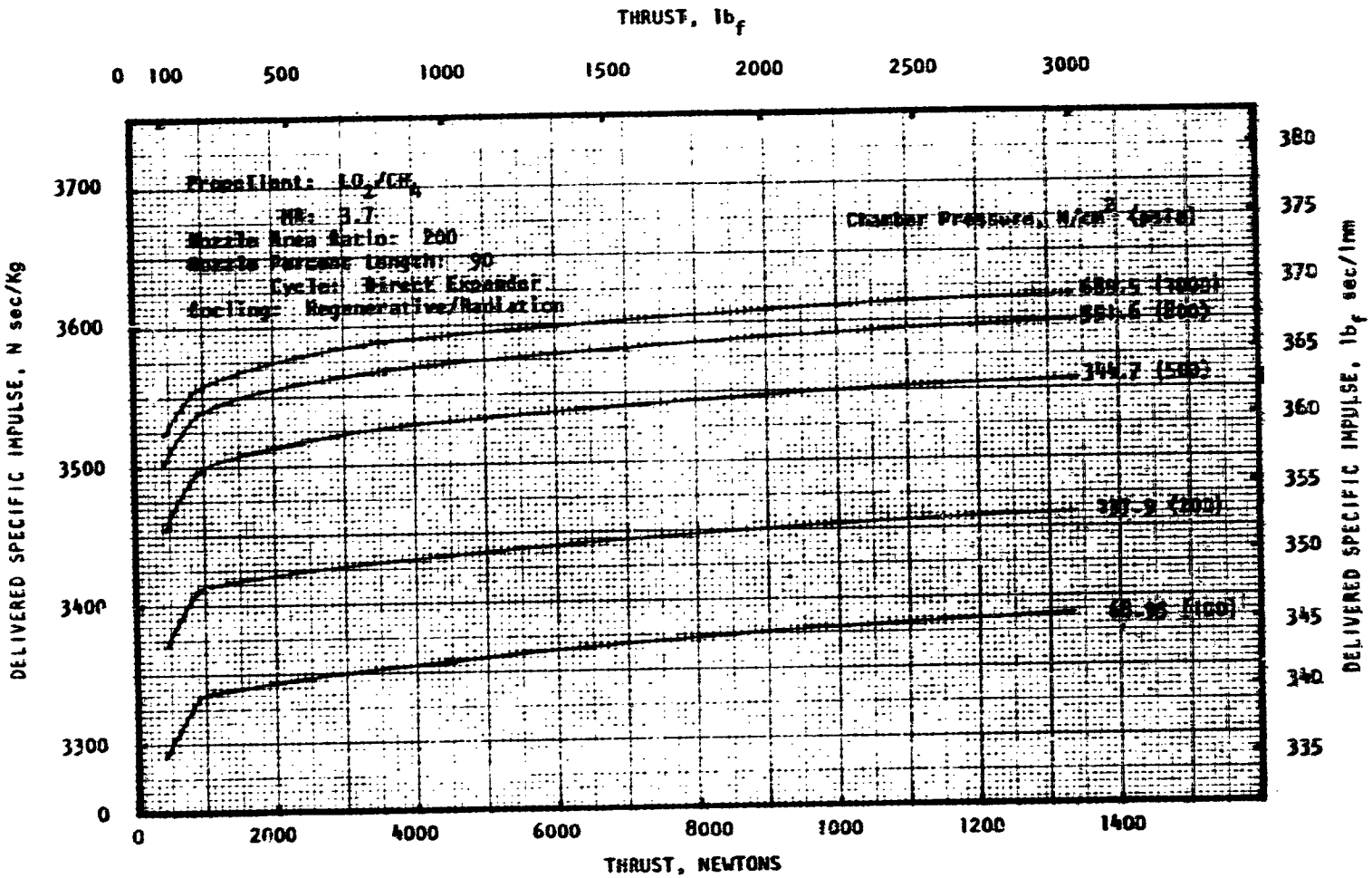

Figure D-19. Delivered LO_2/CH_4 Expander Cycle Engine Specific Impulse Variation With Thrust and Chamber Pressure (Nozzle Area Ratio 200)

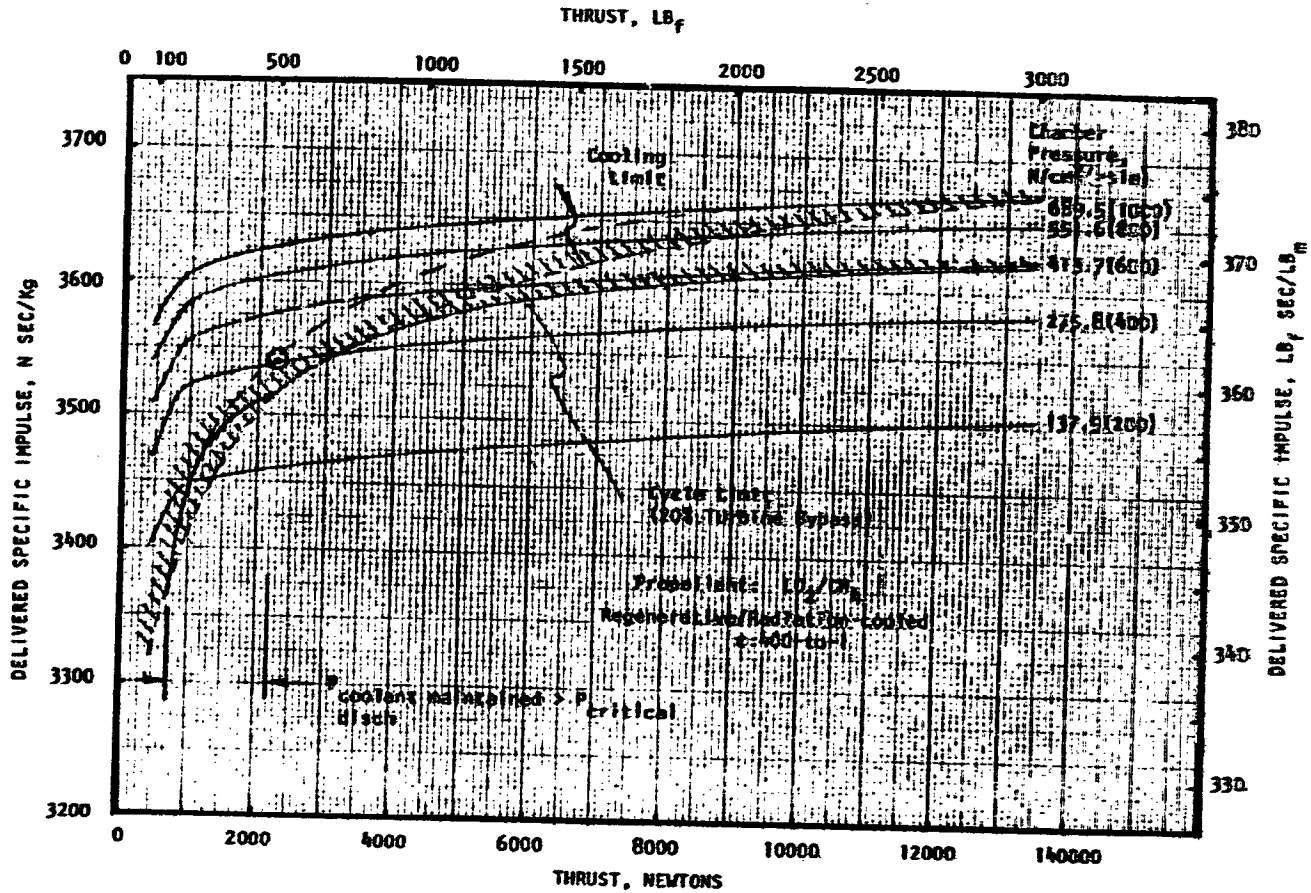

FIGURE D-20. LO_2/CH_4 Direct Expander Cycle Engine Delivered Specific Impulse

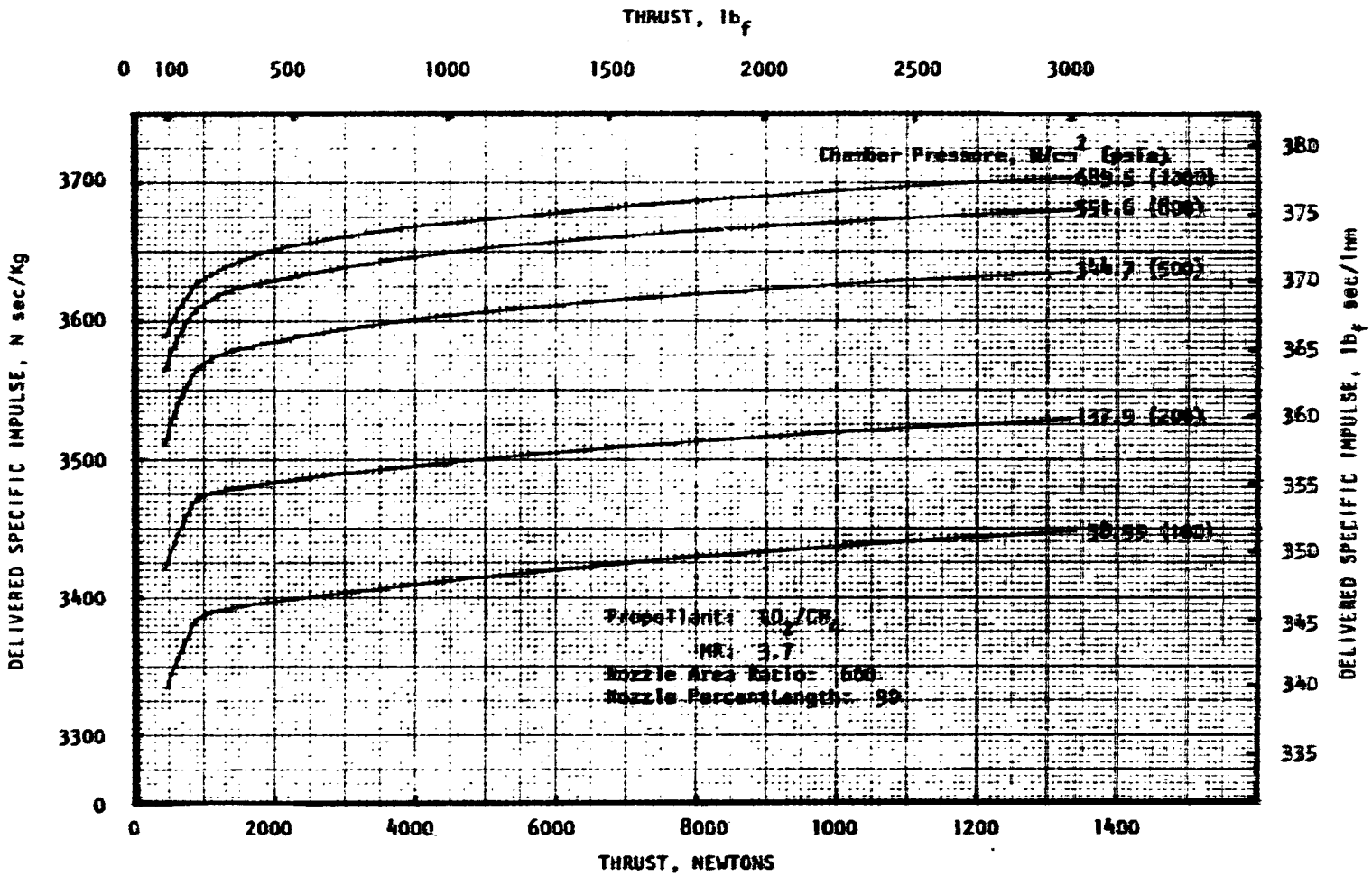

Figure D-21. Delivered LO_2/CH_4 Expander Cycle Engine Specific Impulse Variation With Thrust and Chamber Pressure (Nozzle Area Ratio 600)

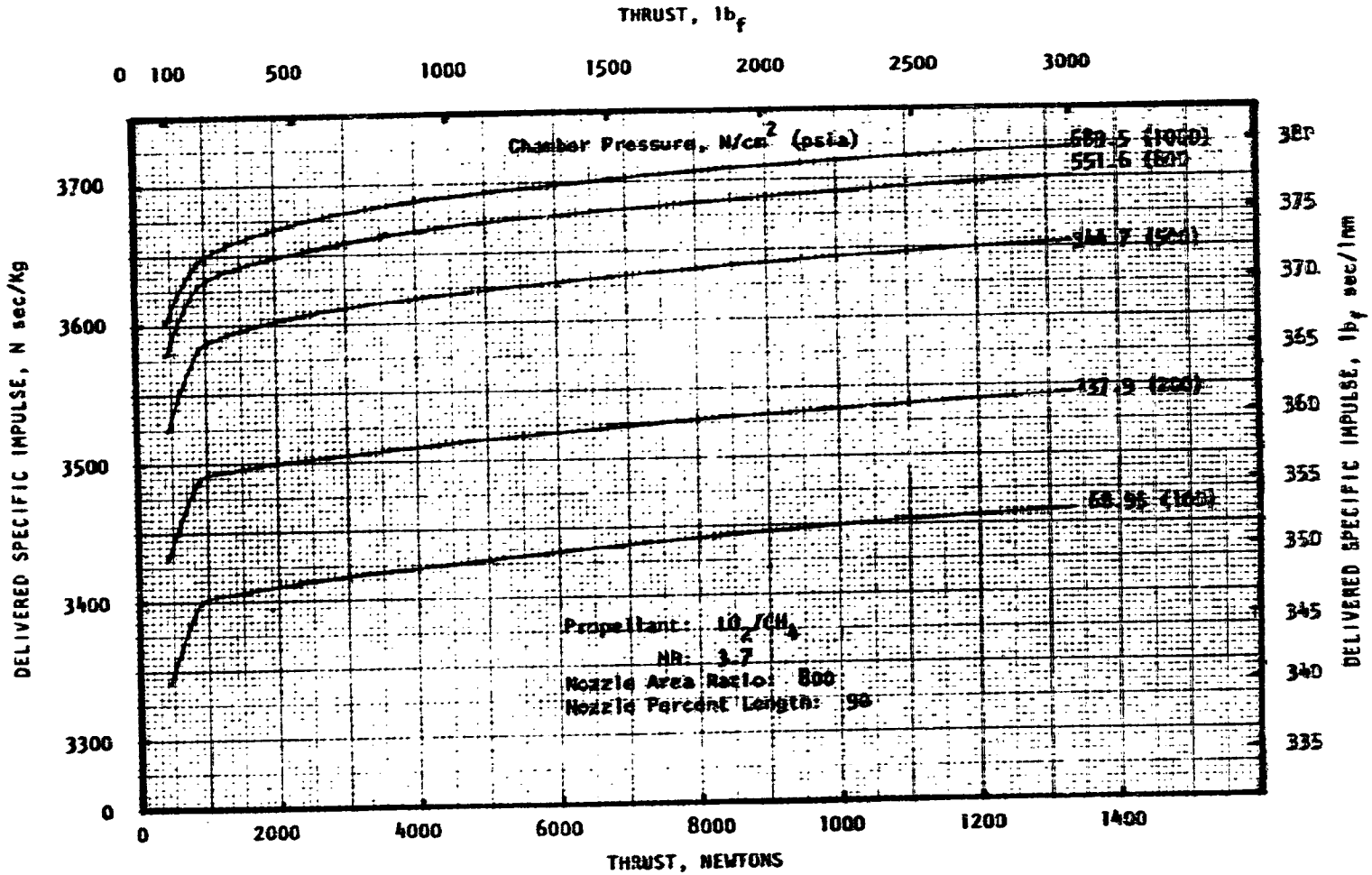

Figure D-22. Delivered LO_2/CH_4 Expander Cycle Engine Specific Impulse Variation With Thrust and Chamber Pressure (Nozzle Area Ratio = 800)

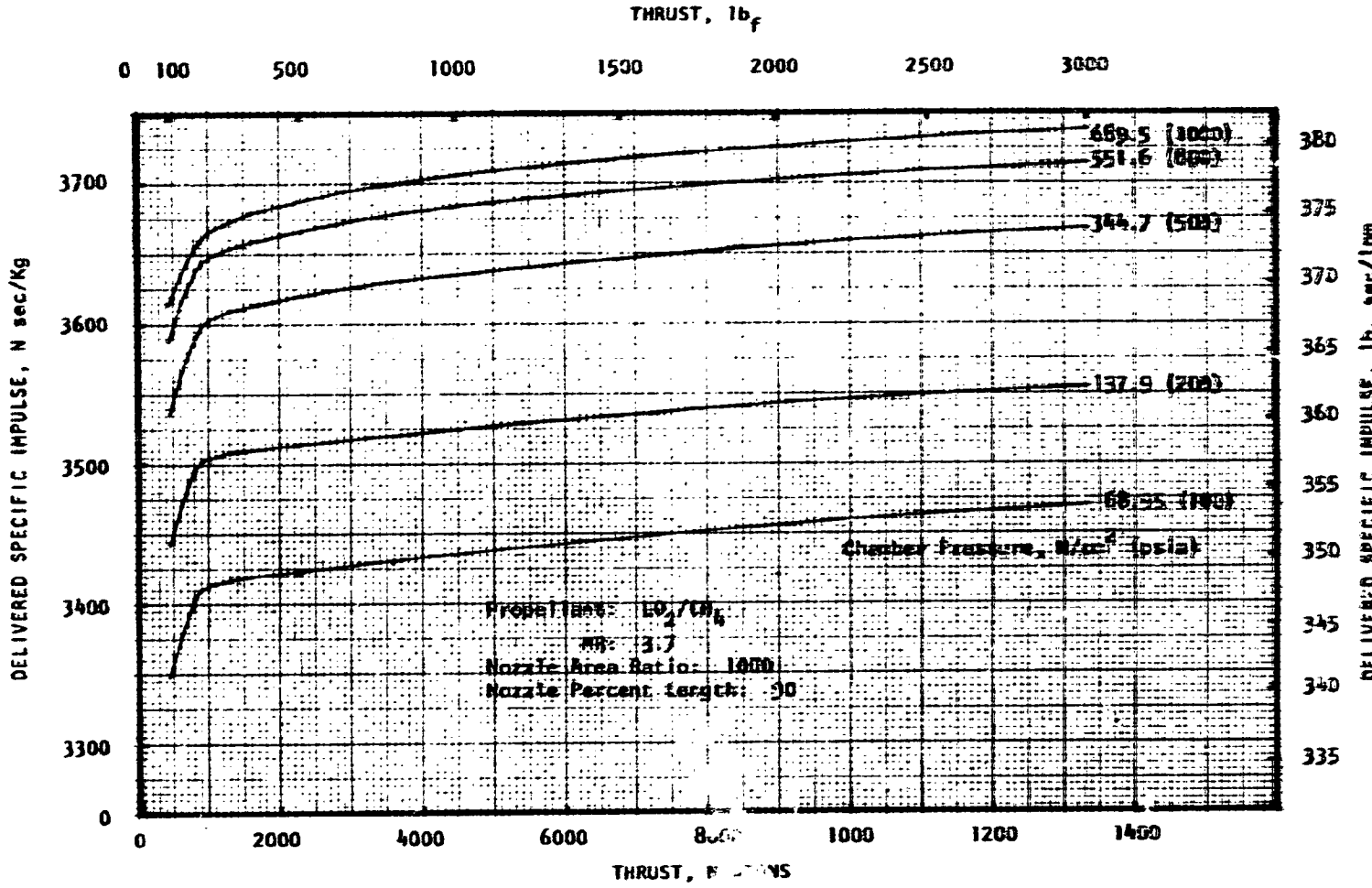

Figure D-23. Delivered LO_2/CH_4 Expander Cycle Engine Specific Impulse Variation With Thrust and Chamber Pressure (Nozzle Area Ratio = 1000)

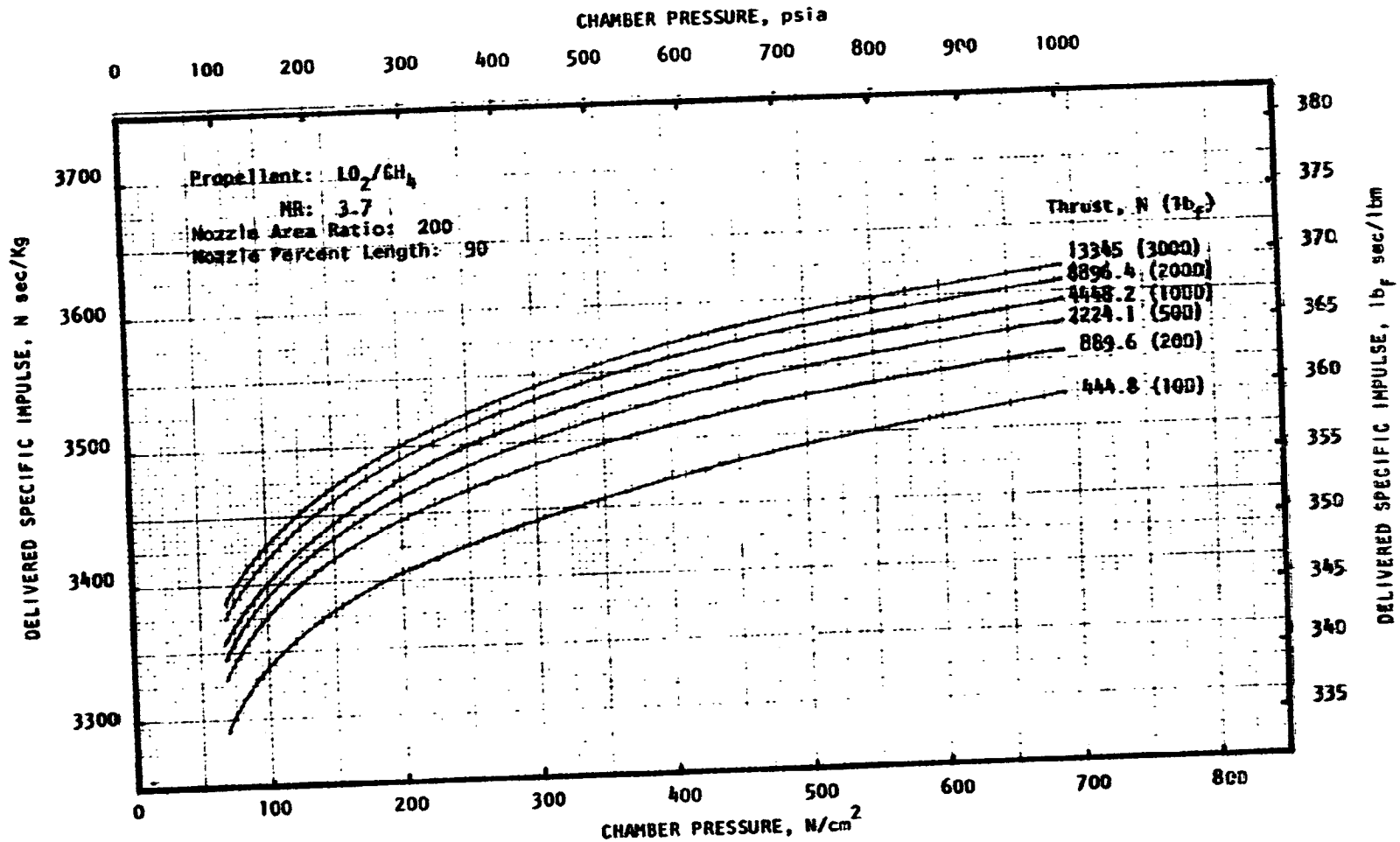

Figure D-24 LO_2/CH_4 Expander Cycle Engine Specific Impulse Variation With Chamber Pressure and Thrust (Nozzle Area Ratio = 200)

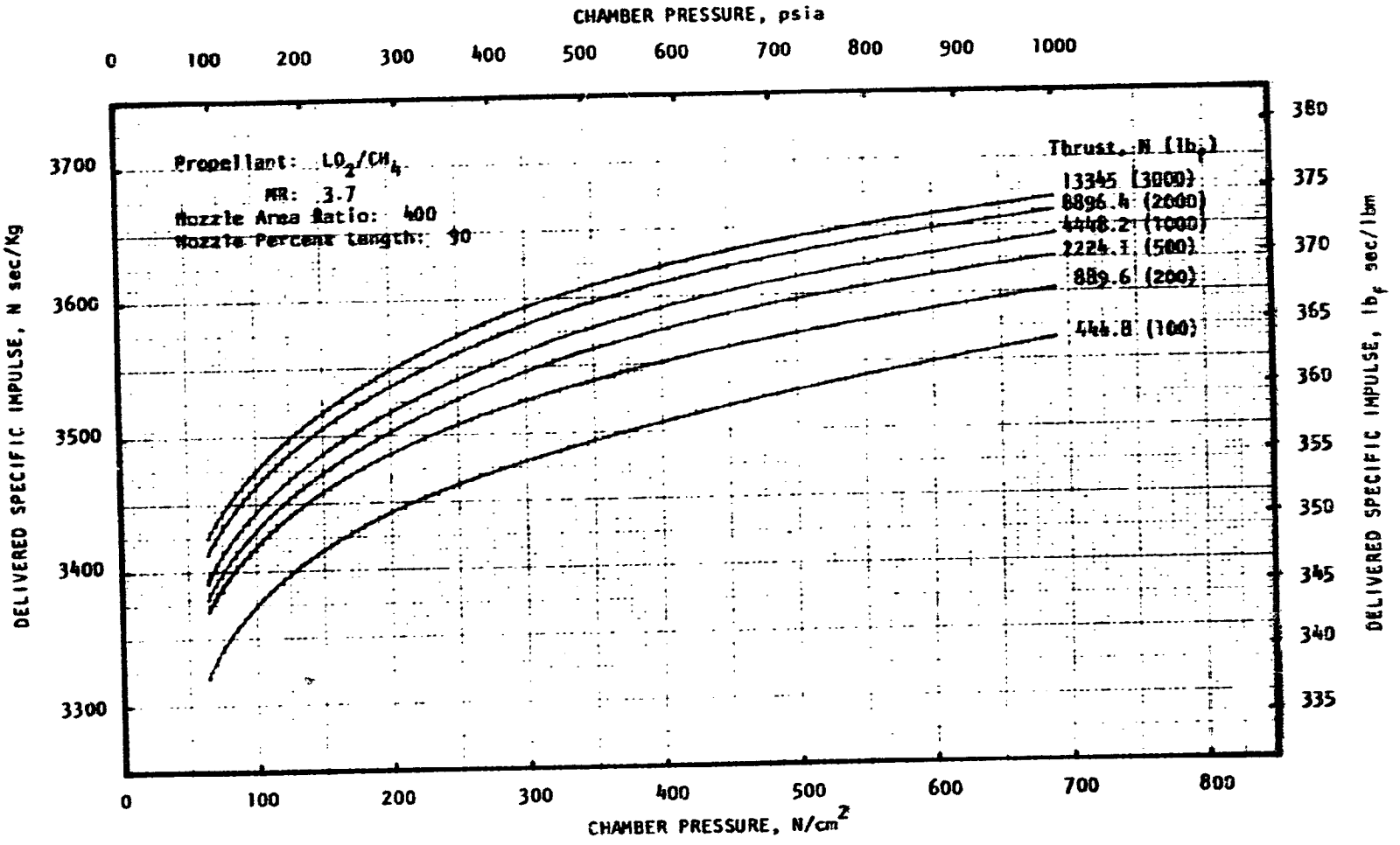

Figure D-25 LO_2/CH_4 Expander Cycle Engine Specific Impulse Variation With Chamber Pressure and Thrust (Nozzle Area Ratio = 400)

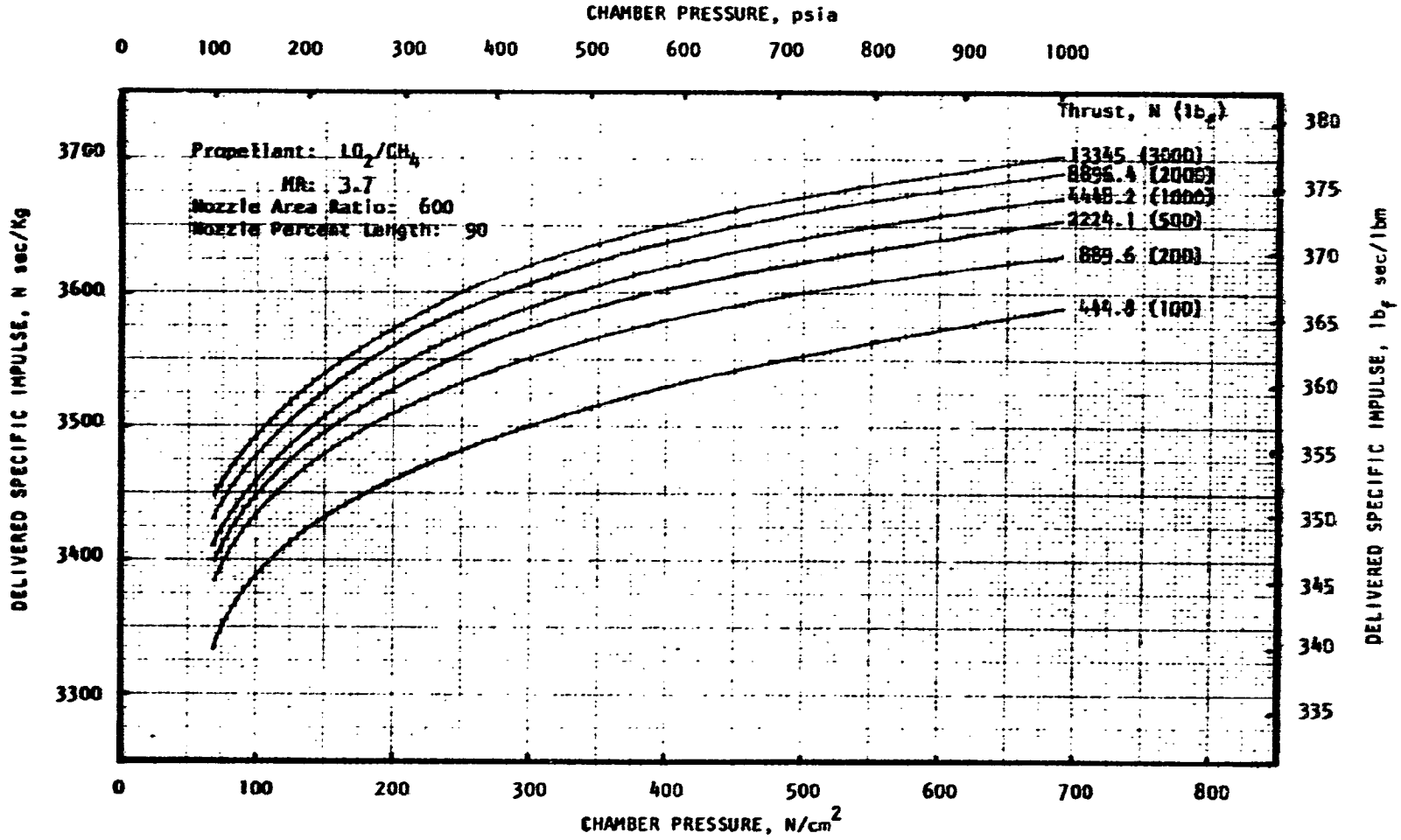

Figure D-26. LO_2/CH_4 Expander Cycle Engine Specific Impulse Variation With Chamber Pressure and Thrust (Nozzle Area Ratio = 600)

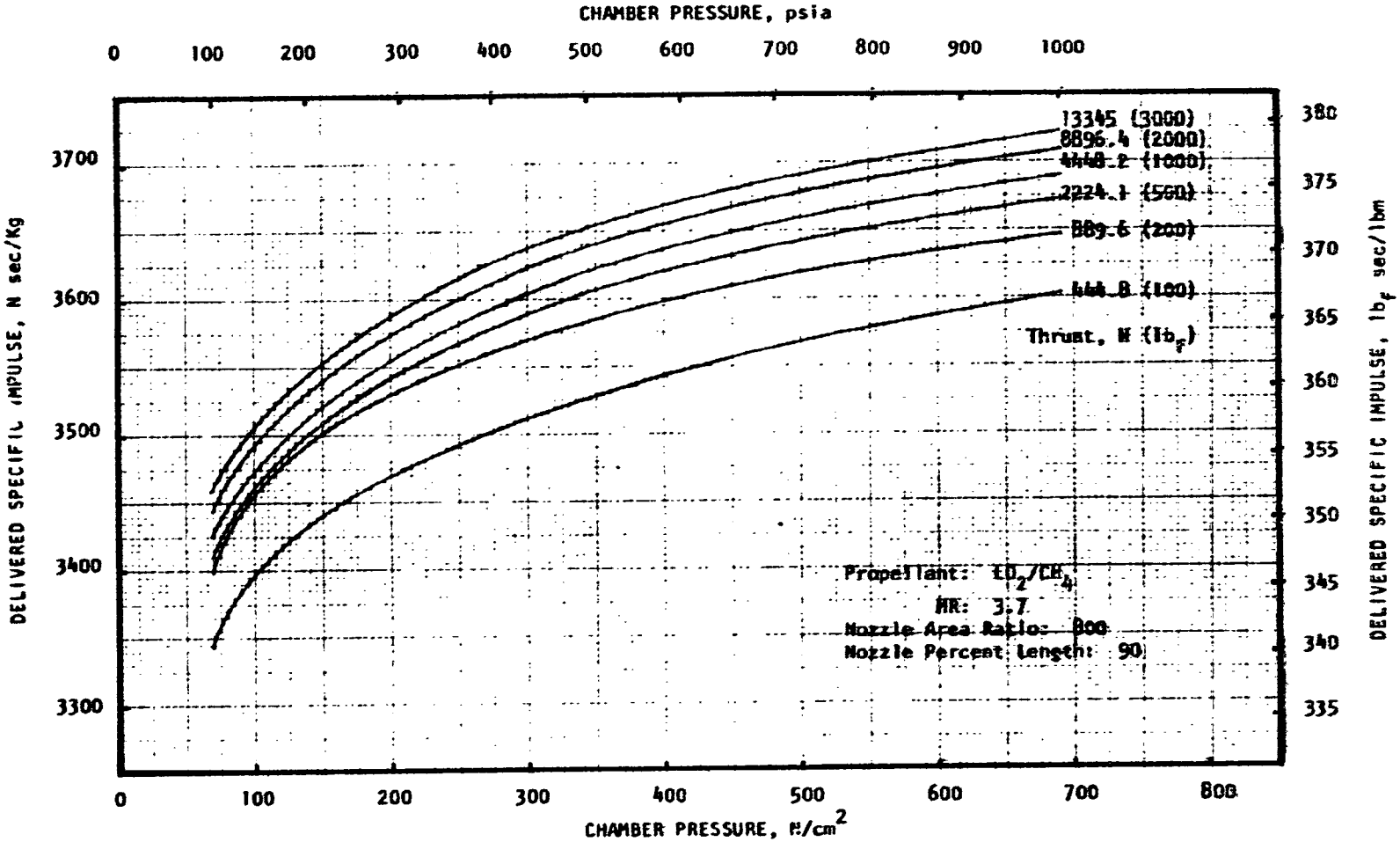

Figure D-27 LO_2/CH_4 Expander Cycle Engine Specific Impulse Variation With Chamber Pressure and Thrust (Nozzle Area Ratio = 800)

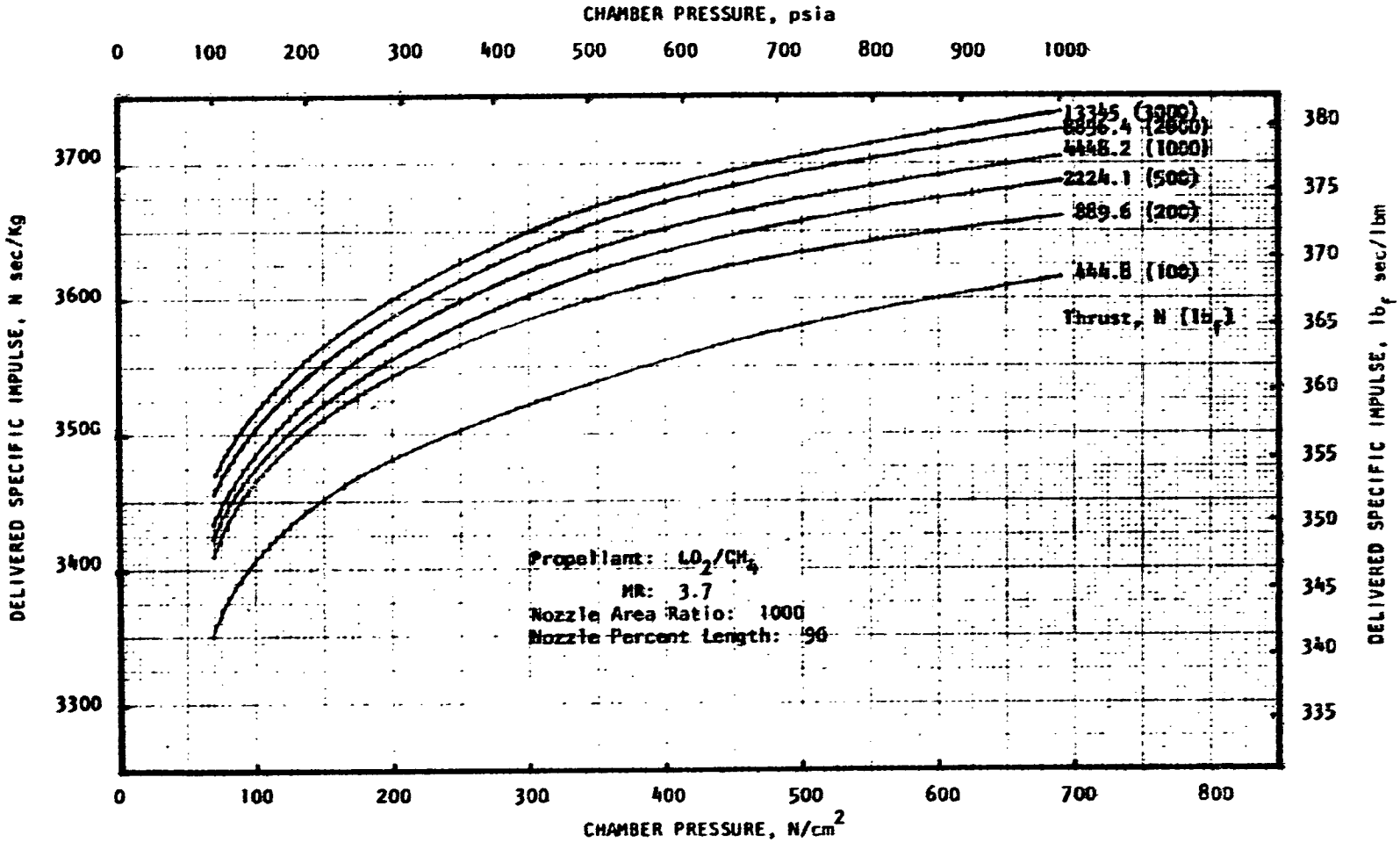

Figure D-28 LO_2/CH_4 Expander Cycle Engine Specific Impulse Variation With Chamber Pressure and Thrust (Nozzle Area Ratio = 1000)

APPENDIX E

PARAMETRIC ENGINE DIMENSIONS

Parametric engine dimension data were generated for both engines, but only the LO_2/H_2 engine data were plotted since the values of engine length and diameter were essentially identical for the two engines. The parametric plots included:

Engine Length: (Fig. E-1 through E-13)

1. Engine length versus nozzle area ratio for parametric chamber pressure at constant thrust

2. Engine length versus chamber pressure for parametric thrust at constant nozzle area ratio

3. Engine length versus chamber pressure for parametric area ratio at constant thrust

Engine Diameter: (Fig. E-14 through E-21)

1. Engine diameter versus nozzle area ratio for parametric chamber pressure at constant thrust

2. Engine diameter versus chamber pressure for parametric area ratio at constant thrust

Note that the parametric data are presented over the entire study range of thrust (444.8 N, 100 Lbf to 13345 N, 3000 Lbf) and chamber pressure (68.95 N/cm^2, 100 psia to 689.5 N/cm^2, 1000 psia). In using these data for mission studies it is important to consider possible engine system design constraints in order to avoid unrealistic design points. The parametric plots of delivered specific impulse versus thrust for the 400-to-1 area ratio LO_2/H_2 and LO_2/CH_4 engines (Figures D-6 and D-20 , Appendix D) show the preliminary design points, thrust chamber cooling constraints, and expander cycle power constraints which resulted from this study. These constraints can be used to conservatively define feasible engine system operating conditions over the range of thrust and chamber pressure.

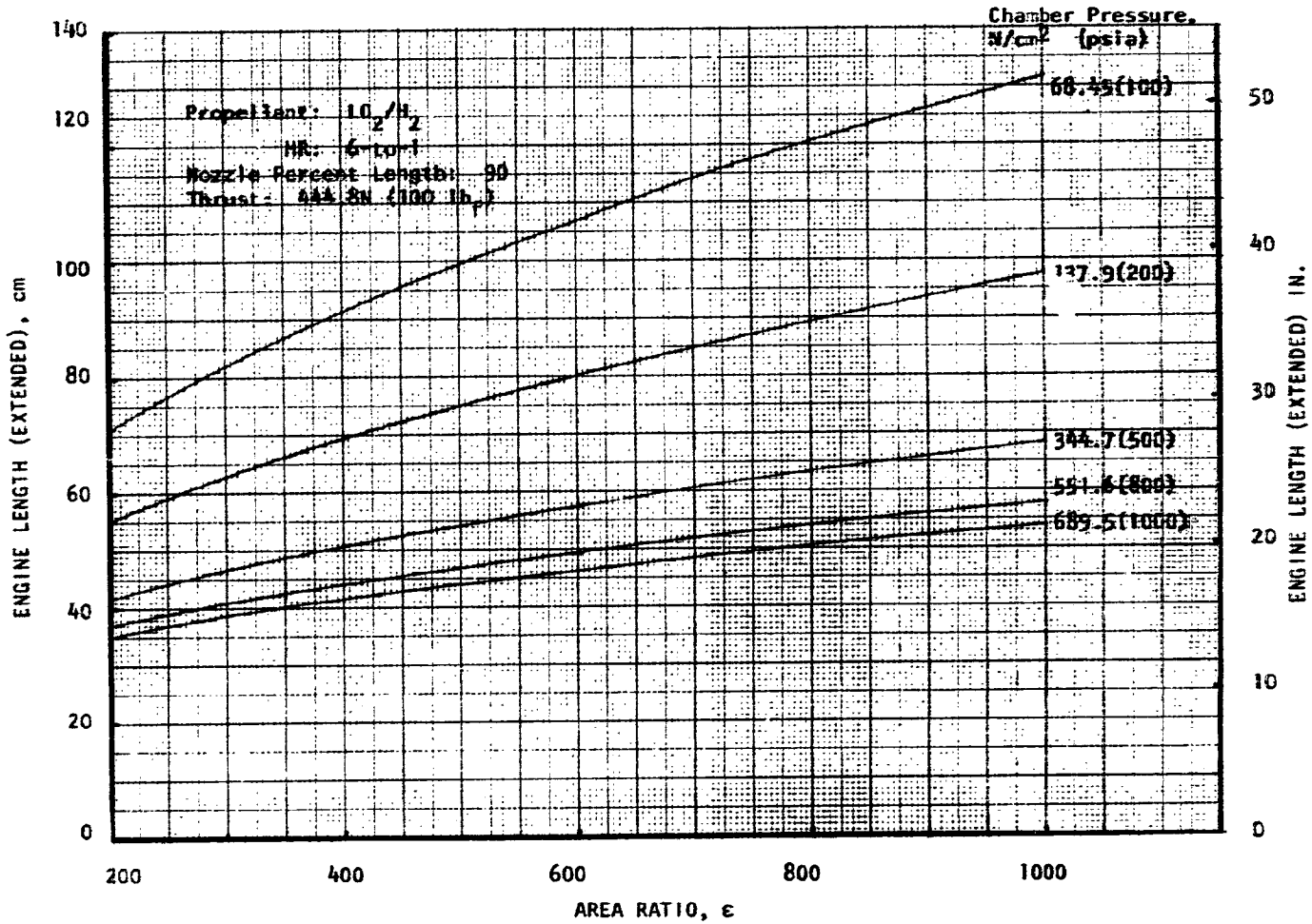

Figure E-1. Total LO_2/H_2 Engine Length Variation with Area Ratio and Chamber Pressure (Thrust = 444.8 N (100 lbf)

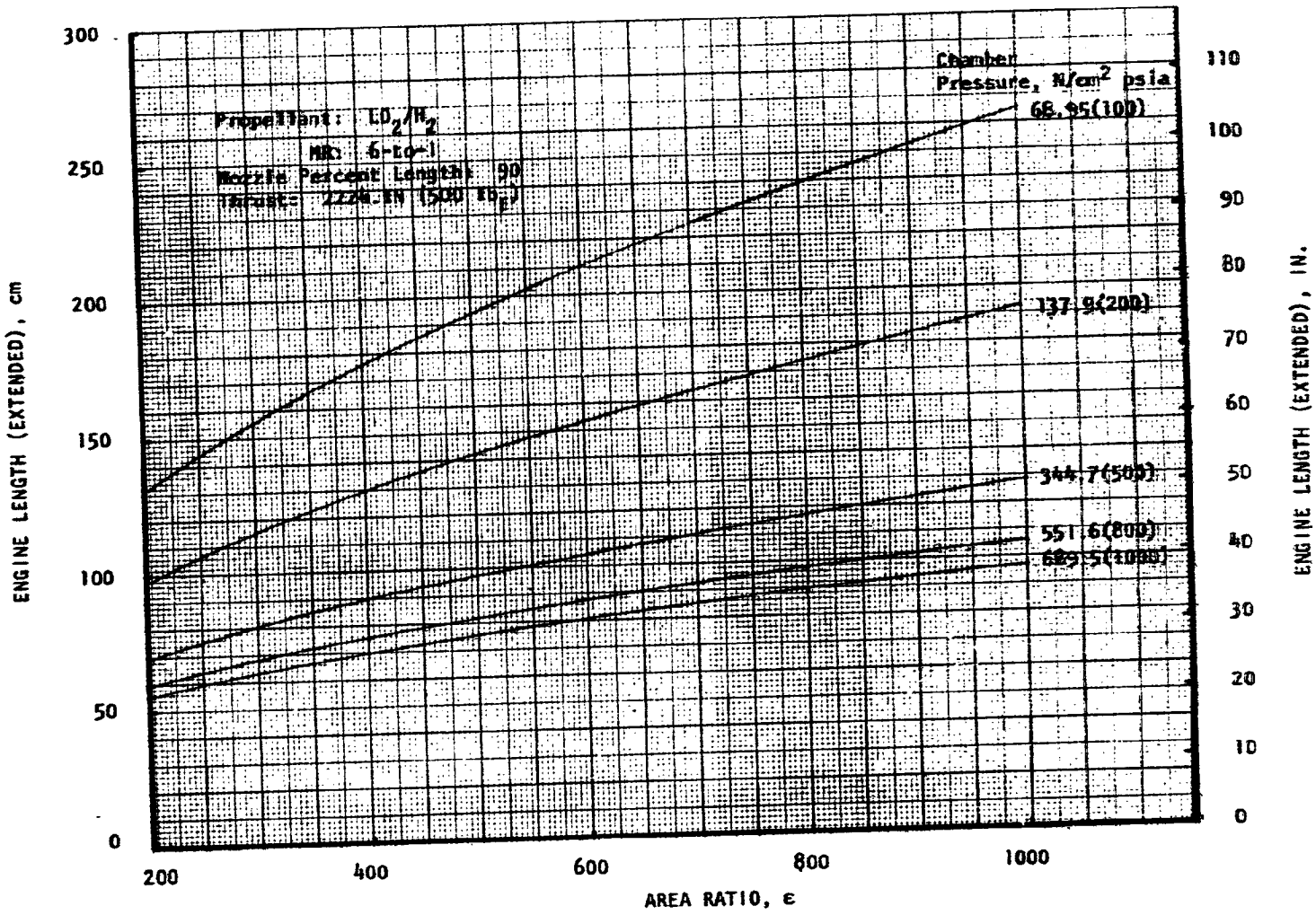

Figure E-2. Total LO_2/H_2 Engine Length Variation with Area Ratio and Chamber Pressure (Thrust = 2224.1 N (500 lbf)

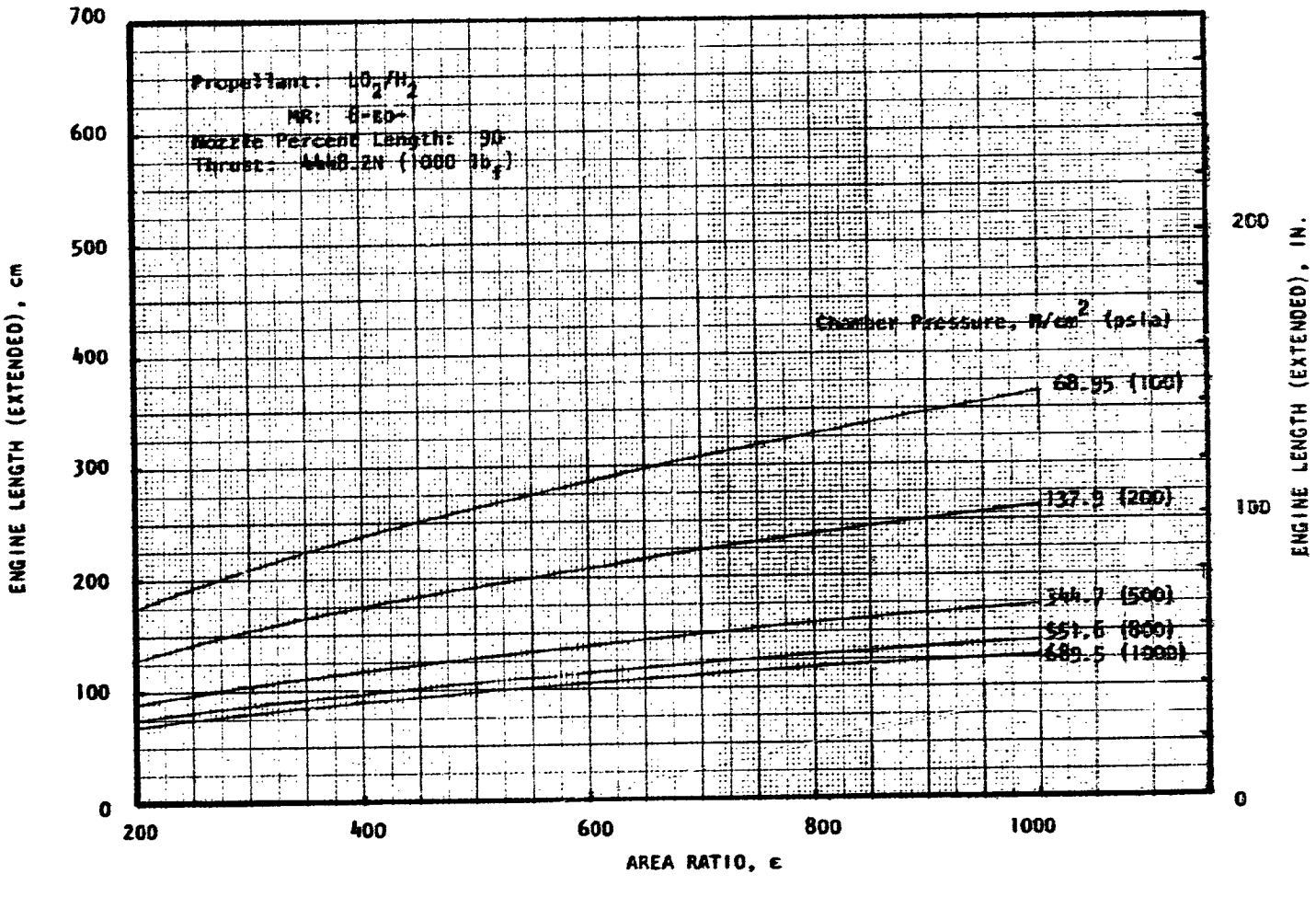

Figure E-3. Total LO_2/H_2 Engine Length Variation with Area Ratio and Chamber Pressure (Thrust = 4448.2 N (1000 lbf)

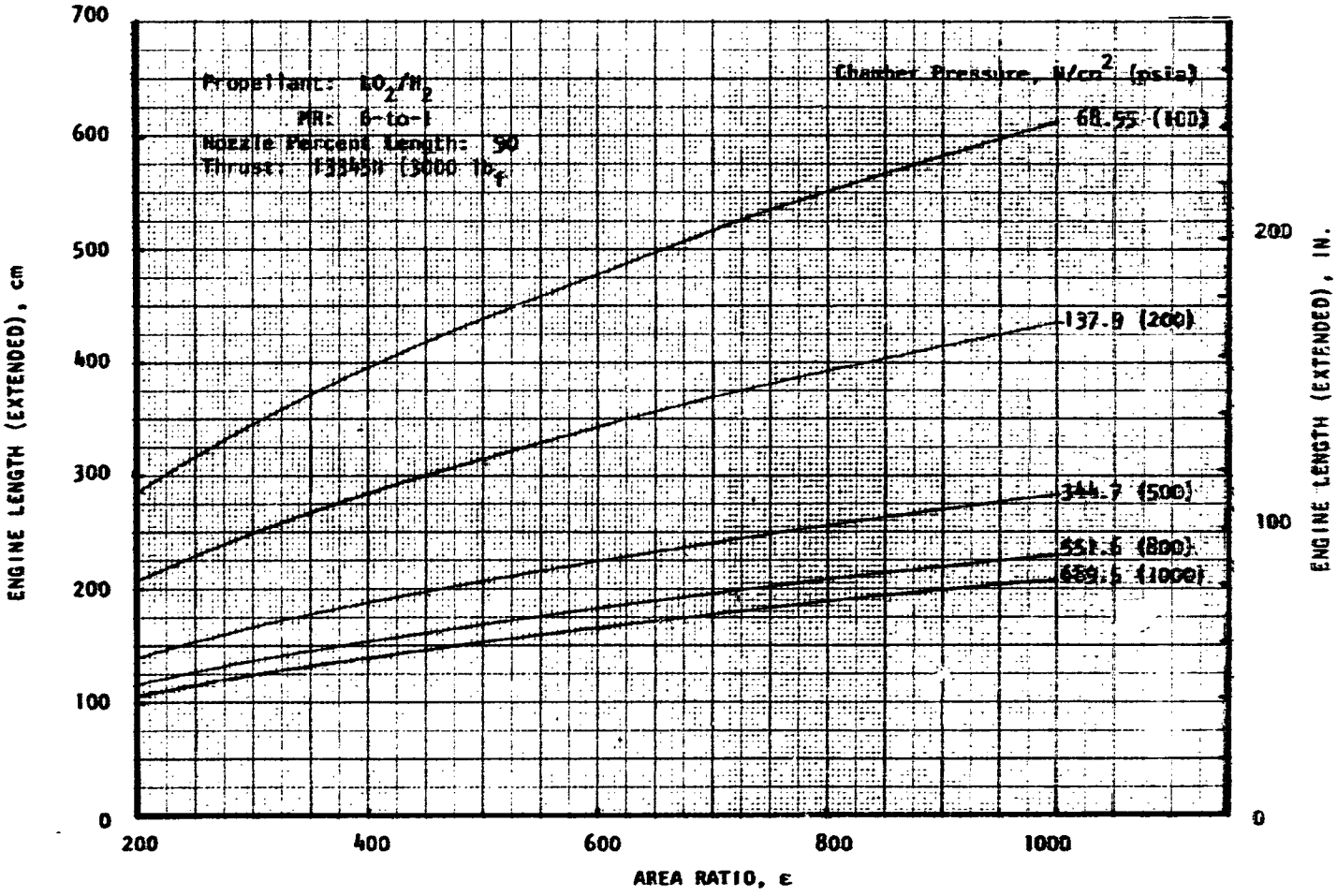

Figure E-4. Total LO_2/H_2 Engine Length Variation with Area Ratio and Chamber Pressure (Thrust = 13345 N (3000 lbf)

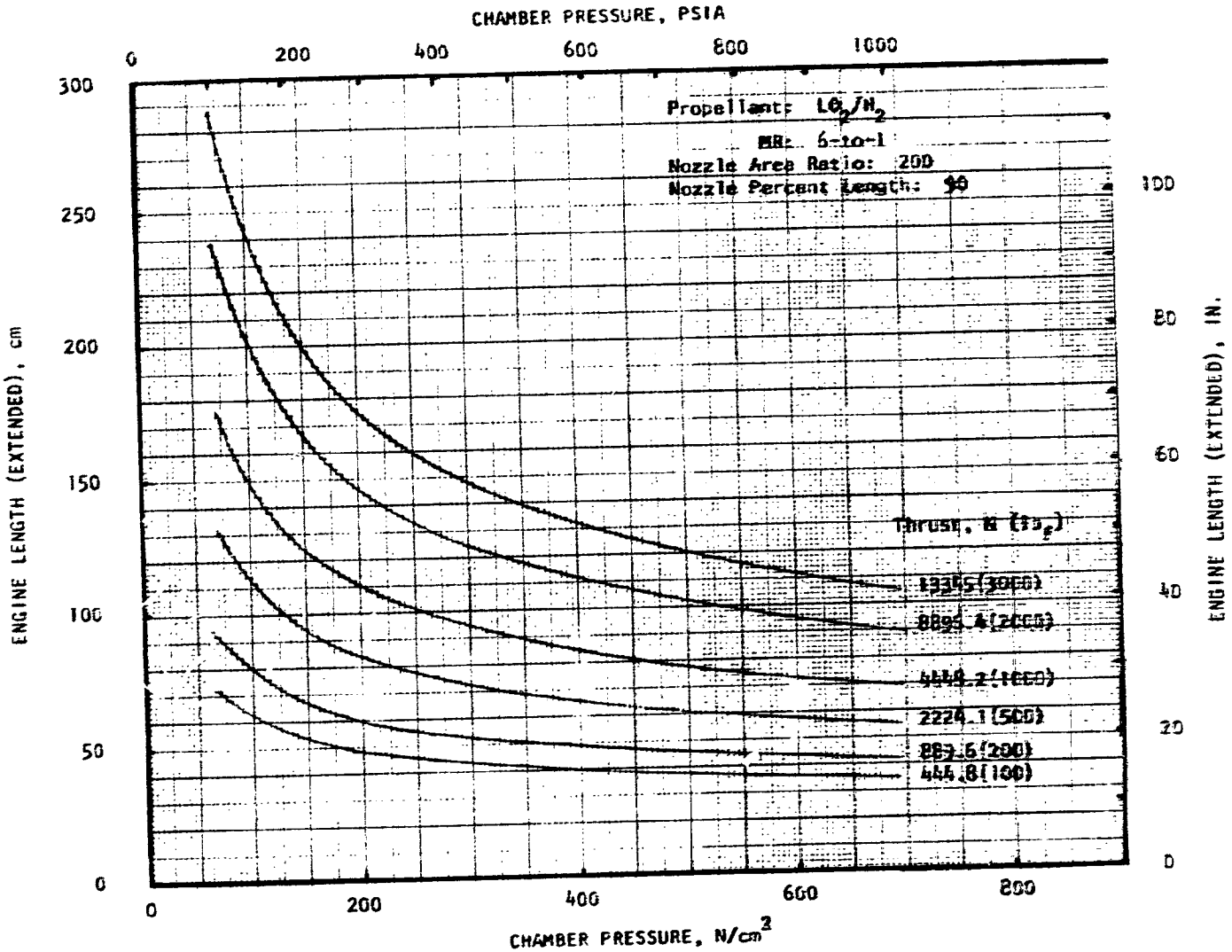

Figure E-5. Total LO_2/H_2 Engine Length Variation with Chamber Pressure and Thrust (Nozzle Area Ratio = 200)

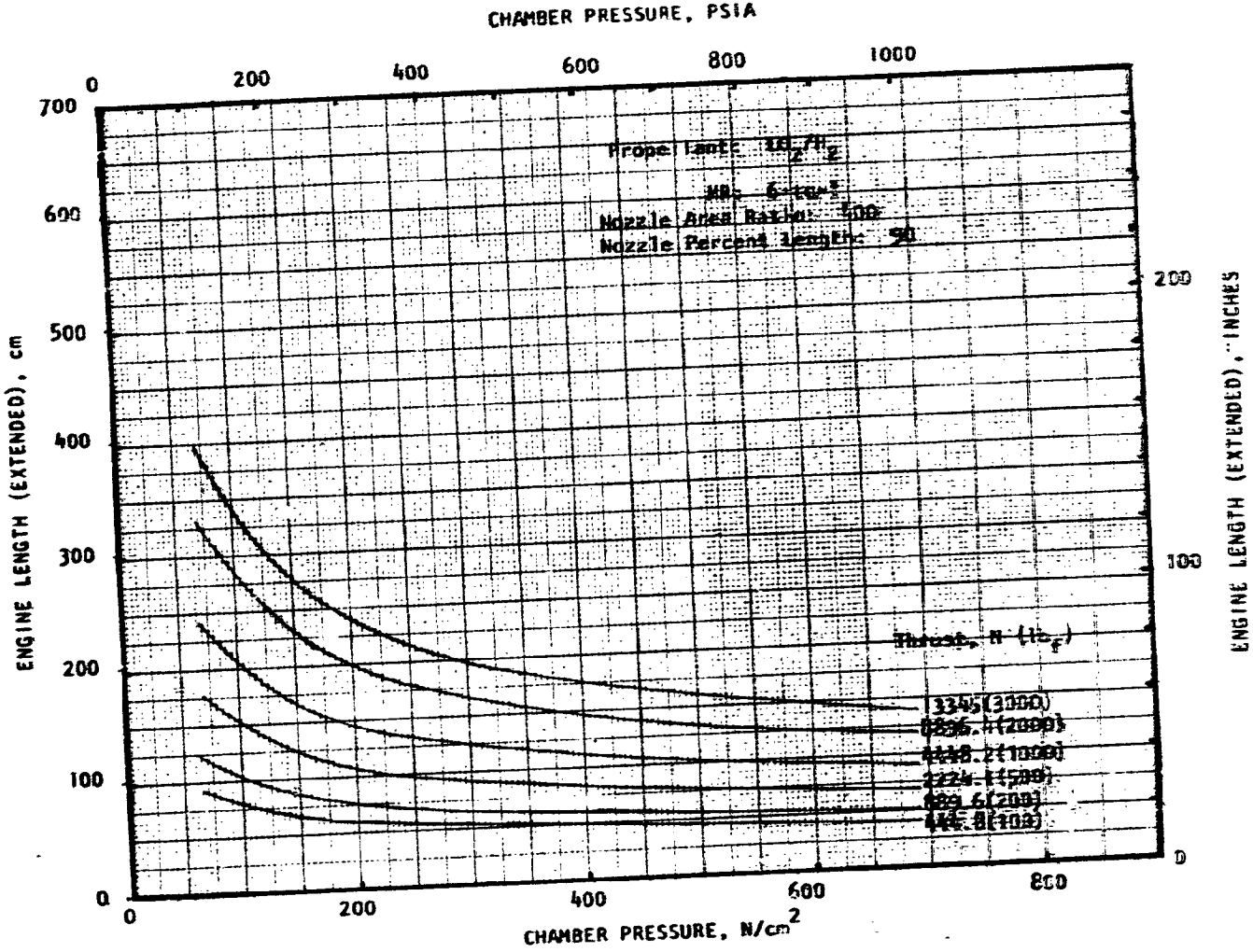

Figure E-6. Total LO_2/H_2 Engine Length Variation with Chamber Pressure and Thrust (Nozzle Area = 400)

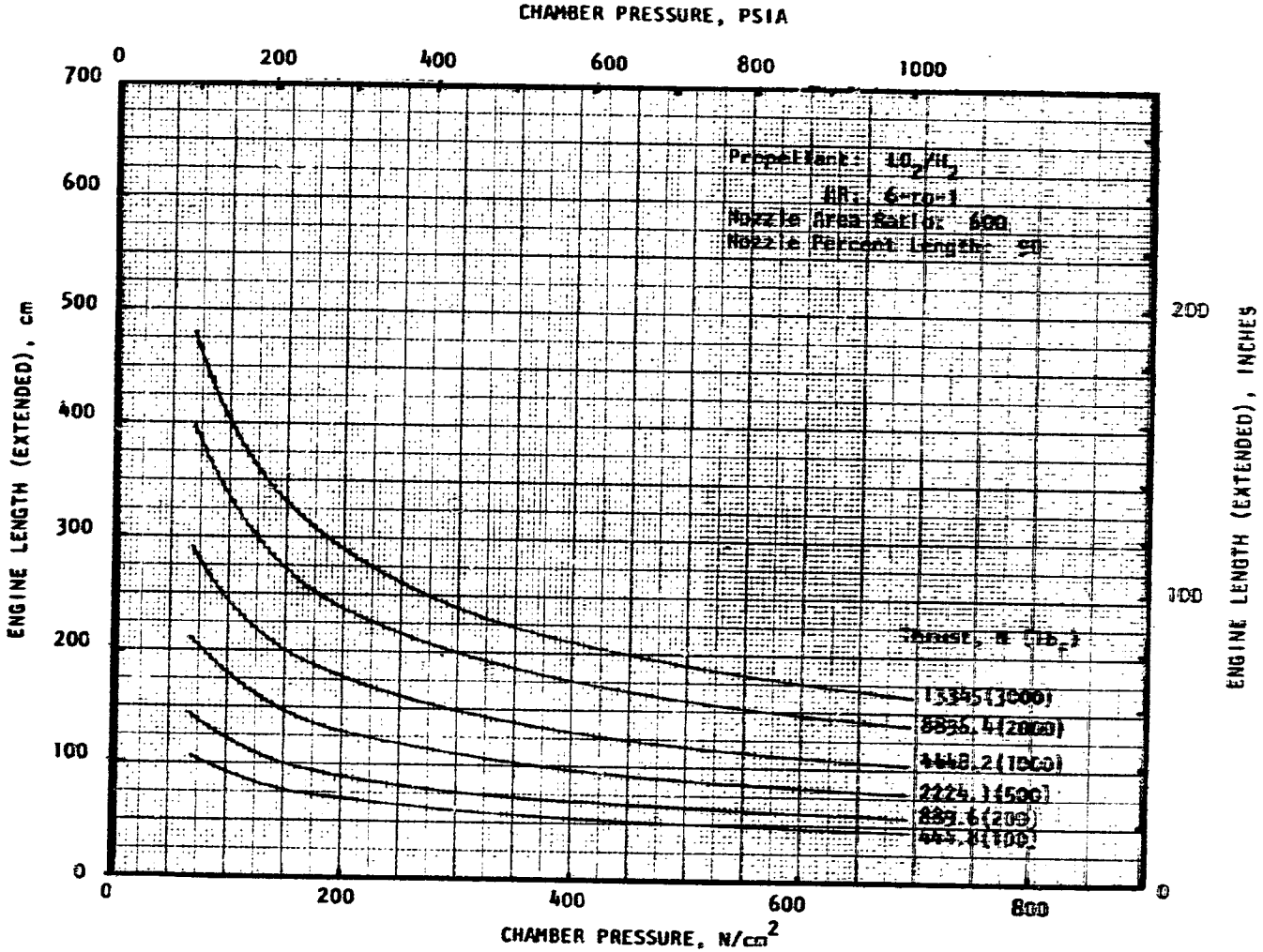

Figure E-7. Total LO_2/H_2 Engine Length Variation with Chamber Pressure and Thrust (Nozzle Area = 600)

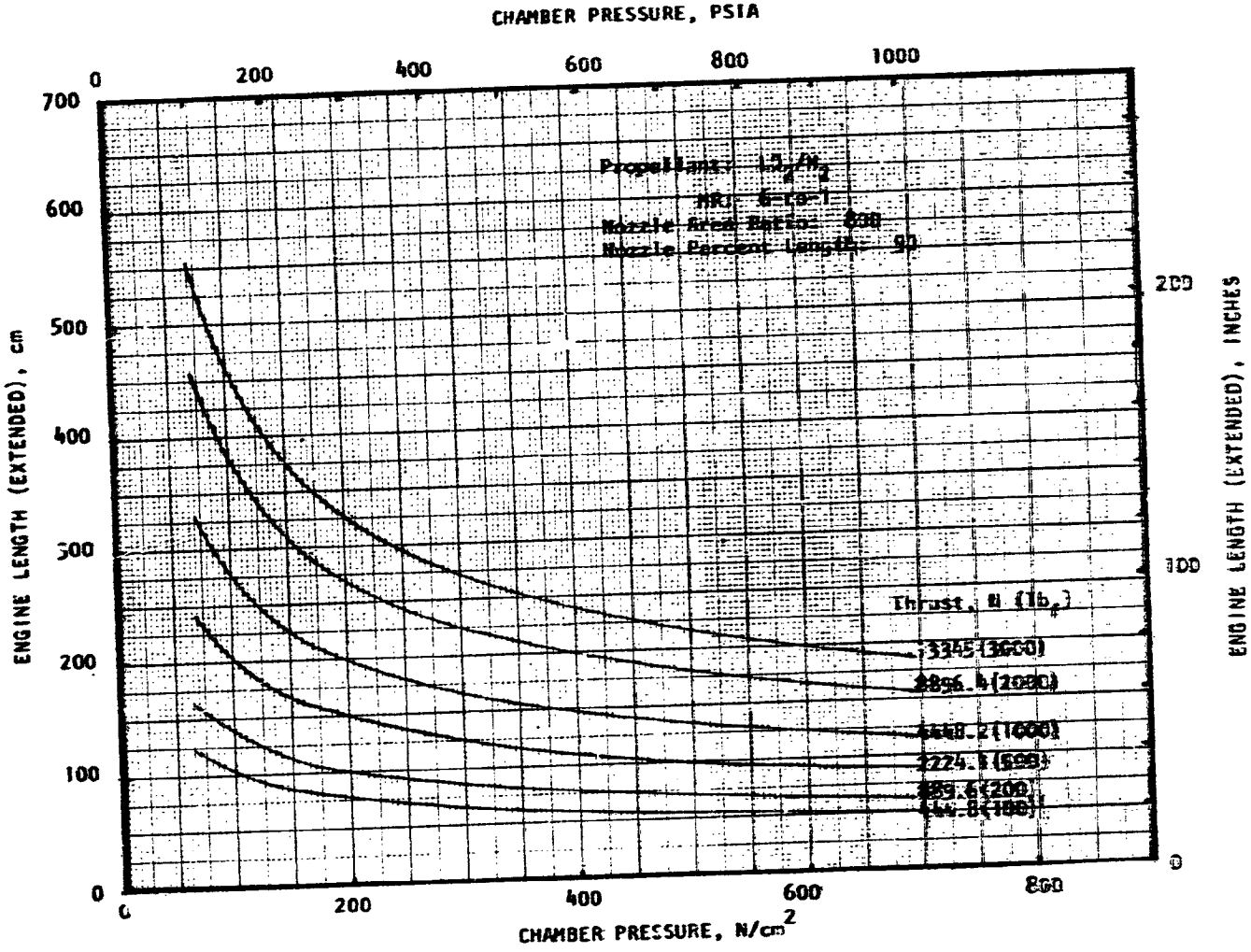

Figure E-8. Total LO_2/H_2 Engine Length Variation with Chamber Pressure and Thrust (Nozzle Area = 800)

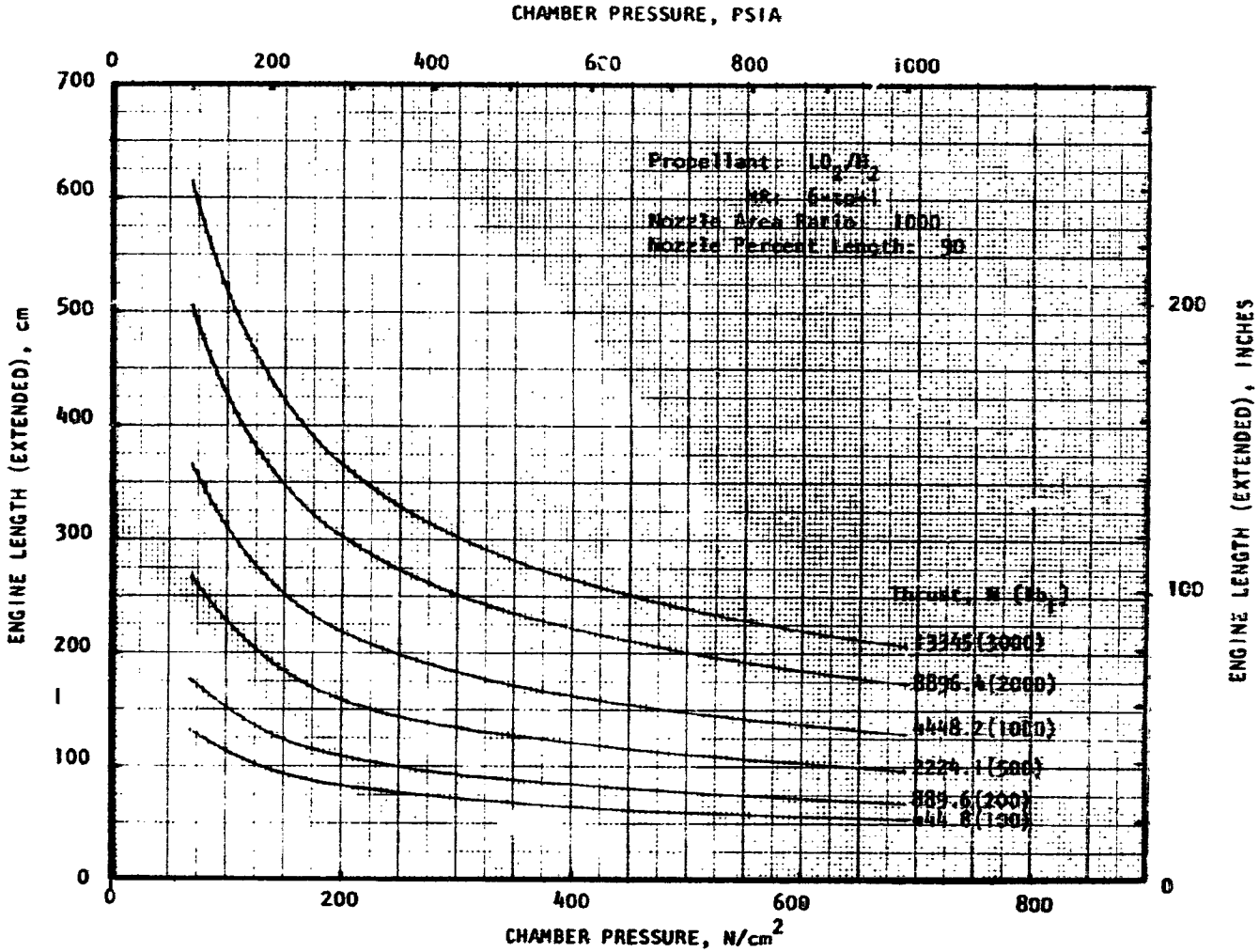

Figure E-9. Total LO_2/H_2 Engine Length Variation with Chamber Pressure and Thrust (Nozzle Area = 1000)

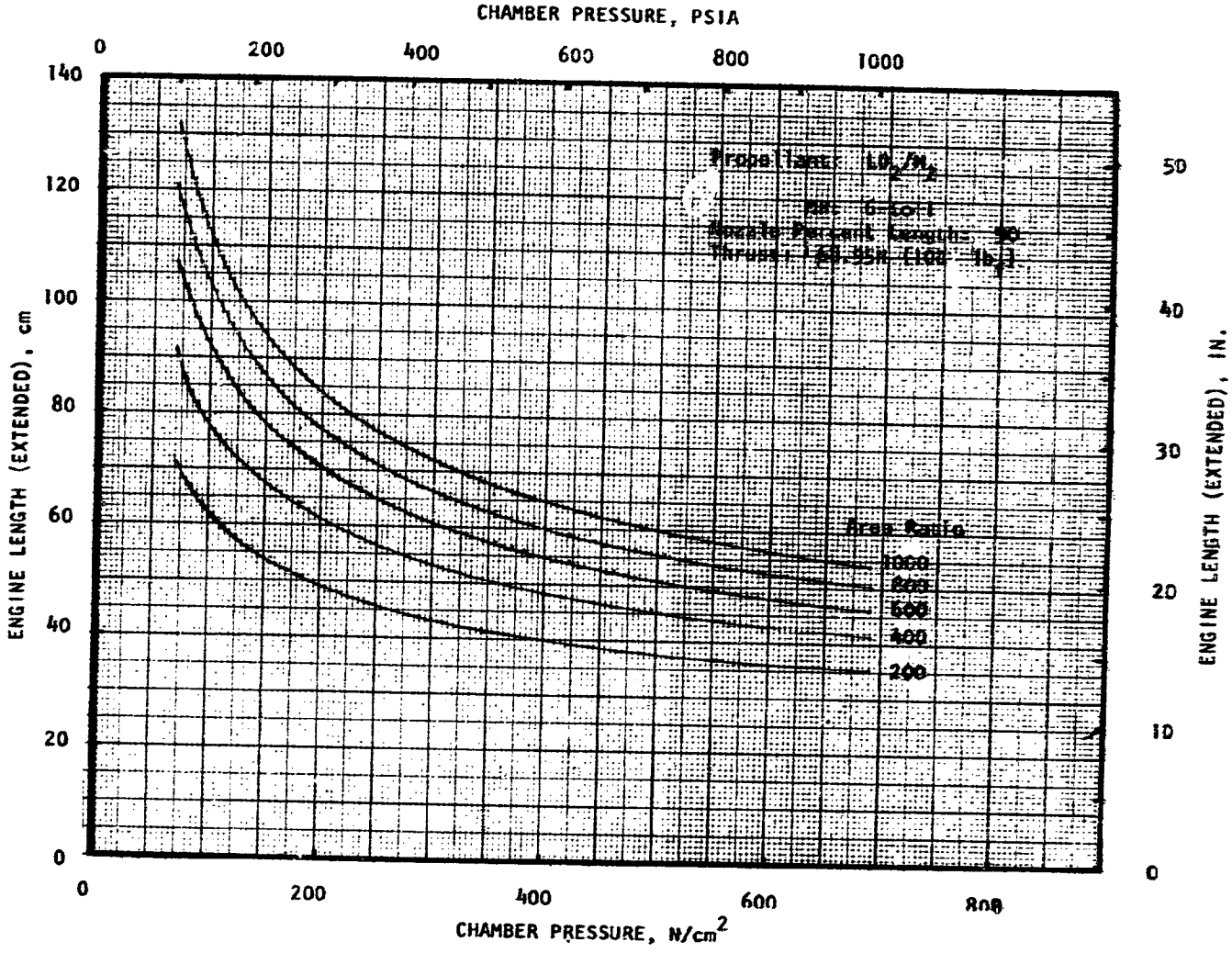

Figure E-10. Total LO_2/H_2 Engine Length Variation with Chamber Pressure and Nozzle Area Ratio (Thrust = 68.95 N (100 lbf)

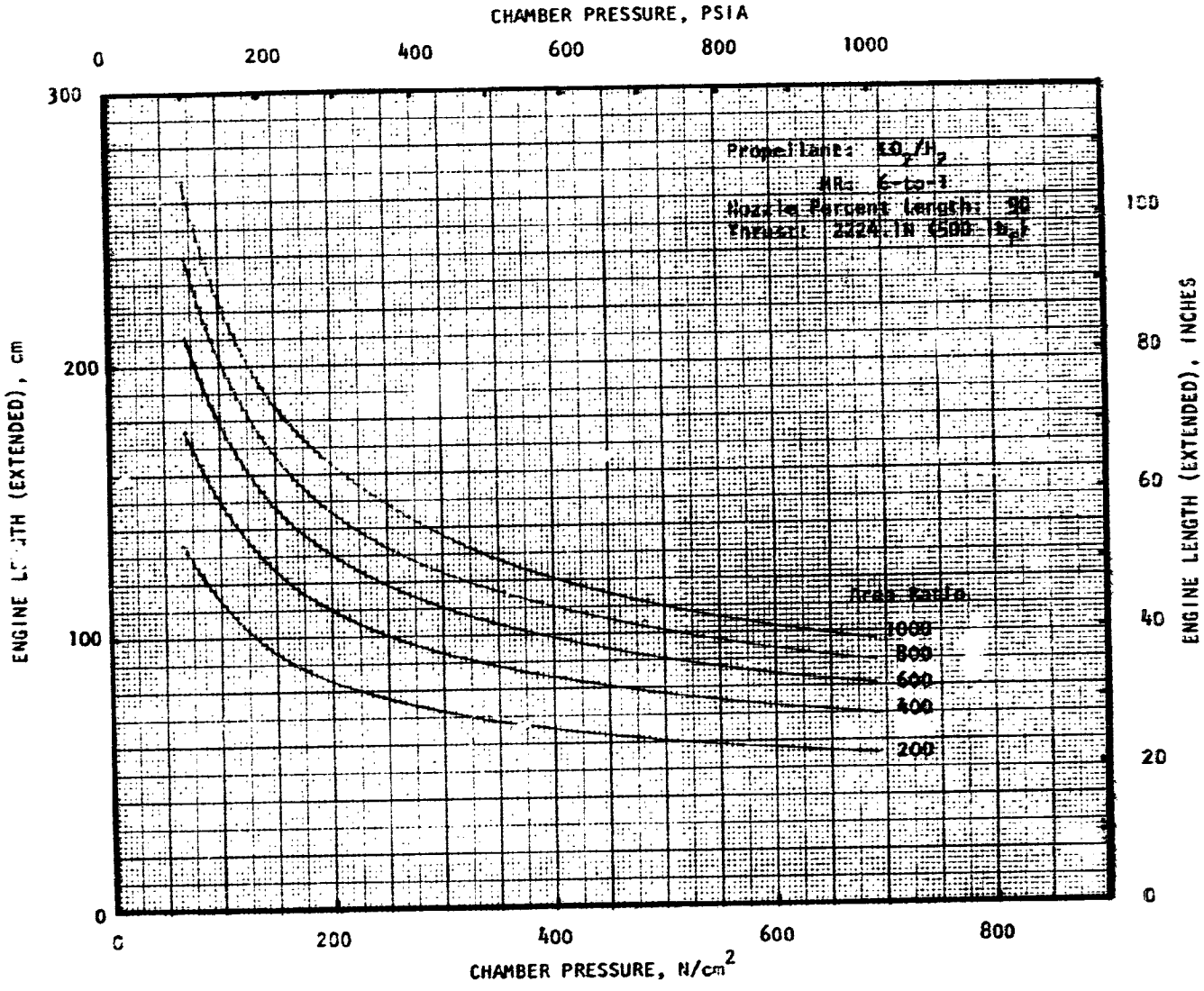

Figure E-11 Total LO_2/H_2 Engine Length Variation with Chamber Pressure and Nozzle Area Ratio (Thrust = 2224.1 N (500 lbf)

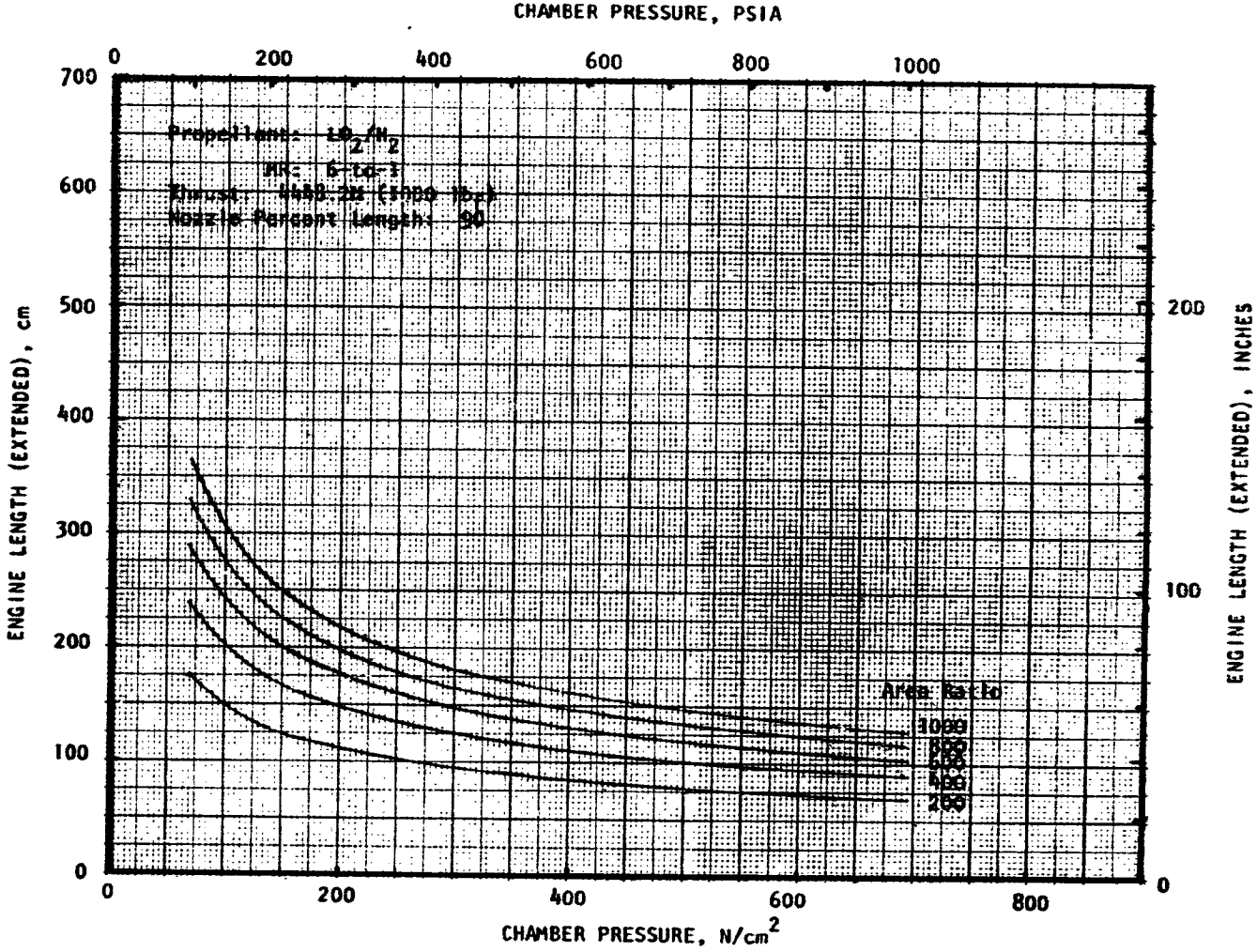

Figure E-12 Total LO_2/H_2 Engine Length Variation with Chamber Pressure and Area Ratio (Thrust = 4448.2 N (1000 lbf)

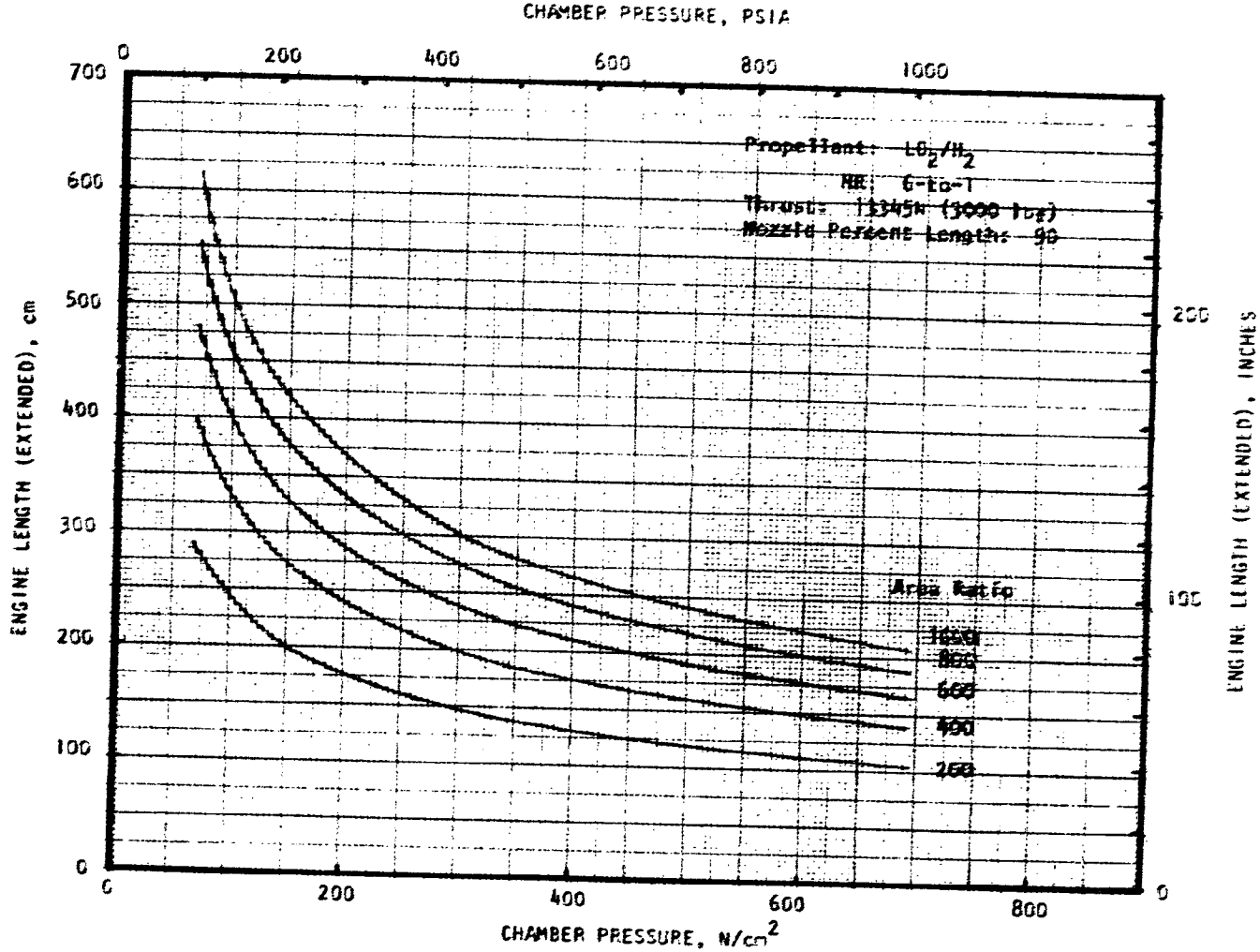

Figure E-13 Total LO_2/H_2 Engine Length Variation with Chamber Pressure and Area Ratio (Thrust = 13345 N (3000 lbf)

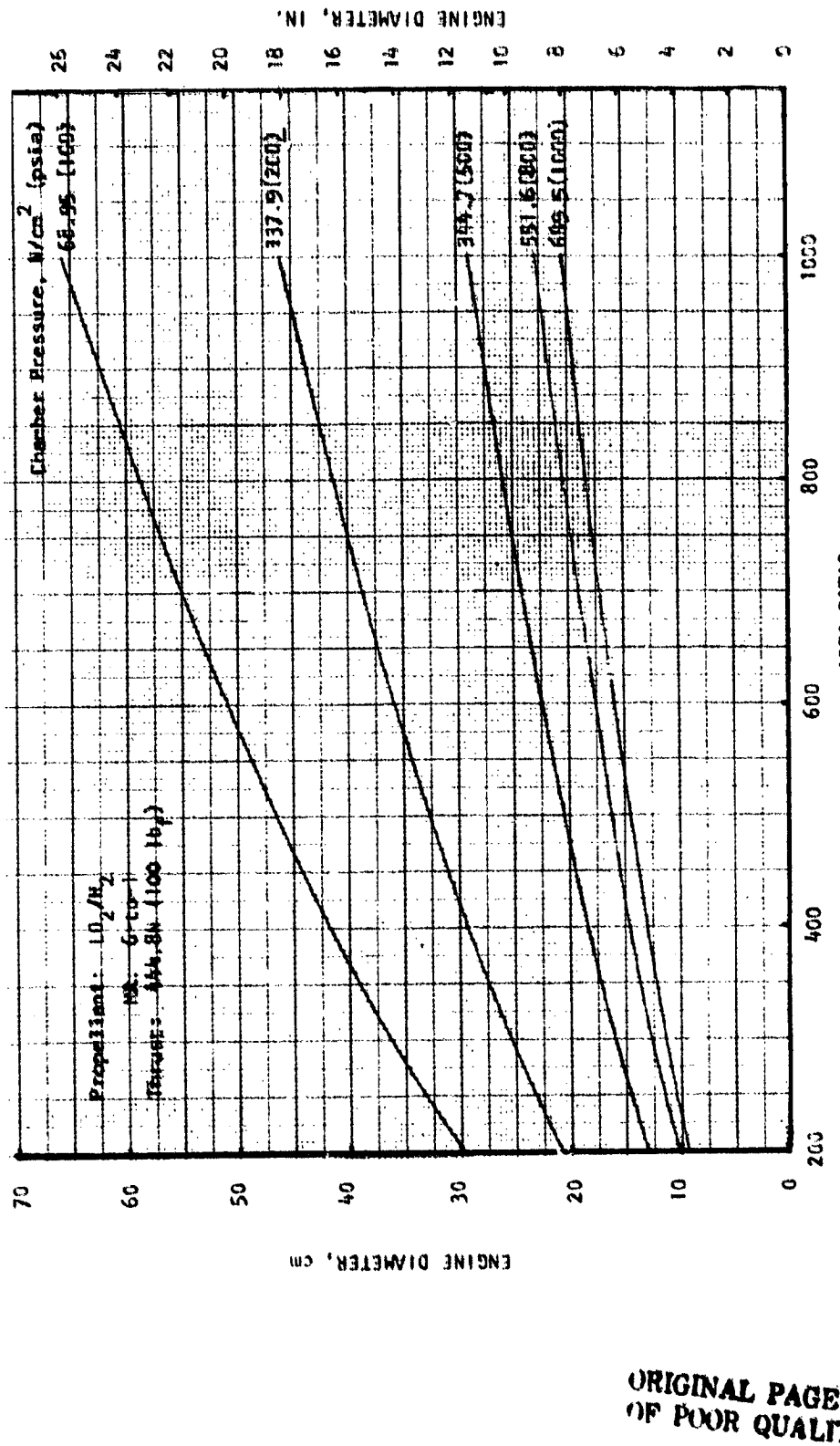

Figure E-14. LO_2/H_2 Engine Diameter Variation with Area Ratio and Chamber Pressure (Thrust = 444.8 N (100 lbf)

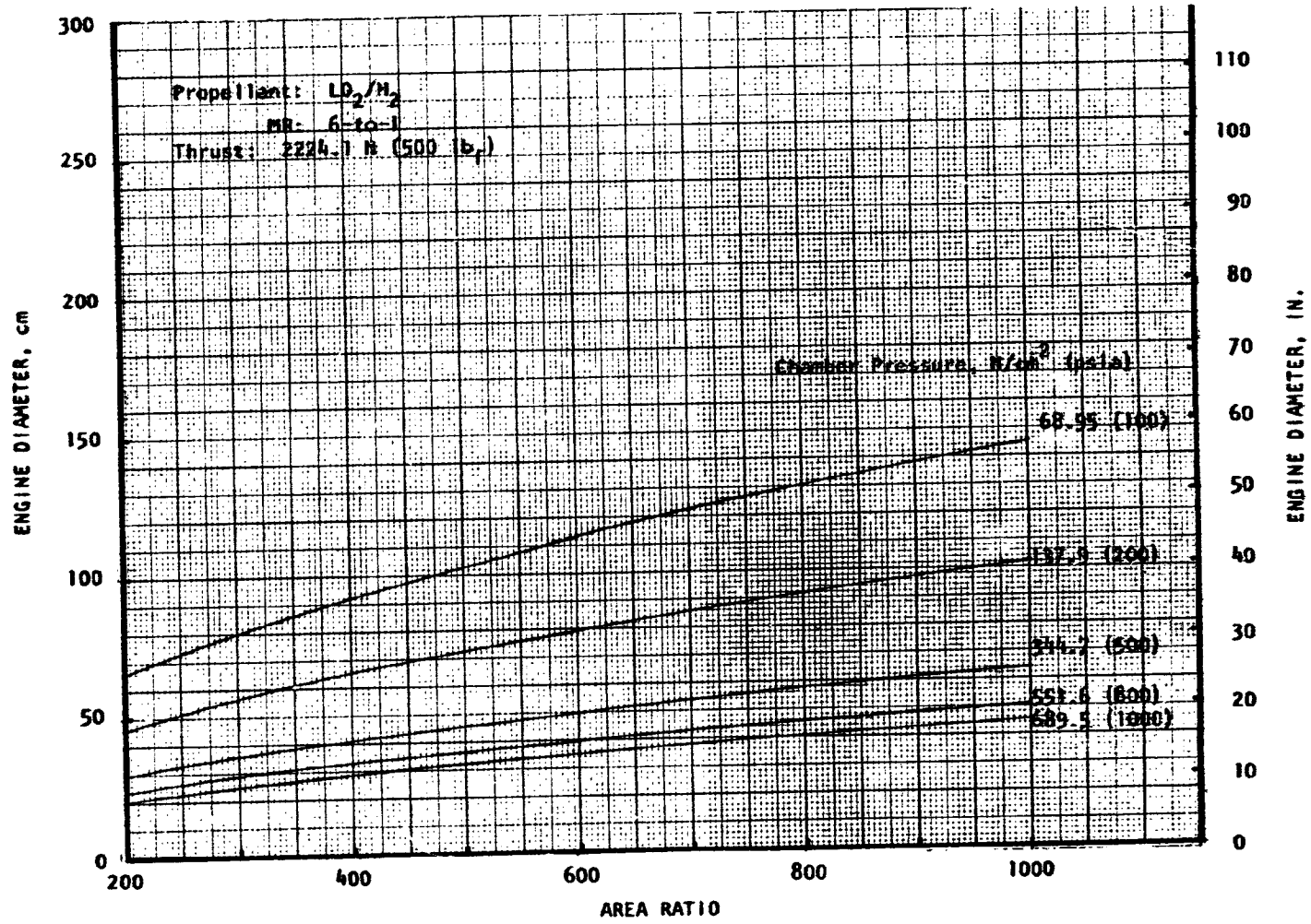

Figure E-15. LO_2/H_2 Engine Diameter Variation with Area Ratio and Chamber Pressure (Thrust = 2224.1 N (500 lbf)

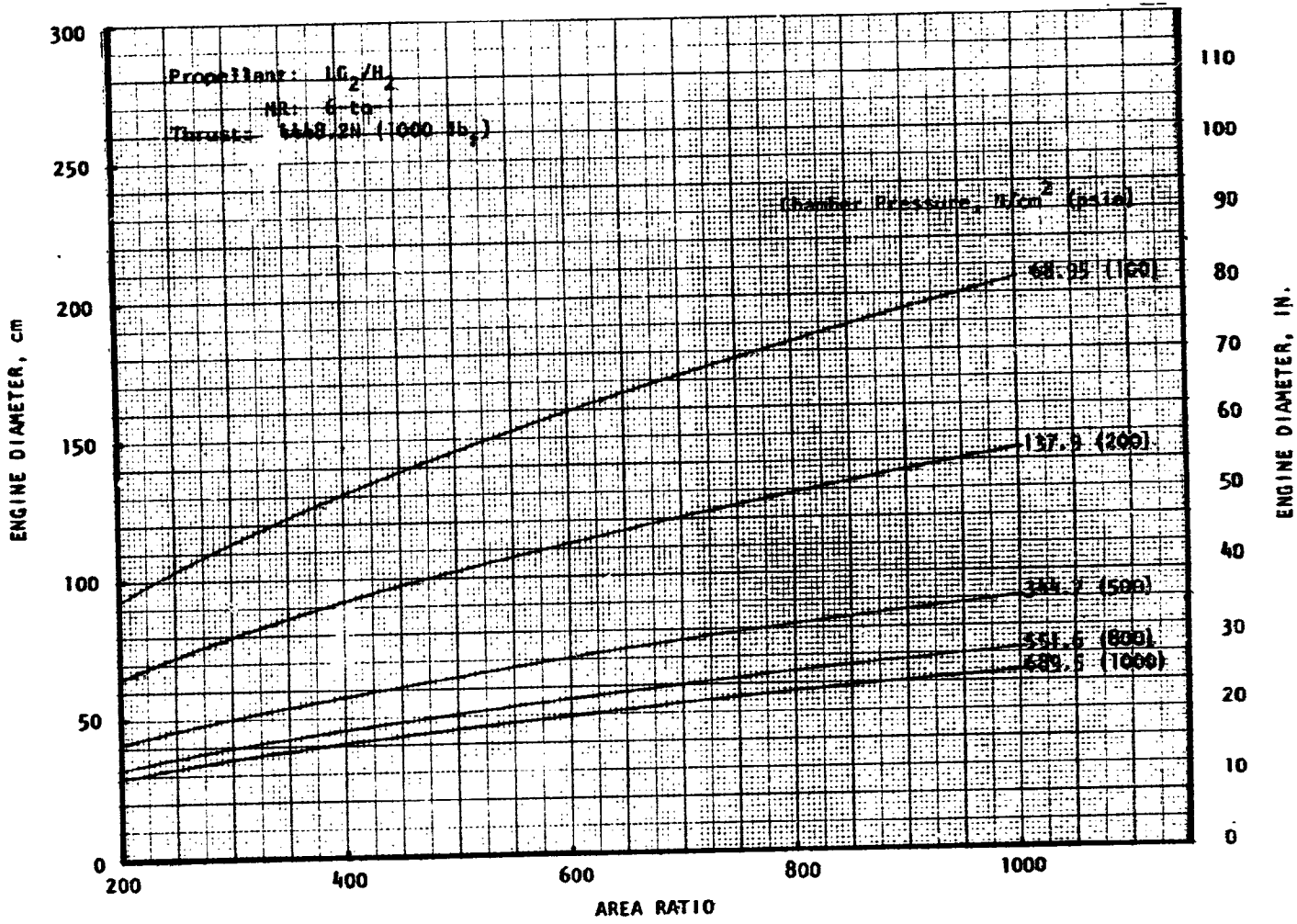

Figure E-16 LO_2/H_2 Engine Diameter Variation with Area Ratio and Chamber Pressure (Thrust = 4448.2 N (1000 lbf)

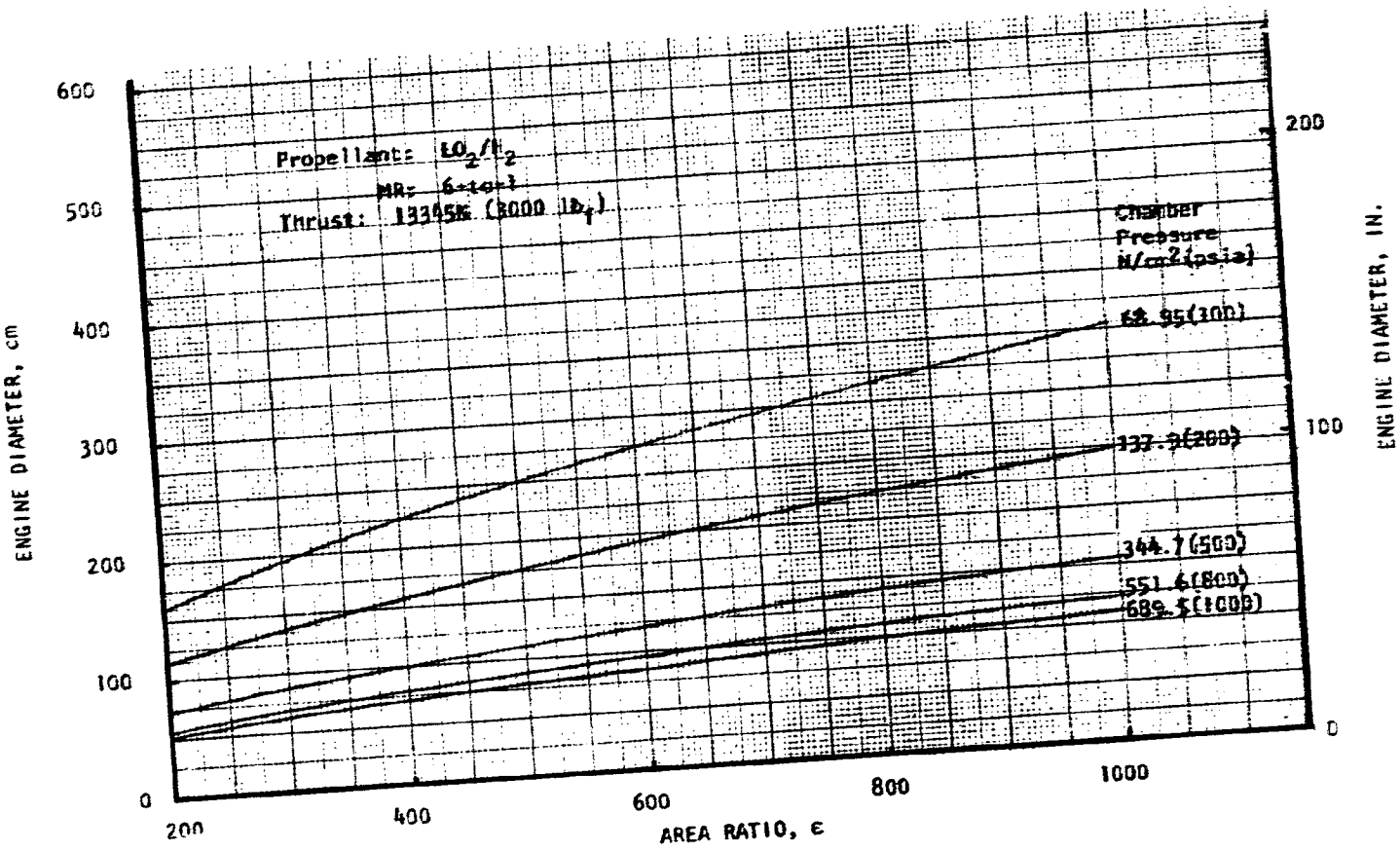

Figure E-17 LO_2/H_2 Engine Diameter Variation with Area Ratio and Chamber Pressure (Thrust = 13345 N (3000 lbf)

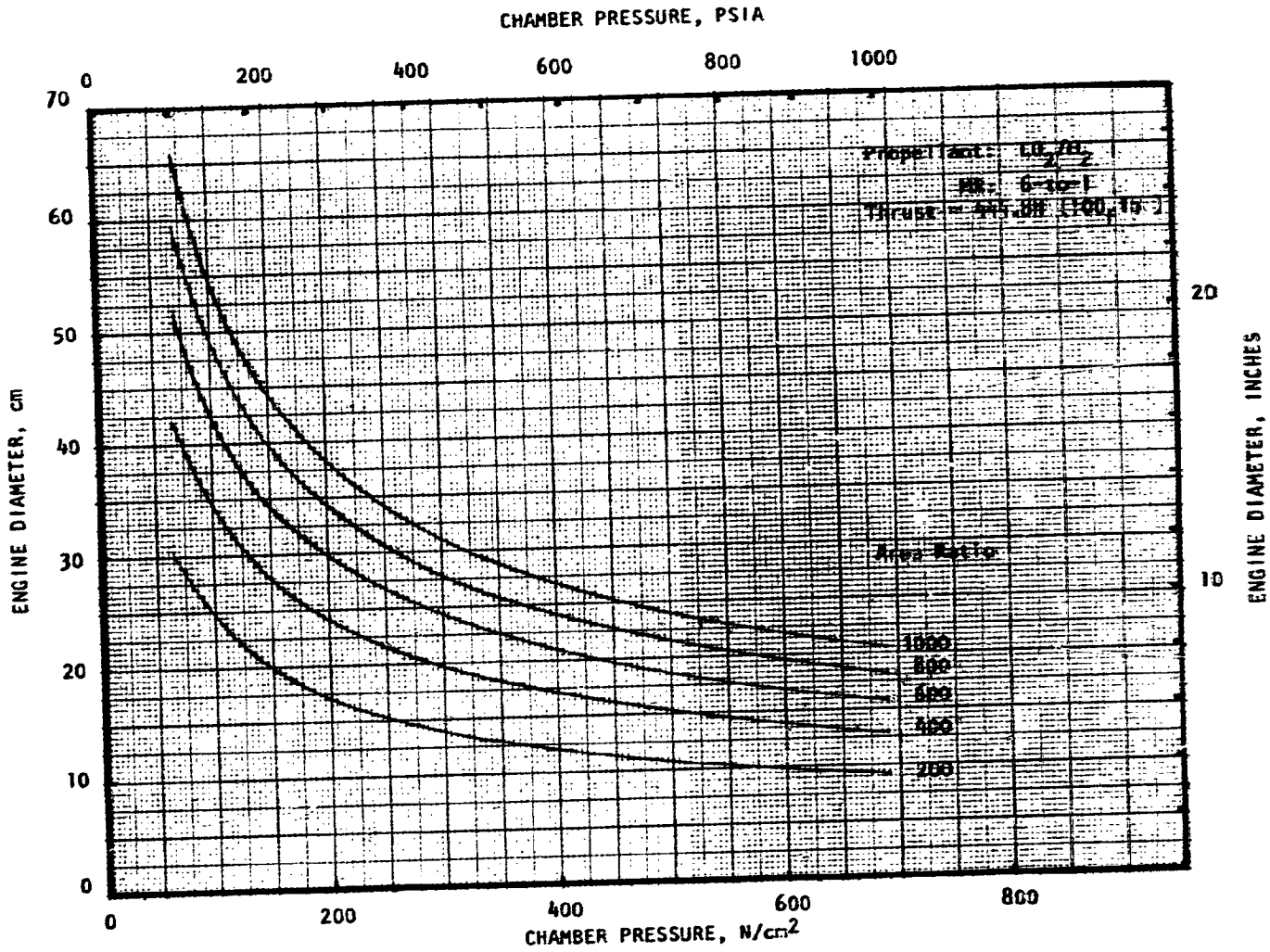

Figure E-18. Total LO_2/H_2 Engine Length Variation With Chamber Pressure and Nozzle Area Ratio (Thrust = 444.8N (100$_f$lb)

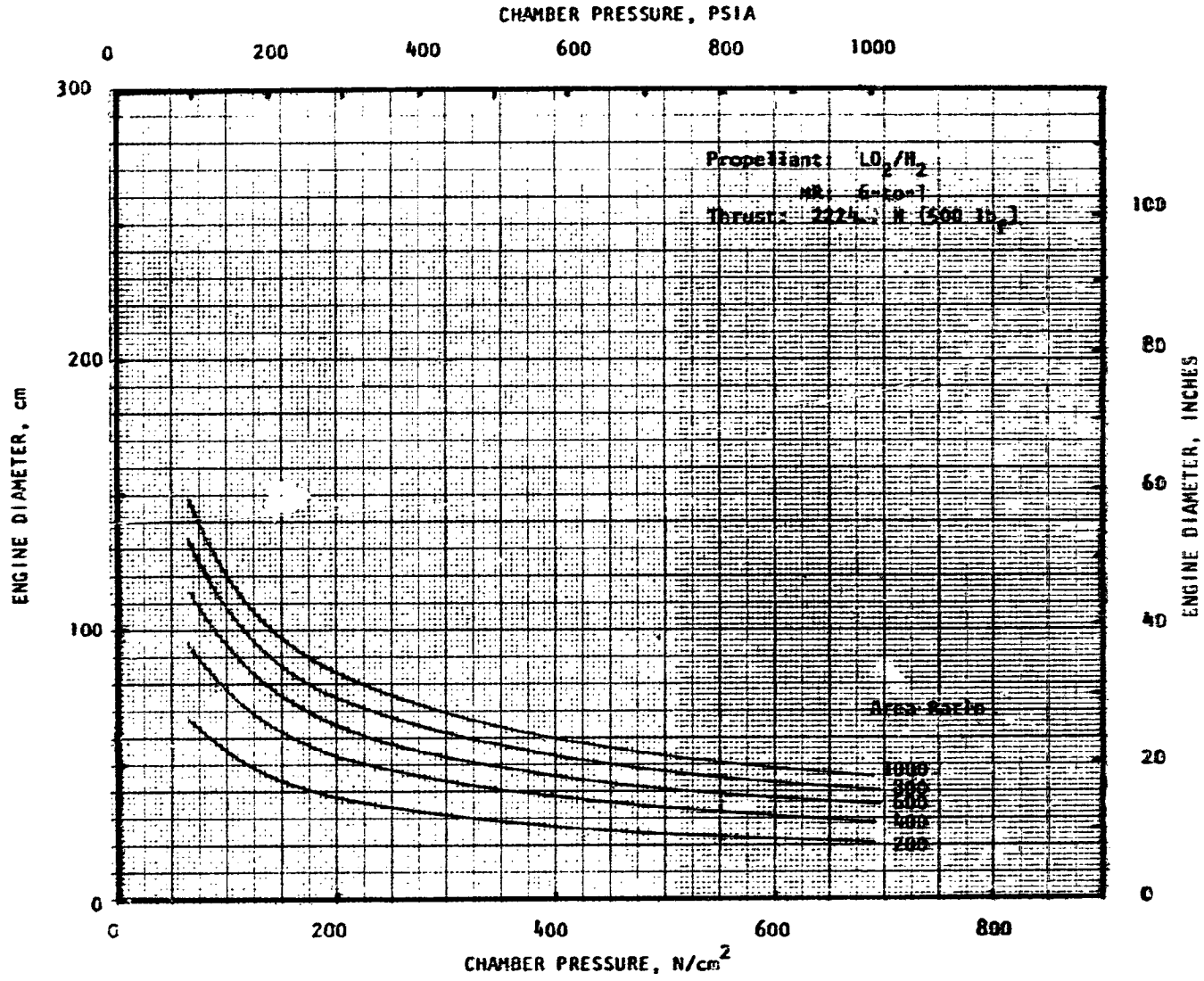

Figure E-19. LO_2/H_2 Engine Diameter Variation With Chamber Pressure and Area Ratio (Thrust = 2224.1 N (500 lb_f)

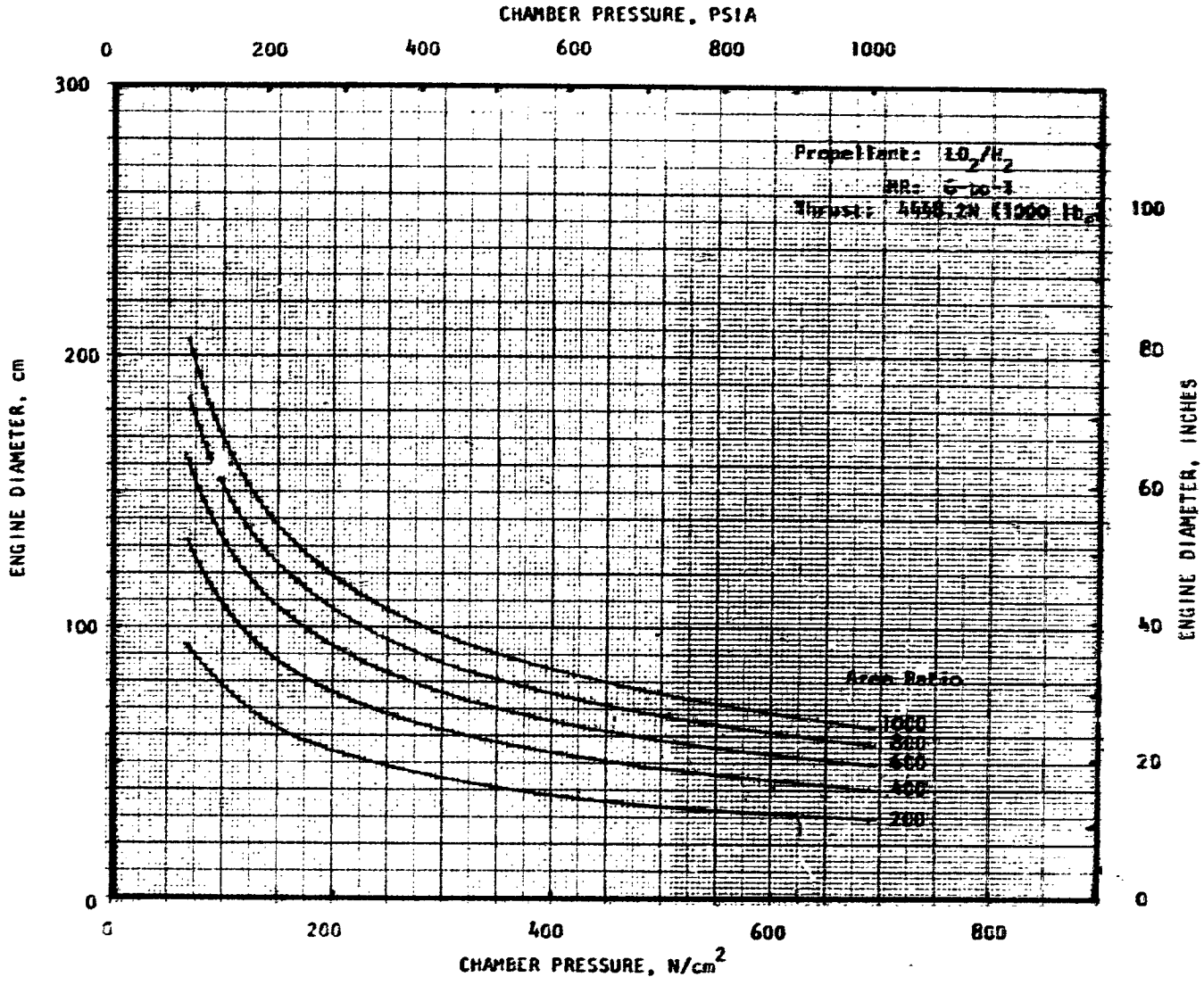

Figure E-20. LO_2/H_2 Engine Diameter Variation With Chamber Pressure and Area Ratio (Thrust = 4448.2N (1000 lb_f)

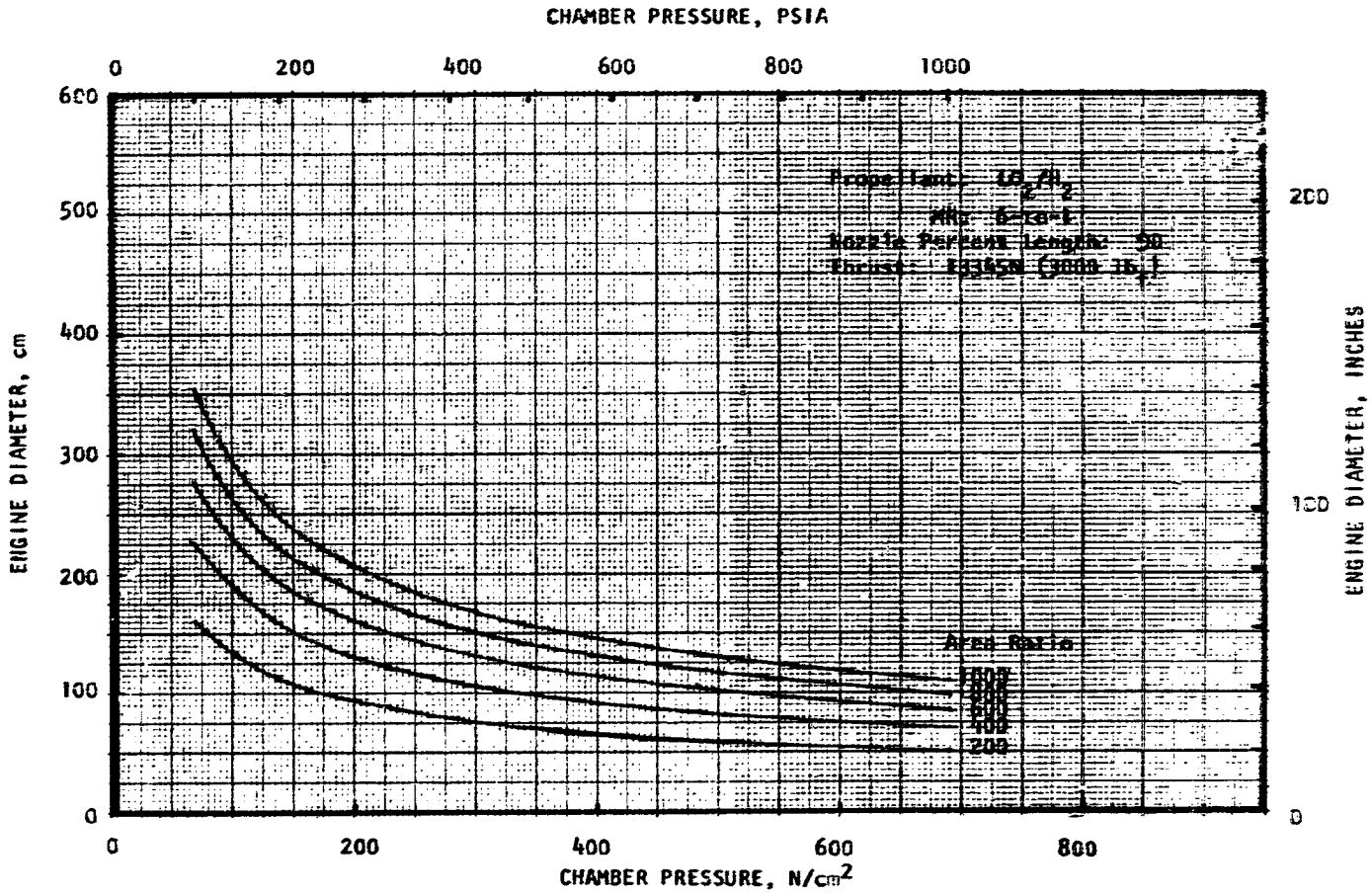

Figure E-21. LO_2/H_2 Engine Length Variation With Chamber Pressure and Nozzle Area Ratio (Thrust = 13345N (3000 lb_f)

APPENDIX F

PARAMETRIC ENGINE WEIGHT

Parametric engine weight for the LO_2/H_2 and LO_2/CH_4 expander cycle engines were generated for the thrust, chamber pressure, and nozzle area ratio of interest. These parametric plots included:

1. Engine weight versus chamber pressure for parametric thrust at constant nozzle area ratio

2. Engine weight versus nozzle area ratio for parametric chamber pressure at constant thrust

Note that the parametric data are presented over the entire study range of thrust (444.8 N, 100 Lbf to 13345 N, 3000 Lbf) and chamber pressure (68.95 N/cm^2, 100 psia to 689.5 N/cm^2, 1000 psia). In using these data for mission studies it is important to consider possible engine system design constraints in order to abold unrealistic design points. The parametric plots of delivered specific impulse versus thrust for the 400-to-1 area ratio LO_2/H_2 and LO_2/CH_4 engines (Figures D-6 and D-20, Appendix D) show the preliminary design points, thrust chamber cooling constraints which resulted from this study. These constraints can be used to conservatively define feasible engine system operating conditions over the range of thrust and chamber pressure.

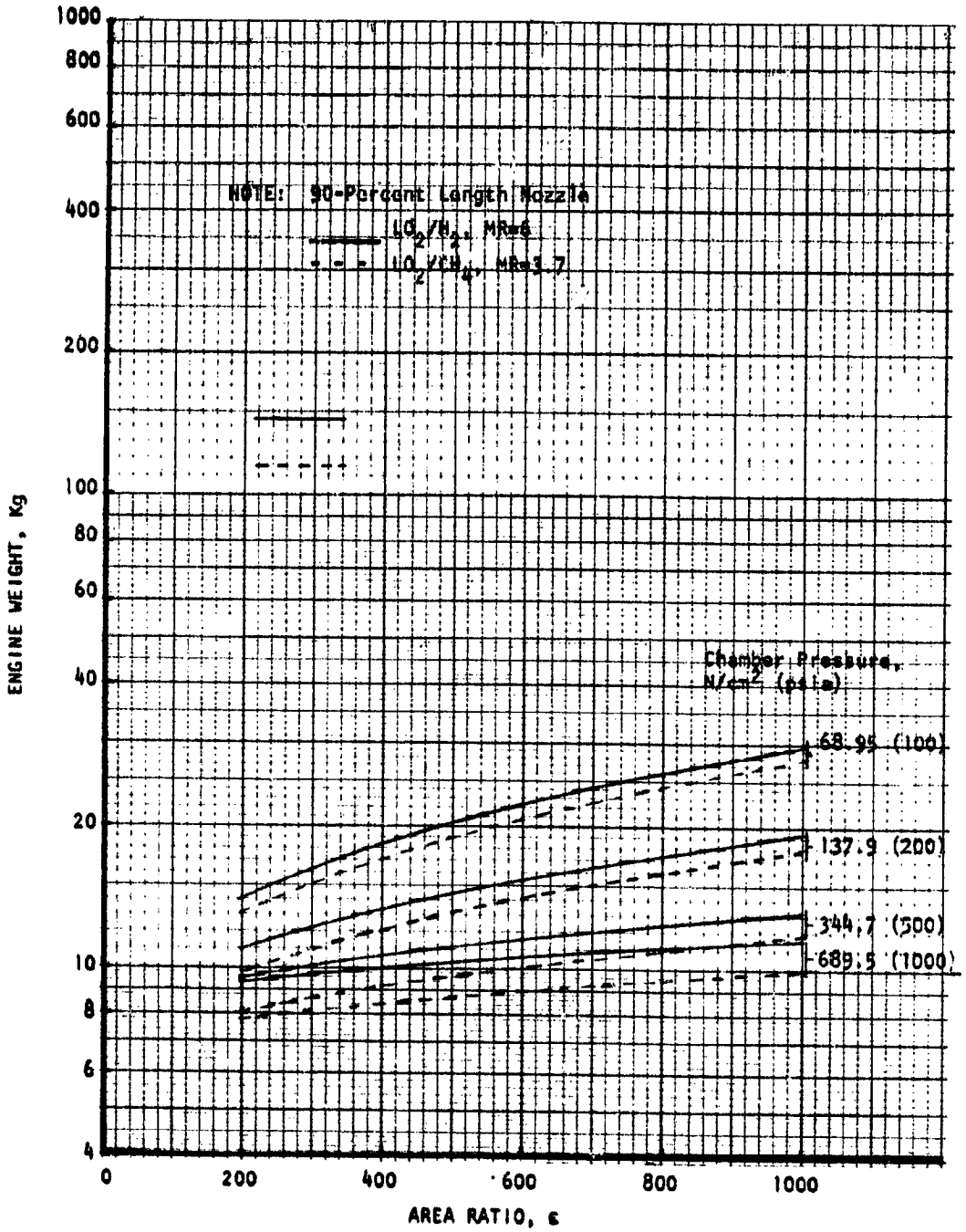

Figure F-1. Engine Weight Variation With Nozzle Area Ratio and Chamber Pressure (Thrust = 444.8N (100_f lb)

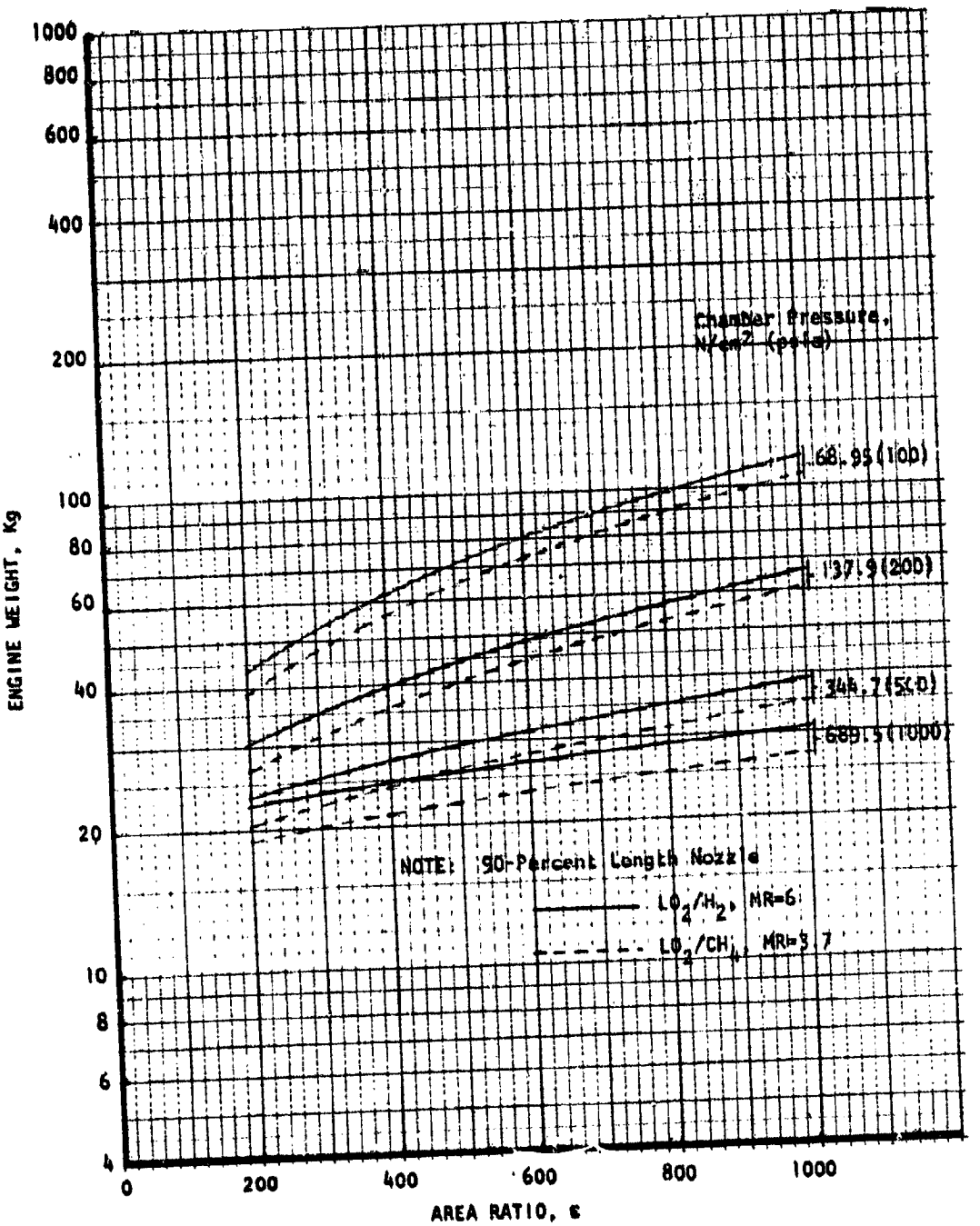

Figure F-2. Engine Weight Variation With Nozzle Area Ratio and Chamber Pressure (Thrust = 2224.1N (500 lb_f)

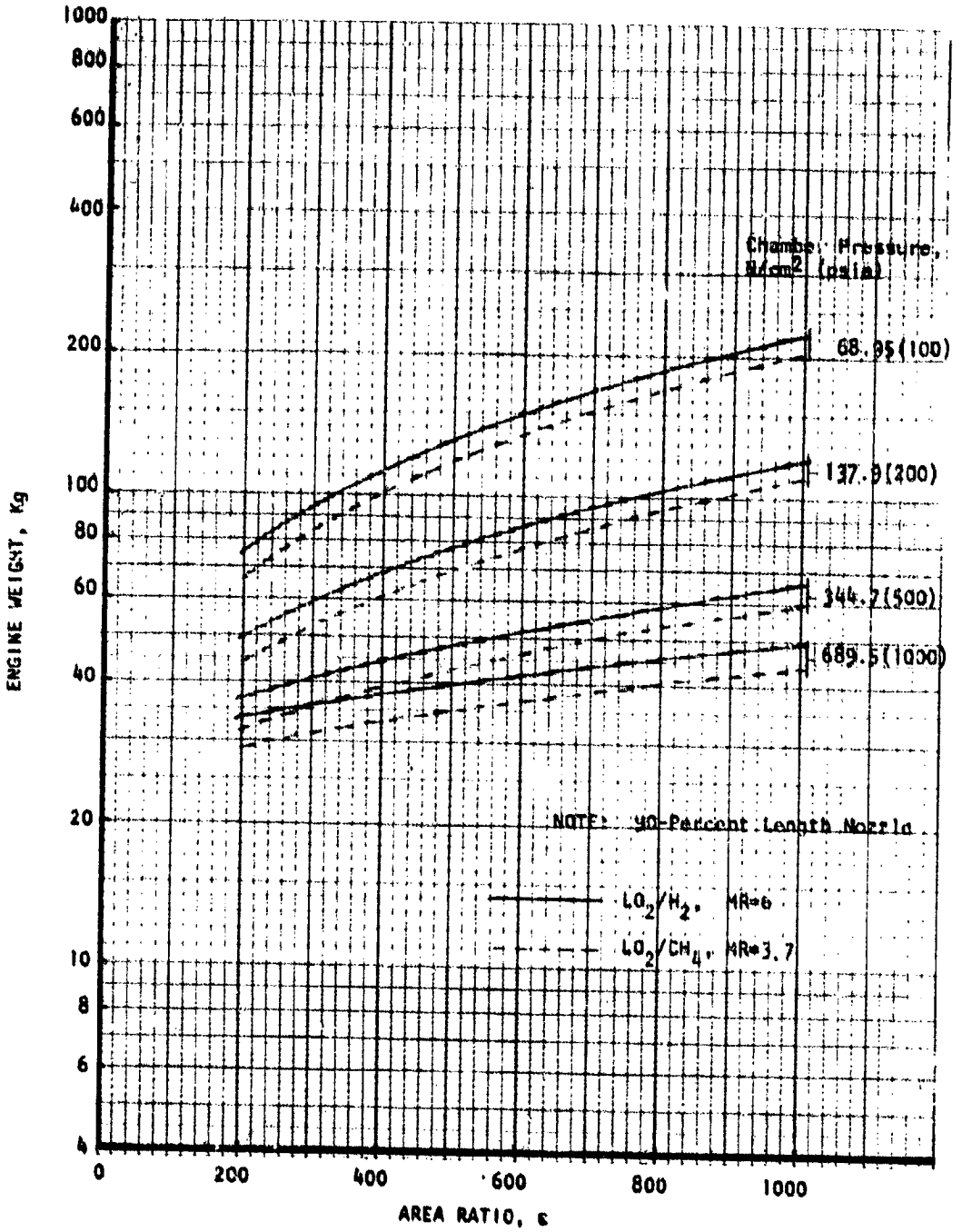

Figure F-3. Engine Weight Variation With Nozzle Area Ratio and Chamber Pressure (Thrust = 4448.2N (1000 lb_f))

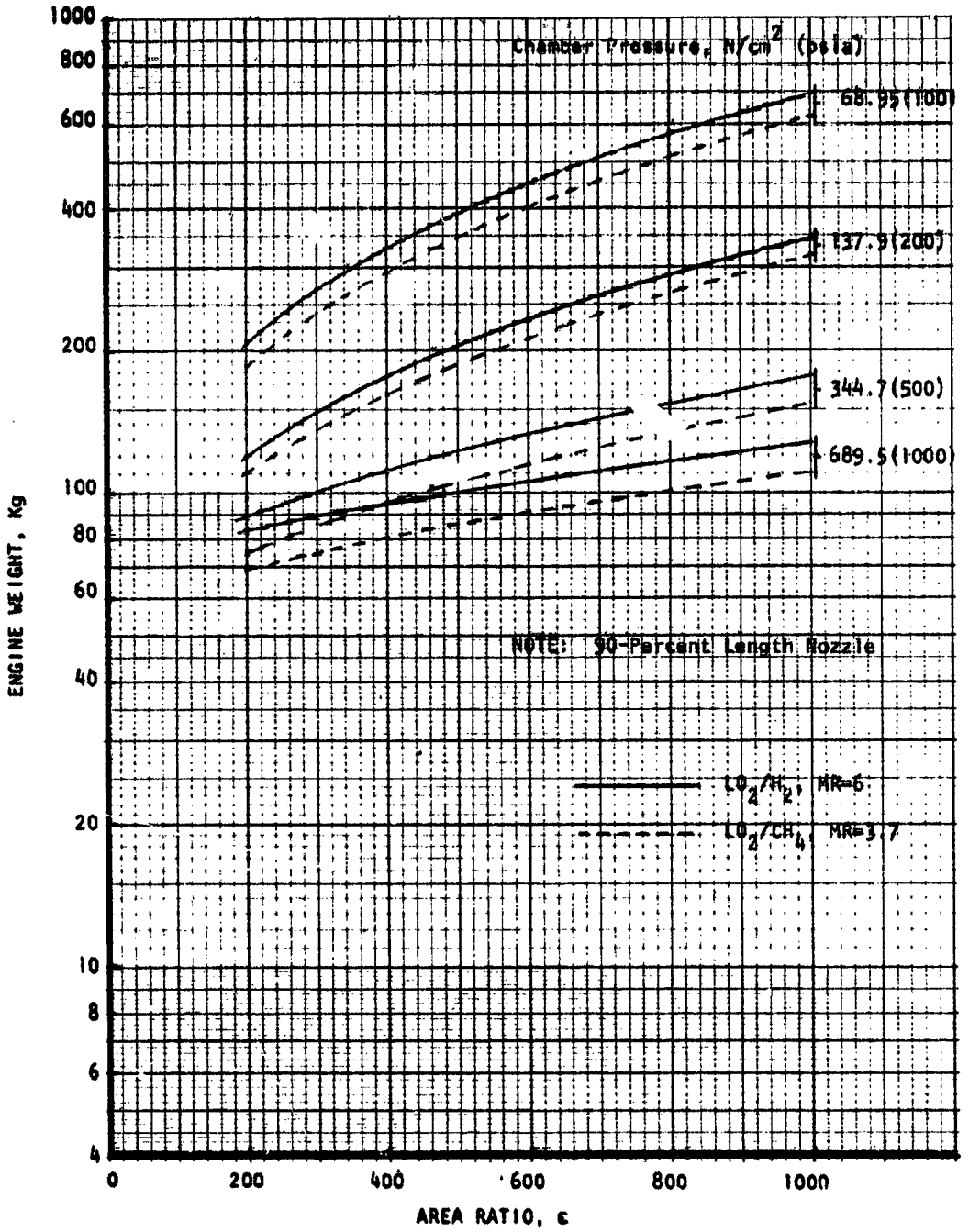

Figure F-4. Engine Weight Variation With Nozzle Area Ratio and Chamber Pressure (Thrust = 13345N (3000 lb)

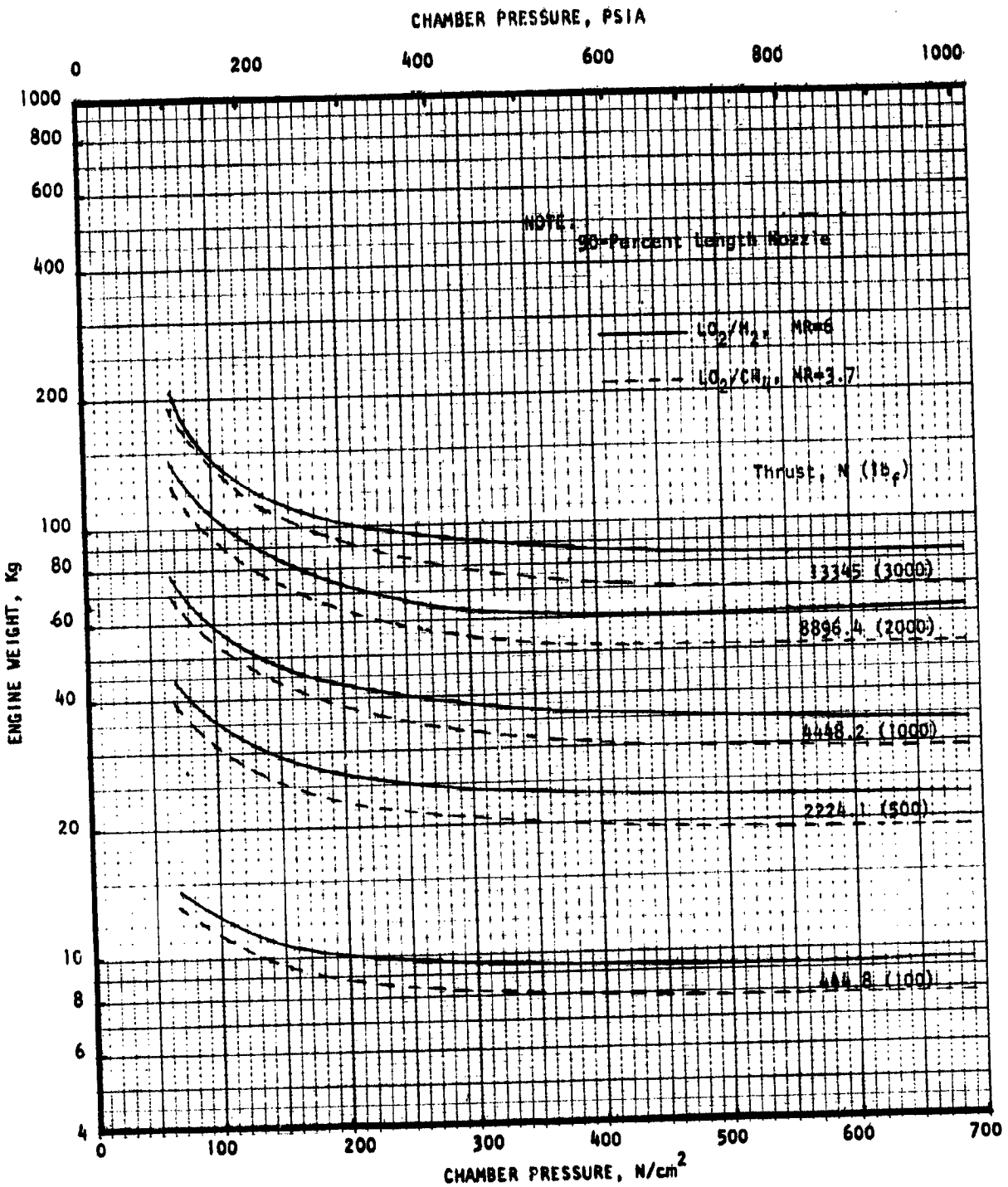

Figure F-5. Engine Weight Variation With Chamber Pressure and Thrust (Nozzle Area Ratio = 200)

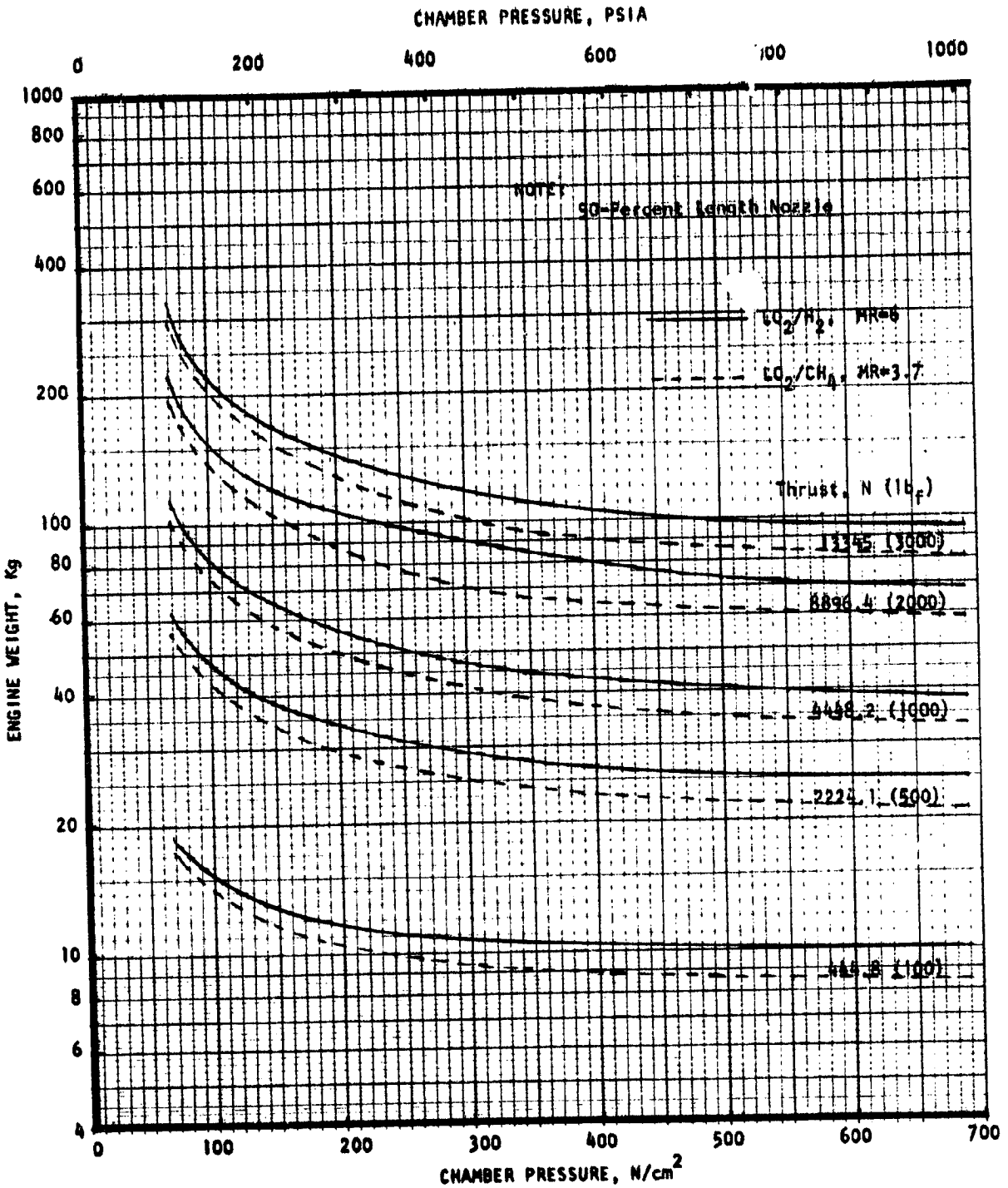

Figure F-6. Engine Weight Variation With Chamber Pressure and Thrust (Nozzle Area Ratio = 400)

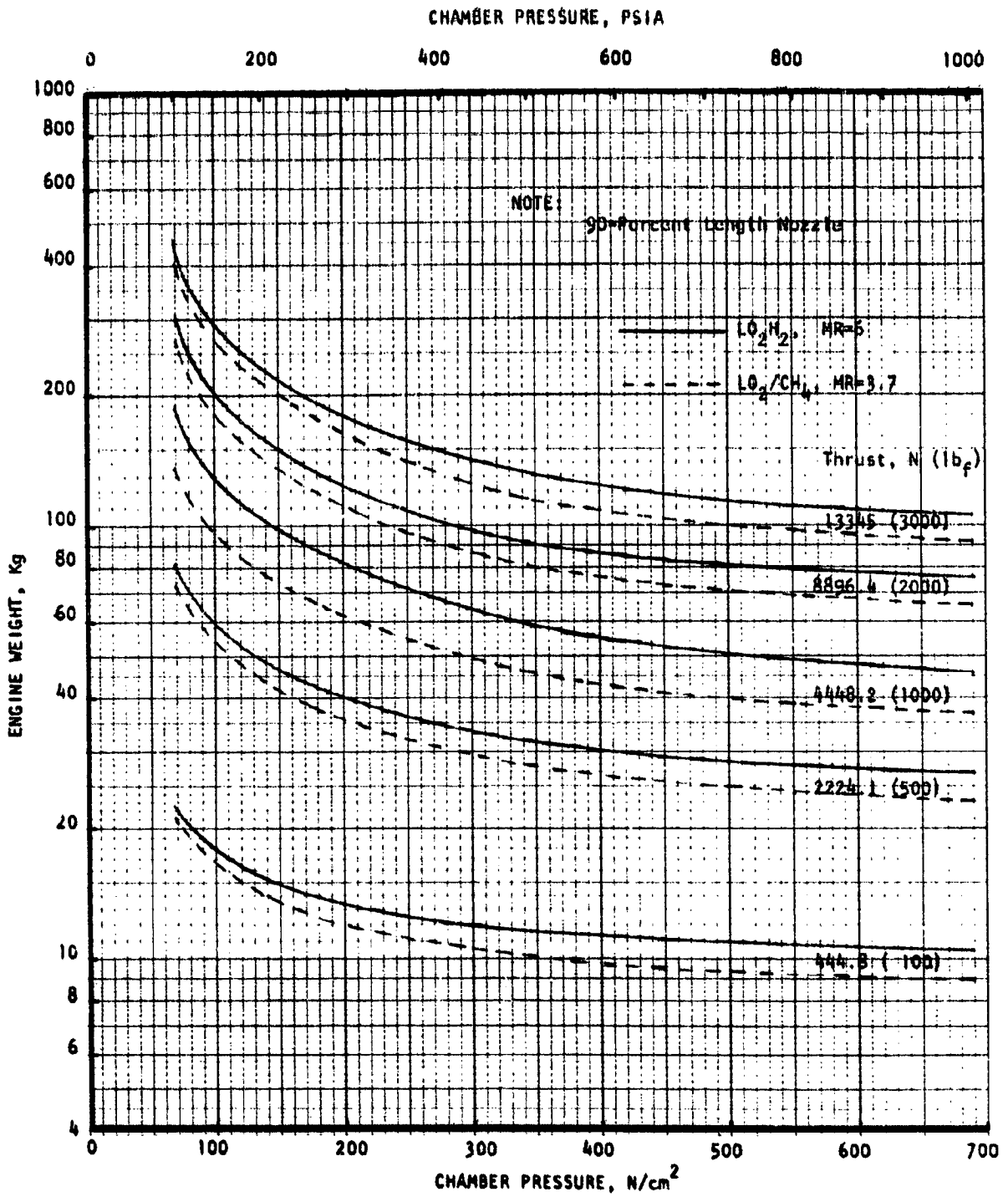

Figure F-7. Engine Weight Variation With Chamber Pressure and Thrust (Nozzle Area Ratio = 600)

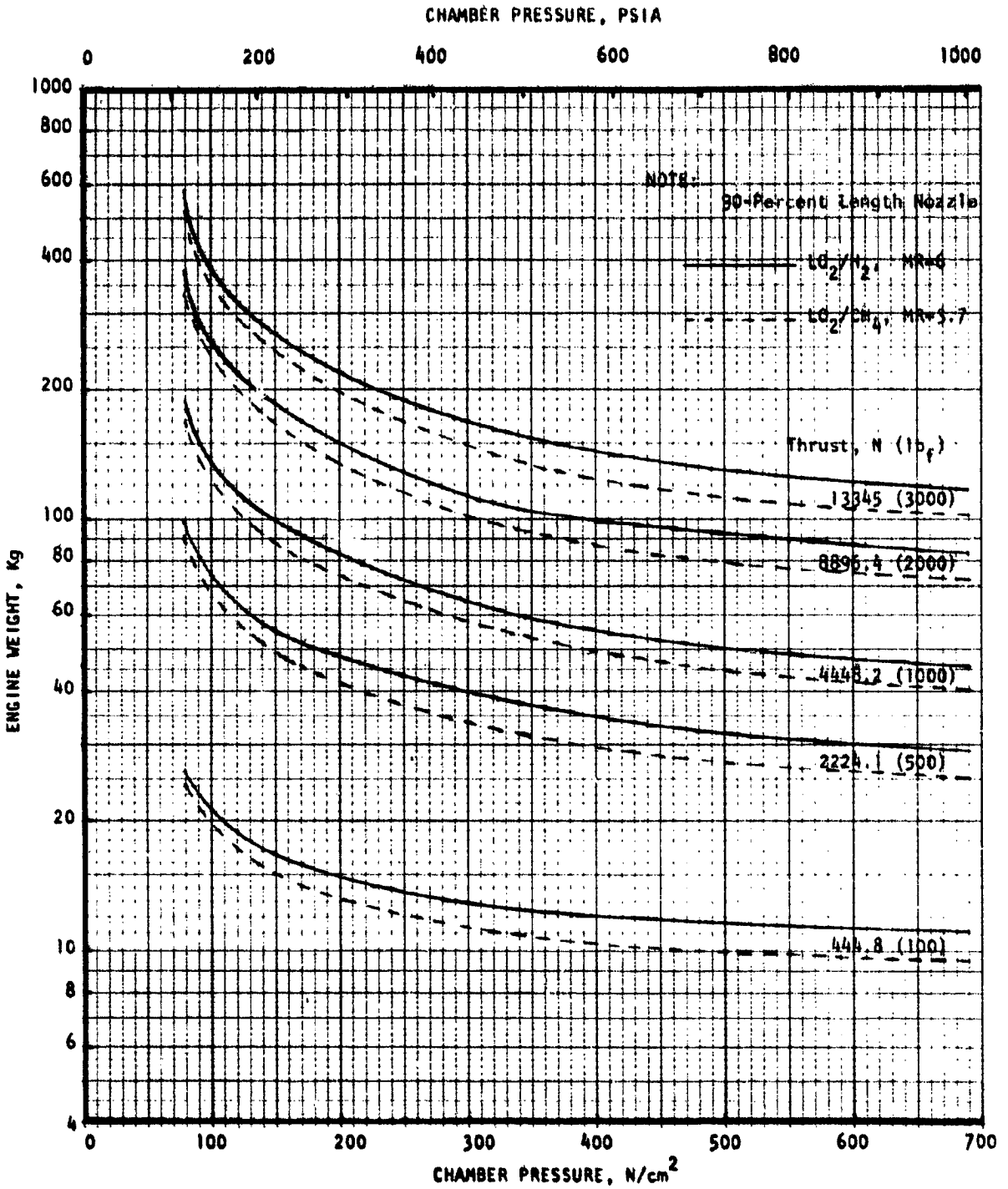

Figure F-8. Engine Weight Variation With Chamber Pressure and Thrust (Nozzle Area Ratio = 800)

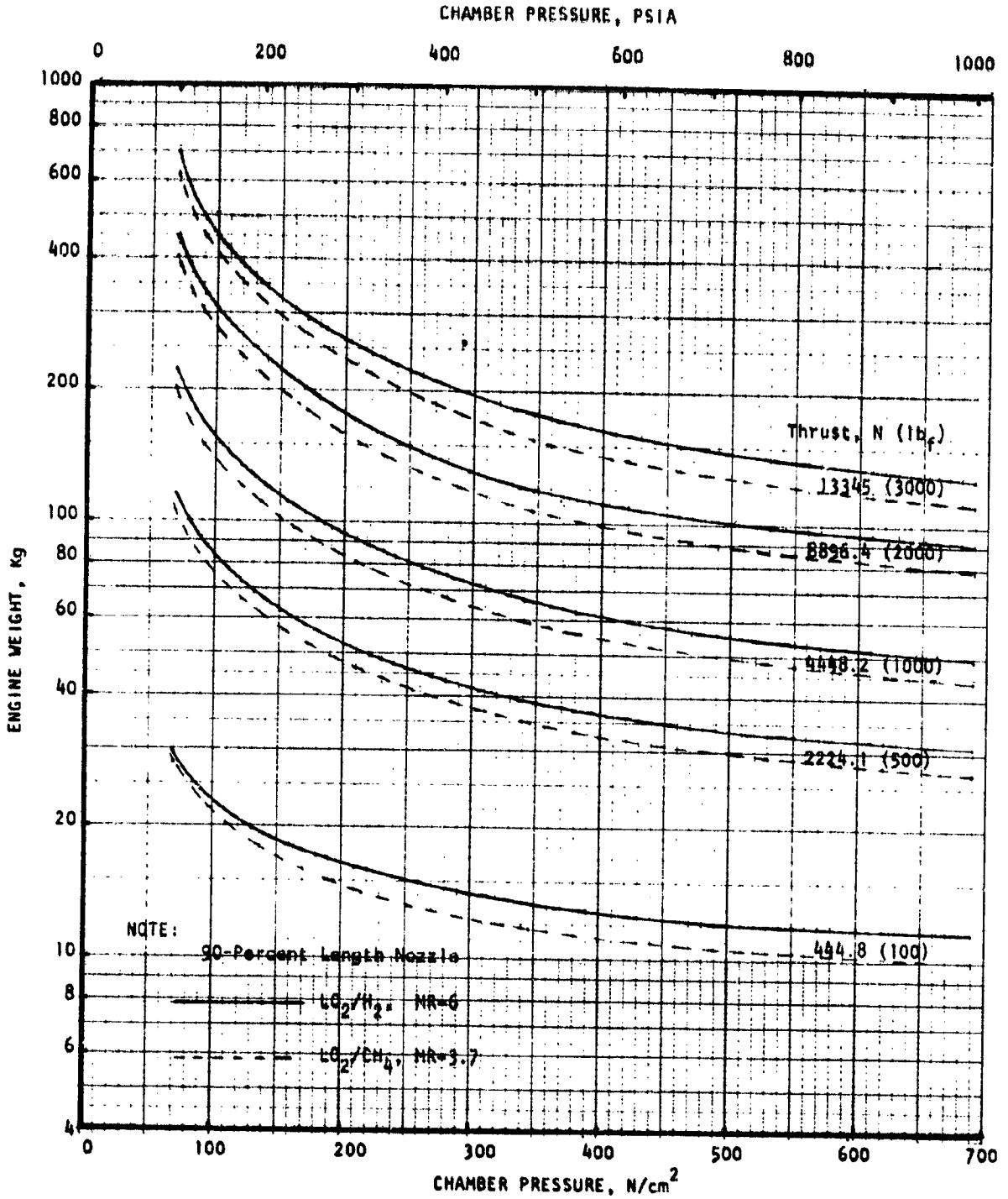

Figure F-9. Engine Weight Variation With Chamber Pressure and Thrust (Nozzle Area Ratio = 1000)